

Hugo Renato Gonçalves da Silva Augusto

CHARACTERIZATION OF THE BEHAVIOUR OF PARTIAL-STRENGTH JOINTS UNDER CYCLIC AND SEISMIC LOADING CONDITIONS

Tese de Doutoramento em Construção Metálica e Mista, orientada pelo Professor Doutor Carlos Alberto da Silva Rebelo e pelo Professor Doutor José Miguel de Freitas Castro, apresentada ao Departamento de Engenharia Civil da Faculdade de Ciências e Tecnologia da Universidade de Coimbra

Abril, 2017



UNIVERSIDADE DE COIMBRA

Hugo Augusto

**CHARACTERIZATION OF THE BEHAVIOUR
OF PARTIAL-STRENGTH JOINTS UNDER
CYCLIC AND SEISMIC LOADING
CONDITIONS**

Tese de Doutoramento em Construção Metálica e Mista, orientada pelo Professor Doutor Carlos Alberto da Silva Rebelo e pelo Professor Doutor José Miguel de Freitas Castro, apresentada ao Departamento de Engenharia Civil da Faculdade de Ciências e Tecnologia da Universidade de Coimbra

Abril, 2017



UNIVERSIDADE DE COIMBRA

CHARACTERIZATION OF THE BEHAVIOUR OF PARTIAL-STRENGTH JOINTS UNDER CYCLIC AND SEISMIC LOADING CONDITIONS

(CARACTERIZAÇÃO DO COMPORTAMENTO DE LIGAÇÕES
DE RESISTÊNCIA PARCIAL SUJEITAS A CARREGAMENTOS
CÍCLICOS E SÍSMICOS)

Hugo Renato Gonçalves da Silva Augusto

Supervisors (Orientadores):

Prof. Doutor Carlos Alberto da Silva Rebelo
(Universidade de Coimbra)

Prof. Doutor José Miguel de Freitas Castro
(Universidade do Porto)

Thesis presented in fulfillment of the requirements for the degree of Doctor of
Philosophy in Steel and Mixed Construction

(Tese apresentada para a obtenção do grau de Doutor em Construção Metálica e
Mista)

Coimbra, Abril, 2017

Institutions and support:



FCTUC DEPARTAMENTO DE ENGENHARIA CIVIL
FACULDADE DE CIÊNCIAS E TECNOLOGIA
UNIVERSIDADE DE COIMBRA



Institute for Sustainability and
Innovation in Structural Engineering

Cofinanciado por:



UNIÃO EUROPEIA
Fundo Europeu
de Desenvolvimento Regional

FCT Fundação para a Ciência e a Tecnologia

MINISTÉRIO DA CIÊNCIA, TECNOLOGIA E ENSINO SUPERIOR



UNIÃO EUROPEIA
Fundo Social Europeu



*“He who is not courageous enough to take risks will
accomplish nothing in life.”*

Muhammad Ali

“Analysis should be as simple as possible, but no simpler”

Albert Einstein

*We can do much in life, but we will only be truly realized
when we do the right things...*

Hugo Augusto

Abstract

This thesis deals with the numerical and analytical modelling of beam-to-column steel joints, when subjected to monotonic, cyclic or dynamic loading, addressing both the global response of the joint and the behaviour of the critical components. End-plate bolted connections are widely used in Europe, due to its attractive manufacturing and erecting costs and its easy integration into the building structure and architecture. Although their design for use in non-seismic regions is fully supported by the design rules in Eurocode 3, current seismic design codes, like the Eurocode 8, do not provide enough information or any design tools to allow their practical use also in seismic regions. The available procedure in the Eurocode 3 based on the Component Method, to characterize the joints behaviour, is only applicable for monotonically loaded joints.

One main goal of this research is to contribute for the developing of an analytical design method, based on the component method, which considers the cyclic behaviour of the joints given by the proper contribution of each dissipative component, assuming that the adequate overstrength is assured for the non-dissipative components (capacity design). A further important goal of this research is to contribute to the development and improvement of displacement-based design procedures, proposing improved ductility-equivalent viscous damping relationships for steel moment-resisting framed (MRF) structures with dissipative beam-to-column partial-strength joints.

In order to achieve the main goals proposed above, a calibrated parametric finite element (FE) model of a double extended beam-to-column end-plate steel joint is developed and calibrated with the available results of experimental work, also examined in here. The set of numerical models generated with the parametric script is developed in Python and use the software package ABAQUS.

The main outputs of the research are: i) the detailed FE model that is capable of simulating, with accuracy, the behaviour of end-plate beam-to-column joints and its components; ii) the several detailed procedures proposed to isolate some of the most relevant and dissipative components that contribute to the joint behaviour, namely: column web panel

in shear, column web in transverse tension and/or compression, column flange in bending and end-plate in bending; iii) the identification of the components' mechanical behaviour in terms of force-displacement relationships by analysing the stress and deformation fields in the FE models, which can be used directly in a component based mechanical model of the joint; iv) improved ductility-equivalent viscous damping relationships (μ -EVD), considering the influence of the several dissipative components involved in the double-extended end-plate joints, which can be used directly in procedures like the Direct Displacement-Based Seismic Design (Priestley *et al.*, 2007).

The proposed procedures to isolate the components behaviour are very flexible in terms of the definition of the integration boundaries; according to the mechanical model chosen. The procedure is able to capture the behaviour of the identified components, including the additional shear resistance provided by the transverse web stiffeners. The use of this stiffeners considerably affects the behaviour of the joints and its components. In the component end-plate in bending the inner bolt rows closer to the beam flanges present stable cycles without pinching, unlike the external rows, which clearly are affected by that phenomenon. The extraction of the components revealed also that the basic component column web panel in shear presented a stable behaviour for all stiffened joints. For the connection components, and in the presence of transverse web stiffeners, only the end-plate in bending significantly contributes to the joint non-linear rotation, with the other connection components response remaining in elastic domain.

Concerning the evaluation of the ductility-equivalent viscous damping (μ -EVD) relationships, conclusions are drawn about the limitation of using the existing expression proposed by Priestley *et al.* (2007), which generally overestimates the levels of equivalent viscous damping, for MRF structures with partial-strength joints. Furthermore, the numerical results obtained in the study revealed no clear dependency of the μ -EVD relationships on the plastic mechanism of the joint type, on the elastic period of vibration of the system or on the soil type. An improved ductility-equivalent viscous damping relationship was derived and proposed.

Resumo

Nesta tese aborda-se a caracterização do comportamento de juntas viga-coluna submetidas a carregamentos monotônicos, cíclicos ou dinâmicos, quer em termos de resposta global da ligação quer ao nível das componentes mais condicionantes. As ligações aparafusadas com chapa de extremidade são utilizadas com frequência na Europa, devido ao seu reduzido custo de fabrico e montagem, mas também devido à sua excelente integração arquitetónica. Apesar do seu dimensionamento estar perfeitamente definido no Eurocódigo 3 para zonas de baixa sismicidade, os mais recentes regulamentos sísmicos, como o Eurocódigo 8, não possuem informação detalhada nem providenciam as ferramentas para o dimensionamento deste tipo de ligações em zonas sísmicas. O procedimento de dimensionamento, baseado no Método das Componentes, presente no Eurocódigo 3 é apenas aplicável a ligações submetidas a carregamentos monotônicos.

Um dos principais objetivos desta investigação é contribuir para o desenvolvimento de uma metodologia analítica, baseada no método das componentes, que tenha em conta o comportamento cíclico das juntas determinado pelo comportamento de cada uma das componentes dissipativas, e garantindo a adequada sobrerresistência das componentes não dissipativas. Outro importante objetivo desta investigação é o contributo para o desenvolvimento e evolução de procedimentos baseados em deslocamentos, propondo relações ductilidade-amortecimento viscoso equivalente melhoradas para pórticos simples que possuam ligações viga-coluna com resistência parcial onde a energia é dissipada.

Para alcançar os objetivos desenvolveu-se um modelo paramétrico de elementos finitos (EF) de uma junta viga-coluna com chapa de extremidade duplamente estendida, calibrado e validado por resultados de ensaios experimentais, disponíveis na literatura. O conjunto de modelos numéricos é gerados através de um script desenvolvido em *Python* e compilado pelo *software* ABAQUS.

Os principais resultados da investigação são: i) o modelo detalhada de EF capaz de simular eficazmente o comportamento de ligações viga-coluna de chapa de extremidade e os seus componentes; ii) os procedimentos desenvolvidos para a caracterização isolada dos

componentes dissipativos que contribuem para o comportamento da junta, nomeadamente: painel da alma de coluna solicitada ao corte, alma de coluna em compressão transversal, alma de coluna em tração transversal, banzo de coluna em flexão e chapa de extremidade em flexão; iii) determinação do comportamento mecânico dos componentes através de curvas força-deslocamento, obtidas por integração de tensões e deformações no modelo de EF, que podem ser usadas diretamente em modelos mecânicos de componentes da ligação; iv) relações ductilidade-amortecimento viscoso equivalente (μ -AVE) melhoradas tendo em conta a influência dos vários componentes dissipativos presentes nas ligações de chapa de extremidade duplamente estendida, e que podem ser usadas diretamente em procedimentos baseados em deslocamentos como o *Direct Displacement-Based Seismic Design* (Priestley *et al.*, 2007).

Os procedimentos propostos para aferir o comportamento isolado das componentes é bastante flexível na definição dos limites de integração, dependendo do modelo mecânico escolhido. O procedimento é capaz de caracterizar o comportamento das componentes identificadas na ligação, incluindo a resistência ao corte adicional devido à existência de reforços transversais na alma. A utilização deste tipo de reforços transversais afeta significativamente o comportamento da ligação e das suas componentes. No caso da componente chapa de topo em flexão as curvas força-deslocamento, associadas às fiadas de parafusos interiores junto aos banzos da viga, apresentam ciclos estáveis, ao contrário das curvas associadas às fiadas exteriores que são mais suscetíveis ao fenómeno de *pinching*. O comportamento do componente básico da alma de coluna solicitada ao corte apresenta um comportamento estável para todas as ligações reforçadas. Na presença de reforços transversais, à alma a componente chapa de extremidade em flexão apresenta um contributo significativo para a rotação da ligação. Ao contrário da componente banzo da coluna em flexão que se mantem em regime elástico.

A determinação das relações μ -AVE permitiu concluir sobre as limitações de usar a expressão proposta por Priestley *et al.* (2007), que geralmente sobrestima o nível de amortecimento viscoso equivalente para pórticos simples com ligações de resistência parcial. Os resultados numéricos permitiram ainda concluir que não existe uma clara dependência das relações μ -AVE com os mecanismos plásticos da ligação, nem do período elástico de vibração do sistema, nem do tipo de solo. No final é proposta uma alteração à expressão existente para a relação ductilidade - amortecimento viscoso equivalente.

Keywords:

Beam-to-Column Steel Joints | Cyclic Behaviour | Partial-Strength | End-Plate | Web Panel | Finite Elements (FE) | Component Method | Moment Resisting Frames | Equivalent Viscous Damping | Direct Displacement Based Design (DDBD).

Palavras-chave:

Ligações Metálicas Viga-Coluna | Comportamento Cíclico | Resistência Parcial | Chapa de Extremidade | Painel da Alma | Elementos Finitos (EF) | Método das Componentes | Pórticos Simples | Amortecimento Viscoso Equivalente | Dimensionamento Sísmico Baseado em Deslocamentos.

Acknowledgements

First of all, I would like to address my acknowledgement to the research group that welcomed me, and gave me the opportunity to embrace this challenge. In particular, to Professor Luís Simões da Silva, head of the group, who believed in me. His valuable guidance and contribution to this work is also acknowledged.

Second I would like also to acknowledge the Foundation for Science and Technology (FCT) that financed this work, through QREN - POPH - Typology 4.1 – Advanced Education, reimbursed by the European Social Fund and Portuguese national funds MEC, under contract grants SFRH/BD/91167/ 2012.

A word of appreciation for my supervisors, Professor Carlos Rebelo and Professor José Miguel Castro, for embracing this challenge with me, putting at my disposal all their valuable knowledge and expertise, which I sincerely appreciate and recognize. Thank you for all the guidance, friendship and also patience to supervise me in the many tasks done in the past years.

I would also like to express my gratitude: to Miguel Serra, for all the valuable discussions taken when we shared the room, and also for all the assistance given during that period; and to Ângela Lemos for the valuable contribution and assistance given to this work, in the final stage.

Although many say that doing a PhD is a lonely journey, I have never been alone, and I have had the opportunity to meet many interesting people. In the inability to list them all, I would like to give a word of appreciation to those who were there in a daily basis, the “roommates”: Guiomar Vicente, Isabel Gomes, Miguel Serra, Rui Matos and Trayana Tankova.

A special thanks to my family that always supported my decision. To my lovely wife Ana Augusto for all the comfort and motivation that really kept me focused without losing the perspective. To my beautiful daughter, Mariana Augusto, for constantly reminding me of the necessary balance between career and family. Although, I recognize that this balance has not always been achieved to its disadvantage. To my parents I sincerely thank you for letting me follow my studies, I really recognize your great effort to do so.

Contents

Abstract	i
Resumo	iii
Acknowledgements	vii
Contents	ix
Notations	xiii
1 Introduction.....	1
1.1 Purpose and Scope of this Research.....	1
1.2 Research Objectives and Main Breakthroughs	10
1.3 Structure and Organization of the Document.....	11
2 Literature Review and Data Collection	17
2.1 Introduction	17
2.2 Behaviour of Steel Joints.....	18
2.2.1 Developments in the Characterization of Steel Joints	18
2.2.1.1 Introduction.....	18
2.2.1.2 Review of Past Experimental Work.....	21
2.2.1.3 Review of Past Analytical Work.....	34
2.2.1.4 Review of Past Numerical Work	37
2.2.2 Analysis of Beam-to-Column Joints by Analytical Methods	43
2.2.2.1 End-Plate Bolted Joints Definitions	43
2.2.2.2 Overview of the Component Method.....	46
2.2.2.3 Column Web Panel Behaviour.....	55
2.2.3 Analysis of Joints by Numerical FE Methods	64
2.2.3.1 Overview of the Finite Element Method.....	64
2.2.3.2 Material Stress-Strain Relationships for the FE Models	67
2.3 Data Collection and Treatment of Experimental Tests on Steel Joints.....	76
2.3.1 Scope	76
2.3.2 Survey of Experimental Results	76
2.3.2.1 Top and Seat Angles Joints Configuration.....	76
2.3.2.2 End-Plate Joints Configuration	78
2.3.3 Organization and Data Processing.....	82
2.3.3.1 Relevant Properties in Analysis	82
2.3.3.2 Stiffness Comparison	83
2.3.3.3 Strength Comparison	85
2.3.3.4 Rotation Capacity Comparison	86
2.3.3.5 Connection Ductility.....	88
2.3.3.6 Summary and Rating of the Examined Joints	90
2.4 Overview of Seismic Design Methods.....	91
2.4.1 General	91
2.4.2 Direct Displacement-Based Design Procedure.....	91
2.4.2.1 Evolution and Recent Developments.....	91
2.4.2.2 Overview of the Direct Displacement-Based Design Procedure	93

2.4.2.3	Ductility-Equivalent Viscous Damping Relationships for Displacement Based Design Procedures	95
2.4.3	Eurocode 8 Recommendations for the Design of Steel Joints	100
2.4.3.1	Design Criteria for Moment-Resisting Frames	100
2.4.3.2	Non Dissipative Beam-to-Column Steel Joints	101
2.4.3.3	Dissipative Beam-to-Column Steel Joints	102

3 Development and Validation of the Finite Element Models to Characterize the Behaviour of Beam-to-Column End-Plate Joints..... 105

3.1	Introduction.....	105
3.2	End-Plate Beam-to-Column Joint Models with Stiffened Columns.....	107
3.2.1	Experimental Tests Used in the Numerical Models Validation	107
3.2.1.1	General Description	107
3.2.1.2	Test Detail, Instrumentation and Procedures.....	109
3.2.1.3	Material Properties	112
3.2.2	Description of the FE Models	113
3.2.3	Numerical Modelling and FE Options	115
3.2.3.1	Modelling Overview	115
3.2.3.2	Finite Element Options	116
3.2.4	Validation of the FE Models Using Experimental Evidence	129
3.2.4.1	Overview.....	129
3.2.4.2	Extraction Procedures for Experimental Tests and Numerical Models.....	129
3.2.4.3	Global Behaviour of the Joints.....	132
3.2.4.4	Components Behaviour.....	139
3.2.4.5	Energy Dissipation.....	144
3.3	End-Plate Beam-to-Column Joint Models with Unstiffened Columns	147
3.3.1	Experimental Tests Used in the Numerical Models Validation	147
3.3.2	FE Model Description.....	148
3.3.3	Validation of the FE Models Using Experimental Evidence	151
3.4	Parameterization of the Beam-to-Column End-Plate Joint Model.....	153
3.4.1	Introduction to Python and Abaqus Interaction	153
3.4.2	Script for the External Beam-to-Column Finite Element Model	154
3.4.2.1	Objective	154
3.4.2.2	Main Body of the Script.....	155
3.5	Isolated T-Stub FE Models	156
3.5.1	The Importance of the T-stub Model	156
3.5.2	Experimental Tests Used in the Numerical Models Validation	157
3.5.3	Description of the Numerical Models.....	159
3.5.4	Constitutive Models (Material options)	160
3.5.5	Results of the FE Models and Experimental Tests	162
3.6	Main Conclusions	166

4 Development of a Methodology for the Characterization of the Joint Components Using the FE Models..... 169

4.1	Introduction.....	169
4.2	Characterization of the Column Web Components	170
4.2.1	Framework.....	170
4.2.2	Components Identification Methodology	173
4.2.3	Application to the Joints	177
4.2.3.1	Joints Loaded Monotonically	177
4.2.3.2	Cyclically Loaded Joints	184
4.3	Characterization of the Connection Components	198
4.3.1	Introduction.....	198

4.3.2	Methodology to Assess the Isolated Contribution of the Connection Components to the Joint Rotation	199
4.3.3	Application of the Methodology to the Joints.....	205
4.3.4	Methodology to Extract the Force-Displacement Relationships of the Connection Components ..	210
4.3.5	Application of the Methodology to the Joints.....	214
4.4	Methodology Walkthrough	217
4.5	Main Conclusions.....	220

5	Application of the Developed Methodologies to Double-Extended End-Plate Joints	223
5.1	Introduction	223
5.2	Beam-to-Column Joints Configuration	224
5.2.1	Requirements.....	224
5.2.2	Configuration and Design of the Joints	225
5.2.3	Finite Element Modelling	228
5.2.4	Load Protocol Adopted.....	229
5.3	Analytical vs Numerical Results	230
5.3.1	Framework.....	230
5.3.2	Moment-Rotation Relationships	230
5.3.3	Stress and Plastic Strain Analysis.....	232
5.3.4	Final Remarks on the Design and Analysis of the Selected Joints	235
5.4	Parametric Study	236
5.4.1	Definition of the Parameters.....	236
5.4.1.1	Framework.....	236
5.4.1.2	Influence of the Continuity Column Web Stiffeners	236
5.4.1.3	Influence of the Middle Bolt Row	237
5.4.1.4	Influence of Two Bolt Rows in the Extended Part of the End-Plate.....	238
5.4.1.5	Sensitivity to the Material Properties of the End-Plate	239
5.4.1.6	Finite Element Models	239
5.4.2	Results and Discussion	241
5.4.2.1	Influence of the Continuity Column Web Stiffeners	241
5.4.2.2	Influence of the Middle Bolt Row	248
5.4.2.3	Influence of Two Bolt Rows in the Extended Part of the End-Plate.....	251
5.4.2.4	Sensitivity to the Material Properties of the End-Plate	257
5.4.3	Final Remarks on the Parametric Study	266
5.5	Comparison With the Experimental Tests Results.....	267
5.5.1	Results and Discussion	267
5.5.2	Final Remarks on the Comparisons with the Experimental Tests Results.....	272
5.6	Component's Behaviour Extraction	273
5.6.1	Framework and Definitions	273
5.6.2	Results and Discussion	274
5.6.2.1	Column Web Components	274
5.6.2.2	Connection Components.....	279
5.7	Main Conclusions.....	283
6	Equivalent Viscous Damping Assessment in MRF with End-Plate Partial-Strength Joints	289
6.1	Introduction	289
6.2	Procedure Developed for the Assessment of Equivalent Viscous Damping.....	290
6.3	Design and Characterization of the End-Plate Joints	292
6.3.1	Joints Description	292
6.3.2	Analytical and numerical Results	294

6.3.3	Final Remarks	301
6.4	Ductility-Equivalent Viscous Damping Relationships	302
6.4.1	Joint Selection	302
6.4.2	Seismic Input	304
6.4.3	Analysis Procedure	308
6.4.4	Ductility-EVD Relationships	310
6.5	Discussion of the Results	312
6.5.1	Influence of the Joint Mechanisms on the Ductility-EVD Relationships	312
6.5.2	Influence of the Elastic Period of Vibration of the System on the Ductility-EVD Relationship ...	315
6.5.3	Influence of the Soil Type on the Ductility-EVD Relationships.....	316
6.5.4	Modification Factor for the Spectral Displacement Response	317
6.6	Main Conclusions	320
7	General Conclusions and Future Work	321
7.1	Final Remarks and Main Conclusions	321
7.2	Summary of the Main Outcomes	326
7.3	Further Developments and Recommendations For Future Work.....	328
7.4	Dissemination and Publications	331
	References	335
	Annexes	349
A	Considerations on the Linearization of Joints Response.....	351
B	Parameterization of the Beam-to-Column End-Plate Joint Model.....	365

Notations

Lowercase

a, b, c and d	Empirical constants for Eqs. (2.52) and (2.53)
a_f	Throat of the beam-to-end-plate fillet weld
b	Width of the T-stub
b_c	Column flange width
b_{class}	Steel grade of the bolts (bolts class)
b_{eff}	Effective width
$b_{eff,c,wc}$	Effective width of the column web in compression
$b_{eff,t,wc}$	Effective width of the column web in tension
$b_{eff,wc}$	Effective width of the column web in compression or tension
b_{iso}	Rate at which the size of the yield surface changes as plastic strain increases
b_p	Width of the end-plate
d	Distance between the loading cells and the connection column flange
d_0	Diameter of the bolts holes
d_1 to d_n	Distance between two aligned displacement transducers
$d_{1,lbf}$	Distance of the bolt row 1 to the lower beam flange
$d_{2,lbf}$	Distance of the bolt row 2 to the lower beam flange
$d_{1,ubf}$	Distance of the bolt row 1 to the upper beam flange
$d_{2,ubf}$	Distance of the bolt row 2 to the upper beam flange
d_b	Distance between the centre of the beam flanges
d_b	Diameter of the bolt
$d_{b,i}$	Diameter of the bolt of the bolt row i
d_{DT20}	Distance between the point DT20 and the connection column flange
e	Distance of the bolt hole to an edge
e_h	Horizontal edge distance
e_u	Ultimate displacement
e_y	Displacement at yielding
e_v	Vertical edge distance
ext	Length of the extended part of the end-plate
f_{el}	Elastic frequency
f_{max}	Maximum stress
f_n	Plastic stress for the n^{th} stage
f_r	Strength at rupture
f_u	Nominal ultimate strength of steel
f_{um}	Mean value of ultimate strength of steel
$f_{u,tru}$	True ultimate strength of steel
f_{uwc}	Nominal value of the ultimate tensile strength for the column web
$f_{r,tru}$	True strength at rupture
f_y	Nominal yield strength of steel

f_{yb}	Nominal yield strength of bolts steel
f_{ym}	Mean value of yield strength of steel
f_{y_tru}	True yield strength of steel
f_{ywc}	Nominal value of the yield tensile strength for the column web
g	Acceleration of gravity
g_N	Amount of penetration in the Penalty method for contact between meshes
h	High of the floor
h	Relative slope of the post elastic linearization ($S_{j,ini}/K_{st}$)
\hat{h}	Shape factor of the inelastic curve
h_b	High of the beam section
h_{bf}	High of the beam section between flanges centre lines
h_c	High of the column section
$h_{c,i}$	Integration length of the compression stresses
h_i	Height of level (floor) i
h_p	Height of the end-plate
h_r	distance from bolt-row r to the centre of compression
ht	Length of the column between supports (FE model)
h_t	Lever arm (Krawinkler model)
$h_{t,i}$	Integration length for the tension stresses
h_{wc}	Height of the column web
h_{shc}	Distance between the column flanges centre lines
i	Component number
k	Coefficient that accounts for the type of loading, and web support conditions in the AJM
k_b	Coefficient for the definition of the stiffness boundaries
k_{bfst}	Post-elastic stiffness for the load-introduction in the AJM
k_{cw}	Parameter used in the calculation of the load-introduction stiffness (AJM)
k_e	Secant (effective) stiffness
k_{eq}	Equivalent stiffness coefficient
k_f	Rate of increase of the additional plastic web capacity resistance V_{cy} .
k_i	Stiffness coefficient for basic joint component
k_p	Post yield stiffness
l_{eff}	Effective length
m	Distance between the bolt axis and the flange-to-web expected location of the plastic hinge
m	Mass of the system
m_e	Seismic mass of the SDOF representation
m_i	Seismic mass of the floor i of the multi degree of freedom structure
mx	Distance of the external bolt row to the beam flange
n	Minimum of the distance between the edge of the flange and the bolts axis or $1.25m$
n	Constant obtained by curve fitting in Krawinkler <i>et al.</i> studies
n	Number of links in the concept of capacity design
n	Number of equations and unknowns in FEM
n	Strain hardening exponent in the Ramberg-Osgood model
n'	Constant obtained by curve fitting for the saturation curve of the material
ph	Horizontal distance between the bolt rows

p_v	Vertical distance between two consecutive bolt rows
r	Bolt-row number
r	Post-yield stiffness coefficient
r	Transition radius between the flange and column
t_l	Thickness of the column web according to the shear area
t_f	Thickness of the flanges
t_{fb}	Thickness of the beam flanges
t_{fc}	Thickness of the column flanges
t_p	Thickness of the end-plate
t_s	Thickness of the transverse web stiffeners
t_w	Thickness of the web
t_{wc}	Thickness of the column web
t_{wp}	Thickness of the supplementary web plate
$[u]$	Vector of displacements in FEM
x	Beam length from the column flange to the measured beam section
z	Distance to the neutral axis in the column flange section
z	Lever arm

Uppercase

A_0	Area of the cross-section of the steel coupon
A_{vc}	Column shear area
B	Length of the T-stub
C	Empirical constant of the cyclic steady state curve (Cofie's model)
C	Coefficient dependent on the hysteresis rule of the hysteretic part of the equivalent viscous damping (ξ_{eq})
C_I	Initial kinematic hardening modulus
$C_{f_{i,1}}, C_{f_{i,2}}$	Pre-defined nodes in the FE mesh for the column flange holes for the bolt row i
C_k	kinematic hardening constant
\dot{C}_k	Rate of change of C_k with respect to temperature and field variables
DT_i	Application point of the displacement transducer or pre-defined node in the FE mesh
E	Young modulus
E	Energy dissipated accumulated
E_0	Initial tangent modulus of the Menegotto-Pinto model
E_{Ed}	Design effort in the column
$E_{Ed,E}$	Effort in the column due to the design seismic action
$E_{Ed,G}$	Effort in the column due to the non-seismic actions
E_h	Hardening modulus of the material
E_m	Mean value for the Young modulus
$E_{m,tru}$	Mean value for the Young modulus of true-stress-true-strain relationship
$Ep_{i,1}, Ep_{i,2}$	Pre-defined nodes in the FE mesh for the end-plate holes for the bolt row i
E_{st}	Strain-hardening modulus
E_{tot}	Total energy dissipated by the joint
E_∞	Secondary tangent modulus of the Menegotto-Pinto model
F	Force

$[F]$	Vector of applied external forces in FEM
F_b	Couple of forces statically equivalent to the moment at the beam end
F_{bb}	Value of F_b when the web panel reaches the instability under compression effects in the AJM
F_{bcr}	Value of F_b for the elastic linear instability load of the web in the AJM
F_{be}	Value of F_b when the web panel reaches the first yielding
F_{bppl}	Value of F_b when the pseudo-plastic moment M_{bppl} of the joint is reached in the AJM
$F_{b,Rd}$	Bearing resistance
F_{buy}	Value of F_b when the web panel reaches the ultimate plastic resistance in the AJM
F_c	Compression forces
$F_{c,fb,Rd}$	Design resistance of the beam or column flange and web in compression
$F_{c,wc,Rd}$	Design resistance of column web in transverse compression
F_e	Design lateral force of the SDOF representation
F_H	Hardening factor
F_i	Design forces to the various discretised masses of the multi degree of freedom structure
F_{load_cell}	Force obtained in the load cell, aligned with hydraulic actuator
F_{max}	Maximum force
F_{min}	Minimum force
F_R	Mean value relaxation factor
$F_{Rd,i}$	Force of the basic component
F_S	Softening factor
F_t	Tension force
$F_{t,b}$	Force in the bolt cross section
$F_{t,ep,Rd}$	Design resistance of end-plate in bending
$F_{ti,Rd}$	Design resistance for the bolt row i
$F_{t,fc,Rd}$	Design resistance of column flange in bending
$F_{t,Rd}$	Design resistance of the tension driving components
$F_{t,Rd,1\ to\ 3}$	Design resistance of the T-stub for mode 1 to 3
$F_{T,Rd,cp}$	Design resistance of the T-stub for circular patterns
$F_{T,Rd,nc}$	Design resistance of the T-stub for non-circular patterns
$F_{tr,Rd}$	Effective design tension resistance of bolt-row r
$F_{t,wb,Rd}$	Design resistance of beam web in tension
$F_{t,wc,Rd}$	Design resistance of column web in transverse tension
$F_{v,Rd}$	Shear resistance per shear plane
$F_{w,Rd}$	Design resistance of welds
F_y	Force at yield
G	Shear modulus
G_{st}	Strain-hardening shear modulus
H_e	Height of the SDOF system representation
I_b	Second moment of area of the beam
I_{fc}	Second moment of area of the section of the column flanges
I_y	Second moment of area of the section around the stronger axis
K	Strength coefficient of the Ramberg-Osgood model
K	Constant obtained by curve fitting in Krawinkler <i>et al.</i> studies

K'	Constant obtained by curve fitting for the saturation curve of the material
K_0	Initial stiffness (measured in the cycle 0)
$K_{1 \text{ to } 3}$	Hardening stiffness's of the Krawinkler <i>et al.</i> multi-linear model
K_{be}	Elastic stiffness for the load-introduction in the AJM
K_{cws}	Axial stiffness of the corresponding spring of the mechanical model for the component column web in shear
$K_{cws,h}$	Axial residual stiffness, due to hardening, of the corresponding spring of the mechanical model for the component column web in shear
$K_{cws,p}$	Axial post-yielding stiffness of the corresponding spring of the mechanical model for the component column web in shear
K_e	Effective stiffness
K_{el}	Initial elastic stiffness
$[K_g]$	System global stiffness square matrix in FEM
K_i	Initial stiffness of the SDOF representation bi-linear response
K_i	Stiffness of the cycle i
K_{ij}	Initial stiffness of a joint response
K_n	Elastic stiffness for the shear AJM
K_{nst}	Post-elastic stiffness for the shear AJM
K_p^{bl}	Plastic stiffness of the bound line
K_p^X	Plastic stiffness at point X
K_{st}	Plastic stiffness with hardening
K_t^X	Tangent stiffness at point X
L	Length of the column between supports
L	Span of the MRF
L_0	Initial position of the coupon specimen
$L1$	Distance between beam end and the column axis
$L2$	Distance between the beam axis and bottom support
$L2$	Distance between the load P and the face of the connected column flange
$L3$	Distance between the column axis and the solid beam limit
$L3$	Distance between the load P and the face of the end-plate
L_b	Span of a beam (centre-to-centre of columns)
L_c	Length of the column
L_b	Length of the beam
$Lb1$	Length of the solid part of the beam
$Lb2$	Length of the wire part of the beam
$Lc1$	Length of the wire upper part of the column
$Lc2$	Length of the intermediate solid part of the column
$Lc3$	Length of the wire lower part of the column
L_{in}	Initial length of the coupon specimen
L_f	Final position of the coupon specimen
M	Bending moment of the joint
M_{1st}	Bending moment for the first bolt row
$M_{1st+2nd}$	Bending moment for the group of first and second bolt rows
$M_{1st+2nd+3rd}$	Bending moment for the group of first, second and third bolt rows
M_a^{pa}	Amplitude of the panel moment of the last half cycle
M_b	Bending moment at the beam end
M_b^{pa}	Normalized moment of the bound line when the rotation is zero

$M_{b,pl,Rd}$	Design value of the plastic resistance to bending moment of the beam
M_c	Bending moment entering in the web from the global system
$M_{c,pl,Rd}$	Design value of the plastic resistance to bending moment of the column
M_{Ed}	Design bending moment in the connection
M_e	First yielding due to the bending moment
M_{el}	Elastic bending moment of a joint
$M_{el,b}$	Elastic bending moment of the beam
M_{fc}	Bending moment of the column flange
M_j	Bending moment of the joint
$M_{j,b}$	Beam plastic capacity to bending moment
$M_{j,Ed}$	Design moment of the joint
$M_{j,Rd}$	Design value of the resistance to bending moment of a joint
M_{nt}^{pa}	Mean panel moment of the last half cycle
M_{max}	Maximum bending moment achieved after lading a joint
M_{min}	Minimum bending moment achieved after lading a joint
M_n^{pa}	Normalizing moment of the column web panel
M_{pd}	Plastic bending moment of a joint, obtained numerically or analytically
M_{pl}	Plastic bending moment of a joint
$M_{pl,Rd}$	Plastic bending moment resistance of a hinge in the T-stub
$M_{p,b}$ or $M_{pl,b}$	Plastic bending moment of the beam
$M_{p,con}$	Plastic capacity of the connection
M_{pcf} or $M_{pl,fc}$	Plastic moment of the column flange
$M_{p,wp}$	Plastic capacity of the web panel in shear due to the bending at the column face
M_r	Bending moment in rupture
M_{Rb}	Design values of the moments of resistance of the beams framing the joint
M_{Rc}	Design values of the moments of resistance of the columns framing the joint
M_s^{pa}	Panel moment on the cycle steady curve
$M_{y(j)}$	Bending moment of the joint for the yielding point
$M_{y(sys)}$	Bending moment of the system for the yielding point
$M_{\theta_{max}}$	Bending moment for the maximum rotation
N	Number of backstresses
N_c	Axial forces entering in the web from the global system
N_{Ed}	Design axial force in the connection
$N_{pl,Rd}$	Design plastic resistance to normal forces of the gross cross-section
P	Applied load in the beam
$P1$	Vertical path in the column web near the connection
$P2$	Vertical path in the column web near the opposite flange to the connection
$P3$	Horizontal path in the column web
$P4$ to $P7$	Paths in the column flanges
P_i and P_{is}	Nominal tensile strength for ductile and brittle material, respectively
P_E	Earthquake-induced tensile force
P_o	Overstrength force
Q	Prying forces
Q_∞	Maximum change in the size of the yield surface
R	Material constant of the Menegotto-Pinto model

R_d	Resistance of the joint
R_{DT20}	Reaction in the beam end support at DT20 position
R_{fy}	Plastic yield resistance of the connected dissipative member
R_ξ	Modification factor for the displacement spectrum
$S_{ini,c}$	Initial stiffness of the connection
$S_{ini,pw}$	Initial stiffness of the column web panel
$S_{ini,pw+c}$	is the initial stiffness of the joint (column web panel and connection)
S_j	Rotational stiffness of a joint
$S_{j,ini}$	Initial rotational stiffness of a joint
T_e	Effective period
T_{el}	Elastic period
$U1$ to $U3$	Translational degrees of freedom
$UR1$ to $UR3$	Rotational degrees of freedom
V	Shear strength
V_{base}	Design base shear force in the DDBD procedure
V_c	Shear strength due to the transverse web stiffeners
V_{c1}	Design shear forces installed in the column at the bottom part of the joint
V_{c2}	Design shear forces installed in the column at the top part of the joint
V_{ce}	Shear forces entering in the web corresponding to the first yielding
V_{cu}	Shear forces entering in the web corresponding to the ultimate resistance
V_{cy}	Additional plastic web capacity, due to the presence of the transverse web stiffeners
V_{Ed}	Design shear force in the connection
V_n	Shear force in the column web panel
V_{ne}	Shear resistance at the first yielding of the column web
V_{nu}	Ultimate shear plastic resistance
V_{ny}	Plastic shear stress uniformly distributed in the whole panel
V_p	Shear force corresponding to the post-yielding of the panel zone
V_{wp}	Shear forces in column web panel
$V_{wp,Ed}$	Design shear force in the column web panel
$V_{wp,Rd}$	Plastic shear resistance of a column web panel
V_y	Shear force corresponding to the first yielding of the panel zone
$W_{c,i}$	Pre-defined nodes in the column flange web for the bolt row i
W_p	Extended part of the end-plate in the AJM
$W_{p,i}$	Pre-defined nodes in the end-plate web for the bolt row i

Lowercase Greek letters

α	Elastic limit factor
α_k or i	Backstress (kinematic strain hardening)
$\dot{\alpha}_k$	Evolution law of the nonlinear isotropic/kinematic hardening model
β	Transformation parameter for the web panel shear force
β	Parameter that relates the strength of the plates and the bolts in the CM
β	Factor to account for the beneficial effect of column shear above and below the joint (Krawinkler model)
β_k	Stiffness-proportional damping

δ	Beam deflection
$\delta_{all,i}$	Sum of the deformations of the components CFB, BT and EPB for each bolt row i , disregarding flip deformation
$\delta_{all,lbf}$	Sum of the deformations of the components CFB, BT and EPB at the lower beam flange level, disregarding flip deformation
$\delta_{all,ubf}$	Sum of the deformations of the components CFB, BT and EPB at the upper beam flange level, disregarding flip deformation
δ_B	Interpolated deformation of the bolts at the beam flanges level
$\delta_{B,i}$	Deformation of the component bolts in tension for each bolt row i
δ_{Cf}	Interpolated deformation of the column flange at the beam flanges level
$\delta_{Cf,i}$	Deformation of the component column flange in bending for each bolt row i
δ_{Ep}	Interpolated deformation of the end-plate at the beam flanges level
$\delta_{Ep,i}$	Deformation of the component end-plate in bending for each bolt row i
$\delta_{flip,lbf}$	Flip deformation of the extended part of the end-plate at the lower beam flange level
$\delta_{flip,ubf}$	Flip deformation of the extended part of the end-plate at the upper beam flange level
δ_{in}	Distance between the beginning of the inelastic curve and the bound line
δ_l	Sum of the deformations of the components CFB, BT and EPB at the lower beam flange level
δ_{P1}	Displacement in the nodes of the path $P1$
δ_{P2}	Displacement in the nodes of the path $P2$
δ_u	Sum of the deformations of the components CFB, BT and EPB at the upper beam flange level
δ_X	Distance between the inelastic curve and the bound line at the point X
δ_y, v_y, e_y	Displacement at yielding
ε	Strain
ε_0	Strain at yielding
ε_e	Elastic strain
ε_{eng}	Engineering strain
ε_N	Penalty coefficient for penetration control
ε_{pl}	Plastic strain
ε^{pl}	Equivalent plastic strain
$\dot{\varepsilon}^{pl}$	Equivalent plastic strain rate
ε_m	Maximum extension
ε_n	Plastic strain for the n^{th} stage
ε_{r_pl}	True plastic strain at rupture
ε_{r_tru}	True strain at rupture
ε_{st}	Strain-hardening steel strain
ε_{tru}	True strain
ε_u	Ultimate strain
ε_{u_pl}	Ultimate true plastic strain
ε_{u_tru}	Ultimate true strain
ε_y	Yield strain
ε_{y_tru}	Yield true strain

ϕ	Strength reduction factor associated to the material
ϕ_c	Connection rotation
ϕ_{Cd}	Rotation capacity of a joint
ϕ_{Ed}	Rotation of the joint associated to $M_{j,Ed}$
ϕ_j	Joint rotation
ϕ_{Xd}	Rotation limit for S_j at which $M_{j,Ed}$ first reaches $M_{j,Rd}$
γ_l	Initial kinematic hardening parameter
γ	Distortion of the column web panel
γ_d^{pa}	Amplitude panel rotation of the last half cycle
γ_k	Rate at which the backstress varies as the plastic strain increases
γ_{MO}	Partial safety factor
γ_{MP}	Material constant of the Menegotto-Pinto model
γ_m^{pa}	Mean panel rotation of the last half cycle
γ_n	Normalizing elastic rotation of the column web panel
γ_{ov}	Overstrength factor
γ_{ovM1} to γ_{ovM4}	Overstrength factors applied to the nominal stress-strain relationship of the structural steel
γ_p	Shear strain corresponding to the post-yielding in the column web panel
γ_{st}	Rotation of the column web panel after strain-hardening appear
γ_u	Rotation of the column web panel at the ultimate web resistance
γ_{wp}	Relative rotation of the column web panel
γ_y	Shear strain corresponding to the first yielding in the column web panel
η	Stiffness modification coefficient
η	Ductility level criterion
η	Displacement reduction factor
φ_i	Ductility index
φ	Rotation of the column web panel due to the load-introduction effect
λ	Relation between the bolts axis and edges or flanges and webs in the CM
λ	Parameter used in the assessment of the column web elastic foundation properties in the AJM
μ	Stiffness ratio in Eq. (2.3)
μ	Parameter used in the assessment of the column web elastic foundation properties in the AJM
μ	Ductility level
ν	Poisson's ratio
θ	Joint (or connection) rotation
θ	Inter-story drift angle in ANSI/AISC 341-10 (2010)
θ_{block}	Contribution of the parasitic displacements from test setup to the global rotation of the joint
θ_{column_web}	Column web panel contribution to the global rotation of the joint
$\theta_{end-plate}$	End-plate contribution to the global rotation of the joint
θ_{elast_column}	Contribution of the elastic deformation of the column to the global rotation of the joint
θ_{elast_beam}	Contribution of the elastic deformation of the beam to the global rotation of the joint

θ_h	Horizontal rotation of the column web panel
θ_{max}	Maximum rotation achieved after lading a joint
θ_{min}	Minimum rotation achieved after lading a joint
θ_p	Accumulated plastic rotation
θ_p	Rotation capacity of the plastic hinge region
θ_{total}	Global rotation of the joint
θ_v	Vertical rotation of the column web panel
θ_y	Yield rotation of a joint
$\theta_{y(j)}$	Yield rotation of a joint
$\theta_{y(sys)}$	Yield rotation of the system
σ	Normal stress
σ^0	Change of the yield surface in isotropic hardening
σ_0	Stress at yielding
$\sigma/0$	Yield stress at zero equivalent plastic strain
σ_{11}	Normal stresses according to the axes xx
σ_{22}	Normal stresses according to the axes yy
σ_{33}	Normal stresses according to the axes zz
σ_{eng}	Engineering stress
σ_i	Horizontal normal stress associated with the load-introduction
σ_{iu}^c	Horizontal normal stress in the Von Mises criterion that induces the ultimate plastic stress state in the web panel
σ_{iy}^c	Horizontal normal stress in the Von Mises criterion that induces the first yielding in the web panel
σ_n	Vertical normal stress due to the axial load and bending of the column
σ_{nu}^c	Vertical normal stress in the Von Mises criterion that induces the ultimate stress in the panel
σ_{ny}^c	Vertical normal stress in the Von Mises criterion that induces the complete yielding of the whole panel
σ_N	Contact stresses
σ_{tru}	True stress
σ_y	Strain at yielding
τ	Shear stress associated with the shear forces on the contour of the column web panel
τ_{23}	Shear stress according to the axes yz
τ_u^c	Horizontal shear stress in the Von Mises criterion that induces the ultimate plastic stress state in the web panel
τ_y^c	Horizontal shear stress in the Von Mises criterion for the first yielding in the web panel
ξ	Parameter used in the assessment of the column web elastic foundation properties in the AJM
ξ	Constant of the cyclic steady state curve (Cofie's model)
ξ_{el}	Elastic viscous damping
ξ_{eq}	Equivalent viscous damping
ξ_{hyst}	Hysteretic damping
ψ	Coefficient for Eq. (2.5)

Uppercase Greek letters

Δ	Deformation
Δ	Deviation to the nominal values
Δ_c	Deformation of the column web in the compression side
Δ_{cw}	Deformation in the column web between the paths $P1$ and $P2$
Δ_d	Target displacement
Δ_e	Column web relative elongation at the first yielding
$\Delta_{el,Te}$	Elastic displacement for a predefined effective period
Δ_f	Displacement at failure
Δ_i	Design displacement profile of the level i
Δ_{in}	Inelastic displacement
Δ_l	Deformation of the link
Δ_{max}	Maximum displacement
Δ_{min}	Minimum displacement
Δ_{P1} or Δ_{P2}	Deformation fields in paths $P1$ and $P2$
Δ_{st}	Column web relative elongation at the apparition of the strain-hardening
$\Delta_{t,i}$	Deformation of the column web in the tension side for the bolt row i
Δ_u	Column web relative elongation at the ultimate web resistance
Δ_y	Beam tip relative displacement
Δ_y	Displacement at yield
$\Delta_{y(sys)}$	Displacement at yield of the system
Ω	Coefficient of utilization of the dissipative elements

Abbreviations

3D	Three Dimensions
2D	Two Dimensions
AISC	American Institute of Steel Construction
AJM	Atamaz-Jaspart model
ANSI	American National Standards Institute
BFWC	Component Beam or Column Flange and Web in Compression
BFC	Component beam flange and web in compression
BT	Component Bolts in Tension
BWT	Component Beam Web in Tension
CAE	Complete ABAQUS Environment
CFB	Component Column Flange in Bending
CM	Component Method
CSM	Capacity Spectrum Method
CWC	Component Column web in compression
CWP	Connection with Cover Welded Plates
CWS	Component Column Web in Shear
CWT	Component Column Web in Tension
DBD	Displacement Based Design

DDBD	Direct Displacement Based Design
DT	Displacement Transducer
ECCS	European Convention for Constructional Steelwork
EC3	Eurocode 3
EC3-1-8	Eurocode 3 part 1-8
EC8	Eurocode 8
EP	End-Plate
EPB	End-Plate in Bending
EPBC	Double sided Extended end-Plate Connections
EPC	Single sided Extended end-Plate Connections
EVD	Equivalent Viscous Damping
FE(A)	Finite Element (Analysis)
FE(M)	Finite Element (Method)
FPC	Flush end-Plate Connections
GUI	Graphical User Interface
LVDT	Linear Variable Differential Transformer
MRF	Moment Resisting Frame
NLTH	Non-Linear Time History
PEEQ	Equivalent plastic strain
RFCS	Research Fund for Coal and Steel
RO	Ramberg-Osgood (hysteresis rule)
SDOF	Single Degree Of Freedom
TF	Takeda-Fat (hysteresis rule)
TSC	Top and Seat angle Connections
TT	Takeda-Thin (hysteresis rule)
UB	Universal Beam
UC	Universal Column
W	Welded connection
XS	Double-sided joint with Symmetrical loading
XU	Double-sided joint with anti-symmetrical loading

1

INTRODUCTION

1.1 PURPOSE AND SCOPE OF THIS RESEARCH

Predicting the behaviour of beam-to-column steel joints remains an important task, as properly detailed steel joints are crucial to achieve safe and economic structures. Double extended end-plate beam-to-column connections have the potential to offer a solution with moderate to low costs, particularly for the cases that do not require full strength/rigid joints. Given that the behaviour of bolted joints influences the overall structural response, simple and reliable models that can be incorporated in advanced structural analyses are essential. Some examples of end-plate bolted joints are illustrated in Figure 1.1.

In the past, and even nowadays, it is common practice to design and detail joints after the analysis and design of the steel structure, as if they did not influence the global behaviour of the structure. This philosophy requires that joints are all treated like rigid or pinned joints (Jaspart and Maquoi, 1990). In the case of rigid joints, their influence on the analysis and design of a steel structure is neglected, and in the case of pinned joints their influence is considered by the introduction of some rotational degrees of freedom in the structural analysis. However, it is known that a joint can hardly be either fully rigid or pinned. A degree of relative rotation is always expected even for stiffened “compact” joints. The evolution of computational technology and the advances in the design codes eased the ability to deal with increasingly complex structures, allowing the member design to be based on non-linear behaviour, even though the analysis of the structure remains linear elastic. Yet, the design of joints is remitted

to a subsequent stage, or included in the global analysis as linear elastic springs to take into account the semi-rigidity nature of the joints.



Figure 1.1: Examples of end-plate bolted joints.

Recently, with the implementation of plastic analysis in specific software packages, engineers and researchers have the opportunity to take advantage of the reserve of plastic resistance of the joints, as well as the possibility to account for the “real” behaviour of the joints in the analysis of the structure. In this way, the analysis and design of the structure and joints can take place simultaneously, in an iterative process, where the complex behaviour of joints is incorporated in the structural analysis. Moreover, the use of more sophisticated design approaches based on performance are easier to implement with more accurate models, where the goal of satisfying performance criteria becomes straightforward after knowing the complete structural behaviour. This procedure requires though some experience from the users as well as the adoption of adequate codes of practice.

Eurocode 3 (EC3) (EN 1993-1-1, 2005) opened the door to the use of advanced analysis in the design of structures. In addition to the current design method, which is based on elastic global analysis, even if the resistance of a cross section is based on its plastic strength, EC3 allows the use of plastic global analysis, provided that some requirements are met: i) the rotation capacity of the members or of the joints is assured, ii) instabilities are prevented from occurring in the parts subject to compression. If these two requirements are fulfilled, plastic hinges are able to develop, ensuring, in this way, a ductile and stable behaviour of the structure.

A rational and efficient seismic design requires the detailed characterization of the members and joints behaviour. Modern design codes, like Eurocode 8 (EC8) (EN 1998-1, 2004), in addition to the standard mode superposition response spectra design procedure, also allow the use of more advanced analysis procedures such as pushover or non-linear time-history analyses. However, these are not thoroughly addressed and there is a lack of information on joints behaviour when these are considered as an important energy dissipation mechanism for the structural system. On the other hand in practical guidelines, such as ASCE/SEI 41-13 (2014), for rehabilitation of existing buildings, the use of advanced analysis is not only allowed, but recommended and proper guidance is provided. Vasilopoulos and Beskos (2006) discuss the opportunity to improve the advanced analysis in current design codes, presenting a comprehensive list of references reflecting the evolution of advanced methods to assist the design of structures. Additionally, a brief evaluation of the limitations of EC8 and EC3 standard design approaches is also discussed and an advanced seismic analysis and design procedure, compatible with the EC3 and EC8 is proposed by the authors. This transition to fully nonlinear analysis requires the complete characterization of the behaviour of the members and joints of the structure. For that, a proper characterization of the joints behaviour is needed, capable of being integrated in the structural analysis and design process.

For a proper and efficient seismic design current codes of practice, like the EC8 (EN 1998-1, 2004) use the concept of hysteretic energy dissipation in some members allowing them to sustain plastic deformations, while other members, designed with an overstrength factor, remain elastic, during the seismic event. Hence, to guarantee that plasticity only occurs at intended locations the so-called capacity design approach is used. This concept is illustrated in Figure 1.2. In the particular case of a moment resisting frame (MRF) structure, plastic hinges should be located in the beams or in the beam-to-column connections, although some specific

columns locations are also allowed, to prevent the formation of undesirable mechanisms, for instance a soft-storey mechanism, as illustrated also in Figure 1.2 (b).

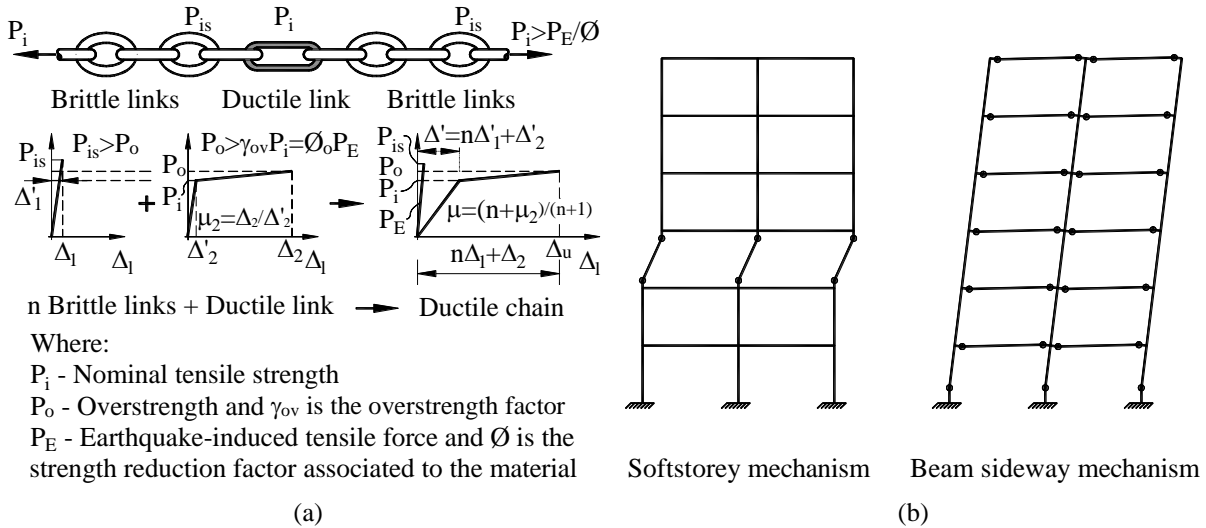


Figure 1.2: (a) A tribute to the basic concept of capacity design: the “weakest link of the chain” concept and (b) its implementation in a frame system with the protection of a soft-storey (brittle) mechanism in favour of a beam side-sway (ductile) mechanism (Paulay and Priestley, 1992, chap.1).

When partial-strength joints are adopted for steel MRF structures, a shift of the plastic hinges from the beams or columns to the joints is expected. In this case, it is necessary to take into account not only the nature of its resisting members, but also of the characteristics of beam-to-column joints. The use of partial-strength joints is a relatively low cost practice to apply in MRF structures, when compared with their full-strength counterpart. Previous studies have shown that, if adequately detailed, these connections can also be attractive to be used in structures located in seismic regions, allowing for the control of the actual location and response of energy dissipative elements (Bernuzzi *et al.*, 1996; Nader and Astaneh-Asl, 1991; Nader and Astaneh-Asl, 1996; Weynand *et al.*, 1998). Additionally, research carried out by Calado (2003), demonstrated the improved behaviour of frames with partial-strength joints due to the period elongation and damping increase resulting from the ductility and friction features of the connections. It is therefore crucial to conduct a proper assessment of the behaviour of partial-strength joints, due to the important role that these joints will play in the structural response during a seismic event, as the main dissipative component of the structure. In current design codes, like EC8 (EN 1998-1, 2004), the use of partial-strength joints is allowed provided that a set of design requirements are met. Advanced structural analyses are required, such as non-linear static (pushover) or non-linear time history (NLTH) analyses, although further detailed

information is missing concerning the adoption of these types of analyses, particularly when one is dealing with steel frames with partial-strength connections. Additionally, EC8 requires experimental evidence of the joints behaviour whenever partial-strength connections are considered in the seismic design process. This requirement is very difficult to accomplish in current engineering practice. It is therefore clear that this kind of joints requires more research aiming at the development of alternative approaches to implement in future design codes.

Many studies have been carried out with the objective of characterising the behaviour of steel connections (e.g. Jaspart (1991), Steenhuis *et al.* (1996), Faella *et al.* (2000)). The classification of steel joints can be divided into three categories, according to the following criteria:

Strength – Full-strength or partial-strength;

Stiffness – Rigid, semi-rigid or pinned;

Rotation capacity – Ductile or non-ductile.

Each one of the properties has a direct impact on the joint behaviour and consequently, on the structural behaviour. The strength requirement determines if the joint is capable of transferring the full connected beam capacity, classified as a full-strength connection, or if the joint is only able to transfer a fraction of the full beam capacity. In the latter case the joint is classified as partial-strength.

The most common partial-strength joints configurations used in European buildings are those composed of an end-plate welded to the beam and which is then bolted to the steel column (Figure 1.4(a)) and the top and seat angle connection (Figure 1.3 (b)).

Normally, partial-strength connections (Figure 1.4) are relatively flexible and hence, are classified as semi-rigid in terms of stiffness. Therefore, the use of this type of connection in seismic zones requires an adequate balance between strength, stiffness and ductility, as they become the main dissipative components in the structure and therefore, additional requirements have to be met in the design process. Hence, as explained in subsequent sections, the joint typology to be discussed in more detail in this thesis is the extended end-plate, Figure 1.3(a), mainly due to its higher stiffness and strength in comparison with the top and seat angle typology.

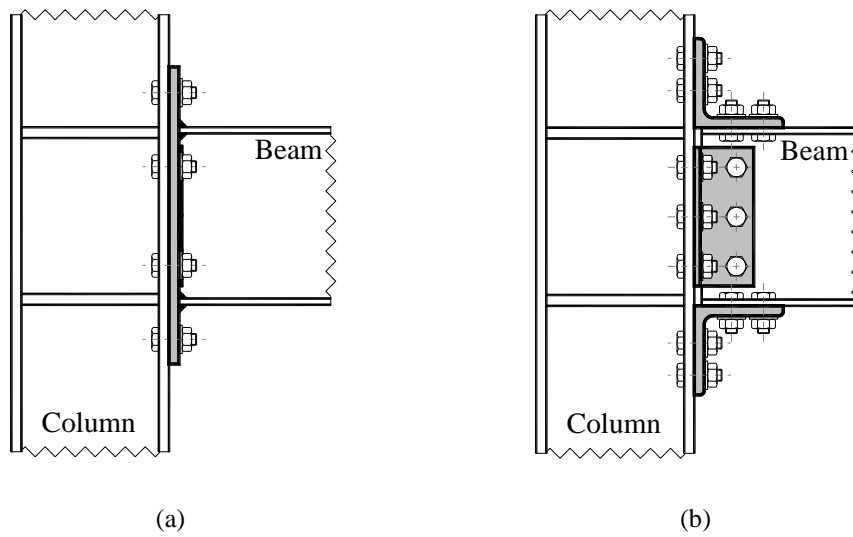


Figure 1.3: Common partial strength joints configurations: (a) end-plate connection; (b) top and seat angle connection.

It can be easily understood that the inelastic behaviour of a bolted joint is far more complex than a welded connection because more components, such as bolts, plates and angles, are introduced into the connection zone. The nonlinear interaction between the connection elements, and the variety of possible failure modes, greatly increases the complexity of the design and the analysis of the joints. However, as realised by Shen and Astaneh-Asl (1999), when designed properly the bolted connection may exhibit high ductility and good energy-dissipation capacity under cyclic loading, provided that proper overstrength is given to the brittle components.

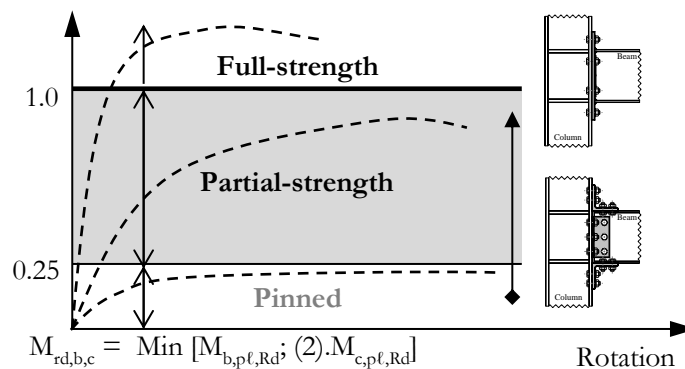


Figure 1.4: Strength and stiffness classification.

It is widely known that predicting the cyclic behaviour of steel bolted joints is quite complex, due to the number of phenomena involved, such as material nonlinearity (plasticity,

isotropic and kinematic strain-hardening), nonlinear contact and slip, geometrical nonlinearity, residual stress conditions, complicated geometrical configurations and also phenomena like pinching, the *Bauschinger* effect, ratchetting effect, among others. All these issues turn the prediction of the connection behaviour into an intricate task. Therefore, experimental testing represents the best way to concisely characterise joint behaviour. However, when extensive parametric studies are required, the limited resources in terms of time and money can be a real problem when one considers performing experimental tests. Allied to the experimental tests, and with the significant development in the computers technology and optimised algorithms provides the opportunity to extend the application of the numerical models to perform parametric studies, as demonstrated by Adány and Dunai (2004), the finite element (FE) method proved so far to be the best numerical approach to characterize the joints behaviour specially for the bolted ones.

Part 1-8 of Eurocode 3 (EC3-1-8) (EN 1993-1-8, 2005) establishes unified procedures concerning the modelling of steel joints as the assembly of basic components. The underlying component method (CM) uses a suitable assemblage of non-linear springs and rigid links to determine the resistance, stiffness and rotation capacity of steel joints. The mechanical characteristics of the components are obtained from experimental tests using specimens similar to the component to be characterized, e.g. T-stub, or using complete full-scale joints. While in the first case acceptable experimental parametric and statistical characterization is possible, in the second case the required number of specimens to have acceptable statistical significance is prohibitively expensive. Therefore, numerical simulations are an effective way to overcome this difficulty, given that the developed FE models reliably reproduce the behaviour of the real joints (Gervásio *et al.*, 2004). Despite the many advantages of the component method, a key limitation is that it is only applicable to monotonic cases, because the mechanical properties of the components cannot deal with the load reversal. This is a major drawback when a structure with partial-strength joints is subjected to cyclic loads, usually due to seismic events. Although this is allowed in structural design codes, like EC 8 (EN 1998-1, 2004), provided that some requirements are met, as discussed before, the design of partial-strength joints is not adequately addressed by seismic codes which often require experimental evidence of the joint behaviour. It is therefore important to find alternative solutions to implement in codes of practice, a

generalized Component Method that can deal with the load reversal conditions, contributing this way to the seismic analysis and design of steel frames with partial-strength joints.

The work developed for this thesis was partially undertaken to fulfil also requirements of two European Projects namely: *DiSTEEL* (RFSR-CT-2010-00029) focused on the development and application to steel frames of the Displacement Based Seismic Design of Steel Moment Resisting Frame Structures, and *EQUALJOINTS* (RFSR-CT-2013-00021) focused on the seismic pre-qualification of steel beam-to-column joints. The first project aimed to set practical performance-based design guidelines for steel moment-resisting frame structures that include performance criteria and a displacement-based design procedure capable of considering different beam-column joint typologies. The second project aimed at the development of design rules for pre-qualified dissipative beam-to-column joints.

As discuss earlier, the methodology prescribed in current seismic design codes consists of a force-based approach, which is largely due to the philosophy adopted for the remaining actions in the structures, where the safety verifications are carried out by comparing the acting forces to the resistance of the members and joints. Besides the fact that this life-safety philosophy can prevent the collapse of a building, recent earthquakes, such as the 2009 L'Aquila earthquake, the 2010 Chile earthquake or the 2011 Christchurch earthquake showed that buildings suffer severe damage during these rare events. These observations revealed the need for seismic design approaches that can also provide damage control, procedures based on the performance of structures as a function of acceptable levels of seismic risk, in order to reduce the direct and indirect costs associated to building repair. Performance-based design has gained awareness internationally, being most possibly the substitute for the current approaches, in the next generation of seismic design codes. The problem however is that force-based procedures present a natural handicap in damage assessment and control, because, as realized by Priestley and his co-workers (Priestley, 1993; Priestley, 2003; Priestley *et al.*, 2007), damage is clearly related to deformations and/or displacements sustained by the structure and not by the relative constant forces that develop in ductile structures, a concept illustrated in Figure 1.5. These findings gave birth to the concept of displacement-based design (DBD).

There is already much work done in the field of displacement-based design, including the most recent publication of a model code (Sullivan, *et al.*, 2012). However, despite the fact that such publications present a comprehensive set of DBD guidelines for reinforced-concrete

structures, the recommendations for moment-resisting steel framed structures are still very limited and had not been fully validated. The *DiSTEEL* project tried to overcome this situation, though the improvement of the design procedure for steel structures, taking into account different beam-column joint typologies, in particular for end-plate bolted connections with partial-strength classification (Calvi *et al.*, 2015).

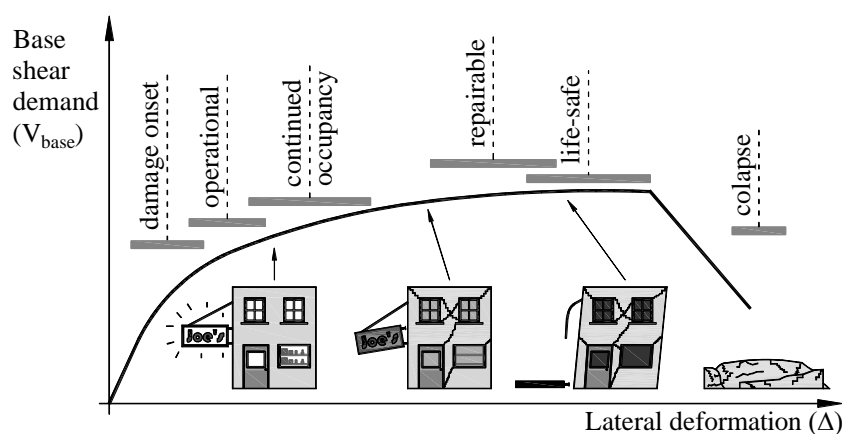


Figure 1.5: Damage relation to the deformation and forces on the structures (Figure from (fib, 2003)).

It is important to mention that the insights gained in the behaviour characterization of extended end-plate joints, allowed to carry out further studies at the components level to characterize their cyclic behaviour. Namely the development of advanced finite elements (FE) models. And the development of a python script of the complete developed FE models compiled by the commercial software package ABAQUS (2014), resulting from the need to perform large parametric studies in the *DiSTEEL* project. The developed tools were naturally applied to the other research project *EQUALJOINTS* concerned with the pre-qualification of steel beam-to-column joints in steel structures. The characterization of the unstiffened end-plate joints by FE analysis, allowed to perform parametric studies, to help design the test setup (Landolfo, 2014).

The purpose of this research is to reduce the gap between the characterization of MRF structures with full-strength joints, and the characterization of MRF structures with partial-strength joints, for seismic design. The focus of the research is on the behaviour of the joints when subjected to cyclic but also dynamic loads. In this case, there are several parts of the joints, considered ductile, able to dissipate energy and others, less ductile, which should be capacity designed. The joint's behaviour and its components are studied with the intention of developing simpler, yet reliable, tools, for the characterization of the joint's behaviour.

1.2 RESEARCH OBJECTIVES AND MAIN BREAKTHROUGHS

The main objective of this thesis is to characterize the monotonic, cyclic and also the dynamic behaviour of beam-to-column joints, both globally and in terms of the critical components, comparing the results of the experimental, numerical and analytical models of beam-to-column end-plate bolted connections.

Based on calibrated and validated FE models, several detailed procedures will be proposed to isolate some of the most relevant components that contribute to the monotonic and cyclic joint behaviour, namely the ones that contribute most to the energy dissipation of the structure. The main achievement will be the identification of the components' mechanical behaviour in terms of force-displacement relationships by analysing the stress and deformation fields in the FE models. Whenever possible, the results are compared with those given by EC3-1-8 (EN 1993-1-8, 2005) and by other models available in the literature. This research has also the objective of contributing to the development of an analytical design method, based on the component method. This method will consider the cyclic behaviour of the joints given by each dissipative component, assuming that adequate overstrength for the non-dissipative components (capacity design) is assured. Such a model can be employed in the global analysis of the structure when the joint cyclic behaviour is to be considered.

Additionally, and based on the calibrated and validated FE models, it is also an objective of this research to contribute to the development and improvement of displacement-based design procedures, proposing improved ductility-equivalent viscous damping relationships for steel moment-resisting framed structures with dissipative beam-to-column partial-strength joints. These relationships can be used directly in procedures like the Direct Displacement-Based Seismic Design (DDBD) (Priestley *et al.*, 2007) that uses effective stiffness, ductility-equivalent viscous damping relationships and period-displacement relationships in a performance-based design approach. The consideration of different joint typologies is essential given that the joint selection significantly affects the seismic behaviour. In the case of steel MRF structures with partial-strength beam-to-column joints, there is a shift of the plastic hinges from the beams to the joints. In this case, the joints are the main source of energy dissipation during a seismic event. Hence, it is necessary to determine how the joints behaviour affects the ductility-equivalent viscous damping relationship, namely the influence of the several

dissipative components involved in the double-extended end-plate joints, as defined in Eurocode 3 Part 1-8 (EN 1993-1-8, 2005).

In order to reach these goals a detailed parametric numerical model for beam-to-column bolted joints is developed in ABAQUS (2014) taking advantage of the Python programming language to develop the scripting interface. The parametric FE model developed considers a three dimensional detailed representation of the various connection components taking into account the several phenomena involved in the connection behaviour, namely the nonlinearities related to the geometry, contact, slip and material properties. A combined isotropic and kinematic material-hardening model is also included in order to characterize the connection behaviour under load reversal.

1.3 STRUCTURE AND ORGANIZATION OF THE DOCUMENT

This document is composed by seven chapters. The organization chart, depicted in Figure 1.6, explains in a concise manner the structure of the document, the topics covered in each chapter and also the interaction between chapters.

The first chapter is crosscutting for the entire document. It contains the introduction and the research objectives. The importance and the motivation of the theme is highlighted, debating the need of further developments in the joints characterization under cyclic loading, due to the lack of consensus around existing procedures, and also the need for further developments for the new displacement based seismic design procedures for moment-resisting frame buildings with beam-to-column partial-strength joints.

Chapter 2 presents the relevant state-of-art and sets the theoretical bases for the research. A literature review of the main topics discussed in the thesis is performed, focusing on the two main subjects addressed in this document: the behaviour of steel joints and the seismic design methods based on displacement. A detailed review of past experimental, analytical and numerical work, to characterize the steel joints behaviour is performed. At the component level, the component method is reviewed focusing on the application to end-plate bolted joints. Particular attention is given to the behaviour of the column web panel, reviewing the available methods to characterize its response, since much of the research is focused on the extraction of

the behaviour of these components. Also, at the components level the equivalent T-stub model is discussed. Since this thesis is based on nonlinear numerical models, an overview of the finite element method is performed in the context of the joints modelling and behaviour characterization. It is also included in this chapter the data collection and treatment of the available experimental tests, found in the literature, used later in Chapter 3 to validate and calibrate the numerical models.

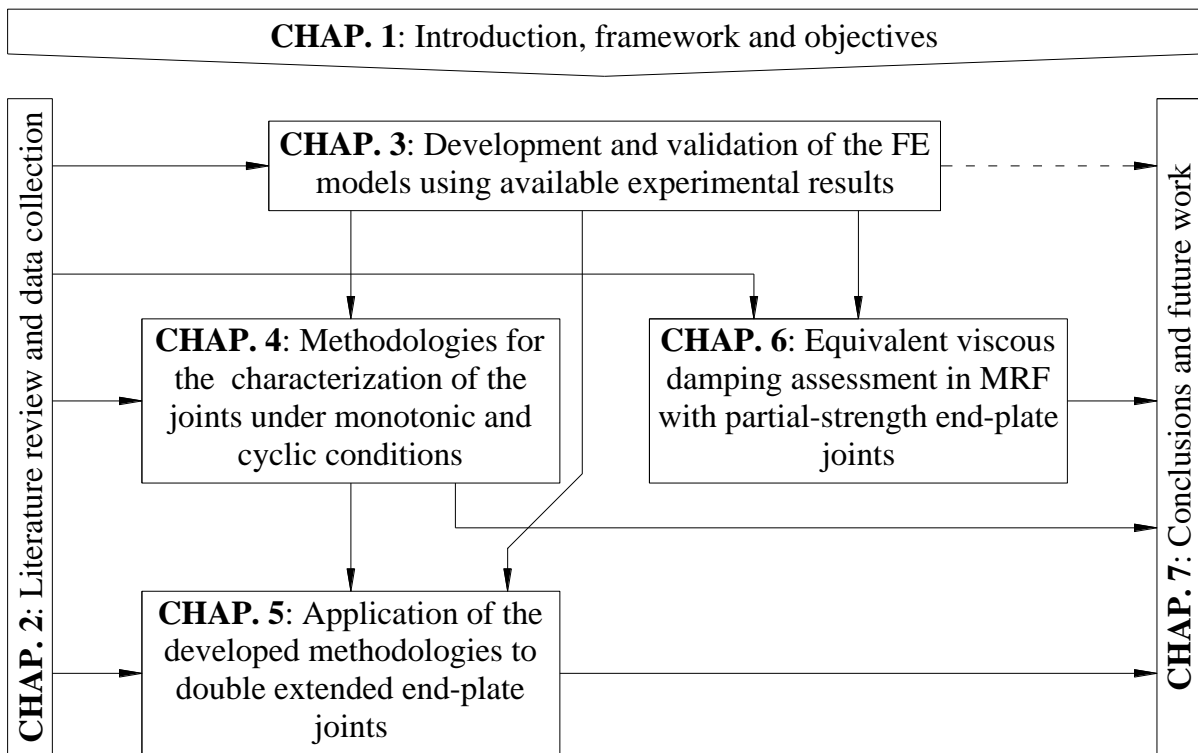


Figure 1.6: Organization of the document.

The third chapter is dedicated to the development and validation of the finite element models to characterize the behaviour of beam-to-column end-plate-joints. The calibration and validation of the numerical model is based on the results of a previously experimental research programme, which is comprehensively described in this document, and on experimental and analytical results available in the literature, collected in the Chapter 2. The monotonic and cyclic behaviour of the joints is characterized, both globally and in terms of the critical components. The results are compared with available experimental, numerical and analytical models. By using the validated FE models, several detailed procedures are described to isolate some of the most relevant components, that contribute to the joint behaviour, namely the ones that

contribute most to the energy dissipation of the structure, and to identify their mechanical behaviour analysing the stress and deformation fields in the FE models. The results are compared with those obtained with EC3-1-8 (EN 1993-1-8, 2005) and with other models available in the literature. In this chapter it is also presented a detailed parametric numerical model developed in ABAQUS (2014) that takes advantage of the Python programming language to develop a scripting interface for ABAQUS. The ability of scripting of beam-to-column end-plate joint, to expedite the execution of large parametric studies, will be used in the subsequent chapters. It is understood that experimental tests are the best tool to characterize joints behaviour. However, the demanding requirements of specialized facilities, equipment, personnel and the amount of resources involved (materials, consumables, time and elevated costs) makes it very difficult to perform large parametric studies. Finite element models are the most viable alternative to extend the results of experimental tests to larger databases. The tools developed in this chapter, namely the numerical models and the proposed methodologies to extract and treat the results, will be used in the following chapters (4, 5 and 6) to characterize the joints behaviour when subjected to monotonic, cyclic or dynamic loading conditions.

In the fourth chapter a methodology is developed to extract the force-displacement response of the individual components behaviour, from the beam-to-column end-plate joints, yet with the potential to be extended to other joint configurations. The use of partial-strength joints in seismic regions, although allowed in current seismic design codes, such as EC8 (EN 1998-1, 2004), is not properly addressed. In the case of partial-strength joints subject to static monotonic loading, they are well characterized in modern codes of practice, such as EC3-1-8 (EN 1993-1-8, 2005) within the framework of the component method. However, in the presence of cyclic load reversals, there is no direct and easy approach to characterize their cyclic behaviour and energy dissipation. With that in mind, a detailed procedure is described to isolate the column web components under cyclic loading, namely the column web panel in shear and the column web in transverse compression or tension, and to identify their mechanical behaviour analysing the stress and deformation fields in the FE models. A similar procedure is developed for the connection components: column flange in bending, end-plate in bending and bolts in tension. It is also based in the integration of the stress fields, that enter into the column web or, in alternative, the stresses in the bolts in tension. The forces are then associated to the components deformation shape. The methodology is also applied to the joints and the

components compared with the analytical procedures available, namely that proposed in EC3-1-8 (EN 1993-1-8, 2005).

In Chapter 5 the previous tools and methodologies are applied to several double-extended end-plate joints configurations tested in the European RFCS project *EQUALJOINTS* referred in Section 1.1. The objective is to study several typical beam-to-column configurations, and for different levels of joint resistance the influence of several parameters that affect joint response in terms of strength, stiffness, ductility and energy dissipation. The joints are subjected to quasi-static monotonic and cyclic loads, and the results are compared with the analytical results of EC3-1-8 (EN 1993-1-8, 2005). To create the basis for the experimental tests carried out in the project, a preliminary parametric study was performed, changing the design configurations for a set of parameters that influence the joints behaviour, using the developed tools in Chapter 3. The methodologies developed in Chapter 4 are applied to the joints under investigation to extract the cyclic force-displacement response of the components, in such a way that they can be directly used in a cyclic component model. Additionally, the numerical results of the preliminary predictions are compared with: the results obtained with the modified numerical models, using the material properties based on the coupon tests; the results of the experimental tests available; and the analytical results provided by the EC3-1-8.

In the sixth chapter the equivalent viscous damping is assessed for moment-resisting frames (MRF) that contain partial-strength joints. For that, and taking advantage of the tools developed in Chapter 3, namely the numerical models, the parametric script and the methodologies to extract the results, a large parametric study is performed. The methodology uses non-linear time history analyses (NLTHA), and a set of real earthquake records, applied to sub-assemblages representative of typical moment-resisting framed structures with several bolted end-plate joints and classified as partial-strength according to EC3-1-8 (EN 1993-1-8, 2005). This large parametric study is part of the European RFCS project *DiSTEEL* referred in Section 1.1. The aim of the study was to evaluate the equivalent viscous damping of MRF structures made with partial-strength end-plate joints. The objective is to improve the existing ductility-equivalent viscous damping relationships for a selection of partial-strength extended end-plate beam-to-column joints of MRF structures, resorting to the same FE modelling approach utilized in the previous chapters, to characterize the behaviour of joints under static and dynamic conditions.

Finally, in the seventh chapter, the overall conclusions are withdrawn, presenting the main findings in a concise manner. Recommendations for future research are also proposed which could complete the characterization of the joints behaviour under cyclic conditions. Furthermore, the main contributions of this thesis to the state-of-the-art are highlighted.

2

LITERATURE REVIEW AND DATA COLLECTION

2.1 INTRODUCTION

This chapter is mainly devoted to literature review and data collection found in the relevant bibliography on partial-strength beam-to-column steel joints. The review and discussion of the main concepts and phenomena involved in the analysis of partial-strength joints as part of steel moment resisting frames is firstly addressed. The focus of the research is on the characterization of the joints behaviour under monotonic, cyclic and dynamic loading conditions including the relevant concepts, in particular for end-plate bolted joints with partial-strength classification. One application of the numerical and analytical models developed for the joints will be to derive important key features needed for displacement-based seismic design methods. In this context, the main features of these methods are also presented in this review as well. Therefore, the literature review is divided into two main subthemes. The first is related to the joints behaviour characterization, under monotonic or cyclic loading, and the second is related to seismic design methods of building structures, in particular steel moment-resisting frame structures with partial-strength joints.

In the joints literature review the current design methods for the beam-to-column joints analysis and design are addressed, including the component method adopted by Eurocode 3 (EN 1993-1-8, 2005). This review focus on joints subjected to monotonic loads, using a component based approach to characterize their behaviour, and also in the efforts done so far to obtain an equally valid procedure for connections subjected to cyclic loads.

The research presented in this document was fully based on numerical simulations performed on FE models properly calibrated and validated by experimental evidence. As such, some background and recent developments on numerical simulation, modelling techniques and analysis are also reviewed in this chapter. The finite element method basic principles, evolution and applications to the joints characterization are discussed.

Additionally, a collection of experimental data on steel joints is also conducted. Since in this research it was not intended to perform new experimental tests, the results of existing experimental tests were used. For that, the available tests results were collected, examined, catalogued and ordered according to degree of relevance. Subsequently, the selected data was analysed and used in the calibration and validation of the several numerical models developed in the following chapters.

The numerical and analytical models developed for the joints are used to derive important key features for displacement-based seismic design methods. Therefore, the second subtheme is related to seismic design methods with the focus on the Direct Displacement Based Design Method, although an overview and comparison of Force and Displacement based methods is given as well.

2.2 BEHAVIOUR OF STEEL JOINTS

2.2.1 DEVELOPMENTS IN THE CHARACTERIZATION OF STEEL JOINTS

2.2.1.1 INTRODUCTION

Beam-to-column joints modelling must deal with a variety of phenomena, mainly in bolted connections that make the prediction of its mechanical behaviour a complex task (Simões da Silva, 2008). As summarized by Faella *et al.* (2000), the methods for predicting the joint behaviour can be divided in five different categories: empirical models, analytical models, mechanical models, finite element models and physical models (experimental testing).

Empirical models are mathematical representations of the response of joints. These empirical mathematical formulations can be obtained by means of curve fitting or regression analysis, presenting though no physical meaning, using data from experimental tests, numerical

simulations, analytical or mechanical models response. This dependency of the data used to define the mathematical formulation makes their applicability limited to the joint configuration from where the data was extracted. Similarly to the empirical models, analytical models also depend on the results of experimental tests or numerical models to validate their response and detect their failure modes, although the degree of dependency, in this case, is lower than in the empirical models case.

Analytical models use the basic concepts of elastic structural analysis and limit design to characterize the joints behaviour, using their geometrical and mechanical properties. From an elastic analysis, the initial stiffness of the joint is assessed, and with the observed failure modes the plastic mechanisms are implemented predicting the ultimate bending moment using the balance between internal and external work. As an example of analytical models the work of Kishi and Chen (1987) and Chen *et al.* (1988), in the characterization of the behaviour of top and seat angles with double angles connections, should be pointed out. On the other hand for extended end-plate connections the work of Yee and Melchers (1986) should be mentioned, identifying several contributions to the joint deformation and failure modes.

Mechanical models have gained wide acceptance because they achieve a good balance between accuracy (accounting for resistance, deformability and ductility) and ease of use. Joints are decomposed in several parts, called components, that represent a specific part of a joint that, depending on the type of loading, make an identified contribution to one or more of its structural properties (Weynand *et al.*, 1996; Jaspart and Weynand, 2016). The constitutive relations of the components and the way they are assembled determine the joint behaviour. The relation between the components and the joint's mechanical properties is determined through equilibrium and compatibility relations. In the framework of EC3-1-8 (EN 1993-1-8, 2005), the implementation of the component method allows for the determination of the resistance, stiffness and rotation capacity of a variety of steel joint configurations. Firstly, the active components are identified, then the force-displacement relationships of each component is derived and, finally, the components are assembled according to the joints geometry, allowing for the assessment of the global joint properties. Typically, the characterization of the behaviour of each component, defined by a force-deformation curve, is obtained either from experimental tests or from numerical or analytical models. The differences for the analytical models is that some components are also obtained by empirical relationships, and, more important, they are

not dependent of curve fitting to be able of simulate the curvilinear shape of the moment-rotation response of the joint, even though bilinear relationships are used for the components force-displacement relationships.

Finite element models (FEM) provide the most sophisticated and realistic representation of joint behaviour, using numerical simulation, but their use in design is very time consuming and cumbersome as they present convergence and calibration problems and is prohibitively expensive if combined with physical models (Gentili *et al.*, 2014). Nevertheless, due to its discretized nature, FEM has the potential to adapt to any joint configuration and to provide information about the whole model. An advantage in relation to the physical models limited to the instrumentation set up to provide information.

Physical models, better known as experimental testing, are the most accurate tool to characterize joints behaviour. This is why they are used to validate empirical, analytical, mechanical and finite element models. However, the demanding requirements of specialized facilities, equipment, personnel and the amount of resources involved (materials, consumables, time and elevated costs) make them impossible to use in current design practice, they are only used in research context with financial support. Notwithstanding the fact that they produce the most accurate results regarding the prediction of the joints moment-rotation curve, they can fail to predict the real joint behaviour in building frames (Faella *et al.*, 2000). Differences like the stress interaction in the column web panel zone, or the modification of the local stresses during the loading process (the point of zero moment is fixed in the experimental tests while in building frames changes during the loading process) or even the interaction with non-structural elements can significantly influence the characterization of the joints behaviour. Moreover, experimental tests can fail to account for other variables that are not easy to recreate in laboratory, like the repercussions of the erection phase or the variability of the loading conditions. Nonetheless, experimental tests are, as mentioned above, the models that produce the most reliable results, and are a key element in any research focusing on joint behaviour.

In the following sections the most relevant work developed in experimental, analytical and numerical models is examined, demonstrating the growing evolution of this theme over the years, with a growing number of research projects devoted to the characterization of the behaviour of steel joints. Despite the numerous investigations developed so far, there is still

room for development in this area, especially in the field of the characterization of behaviour of steel joints under special loads, namely cyclic, dynamic, impact, fire, etc.

2.2.1.2 REVIEW OF PAST EXPERIMENTAL WORK

A considerable amount of experimental work was carried out in the past to characterize the cyclic behaviour of steel joints in several fields of application. Korol *et al.* (1990) and Ghobarah *et al.* (1992) studied the cyclic behaviour of extended end-plate joints in terms of strength, stiffness, ductility and energy dissipation, both for the global response and in terms of their individual components. Several factors that can influence the behaviour of joints were examined, such as end-plate thickness, bolt pre-tension forces, column flange slenderness, the presence of transverse web stiffeners and supplementary web plates in the column web, and the presence of end-plate rib stiffeners. Several geometries were tested changing the beams and columns and also the presence of stiffeners, see Figure 2.1. In the first study the column stub was rigidly fixed to the testing frame, so only the deformations due to the beam and the connection was analysed. In this conditions all specimens experienced degradation in their stiffness with load cycling, see Figure 2.2 a), b) and d). The possible excessive contribution of the connection to the interstorey drift should be taken into account. The authors alert to the risks of employing thin end-plates that can lead to premature failure under cyclic loading. Furthermore it was observed that with proper detail of the connections it is possible to dissipate sufficient energy without substantial loss of strength and stiffness, see Figure 2.2 c).

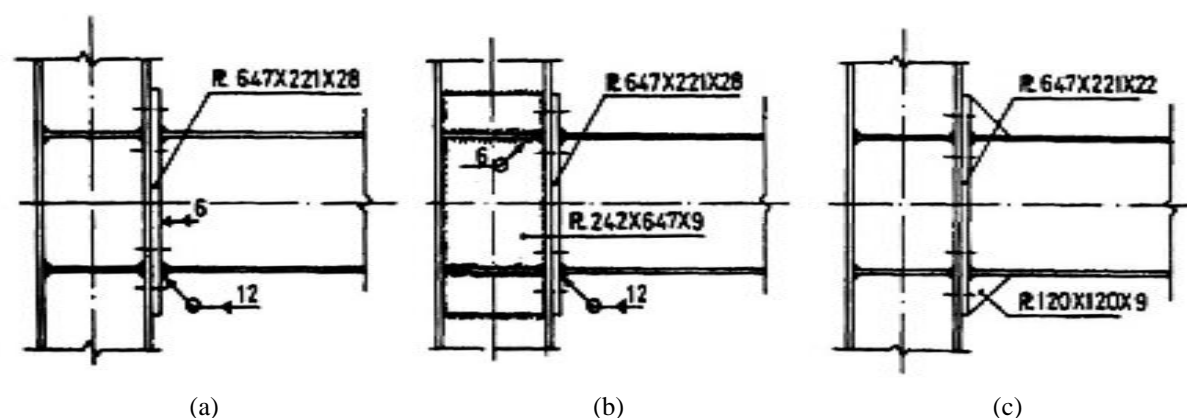


Figure 2.1: Detail of the specimens tested (Ghobarah *et al.*, 1992).

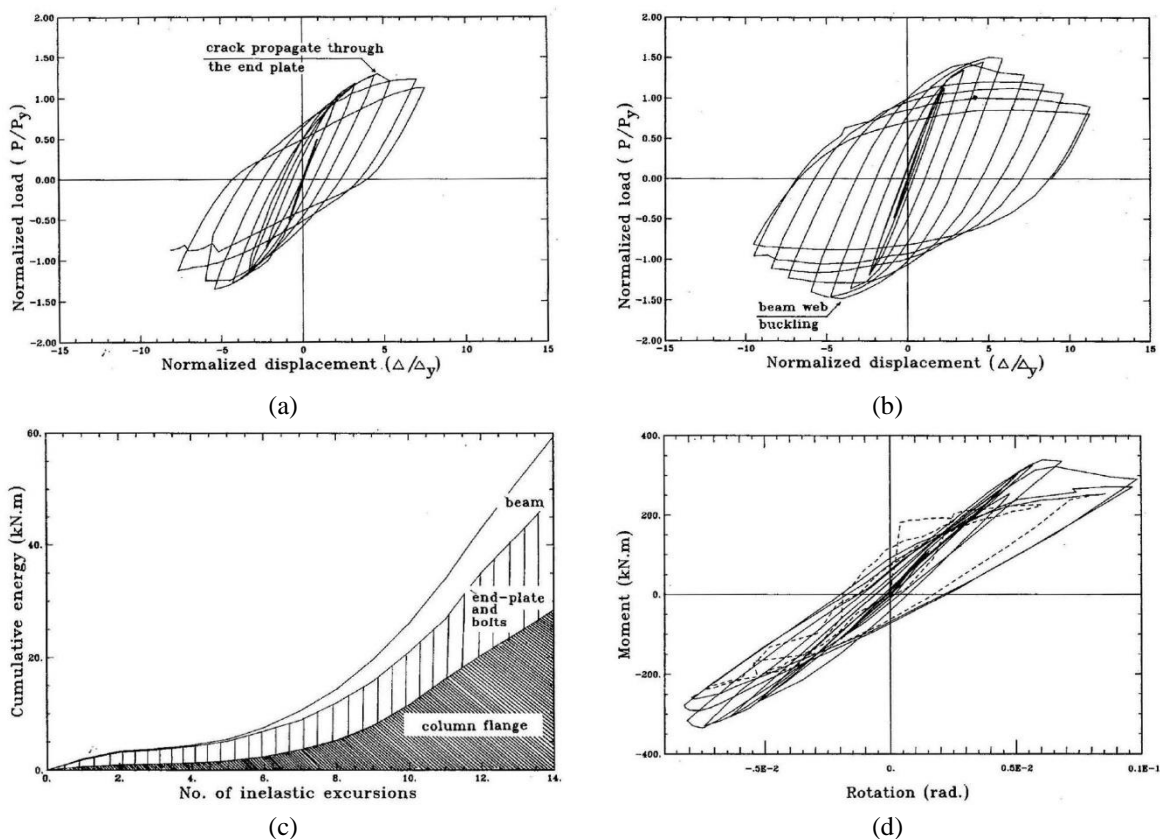


Figure 2.2: Normalized beam load vs. normalized beam tip displacement for a) a specimen without continuity and end-plate rib stiffeners and b) for specimen with all stiffeners. (c) Cumulative energy dissipation by each component and d) beam moment vs. connection rotation hysteresis curves for a joint with stiffeners (Korol *et al.*, 1990).

In the second study Ghobarah *et al.* (1992) the test setup already allowed to take into account the contribution of the column panel zone to the joint rotation. For all the specimens the response curves, of the joints, showed stable behaviour during the load history. In this tests panel zone had great influence, especially in the joints without supplementary web plates, see Figure 2.3, and it was confirmed the large ductility achieved by the panel zone with stable behaviour. The supplementary web plates revealed to be very effective in increasing the shear capacity of the panel zone when they are filled welded all around to the column web. It was also found that the participation of the end-plate, in the inelastic range, provides an additional strength to the panel zone resistance, this conclusion was confirmed when the experimental results were compared with the Krawinkler *et al.* (1975) model developed for welded joints. The authors also question the direct application of the design criteria, to the panel zone, imposed by the codes, for fully welded connections, in the presence of an end-plate connection. As a final conclusion it is stated that extended end-plate joints, when properly detailed and designed,

can perform well during severe earthquakes.

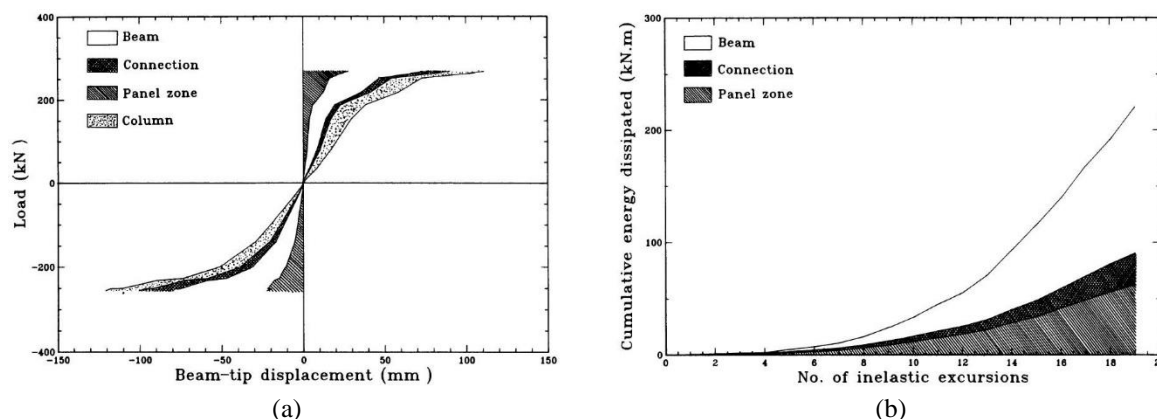


Figure 2.3: a) contribution of specimen (c) components to the beam-tip deflection, and b) cumulative energy dissipated by each component in the same specimen (Ghobarah *et al.*, 1992).

Plumier and Schleich (1993) studied the contribution of the column shear panel to the energy dissipation, strength and rotation capacity of the joints. Several joints typologies were tested, for simple and moment connections, for pure steel and composite structures and also considering internal and external nodes in a large sub-assembly of a one-storey cell of a multi-storey building. Several parameters were investigated, as such stiffness, ductility, three dimensional joints (four beams connecting to the column), the easiness of assembly, the optimization of concrete and welding, manufacturing and assembling costs. The main conclusions revealed that the contribution of the shear panel to the overall energy dissipation should not be neglected, however should be balanced with the energy dissipation from other sources, like beam plastic hinges. The shear panel should be capacity designed to the beam or connection resistance. The additional shear resistance, provided by the frame formed by the column flanges and the transverse web stiffeners, should be consider in the panel strength assessment, as well as the additional resistance provided by the reinforced concrete in composite structures. Some rules for the connections design were also proposed, such that sufficient rotation is possible without loss of strength: in end-plate joints welds and bolts should be ‘capacity designed’ imposing that only the end-plate should sustain plastic deformations; welded connections should also be ‘capacity designed’; the semi-rigid joints, designed accordingly to the specimens tested, can be used as safe dissipative zones.

Bernuzzi *et al.* (1996) analysed the influence of the load history and the key geometrical and mechanical parameters on the cyclic performance of some connections types, namely top and seat angle connections (TSC), flush end-plate connections (FPC), single (EPC) and double

sided extended end-plate connections (EPBC). The main parameters identified, in the first series (only TSC and FPC), were the influence of the loading history and the main stiffness and strength parameters, whereas in the second series the study focused on the influence of the key geometrical and mechanical parameters in the cyclic performance, and also on the energy dissipation capacity. The work on extended end-plate connections intended to study the overall joint response and the individual contribution of the basic components. On the other hand, the study on top and seat angle connections intended to assess the problem of the cumulative damage. The ECCS (1986) loading protocol and three additional loading histories were used for the cyclic loading pattern, and a parametric study was undertaken in the connection components. All specimens consisted of a long beam stub with IPE 300 section, attached through the connection to be tested to a rigid counter-beam, see Figure 2.4.

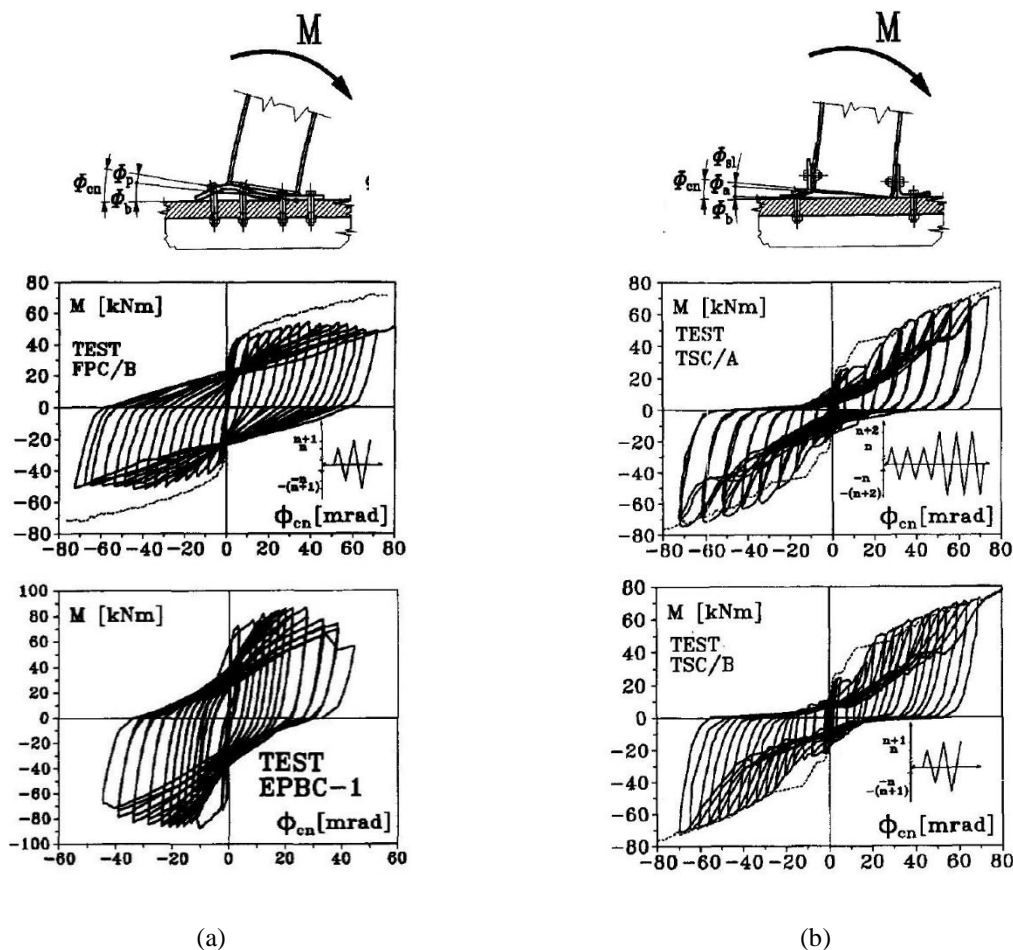


Figure 2.4: (a) Response of some flush and extended end-plate connection tested; (b) response of a top and seat angles connection, under two of the four different load protocols used (Bernuzzi *et al.*, 1996).

From the TSC, the results showed that the correlation between the monotonic tests and the envelopes of the cyclic ones correlate well in the initial elastic range and in the final inelastic

ranges, whereas in the intermediate range differences were remarkable mostly because of the slippage. For the flush end-plate connections (FPC), the correlation between the monotonic tests and the envelope of the cyclic ones differ remarkably, although this difference was explained by the earlier plastic deformation of the end-plate in the vicinity of the beam flanges affecting the contact with the counter-beam. The main contribution to the rotation of nodal zone is the end-plate deformation (close to 90%).

For the second series of tests, the steel grade was changed among other parameters. For the flush end-plate connections, such influence appeared to be insignificant, but the deformation of the cleats in the TSC specimens was fairly affected by the steel beam grade and also the fracture mechanism changed to one occurring in the cleats. In addition, the TSC connections showed lower pinching and higher resistance (of about 14%). For the extended end-plate connections (EPBC), the results revealed that the plate extension ensures a noticeable increase in the stiffness and strength when compared to the FPC connections. The key features of the behaviour were nonetheless the same, with the plate contributing the most to the response in both the elastic and inelastic range. If the thickness of the end-plate increased, the behaviour of the connection changed, with bolt inelastic elongation and pinching behaviour becoming more prominent. The failure mode differed also for the lower end-plate thickness, where failure occurred in the plate welds and with the thickness increase, the bolts were seen to fail first. As for the energy dissipation capacity, TSC and EPBC-1 connections exhibited remarkably higher energy dissipation compared to both flush end-plate connections, but only in the high rotation range. The EPBC1 connection therefore showed the better balance between the stiffness and rotation ductility. As a general conclusion, the cyclic response of semi-rigid connections can be generally considered quite satisfactory in terms of stiffness, strength and rotational ductility. A simple prediction model was also proposed taking into account the results of the tests under reversal loading, considering only the results for FPC. The energy dissipated E was adopted as the reference variable for the assessment of the degradation of stiffness in the loading and unloading branches of the connections response. After observing that loading and unloading branches were nearly linear, a linearization of the responses was undertaken. Considering E_{tot} (total energy dissipated) as the reference parameter, K_i and K_0 the stiffness of the cycle i and the initial stiffness value, respectively. For further simplification the unloading stiffness is considered as a function of the loading one, see Figure 2.5 a) and b). The authors also realised that for the cycles with the same amplitude a simple relationship exists between partial ductility

ratio and the mean dissipated energy, thus allowing assess the E_{tot} by the loading history, see Figure 2.5 c). In Figure 2.5 d) is depicted one of the comparisons revealing an overestimation of the connection maximum moment for low partial ductility ratios.

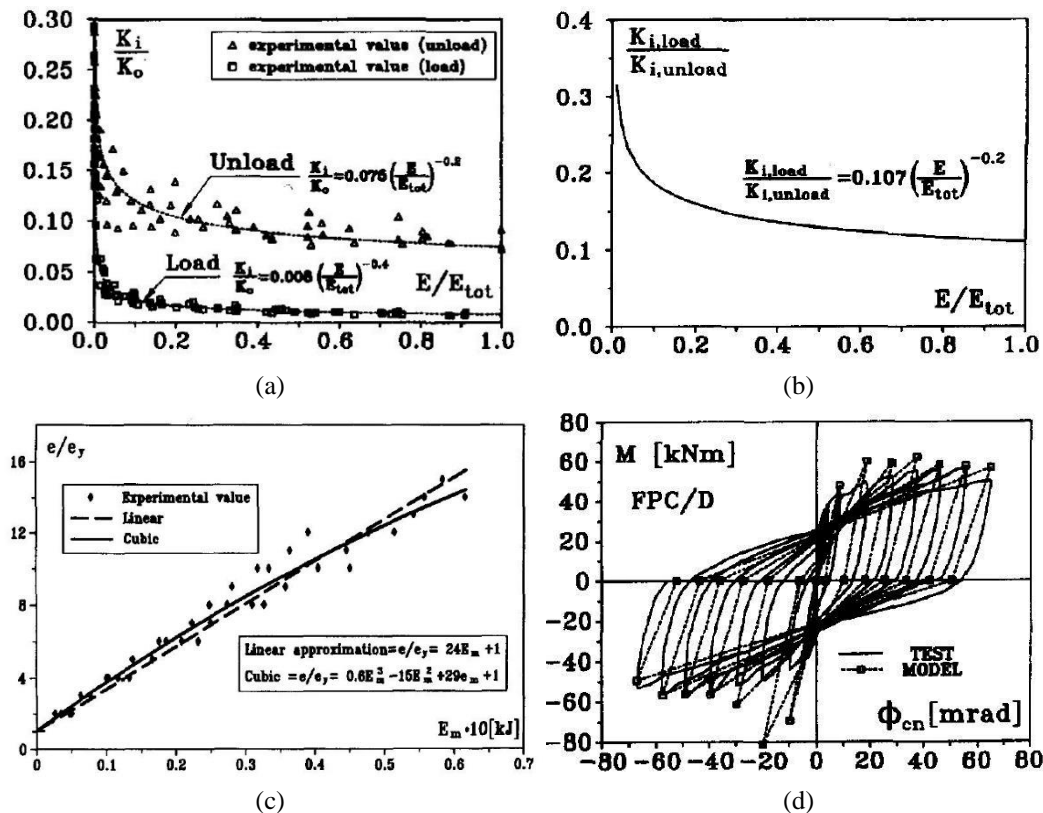


Figure 2.5: a) and b) Stiffness degradation versus dissipated energy; c) partial ductility ratio versus mean dissipated energy and d) application of the procedure (Bernuzzi *et al.*, 1996).

Adey *et al.* (1998) and in more detail in (Adey, 1997) studied the effect of the beam size, bolt layout tight and relaxed), end-plate thickness, the presence of transverse web stiffeners and welding techniques. As in some of the previous tests also in this the column was prevented to deform, the main contributions to the deformation was concentrated in the connection and in the beam. Three series of tests were designed (S, M and B). For the S (small) series three joints were tested with W360x51 beams size and a weak end-plate; for the M (medium) series seven joints were tested with W460x97 beam size; and for the B series five joints were tested using larger beams (W610x125) to study the effect of the beam size. For the column in the S series W310x118 were used and for the rest of the tests W310x143 were used. The thicknesses of the end-plates ranging from 13 to 19mm. Several configurations of stiffeners were used in the column and in the end-plates. The results indicate that an increase in the beam size results in a reduction in the energy dissipation. On average the energy dissipation per inelastic incursion

increases with the increase of the end-plate thickness. Although this increase may not be reflected in the total energy dissipation. Bolts layout affects significantly the moment capacity of the joints. The stiffened end-plate connections dissipated more energy than the other types of joints tested, combining a high moment capacity and good degree of ductility. The results of tests left to foresee that if properly designed the extended end-plate connections are capable of developing the plastic moment capacity of the beam under cyclic loading. In Figure 2.6 is depicted the response of the end-plate connection of two of the medium series tests. The failure of the joints, in M and B series, was always by cracking of the end-plate in the heat affected zone at the toe of the full penetration groove welds.

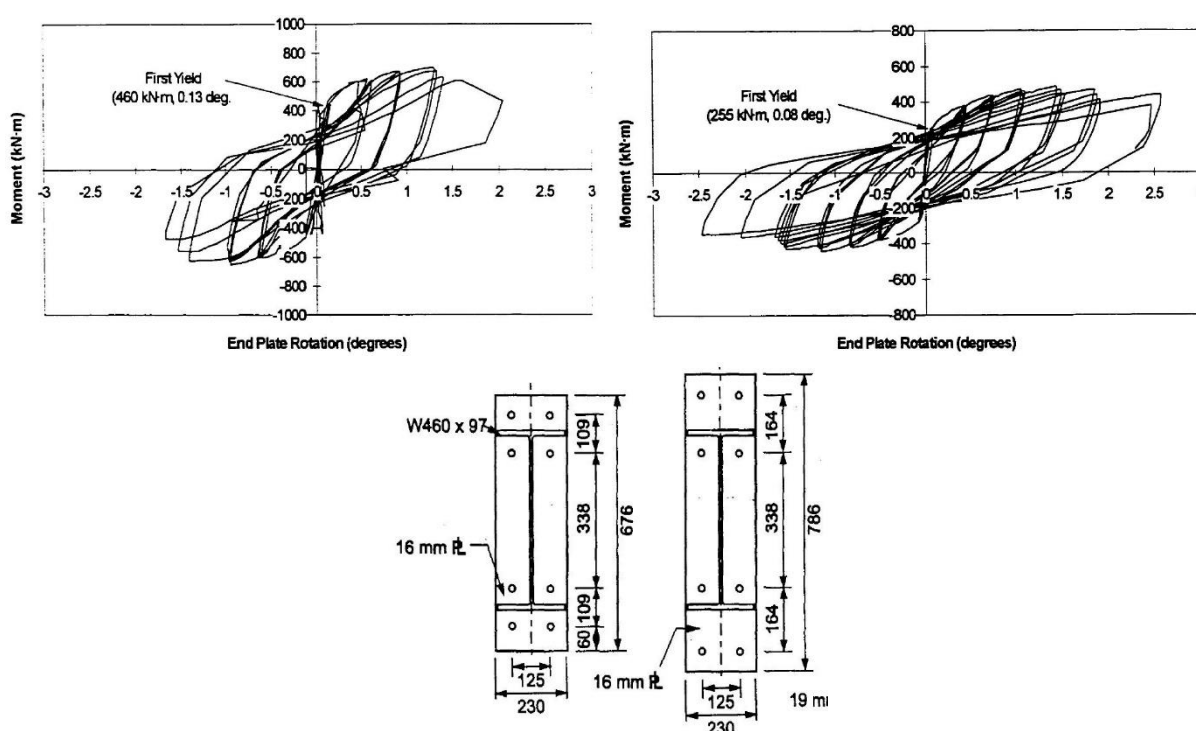


Figure 2.6: Bending moment vs. end-plate rotation (Adey, 1997).

Yorgun and Bayramoglu (2001) analysed the effect of the gap between the end-plate and the column flange on the joint performance. An innovative end-plate connection was proposed, using a gap between the end-plate and the column flange, filled with an I-shaped element. Two types of specimens were analysed, with a gap of 15mm and without gap (EP-15 and EP-00, respectively). Due to the fact that the specimens were made from welded plates the thickness of the web panel zone of the column was selected as twice the thickness of the column web to reduce the deformations in this zone. The recommendations of the ECCS (ECCS, 1986) were used for the load protocol implementation. The results, see Figure 2.7, revealed that there was

no deformation in the I-shape element spacer, and that the two specimens revealed stable hysteresis loops, however with different ductility ratios. The innovative end-plate connection showed better performance than the standard one. Due to the additional thickness in the column web panel no sign of yielding was detected during the loading history.

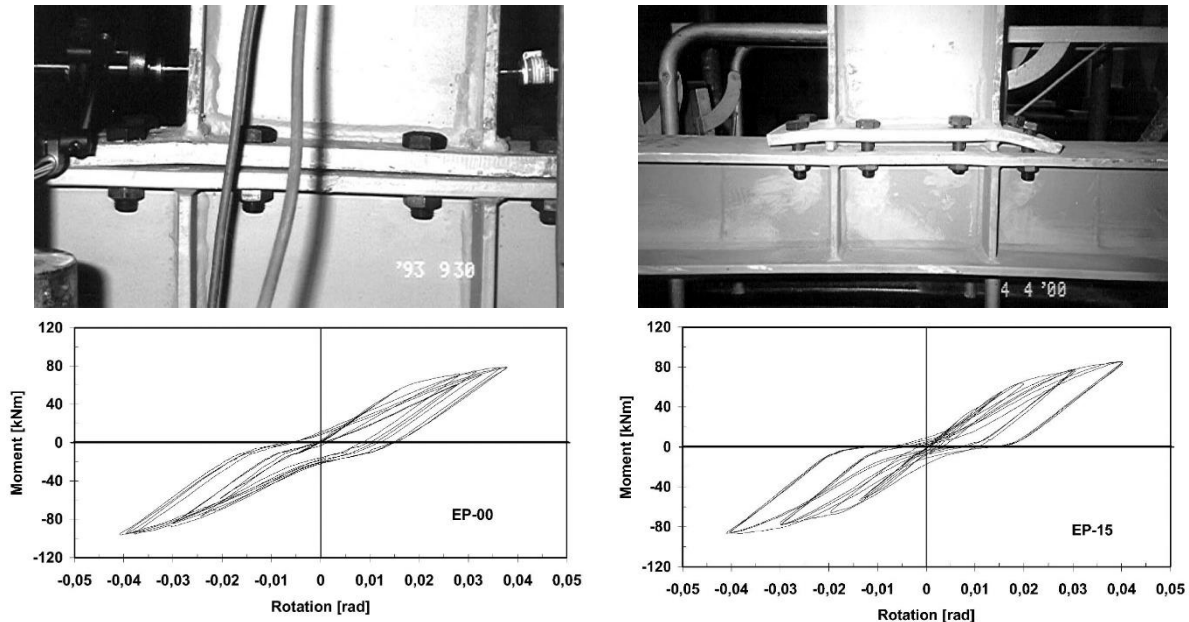


Figure 2.7: Response of the joints (Yorgun and Bayramoğlu, 2001).

The studies undertaken by Dubina *et al.* (2001; 2000) analysed the influence of symmetric and antisymmetric cyclic loading. Three connections typologies were tested, extended end-plate (EP), welded (W) and with cover plates (CWP). The beam-to-column joints were double-sided and each typology was tested twice under symmetrical (XS) and anti-symmetrical (XU) cyclic loading. An additional series of tests were done using built up sections, “I” in the beam and “X” in the column. The main parameters considered in the study were the initial stiffness, moment capacity and plastic rotation capacity and the results of the experiment were compared with the Eurocode 3 (EN 1993-1-1, 1992), Annex J. In addition, the anti-symmetrical loading tests were compared with the symmetrical loaded ones due to the panel zone plastic mechanism developed in the anti-symmetrical ones. This resulted in the following differences for the XU tests: increase of ductility; decrease of moment capacity; and initial stiffness; and more stable energy dissipation through hysteretic loops, see Figure 2.8. The ECCS (ECCS, 1986) procedure was used for the applied loading history. The failure of the specimens was defined as when the force applied to the joint fell below 50% of the maximum load applied during the loading history. The test results for the XS-EP specimens showed that the end-plate was the weakest

component with visible deformation in the vicinity of the beam flanges. In the case of XU-EP the main source of ductility was the column panel zone with stable hysteretic loops over the entire loading history, with an important strain hardening. A degradation of strength and stiffness was observed throughout the entire loading history of the extended end-plate tests.

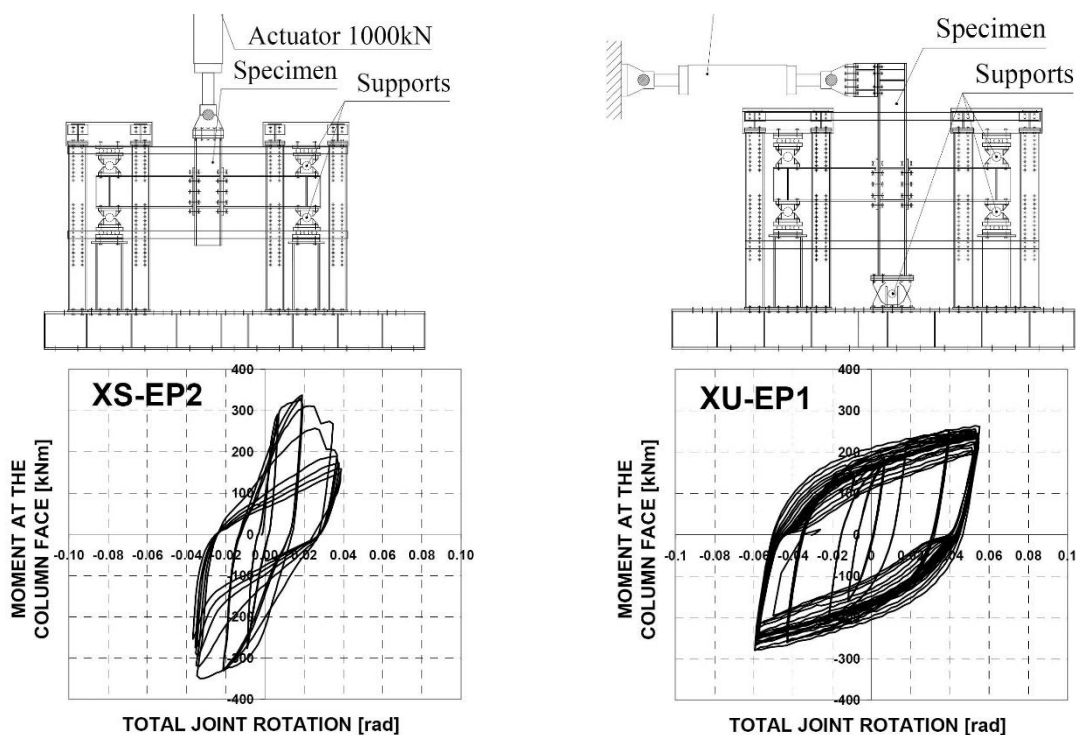


Figure 2.8: Teste setup and moment-rotation response for the XS and XU end-plate joints (Dubina *et al.*, 2000).

The main conclusions were that the loading type (symmetrical and anti-symmetrical) significantly affected the connection response, where the column panel zone was the component that differentiated their behaviour. Unbalanced moments affect the column panel zone by reducing the stiffness and strength of the connection. A joint classified as rigid and full-strength in a symmetrical loading case can be classified as semi-rigid and partial-strength in an anti-symmetrical loading case. In the comparison with Annex J of EC3, similar values were found for the XS series for the plastic moments. On the other hand for the XU series, all experimental values were lower than the ones computed with the Annex J of EC3-1-1. For what concerns the initial stiffness, numerical and experimental results agreed for the XU series, but were very different for the XS series. In general, bolted end-plate connections showed good rotation capacity and more ductile behaviour when compared to welded connections, but with a reduced initial stiffness. The plastic rotation of the XU series showed to be higher than the values generally accepted by codes (30%). Furthermore the conclusions revealed the importance of a

proper welding procedure and design. The use of X-shaped columns increases the stiffness and moment resistance for the anti-symmetrical loading when compared to the usual I and H shaped columns.

The work developed by Guo *et al.* (2006) on the cyclic behaviour of stiffened and unstiffened extended end-plate connections of beam-to-column joints, investigated the influence on the hysteretic behaviour, stiffness and strength when the transverse web stiffeners of the column web and the rib stiffeners of the end-plate are considered. During the tests the column was under uniform axial load, and the joint was subjected to cyclic load using the yield displacement, recorded, as incrementation measure, until the failure criteria were reached. For the same beam-to-column configuration, along with the end-plate thickness variation, several stiffeners, in the column web and in the end-plate were tested. The results allowed concluding that the stiffeners have a remarkable influence, contributing to increase the strength of the joint as well as the energy dissipation capacity. For the thinner end-plates the presence of the stiffeners can actually prevent the brittle fracture of connections. The tests results also allowed to conclude that the use of stiffeners is more effective than the increase of the end-plate and column web thicknesses, to improve the stiffness and strength of the joint.

The work developed by Nogueiro (2009) presented a set of 13 tests performed on external beam-to-column extended end-plate joints under monotonic and cyclic loads. The aim of the research was to characterise the behaviour of the connections under cyclic loading and the numerical implementation of a mathematical model capable of simulating real connections behaviour. These tests results are used later on in this thesis to validate the numerical models developed in this research, and therefore a detailed review of the experimental tests is undertaken in Chapter 3.

The work by Elnashai and Elghazouli (1994) on the dynamic behaviour of frames with semi-rigid / partial-strength joints, subjected to seismic loading, concluded that the frame behaviour exhibited a ductile and stable response, confirming the improved behaviour of semi-rigid frames in seismic regions. Five monotonic, cyclic and pseudo-dynamic tests were carried out. Half of two-storey single-bay frame, with top and seat angle plus double web angle joints, was tested, for the pseudo-dynamic tests additional masses were considered at both stories. It is also concluded that, in many cases, the response of the frames with semi-rigid joints is superior to frames with rigid joints, provided that stable hysteretic behaviour is ensured. Shen and Astaneh-Asl (1999) and Yang and Kim (2007b; 2007a) worked on the same type of top and

seat joints, aiming at investigate their hysteretic behaviour, failure modes, energy dissipation and in the case of the later studies it was also intended to performed comparisons with their fully welded counterpart. The results revealed that the test specimens demonstrated stable cyclic response and reliable energy dissipation capacity. The comparisons with the fully welded joints revealed that the permanent deformation of the column in the bolted joints was undetected unlike the deformation of the column of the welded joints that was seriously deformed. Although the initial stiffness and capacity were smaller in the bolted joints, they reached higher ductility levels and overstrength factors.

The work developed by Iannone *et al.* (2011) in the ultimate behaviour of bolted beam-to-column partial-strength joints under cyclic loading, aiming at extending the component method to cyclic loading, gave an important contribution to the subject. The study comprised three joint typologies, two partial-strength extended end-plate joints, whose geometry is presented in Figure 2.9, one full-strength extended end-plate joint with a dog-bone in the beam and a partial-strength joint using a couple of T-stubs bolted to the beam and column flanges. This work allowed the authors to conclude that the overall energy dissipation of the joint can be obtained by the sum of the energy dissipation capacity of the single joint components. Thus allowing to state that the extension of the component approach, codified in the EC3-1-8 (EN 1993-1-8, 2005), could be practically applied to cyclic loaded joints, if the dissipative components were properly identified and properly modelled.

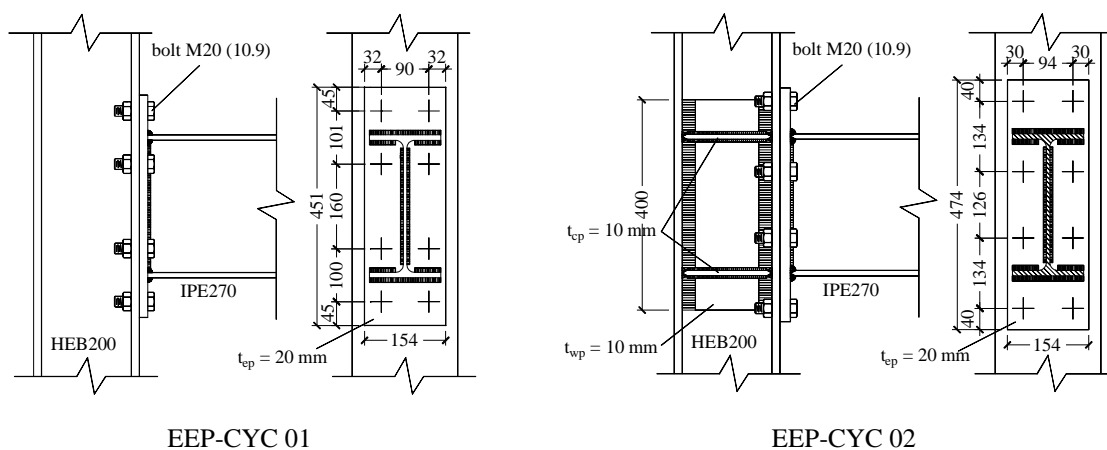


Figure 2.9: Extended- end-plate joints tested (Iannone *et al.*, 2011).

EEP-CYC 01 was a partial-strength joint governed by the column web panel zone, and the EEP-CYC 02 was a partial-strength joint governed by the end-plate in bending. All specimens tested were constituted by and HEB200 in the column (S355) and an IPE270 in the

beam (S275). The response of the two partial-strength joints with end-plate connections is depicted in Figure 2.10. The isolated response of the dissipative components is depicted in the Figure 2.11 for the joint EEP-CYC 01 and in the Figure 2.12 for the joint EEP-CYC 02. The failure of the unstiffened joint was the brittle failure of the welds, and for the stiffened joint was the fracture of the end-plate.

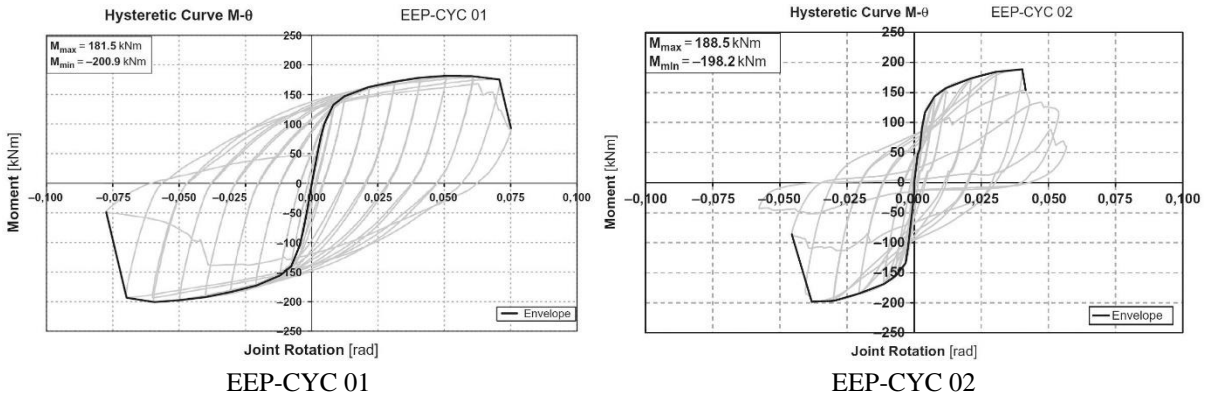


Figure 2.10: Cyclic response of the partial-strength extended end-plate joints tested (Iannone *et al.*, 2011).

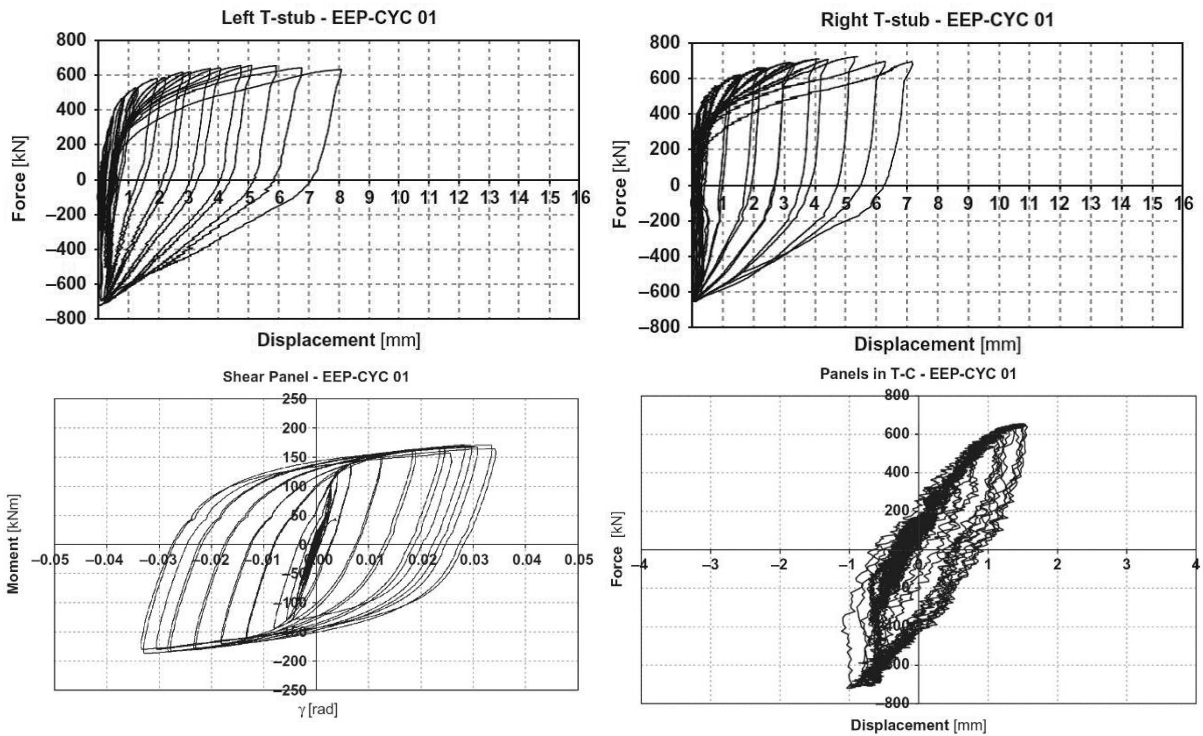


Figure 2.11: Isolated response of the dissipative components for the EEP-CYC 01 (Iannone *et al.*, 2011).

The hysteretic behaviour of the components in the joint EEP-CYC 01 revealed that the energy dissipation was governed by the column web panel in shear, as expected, although a lower contributions of the component end-plate in bending was also observed, with a behaviour

closer to type-1 mechanism (EN 1993-1-8, 2005). The contribution of the components column web in transverse tension or compression was practically negligible. In the case of the joint EEP-CYC 02, due to the presence of the column web stiffeners the column web components does not provide a significant energy dissipation. The only component in the energy dissipation is, as expected, the end-plate in bending, presenting a collapse mechanism of the type-1, imposing some degree of pinching in the global response. The energy dissipated by this joint was quite limited when compared with the EEP-CYC 01. It is also important to refer that the flexural strength and plastic rotation, measured, had a good agreement with the predictions during the design of the joints.

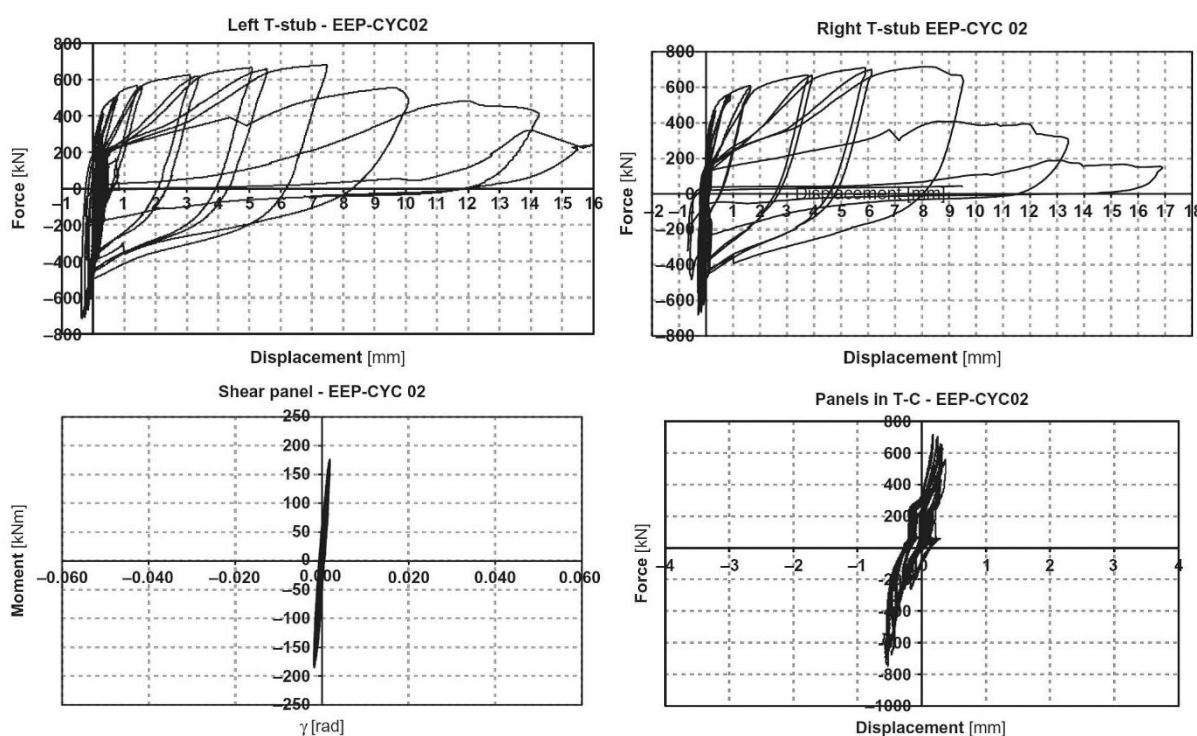


Figure 2.12: Isolated response of the dissipative components for the EEP-CYC 02 (Iannone *et al.*, 2011).

A research group at the University of Salerno has been developing studies on the cyclic characterization of beam-to-column joints (Latour, and Rizzano, 2015), working with traditional and innovative joints configurations, including free from damage ones (Latour, *et al.*, 2015). They have further developed the concept and implementing them in full scale frames (Francavilla *et al.*, 2015).

A detailed review of the experimental work on steel joints subjected to cyclic loading can be found in Sullivan and O'Reilly (2014).

2.2.1.3 REVIEW OF PAST ANALYTICAL WORK

Extensive experimental research work has been conducted, over the years, seeking the characterization of the behaviour of steel joints. The results of the research studies allowed the development of empirical models, relating the parameters found in the response to the geometrical and mechanical properties of the joints. They allowed also the validation of mechanical models based on rigid and flexible components, the Component Model, which is able to predict the joints behaviour main features and allows for the extension of the experimental results to a wider range of joints and applications.

There are several examples of models available in the literature that are proposed based on experimental results. Frye and Morris (1975) is one of the first empirical models known in which the representation of the $M-\theta$ rotation curve is obtained by an odd-power polynomial function, where the rotation depends on parameters that are defined by the geometrical and mechanical properties of the structural details and also relies on curve-fitting constants. Ten years later, Azizinamini *et al.* (1985) improved the model to tackle the undesirable problem of having a negative $M-\theta$ slope. Other research work followed, such as that by Krishnamurthy (1978), Kukreti *et al.* (1987) and Faella *et al.* (1997). The last used the same component based approach of that implemented in Eurocode 3 (EN 1993-1-8, 2005) to develop a mechanical model capable of obtaining the data for reliable regression analyses for all the parameters affecting the joint rotation behaviour requiring less computational effort. Also, the work of Jaspart (1991) on the mechanical models based on the components approach should be pointed out, contributing significantly to the development of the Eurocode 3 (EN 1993-1-8, 2005) methodology for the characterisation of joint behaviour and the strength, stiffness and rotation capacity design. More recent models have been proposed over the years, such as the Flejou and Colson (1992) model. It followed a different approach to characterise the behaviour of several joint typologies and materials, associating to each type of joint the phenomena involved in the constitutive material, like the kinematic hardening for steel and the damage for concrete and timber, using then a multi-surface model to activate each one of the phenomena. Furthermore, with that model it is possible to simulate the joint cyclic behaviour. More recently, Del Salvio *et al.* (2009) proposed a component-based mechanical model for semi-rigid beam-to-column connections that combines the effect of axial force and bending moment by assuming a tri-linear characterisation of the joint response.

The extensive experimental research work summarized in the previous section led to the development of several approaches to establish, and ultimately to predict, the behaviour of steel joints under cyclic loading.

Many authors proposed mathematical models (bilinear hysteretic, Ramberg-Osgood based models, Richard-Abbott based models or multi-linear deterioration models) to fit the global moment-rotation curves of steel joints. Ramberg and Osgood (1943) model, consist of mathematical relations that express strain (generalised displacement) as a nonlinear function of stress (generalised force). A valid alternative is the Richard and Abbott (1975) model that relates the generalised force (stress) with generalised displacement (strain). As demonstrated by Nogueiro *et al.* (2007) these two mathematical models have provided the basis for most of the models that have been proposed in the literature, like the Mazzolani (1988) comprehensive model, based on the Ramberg-Osgood expressions, but allowing for pinching effects and later modified further by Simões *et al.* (2001) to allow for pinching in the unloading zone. Based on the Richard-Abbott expressions, Della Corte *et al.* (2000) also proposed a model that was able to simulate the pinching effect. Ramberg-Osgood expressions present the disadvantage of expressing strain as a function of stress which, in the context of finite element analysis, clearly complicates the integration in displacement-based, or for the calibration of tests results generally carried out under displacement-control once they reach the nonlinear stage. Several other relevant mathematical models can be pointed out like Clough and Johnston (1966), Popov and Pinkney (1968), De Martino *et al.* (1984), Della Corte *et al.* (2002), Ibarra *et al.* (2005), Lignos and Krawinkler (2011).

Bernuzzi *et al.* (Bernuzzi, 1992; Bernuzzi *et al.*, 1996) developed a mathematical model that relates the stiffness values for several $M-\theta$ branches to the energy dissipation, while Bursi and Galvani (1997) relates the strength obtained in the monotonic tests to the degradation and pinching of the cyclic ones and both are based on experimental evidence.

Kukreti and Abolmaali (1999) proposed an analytical model to predict the moment-rotation hysteretic response, including the initial stiffness, ultimate moment capacity, ultimate rotation of the top and seat angles connections. More recently, based on mechanical-based models for the prediction of the initial stiffness and moment resistance of steel joints subject to static monotonic loading, these models were calibrated to obtain relevant cyclic parameters such as stiffness, strength degradation and pinching, whenever relevant. An example is the

model proposed by Sivaselvan and Reinhorn (2000), which is able to take into account the stiffness and strength degradation of the joint, derived from inelastic material behaviour, as well the pinching phenomenon. A drawback of the model is that it does not include a negative backbone tangent stiffness. Song and Pincheira (2000) developed a model capable of representing the cyclic strength and stiffness deterioration based on the dissipated hysteretic energy. That same model is also able to account for pinching based on deterioration parameters. The backbone curve includes a post-capping negative tangent stiffness and a residual strength branch. Ibarra *et al.* (2005) proposed a model that based on a backbone curve capable of representing the cyclic deterioration of strength and stiffness, bilinear, peak-oriented and pinched hysteretic systems, with four modes of deterioration. Della Corte *et al.* (2000; 2002) extended the Richard-Abbott model to cyclic behaviour, based on several parameters that should be defined according to experimental and numerical results. The model is also able to take into account the strength and stiffness degradation as well as pinching effects. Subsequently, Nogueiro *et al.* (2007; 2009) simulated the cyclic behaviour of steel joints based on the improved version of the Richard-Abbott expression proposed by Della Corte *et al.* (2000).

In addition to the mathematical formulations described above, some authors focussed on establishing empirical damage accumulation laws to assess the low-cycle fatigue behaviour of steel joints. Calado and Castiglioni (1996) developed a cumulative damage model and a general failure criterion to assess the low-cyclic fatigue of steel joints. Bursi *et al.* (2002) studied the fracture behaviour of isolated T-stub connections with partial fillet welds, and characterized cracks for the low-cyclic fatigue assessment of isolated T-Stubs of steel joints. Deng *et al.* (2000) worked on a finite element formulation of a non-linear element that takes into account both stiffness and strength degradation and pinching, expressed as a function of damage state variables, using a damage index to detect failure.

There is a growing interest on the implementation of cyclic component models, whereby the global moment-rotation behaviour of the joint is obtained from the cyclic behaviour of the individual components. Mechanical models, such as those developed by Madas and Elnashai (1992), can be considered one of the first attempts to apply the component approach to characterise the cyclic behaviour of beam-to-column joints. Calado and Ferreira (1994) considered the monotonic behaviour of the component to assess the cyclic response. However,

the model does not account for pinching or strength and stiffness degradation. A few years later, Calado (2003) proposed a model for top and seat web angle for steel beam-to-column connections with damage accumulation, considered in the stress-strain relationship of the material, and including also the behaviour of the bolts in cyclic shear, taking into account the slip between the connected elements, although it disregards the ovalisation of the hole and the changes in preloading force. An important issue affecting the connection behaviour is the internal force interaction, namely the axial and bending moment interaction. Simões da Silva *et al.* (2009) proposed an extension to the component method for the cyclic behaviour of end-plate joints. Latour *et al.* (2011) proposed a simplified cyclic model based on a lumped approach for the tensile and compressive zones, considering that the overall energy dissipation of the connection can be obtained by summing the energies dissipated by the various joint components. Using the insights gained in this research, Latour and Rizzano (2013) extended the proposed model to column base-plate joints using a component-based approach to predict the cyclic behaviour. More recently, Simões da Silva *et al.* (2016) detailed a cyclic component model fully compatible with the static monotonic implementation in EC3-1-8 (EN 1993-1-8, 2005).

2.2.1.4 REVIEW OF PAST NUMERICAL WORK

Although the prediction of the joint behaviour by analytical procedures is a subject with remarkable advances in the last few decades, and despite a large number of proposed models to predict the moment-rotation relationship of the joints, they present still some limitations. In order to find a generalised procedure able to characterise every type of joints or loading (monotonic, cyclic, dynamic, etc.) the finite element analyses represent a powerful technique that can be used to improve analytical models.

Numerous publications can be found in the literature, which use finite element (FE) models to predict the behaviour of different joint types. Krishnamurthy and Graddy (1976) was the earliest work that used the FE method to predict the behaviour of end-plate connections. Due to the limited computer resources available at the time, there were several limitations in the analyses performed. The authors attempted to correlate the results from an elastic three-dimensional FE analysis to those from an elastic two-dimensional FE analysis. Also in the early use of the FE method to model connections, Kukreti *et al.* (1987) used a similar approach

developing moment-rotation relationships for bolted steel end-plate connections, focusing the research on the prediction of maximum end-plate separation through parametric analyses covering the various geometric and force related variable found in practical ranges. Later, with the development of computational resources and tools, several works have been conducted in the field of bolted beam-to-column behaviour characterization using 3D FE models. This improvement was well accepted due to the proved inadequacy of the 2D displacement-based FE models to characterise the behaviour of bolted joints, which were known to predict stiffer and stronger solutions in comparison with the corresponding 3D models (Bursi and Jaspart, 1997a). Ziomek *et al.* (1992) used 3D models with several types of shell and modelling approaches to simulate the one side extended end-plate experimental tests and to determine the best modelling approaches to be used in the behaviour assessment. The authors concluded mostly what is nowadays taken for granted, namely the influence of the material, mesh refinement, the bolts loading and the influence of nonlinearities on the results. A similar approach was adopted by Sherbourne and Bahaari (1994) using the ANSYS software package to develop 3D shell models trying to overcome the limited ability of the 2D models to deal with thin plates in which yielding occurs due to biaxial bending. The authors aimed to study the distribution and magnitude of the prying forces at the free edge of the end-plate and concluded that the extended end-plate connections can be successfully simulated with complete 3D model up to the ultimate load, and that the model developed was adequate for thin plates but also gave satisfactory results for thick plates. In the same line of research, and using the same techniques, (Sherbourne and Bahaari, 1996; Bahaari and Sherbourne, 1996) they conducted the first study on bolted T-stub connections, and proceeding the studies on complete extended end-plate connections in order to study the stiffness and strength of the joints with unstiffened column flanges. The authors concluded that only a 3D model could satisfactorily predict the interaction between the T-stub and the column flange, since the maximum bending stresses were perpendicular to each other, and that the prying forces in the T-hanger increased with the decrease in relative stiffness of flange to bolt. It was also concluded that the lack of the stiffeners changed the behaviour of the connections in the tensile and compression zones of the column flange. A few years later, Bahaari and Sherbourne (2000) used the same modelling approach and conducted a study on eight-bolt extended end-plate connections to analyse the large capacity of this solution, in terms of stiffness and strength, when no stiffeners in either tension or compression region were used in the column. Later, Maggi *et al.* (2003; 2005) performed

some parametric analyses on the behaviour of bolted extended end-plate connections using FE modelling tools, using solids and beam elements as depicted in Figure 2.13, which were validated by the experimental tests performed. Studying the interaction between the end-plate and bolts, the authors concluded that the T-stub failure mode type 2 presented levels of interaction between the end-plate and bolts that is difficult to predict accurately. It was also found that there are some limitations in the T-stub analogy for the yield lines representation at the end-plate, leading to limitations both in accounting for prying action and in predicting values for strength and stiffness of the connection.

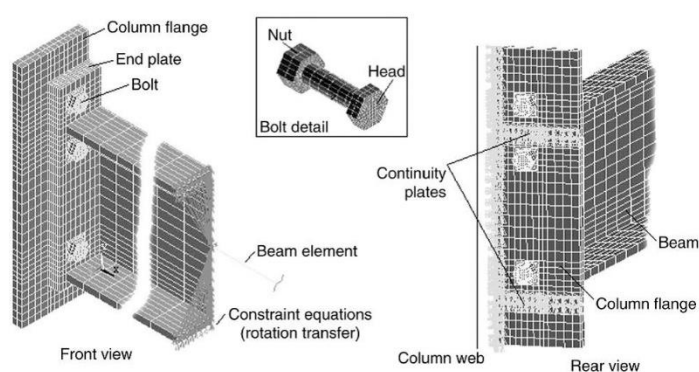


Figure 2.13: General view of the FE models (Maggi *et al.*, 2005).

Shi *et al.* (2008) also studied the end-plate joints loaded monotonically with the development of a FE model to simulate the mechanical behaviour of different types of beam-to-column joints with pre-tensioned bolts. With the intention of providing a basis for developing mechanical models consistent with the Eurocode component method, since FE results can give additional valuable data for the joint's behaviour which are difficult to measure in experimental tests. For instance the distribution of pressure caused by bolt pretension, the friction between the end-plate and the column flange and the principal stress flow in the connection. Recently, Tartaglia *et al.* (2015) studied the influence of rib stiffeners in bolted extended end-plate beam-to-column joints, and also the influence of the bolt row located in the symmetry axis of the connection. The study comprised a parametric numerical analysis based on FE models of the joints. The conclusions revealed that the thickness of the rib stiffeners influences the beam ductility, and that the bolt row located at the symmetry axis does not affect the global behaviour of the joint in terms of both stiffness and strength. Dealing also with rib stiffeners, Pirmoz *et al.* (2016) studied the applicability of extended stiffened end-plate joints, with ribs, in eccentrically braced frames acting as link-to-column connections, with long flexural yielding,

using FE models of the joints, demonstrating that they are a good alternative to other connections typologies currently used, e.g. welded, achieving the required rotations. Also in the stiffened end-plate joints field Shi and Chen (2017) proposed a new component, referred to as cruciform, to deal with ultra-large capacity end-plate joints, based on the component method specified in the EC3-1-8 (EN 1993-1-8, 2005) to determine the moment resistance and rotational stiffness of the joint.

In the field of composite end-plate joints, the work of Ahmed *et al.* (1996) can be pointed out. They use the ABAQUS software package to simulate semi-rigid composite connections, aiming to develop a FE model that realistically represents all aspects of the physical behaviour of composite end-plate connections, observed in tests, and examine the effects of varying the reinforcement ratio and the shear interaction.

The achievements in FE modelling and analyses by Bursi and Jaspart (1997a; 1997b; 1998) in the field of end-plate joints and T-stub component behaviour assessment should also be pointed out. Trying to deal with and overcome the complex nonlinear phenomena, which are commonly observed in the FE joint models, and study the best ways to improve the degree of accuracy of the FE models, using their simulations as benchmarks in the validation process of FE software packages.

Regarding the field of beam-to-column top and seat-angle connections, Kishi *et al.* (2001) and Komuro *et al.* (2004) modelled FE connections using different technics aiming to find the one that best estimates $M-\theta$ relationship. Furthermore, a three-parameter power model was also used based on the Richard and Abbott's power function (Richard and Abbott, 1975), to compare the nonlinear $M-\theta$ curves. They concluded that the three-parameter power model and the FE model can be used as an efficient and reasonably accurate prediction of the joints behaviour, but with considerable differences at the computing time. In the same field of work, Pirmoz *et al.* (2008; Pirmoz and Mohammadrezapour, 2008; 2009) studied the effect of the web angle dimensions on moment-rotation behaviour of bolted top and seat angle connections. Studying also the connections behaviour under combined axial and tension force, it was concluded that the axial tension load reduces the initial connection stiffness and moment capacity. A tri-linear semi-analytical method was proposed to estimate the connection response under combined tension and monotonic moment loading demonstrating sufficient accuracy, especially for relatively low levels of axial tension loads. In the same research group, Danesh *et al.* (2007)

studied the moment–rotation behaviour of bolted top and seat angles with double web angle connections under the combination of shear force and bending moment. They concluded that connections with low shear capacity of their web angles are more sensitive to shear force and have a large value for the initial stiffness reduction factor.

In another typology of joints, which are not so common in European countries is the half laminated H sections, T-stubs were used to connect the flanges of the beam, by fillet weld, and the column, using four columns of bolts. Takhirov and Popov (2002) studied, by means of FE analysis, a specimen with rectangular-shaped stems. Using this, a solid element analysis of the T-stub under tension in the stem was performed and a shell element modelling with buckling and instability analysis.

In the field of cyclic loading simulations, far less work can be found in the literature. For example, Nemati *et al.* (2000) presented a methodology based on FE techniques with a combination of several other methods to extend the component-based design philosophy of EC3-1-8 (EN 1993-1-8, 2005) to the cyclic behaviour of end-plate connections. In that study, monotonic and cyclic loaded models of T-stubs were performed following the geometry of the experimental tests and comparing their results. Following that, a mathematical energy balance model was proposed by approximating the nonlinear response by six lines representing the slopes of the unloading and reloading branches. By using the FE curves, it was possible to find the common points in the hysteresis and use the energy balance method again. To extend the model to a mechanical model for the end-plate connection, the connection was divided into independent T-stubs, which can be replaced by a spring with the constitutive law of the mathematical energy balance model, adopted for the isolated T-stub. Also in the field of T-stubs behaviour assessment, Bursi *et al.* (2002) presented some work based on numerical analysis of the low-cycle fracture behaviour of T-stubs with partial fillet welds, which attempted to assess the seismic performance of bolted partial strength beam-to-column joints under seismic loading. Several FE models were undertaken in order to tune model material parameters connections in FE models, see Figure 2.14, because the cyclic response was much more difficult to model than the monotonic one due to the nonlinear hardening behaviour involved. In this case, the combined nonlinear isotropic/kinematic hardening model available in the ABAQUS code was used. This model was proposed by Lemaitre and Chaboche (1990) and relies on small

deformations and associate flow rule, this model will be discussed in more detail later in this chapter.

Lastly, a parametric study was conducted in order to define details able to reduce loading-induced toughness demands, namely the effects of the weld-to-base metal yield strength ratio, the residual stress influence and the end-plate yield-to-ultimate strength ratio. The conclusions showed that the overall behaviour of the specimens was governed by the material provided with the lowest strength, which is the base metal, in which yielding occurs effectively. Bravo and Herrera (2014) studied built-up T-stubs under cyclic loading to demonstrate that the failure modes and limit states that control the behaviour of built-up T-stubs are the same that control the hot rolled T-stubs behaviour. The twenty specimens were tested and numerically modelled resorting to 3D FE analysis subjected to cyclic loading conditions. The results revealed that the weld has no effect on the response of the built-up T-stubs.

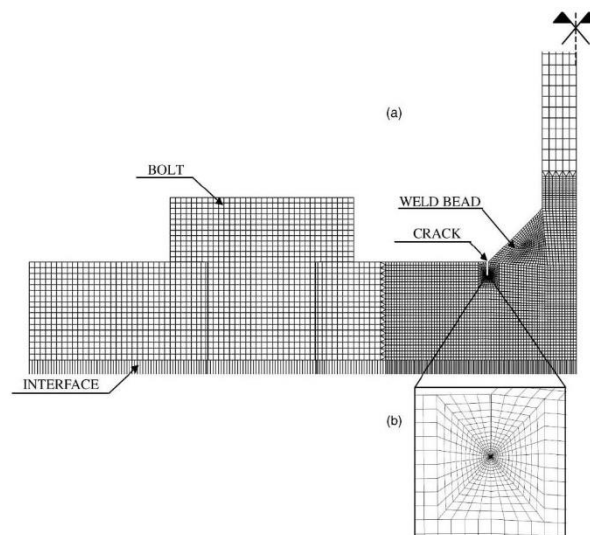


Figure 2.14: 2D FE models of isolated T-stub connections (Bursi *et al.*, 2002).

Ádány and Dunai (2004) presented some work in the field of FE modelling and analysis of end-plate joints in steel frames under monotonic and cyclic loading conditions which tried to deal with the main features involved in the joints modelling and validation, such as the applicable material models or the nonlinear solution algorithms. The main conclusion was that the models cannot be tested in a single step but instead, a multi-step verification is recommended, presenting a step-by-step checking procedure for the cyclic models and computational methods. Gerami *et al.* (2011) conducted a series of FE simulations using the experimental tests of Sumner and Murray (2002), which looked at end-plate and rectangular-

shaped T-stub connections to compare the cyclic behaviour of fourteen specimens by changing the horizontal and vertical arrangement of bolts. It was intended to study the cyclic behaviour influence when the parameters used in the design of bolted connections suffer undesirable changes such as the imperfections in construction. The objective of this study was to help the designers to choose appropriate connections according to the construction conditions. The results revealed that moment capacity and rotational stiffness of T-stubs bolted connections are higher than that of end-plate bolted connections, considering the total energy dissipation of both groups to be approximately the same. It was also concluded that under cyclic loading the probability of failure mode change is higher in T-stub connections than that of the end-plate ones, due to the arrangement variation of bolts; as such end-plate connections are suggested for conditions where the imperfections in construction are probable. Recently D'Aniello *et al.* (2017) studied the design rules and analytical models, present in Eurocodes 3 and 8 (EN 1993-1-8, 2005; EN 1998-1, 2004) of bolted extended stiffened end-plate beam-to-column joints, supported by a parametric study with detailed FE simulations of the joints. The authors proposed new design criteria for seismic resistant extended end-plate joints with ribs. A capacity design procedure was also proposed to control the joint response for different performance levels. A new ductility criterion was presented to avoid brittle behaviour of the joints. The same authors also concluded that the end-plate rib stiffener significantly contributes to the joint strength and stiffness, and that the presence of this stiffener changes the location of the centre of compression, increasing the lower arm of the joint. The lower position of the centre of compression is beneficial to the design of the column web panel, due to the lower design shear forces.

From the review presented above it can be concluded that much work still needs to be performed in the field of the assessment of joints behaviour when subjected to cyclic loadings, although the recent advances in this field have greatly improved the state of knowledge.

2.2.2 ANALYSIS OF BEAM-TO-COLUMN JOINTS BY ANALYTICAL METHODS

2.2.2.1 END-PLATE BOLTED JOINTS DEFINITIONS

The prediction of the behaviour for end-plate bolted connections is available, in the current version of the EC3-1-8 (EN 1993-1-8, 2005), in a component based approach. This type

of connection, whose geometry is illustrated in Figure 2.15, is used to transfer the internal forces from the beam to the column, like the axial forces, bending moments and shear forces, providing normally a semi-continuous solution. The connection is composed of an end-plate welded to the beam ends, and bolted to the column flange, using the pre-drilled holes in the plate and flange. Normally, high strength bolts are used in this type of connection, because it is expected to transmit some degree of bending moments from the beam to the column, and these are usually pre-stressed, to avoid undesirable movements due to the bolts holes clearances. It is also common to add stiffeners to the joint in order to improve their stiffness and/or strength, examples include the transverse stiffeners (*f*) or the supplementary web plates (*h*), used to improve the column web behaviour.

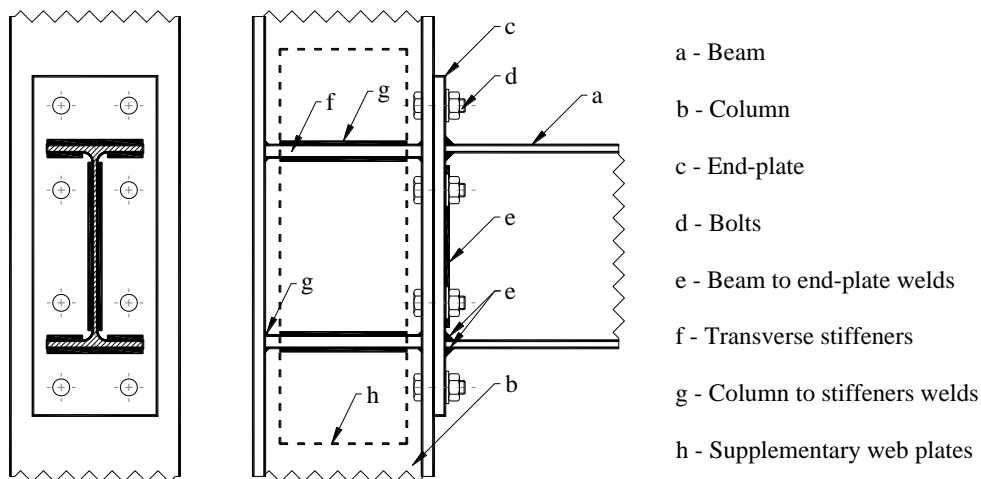


Figure 2.15: Typical beam-to-column double-extended end-plate bolted connection.

The mechanical behaviour of these joints, when subjected to axial forces, shear forces and bending moment is simple, and the assumed stress flow is schematically represented in Figure 2.16. The axial forces are transferred directly by the bolts in case of tension, or in case of compression directly by the contact between the end-plate and the connected column flange. Shear is normally transferred by friction caused by the pre-tightening of the bolts, or if the bolts do not have a controlled grip, the shear is transferred directly by the contact of the bolts shank to the edges of the bolts holes. Normally, the design option is to choose the bolts in the compression zone, to resist shear forces, this way the friction is not affected by the tension, which can reduce resistant force due to friction. In the case of bending moment, a part of the connection will be in compression and the other part in tension. In the compression part, normally aligned with the compressed beam flange, the contact between the end-plate and the

column flange ensures the transfer of effort. In the tension part the effort is transferred from the beam to the end-plate by the welds (e), and through the bolts (d) from the end-plate to the column flange.

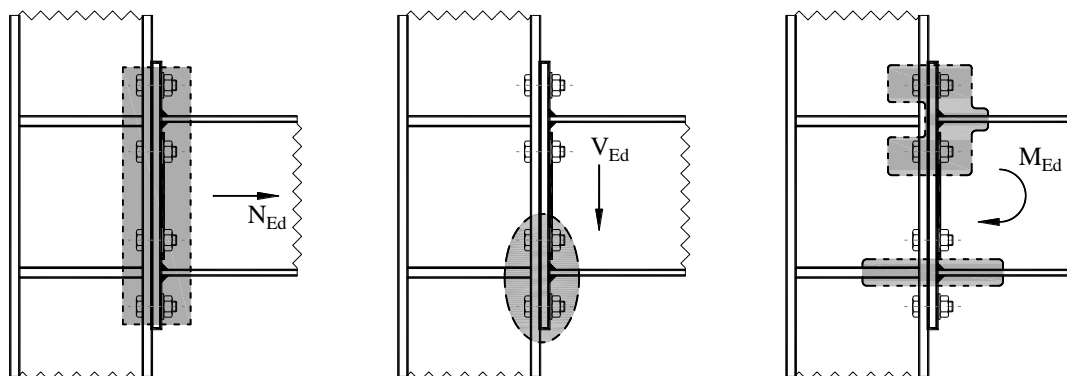


Figure 2.16: Stress flow under axial forces (in tension), shear and hogging bending moment.

The deformability of beam-to-column joints was subject of several studies and publications, e.g. Girão Coelho (2004), Jaspert and Weynand (2016), etc., and, currently, is quite consensual the sources of deformability that contribute to the joint rotation. Beam-to-column joints can be divided in two zones: panel zone and connection zone, identified in Figure 2.17. The connection zone can be one or more, according to the beams connected to the column in the node. The joint deformability results from the contribution of the panel zone and from the connection. The deformation of the connection includes the deformation of the connection elements (bolts, column flange, end-plate, etc.) and the load-introduction deformation of the column web, resulting from the transverse forces F_b acting on the column web. The couple of F_b forces are statically equivalent to the moment M_b at the beam end. The connection rotation ϕ_c is determined by the relative rotation between the beam and the column axes. The other source of deformability is the shear deformation of the column web panel associated to the shear forces V_{wp} , leading to a relative rotation γ_{wp} between the beam and the column axes. In terms of modelling, in current design practice, this separation is normally difficult to accomplish. To overcome this difficulty EC3-1-8 (EN 1993-1-8, 2005) simplified the problem using a transformation parameter β . First the V_{wp} - γ_{wp} curve is transformed into an M_b - γ_{wp} curve using the transformation parameter. This parameter relates the web panel shear force to the (load-introduction) transverse compression and tensile forces. The global joint behaviour is obtained by summing the contributions of the connection rotation (ϕ_c) and from

the shear panel (γ_{wp}), and the response curve is given by $M_j - \phi_j = M_b - \phi_c + M_b - \gamma_{wp}$ Jaspart and Weynand (2016, chap.2), located at beam-to-column interaction. The shear force in the web panel is defined by Eq. (2.1), where V_{c1} and V_{c2} are design shear forces installed in the column at bottom and top of the joint, respectively, and z is the level arm of the internal forces. For a welded connection z is the distance between the beam flanges centre lines and for bolted end-plate connections z will depend on the bolt rows location and on the location of the centre of compression. Because the transformation parameter β relates the web panel shear force V_{wp} with the internal actions, its accurate determination requires an iterative process in the global frame analysis. Conservative values for β , neglecting the effect of shear force in the column, are suggested in EC3-1-8 (EN 1993-1-8, 2005) in *Table 5.4*, e.g. $\beta = 1$ for single-sided joints.

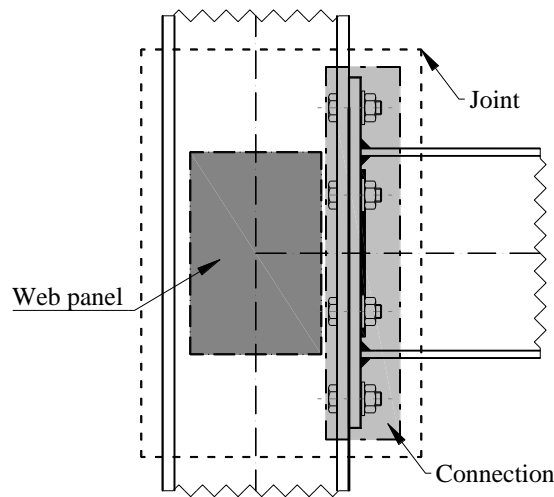


Figure 2.17: Division of a beam-to-column joint into zones (single-sided configuration).

$$V_{wp} = \frac{M_b}{z} \left[1 + \frac{z}{2M_b} (V_{c1} + V_{c2}) \right] = \frac{M_b}{z} \beta \quad (2.1)$$

2.2.2.2 OVERVIEW OF THE COMPONENT METHOD

The component method is a mechanical procedure to estimate global joint response using the properties of its individual basic components. Basic components are equivalent simple parts of the joint that can be translated by their isolated response, i.e. strength and stiffness either in tension, compression or shear. This procedure has become the most consensual analytical approach to evaluate the mechanical properties of steel and composite joints, in part due to its adoption by the Eurocodes. The procedure was firstly developed for steel joints and had its first

developments with the work of Zoetemeijer (Zoetemeijer, 1974) on bolted beam-to-column joints. Several research programs followed the development of this method, e.g. Jaspart (1991), Weynand *et al.* (1996), Jaspart and Vandegans (1998) leading to the implementation of the current European code (EN 1993-1-8, 2005). From a theoretical point of view, this methodology can be applied to any joint configuration and loading conditions provided that the basic components are properly characterized.

The complex behaviour of the joint is normally represented by its response curve ($M-\theta$), generally non-linear. In the component method this response is obtained by the subdivision of the joint into single parts, called components. The components are modeled by means of translational springs with non-linear force-deformation ($F-\Delta$) response, in this way the method deals with forces and deformations instead of stress and strains. The assembly of the several activated components, according to the joints geometry and loading conditions, determines the mechanical behaviour of the joint. That requires to find a statically admissible system to define how the external forces, acting on the joint, distribute into internal forces, acting on the components, in order that satisfies the equilibrium and respects the behaviour of the components. To become a direct method, some simplifications were introduced to the procedure (Weynand *et al.*, 1996) which avoid an iterative assembly, eg. the interdependency between tension and compression in the web panel zone is prevented. The errors introduced with this simplifications have been observed to be acceptable, and the advantages are clear by avoiding an iterative procedure.

At the components level, an accurate characterization of the behaviour is crucial for the performance of the described model. The weakest component in the assembly will govern the response of the joint, a poor characterization of their behaviour can contaminate the all system, an expected ductile behaviour can in turn be a fragile one. The assessment of the $F-\Delta$ curves of the basic components response can be performed through experimental tests, numerical models and / or analytical models.

The procedure, prescribed in EC3-1-8 (EN 1993-1-8, 2005), can be summarized in the following steps:

1. Identify the active components that contribute for the strength and stiffness, the components are described in the *Table 6.1* of the EC3-1-8 (EN 1993-1-8, 2005);

2. Evaluate the mechanical properties / model of each one of the individual components (strength, initial stiffness, rotation capacity or the whole deformability curve);
3. Assembly of the components, and evaluate the connection strength, initial stiffness, rotation capacity or the whole moment-rotation curve;
4. Classification of the joint.

The component method, adopted by EC3-1-8 (EN 1993-1-8, 2005), allows to determine the bending moment resistance ($M_{j,Rd}$), the rotational stiffness (S_j) and the rotation capacity (ϕ_{Cd}), according to the scheme of Figure 2.18 a). The design moment resistance ($M_{j,Rd}$) is equal to the maximum moment of the design moment-rotation characteristic, and is defined by the Eq. (2.2). The rotational stiffness S_j is the secant stiffness, as indicated in Figure 2.18, and is dependent on the design moment $M_{j,Ed}$ until ϕ_{Xd} is reached, i.e. for $M_{j,Ed} = M_{j,Rd}$. S_j is defined by Eq. (2.3). The design rotation capacity ϕ_{Cd} of a joint is equal to the maximum rotation of the design moment-rotation characteristic. Contrary to the other two properties for the deformation capacity, only a qualitative evaluation can be performed where sufficient or insufficient joint rotation capacity may be assumed for a plastic design.

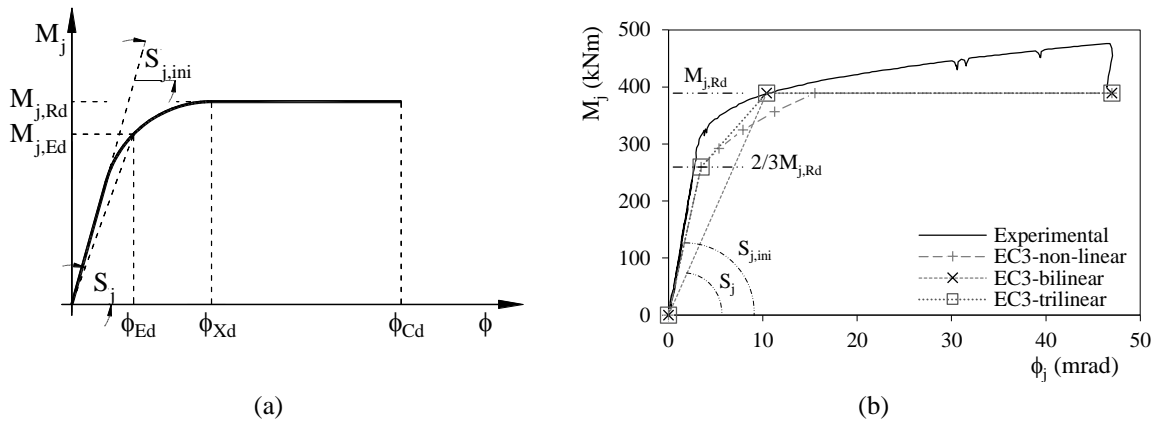


Figure 2.18: a) Design moment-rotation characteristics for a joint (EN 1993-1-8, 2005); b) application of the component method to a beam-to-column end-plate joint.

$$M_{j,Rd} = \sum_r h_r F_{tr,Rd} \quad (2.2)$$

where $F_{tr,Rd}$ is the effective design tension resistance of bolt-row r , h_r is the distance from bolt-row r to the centre of compression and r is the bolt-row number. If the bolt-rows in tension are

more than one, then they are numbered starting from the bolt-row farthest from the centre of compression.

$$S_j = \frac{Ez^2}{\mu \sum_i \frac{1}{k_i}} \quad (2.3)$$

where E is the Young's modulus, k_i is the stiffness coefficient for basic joint component i , z is the lever arm, for two or more bolt rows an equivalent lever arm may be determined, and μ is the stiffness ratio $S_{j,ini}/S_j$, where $S_{j,ini}$ is given by Eq. (2.3) with $\mu = 1.0$. The stiffness ratio μ should be determined from the following:

$$\text{- if } M_{j,Ed} \leq 2/3M_{j,Rd} \rightarrow \mu = 1 \quad (2.4)$$

$$\text{- if } 2/3M_{j,Rd} < M_{j,Ed} \leq M_{j,Rd} \rightarrow \mu = \left(1.5M_{j,Ed} / M_{j,Rd}\right)^\psi \quad (2.5)$$

in which the coefficient ψ is obtained from Table 2.1.

Table 2.1: Value of the coefficient ψ and the stiffness modification coefficient η for beam-to-column joints.

Type of connection	ψ	η
Welded	2.7	2
Bolted end-plate	2.7	2
Bolted angle flange cleats	3.1	2
Base plate connections	2.7	-
Composite (contact plate joint) in (EN 1994-1-1, 2004)	1.7	1.5

The idealized behaviour, obtained by applying the previous methodology to a beam-to-column end-plate joint, is depicted in Figure 2.18 b). Depending on the type of global analysis to be performed in the frame, the behaviour of the joint may be assumed as elastic or plastic. For the elastic analysis, if the design bending moment of the joint ($M_{j,Ed}$) remains under $2/3M_{j,Rd}$, the initial rotational stiffness of the joint ($S_{j,ini}$) may be used. In any other case a modified rotational stiffness ($S_{j,ini}/\eta$) should be consider, the stiffness modification coefficient η is defined in the Table 2.1 for beam-to-column joints. For a plastic analysis, three different approaches may be used: i) bilinear moment-rotation characteristic, where the joint modified rotational stiffness $S_{j,ini}/\eta$ is used for the elastic branch until $M_{j,Rd}$ followed by a plateau; ii) trilinear moment-rotation characteristic, where the initial rotational stiffness $S_{j,ini}$ is used, for the elastic branch until $2/3M_{j,Rd}$ followed by a second line branch up to $M_{j,Rd}$, and finally a plateau; iii) non-linear moment-rotation characteristic, where a linear elastic branch is consider

until $2/3M_{j,Rd}$ is reached, then a non-linear branch is obtained using Eq. (2.3) for several values of $M_{j,Ed}$, followed by a plateau. The three possible representations of the moment-rotation characteristic are depicted in Figure 2.18 b), as well as the moment-rotation response of the joint tested experimentally. It is possible to observe that the method is well adjusted to the actual response of the joint, however the procedure does not take into account the hardening of the steel, and consequently does not captures the increase of strength provided by that hardening in the plastic range.

The assessment of the joints properties, namely stiffness and strength, allows the classification of the joint according to the limits imposed in the code. The stiffness classification is performed by comparing the initial rotational stiffness ($S_{j,ini}$) with two stiffness boundaries, see Figure 2.19 a), where $k_b = 8$ for braced frames and $k_b = 25$ for unbraced frames. The strength classification simply consists in comparing the joint design moment resistance $M_{j,Rd}$ with the design plastic moment resistance of the connected beam ($M_{b,pl,Rd}$) and column ($M_{c,pl,Rd}$), see Figure 2.19 b).

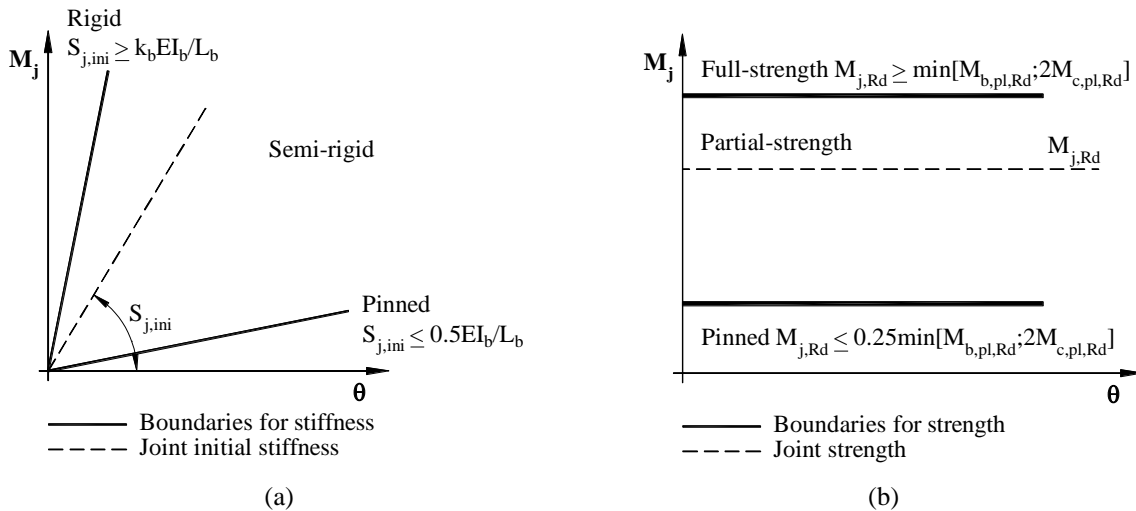


Figure 2.19: a) Stiffness and b) strength classification boundaries.

The field of application is limited at this time to “H” or “I” sections hot-rolled or shop-welded profiles, and the connections typologies that can be design by the procedure are: welded joints; bolted end-plate joints; bolted flange cleat joints; base plate joints; steel-concrete composite joints and joints with beam haunches.

There are twenty components available in Table 6.1 of EC3-1-8 (EN 1993-1-8, 2005), for the particular case of end-plate beam-to-column joint the relevant components are identified in

Table 2.2, according to Figure 2.20 distribution. The mechanical model, with the assembling of the components, is also depicted in the same figure. Note that normally the bolt rows located near to the compressed beam flange are neglected for the components in tension, without losing precision due to their smaller level arm, although in a systematic procedure all rows above the compression flange may be consider for the components in tension.

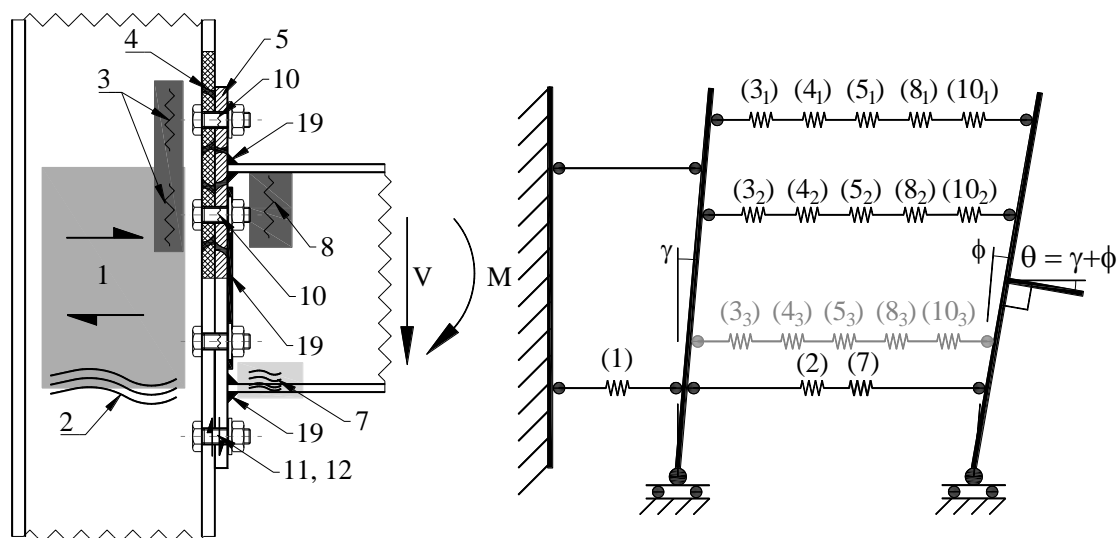


Figure 2.20: Basic components identification and idealized mechanical model of the joint.

Table 2.2: Basic end-plate beam-to-column components.

Type	Ref.	Notation	Component description	Ductility
Tension	3	$F_{t,wc,Rd}$	Column web in transverse tension	Limited
	4	$F_{t,fc,Rd}$	Column flange in bending	High
	5	$F_{t,ep,Rd}$	End-plate in bending	High
	8	$F_{t,wb,Rd}$	Beam web in tension	High
	10	$F_{t,Rd}$	Bolts in tension	Brittle
	19	$F_{w,Rd}$	Welds in tension	Brittle
Horizontal shear	1	$V_{wp,Rd}$	Column web panel in shear	High
Compression	2	$F_{c,wc,Rd}$	Column web in transverse compression	Limited
	7	$F_{c,fb,Rd}$	Beam flange and web in compression	Limited
Vertical shear	11	$F_{v,Rd}$	Bolts in shear (for non-preloaded bolts)	Brittle
	12	$F_{b,Rd}$	Bolts in bearing (column flange, or end-plate for non-preloaded bolts)	-
	19	$F_{w,Rd}$	Welds in shear	Brittle

Assuming that the connection is subjected to bending and the centre of compression is located in the mid-thickness of the beam compression flange, the joint strength is governed by the resistance of the weakest component in tension, for a bolt-row r or for a group of bolt rows, but not greater than the weakest component in horizontal shear or compression.

The evaluation of the design resistance of basic components under tension or compression is defined by the strength capacity of a plate with an effective width (b_{eff}). In the case of column web panel in shear, a detail review is performed in the next section. The evaluation of the design resistance of basic components under bending or subjected to transverse forces is based on equivalent T-stubs: a geometrical idealization of a T profile made of a web in tension and a flange in bending bolted by the flange. This well-known idealization, explained in detail in several publications, e.g. Girão Coelho (2004) or Jaspart and Weynand (2016), is the key for the evaluation of the design plastic strength of those basic components. The T-stub components have three possible collapse mechanisms, represented in Figure 2.21. Failure mode type 1 is characterized by the formation of four plastic hinges, see Eq. (2.6); failure mode type 2 is characterized by the formation of two plastic hinges in the flange-to-web connections and by the failure of the bolts. The increasing prying forces, Q , lead to the bolts fracture before the complete hinge formation in the flange zone near the bolts axis, see Eq. (2.7); failure mode type 3 is characterized by the bolts failure, without prying forces, see Eq. (2.8).

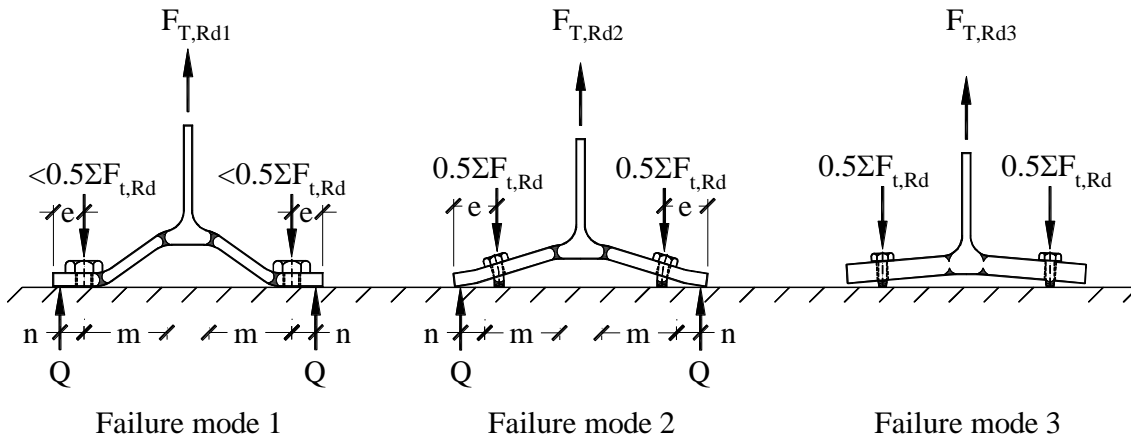


Figure 2.21: Collapse mechanisms for T-stub.

$$F_{T,1,Rd} = \frac{4M_{pl,1,Rd}}{m} \quad (2.6)$$

$$F_{T,2,Rd} = \frac{2M_{pl,2,Rd} + n\Sigma F_{t,Rd}}{m+n} \quad (2.7)$$

$$F_{T,3,Rd} = \Sigma F_{t,Rd} \quad (2.8)$$

The ratio between the flexural strength of the flanges and the axial bolts strength governs the collapse, In Figure 2.22, β is defined by Eq. (2.9) and $\lambda = n/m$, m is the distance between

the bolt axis and the flange-to-web expected location of the plastic hinge and n is the minimum of the distance between the edge of the flange and the bolts axis or $1.25m$, according to Figure 2.21.

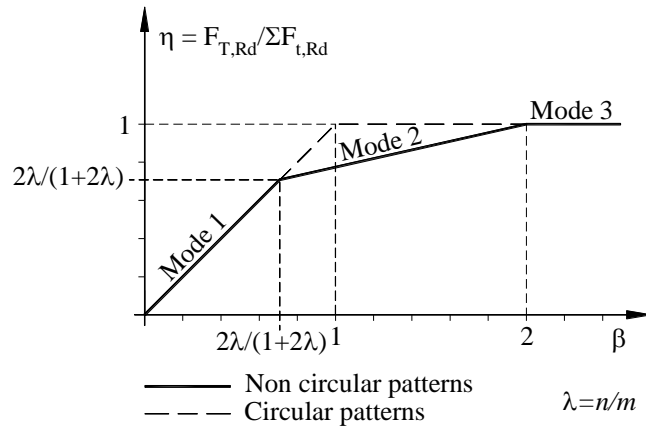


Figure 2.22: Collapse mechanisms.

$$\beta = \frac{4M_{pl,Rd}}{m \sum F_{t,Rd}} = \frac{l_{eff} t^2 f_y / \gamma_{M0}}{m \sum F_{t,Rd}} \quad (2.9)$$

The design resistance of the T-stub is defined by the lower of Eq. (2.10) and Eq. (2.11):

$$F_{T,Rd,nc} = \min(F_{t,Rd,1}; F_{t,Rd,2}; F_{t,Rd,3}) \text{ for non-circular patterns} \quad (2.10)$$

$$F_{T,Rd,cp} = \min(F_{t,Rd,1}; F_{t,Rd,3}) \text{ for circular patterns} \quad (2.11)$$

The initial stiffness of each basic components is evaluated using the formulations in *Table 6.11* of EC3-1-8 (EN 1993-1-8, 2005).

Besides the simplified force-displacement ($F-\Delta$) relation, defined by the design resistance and the initial stiffness of each basic component, a more realistic characterization of their behaviour can be achieved. This relation can be translated by non-linear behaviour or simplified for a bi-linear approximation, characterized by an initial stiffness, yielding limit, post-limit stiffness and a collapse displacement, as depicted in Figure 2.23, although the information regarding of this last parameter cannot be quantified for most of the components in the current version of the EC3-1-8.

As identified by Kuhlmann *et al.* (1998), each one of the basic components in Table 2.2 can fall in one of the three ductility classes, illustrated in Figure 2.23: Components with high ductility, components with limited ductility and components with brittle failure. Following this

classification Simões da Silva *et al.* (2002) proposed a ductility index φ_i (that relates the failure displacement with the yield displacement) for each one of the components, according to the following ductility limits: i) components with high ductility $\varphi_i \geq 20$; ii) components with limited ductility $3 \leq \varphi_i < 20$; iii) components with brittle behaviour $\varphi_i < 3$.

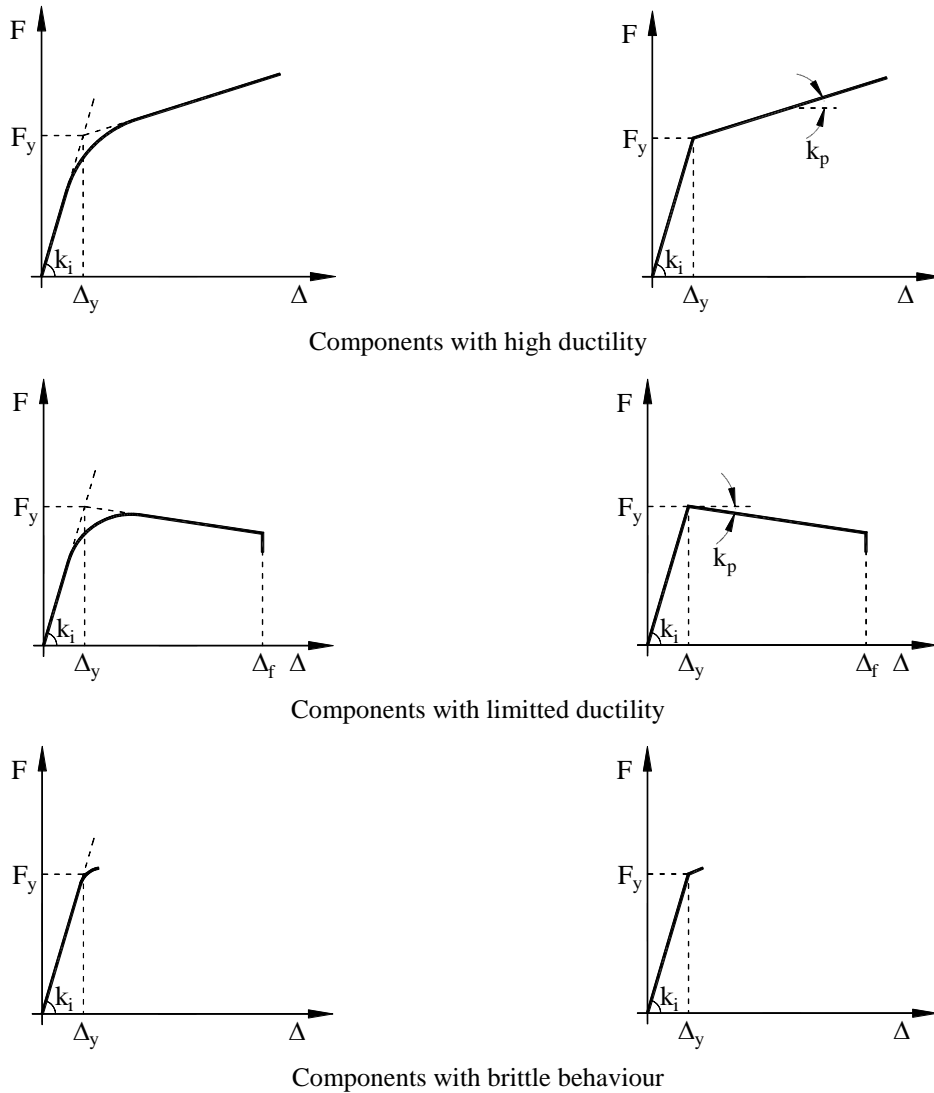


Figure 2.23: Force-displacement curves of components of different ductility classes. Non-linear behaviour and bi-linear approximation (Simões da Silva *et al.*, 2002).

Recently, Francavilla *et al.* (2016) proposed a new theoretical model for predicting the global behaviour of bolted T-stubs under monotonic loading conditions up to failure. The comparisons with experimental results revealed a good accuracy of the proposed model.

2.2.2.3 COLUMN WEB PANEL BEHAVIOUR

In many situations, the column web panel controls the behaviour of the joint. Especially under cyclic loading conditions, the column web panel provides large energy dissipation. In this thesis special attention is paid to deriving the components associated with the column web in double extended bolted end-plate joints. Thus, a review is performed in the following sections, focusing on the most relevant studies on the column web panel behaviour.

Figure 2.24 illustrates the contributions to the deformation of the column web panel resulting from the combined effect of tensile and compressive forces generated by the bending moment in the beam. The load-introduction and shear effects are identified in Figure 2.24; they require appropriate characterization of the components behaviour, which are associated to the column web in tension, column web in compression and the column web in shear.

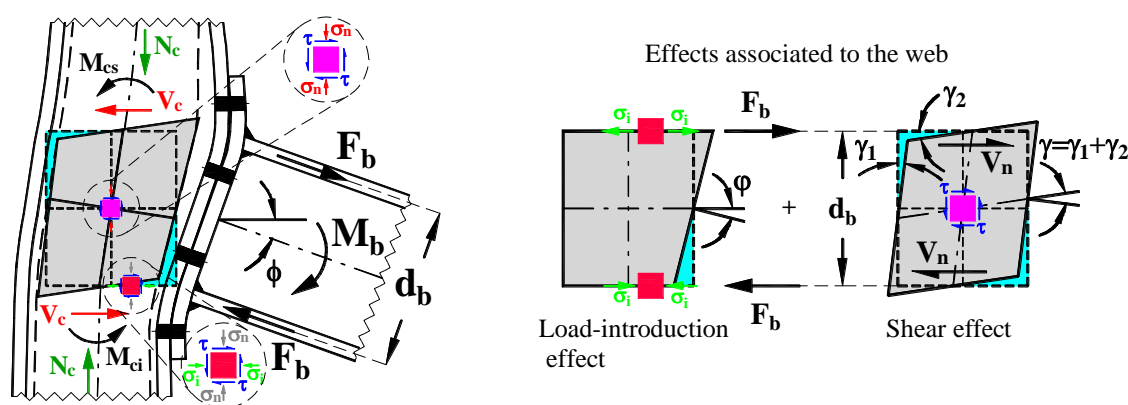


Figure 2.24: Behaviour of the unstiffened column web panel in an external node end-plate connections.

The characterization of the column web panel was the subject of relevant research work conducted by Krawinkler and his co-workers (Krawinkler *et al.*, 1975) who studied the column web behaviour, mainly subjected to shear, using experimental tests on welded joints stiffened with continuity plates. They concluded about the significant post-yielding resistance, due to the strain hardening and the bending contribution of the boundary elements composed by the column flanges and the transverse stiffeners, and proposed a trilinear model for the shear force versus distortion of the panel zone. The relevant features of the model are illustrated in Figure 2.25 and the formulation is summarized in Table 2.3, using the notation adopted by Faella *et al.* (2000). This model can be inserted directly in possible mechanical models as the one depicted in the same figure, where CWS represents the component column web in shear, CWT the component column web in tension CFB the component column flange in bending,

CWC the component column web in compression and BFC represents the components beam flange and web in compression. The properties of the models are determined for the first yielding of the panel zone, note that the rotational stiffness is defined by $K_{cws}h_t^2$, where K_{cws} is the axial stiffness of the corresponding spring of the mechanical model depicted in Figure 2.25. After yielding, and according to Krawinkler *et al.* (1975), the rotational stiffness of the panel zone $K_{cws,p}h_t^2$ can be attributed to the bending of the column flanges, developed up to the yielding of the column flanges, assumed to be equal to shear deformation of 4γ . After that point a plastic resistance increase is observed due to the strain hardening of the panel zone.

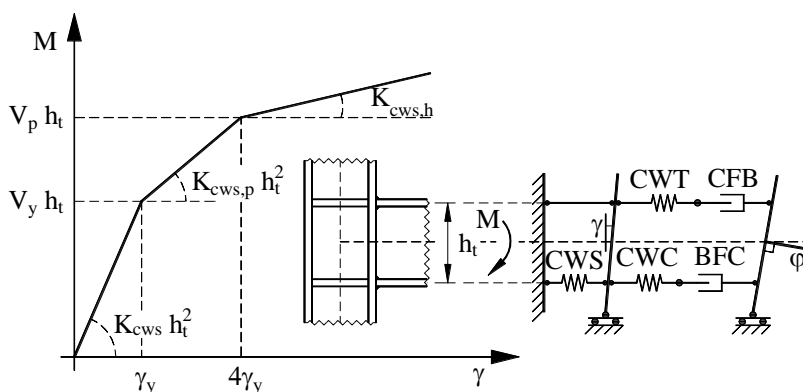


Figure 2.25: Krawinkler model and an associated mechanical model (Faella *et al.*, 2000).

Table 2.3: Krawinkler formulation (Faella *et al.*, 2000).

	Stiffness (K)	Resistance (M)	Rotation (γ)
Yielding of the panel zone	$K_{cws} h_t^2 = \frac{G t_{wc} h_c h_b}{\beta}$	$V_y h_t = \frac{f_y}{\sqrt{3}} \frac{t_{wc} h_c h_b}{\beta}$	$\gamma_y = \frac{f_y}{\sqrt{3} G}$
Yielding of the column flanges in bending	$K_{cws,p} h_t^2 = \frac{24 E I_{fc}}{5 t_{fc}} \frac{1}{\beta}$	$V_p h_t = V_y h_t + 3 K_{cws,p} h_t^2 \gamma_y$	$\gamma_p = 4 \gamma_y$
Strain hardening of the panel zone	$K_{cws,h} h_t^2 = \frac{E_h}{E} K_{cws} h_t^2$	-	-

Where

- h_t – lever arm
- E_h – is the hardening modulus of the material;
- I_{fc} – is the inertia moment of the column flanges ($I_{fc} = b t_{fc}^3 / 12$)
- β – is a factor to account for the beneficial effect of column shear above and below the joint, it can be taken equal to 1
- E – modulus of elasticity
- G – shear modulus

Following Zoetemeijer’s work (Zoetemeijer, 1975) on the definition of the relevant stress interactions when the load-introduction effect due to the beam forces is considered, a research programme was conducted at the University of Innsbruck to separately characterize the components due to shear and load-introduction effects in the column web panel using experimental tests on welded joints. The insights gained in the characterization of the web panel

behaviour were exploited by Jaspart (1990; Jaspart, 1991) to develop multi-linear analytical models, hereinafter referred to as the Atamaz-Jaspart model (AJM). The models were developed for the two identified deformation modes in the web panel, namely the load-introduction, due to the beam moment binary forces, and the distortion due to the pure shear installed in the panel. The induced forces in the web panel produce a complex stress state with three stress components, as depicted in Figure 2.24. In this figure, τ is the shear stress associated with the shear forces on the contour of the column web panel; σ_i is the horizontal normal stress associated with the load-introduction and σ_n is vertical normal stress due to the axial load and bending of the column. The analytical model determines the strength of the column web panel by analysing its stress state. In the application of the Von Mises yield criterion, some simplifications were proposed by Zoetemeijer (1975) and Jaspart (1990) for the stress interactions, which are:

- i) due to the localized effect of the σ_i stresses in the assessment of the shear resistance only the $\tau - \sigma_n$ interaction needs to be considered; and
- ii) for the assessment of the load-introduction resistance only the $\tau - \sigma_i$ interaction needs to be considered, because σ_n has a low influence on the load-introduction resistance for axial load in the column lower than $0.7N_{pl,Rd}$.

Subsequently, analytical models were developed for welded joints (Jaspart, 1990) and further adjusted for bolted joints in the case of the load-introduction, summarized in Figure 2.26, Table 2.4, Table 2.5 and Table 2.6. In the extrapolation from welded joints to bolted end-plate joints there are relevant differences that must be taken into account (Jaspart, 1990). For the load-introduction effect, based on a beam on elastic foundation model, the deformation in welded joints is similar in the tension and compression zones. However, for bolted end-plate joints, because of the different ways of applying the tension and compression loads by the beam (see Figure 2.24) the corresponding $F_b-\Delta$ curves are distinct, as shown in Table 2.4. Differences in the bolt rows change the deformed configuration and the position of the neutral axis. Therefore, the rotation needs to be computed considering the deformation contributions of each component: bolts, end-plate, column flange and column web. Also for the load-introduction effect, the infinitely stiff condition for the column flange provided by the welding of the beam web to the column flange cannot be considered valid in bolted end-plate

Recent studies on the column web panel extended its scope of application by proposing new and more sophisticated models. Castro *et al.* (2005) proposed a model for steel and composite joints suitable for use within frame analysis procedures. The model accounts for the effect of different boundary conditions, as well as shear and flexural deformation modes, in the evaluation of the elastic and inelastic response. Jordão *et al.* (2013) based their studies on the work done by Zoetemeijer (1975) and Jaspart (1991) and proposed new behaviour models for internal joints with beams of unequal depth, based on experimental and numerical work. Due to the unequal beam depths, the column web panel is divided into two sub-panels and three levels are considered for the load-introduction effect. An appropriate mechanical model was then proposed to determine the overall response of the joint (Jordão *et al.*, 2013).

Table 2.5: Multi-linear model values due to the shear effect of steel joints.

	Stiffness (K)	Resistance (V)	Rotation (γ)	Stiffeners
a)	$K_n = GA_{vc}$ with: $G = E/2(1 + \nu)$ $\lambda = 4\sqrt{k_{cw}/4EI_{fc}}$ $\xi = b_{eff,wc} \lambda/2$	$V_{ne} = \min(\tau_{y(tens)}^c; \tau_{y(comp)}^c) A_{vc}$ with: $\sqrt{(\sigma_{iy}^c)^2 + 3(\tau_y^c)^2} = f_{ywc}$ $\tau_y^c = \frac{F_{be} - V_{ce}}{A_{vc}}$	$\gamma_y = \frac{V_{ne}}{K_n}$	
b)	Adopted material uniaxial response 	$V_{ny} = \tau_y^c A_{vc}$ with: $\sqrt{(\sigma_{ny}^c)^2 + 3(\tau_y^c)^2} = f_{ywc}$ $\tau_y^c = \frac{F_{by} - V_{cy}}{A_{vc}}$ $\sigma_{ny}^c = \frac{M_c}{W_{cy}} + \frac{N_c}{A_c}$	$\gamma_y = V_y / K_n$ $\gamma_{st} = 0.5\sqrt{3}(\varepsilon_{st} - \varepsilon_y) + \gamma_y$ with: $\varepsilon_y = f_y / E$	$K_f = \frac{24EI_{fc}}{d_b^2}$ $V_{cy} = \frac{4M_{pl,fc}}{d_b}$
c)	$K_{nst} = G_{st} A_{vc}$ with: $G_{st} = E_{st} / 3$ $E_{st} \cong E/50$	$V_{nu} = \tau_u^c A_{vc}$ with: $\sqrt{(\sigma_{nu}^c)^2 + 3(\tau_u^c)^2} = f_{uwc}$ $\tau_u^c = \frac{F_{bu} - V_{cu}}{A_{vc}}$ $\sigma_{nu}^c = \frac{M_c}{W_{cu}} + \frac{N_c}{A_c}$	$\gamma_u = \sqrt{3}(\varepsilon_u - \varepsilon_{st}) + \gamma_{st}$	

- a) First yielding of the of the web under the combined stresses τ - σ ;
b) Plastic shear stress uniformly distributed in the whole panel, using the interaction of stresses τ - σ , followed by the apparition of the strain hardening in the web, γ_{st}
c) Ultimate shear force, V_{nu}

Table 2.6: Specific notation for the multi-linear model AJM (Jaspart, 1990).

k_{cw}	- is a parameter used in the calculation of the load-introduction stiffness;
λ , ξ and μ	- are parameters related with the assessment of the column web elastic foundation properties, for the calculation of column flanges bending resistance in the load-introduction effect;
A_{vc}	- is the column web shear area;
I_{fc}	- is the inertia of the column flanges plus the web transition radius;
$b_{eff,wc}$	- is the effective width of column web in compression or in tension, for tension the EC3-1-8 (EN 1993-1-8, 2005) effective width recommendations should be used;
a_f	- is the throat of the beam-to-end-plate fillet weld
W_p	- is the extended part of the end-plate
K_{be} and k_{bjst}	- is the elastic and post-elastic stiffness for the load-introduction model, respectively;
K_n and k_{nst}	- is the elastic and post-elastic stiffness for the shear model, respectively;
F_{be}	- is the value of F_b when the web panel reaches the first yielding (associated to the biaxial stress state σ_{iy}^c vs τ_y^c) for the load-introduction model;
$F_{b ppl}$	- is the value of F_b when the pseudo-plastic moment $M_{b ppl}$ of the joint is reached, for the load-introduction model;
F_{buy}	- is the value of F_b when the web panel reaches the ultimate plastic resistance (associated to the biaxial stress state σ_{iu}^c vs τ_u^c) for the load-introduction model;
F_{bb}	- is the value of F_b when the web panel reaches the instability under compression effects, for the load-introduction model;
F_{bcr}	- is the value of F_b for the elastic linear instability load of the web, for the load-introduction model;
k	- is a coefficient that accounts for the type of loading, and web support conditions (1 for cross nodes symmetrically loaded and 2 for external nodes);
V_{ce} and V_{cu}	- shear forces entering in the web from the global system, corresponding to the first yielding and the ultimate resistance of the web;
f_{ywc} and f_{uwc}	- are the nominal values of the yield strength and the ultimate tensile strength of the steel grade adopted for the column web;
σ_{iy}^c and τ_y^c	- are the horizontal normal stress and shear stress, respectively, in the Von Mises criterion that induces the first yielding in the column web panel;
σ_{iu}^c and τ_u^c	- are the horizontal normal stress and shear stress, respectively, in the Von Mises criterion that induces the ultimate plastic stress state in the column web panel;
Δ_e , Δ_{st} and Δ_u	- are the column web relative elongation, between the axis of the web and the introduction-load zone, at the first yielding in the web, the apparition of the strain-hardening in the web and at the ultimate web resistance;
ε_y , ε_{st} and ε_u	- are the strains at the first yielding in the web, the apparition of the strain-hardening in the web and at the ultimate web resistance, respectively;
V_{ne} , V_{ny} and V_{nu}	- are the column web shear resistance at the first yielding, at the complete yielding of the whole panel and at the ultimate plastic resistance, respectively, for the shear model;
γ_y , γ_{st} and γ_u	- are the column web shear rotation at the first yielding in the web, the apparition of the strain-hardening in the web and at the ultimate web resistance, for the shear model, respectively;
σ_{ny}^c and τ_y^c	- are the vertical normal stress and shear stress, respectively, in the Von Mises criterion that induces the complete yielding of the whole panel;
σ_{nu}^c and τ_u^c	- are the vertical normal stress and shear stress, respectively, in the Von Mises criterion that induces the ultimate plastic stress state in the column web panel;
M_c and N_c	- are the bending moment and axial forces entering in the web from the global system;
V_{cy}	- is the additional plastic web capacity, due to the presence of the transverse stiffeners aligned with the beam flanges, that forms with the column flanges a frame with additional shear resistance;
k_f	- is the rate of increase of the additional plastic web capacity resistance V_{cy} .

Concerning the cyclic behaviour of components, Kim and Engelhardt (2002) proposed a model to characterize the behaviour of the column web panel in shear under cyclic loading, after observing the limitations of the bilinear model to replicate the full loading history of the

panel zone. It is a model based on the Dafalias' (1975) bounding surface theory, that uses the Cofie and Krawinklers's (1985) rule for the movement of the bound line. Moreover, it is assumed that the moment-rotation relationship of the panel zone can be determined from its material properties using the Cofie's rule. Figure 2.27 and Table 2.7 summarizes the model main features.

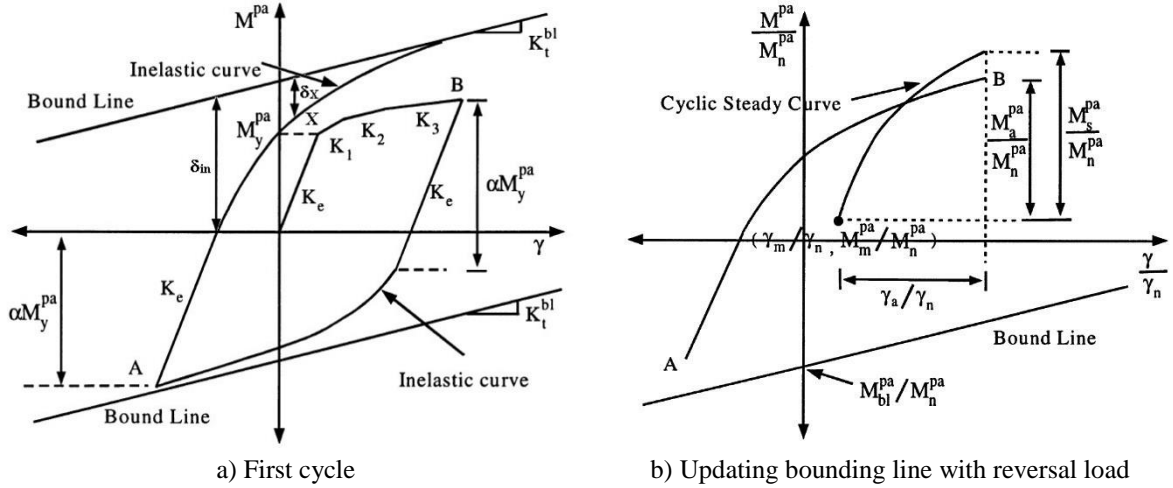


Figure 2.27: Cyclic model to characterize the behaviour of the column web panel (Kim and Engelhardt, 2002).

Table 2.7: Kim and Engelhardt (2002) model main features.

First cycle	Updating bounding line with reversal load
Movement of the bounding line	For the last half cycle of loading history
$\frac{\gamma}{\gamma_n} = \frac{M^{pa}}{M_n^{pa}} + \left(\frac{M^{pa}}{\xi M_n^{pa}} \right)^C \quad (2.12)$	$M_m^{pa} = 0.5(M_A^{pa} + M_B^{pa}) \quad (2.13)$
$C = 7; \xi = 1.1-1.2$ (empirical values)	$\gamma_m^{pa} = 0.5(\gamma_A^{pa} + \gamma_B^{pa}) \quad (2.14)$
$M_n^{pa} = M_y^{pa} + 2M_{pcf} \quad (2.16)$	$M_a^{pa} = 0.5 M_A^{pa} - M_B^{pa} \quad (2.15)$
$\gamma_n = M_n^{pa} / K_e \quad (2.18)$	$\gamma_a^{pa} = 0.5 \gamma_A^{pa} - \gamma_B^{pa} \quad (2.17)$
Initial half-cycle	If $\Delta M^{pa} > 0$
K_1, K_2 and $K_3 \rightarrow$ Krawinkler <i>et al.</i> (1975) model $\alpha = 1.4$	$\left(\frac{M_{bl}^{pa}}{M_n^{pa}} \right)_{new} = \left(\frac{M_{bl}^{pa}}{M_n^{pa}} \right)_{old} - 2F_H \left(\frac{\Delta M^{pa}}{M_n^{pa}} \right) \quad (2.20)$
Inelastic curve shape factor	If $\Delta M^{pa} < 0$
$\hat{h} = 40 + \frac{(20-40)}{\left[1 + e^{(\theta_p - 0.213)/0.074} \right]} \quad (2.21)$	$\left(\frac{M_{bl}^{pa}}{M_n^{pa}} \right)_{new} = \left(\frac{M_{bl}^{pa}}{M_n^{pa}} \right)_{old} - 2F_S \left(\frac{\Delta M^{pa}}{M_n^{pa}} \right) \quad (2.22)$
Bound line	Move the bound by $F_R M_m^{pa}$
$K_p^{bl} = 0.008 K_{el} \quad (2.23)$	$F_H = 0.45; F_S = 0.07$ and $F_R = 0.05$
For a point X that $0.1 \leq \delta_X / \delta_{in} \leq 0.5$	

First cycle	Updating bounding line with reversal load
$K_p^X = K_p^{bl} \left[1 + h \frac{\delta_X}{\delta_{in} - \delta_X} \right] \quad (2.24)$	$\left(\frac{M_{bl}^{pa}}{M_n^{pa}} \right)_{new} = \left(\frac{M_{bl}^{pa}}{M_n^{pa}} \right)_{old} - 2F_R M_m^{pa} \quad (2.25)$
$K_t^X = \frac{K_{el} K_p^X}{K_{el} + K_p^X} \quad (2.26)$	

Where

M_p^{pa}	is the panel elastic moment
M_{bl}^{pa}	is moment of the bound line when the rotation is zero
γ_n	is the panel elastic rotation
ξ	is a constant of the cyclic steady state curve
C	is an empirical constant of the cyclic steady state curve
M_{pcf}	is the thecolumn flanges plastic moment
K_{el}	is the initial elastic stiffness
$K_{1 \text{ to } 3}$	are the hardening stiffness's of the Krawinkler <i>et al.</i> multi-linear model
α	is the elastic limit factor
\hat{h}	is the shape factor of the inelastic curve
θ_p	is the accumulated plastic rotation
K_p^{bl}	is the plastic stiffness of the bound line
K_p^X	is the plastic stiffness at the point X
δ_X	is the distance between the inelastic curve and the bound line at the point X
δ_{in}	is the distance between the beginning of the inelastic curve and the bound line
K_t^X	is the tangent stiffness at point X
M_m^{pa}	is the mean panel moment of the last half cycle
M_d^{pa}	is the amplitude of the panel moment of the last half cycle
γ_m^{pa}	is the mean panel rotation of the last half cycle
γ_d^{pa}	is the amplitude panel rotation of the last half cycle
M_s^{pa}	is the panel moment on the cycle steady curve
F_H	is the hardening factor
F_R	is the mean value relaxation factor
F_S	is the softening factor

Simões da Silva *et al.* (2009) applied the Richard-Abbot model to simulate the cyclic behaviour of individual components, such as the column web panel in shear and the end-plate in bending. Finally, Latour *et al.* (2011) extended the application of the Kim and Engelhardt (2002) model to the load introduction components. The difference between this model and the one developed for the panel zone is the assumption of a constant shape factor \hat{h} and of a nonlinear monotonic law. However, they did not separate load-introduction in tension and in compression, therefore disregarding the fact that, in bolted joints, the bolts at discrete positions transfer tension while compression is transferred within a tributary area, approximately centred on the beam-compressed flanges. Figure 2.28 and Table 2.8 summarizes the model main features.

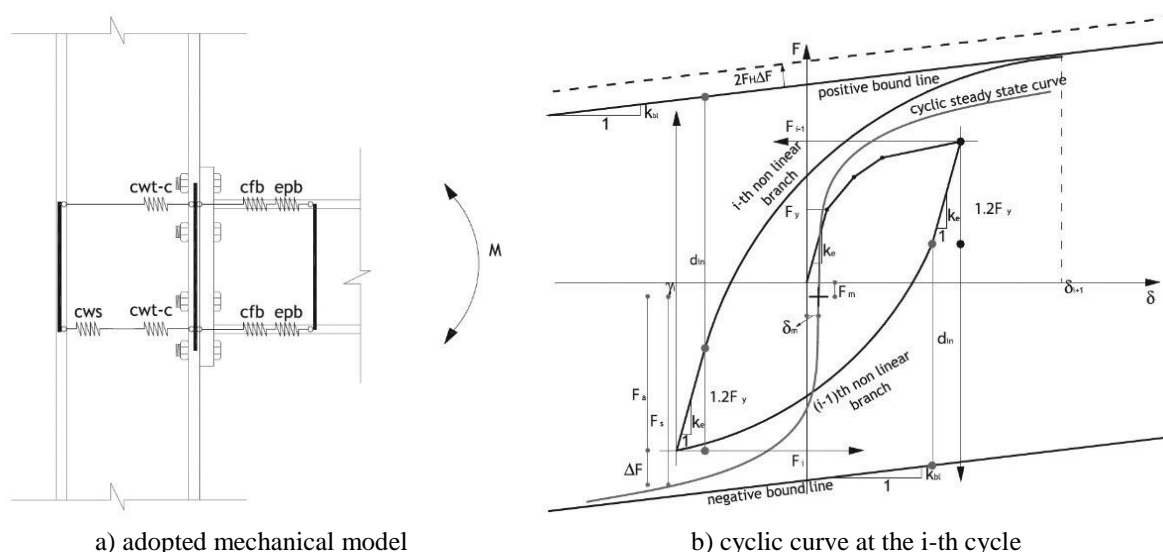


Figure 2.28: Cyclic model to the components column web panel in transverse tension and compression (Latour, et al., 2011).

Table 2.8: Extended the application of the Kim and Engelhardt (2002) model to the load introduction components (Latour, et al., 2011).

Monotonic curve	Cyclic steady state curve (representing the saturation curve of the material)
$\sigma = E\varepsilon \text{ for } 0 < \varepsilon < \varepsilon_y \quad (2.27)$	$\frac{\varepsilon}{\varepsilon_y} = \frac{\sigma}{f_y} + \left(\frac{\sigma}{K'f_y} \right)^{1/n'} \quad (2.28)$
$\sigma = f_y \text{ for } \varepsilon_y < \varepsilon < 14\varepsilon_y \quad (2.29)$	
$\frac{\varepsilon}{\varepsilon_y} = \frac{\sigma}{f_y} + \left(\frac{\sigma}{Kf_y} \right)^{1/n} \text{ for } \varepsilon > 14\varepsilon_y \quad (2.30)$	
$K=0.51$ and $n = 0.23$ (obtained from curve fitting of experimental data in Krawinkler et al. studies)	$K'=0.9$ and $n' = 0.19$ (determined by Cofie and Krawinkler by means of constant amplitude cycles, and described by a Ramberg-Osgood relationship)
Empirical parameters for the application of Krawinkler et al. model	
$h = 45$	$F_H = 0.45$
	$F_S = 0.07$
	$F_R = 0.05$

Where

- K is a constant obtained by curve fitting
- n is a constant obtained by curve fitting
- K' is a constant obtained by curve fitting for the saturation curve of the material
- n' is a constant obtained by curve fitting for the saturation curve of the material
- E is the Young modulus
- f_y is the yield strength
- σ is the normal stress
- ε is the strain associated to the stress
- ε_y is the yield strain
- F_H is the hardening factor
- F_S is the softening factor
- F_R is the mean value relaxation factor

2.2.3 ANALYSIS OF JOINTS BY NUMERICAL FE METHODS

2.2.3.1 OVERVIEW OF THE FINITE ELEMENT METHOD

According to Hutton (2003) the finite element (FE) method is a powerful numerical tool, normally requiring computational assistance, used to obtain approximate solutions of boundary value problems in engineering. In a simplified way a boundary value problem is a mathematical problem in which one or more dependent variables must satisfy a differential equation everywhere within a known domain of independent variables and satisfy specific conditions on the boundary of the domain.

As realised by Bhatti (2005) to solve a finite element problem the following procedure should be followed:

1. Development of the element equations;
2. Discretization of solution domain into a finite element mesh;
3. Assembly of element equations;
4. Introduction of boundary conditions;
5. Solution of nodal unknowns;
6. Computation of solutions and related quantities over each element.

The procedure intends to reduce the solution domain into simpler domains that are parts of overall domain called elements. The solution for each element is determined at selected points called nodes. Hence, the finite element process is not more than a large system of equations that must be solved for determine nodal unknowns.

The choice of the elements type is very important, because the number of differential equations is related to the element shape and node distribution. There are several types of elements depending on the problems complexity, so for a problem that can be governed by a one-dimensional ordinary differential equations linear elements can be used, for problems governed by two-dimensional partial differential equations the elements are usually of triangular or quadrilateral shape. Three-dimensional problems use normally tetrahedral or solid brick-shaped elements, in the Figure 2.29 it's shown an example of the elements, where the nodes are also represented by the dark circles.

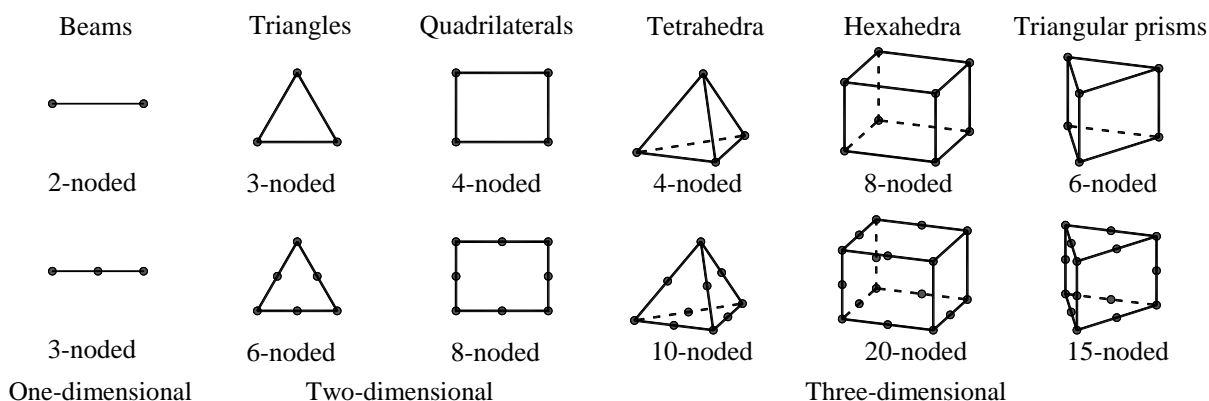


Figure 2.29: Typical finite element shapes.

Normally the number and arrangement of elements used in the finite elements analysis is related to the accuracy of the results, but also with the computational effort. It is important to concentrate more elements where the solution changes rapidly and fewer elements where it is expected less variation in the solutions, so the calculation effort can be balanced. It is important to have in mind some good practical rules on the FE discretization:

- Number of elements vs accuracy – a proper number of elements should be choose;
- Element formulations – some elements produced more accurate solutions than others, so in some cases more elements should be needed;
- Available computational resources – if the number of elements required for an accurate solution is too high, dividing the model domain can be a useful solution;
- Element interfaces – it is important to create a regular and effective mesh in the model;
- Symmetry – in many practical applications the solution domain and the boundary conditions are symmetric, so it is important to model only the symmetric portion of the solution domain that gives information for the entire model.

It is on the assembly process that the elementary solutions, from each element, are assembled to obtain the overall solution domain back together, along with the boundary conditions. This process is achieved by making for several elements the same nodal solution if they share the node. Thus contributions to that degree of freedom from all adjacent elements must be added together.

After the definition of the boundary conditions a global system of n equations in n unknowns is obtained, in most of structural problems is used:

$$[K_g][u] = [F] \quad (2.31)$$

where $[K_g]$ is the system global stiffness square matrix, $[u]$ is the vector of displacements resulting from the application of the forces and $[F]$ is the vector of applied external forces. In most practical applications the equations system is often very large, due to the number of elements, and so it is necessary to use computer algebra systems with sophisticated built-in functions for solving large systems of linear equations.

The numerical methods used in the resolution of the large equation systems produce normally approximate solutions to real one. The accuracy of the results will depend on how the FE model is developed and lies in the specific options taken according to the nature of the problem. Therefore, it is important to be aware of the difficulties and limitations that the numerical models exhibit like the *Hourglassing* and the *Shear Locking* numerical problems in stress analysis, which can affect the solution depending on the element type chosen. *Hourglass* occurs when reduced integration elements are used (normally is used a scheme one order less than the full scheme to integrate the element's internal forces and stiffness with only 1 Gauss point) and tends to be excessively flexible, because in bending the integration point remain unchanged what implies that the normal stress and shear stress are wrongly zero, see Figure 2.30. And in the *shear lock* phenomenon occurs the opposite. When first order fully integrated elements are used, and tends to become overly stiff in bending, because the brick isn't able to bend its faces and the angle A doesn't remain at 90° leading to an incorrect artificial shear stress, as illustrated in Figure 2.31. To control these phenomena several actions can be taken, for example to control the *Hourglassing*, in bending dominant problems, several elements in thickness of the plated parts should be consider, so integration points have relative strains between the thickness elements. To control the *shear lock* the use of fully integrated second order elements that take into account the elements curvature will avoid the numerical problem. More than the awareness of the phenomena the detection and interpretation of the results are crucial to achieve good solutions.

The previous overview of the FE method is only a descriptive approach because the intention was to review the general concepts associated with the method, that allowed a good

understanding of the phenomena involved, rather than a the mathematical formulation widely disseminated in the specialized literature like the ones mentioned above.

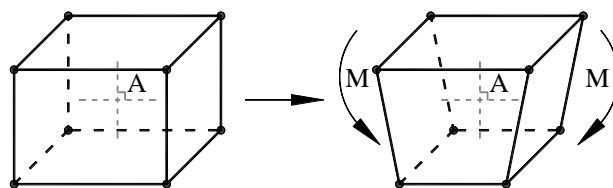


Figure 2.30: Shape of reduced integration linear (first order) element in bending (Sun, 2006).

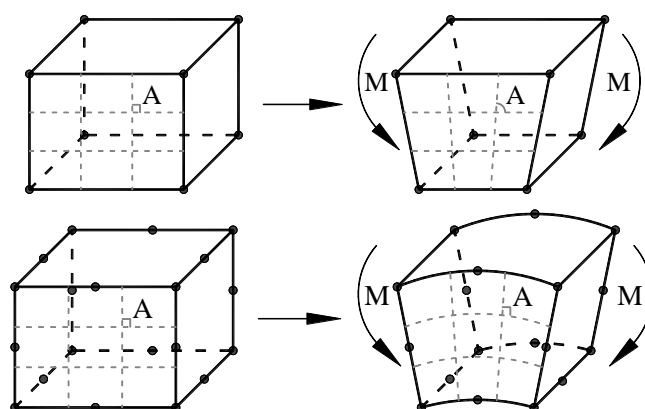


Figure 2.31: Comparison of the shape of linear (first order) elements and the fully integrated quadratic (second order) elements in bending (Sun, 2006).

2.2.3.2 MATERIAL STRESS-STRAIN RELATIONSHIPS FOR THE FE MODELS

i) Monotonic Loaded Models

In complex joint models the characterization of the behaviour requires to deal with physical nonlinearities, in this case spread of plasticity is expected, and is necessary to implement the proper stress-strain relationships in the finite elements models. Two approaches can be drawn to define the stress-strain relationships for steel: using real properties obtained from coupon tensile tests, which implies to have access to results of previous material tests; or the use of theoretical stress-strain relationships, for the material characterization, already available in literature, like bilinear approach, Ramberg-Osgood model or Menegotto-Pinto model.

The bilinear approach is a simple material model definition represented by two linear expressions where the initial stiffness governs the first one, until the yield strength and the second one is the hardening stiffness, typically defined as a ratio E_h to the initial stiffness, see Figure 2.32. Due to its linearity and simplicity, this approach requires relatively little

computational effort and is very attractive for use in numerical and analytical simulations. For the bilinear model's definition, the following data are required: $f_y, f_u, \epsilon_y, \epsilon_u, E$ and E_h .

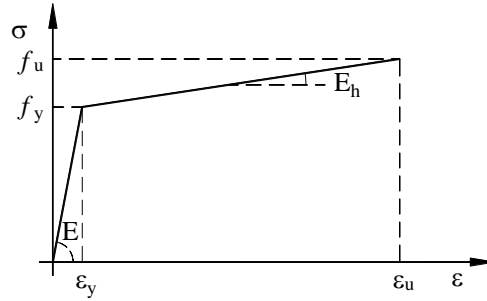


Figure 2.32: Bilinear model.

The Ramberg-Osgood approach is a stress-strain relationship normally used for materials of round-house type and it is based on the observation that a representation in a log-log coordinates of the true stress against true plastic strain results is a straight line and can be represented by a power function:

$$\sigma = K(\epsilon_{pl})^n \quad (2.32)$$

where ϵ_p is the true plastic strain, σ is the true stress, K is the strength coefficient and n is the strain hardening exponent. If the elastic strain, ϵ_e , is included and the total strain, ϵ , is made explicit the relationship proposed by Ramberg and Osgood (1943) is obtained:

$$\epsilon = \epsilon_e + \epsilon_{pl} = \frac{\sigma}{E} + \left(\frac{\sigma}{K}\right)^{1/n} \quad (2.33)$$

According to De Martino *et al.* (1990) the exponent n is determined in accordance to the reference points for the elastic limit and the ultimate stress, or other two intermediate points. In this case n is determined as follows:

$$n = \frac{\log(\epsilon_u / \epsilon_y)}{\log(f_u / f_y)} \quad (2.34)$$

the Menegotto-Pinto model consists of an expression that relates inelastic stress-strain in the hardening phases of sharp knee metals at yielding and is represented by:

$$\sigma = \left\{ E_\infty + (E_0 + E_\infty) / \left[1 + \left(\frac{\epsilon}{\epsilon_0} \right)^R \right]^{1/R} \right\} \epsilon \quad (2.35)$$

where E_0 is the initial tangent modulus of the stress-strain curve, E_∞ is the secondary tangent modulus of the stress-strain curve, R is a material constant and $\varepsilon_0 = \sigma_0/E_0$ is the strain at the stress σ_0 as shown in Figure 2.33 (a). According to Kato *et al.* (1990), when the gradient of the nominal engineering stress-strain curve becomes zero at the maximum load, the secondary tangent modulus E_∞ is set to zero at the maximum stress $\sigma_0(MP) = E\varepsilon_0 = f_{max}$, as shown in Figure 2.33 (b). Furthermore, the initial tangent modulus E_0 can be assumed to be equal to the modulus of elasticity E . The previous equation is then simplified as follows:

$$\sigma = \left\{ E / \left[1 + \left(\frac{\varepsilon}{\varepsilon_0} \right)^R \right]^{1/R} \right\} \varepsilon \quad (2.36)$$

Using the $\varepsilon_0 = f_{max}/E$ introduces a large error at the maximum load, as can be seen in Figure 2.33 (b), and therefore another material constant is introduced to improve the fitness of the Eq. (2.36), becoming $\varepsilon_0 = \gamma_{MP} f_{max}/E$ or:

$$\sigma_0(MP) = \gamma_{MP} f_{max} = E\varepsilon_0 \quad \gamma_{MP} > 1 \quad (2.37)$$

To determine the parameters R and γ_{MP} it is sufficient to use the coordinates of two points of the strain-hardening curve $P_A(\sigma_A, \varepsilon_A)$ and $P_B(\sigma_B, \varepsilon_B)$, R can be determined with the following equation:

$$\left(\frac{\sigma_A \sigma_B}{E} \right)^R \left[\left(\frac{1}{\varepsilon_A} \right)^R - \left(\frac{1}{\varepsilon_B} \right)^R \right] + (\sigma_A^R - \sigma_B^R) = 0 \quad (2.38)$$

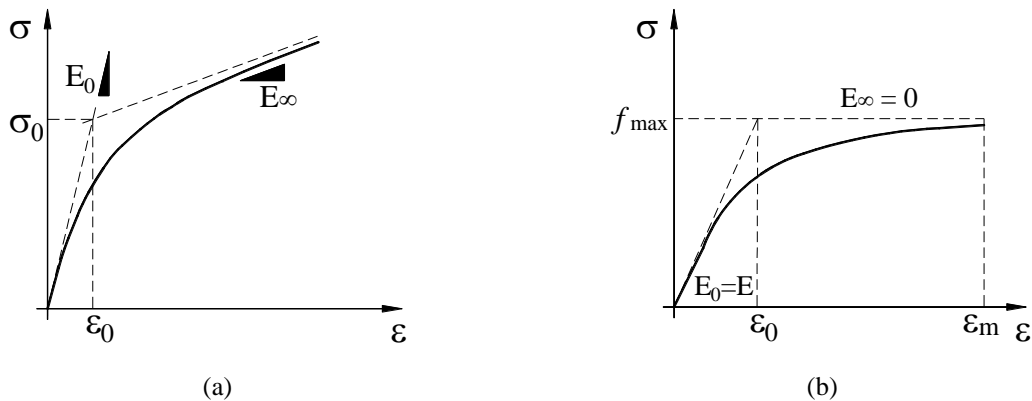


Figure 2.33: (a) Menegotto-Pinto model; (b) the case of $E_0 = E$ and $E_\infty = 0$.

ii) Cyclic Loaded Models

When reversal cyclic load reaches the inelastic field of the steel the definition of the material behaviour as to be different from the monotonically loaded specimen, since now the cyclic plasticity is dependent on the load history.

Two phenomena have to be taken into account for the hardening model: the Isotropic hardening and the Kinematic hardening. Hardening is a phenomena common too many metals, that consists in the stress required to cause further plastic deformation, often as a function of accumulated plastic strain. When the expansion on the yield surface is uniform in all directions in stress space it is called the isotropic hardening, Figure 2.34. The loaded point, in the 2-direction, moves from zero to σ_y , the yield occurs at this point, in order to hardening take place the yield surface must expand as σ_2 increases to maintain the loaded point on the yield surface (Dunne and Petrinic, 2006, sec. 2.5).

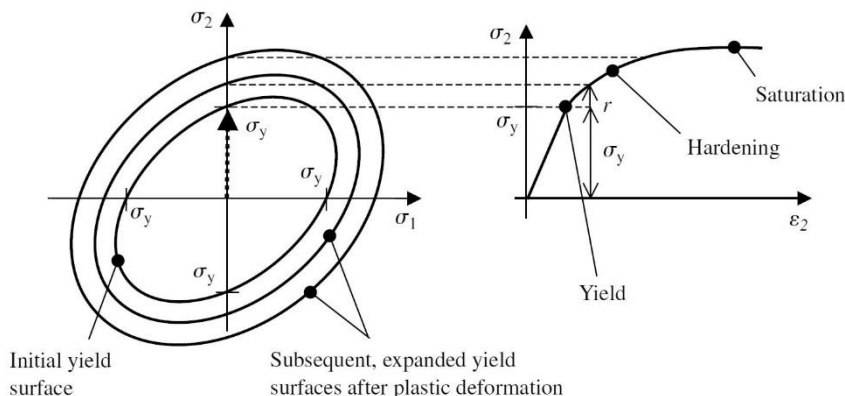


Figure 2.34: Isotropic hardening, in which the yield surface expands with plastic deformation, and the corresponding uniaxial stress-strain curve (Dunne and Petrinic, 2006, sec.2.4).

Although for the monotonic loading conditions, the consideration of the isotropic hardening is reasonable, when reversal load occurs in the plastic range, this may not be appropriate. In Figure 2.35 is depicted a material that hardens isotropically, for the load point (1) the strain ϵ_i is reached, when the load is reversed until the load point (2) reaching again the expanded yield surface, isotropic hardening leads to a very large elastic region, as observed in Figure 2.35 (b), which is not verified in experimental results. In fact, experimental results have showed that the elastic region is much smaller due to the *Bauschinger effect*. In kinematic hardening the yield surface translates in stress space rather than expanding, see Figure 2.36. The stress increases until the yield stress, σ_y (or σ_0), after that point the material deforms

plastically and the yield surface translates. When the load is reversed the material deforms elastically until the point is again in contact to the yield surface, and the elastic region is much smaller than the isotropic hardening one (Dunne and Petrinic, 2006, sec. 2.5).

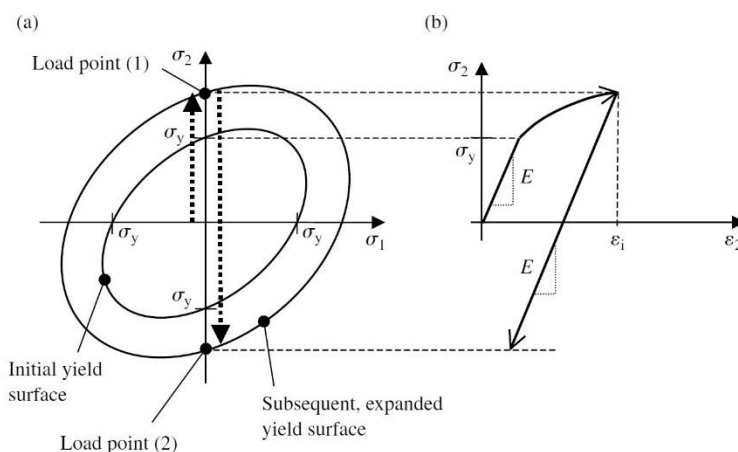


Figure 2.35: Reversed loading with isotropic hardening showing (a) the yield surface and (b) the resulting stress-strain curve (Dunne and Petrinic, 2006, sec.2.5).

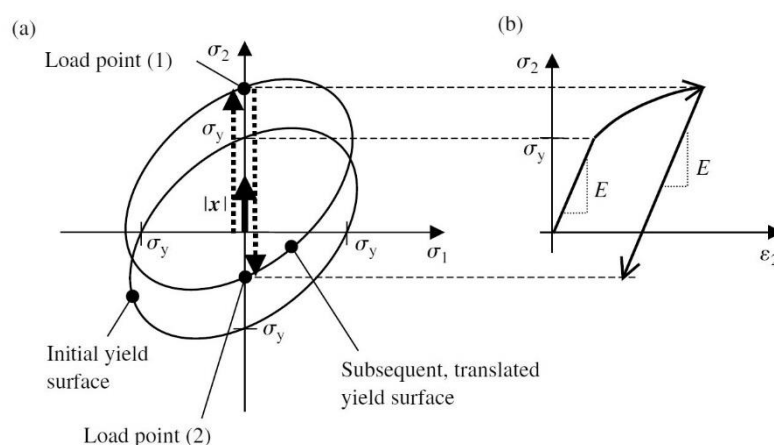


Figure 2.36: Kinematic hardening showing (a) the translation of the yield surface with plastic strain, and (b) the resulting stress-strain curve with shifted yield stress in compression - the *Bauschinger effect* (Dunne and Petrinic, 2006, sec.2.5).

For joint models subjected to cyclic loading conditions, combine the isotropic and kinematic hardening model is recommended. ABAQUS (2014) allows a combined isotropic/kinematic model for the simulation of the material hardening when subjected to cyclic loads. This constitutive model is based on the work of Lemaitre and Chaboche (1990, chap.5) and uses the Von Mises yield criterion and an associative flow rule is assumed.

The isotropic component of the model defines the change of the size of the yield surface σ_0 as a function of equivalent plastic strain ε^{pl} , and is given by:

$$\sigma^0 = \sigma|_0 + Q_\infty \left(1 - e^{-b_{iso}\epsilon^{pl}} \right) \tag{2.39}$$

where $\sigma|_0$ is the yield stress at zero equivalent plastic strain, Q_∞ is the maximum change in the size of the yield surface and b_{iso} is the rate at which the size of the yield surface changes as plastic strain increases.

The kinematic component of the model defines the changes of backstress α_k , which is expressed as:

$$\alpha_k = \frac{C_k}{\gamma_k} + \left(1 - e^{-\gamma_k \epsilon^{pl}} \right) + \alpha_{k,1} e^{-\gamma_k \epsilon^{pl}} \tag{2.40}$$

where C_k and γ_k are material constants. The ratio C_k/γ_k is the maximum change in backstress and γ_k determines the rate at which the backstress varies as the plastic strain increases.

If α_k is considered to be 0 at $\epsilon^{pl} = 0$ Eq. (2.40) becomes:

$$\alpha_k = \frac{C_k}{\gamma_k} + \left(1 - e^{-\gamma_k \epsilon^{pl}} \right) \tag{2.41}$$

In this case the non-linear kinematic hardening increases as the plastic strain ϵ^{pl} increases until the saturation is reached for maximum backstress of C_k/γ_k giving a maximum saturated stress of $\sigma|_0 + C_k/\gamma_k$, as depicted in Figure 2.37.

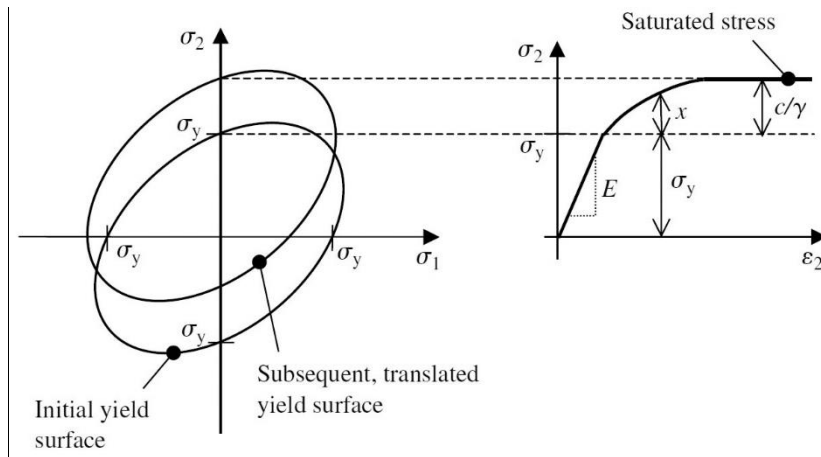


Figure 2.37: Non-linear kinematic hardening and the associated stress-strain curve (Dunne and Petrinic, 2006, sec.2.5).

If we now consider the combined effect of both Kinematic and isotropic hardening, appropriate for cyclic loading, where for the first cycle's kinematic hardening is the dominant

hardening process, considering the *Bauschinger effect*, however with the increase of the number of cycles the material also hardens isotropically, the peak stress in tension and compression increases until saturation is achieved. This process is represented in Figure 2.38. The stress increase until point A, where the yielding is reached, from that point on the material hardens kinematically, leading to a translation of the yield surface. When the point B is reached the strain reversal occurs and the material is again governed elastically until the load point reaches the yield surface again at point C. From this point forward plastic deformations take place again until point D with kinematic hardening and a translation of the yield surface. If the combined effect of both kinematic and isotropic hardening occurs, then superimposed upon the translation of the yield surface is a progressive expansion, represented by the dashed line hysteresis loop in Figure 2.38.

In ABAQUS (2014) the combined kinematic and isotropic hardening behaviour is computed determining the overall backstress, which is composed of multiple backstress components, where the evolution of the backstress components of the model is defined in Eq. (2.42) and the overall backstress is computed by the Eq. (2.43).

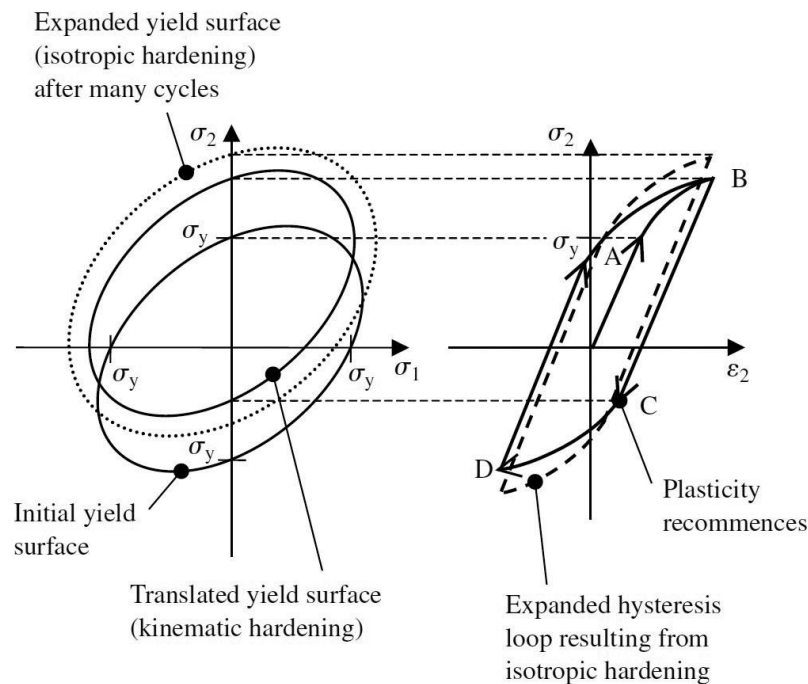


Figure 2.38: Combined kinematic and isotropic hardening (Dunne and Petrinic, 2006, sec.2.5).

$$\dot{\alpha}_k = C_k \dot{\epsilon}^{pl} \frac{1}{\sigma_0} (\sigma - \alpha) - \gamma_k \alpha_k \dot{\epsilon}^{pl} + \frac{1}{C_k} \alpha_k \dot{C}_k \quad (2.42)$$

$$\alpha = \sum_{k=1}^N \alpha_k \tag{2.43}$$

Where N is the number of backstresses, C_k and γ_k are material parameters, and \dot{C}_k is the rate of change of C_k with respect to temperature and field variables.

iii) Other Phenomena Related to Cyclic Material Behaviour of Joints.

According to ABAQUS (2014) the following phenomena are covered when the combine nonlinear isotropic/kinematic hardening model is used:

- Bauschinger effect: already seen in the previous point. This phenomenon decreases with continued cycling. The use of multiple backstresses can improve the shape of the cycle;

- Cyclic hardening with plastic shakedown: this phenomenon usually appears in the symmetric stress or strain controlled experiments. Usually the soft metals tend to harden towards a stable limit, Figure 2.39, and on the contrary the hardened metals tend to soften in the beginning. The combine isotropic/kinematic model predicts shakedown after several cycles.

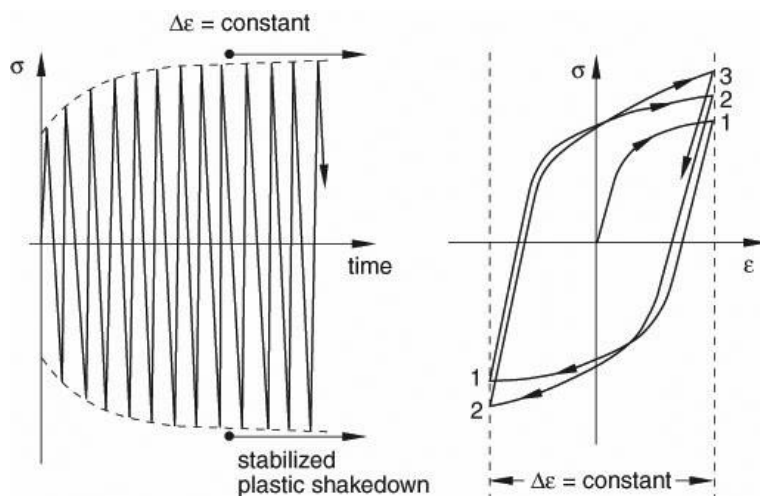


Figure 2.39: Plastic shakedown – hardening under prescribed symmetric strain cycles (ABAQUS, 2014, fig.23.2.2-4).

- Ratchetting effect: progressive ratchetting in the direction of the mean stress may occur when unsymmetrical cycles of stress between prescribed limits are applied, Figure 2.40. For low mean stress typically the transient ratchetting is followed by stabilization, while, at high mean stresses, a constant increase in the accumulated ratchet is observed. The combined model predicts better this effect than the isolated kinematic model, but the ratchet strain may decrease until it becomes constant.

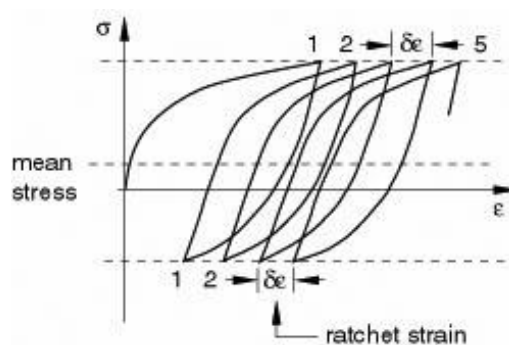


Figure 2.40: Ratchetting effect (ABAQUS, 2014, fig.23.2.2-5).

- Relaxation of the mean stress: this phenomenon is characteristic of an unsymmetrical strain experiment, as the number of cycle's increases the mean stress tends to zero, as shown in Figure 2.41. This phenomenon is taking into account by the nonlinear kinematic hardening component of the nonlinear isotropic/kinematic model.

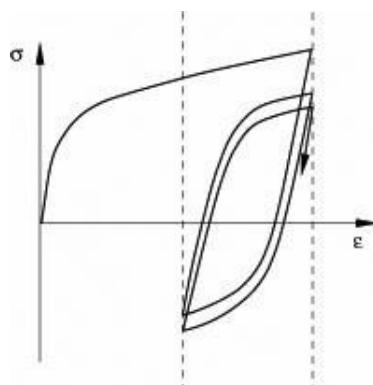


Figure 2.41: Relaxation of the mean stress (ABAQUS, 2014, fig.23.2.2-6).

Although the nonlinear isotropic/kinematic hardening model can be more accurate in many cases that involve cyclic loading, it still has the following limitations:

- For all strain ranges, the isotropic hardening is the same. However, physical observations indicate that the strain range influences the amount of the isotropic hardening. In addition, if the specimen is cycled at two consecutive and different strain ranges the deformation in the first cycle affects the isotropic hardening in the second cycle.
- Proportional and non-proportional load cycles generate the same cyclic hardening behaviour. However, physical observations indicate that the cyclic hardening behaviour at similar strain amplitude may be very different for the non-proportional loading when compared to the uniaxial behaviour.

As in any other problems solver knowing their limitations is an important step to better control the results.

2.3 DATA COLLECTION AND TREATMENT OF EXPERIMENTAL TESTS ON STEEL JOINTS

2.3.1 SCOPE

As referred previously, it was not objective of this work to perform new experimental tests. Instead, the considerable amount of test results available should be collected and treated, which has been already done in some extent in Section 2.2.1.2.

Notwithstanding the detail review of the tests performed there, a survey of experimental tests, since 1990, in end-plate and top and seat angle joints configurations, subjected to cyclic loading, will be presented, catalogued and analysed here.

The objective is to identify the characteristic hysteresis of the considered joint typology and to choose the most suitable tests to use in the calibration/validation of parametric numerical models, which will then be used to study joint hysteretic behaviour. Thirty-two experimental tests were analysed and the results compared.

2.3.2 SURVEY OF EXPERIMENTAL RESULTS

2.3.2.1 TOP AND SEAT ANGLES JOINTS CONFIGURATION

Following the work developed by Nogueiro (2009) in the collection of research projects with experimental tests of joints under cyclic loading conditions, in Table 2.9 are summarized 14 research projects, 84 tests and 11 different cyclic load protocols for steel bolted top and seat angle joints.

Table 2.9: Top and seat steel joints.

Authors	No. tests	Joint characterization	Load history	Main parameters investigated	Country
Elnashai and Elghazouli (1994)	2	One half of two storey frame. Columns in H150x150x7x10, beams in H250x130x9x9 and column web stiffeners. 1 cyclic test and 1 pseudo-dynamic.	(1) - Based in the second-storey yield displacement (δ_y), 3 cycles were applied at each displacement of δ_y , $2\delta_y$, $4\delta_y$, $6\delta_y$, etc.	Investigate the effect of the semi-rigid joints on the member as well as the frame behaviour. Study the hysteretic joint behaviour.	UK
Calado (Calado, 1995)	4	Top and seat angles connecting the column and beam, which in all specimens was a HEA140. The angles were 100x100 with two different thickness, 10 mm and 12 mm. Bolts used: M16 grade 8.8.	(2) - ECCS procedure.	Investigate the influence of the connection components (i.e. number of bolts, thickness of the angles and change bolts through welding) in the cyclic behaviour of the joints.	Portugal
Calado and Castiglioni (1996)	3	Bolted web and flange cleats joints. Columns and Beams in HEA120 (Fe360) and cleats 100x100x10 angles (Fe360), bolts M16 (8.8) without preloading.	(3) - In the elastic range: 4 cycles with $0.5v_y$, $1.5v_y$ and $2v_y$. In the plastic range: total amplitudes comprised between 5 and $12v_y$, where v_y is the yield displacement of the connection.	Development of a cumulative damage model, the identification of a unified failure criterion and also the assessment of classes of low cycle fatigue resistance for connections.	Portugal / Italy
Bernuzzi <i>et al.</i> (1996)	5 + (1)	External top and seat angle joints, with beam IPE300 attached to a rigid counter beam. (5 tests loaded cyclically and 1 test loaded monotonically).	(2) - ECCS procedure. (4) - ECCS with only 2 cycles at the same level of amplitude. (5) - ECCS with an increase of $1.5e/e_y$ in the cycles amplitude, and only 1 cycle in each amplitude. (6) - (4) but with $2.5e/e_y$.	In the first series studied the influence of load history. The second series studied the influence of the key geometrical and mechanical parameters in the cyclic performance.	Italy
Elnashai <i>et al.</i> (1998)	5	Tests on two-storey steel frames with semi-rigid joints comprising of top and seat and web angles. Beams in H250x130x9x9 and UB 254x146x31 sections and columns in H150x150x7x10 and UC 203x203x6 sections.	(1) - Based in the second-storey yield displacement (δ_y), 3 cycles were applied at each displacement of δ_y , $2\delta_y$, $4\delta_y$, $6\delta_y$, etc.	Effect of the joint stiffness and capacity on frame response. In addition, a comparison between the behaviour of frames with bolted semi-rigid and fully welded rigid joint is carried out.	UK
Shen and Astaneh-Asl (1999)	6	Bolted-angle beam-to-column joints, with W360x179 column size.	(7) - Three phases of loading history: displacement increased to 5-10 mm to 15-20 mm, then decreased to the starting displacement.	Inelastic behaviour under large cyclic deformation, failure modes and energy dissipation capacity.	USA
Kukreti and Abolmaali (1999)	12	Bolted top and seat angle steel joints with column W200x100 and beam sizes W360x64 and W410x67.	(8) - 3 cycles of 4.45 kN loops, 3 cycles of 8,9 kN loops, 3 cycles of 13.35 kN loops, 2 cycles of 17.8 kN loops.	Study of the initial stiffness, ultimate moment capacity, ultimate rotation. To derive analytical models.	USA

Authors	No. tests	Joint characterization	Load history	Main parameters investigated	Country
Calado and Mele (2000)	15 + (3)	External top, seat and web angle joints with beams in IPE300 and columns in HEB160, HEB200 and HEB240 (S235). L120x120x10 for the angles, with two rows of bolts on each leg of the flange angles.	(2) - ECCS procedure. (9) - Constant amplitude. (15 tests under cyclic loading and 3 tests under monotonic loading).	Compare the behaviour of welded and bolted joints, the effect of column size, the effect of the loading history and the accuracy of the "component method" of the Eurocode 3 Annex J.	Portugal
Abolmaali <i>et al.</i> (2003)	20	Double web angle external joints, with bolted angles and welded-bolted angles. W410x67 beam size and W200x100 column size.	(8) - 3 cycles of 4.45 kN loops, 3 cycles of 8,9 kN loops, 3 cycles of 13.35 kN loops, 2 cycles of 17.8 kN loops.	Moment-rotation hysteresis loops and the failure modes.	USA
Calado (2003)	1	External top, seat and web angle joints with beam IPE300 and column HEB200.	(2) - ECCS procedure.	Cyclic behaviour, modes of failure.	Portugal
Komuro <i>et al.</i> (2003)	3	External top, seat and web angle joints with H400x200x13x8, L150x100x12 and L90x90x7. Pre-loaded F10T high strength bolts with 20 mm diameter.	(10) - Lateral displacement corresponding to the relative rotation of $\pm 1, 2, 5, 10, 20, 30, 40, 60, 80$ mrad.	Dynamic characteristics of semi-rigid connections: Initial connection stiffness; ultimate moment capacity and pinching phenomenon.	Japan
Leon <i>et al.</i> (2004)	2	Top, web and seat angle external joints with W460x60 beam size and W360x216 column size.	(11) - Full reversal cycles at 0.1, 0.25, 0.50, 0.75, 1.0, 1.5, 2.0 and 3.0% interstorey drifts.	Strength, stiffness and rotation capacity.	USA
Yang and Kim (2007b)	4	A single-storey and bay steel frame with connections: top-seat angle (L75x75x6) and double web angle (L50x50x6). 12mm bolts. Column H-125x125x6.5x9, and beam H-250x125x6x9, in SS400.	(12) - SAC procedure.	Investigation of cyclic behaviour; failure modes of each connection; and the capacity of the high-strength bolted angle connections compared with the fully welded counterpart.	Korea
Yang and Kim (2007a)	2	Three external joints, with similar geometry to the previous tests, were compared. One top-seat-double web angles, one double web angle and one welded.	(12) - SAC procedure.	Experimental investigation on the cyclic behaviour of the steel sub-assemblages with fully welded and high-strength bolted joints with angles.	Korea

2.3.2.2 END-PLATE JOINTS CONFIGURATION

As in the previous section in Table 2.10 are summarized 23 research projects, 203 tests and 14 different load protocols, however in this case for steel end-plate bolted joints also loaded cyclically.

Table 2.10: End-plate steel joints.

Authors	No. tests	Joint characterization	Load history	Main parameters investigated	Country
Tsai and Popov (1990)	3	3 external extended end-plate connections were tested (of the 19 in Tsai (1988)). One was modified to accommodate rib stiffeners in the end-plate. Two beam sections: W18x40 and W21x44, and two thicknesses dimensions 1(3/8) and 1(1/4).	Cyclic moments were generated in the test specimens by applying increasing cyclic forces or displacements at the end of the cantilever.	Test the end-plate joint properties under severe cyclic loading. Deal with the premature fracture of one of the inner bolts in typical joints. Assess the improvements of using rib stiffeners in the end-plate and stronger bolts.	USA
Korol <i>et al.</i> (1990)	7	External extended end-plate joints, with or without several stiffeners, as such transverse column web stiffeners, additional column web plates and end-plate rib stiffeners. Beams in W360x45 and W360x57, and columns in W360x64 and W360x79. In this study, the column stub was rigidly fixed to the testing frame.	(13) - 4 cycles in the elastic range, with $\Delta_y/2$, then 2 cycles with Δ_y . For subsequent loading cycles, the beam tip displacement was incrementally increased by $\Delta_y/2$ up to $4\Delta_y$. If no failure was detected two additional cycles were applied: one at $5\Delta_y$ and another at $6\Delta_y$.	Seismic performance in terms of strength, stiffness, energy dissipation, and ductility. Influence of end-plate thickness, bolt pre-tension forces, column flange slenderness and column flange stiffeners.	Canada
Ghobarah <i>et al.</i> (1992)	4	External double extended end-plate joints, with several stiffeners arrangement in the end-plate and in the column web panel. Beams in W360x57 and W410x60, and columns in W360x64 and W310x129.	(14) - N=2000kN applied to the column. 12-14 cycles: 2 cycles in the elastic range, then 2 cycles with Δ_y . For the next 10 cycles, the displacements were increased by $\Delta_y/2$ for each cycle.	Investigate the performance of the sub-assemblages and their individual components in terms of stiffness, strength, ductility, and energy dissipation capacity.	Canada
Plumier and Schleich (1993)	4	Two external joints and two internal joints, combining columns in sections HEB300 and beams in section HEA260.	(2) - ECCS procedure.	Contribution of the shear panel in the energy dissipation. Study the strength and rotation capacity of the joint.	Belgium
Pradhan and Bouwkamp (1994)	-	High-strength bolted joints. Beams in HEA260 and columns in HEB300. Some tests are with beam and column filled-in reinforce concrete.	-	Interactive yielding of the beam-end and column shear web panel, shear panel thickness and contribution of the concrete.	UK
Calado and Castiglioni (1996)	3	Extended end-plate joints. Columns and Beams in HEA120 (Fe360), M16 (8.8) bolts preloaded, according to EC3 provisions, at 224Nm of torque. All welds were full penetration butt welds.	(3) - In the elastic range: 4 cycles with $0.5v_y$, $1.5v_y$ and $2v_y$. In the plastic range: total amplitudes comprised between 5 and $12v_y$, v_y is the yield displacement.	Develop a cumulative damage model, the identification of a unified failure criterion and also the assessment of classes of low cycle fatigue resistance for connections.	Portugal / Italy

Authors	No. tests	Joint characterization	Load history	Main parameters investigated	Country
Bernuzzi <i>et al.</i> (1996)	9 + (1)	External flush and extended end-plate joints, with beam IPE300 attached to a rigid counter beam.	(2) - ECCS procedure. (9 tests under cyclic loading and 1 test under monotonic loading).	Studied the influence of load history and the key geometrical and mechanical parameters in the cyclic performance.	Italy
Adey (1997) and Adey <i>et al.</i> (1998)	15	Extended end-plate moment joints with several beam sections: 3 joints with W360x51 (S); 7 joints with W460x97; and 5 joints with W610x125. For the columns: W310x118 (S) and for the rest W310x143. The thicknesses of the end-plates ranging from 13 to 19mm. Several configurations of stiffeners were used.	(15) -Applied Technology Council Guidelines for Testing of Components of Steel Structures (ATC-24, 1992).	Effect of the beam size, bolt layout, use of transverse web stiffeners, end-plate thickness and rib stiffeners and welding techniques. Twelve specimens were designed to fail by the end-plate, and three were designed to fail by the beam and end-plate.	Switzerland / Canada
Plumier <i>et al.</i> (1998)	4	External extended end-plate moment joints, with beam IPE450 attached to a rigid column HEB300. (4 tests with end-plate in 16 tests performed).	(16) - Constant amplitude loading history in the plastic range, after a few cycles in the elastic range.	Development of a cumulative damage model for assessing the performance of structural components under arbitrary loading histories and evaluating the effects of inelastic cycles on a limit state of acceptable behaviour.	Belgium
Boorse (1999)	7	Flush end-plate connections, using built up sections. Bolts in A325 and for the plates A572 Gr50 steel were used.	(12) SAC protocol. (15) - ATC-24 (1992).	Study the inelastic rotation capability of flush end-plate moment connections.	USA
Ryan (1999)	7	Extended stiffened and unstiffened end-plate connections, using built up sections. Bolts in A325 and for the plates A572 Gr50 steel were used.	(12) - SAC procedure.	Find the rotational capacity for the three end-plate configuration under cyclic loading.	USA
Ádány <i>et al.</i> (2001)	6	Extended end-plate representing a column-base joint. Rigid counter-beam retained to the rigid base, connected to the columns in HEA200 and a welded section (S235). Two external bolt rows were considered and several end-plate thicknesses. Bolts M16 (8.8).	(4) - ECCS with only 2 cycles at the same level of amplitude.	Provide information on the joint behaviour, namely: end-plate, bolts, beam/column and the interaction of these elements. The concrete behaviour is not within the scope of this study. It is also intended to calibrate the numerical models.	Portugal

Authors	No. tests	Joint characterization	Load history	Main parameters investigated	Country
Yorgun and Bayramoğlu (2001)	4	Bolted fabricated beam-to-column end-plate joints. (110x195) for beam and (160x135) column sizes.	(2) - ECCS procedure.	Effect of the gap between the end-plate and the column flange on the cyclic performance of the joint.	Turkey
Dubina <i>et al.</i> (2000) Dubina <i>et al.</i> (2001)	8 + (2)	Bolted with extended end-plate beam (IPE360) to column (HEB300) internal joints	(2) - ECCS procedure. (8 tests under cyclic loading and 2 tests under monotonic loading).	Evaluate the performance of internal node joints. The main parameters considered are: Initial stiffness, moment capacity and plastic rotation capacity.	Romania
Broderick and Thomson (2002)	6 + (2)	Flush end-plate steel external joints. UC 203x203x86 column sizes, 254x102x22UB and 254x146x37 UB beam sizes.	(2) - ECCS procedure. (6 tests under cyclic loading and 2 tests under monotonic loading).	Stiffness, moment capacity, rotation capacity and hysteretic behaviour.	Ireland
Bursi <i>et al.</i> (2002)	18	Bolted extended end-plate beam-to-column external joints. IPE300 beams size, HEA180, HEB180 and HEA280 columns sizes.	(2) - ECCS procedure.	Joint geometry and loading history.	Italy
Sumner and Murray (2002) Sumner (2003)	10 + (9)	Four different beam-to-column combinations were used: W24x68, W30x99 and W36x160 for beams, and W14x120, W14x257, W14x193 and W14x257 for columns. 6 unstiffened end-plate connections and 4 stiffened end-plate connections.	(12) - SAC procedure. (10 tests under cyclic loading and 9 tests under monotonic loading).	Investigate the strength and inelastic rotation capacity of the connection assemblies and to determine if extended end-plate moment connections were suitable for use in seismic force resisting moment frames.	USA
Dunai <i>et al.</i> (2004)	19	End-plate joints with or without encased column in HEA200 or welded. Changing the end-plate thickness, class and bolt diameters.	(2) - ECCS procedure.	Study and characterise the typical cyclic behaviour failure modes of this type of joints.	Hungary / Portugal
Guo <i>et al.</i> (2006)	6	Extended end-plate joints. The length of beam and column were 1600 and 1800 mm, respectively. Eight high-strength bolts M20, grade 10.9 were used, fully tightened up to 155 kN. All materials, except bolts, were from Q235. Beam I200x150x6x10, column H200x200x12x18.	(17) - Axial force in the column of 20% of the yield load. 2 cycles of load with 10 kN, increments were applied until the specimen reached the yielding point. After that the displacement was incremented at the yield displacement recorded, e_y .	Compare the hysteretic behaviour, stiffness, and strength of stiffened and unstiffened extended end-plate connections of beam-to-column joints.	China

Authors	No. tests	Joint characterization	Load history	Main parameters investigated	Country
Shi <i>et al.</i> (2007)	8	External extended and flush end-plate connection. Welded I-shaped cross-section beam (300x200x8x12) and column (300x250x8x12), end-plate thickness 12mm. Steel grade Q345 and bolts grade 10.9.	(18) - JGJ 101-96. Specification for building seismic testing method (1996).	End-plate thickness, bolt diameter, end-plate extended stiffener, column stiffener, type of flush and extended end-plate.	China
Nogueiro <i>et al.</i> (2006) Nogueiro (2009)	9 + (4)	External end-plate joints, with transverse web column stiffeners. End-plates, 18 mm thick. Hand tightened, full-threaded M24, 10.9 grades were employed in all joints. All the material is steel grade S355. 7 Beams in IPE 360 and HEA280, columns in HEA 320 and HEB 320. (9 tests under cyclic loading and 4 tests under monotonic loading).	(19) - θ_y is the yield rotation. In the elastic range: $(\theta_y \times 6)/4$; $2(\theta_y \times 6)/4$; $3(\theta_y \times 6)/4$, with $\theta_y \times 6$ (20) - $(\theta_y \times 3)/4$; $2(\theta_y \times 3)/4$; $3(\theta_y \times 3)/4$ with $\theta_y \times 3$ for 20 cycles then $\theta_y \times 3 + 2.5$ for 20 cycles and so on.	Set the bases for pre-qualification beam-column connections suitable for the European practice. Like in the American codes.	Portugal
Iannone <i>et al.</i> (2011)	2	External end-plate joints using HEB200 (S355) for the columns and IPE270 (S275) for the beams, and bolts M20 (10.9): Partial strength extended end-plate joints governed by the panel zone or by the end-plate.	(21) - AISC provisions.	Investigate the extension of the component approach to cyclic loading. For that it is intended to evaluate the overall energy dissipated by the some of the energy dissipation of the single joint components.	Italy
Landolfo (2016) Landolfo <i>et al.</i> (2017)	44 + (4)	16 unstiffened + 16 stiffened external extended end-plate joints and 6 unstiffened + 6 stiffened internal extended end-plate joints. With IPE360, IPE450 and IPE600 for the beams, and HEB280, HEB340, HEB5000 and HEB650 for the columns.	(22) - AISC provisions (23) - Alternative EQUALJOINTS cyclic protocol. (44 tests under cyclic loading and 4 tests under monotonic loading).	The EQUALJOINTS research project aims to provide pre-qualification criteria of a set of selected seismic resistant steel beam-to-column joints.	Belgium

2.3.3 ORGANIZATION AND DATA PROCESSING

2.3.3.1 RELEVANT PROPERTIES IN ANALYSIS

In order to make adequate use of the collected test data, it is necessary to choose the tests that best fit the needs of the adopted methodology for the assessment of the partial-strength joints characterisation, and consequently lead to justifiable outcome in this research.

Firstly, it was important to determine the relevant properties in the tested specimens, so that they could be properly grouped.

The main properties of the collected tests that are relevant to this study are:

- Initial stiffness (K_0) - it is important to know the elastic stiffness of the joint since this is a key parameter to ensure adequate behaviour of a MRF structure when subject to seismic loads and other horizontal loads, such as wind.
- Strength ($M_{max}/M_{pl,Rd,b}$) - as stated before, strength is an important factor to take into account in the design of a connection because its relation with ductility is crucial for a good connection behaviour under seismic actions.
- Rotation capacity (θ_u) - this is an important property associated to the dissipative elements in an MRF; it is necessary to ensure that connections have sufficient rotational capacity in order to withstand the acceptable demands without collapse.
- Ductility (e_u/e_y or θ_u/θ_y) - this property represents the capacity of the connection for dissipating energy and for sustaining plastic deformations. Hence, it is an important factor to take into account in the selection of connections.

By focusing these properties, it was possible to determine the most suitable joints based on the following comparisons.

2.3.3.2 STIFFNESS COMPARISON

In order to compare the test results, a beam span L_b of $6m$ was assumed and the Young's modulus was taken equal to $210GPa$. Figure 2.42 and Table 2.11 show the stiffness of the joints tested and also the EC3-1-8 limits for the joints classification as rigid or pinned. It is important to mention that the original test codes used in the research projects were kept here.

This classification is as follows:

$$\text{Rigid: } S_{j,ini} \geq 25 EI_b / L_b$$

$$\text{Pinned: } S_{j,ini} \leq 0.5 EI_b / L_b$$

It is possible to see that the majority of the joints analysed exhibited a semi-rigid nature based on their initial stiffness.

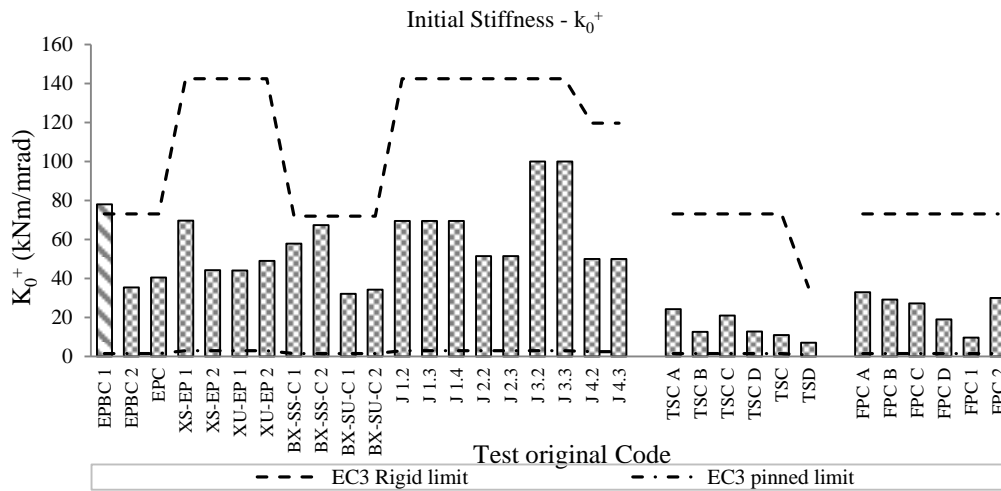


Figure 2.42: Initial stiffness comparison.

Table 2.11: Initial stiffness comparison.

Test code	Author	Typology	K_0^+ (kNm/mrad)	Classif.
EPBC 1	Bernuzzi <i>et al.</i> (1996)	Extended End-plate	78.00	Rigid
EPBC 2	Bernuzzi <i>et al.</i> (1996)	Extended End-plate	35.40	Semi-rigid
EPC	Bernuzzi <i>et al.</i> (1996)	Extended End-plate One Side	40.50	Semi-rigid
XS-EP 1	Dubina <i>et al.</i> (2001)	Extended End-plate	69.54	Semi-rigid
XS-EP 2	Dubina <i>et al.</i> (2001)	Extended End-plate	44.21	Semi-rigid
XU-EP 1	Dubina <i>et al.</i> (2001)	Extended End-plate	44.08	Semi-rigid
XU-EP 2	Dubina <i>et al.</i> (2001)	Extended End-plate	49.00	Semi-rigid
BX-SS-C 1	Dubina <i>et al.</i> (2000)	Extended End-plate	57.76	Semi-rigid
BX-SS-C 2	Dubina <i>et al.</i> (2000)	Extended End-plate	67.37	Semi-rigid
BX-SU-C 1	Dubina <i>et al.</i> (2000)	Extended End-plate	32.08	Semi-rigid
BX-SU-C 2	Dubina <i>et al.</i> (2000)	Extended End-plate	34.18	Semi-rigid
J 1.2	Nogueiro (2009)	Extended End-plate	69.50	Semi-rigid
J 1.3	Nogueiro (2009)	Extended End-plate	69.50	Semi-rigid
J 1.4	Nogueiro (2009)	Extended End-plate	69.50	Semi-rigid
J 2.2	Nogueiro (2009)	Extended End-plate	51.50	Semi-rigid
J 2.3	Nogueiro (2009)	Extended End-plate	51.50	Semi-rigid
J 3.2	Nogueiro (2009)	Extended End-plate	100.00	Semi-rigid
J 3.3	Nogueiro (2009)	Extended End-plate	100.00	Semi-rigid
J 4.2	Nogueiro (2009)	Extended End-plate	50.00	Semi-rigid
J 4.3	Nogueiro (2009)	Extended End-plate	50.00	Semi-rigid
TSC A	Bernuzzi <i>et al.</i> (1996)	Top and Seat Angles	24.20	Semi-rigid
TSC B	Bernuzzi <i>et al.</i> (1996)	Top and Seat Angles	12.50	Semi-rigid
TSC C	Bernuzzi <i>et al.</i> (1996)	Top and Seat Angles	21.00	Semi-rigid
TSC D	Bernuzzi <i>et al.</i> (1996)	Top and Seat Angles	12.80	Semi-rigid
TSC	Bernuzzi <i>et al.</i> (1996)	Top and Seat	11.00	Semi-rigid
TSD	Yang and Kim (2007a)	Top and Seat Angles	6.98	Semi-rigid
FPC A	Bernuzzi <i>et al.</i> (1996)	Flush End-plate	32.90	Semi-rigid
FPC B	Bernuzzi <i>et al.</i> (1996)	Flush End-plate	29.20	Semi-rigid
FPC C	Bernuzzi <i>et al.</i> (1996)	Flush End-plate	27.10	Semi-rigid
FPC D	Bernuzzi <i>et al.</i> (1996)	Flush End-plate	19.00	Semi-rigid
FPC 1	Bernuzzi <i>et al.</i> (1996)	Flush End-plate	9.70	Semi-rigid
FPC 2	Bernuzzi <i>et al.</i> (1996)	Flush End-plate	30.00	Semi-rigid

2.3.3.3 STRENGTH COMPARISON

Figure 2.43 show a comparison of the envelope of maximum bending moments for the positive branches of the moment-rotation response. Figure 2.44 is depicted the same comparison for the negative branches. The EC3-1-8 limits for the full-strength and pinned classification are also depicted in the charts. In addition, it is also depicted a reference line for a proposed minimum strength of 70% of the beam strength needed for a joint be able to fulfil the seismic design requirements of a medium-rise building i.e. the 0.7 to 1.0 range considered for the strength ratio was deemed to be acceptable in regions of moderate to high seismicity. Table 2.12 shows the detail results.

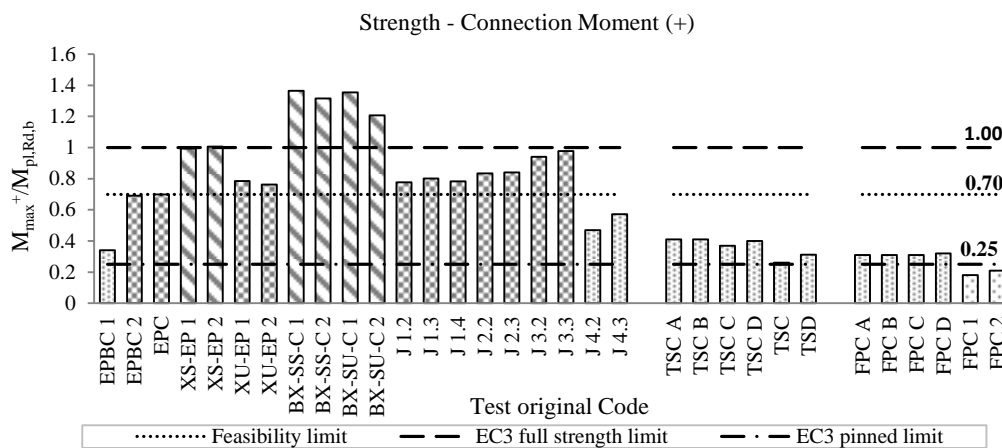


Figure 2.43: Strength comparison for the envelope maximum positive moments achieved.

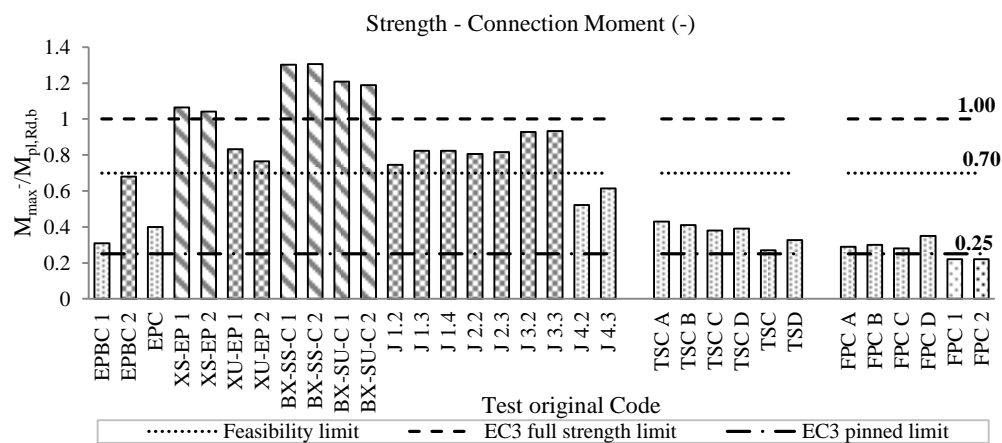


Figure 2.44: Strength comparison for the envelope maximum negative moments achieved.

There are only nine joints that fulfil the imposed requirements.

Table 2.12: Strength comparison for the envelope maximum moments achieved.

Test ID	Author	Typology	$M_{max}^+/M_{pl,Rd,b}$	$M_{max}^-/M_{pl,Rd,b}$
XS-EP 1	Dubina <i>et al.</i> (2001)	Extended End-plate	0.99	1.06
XS-EP 2	Dubina <i>et al.</i> (2001)	Extended End-plate	1.01	1.04
BX-SS-C 1	Dubina <i>et al.</i> (2000)	Extended End-plate	1.36	1.30
BX-SS-C 2	Dubina <i>et al.</i> (2000)	Extended End-plate	1.32	1.31
BX-SU-C 1	Dubina <i>et al.</i> (2000)	Extended End-plate	1.35	1.21
BX-SU-C 2	Dubina <i>et al.</i> (2000)	Extended End-plate	1.21	1.19
EPBC 2	Bernuzzi <i>et al.</i> (1996)	Extended End-plate	0.69	0.68
XU-EP 1	Dubina <i>et al.</i> (2001)	Extended End-plate	0.78	0.83
XU-EP 2	Dubina <i>et al.</i> (2001)	Extended End-plate	0.76	0.76
J 1.2	Nogueiro (2009)	Extended End-plate	0.78	0.75
J 1.3	Nogueiro (2009)	Extended End-plate	0.80	0.82
J 1.4	Nogueiro (2009)	Extended End-plate	0.78	0.82
J 2.2	Nogueiro (2009)	Extended End-plate	0.83	0.80
J 2.3	Nogueiro (2009)	Extended End-plate	0.84	0.82
J 3.2	Nogueiro (2009)	Extended End-plate	0.94	0.93
J 3.3	Nogueiro (2009)	Extended End-plate	0.98	0.93
EPBC 1	Bernuzzi <i>et al.</i> (1996)	Extended End-plate	0.34	0.31
EPC	Bernuzzi <i>et al.</i> (1996)	Extended End-plate One Side	0.70	0.40
J 4.2	Nogueiro (2009)	Extended End-plate	0.47	0.52
J 4.3	Nogueiro (2009)	Extended End-plate	0.57	0.61
TSC A	Bernuzzi <i>et al.</i> (1996)	Top and Seat Angles	0.41	0.43
TSC B	Bernuzzi <i>et al.</i> (1996)	Top and Seat Angles	0.41	0.41
TSC C	Bernuzzi <i>et al.</i> (1996)	Top and Seat Angles	0.37	0.38
TSC D	Bernuzzi <i>et al.</i> (1996)	Top and Seat Angles	0.40	0.39
TSC	Bernuzzi <i>et al.</i> (1996)	Top and Seat	0.26	0.27
TSD	Yang and Kim (2007b)	Top and Seat Angles	0.31	0.33
FPC A	Bernuzzi <i>et al.</i> (1996)	Flush End-plate	0.31	0.29
FPC B	Bernuzzi <i>et al.</i> (1996)	Flush End-plate	0.31	0.30
FPC C	Bernuzzi <i>et al.</i> (1996)	Flush End-plate	0.31	0.28
FPC D	Bernuzzi <i>et al.</i> (1996)	Flush End-plate	0.32	0.35
FPC 1	Bernuzzi <i>et al.</i> (1996)	Flush End-plate	0.18	0.22
FPC 2	Bernuzzi <i>et al.</i> (1996)	Flush End-plate	0.21	0.22

2.3.3.4 ROTATION CAPACITY COMPARISON

A comparison of the rotational capacity can be seen in Figure 2.45 for the positive branches of the moment-rotation response, in Figure 2.46 for the negative branches of the moment-rotation response and in detail in Table 2.13. Also shown in the charts are the 25 *mrad* and 35 *mrad* which correspond to the minimum limits required in EC8 [CEN, 2004] for medium and high ductility connections, respectively.

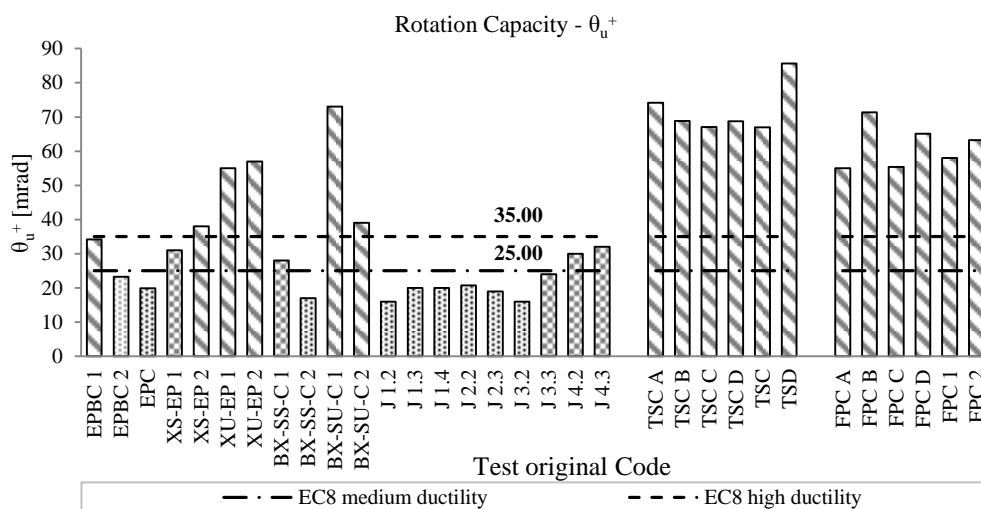


Figure 2.45: Rotation comparison for the positive envelope.

As expected, the joints with the highest rotation capacities are also the ones that achieved the lowest values of strength. A balance between these two properties is always needed to be able to fulfil the codes requirements in seismic regions.

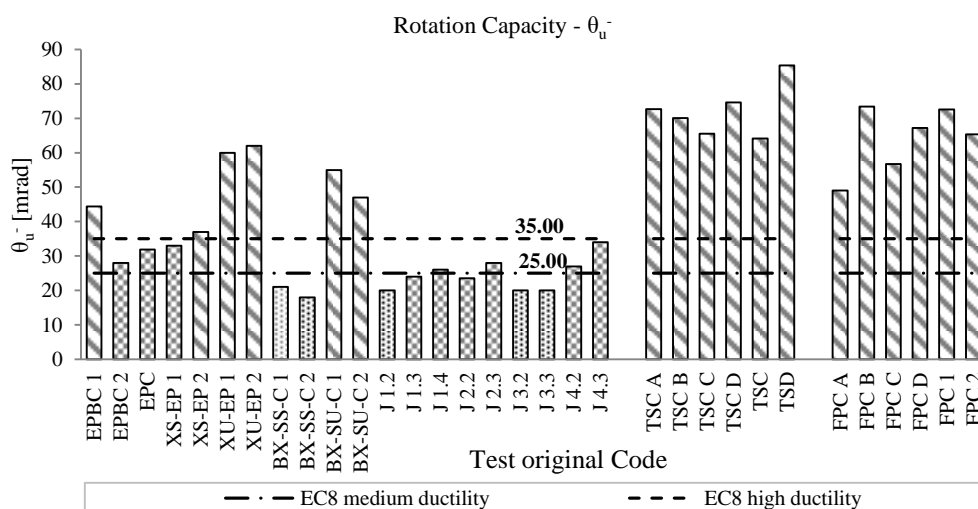


Figure 2.46: Rotation comparison for the negative envelope.

Table 2.13: Rotation comparison.

Test ID	Author	Typology	θ_u^+ (mrad)	θ_u^- (mrad)
EPBC 1	Bernuzzi <i>et al.</i> (1996)	Extended End-plate	34.20	44.40
XS-EP 2	Dubina <i>et al.</i> (2001)	Extended End-plate	38.00	37.00
XU-EP 1	Dubina <i>et al.</i> (2001)	Extended End-plate	55.00	60.00
XU-EP 2	Dubina <i>et al.</i> (2001)	Extended End-plate	57.00	62.00
BX-SU-C 1	Dubina <i>et al.</i> (2000)	Extended End-plate	73.00	55.00
BX-SU-C 2	Dubina <i>et al.</i> (2000)	Extended End-plate	39.00	47.00
TSC A	Bernuzzi <i>et al.</i> (1996)	Top and Seat Angles	74.20	72.70
TSC B	Bernuzzi <i>et al.</i> (1996)	Top and Seat Angles	68.80	70.10

Test ID	Author	Typology	θ_u^+ (mrad)	θ_u^- (mrad)
TSC C	Bernuzzi <i>et al.</i> (1996)	Top and Seat Angles	67.10	65.50
TSC D	Bernuzzi <i>et al.</i> (1996)	Top and Seat Angles	68.70	74.60
TSC	Bernuzzi <i>et al.</i> (1996)	Top and Seat	67.00	64.10
TSD	Yang & Kim [2007b]	Top and Seat Angles	85.60	85.40
FPC A	Bernuzzi <i>et al.</i> (1996)	Flush End-plate	55.00	49.00
FPC B	Bernuzzi <i>et al.</i> (1996)	Flush End-plate	71.40	73.40
FPC C	Bernuzzi <i>et al.</i> (1996)	Flush End-plate	55.40	56.70
FPC D	Bernuzzi <i>et al.</i> (1996)	Flush End-plate	65.10	67.20
FPC 1	Bernuzzi <i>et al.</i> (1996)	Flush End-plate	58.00	72.60
FPC 2	Bernuzzi <i>et al.</i> (1996)	Flush End-plate	63.20	65.30
XS-EP 1	Dubina <i>et al.</i> (2001)	Extended End-plate	31.00	33.00
J 4.2	Nogueiro (2009)	Extended End-plate	30.00	27.00
J 4.3	Nogueiro (2009)	Extended End-plate	32.00	34.00
EPBC 2	Bernuzzi <i>et al.</i> (1996)	Extended End-plate	23.30	28.00
EPC	Bernuzzi <i>et al.</i> (1996)	Extended End-plate One Side	19.90	31.90
BX-SS-C 1	Dubina <i>et al.</i> (2000)	Extended End-plate	28.00	21.00
BX-SS-C 2	Dubina <i>et al.</i> (2000)	Extended End-plate	17.00	18.00
J 1.2	Nogueiro (2009)	Extended End-plate	16.00	20.00
J 1.3	Nogueiro (2009)	Extended End-plate	20.00	24.00
J 1.4	Nogueiro (2009)	Extended End-plate	20.00	26.00
J 2.2	Nogueiro (2009)	Extended End-plate	20.78	23.50
J 2.3	Nogueiro (2009)	Extended End-plate	19.00	28.00
J 3.2	Nogueiro (2009)	Extended End-plate	16.00	20.00
J 3.3	Nogueiro (2009)	Extended End-plate	24.00	20.00

2.3.3.5 CONNECTION DUCTILITY

The ductility of a connection can be evaluated in different ways and it is inherent that different authors report ductility using different calculation approaches. Figure 2.47 and Table 2.14 show the different ductility demands achieved for the different connections. Although a direct comparison cannot be made, it allows visualising the evolution of the ductility in the various groups.

The ductility demands represented in the figure were obtained directly from the cyclic tests, and this corresponds to the ratio between the maximum displacement/rotation and the elastic displacement/rotation, with an exception for the darker bars where the ductility demands were obtained from the monotonic tests according to the same ratio.

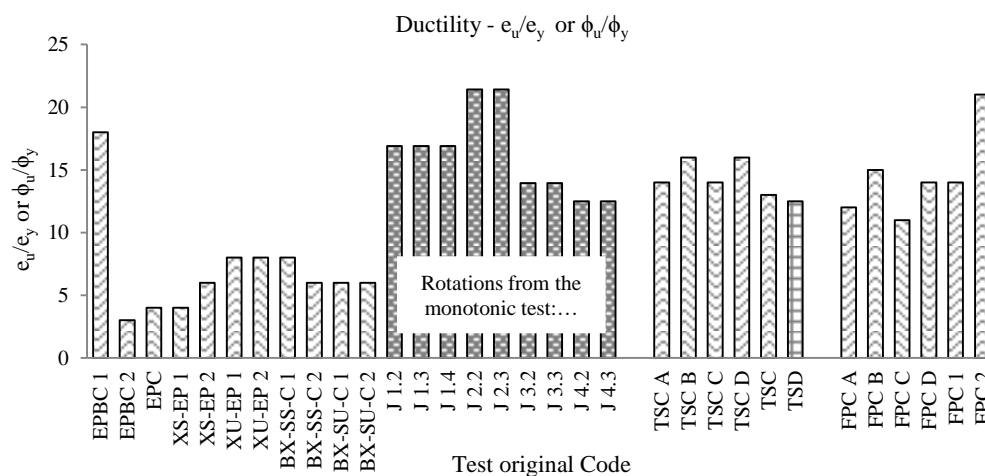


Figure 2.47: Ductility capacity.

Table 2.14: Ductility capacity

Test ID	Author	Typology	e_u/e_y or θ_u/θ_y
EPBC 1	Bernuzzi <i>et al.</i> (1996)	Extended End-plate	18.00
EPBC 2	Bernuzzi <i>et al.</i> (1996)	Extended End-plate	3.00
EPC	Bernuzzi <i>et al.</i> (1996)	Extended End-plate One Side	4.00
XS-EP 1	Dubina <i>et al.</i> (2001)	Extended End-plate	4.00
XS-EP 2	Dubina <i>et al.</i> (2001)	Extended End-plate	6.00
XU-EP 1	Dubina <i>et al.</i> (2001)	Extended End-plate	8.00
XU-EP 2	Dubina <i>et al.</i> (2001)	Extended End-plate	8.00
BX-SS-C 1	Dubina <i>et al.</i> (2000)	Extended End-plate	8.00
BX-SS-C 2	Dubina <i>et al.</i> (2000)	Extended End-plate	6.00
BX-SU-C 1	Dubina <i>et al.</i> (2000)	Extended End-plate	6.00
BX-SU-C 2	Dubina <i>et al.</i> (2000)	Extended End-plate	6.00
J 1.2	Nogueiro (2009)	Extended End-plate	16.90
J 1.3	Nogueiro (2009)	Extended End-plate	16.90
J 1.4	Nogueiro (2009)	Extended End-plate	16.90
J 2.2	Nogueiro (2009)	Extended End-plate	21.42
J 2.3	Nogueiro (2009)	Extended End-plate	21.42
J 3.2	Nogueiro (2009)	Extended End-plate	13.95
J 3.3	Nogueiro (2009)	Extended End-plate	13.95
J 4.2	Nogueiro (2009)	Extended End-plate	12.50
J 4.3	Nogueiro (2009)	Extended End-plate	12.50
TSC A	Bernuzzi <i>et al.</i> (1996)	Top and Seat Angles	14.00
TSC B	Bernuzzi <i>et al.</i> (1996)	Top and Seat Angles	16.00
TSC C	Bernuzzi <i>et al.</i> (1996)	Top and Seat Angles	14.00
TSC D	Bernuzzi <i>et al.</i> (1996)	Top and Seat Angles	16.00
TSC	Bernuzzi <i>et al.</i> (1996)	Top and Seat	13.00
TSD	Yang and Kim (2007b)	Top and Seat Angles	12.50
FPC A	Bernuzzi <i>et al.</i> (1996)	Flush End-plate	12.00
FPC B	Bernuzzi <i>et al.</i> (1996)	Flush End-plate	15.00
FPC C	Bernuzzi <i>et al.</i> (1996)	Flush End-plate	11.00
FPC D	Bernuzzi <i>et al.</i> (1996)	Flush End-plate	14.00
FPC 1	Bernuzzi <i>et al.</i> (1996)	Flush End-plate	14.00
FPC 2	Bernuzzi <i>et al.</i> (1996)	Flush End-plate	21.00

2.3.3.6 SUMMARY AND RATING OF THE EXAMINED JOINTS

From the above comparisons, it is possible to state that there are clearly a wide range of behaviours for the different connection typologies examined, with the extended end-plates being the ones that exhibited improved properties to be used in steel moment resisting frames of medium to high-rise buildings. For that reason, in the subsequent studies only the extended end-plate joints will be addressed.

In order to choose the most feasible joints to validate and subsequently calibrate the numerical models, a binary classification was assigned for each one of the tests analysed according to their performance, where 1 represented the joint behaviour achieving the imposed criteria and 0 if not, and these are shown in Table 2.15. It is highlighted in the table that the connections which presented the best classification are those that are most suitable for the validation of the FE models.

Table 2.15: Joints ranking table.

Test ID	Author	K_0^+	$M_{\text{max}}^+/M_{\text{pl,Rd,b}}$	$M_{\text{max}}^-/M_{\text{pl,Rd,b}}$	θ_u^+	θ_u^-	e_u/e_y	Sum
EPBC 1	Bernuzzi <i>et al.</i> (1996)	1	0	0	1	1	1	4
EPBC 2	Bernuzzi <i>et al.</i> (1996)	0	1	1	0	1	0	3
EPC	Bernuzzi <i>et al.</i> (1996)	1	1	0	0	1	0	3
XS-EP 1	Dubina <i>et al.</i> (2001)	0	0	1	1	1	0	3
XS-EP 2	Dubina <i>et al.</i> (2001)	0	0	1	1	1	0	3
XU-EP 1	Dubina <i>et al.</i> (2001)	0	1	1	1	1	0	4
XU-EP 2	Dubina <i>et al.</i> (2001)	0	1	1	1	1	0	4
BX-SS-C 1	Dubina <i>et al.</i> (2000)	1	0	0	1	0	0	2
BX-SS-C 2	Dubina <i>et al.</i> (2000)	1	0	0	0	0	0	1
BX-SU-C 1	Dubina <i>et al.</i> (2000)	0	0	0	1	1	0	2
BX-SU-C 2	Dubina <i>et al.</i> (2000)	0	0	0	1	1	0	2
J 1.2	Nogueiro (2009)	0	1	1	0	0	1	3
J 1.3	Nogueiro (2009)	0	1	1	0	1	1	4
J 1.4	Nogueiro (2009)	0	1	1	0	1	1	4
J 2.2	Nogueiro (2009)	0	1	1	0	1	1	4
J 2.3	Nogueiro (2009)	0	1	1	0	1	1	4
J 3.2	Nogueiro (2009)	1	1	1	0	0	1	4
J 3.3	Nogueiro (2009)	1	1	1	1	0	1	5
J 4.2	Nogueiro (2009)	0	0	0	1	1	1	3
J 4.3	Nogueiro (2009)	0	0	0	1	1	1	3

2.4 OVERVIEW OF SEISMIC DESIGN METHODS

2.4.1 GENERAL

Seismic design codes have already evolved over four generations. Since the first ones with basic instructions, in which the design of the structure were based on the application of a uniform accelerations of $0.1g$. Passing through the second generation codes that had already included the amplification effects due to dynamic behaviour of the structure and the energy dissipation, although this last concept had been introduced in an elementary form. Nowadays we have the third generation codes that accounts already with the energy dissipation of the structure according to the lateral bracing system used and the different structural materials. This generation of codes already accounts also with the interactions with other domains like geotechnical aspects. Moreover, for verification of safety, these rules considers the semi-probabilistic approach, as defined in Eurocode (EN 1990, 2002). The fourth generation codes are now being developed with the appearance of the performance-based and displacement-based seismic analysis methods, like the Direct Displacement-Based seismic Design (DDBD) proposed by Priestley *et al.* (2007), reviewed in detail further ahead. The performance requirement will allow a better damage control by controlling the energy dissipated during a seismic event. EC8 (EN 1998-1, 2004) can be considered an intermediate code of third and fourth generation, because it is based on the third generation codes but already includes fundamental requirements and damage limitation of the fourth generation codes (Elghazouli, 2009, chap.1).

Next is performed a review of the evolution of the DDBD methodology and the recent developments are analysed. In the end, the DDBD methodology will be reviewed, with a greater focus on the way the energy dissipation is approached through the equivalent viscous damping, which will be object of study, later on, in this thesis.

2.4.2 DIRECT DISPLACEMENT-BASED DESIGN PROCEDURE

2.4.2.1 EVOLUTION AND RECENT DEVELOPMENTS

In current seismic codes ductile structures are allowed to develop plastic deformations in order to dissipate energy, aiming to mitigate forces to which the structure is subjected and,

consequently, allowing for a more economical structural design, particularly in regions of high seismicity. Notwithstanding, there has been a growing acknowledgement by the scientific community that, in ductile structures, structural and non-structural damages are related with deformations and displacements (Villaverde, 2004; Filiatrault and Sullivan, 2014). Hence, there is a need for the development of new or improved design procedures based on displacements that, coupled with performance-based requirements, allow for the economical and rational seismic design of structures. Existing displacement-based procedures are normally based on the structure's stiffness and the energy dissipated during the event for a predefined performance level, normally related to the building importance class. It is therefore important to have some key features that relate the displacements, ductility and energy dissipation, as inputs for the procedures. Several procedures were proposed in the last decades that try to enforce performance-based requirements through the implementation of displacement based design philosophy. Sullivan *et al.* (2003) studied the most relevant procedures, concluding that all have limitations and potential for improvement. The authors referred the direct displacement-based seismic design procedure (DDBD), proposed by Priestley *et al.* (2007) as the most adequate for the design of regular structures due to its most complete set of recommendations. The DDBD procedure is based on the substitute structure approach proposed by Gulkan and Sozen (1974). The procedure has several aspects in common with the Capacity Spectrum Method (CSM) that was proposed by Freeman (1978; 1998) for the seismic assessment of existing buildings. Both the CSM and the DDBD procedures are commonly designated by secant stiffness methods as they resort to the use of the equivalent linearization technique and to damping-equivalent viscous damping relationships. In DDBD, the effective period, T_e , at maximum response is determined and using the equivalent linearization technique an equivalent SDOF structure, with the same elastic period, is determined. The structure stiffness, K_e , and consequently the required strength, for the design, at the target displacement are determined, using the equivalent viscous damping to account for the inelastic behaviour. Recent studies by Sullivan *et al.* (2012) proposed a more refined approach in the consideration of the equivalent viscous damping (EVD) for each storey in which the storey damping values are then combined to obtain the global system damping. The DDBD procedure significantly evolved throughout the years, as the result of several research projects.

In the beginning of the 1990's performance-based methodologies began to be disseminated mainly for reinforced concrete structures and masonry structures (Paulay and Priestley, 1992). because the detected problems associated to force-based seismic design were particularly evident for this kind of structures, mainly due to the choice of the appropriate member stiffness, gross (uncracked section) or reduced sections (cracked section). As mentioned above, Force-based methods are essentially based on the concept of elastic stiffness which, for concrete or masonry buildings, raises an additional problem, since after the first incursion in the inelastic response, the stiffness may observe a severe reduction. This situation raises important questions related to the procedures that should be adopted for the estimation of structural deformations caused by a seismic event, since the widely used equal displacement rule, which depends on a reliable estimation of the elastic period of the structure, is only applicable to systems with stable inelastic behaviour. Performance-based methodologies were later extended to bridges (Priestley *et al.*, 1996), and only recently have been applied to steel structures. Some authors focused on steel concentrically braced frames (Della Corte and Mazzolani, 2008; Sullivan and Goggins, 2009; Della Corte, *et al.*, 2010; Wijesundara *et al.*, 2011; Salawdeh, 2012; Grande and Rasulo, 2013) whereas Sullivan (2013) and O'Reilly and Sullivan (2016) addressed the design of eccentrically braced frames. The design of steel moment-resisting frames have been studied by Sullivan *et al.* (2011), Sullivan and O'Reilly (2014), Nievas and Sullivan (2015) and, more recently, by Roldán *et al.* (2016). Dual systems have been the subject of study by Maley *et al.* (2010) and Garcia *et al.* (2010). It should be noted that the design displacement profiles for steel moment-resisting frames (Priestley *et al.*, 2007), were derived based on results obtained for reinforced concrete frames. Moreover, the current guidelines were developed for steel MRFs structures featuring stable hysteretic behaviour, which can be characterised by a Ramberg- Osgood model.

2.4.2.2 OVERVIEW OF THE DIRECT DISPLACEMENT-BASED DESIGN PROCEDURE

The basic formulation of the displacement-based seismic design of structures (DDBD), proposed by Priestley *et al.* (2007), is illustrated with reference to Figure 2.48 where the first step is to reduce the frame structure to a SDOF representation, Figure 2.48 (a). Note that, in this way, the method can be applied to all structural types. A lateral force, representing the forces in the building, is then applied to the SDOF representation and the response is registered in a

force-displacement diagram, Figure 2.48 (b). The nonlinear response is then translated by a simpler bi-linear envelop, defined by the initial stiffness K_i and the post yield stiffness rK_i , this representation allows the assessment of the elastic limit Δ_y necessary to determine the displacement ductility μ . Unlike the force-based seismic design the DDBD characterizes the structure by secant stiffness K_e at maximum displacement Δ_d , instead of the initial stiffness K_i , see Figure 2.48 (b). To consider the combination of elastic damping and the hysteretic energy absorbed during inelastic response, a level of equivalent viscous damping ξ_{eq} is considered taking into account the structure ductility and typology, Figure 2.48 (c). With the maximum displacement and the damping estimated from the expected ductility, for the effective height H_e , the effective period T_e can be determined from a set of displacement spectra for different levels of damping, Figure 2.48 (d). For that is required a modification factor, R_ξ , which is a function of the EVD, to take into account the inelastic displacement associated with the effective period. To determine the effective stiffness K_e and the design lateral force, which is also the design base shear force V_{Base} for the SDOF structure the following expressions are used:

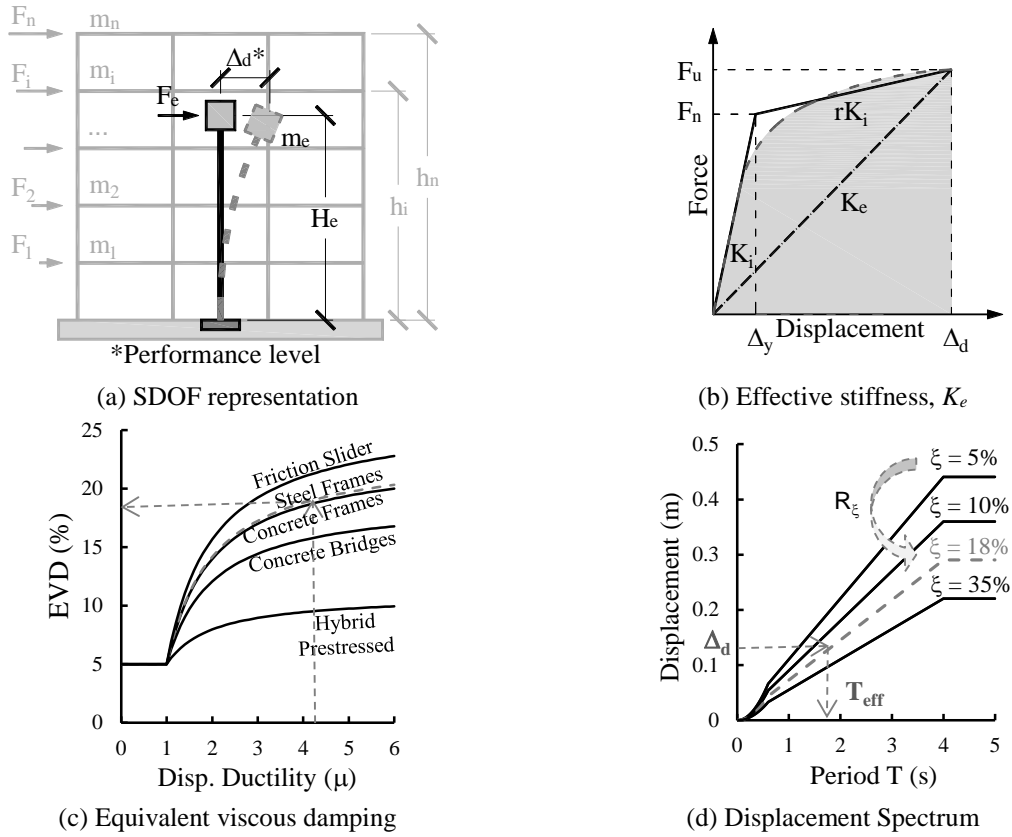
$$K_e = \frac{4\pi^2 m_e}{T_e^2} \quad (2.44)$$

$$F_e = V_{Base} = K_e \Delta_d \quad (2.45)$$

The base shear force is then distributed as design forces to the various discretised masses of the multi degree of freedom structure, in order the moments for potential plastic hinges can be established. The base shear is then distributed in proportion to mass and displacement at discretized mass locations according to Eq. (2.46).

$$F_i = V_{base} \frac{m_i \Delta_i}{\sum_{i=1}^n m_i \Delta_i} \quad (2.46)$$

It is also worth mentioning how to define the SDOF representation of the frame, this is perhaps the most complex part of the entire process, because it lies principally in the identification of the design displacement profile, Δ_i . The characteristics of the SDOF system are obtained by the following relationships:

Figure 2.48: Fundamentals of DDBD (Priestley *et al.*, 2007).

$$\Delta_d = \frac{\sum_{i=1}^n m_i \Delta_i^2}{\sum_{i=1}^n m_i \Delta_i} \quad (2.47)$$

$$m_e = \frac{\sum_{i=1}^n m_i \Delta_i}{\Delta_d} \quad (2.48)$$

$$H_e = \frac{\sum_{i=1}^n m_i \Delta_i h_i}{\sum_{i=1}^n m_i \Delta_i} \quad (2.49)$$

where Δ_i is the design displacement, m_i and m_e are the seismic mass and h_i is the height of level i .

2.4.2.3 DUCTILITY-EQUIVALENT VISCOUS DAMPING RELATIONSHIPS FOR DISPLACEMENT BASED DESIGN PROCEDURES

The equivalent viscous damping (EVD), ξ_{eq} , consists of the elastic viscous damping, ξ_{el} , and the damping associated with the energy dissipated (hysteretic damping ξ_{hyst}) during the inelastic response, given by:

$$\xi_{eq} = \xi_{el} + \xi_{hyst} \quad (2.50)$$

where the hysteretic damping, ξ_{hyst} , depends on the hysteresis characteristics of the structure. The elastic viscous damping, ξ_{el} , represents the energy dissipated by internal friction within the material particles, and is commonly employed in engineering practice to account also for all sources of energy dissipation prior to the development of significant plastic deformations, such as that associated with the behaviour of non-structural elements and/or secondary structural elements attached to the main structure.

The DDBD procedure uses the EVD to account for the energy dissipated during the inelastic response of the structure, when subjected to a seismic event. It was in the earlier 30's that Jacobsen (1930) proposed the concept of equivalent viscous damping to represent the inelastic energy dissipated as an equivalent viscous damping ratio. This concept was based in the approximation of a steady state solution of a nonlinear SDOF system by a linear system with EVD, comparing the energy dissipated by the nonlinear system to the energy dissipated by one cycle of sinusoidal response of that linear system. Three decades later, Rosenblueth and Herrera (1964) introduced the concept of equivalent linear system to characterize the non-linear response, using the effective period at maximum response and an equivalent viscous damping ratio. In that approach, the nonlinear system was treated as quasilinear, and the equivalent stiffness was defined under the condition that the corresponding load deformation relation of the linear system, under static loading, passed through the extreme points of the nonlinear response. As highlighted by Dwairi *et al.* (2007), the DDBD procedure also adopted this concept due to its simplicity, the single dependency of the equivalent damping on the hysteretic shape and the familiarity of practitioners with elastic spectra seismic design. Blandon and Priestley (2005) proposed a modification to the equations obtained using the Jacobsen's approach by making them dependent of the effective period.

The most recent developments in the field of the equivalent viscous damping were made during the development of the DDBD procedure (Priestley *et al.*, 2007; Sullivan, *et al.*, 2012), and were based on three independent studies Grant *et al.* (2005), Dwairi *et al.* (2007) and Pennucci *et al.* (2011). In all studies, the calibration of the EVD for different hysteresis rules was obtained matching the peak displacement of inelastic time-history analyses to the displacement obtained with the equivalent structure responding according to the predefined

hysteresis rules and the calibrated EVD. Nevertheless, the studies followed different methodologies to derive the values of EVD in terms of hysteretic rules used and the type (real or artificial) and number of the accelerograms. The first study, carried out by Grant *et al.* (2005), used a range of six hysteresis rules (Elasto-Plastic, Bi-linear with hardening parameter of $r=0.2$, Takeda “thin”, Takeda “fat”, Ramberg-Osgood and Flag-Shape), each one associated with a type of structural behaviour and five artificial accelerograms compatible with a given target spectrum. The results of elastic and inelastic analyses were separately averaged and compared, changing the EVD until the responses matched. In the study conducted by Dwairi *et al.* (2007), presented as an extensive evaluation of Jacobsen’s damping approach (Jacobsen, 1930) combined with the secant stiffness method, a large number of real earthquake accelerograms (100 ground motion records) were used, and only four hysteresis rules (Ring-Spring, Large Takeda, Small Takeda and Elasto-plastic). Successive NLTH analyses were undertaken for each individual record, ductility level, effective period and hysteresis rule separately. The authors concluded that, on average, the EVD is overestimated and consequently, the displacement is underestimated for intermediate and long period structures. It was also evident that, on average, the EVD was largely underestimated for short effective periods, particularly for periods lower than 0.4 seconds. The scatter observed was between 20% and 40% for intermediate and long periods. In that study, the proposed expressions for the EVD have the form of Eq. (2.51), where the coefficient C depends on the hysteretic shape and is a constant for effective periods (T_e) greater or equal to 1s. However for shorter periods ($T_e < 1.0s$) EVD is presented as a function of the effective period itself (see Eq. (2.52)), which complicates the direct design of the structure. Nevertheless, Priestley *et al.* (2007), did not consider this scenario and adopted Eq. (2.51) in the context of the DDBD procedure, arguing that the vast majority of the structures will have effective periods greater than 1s and hence, the adoption of an expression independent of the effective period will generally be adequate, and even conservative if a period lower than 1 second is achieved as a low estimate of damping will be obtained.

$$\xi_{eq} = \xi_{el} + C \left(\frac{\mu - 1}{\mu \pi} \right) \quad (2.51)$$

$$\xi_{eq} = \xi_{el} + (c + d(1 - T_e)) \left(\frac{\mu - 1}{\mu \pi} \right) \quad \text{for } T_e < 1.0s \quad (2.52)$$

On the other hand, Grant *et al.* (2005) used a more complex formulation to represent the hysteretic component of the EVD, see Eq. (2.53). Note that in this case Grant *et al.* (2005) proposed a correction factor for the elastic damping value based on whether initial-stiffness damping or tangent-stiffness damping was adopted in the time-history analyses, to ensure compatibility between the “real” and “substitute” structures.

$$\xi_{hyst} = a \left(1 - \frac{1}{\mu^b} \right) \left(1 + \frac{1}{(T_e + c)^d} \right) \quad (2.53)$$

In spite of the differences, the two studies arrived at very similar results, with important differences only observed for the elasto-plastic hysteretic behaviour. The average of the two studies was adopted by Priestley *et al.* (2007) to generate the EVD design curves, which, for the sake of simplicity, followed the form of Eq. (2.51). For steel moment-resisting frame buildings, assuming the Ramberg-Osgood hysteresis rule, and setting the tangent-stiffness elastic damping to 5% ($\xi_{el}=0.05$) the calibrated constant C was proposed to be equal to 0.577, without effective period restrictions. On the other hand, some pinching effect and deterioration of strength and stiffness is often observed in partial-strength end-plate joints. In these conditions the Ramberg-Osgood hysteresis rule is clearly not applicable. For that reason, it is also necessary to take into account other EVD equations derived based on hysteresis rules which are able to account for the pinching effect, like the Takeda-Fat (TF) or even the Takeda-Thin (TT), for which the calibrated constant C was proposed to be equal to 0.565 and 0.444, respectively. Note that the initial elastic damping in the nonlinear system is added directly to the hysteretic damping, as Priestley *et al.* (2007) preferred to calibrate the Eq. (2.51) coefficients C since that the elastic damping ξ_{el} remain equal to 5% in the proposed expressions. In this way, the expressions cannot be altered for different elastic damping coefficients.

Pennucci *et al.* (2011) replicated the analyses of Grant *et al.* (2005) and Dwairi *et al.* (2007), and also ran additional non-linear time history analyses with a new set of real records. They found that the calibration of the EVD is considerably affected by the type of accelerogram (real or artificial) and also by the spectral shape. According to Pennucci *et al.* (2011), the differences in the two previous studies were not detected, because the differences in the spectral shape and the accelerogram type lead to identical equivalent viscous damping results.

Due to the fact that the DDBD procedure uses the effective period for the representation of the structural response, a modification factor is required to be applied to the displacement response spectrum to account for ductile response (Priestley *et al.*, 2007).

The recent developments in the DDBD approach, namely the latest model code (Sullivan, *et al.*, 2012) suggest that in order to take the effects of the energy dissipation and/or non-linear structural response into account, the displacement spectrum should be reduced by a modification factor, R_ξ , which is a function of the EVD. This way, the EVD represents a simplified means of identifying the inelastic displacement spectra associated with the effective period.

It is therefore important to have a robust damping modifier R_ξ to be applied to the elastic spectrum for different levels of damping. The problem is that there have been some uncertainties in this area, where there are several expressions presented thus far, like the EC8 expression presented earlier (EN 1998-1, 1994), which is given by:

$$R_\xi = (0.07/(0.02 + \xi))^{0.5} \geq 0.7 \quad (2.54)$$

where ξ is a ratio of the elastic critical damping. In the 2003 revision of EC8, this expression was replaced by:

$$R_\xi = (0.1/(0.05 + \xi))^{0.5} \geq 0.55 \quad (2.55)$$

Newmark and Hall (1982) proposed a different expression, which is given below.

$$R_\xi = (1.31 - 0.19 \ln(100\xi)) \quad (2.56)$$

However, this expression revealed to be very conservative in comparison with that proposed in EC8. Priestley (2003) proposed another expression, based on limited data, for sites where forward directivity velocity pulse characteristics might be expected (Eq. (2.57)) and it is similar to the expression of EC8 (EN 1998-1, 1994) but with a change of power from 0.5 to 0.25 in this case, as shown below.

$$R_\xi = (0.07/(0.02 + \xi))^{0.25} \quad (2.57)$$

Recent studies, through numerous NLTH analyses, such as that conducted by Pennucci *et al.* (2011), revealed that for structures responding in the inelastic range, the use of expressions that relate directly the ductility and inelastic reduction factor, which essentially bypasses the

EVD expression step, leads to an improvement in the displacement estimates. Pennucci *et al.* (2011) also studied how the inelastic displacement reduction factor, defined by the ratio between the inelastic displacement (Δ_{in}) and the elastic displacement for the same effective period ($\Delta_{el,Te}$), according to Eq. (2.58), is affected by the spectral shape and response spectra sensitivity to damping.

$$\eta = \frac{\Delta_{in}}{\Delta_{el,Te}} \quad (2.58)$$

This displacement reduction factor (η) represents the same ratio that should be obtained using, for example, Eq. (2.51) in to Eq. (2.54) as part of the DDBD process. Pennucci *et al.* (2011) found that this factor appears to be independent of the record type. As a consequence, these findings seem to imply that the EVD expressions should be used with the spectral damping reduction expression that best characterize the records used in the NLTH analyses used in the assessment of the those EVD expressions.

2.4.3 EUROCODE 8 RECOMMENDATIONS FOR THE DESIGN OF STEEL JOINTS

2.4.3.1 DESIGN CRITERIA FOR MOMENT-RESISTING FRAMES

As mentioned earlier, the current codes of practice allow for plastic hinges to occur in specific locations of the structure of the lateral resisting system, in order to dissipate energy and provide a more economical and rational design. In the particular case of EC8 (EN 1998-1, 2004), for moment-resisting frames, plastic hinges are allowed to develop in the beams or in the beam-to-column joints. The plastic hinges in the columns are not allowed, except in the base of the frame, at the top level of multi-storey buildings and for single storey buildings. In either case, plastic hinges on the beams or in the beam-to-column connections, columns should always be capacity designed to be stronger.

This design philosophy intends that a beam-sway mechanism develops and hence that a soft storey is prevented. This implies that the structure possess adequate ductility, in order to obtain the hierarchy of resistance of the various structural components, necessary for ensuring the intended configuration of plastic hinges and for avoiding brittle failure modes. In this situation, columns should verify the condition of Eq. (2.59) for all combination of efforts. In

that condition, E_{Ed} represents the design effort in the column, $E_{Ed,G}$ is the effort in the column due to the non-seismic actions included in the combination of actions for the seismic design situation, $E_{Ed,E}$ is the effort in the column due to the design seismic action, γ_{ov} is the overstrength factor, Ω is a coefficient determined as the minimum ratio between the plastic strength and the design effort of the dissipative elements under seismic design situation. The safety coefficient 1.1 ensures that the plastic hinges occur in the foreseen locations. The overstrength factor γ_{ov} is a coefficient based on statistics of yield stresses characterizing steel products, and it intends to transform the lower bound nominal yield stress f_y to a upper bound value, which may vary with the steel manufacturer, because to assign a steel grade to an element only the lower bound properties are required.

$$E_{Ed} = E_{Ed,G} + 1.1\gamma_{ov}\Omega E_{Ed,E} \quad (2.59)$$

In accordance with clause 4.4.2.3(3) of the EC8 (EN 1998-1, 1994) for frame buildings with two or more storeys, the following condition should be satisfied at all joints of primary or secondary seismic beams with primary seismic columns:

$$\sum M_{Rc} \geq 1.3 \sum M_{Rb} \quad (2.60)$$

where $\sum M_{Rc}$ is the sum of the design values of the moments of resistance of the columns framing the joint. The minimum value of column moments of resistance within the range of column axial forces produced by the seismic design situation should be used in Eq. (2.60); and $\sum M_{Rb}$ is the sum of the design values of the moments of resistance of the beams framing the joint. When partial-strength connections are used, the moments of resistance of these connections are taken into account in the calculation of $\sum M_{Rb}$.

2.4.3.2 NON DISSIPATIVE BEAM-TO-COLUMN STEEL JOINTS

If the structure is designed to dissipate energy in the beams, the beam-to-column joints should be designed for the required degree of overstrength to prevent them from damage. For that, and according to EC8 (EN 1998-1, 1994) clause 6.5.5(3), the following expression should be satisfied:

$$R_d \geq 1.1\gamma_{ov}R_{fy} \quad (2.61)$$

were R_d is the resistance of the joint in accordance with EC3 (EN 1993-1-8, 2005), R_{fy} is the plastic resistance of the connected dissipative member based on the design yield stress of the material as defined in EC3 (EN 1993-1-1, 2005) and γ_{ov} is the overstrength factor, as defined previously.

2.4.3.3 DISSIPATIVE BEAM-TO-COLUMN STEEL JOINTS

In the case of dissipative joints the structure should be designed with semi-rigid and/or partial-strength joints. In this case the EC8 (EN 1998-1, 1994) in clause 6.6.4(2) requires that the following conditions are verified:

1. The joints have a rotation capacity consistent with the frame deformations;
2. The members connected are demonstrated to be stable at the ultimate limit state;
3. The global drift should be determined considering the effect of joint deformation, the global drift should be determined by non-linear static (pushover) global analysis or non-linear time history analysis.

Additionally, the joint design should be such that the rotation capacity of the plastic hinge region θ_p , defined by Eq. (2.62), is not less than 35 *mrad* for structures of high ductility class and 25 *mrad* for structures of medium ductility class. This rotation capacity of the plastic hinge region should be ensured under cyclic loading without degradation of strength and stiffness greater than 20%. This requirement is independent of the intended location of the dissipative zones. Note that the column elastic deformation should not be included in the evaluation of θ_p .

$$\theta_p = \delta / 0.5L_b \quad (2.62)$$

Where δ is the beam deflection at mid span, and L_b is the beam span.

Furthermore, EC8 (EN 1998-1, 1994) requires that θ_p should be determined by experiments, where the column web panel shear resistance should satisfy Eq. (2.63) and that the column web panel shear deformation should not contribute for more than 30% of the plastic rotation capability θ_p .

$$V_{wp,Ed} / V_{wp,Rd} \leq 1.0 \quad (2.63)$$

Where $V_{w,Ep}$ is the design shear force in the web panel due to the action effects and $V_{wp,Rd}$ is the shear resistance of the web panel in accordance with EC3-1-8 (EN 1993-1-8, 2005). EC8 also imposed that when partial-strength connections are used, the column capacity design should be derived from the plastic capacity of the connections.

In addition to the previous requirements, in the design rules for connections in dissipative zones, EC8 also demands that for each structural type and structural ductility class the adequacy of design should be supported by experimental evidence. Also, the resistance and ductility of the members and their connections must also be tested under cyclical loads, in order to meet the specific requirements stated above. This applies to partial and full-strength connections in or adjacent to dissipative zones. Nonetheless, experimental evidence may be based on existing data. Otherwise, tests should be performed.

3

DEVELOPMENT AND VALIDATION OF THE FINITE ELEMENT MODELS TO CHARACTERIZE THE BEHAVIOUR OF BEAM-TO-COLUMN END-PLATE JOINTS

3.1 INTRODUCTION

This chapter describes in detail the developed numerical models, in order to study and characterize the joints behaviour and its components. The options in terms of finite element will be explored and explained, sensitivity analyses will be used to support the choices. It is also explained in detail the systematization of the complete model for end-plate joints, using available programming language in order to ease the execution of large parametric studies, presented in detail later. In the end, the models will be validated and calibrated against the results of experimental data previously collected.

The main tools used in this research are the numerical models of beam-to-column end-plate steel joints, or its isolated components, subjected to cyclic loading, using the finite element method approach. The final objective of the research is the derivation of mechanical properties of several connection components, an essential requirement for the development of a component based approach to use in the context of seismic design of steel frames. The numerical modelling of the joints requires the interaction of various domains of high complexity, such as solving the complex geometry of the connections, material nonlinearity and nonlinearity in the interface between elements, mainly through the contact between the end-

plate and the column flange and the contact between bolts and end-plate or column flanges. When the cyclic behaviour is considered, new requirements have to be taken into account as recommended by Ádány and Dunai (2004) who pointed out the following:

- The model should consider the complex 2D or 3D geometry of the joint.
- The load model should represent appropriately the cyclic loading history.
- The material model should take into account the cyclic behaviour of the steel material (isotropic and kinematic hardening).
- The model should be able to represent the local buckling of the slender plate elements subjected to load reversal.
- The conditional connections between the joint components should be modelled under cyclic effects (contact-separation-re-contact).

The component method currently implemented in EC3-1-8 (EN 1993-1-8, 2005) allows for the assessment of the stiffness, strength and rotation capacity, when a joint is subjected to monotonic loading conditions. As seen above the method consists of a mechanical model based on the assemblage of a series of springs, representing the various components of the joint, each one with an associated value of stiffness and strength. This allows the determination of the joint's properties. The extension of this methodology to joints subjected to cyclic loading requires additional information regarding the characterization of each component, namely the description of the behaviour under unloading and reloading conditions, the stiffness and/or strength degradation rules, the potential for pinching, among other effects. It is therefore clear the increased complexity of the mechanical model.

Typically, the characterization of the behaviour of each component, defined by a force-deformation curve, is obtained either from experimental tests or from numerical or analytical models. In this work finite element models of T-stub components, representative of the end-plate and the column flange in bending, and detailed models of complete extended end-plate connections are developed with the objective of obtaining the behaviour of key joint components under cyclic loading. The FE models were developed with the ABAQUS (2014) software package, and were validated with experimental data available in the literature.

The experimental data survey allowed to identify the joint typologies that present the most adequate characteristics to be applied in MRF structures located in moderate to high seismic regions. In this section, some of the experimental tests will be used in the validation and also in the calibration of the FE models, in order to gain the necessary confidence in the models outputs. Double-extended end-plate bolted connections configuration were identified as the most adequate to fulfil the compromise between strength, stiffness and rotation capacity, during a seismic event. Hence, from now on, only this type of connection will be studied.

3.2 END-PLATE BEAM-TO-COLUMN JOINT MODELS WITH STIFFENED COLUMNS

3.2.1 EXPERIMENTAL TESTS USED IN THE NUMERICAL MODELS VALIDATION

3.2.1.1 GENERAL DESCRIPTION

A set of experimental tests (Nogueiro, 2009) carried out at the University of Coimbra were used to calibrate the numerical model of complete end-plate joint. The tested joints were designed aiming to study the behaviour of several external bolted beam-to-column partial-strength joint typologies with double extended end-plates. The relevant features of these tests are described in the following sections.

The experimental programme comprised thirteen external double-extended bolted end-plate joints, see Table 3.1. It is divided in four groups, whereby the column section size and/or the beam size were varied, as well as the presence of axial force in the column in J2 group, as can be observed in Table 3.1. Each group has the first test with the loading applied monotonically, and two more tests with cyclic loading, except in the first group which has one more cyclic test, with arbitrary loading. The specimens reproduced joints of a moment-resisting frame system and included transverse stiffeners in the column aligned with the beam flanges. The joint's details are illustrated in Figure 3.1 to 3.3. The configurations of the joints differ mainly in the column and beam cross-sections. For all cases, 18 mm thick end-plates were chosen, connected to the beam-ends by full strength 45° continuous fillet welds, shop welded in a down and up position. A manual metal arc welding procedure was used, with Aural Gold 70S electrodes. Hand tightened, full-threaded M24, grade 10.9, in 26 mm diameter drilled holes

were employed in all joints. The columns were 3.0 m high and the beams were approximately 1.2 m long.

The groups of tests J2 are very similar to test J1.1 except for the presence of axial force in the column, so these tests will not be characterized by a FE model.

Table 3.1: Bolted beam-to-column double extended end-plate joints test programme.

Group J1	Beam	Column	Type*	Bending	Axial
Test J1.1	IPE360	HEA320	Monotonic	M-	-
Test J1.2	IPE 360	HEA 320	Cyclic S1	M-/M+	-
Test J1.3	IPE 360	HEA 320	Cyclic S2	M-/M+	-
Test J1.4	IPE 360	HEA 320	Cyclic SA	M-/M+	-
Group J2	Beam	Column	type	Bending	Axial
Test J2.1	IPE360	HEA320	Monotonic	M-	N- (800 kN)
Test J2.2	IPE 360	HEA 320	Cyclic S1	M-/M+	N- (1200 kN)
Test J2.3	IPE 360	HEA 320	Cyclic S2	M-/M+	N- (800 kN)
Group J3	Beam	Column	type	Bending	Axial
Test J3.1	IPE360	HEB320	Monotonic	M-	-
Test J3.2	IPE 360	HEB 320	Cyclic S1	M-/M+	-
Test J3.3	IPE 360	HEB 320	Cyclic S2	M-/M+	-
Group J4	Beam	Column	type	Bending	Axial
Test J4.1	HEA280	HEA320	Monotonic	M-	-
Test J4.2	HEA 280	HEA 320	Cyclic S1	M-/M+	-
Test J4.3	HEA 280	HEA 320	Cyclic S2	M-/M+	-

See also Table 3.2

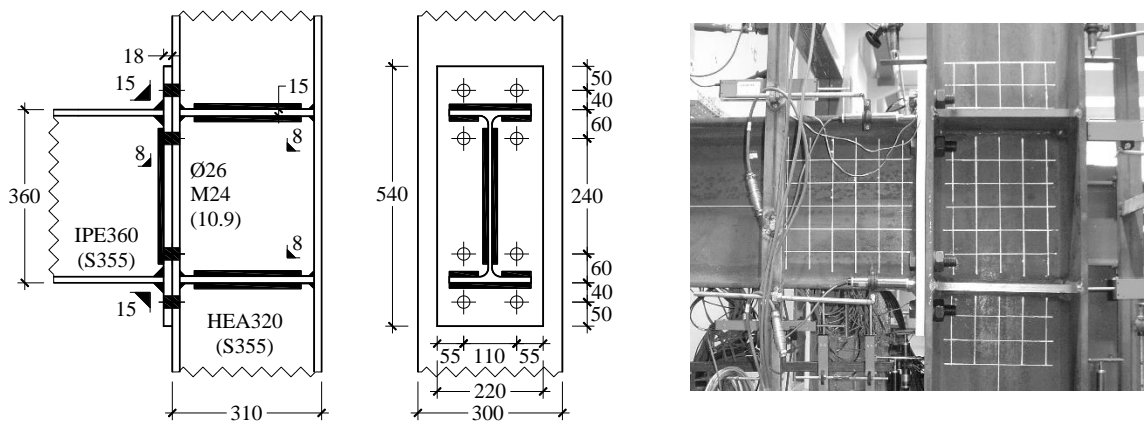


Figure 3.1: Detail of the joint for Groups 1 and 2 (dimensions in mm).

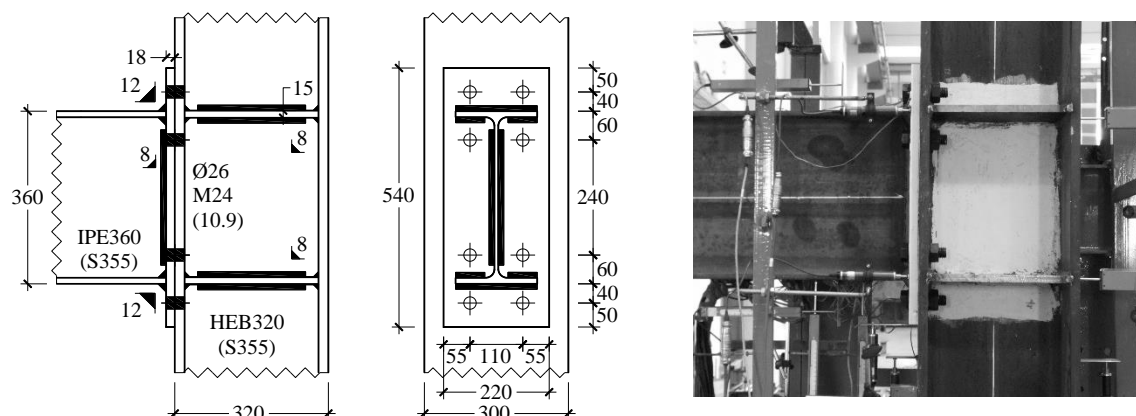


Figure 3.2: Detail of the joint for Group 3 (dimensions in *mm*).

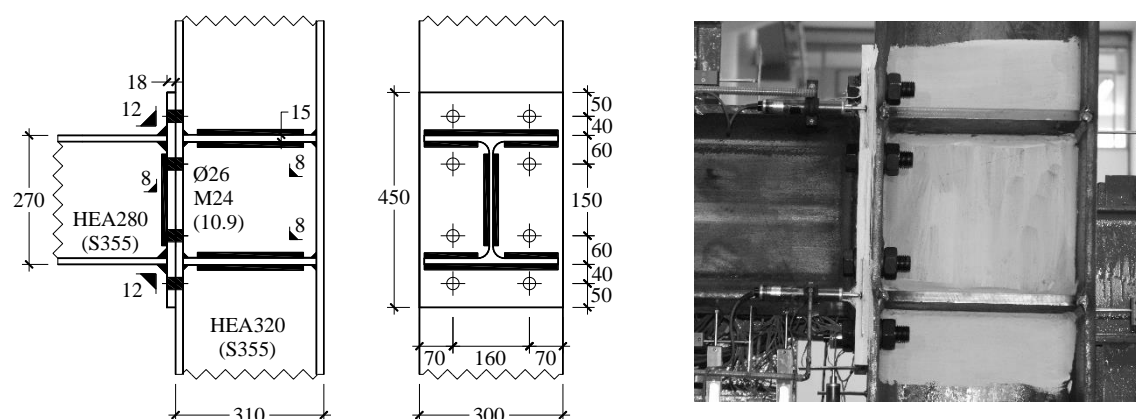


Figure 3.3: Detail of the joint for Group 4 (dimensions in *mm*).

3.2.1.2 TEST DETAIL, INSTRUMENTATION AND PROCEDURES

The loading was applied monotonically, in the first joint of each group in a displacement-controlled procedure. The loading was applied in the vertical direction, at the end of the cantilever beam by means of a 100 *ton* hydraulic actuator, as shown in Figure 3.4a). Figure 3.4b) shows the test setup for joint J-3.3 that comprised a reaction wall on the left side, a loading steel beam at the top and a steel frame on the right side anchored to the floor. The specimens were supported by a concrete block with a pinned joint at the bottom. At the top of the model the connection to the steel beam had the vertical displacement free.

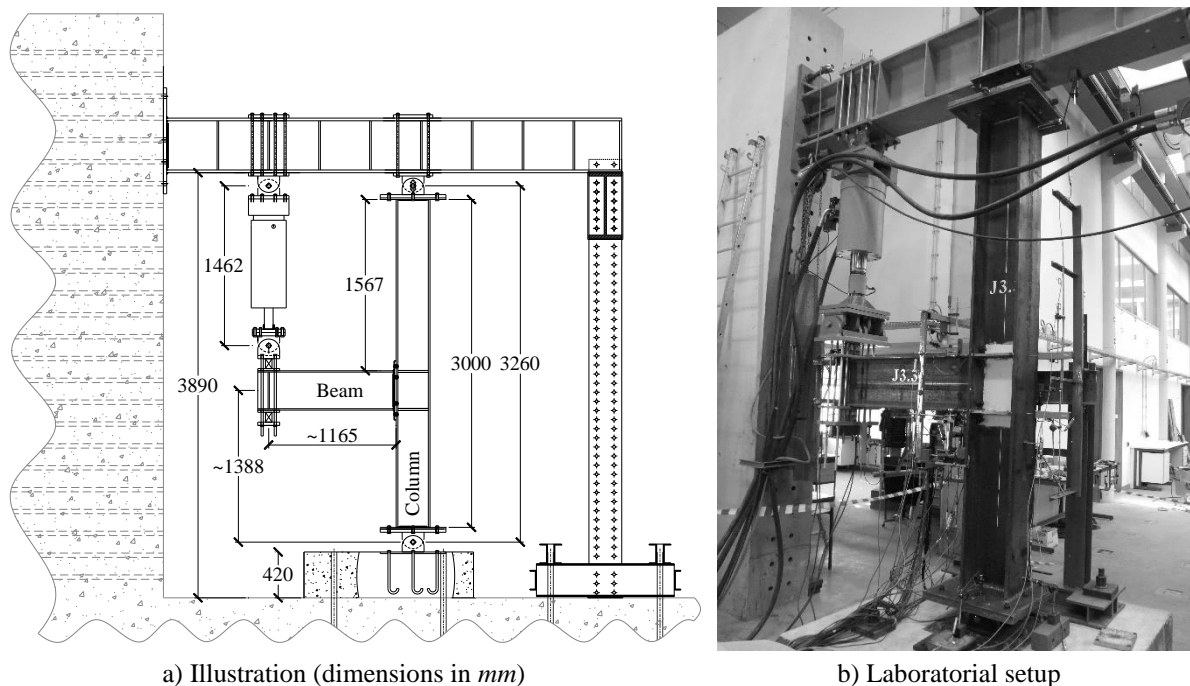


Figure 3.4: Test's setup.

Two additional tests, with two alternative cyclic loading protocols, were also performed, except in the first group where an additional cyclic test was conducted, J-1.4, with arbitrary loading (SA). The two cyclic loading strategies, are illustrated in Figure 3.5, and described in Table 3.2.

Table 3.2: Cyclic loading strategies.

Cycle	Strategy 1 (S1)	Strategy 2 (S2)
1	$0.75\theta_y$	$1.5\theta_y$
2	$1.5\theta_y$	$3.0\theta_y$
3	$2.25\theta_y$	$4.5\theta_y$
4 (and following)	$3.0\theta_y$	$6.0\theta_y$
20 (and following)	$3.0\theta_y + 2.5 * 1\text{mrad}$	$6.0\theta_y$
40 (and following, and so on)	$3.0\theta_y + 2.5 * 2\text{mrad}$	$6.0\theta_y$

The tests were carried out in displacement control, with constant speed of 0.02 mm/sec for the monotonic tests, 0.2 mm/sec for the first cyclic tests and 0.4 mm/sec for the second cyclic tests. Group 2 was tested with a constant level of axial force in the column: i) 800 kN , corresponding to 18% of the plastic axial resistance of the column; and ii) 1200 kN , corresponding to 27% of the plastic axial resistance of the column section.

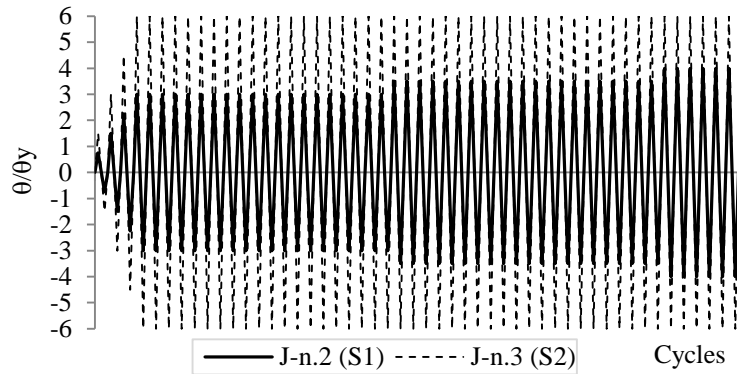


Figure 3.5: Cyclic loading strategies used in the experimental tests.

To extract the relevant test information, the sub-assemblages were instrumented according to the scheme shown in Figure 3.6. All the instrumentation and load cells were connected to a data logger and measurements were taken every 10 seconds. The displacements were measured by means of TML displacements transducers. Strain gauges TML PFL-10-11-1L, FLK-1-11 and FRA-6-11 (general use, with 2%, 3% and 3% maximum strain, respectively) were used to measure the surface deformation. The bolt deformations were measured with special TML BTM 1C strain gauges embedded in the bolt shaft, as shown in Figure 3.7.

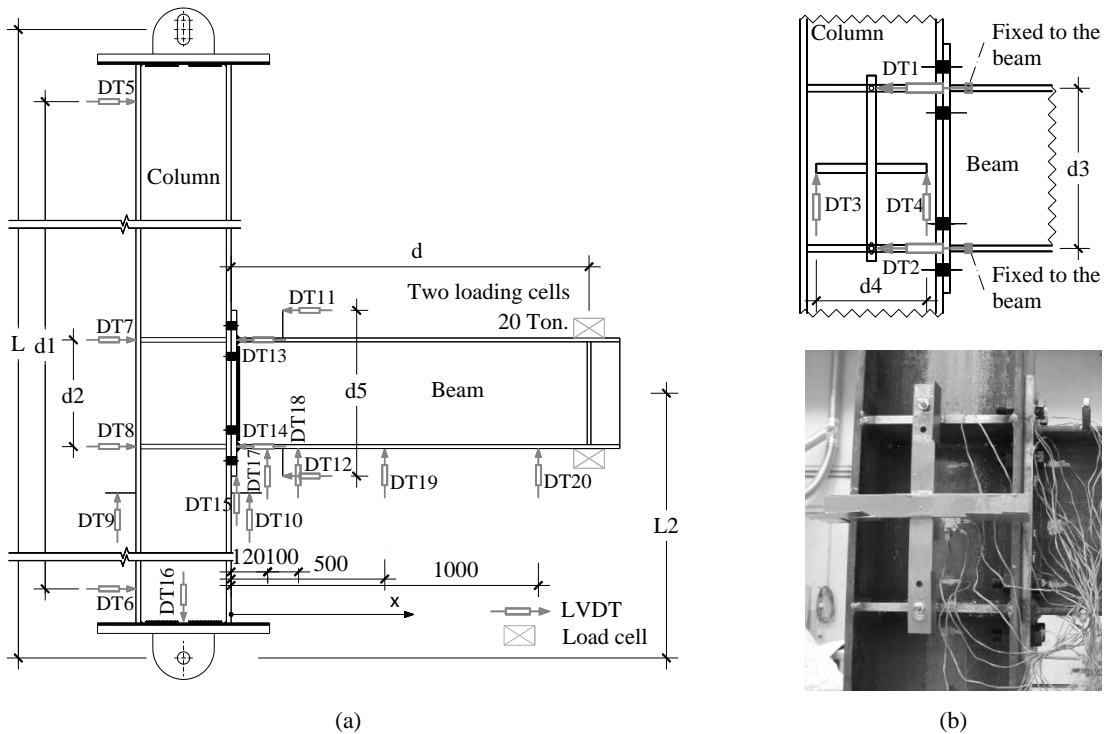


Figure 3.6: a) Instrumentation apparatus (dimensions in mm), and b) detail of the instrumentation in the column web using a crosshead.

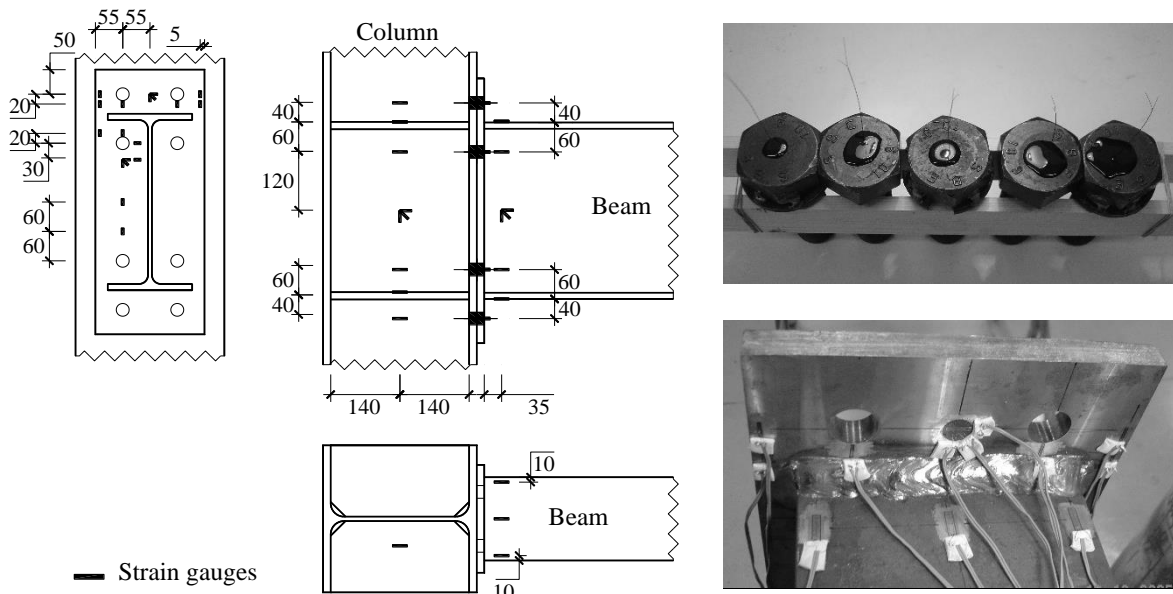


Figure 3.7: Strain gauges disposition (dimensions in *mm*).

3.2.1.3 MATERIAL PROPERTIES

The material properties were obtained from steel coupons extracted from the web and flanges of the beams and columns and also from the end-plates and were subjected to uniaxial tensile tests. Some bolts were also subjected to tensile tests until rupture occurred.

Table 3.3 and Table 3.4 reproduce the mean of the measured values of the steel mechanical properties for the steel components and the bolts. An average overstrength in the range of 10% to 30% is noted for the yield stress of the steel profiles. The real dimensions of the prototypes were also measured, without significant deviations. By observing the results of coupon tests, it is possible to state that there are considerable differences between the nominal yield stress and the actual yield stress measured. A direct consequence of this discrepancy lies in the application of the capacity design procedure, to allow only the dissipative components to sustain plastic deformation, and ensuring that non-dissipative components, or fragile components, remain in the elastic domain. In fact, EC8 (EN 1998-1, 2004) already takes into account the possibility that the actual yield strength of steel can be higher than the nominal yield strength, so an material overstrength factor γ_{ov} is defined for the capacity design checks, being the recommended value set to $\gamma_{ov} = 1.25$. Although the value ascribed to γ_{ov} can be defined by each country in its National Annex, it is common to adopt the general recommendation of the 1.25. By examining the values in Table 3.3, it is possible to conclude that the overstrength

factor is exceeded in some cases, like in the webs of the IPE360, HEA 320 and HEA280, where an overstrength of 1.26, 1.27 and 1.30 can be found, respectively.

Table 3.3: Average mechanical properties of the tested steel coupons.

Section Size	Component	Yield Stress (MPa)	Nominal yield (MPa)	Δ (%)	Young's Modulus (GPa)	Nominal value (GPa)	Δ (%)	Ultimate stress (MPa)	Nominal value (MPa)	Δ (%)
		f_{ym}	f_y		E_m	E		f_{um}	f_u	
IPE360	Flanges	430,0	355	+21,1	206,0	210	-1,9	554,2	490	+13,1
	Web	448,2	355	+26,3	213,6	210	+1,7	552,9	490	+12,8
HEB320	Flanges	393,9	355	+11,0	208,8	210	-0,6	520,7	490	+6,3
	Web	398,8	355	+12,3	216,1	210	+2,9	521,1	490	+6,3
HEA320	Flanges	414,8	355	+16,8	204,9	210	-2,5	531,4	490	+8,4
	Web	449,6	355	+26,7	207,4	210	-1,3	553,4	490	+12,9
HEA280	Flanges	439,7	355	+23,9	209,4	210	-0,3	547,7	490	+11,8
	Web	461,7	355	+30,1	210,2	210	+0,1	575,9	490	+17,5
	End-plate 220x18	405,1	355	+14,1	210,3	210	+0,1	534,0	490	+9,0
	End-plate 300x18	392,9	355	+10,7	208,4	210	-0,8	523,0	490	+6,7
	Stiffeners	286,4	235	+21,9	205,9	210	-2,0	451,8	360	+25,5

Table 3.4: Average mechanical properties of the tested bolts.

Bolt	Young's Modulus (GPa) E_m	Ultimate Stress (MPa) f_u	Ultimate strain ϵ_u
M24 (10.9)	213	1170	0,030

3.2.2 DESCRIPTION OF THE FE MODELS

Beam-to-column joints behaviour is a three dimensional problem, so in this, and in all other models present in this document, the FE models use solid three-dimensional elements, contact elements. Geometrical and material nonlinearities are also taken into account as discussed later in this thesis.

A set of models were developed according to the tests set up, using the same geometry, see Figure 3.8, Figure 3.9 and Table 3.5, using the same boundary conditions and the applied loading as in the test procedure. For each group of tests a monotonic and a cyclic loaded joint was chosen to be modelled with a finite element approach. Except for the group J2 due to the similar geometry as for the group J1. The bolts were preloaded with 20% of the ultimate bolt strength for the J1 and J3 groups. In the J4 group only a small percentage of the ultimate bolt

strength was applied because the bolts were not pre-stressed in the experimental test, whereas in the model a residual value is needed to initiate the contact between the parts. The elasto-plastic material properties were based on the mean values of the coupon tests, listed in Table 3.3 and Table 3.4.

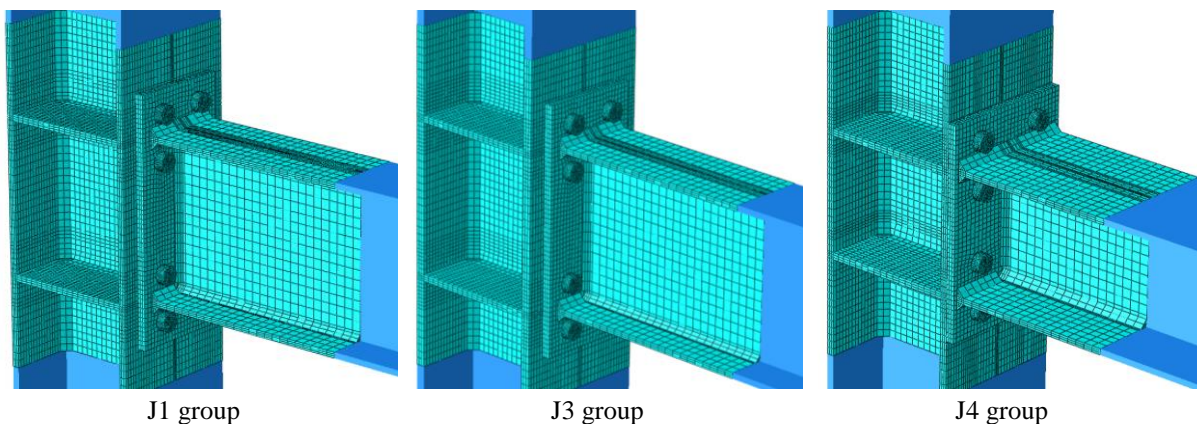


Figure 3.8: Detail view of the joint zone of the FE models used in the validation

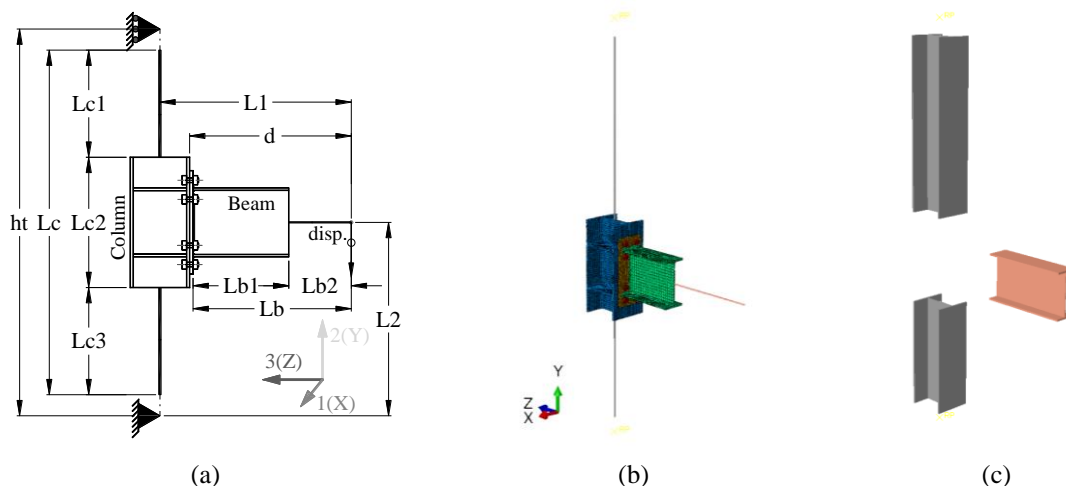


Figure 3.9: a) Geometrical properties of the FE model; b) global FE model; c) detail of the cross sections of the wire elements.

Table 3.5: Geometrical properties of the FE models.

	Column	Beam	ht (mm)	Lc (mm)	Lc1 (mm)	Lc2 (mm)	Lc3 (mm)	L1 (mm)	L2 (mm)	Lb1 (mm)	d (mm)
J1.1	HEA320	IPE360	3260	3000	1375	740	885	1322	1385	468	1166
J1.3	HEA320	IPE360	3220	3000	1395	720	885	1331	1355	467	1175
J3.1	HEB320	IPE360	3260	3040	1395	740	905	1340	1385	468	1180
J3.2	HEB320	IPE360	3260	3040	1395	740	905	1320	1385	468	1160
J4.1	HEA320	HEA280	3260	2991	1298	690	1003	1316	1483	358	1159
J4.3	HEA320	HEA280	3260	2894	1249	690	955	1329	1483	357	1173

3.2.3 NUMERICAL MODELLING AND FE OPTIONS

3.2.3.1 MODELLING OVERVIEW

The various aspects related with the development of the FE models are discussed next, such as the geometry and boundary conditions, the element types, the constraints, the interactions and the nonlinear solver. The main options adopted are explained and justified, and the models results are validated with available experimental tests results.

The numerical model developed in ABAQUS (2014) consists of sub-assemblages of a column and a beam connected to each other by means of an end-plate welded to the beam and bolted to the column flange and are representative of an external node of a moment-resisting framed structure with double-extended end-plate joints. The lengths of the beam and the column are established according to the experimental tests setup used in the validation of the FE models, and described before.

The models are composed of solid (mainly C3D8RH) finite elements in the joint region. Beam elements (B31) are used in the adjacent regions of the joint, i.e., in the beam and column segments, aiming at reducing the computational time. The technique adopted is similar to the one used in Maggi *et al.* (2005), the kinematic relations being transferred from the solid to the beam elements by multi-point constraint equations. The model and its parts are illustrated in Figure 3.10, with the corresponding adopted mesh, namely the wire columns, the wire beam, the solid column with or without stiffeners and with the bolt holes in the flange, the solid beam with the corresponding fillet welds, the end-plate with the bolt holes and the bolts composed by the shank, head and nut. The various parts interact with each other by constraints or contact interactions, to form the beam-to-column end-plate joint mechanism.

The model is prepared to deal with monotonic and cyclic loads and also dynamic excitation. In the first two cases the “loads” are applied in a displacement control bases, i.e., a displacement is imposed in the end of the cantilever formed by the beam. The applied load will depend on the intended analysis.

All of these features, and other relevant modelling approaches, for the beam-to-column end-plate bolted steel joints behaviour characterization, are analysed in more detail hereafter.

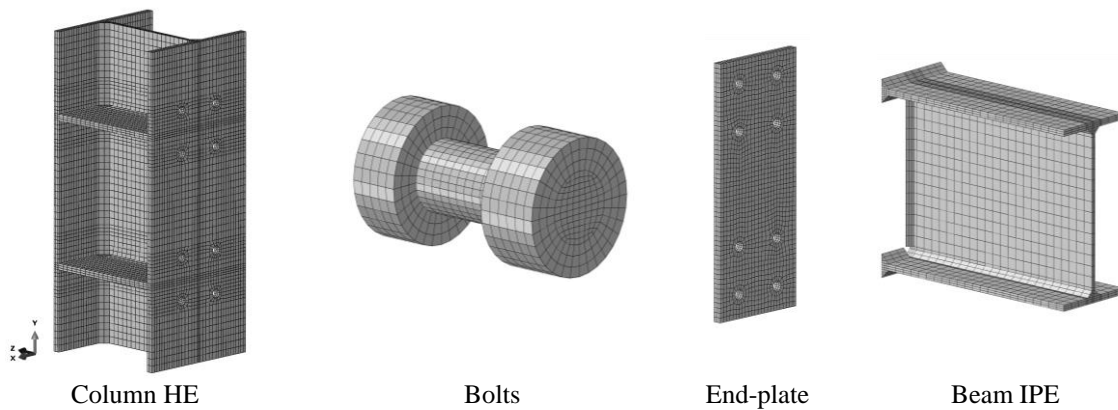


Figure 3.10: Meshed parts of the FE model.

3.2.3.2 FINITE ELEMENT OPTIONS

The software package adopted for the resolution of this highly non-linear problem was the Abaqus Unified FEA software, version 6.14 (ABAQUS, 2014). It is a generic finite element program that can be used for the calculation of a large range of problems. It can be used in a general (standard) implicit or in a dynamic explicit purpose, and also as a general-purpose computational fluid dynamics program. In this research only Abaqus/standard will be used. This product can deal with a wide range of linear and nonlinear problems involving the static, dynamic, thermal, electrical, and electromagnetic response of components. For pre-processing and post-processing the interfaces Abaqus/CAE and Abaqus/Viewer are used, respectively, with the ability for creating, submitting, monitoring, and evaluating results from Abaqus simulations.

The selection of this software was based on the large number of solutions available, like the wide range of finite element types, the available non-linear geometric and material options, the automatic or manual mesh generation and the different available numerical techniques to solve the problems. This versatility makes it one of the most complete generic software available. Moreover, its widespread use in research projects and practical applications, along with their extended benchmarks, gives us the confidence to use it. Of course, its widespread use is not a guarantee in itself, and should not dismiss the proper validation of input data and results. With that in mind, a brief description and validation of the most relevant modelling options, used in the numerical simulation of the joints, is given hereafter.

i) Element types and mesh

The solid elements used are mainly quadrilateral and hexahedra that are the standard volume elements available in ABAQUS. For complex nonlinear analyses involving contact, plasticity and large deformations, and taking into account the recommendations of Bursi and Jaspart (1997a; 1997b), three finite elements available in ABAQUS (2014) were considered, Table 3.6 provides a summary of the main characteristic of these elements, according to Figure 3.11 (a).

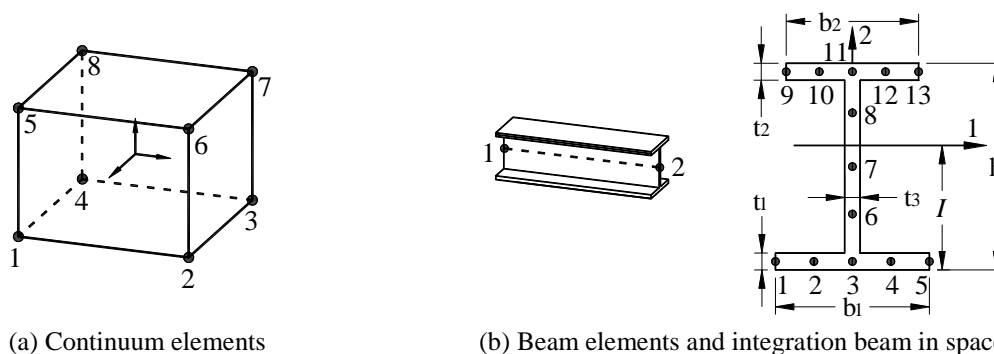


Figure 3.11: (a) Brick linear element with 8 nodes, and (b) beam element with 2 nodes

Table 3.6: Main properties for the finite elements selected for numerical calculations.

Finite element	Main properties
C3D8H	8 nodes
	8 integration points
	3 degrees of freedom per node Shear lock problems (tends to become overly stiff in bending)
C3D8RH	8 nodes
	1 integration point
	3 degrees of freedom per node Hourglassing problems (zero strain in integration point in bending problems)
C3D8IH	8 nodes
	1 integration point
	3 degrees of freedom per node + 13 incompatible modes in the element More expensive than the regular first-order elements, but more economical than the second-order elements

C3D8H is a 8-node linear or first-order brick element (nodes only at corners) with full integration (8 Gauss points), hybrid formulation and featuring constant pressure; C3D8RH is also a 8-node linear brick element but with reduced integration (normally using a scheme one order less than the full scheme to integrate the element's internal forces and stiffness with only 1 Gauss point) (ABAQUS, 2014), hourglass control using the artificial stiffness method given in Flanagan and Belytschko (1981) and hybrid formulation; and C3D8IH, a first-order full

integrated (8 Gauss points) element enhanced by incompatible modes to improve its bending behaviour, allowing to overcome the overly stiff condition due to the parasitic shear stresses. Due to the 13 additional degrees of freedom, these elements are more computationally demanding than the regular first-order displacement elements, but less demanding than second-order elements (ABAQUS, 2014). Following the recommendations of the benchmark proposed in Bursi and Jaspart (1997a), a sensitivity study was conducted to analyse the response of the 3 solid brick elements, which, according to the previous statement, are the ones that might best solve the specific problem. Using the J1.1 and the J3.1 models, for which the geometric properties are shown in Table 3.1, in Figure 3.1 and in Figure 3.2, Figure 3.12 shows a comparison of the numerical response using the 3 different element types with the corresponding experimental response. It was concluded that the element that best predicts the real behaviour for large rotations is C3D8RH. In the linear elastic branch all the elements presented similar and satisfactory results. The results lead to a logical choice for the solid element to use in the FE analyses, C3D8RH, because of its better efficiency.

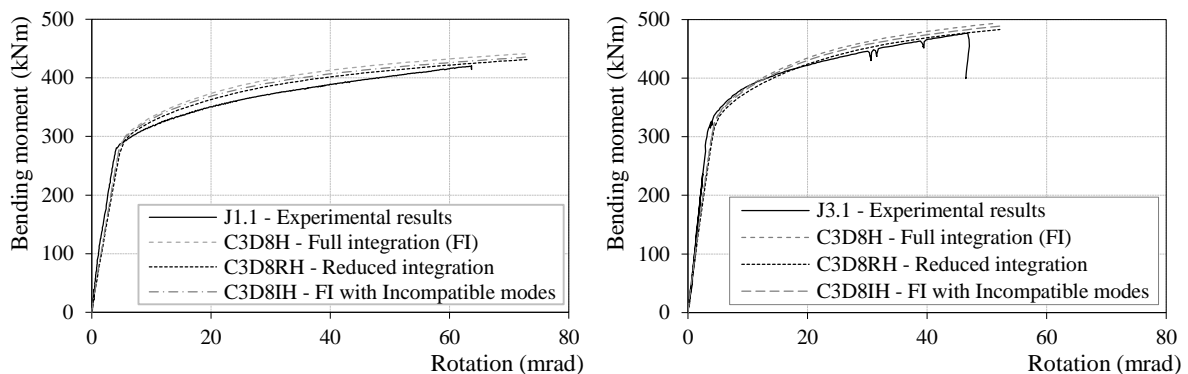


Figure 3.12: Sensitivity study on the ABAQUS solid elements

The preferential use of quadrilaterals and hexahedral elements was due to the better convergence rate of these elements in comparison with the triangles and tetrahedral elements, providing equivalent accuracy with less computational effort, for regular meshes, which is the case in most of the model zones. As first-order (linear) triangles and tetrahedral are usually overly stiff, these elements can only provide accurate results with very refined meshes. With the intent of saving computational time, reduced integration elements were adopted using a lower-order integration to form the element stiffness. Although in this case the numerical problem concerning shear locking is overcome, the hourglass can be a real problem for the linear reduced-integration elements. As the elements only have one integration point, it is

possible to have distortional deformation modes in such a way that their stiffness is severely reduced, as represented in Figure 3.13. In problems governed by bending deformations this effect can have a direct influence on the accuracy of the results. To avoid this problem, at least 3 layers of elements were considered across the thickness, see Figure 3.13, and also the hourglass control formulation was activated for these elements. In their convergence study, Bursi and Jaspart (1997a) concluded, using 1, 2, 3, 5 and 8 layers of elements in clamped and simply supported beam models subjected to bending, that at least 3 layers should be considered in bending-dominated problems. The elements chosen have also hybrid formulation, normally used for fully incompressible material behaviour or, as in this case, if severe plastic deformation is expected, because the rate of total deformation becomes incompressible as the plastic deformation starts to dominate the response (ABAQUS, 2014). For the non-solid column and beam parts, the B31 element available in ABAQUS is used, i.e., a three-dimensional first-order linear beam element with 2 nodes, using a beam section integrated during the analysis to define the section behaviour, with 13 wall points in total, because it is a spatial model, see Figure 3.11 (b). It is not expected that the beam elements develop large plasticity due to their location, hence the standard number of points in the section seems to be reasonable in these circumstances.

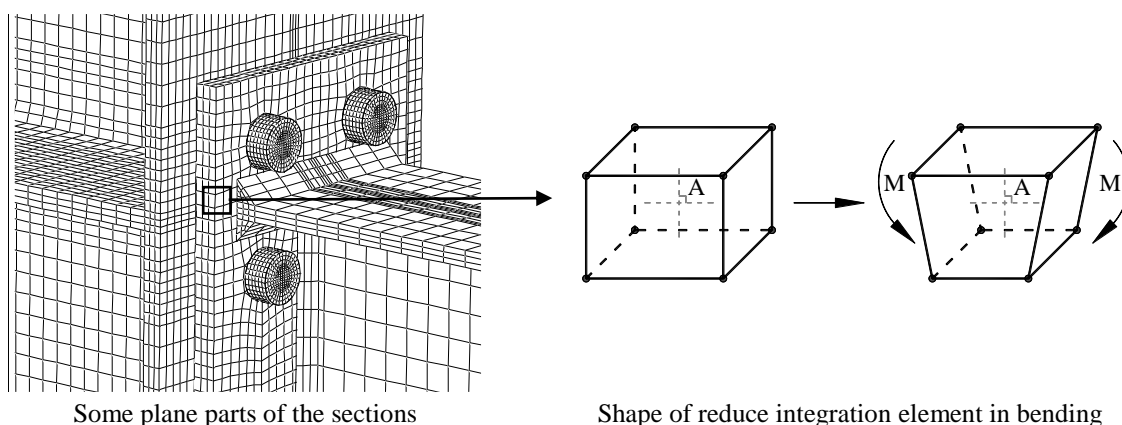


Figure 3.13: Detail for the elements in the thickness and hourglass phenomenon.

The mesh was automatically generated. To ensure a regular mesh distribution it is necessary to impose some pre-defined conditions. The parts are composed by plane surfaces where a regular distribution of the mesh is usually generated. The major problem are the perturbations in the plane surfaces by the bolts holes or in the intersections with non-orthogonal surfaces. In those cases, the problem should be divided in such a way that a regular mesh is allowed. Figure 3.14 (a) shows an example of the partitions created in the J3.1 model to allow for a regular automatic generation of the mesh. Partitions is a tool available in ABAQUS that

allows setting some mesh boundaries without actually break the part. In addition to the created partitions, it is also required to define, in some cases, a more refine mesh in some particular zones of the mesh, for example in the edge of the bolts holes, see Figure 3.14 (b) the seed in pink are the additional ones. In those cases, the seed option available in ABAQUS, can be used, the automatic generation of the mesh will try to create the additional number of elements required around the bolts holes, without refining the rest of the mesh of the end-plate.

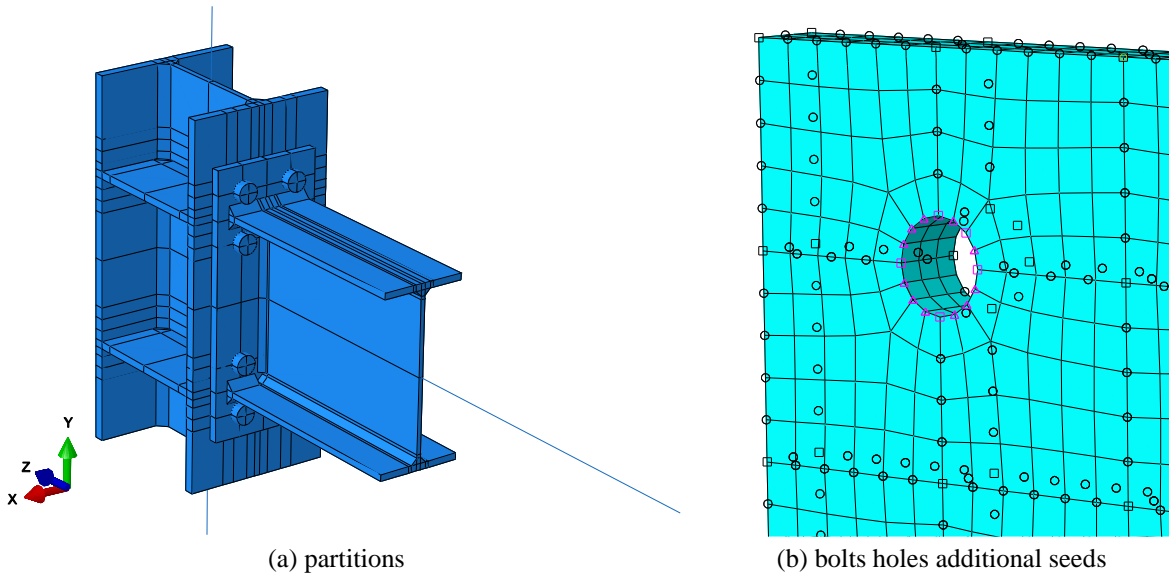


Figure 3.14: Partitions representation for a regular mesh distribution.

After defining all the required inputs and the proper conditions for a regular mesh, it is possible to automatically generate the mesh.

ii) Constraints and contact interactions

As previously mentioned, the various parts of the model interact with each other by continuity links, called constraints in ABAQUS (e.g. between the beam and the end-plate) or defining contact properties, called interactions in ABAQUS (e.g. between the end-plate and the column flange), see Table 3.9. The beam elements are constrained to the solid column and beam parts by a multi-point constraint beam formulation that uses the concept of slave and master nodes to define the same degrees of freedom between both. Between the end-plate and the solid beam a *tie* constraint is imposed, using the same master and slave philosophy, the degrees of freedom of the dependent nodes are eliminated; the two surfaces will have the same values of their degrees of freedom. The interactions between the end-plate and the column flange and the interactions between the bolts and the end-plate or column flange are imposed by the general

contact algorithm, which uses “hard contact” formulation, using the penalty method to approximate the hard pressure-overclosure behaviour that acts in the normal direction to resist penetration. The contact force being proportional to the penetration distance g_N is controlled by a penalty coefficient ε_N , the greater ε_N the smaller the penetration, see Figure 3.15 and tangential behaviour to take into account the friction between surfaces. It is important to note that Lagrange multipliers will be automatically added to the solution if the comparison of the contact stiffness to the underlying element stiffness is overcome in 1000 times, at the expense of solution cost, but avoiding numerical errors related to ill-conditioning of the stiffness matrix.

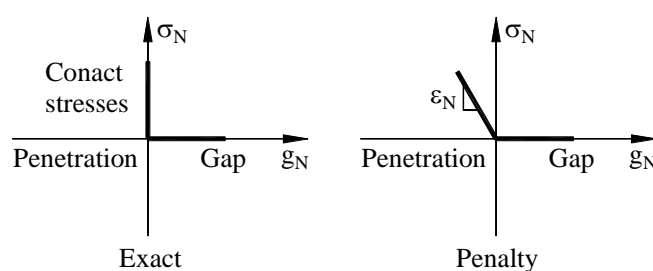


Figure 3.15: Penalty method representation.

iii) Constitutive models

For the material properties, the combined isotropic/kinematic hardening model available in ABAQUS was adopted. Although for monotonic loading models isotropic hardening approach is sufficient, the model is prepared also to deal with cyclic loading cases. Experimental evidence has shown the difference between the material properties obtained from the monotonic and cyclic specimens, and therefore simple elasto-plastic isotropic or kinematic hardening models are not adequate to deal with load reversal. This constitutive model (Lemaitre and Chaboche, 1990, chap.5) uses the von Mises yield criterion and an associative flow rule is assumed. The monotonic coupon test results are used to obtain key coordinates in the stress-strain relationship (see Table 3.3 and Table 3.4). In all parts of the model the elasto-plastic constitutive material relationships were used, non-linear in the solid elements and tri-linear in the beam elements.

ABAQUS expects the stress strain data to be entered as true stress and true plastic strain. The tensile coupon tests engineering stress-strain relationship is achieved by dividing the load at any instant by the initial cross area of the coupon. However, when the coupon is tensioned the length increases, but the width and thickness shorten. At a given load level, the true stress is obtained by dividing the load by the cross-area at that instant. Unless thickness and width are

being monitored continuously during the test, the true stress cannot be calculated. It is, however, a much better representation of how the material behaves as it is being deformed.

If during deformation the volume of the sample is preserved one may relate true stress and engineering stress using Eq. (3.1). In the same way, if the uniaxial case is considered, small increments should be taken to solve a plastic analysis with large displacements. Hence, between the initial position L_0 and the final position L_f , and being L_{in} the initial length of the specimen, the total strain is given by Eq. (3.2). Consequently, the true strain is given by Eq. (3.3) (Ling, 1996).

$$\sigma_{tru} = \sigma_{eng} (1 + \varepsilon_{eng}) \quad (3.1)$$

$$\varepsilon = \int_{L_0}^{L_f} \frac{dL_{in}}{L_{in}} = \ln\left(\frac{L_f}{L_0}\right) \quad (3.2)$$

$$\varepsilon_{tru} = \ln(1 + \varepsilon_{eng}) \quad (3.3)$$

Where σ and ε represents the stress and strain, respectively. In ABAQUS the modulus of elasticity E has also to be updated, corresponding to the slope defined by the first point (the yield point). This can be obtained by dividing the first nonzero true stress by the first nonzero true strain. Finally, to convert the true strain to true plastic strain Eq. (3.4) is used.

$$\varepsilon_{pl} = \varepsilon_{tru} - \frac{\sigma_{tru}}{E} \quad (3.4)$$

In fact, the uniaxial stress state is one of the few simple cases where the stress-strain relation can be verified experimentally. That is why, in the case of large plastic deformations, it is necessary to relate stresses and strains in a general state to the uniaxial observations. In such cases, it is assumed that, for a given stress state, there exists an equivalent uniaxial stress state. The von Mises criterion is generally used for this equivalency (Ling, 1996).

To build the non-linear and multi-linear constitutive material relationships to implement in ABAQUS, three relevant points from the coupon tests stress-strain curves were chosen, which are listed in Table 3.3. Table 3.7 shows the conversion of the engineering properties to the true stress-true strain material properties, using Eqs. (3.1), (3.3) and (3.4), for the several members that constitute the joints. The achieved true stress vs true strain relationships for the constitutive material models are depicted in Figure 3.16, for the several joint members.

Table 3.7: True stress true strain main material properties

Joint members		Elastic modulus (GPa)	Yield true stress (MPa)	Yield true strain (%)	Ultimate true stress (MPa)	Ultimate true strain (%)	Ultimate true plastic strain (%)	True stress at rupture (MPa)	True strain at rupture (%)	True plastic strain at rupture (%)
		E_{m_tru}	f_{y_tru}	ϵ_{y_tru}	f_{u_tru}	ϵ_{u_tru}	ϵ_{u_pl}	$f_{r_tru}^*$	ϵ_{r_tru}	ϵ_{r_pl}
IPE360	Flanges	206.65	430.90	0.209	637.33	13.976	13.668	671.97	22.314	21.989
	Web	214.27	449.14	0.210	641.36	14.842	14.543	675.75	23.111	22.796
HEB320	Flanges	209.39	394.64	0.188	609.22	15.700	15.409	656.60	26.236	25.923
	Web	216.70	399.54	0.184	609.69	15.700	15.419	641.94	23.902	23.605
HEA320	Flanges	205.52	415.6	0.202	621.74	15.700	15.398	664.94	25.464	25.141
	Web	208.07	450.57	0.217	636.41	13.976	13.670	665.63	21.511	21.119
HEA280	Flanges	210.06	440.62	0.210	640.81	15.700	15.395	674.71	23.902	23.580
	Web	210.89	462.71	0.219	662.29	13.976	13.662	692.69	21.511	21.183
End-plate 220x18		210.91	405.88	0.192	608.76	13.103	12.814	642.30	21.511	21.207
End-plate 300x18		208.99	393.64	0.188	596.22	13.103	12.818	629.06	21.511	21.210
Stiffeners		206.33	286.80	0.139	542.16	18.232	17.969	569.72	26.236	25.960
Bolts		214.49	994.59	0.464	1182.87	1.094	0.542	1242.44	3.343	2.764
Welds		213.66	440.91	0.206	659.88	20.049	19.740	687.20	23.111	22.790

* – f_r values were achieved reducing f_u values by 3%.

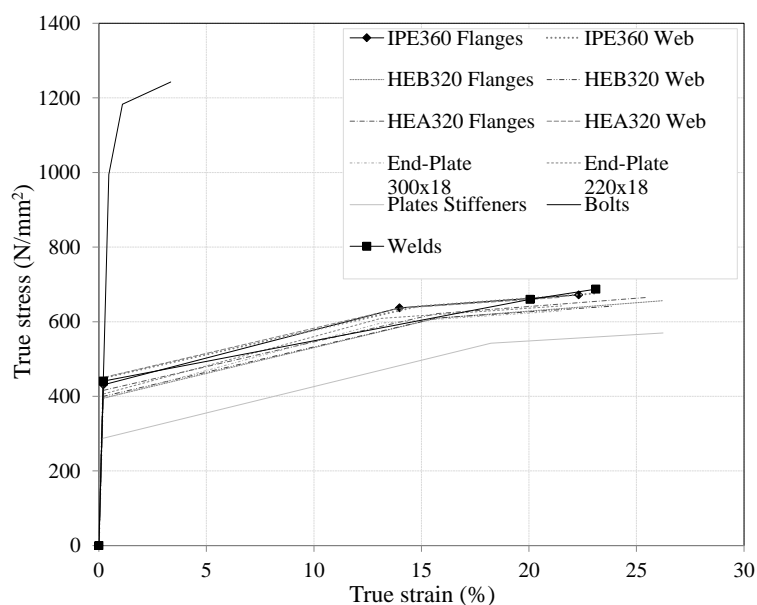


Figure 3.16: Idealized tri-linear true stress vs true strain constitutive material models

In the process of defining the material cyclic properties, and for the calibration of the isotropic part of the combine hardening model, the default ABAQUS values were defined, due

to the absence of cyclic material tests. For the kinematic hardening calibration an approximate procedure was used that adjusts the C_k and γ_k values, of the first backstress α , according to Eq. (3.5), through the known reference values of the monotonic coupon tests determined in Table 3.7. This procedure is well explained in Imaoka (2008) and is illustrated in Figure 3.17. The yield stress value f_y is used to find the plastic stress $\alpha^* = f_n - f_y$, where n denotes the several plastic stress stages, and also the corresponding equivalent plastic strain $\epsilon^{pl} = \epsilon_n - f_n/E$ is determined. The results of α are fit to α^* , finding the pair of values C_1 and γ_1 that minimizes the error between the analytical solution and the experimental values, using least-squares method. This can be done, for example, in Microsoft Excel using the Solver Add-In. Normally, curve-fitting procedures are sensitive to the initial input values. Since C_1 is the initial hardening modulus, the slope after yielding can be a reasonable initial estimate for C_1 , and with the asymptotic value, translated by the relation C_1/γ_1 an initial value can be assessed for γ_1 .

$$\alpha_i = \frac{C_1}{\gamma_1} + \left(1 - e^{-\gamma_1 \epsilon^{pl}} \right) \tag{3.5}$$

A summary of the kinematic hardening calibration parameters, for the member of the joints, are shown in Table 3.8, and in Figure 3.18 is depicted the curve-fit of the backstress curves to the experimental values, using the assessed C_1 and γ_1 values.

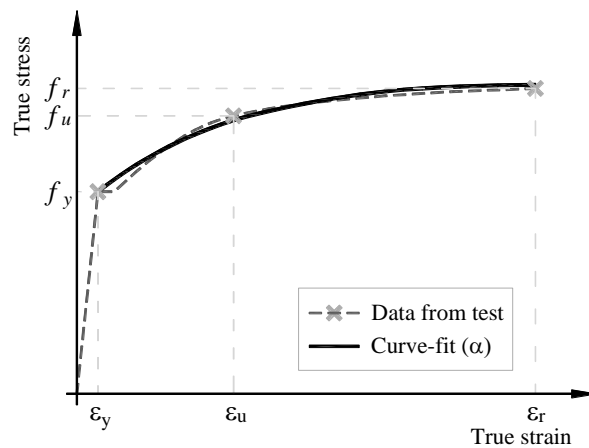


Figure 3.17: Curve-fit the backstress expression to the experimental data changing C and γ values.

Table 3.8: Kinematic hardening calibration.

Joint members	f_y (MPa)	f_{u_tru} (Mpa)	ϵ_{pl}	α^* (MPa)	α (MPa)	$(\alpha^*-\alpha)^2$	$\Sigma(\alpha^*-\alpha)^2$	C_1	γ_1	C_1/γ_1
IPE360	Flanges	430.9	430.897	0.000	0.000	0.000	0	2947.485	11.180	263.633
		637.330	0.137	206.433	206.438	2.23E-05	3.59E-05			
		671.968	0.220	241.071	241.075	1.36E-05				
	Web	449.1	449.139	0.000	0.000	0.000	0	2459.437	9.650	254.866
		641.364	0.145	192.225	192.227	8.63E-06	3.21E-05			
		675.754	0.228	226.615	226.620	2.35E-05				
HEB320	Flanges	394.6	394.642	0.000	0.000	0.000	0	2486.864	8.424	295.228
		609.219	0.154	214.577	214.609	1.08E-3	1.31E-03			
		656.603	0.259	261.960	261.976	2.34E-4				
	Web	399.6	399.556	0.000	0.000	0.000	0	2663.698	9.936	268.078
		609.687	0.154	210.131	210.105	6.88E-4	8.38E-04			
		641.943	0.236	242.388	242.375	1.50E-4				
HEA320	Flanges	415.6	415.639	0.000	0.000	0.000	0	2394.122	8.458	283.062
		621.738	0.154	206.099	206.099	3.13E-12	9.86E-12			
		664.941	0.251	249.302	249.302	6.73E-12				
	Web	450.6	450.574	0.000	0.000	0.000	0	2655.055	11.194	237.178
		636.410	0.137	185.836	185.836	2.04E-09	5.47E-09			
		665.630	0.212	215.056	215.056	3.43E-09				
HEA280	Flanges	440.6	440.622	0.000	0.000	0.000	0	2432.243	9.204	264.247
		640.809	0.154	200.187	200.186	2.13E-07	2.90E-07			
		674.712	0.236	234.089	234.090	7.74E-08				
	Web	462.7	462.713	0.000	0.000	0.000	0	2892.625	11.470	252.191
		662.285	0.137	199.572	199.569	1.082E-05	1.35E-05			
		692.693	0.212	229.980	229.981	2.701E-06				
End-plate	393.6	393.640	0.000	0.000	0.000	0	3184.993	12.593	252.919	
	596.220	0.128	202.580	202.580	3.827E-10	1.08E-09				
	629.064	0.212	235.424	235.424	6.965E-10					
Stiffeners	286.8	286.798	0.000	0.000	0.000	0	3078.647	10.089	305.159	
	542.160	0.180	255.362	255.362	2.545E-09	6.29E-09				
	569.720	0.260	282.922	282.922	3.747E-09					
Bolts	994.6	994.591	0.000	0.000	0.000	0	65074.654	262.366	248.030	
	1182.87	0.005	188.279	188.277	3.491E-06	4.72E-06				
	1242.44	0.028	247.853	247.854	1.232E-06					
Welds	440.9	440.908	0.000	0.000	0.000	0	1321.347	1.827	723.103	
	659.880	0.197	218.972	218.972	1.036E-10	2.41E-10				
	687.204	0.228	246.296	246.296	1.369E-10					

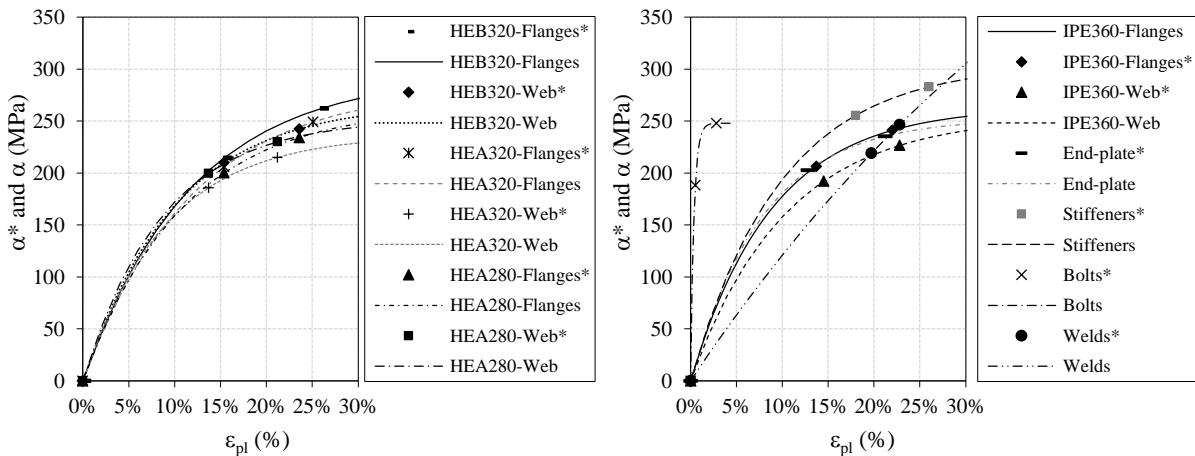
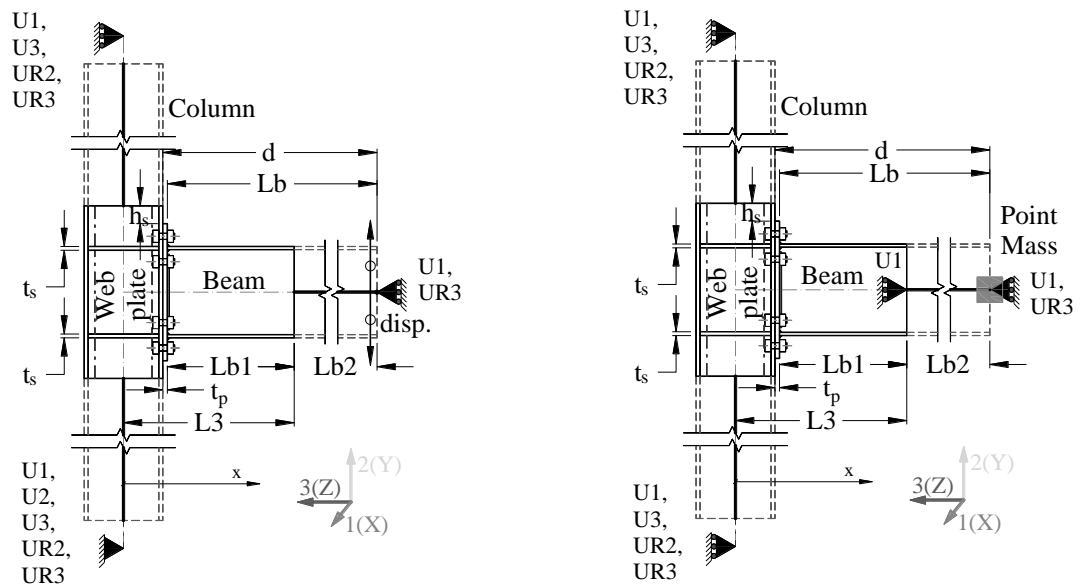


Figure 3.18: Curve-fit representation for the assessed C_1 and γ_1 parameters.

The assessed values of f_y , C_1 and γ_1 can be introduced directly in ABAQUS software in a tabulated format, along with the corresponding E values determined for the true stress true strain condition.

iv) Loading

The models were loaded following the protocol adopted in the tests, which consisted of an imposed displacement applied at the beam end, according to the scheme shown in Figure 3.19 (a). The models are prepared to deal with monotonic and cyclic loads and also dynamic excitation. In the first two cases, the “loads” are applied in a displacement control way, i.e., a displacement is imposed at the tip of the cantilever beam, see Figure 3.19 (a). The loading protocol is defined by the direction (along the three global axis, although in this research only the YY axis direction was used), orientation, amplitude of the displacement, and number of cycles at the same amplitude. For the dynamic excitation, an acceleration spectrum is normally considered. To generate the necessary inertia forces in the structure, the mass of the sub-assembly elements is defined (by the mass density property). However, to generate a significant level of inertia forces in the structure a point mass can be added to the tip of the cantilever beam, so that it can be excited and generate bending moment in the system, see Figure 3.19 (b). In this case, the boundary conditions also need to be changed to accommodate the global motion of the system.



(a) Monotonic and cyclic loading.

(b) Dynamic excitation.

Figure 3.19: Boundary conditions for the several load possibilities.

ABAQUS divides the problem history into steps. A step is any convenient phase of the history and, in its simplest form, a step can be just a static analysis, a load change from a magnitude to another, an initial pre-stress operation of a part of the structure or the change of a boundary condition in the model. In this particular case, the solution of the problem is obtained in 3 steps. The first step is used to formulate the boundary conditions and prepare the contact interactions defined previously. The second step corresponds to the pre-loading of the bolts using the adjust length option and determining the length magnitude by the elastic elongation needed to produce the required amount of force in the bolts, normally a percentage of the ultimate strength. Figure 3.20 shows the plane where the adjust length option is applied. In the third step the bolts current length are fixed so the magnitude is computed during the analyses. This option allows maintaining the pre-defined load in the bolts during the third step. It is in the third step that the pushover begins, changing the boundary conditions on the tip of the cantilever by imposing a displacement in the boundary condition parallel to the beam web. Or, in the case of a dynamic excitation, the acceleration spectrum accelerates the mass of the structure, and the boundary condition of the bottom support is changed to allow the movement of the system.

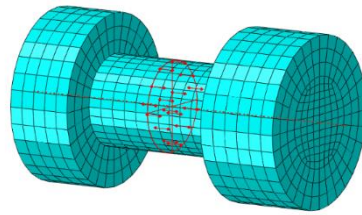


Figure 3.20: Bolts pre-load plane.

v) FE options summary

The options described above are summarised in Table 3.9 for the groups of joints modelled according to the experimental tests (groups 1, 2 and 3). The several parts that comprise the model are listed in the same table along with the identification of the distribution of the different material properties. The constraints and interactions are also illustrated in the table, showing the relationships between the parts. The necessary partitions, defined for a regular mesh, were used to create the interactions between the movable parts, namely the interactions between the bolts and the end-plate or the column flanges.

Table 3.9: FE options summary.

Model	Parts	Materials	Constraints	Interactions
J1 group				
J3 group				
J4 group				
	7 different parts	10 different materials	4 constraints	3 interactions
	(a)	(b)	(c)	(d)

vi) Numerical strategy for resolution of the non-linear problem

The analyses were performed using the ABAQUS/Standard solver that iteratively solves a system of equilibrium equations implicitly for each solution increment (ABAQUS, 2014).

Second-order effects were considered in all the analyses to account for large displacements effects. Due to the several nonlinearities present in the models, namely material nonlinearity, geometric nonlinearity and contact nonlinearity, general analysis steps were adopted with automatic control for the increments, i.e. the increment size was determined according to the response of the model.

3.2.4 VALIDATION OF THE FE MODELS USING EXPERIMENTAL EVIDENCE

3.2.4.1 OVERVIEW

In this section, a detailed analysis of the joints will be performed both for the global and components behaviours. The results from the numerical and analytical models, loaded monotonically, are compared with the experimental test results described in Section 3.2.1. The analytical models proposed in EC3-1-8 (EN 1993-1-8, 2005) are used in the comparisons, using the real material properties of the steel obtained in the coupon tests and adopting partial safety factors equal to unity. Then, the numerical results of the cyclic loaded models are also analysed and compared with the experimental test results.

A special attention is also given to the energy that joints are able to dissipate, in terms of the global behaviour, and in terms of the main dissipative components. The identification of the components is conditioned by the experimental tests setup. The numerical results will be compared with the ones recorded in the experimental tests, to evaluate the accuracy of models in terms of energy dissipated during the load protocols.

3.2.4.2 EXTRACTION PROCEDURES FOR EXPERIMENTAL TESTS AND NUMERICAL MODELS

In order to compare experimental and numerical results, forces, bending moments, displacements and rotations were determined according to the procedure described hereafter. For the experimental tests, the load cells and the displacement transducers (DT) indicated in Figure 3.6, with a reminder of the most relevant DT in Figure 3.21 (a), were used. In the same

way, for the FE models, the reactions and the displacement of some predefined nodes were selected, as shown in Figure 3.21 (b). The strain gauges were used to determine the column web strains, in the experimental tests, according to the scheme of Figure 3.7, and the logarithmic strain were extracted from the FE models. The equations used to obtain the $M-\theta$ relationships in this section can be found in Table 3.10. The left column of the table lists the equations for the experimental tests and in the right column the ones for the FE models.

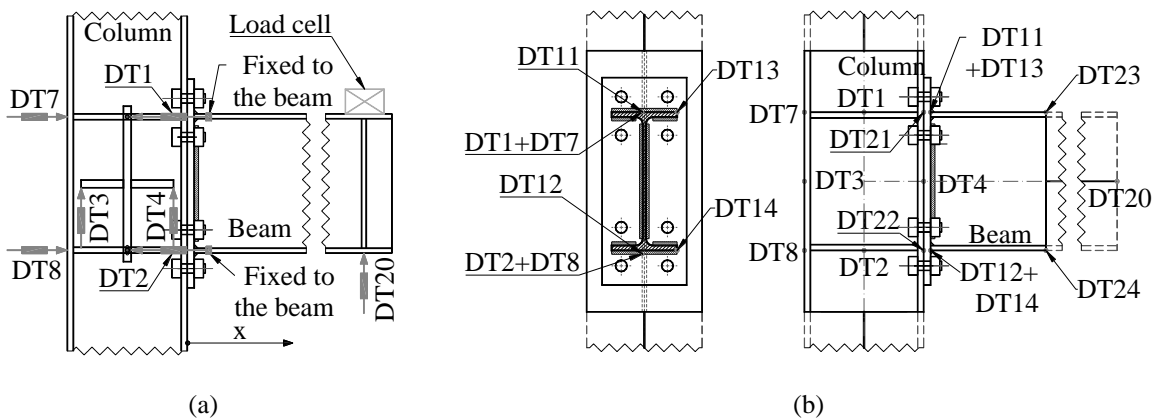


Figure 3.21: Points of interest in (a) experimental and (b) FE models.

There are several ways to measure the global rotations. For the experimental tests, the one that has the best results is given by Eq. (3.9), since it can capture all the deformability sources and is sufficiently near to the joint to avoid larger contributions of the beam elastic deformation. Due to the lesser instrumented J3.1 specimen, it was necessary to use Eq. (3.10) to obtain the total rotation. Because in the numerical models the corresponding location of $DT11$ and $DT12$ were outside the beam mesh, and also because it was intended to isolate the rotation components (column web panel and end-plate) in the experimental/numerical comparisons the Eq. (3.11) and Eq. (3.12) were adopted.

Eq. (3.14) and Eq. (3.15) were used for the experimental and numerical results, respectively, to extract the components behaviour for the column web component in shear. The grouped behaviour of the components in bending and the bolts in tension are all included in Eq. (3.16) and Eq. (3.17) for the experimental and numerical results, respectively. Eq. (3.18) and Eq. (3.19) were used to analytically determine the elastic deformation of the column and beam (according to the measuring position in the beam), respectively. This deformation is subtracted to the initial joint rotation to obtain the contribution of the joint to the rotation.

Table 3.10: Equations for the extraction of the M - θ curves from the experimental and numerical results.

Experimental	FE
$M_{Ed} = F_{load_cell} \cdot d$ (3.6)	$M_{Ed} = R_{DT20} \cdot d_{DT20}$ (3.7)
$\theta_{total} = \theta_{column_Web} + \theta_{end-Plate} - \theta_{elast_column} - \theta_{elast_beam} - \theta_{block}$ (3.8)	
$\theta_{total} = \arctan\left(\frac{DT11 - DT12}{d5}\right) -$ $-\theta_{elast_beam} - \theta_{elast_column} - \theta_{block}$ or $\theta_{total} = \arctan\left(\frac{DT20}{L_1}\right) - \theta_{elast_beam} -$ $-\theta_{elast_column} - \theta_{block}$ or $\theta_{total} = \arctan\left(\frac{DT3 - DT4}{d4}\right) +$ $+ \arctan\left(\frac{DT1 - DT2}{d3}\right) - \theta_{elast_column} - \theta_{block}$ (3.11)	$\theta_{total} = \arctan\left(\frac{DT1_{U3} - DT2_{U3}}{DT1DT2}\right) +$ (3.12) $+ \theta_{end-plate} - \theta_{elast_column}$ or $\theta_{total} = \arctan\left(\frac{DT11_{U3} - DT12_{U3}}{DT11DT12}\right) -$ $-\theta_{elast_column}$ (3.13)
$\theta_{column_web} = \arctan\left(\frac{DT3 - DT4}{d4}\right) -$ $-\theta_{elast_column} - \theta_{block}$ (3.14)	$\theta_{column_web} = \arctan\left(\frac{DT1_{U3} - DT2_{U3}}{DT1DT2}\right) -$ $-\theta_{elast_column}$ (3.15)
$\theta_{end-plate} = \arctan\left(\frac{DT1 - DT2}{DT1DT2}\right) -$ $-\theta_{elast_beam}$ (3.16)	$\theta_{end-plate} = \arctan\left(\frac{DT13_{U3} - DT14_{U3}}{DT13DT14}\right) -$ $-\theta_{column_web}$ (3.17)
$\theta_{elast_column} = \frac{F_{load_cell} \cdot d \cdot L^2}{L} + \frac{2 \cdot F_{load_cell} \cdot d \cdot L}{6} - F_{load_cell} \cdot d \cdot L2$ $E \cdot I_{y(Colunn)}$ (3.18)	
$\theta_{elast_beam} = \frac{F_{load_cell} \cdot d \cdot x - F_{load_cell} \cdot \frac{x^2}{2}}{E \cdot I_{y(Beam)}}$ (3.19)	
$\theta_{block} = \arctan\left(\frac{DT5 - DT6}{d_1}\right)$ (3.20)	-

See also Figure 3.6 and Figure 3.21.

Rotation definition:

θ_{block}	Parasitic displacements (global rotation of the setup due to the gaps)
θ_{elast_beam}	Elastic deformation of the beam
θ_{elast_column}	Elastic deformation of the column
θ_{column_web}	Column web panel rotation
$\theta_{end-plate}$	End-plate rotation

Eq. (3.20) was used to determine the block deformation of the test setup due to the clearances in the support devices of the sub-assembly.

3.2.4.3 GLOBAL BEHAVIOUR OF THE JOINTS

Figure 3.22 (a), (b) and (c), compares the experimental, numerical and analytical moment-rotation curves for the 3 joints configurations, J1, J3 and J4 groups, respectively.

The joints were analysed according to the component-based procedure given in EC3-1-8 (EN 1993-1-8, 2005), using the web and flanges measured material properties, from Table 3.3 and Table 3.4. The main results are shown in Table 3.11, highlighting the critical design components. It is noted that the failure mode found among all the components in tension was always related to the T-Stub components, mode 2.

Table 3.11: Main design properties of the joints according to EN1993-1-8.

Test	Global prop.		Component properties																
			Shear comp.	Compr. comp.	Tension comp.														
	$S_{j,ini}$	$M_{j,Rd}$			$V_{wp,Rd}$	$F_{c,fb,Rd}$	1st Row			2nd Row			3rd Row						
kNm/rad	kNm	kN	kN	$F_{t,wc,Rd}$	$F_{t,fc,Rd}$	$F_{t,ep,Rd}$	$F_{t,wb,Rd}$	$F_{t,Rd}$	$F_{t,wc,Rd}$	$F_{t,fc,Rd}$	$F_{t,ep,Rd}$	$F_{t,wb,Rd}$	$F_{t,Rd}$	$F_{t,wc,Rd}$	$F_{t,fc,Rd}$	$F_{t,ep,Rd}$	$F_{t,wb,Rd}$	$F_{t,Rd}$	
J1	60246	355	1025	1288	846	601	534	-	534	835	598	604	988	<u>491</u>	835	598	604	986	<u>0</u>
J3	72950	389	1166	1288	929	727	534	-	534	918	722	604	966	604	918	722	604	986	<u>27</u>
J4	37865	271	1050	1776	1110	568	574	-	568	1080	560	591	1680	<u>483</u>	1080	560	591	1680	<u>0</u>

For the experimental results, the bending moment was obtained using Eq.(3.6) and the joint rotation was obtained by Eq. (3.11). Similarly, for the FE models, Eq.(3.7) was used, where d_{DT20} is the distance between the point where the imposed displacement occurs ($DT20$) and the column flange, and R_{2DT20} is the reaction force obtained at the same point. The total rotation of the joint is obtained from Eq.(3.12), the sum of the column web contribution with the other components contributions (end-plate, column flanges and bolts).

Figure 3.22 (d) depicts the adopted criterion for extracting the initial stiffness and moment resistance from the experimental and numerical $M-\theta$ curves. The initial stiffness is easier to identify as it may be estimated by adjusting a straight line between the point of zero loading and the elastic moment of the joint (M_{el} , first yield in the joint). It is noted that the experimental procedure should always contemplate elastic unloading during this stage and the elastic stiffness

should be fitted to the unloading branch. Assessing the plastic resistance from experimental or FE numerical results is a more complex task, as yielding of the joint is a gradual process, typically occurring between points A and B in Figure 3.22 (d). Furthermore, in many cases, the behaviour of the joint is not only driven by plasticity and a plastic plateau is less obvious, either because of membrane effects and/or strain hardening. According to the literature (ECCS, 1986), it is common to define the plastic moment resistance at the intersection of the two straight lines corresponding to the initial stiffness of the joint and a post-limit stiffness. The latter can only be properly established on a case-by-case basis, directly from the full $M-\theta$ curve. In this work it is defined as the tangent to the $M-\theta$ curve with a slope given by $S_{j,ini}/h$, where h is adjusted for each case. Finally, it is noted that this procedure is very sensitive to the adjustment of the tangent point and the slope, in comparison to analytical procedures. An attempt to systematize this procedure is presented in Annex A, modifying the ECCS (ECCS, 1986) procedure, to consider different plastic mechanisms in the joints according to EC3-1-8 (EN 1993-1-8, 2005).

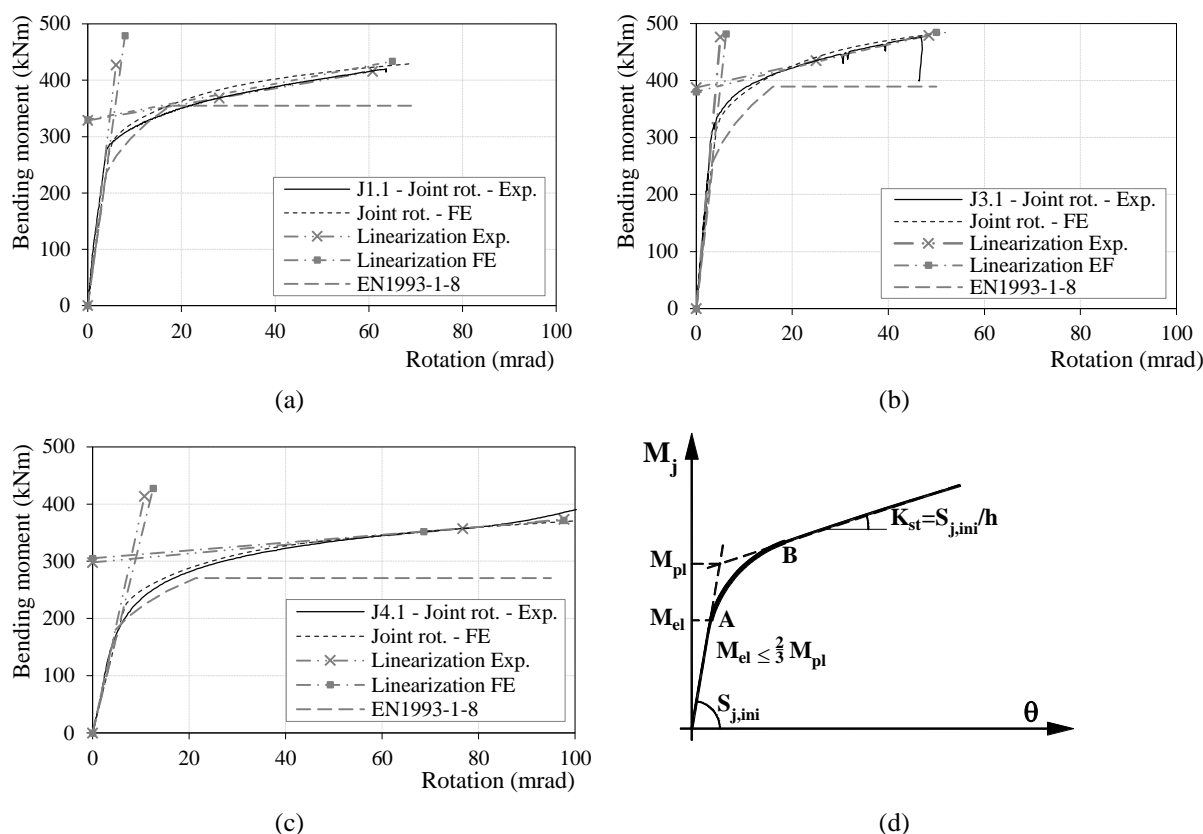


Figure 3.22: Global experimental, numerical and analytical results.

Table 3.12 compares the moment resistance and initial stiffness (equal for hogging and sagging because of the symmetry of the connection), using the linearized responses of the experimental and numerical results.

The experimental moment-rotation curves, including now the cyclic loaded joints, are depicted in Figure 3.23 for each group, using the load cells and displacement transducers *DT11*, *DT12* for the groups J1 to J4 tests and *DT20* for the lesser instrumented J3.1. The analysis of the results of the J1 group allows to conclude that for all cyclic loading strategies, the hysteretic response was very stable. No pinching or strength degradation was detected and only small stiffness degradation was observed (Figure 3.23 a). For joint configuration J2, no pinching or stiffness degradation was observed (Figure 3.23 b). For joint configuration J3, a small strength degradation was observed; however, no pinching was detected (Figure 3.23 c). Failure occurred either by cracking of the end-plate (J.3.2) or cracking of the weld (J.3.3). Noticeable strength and stiffness degradation and pinching were observed for joint configuration J4 (Figure 3.23 d). Table 3.13 summarises the nine results for all cyclic tests, including the identification of the failure modes and the corresponding number of cycles.

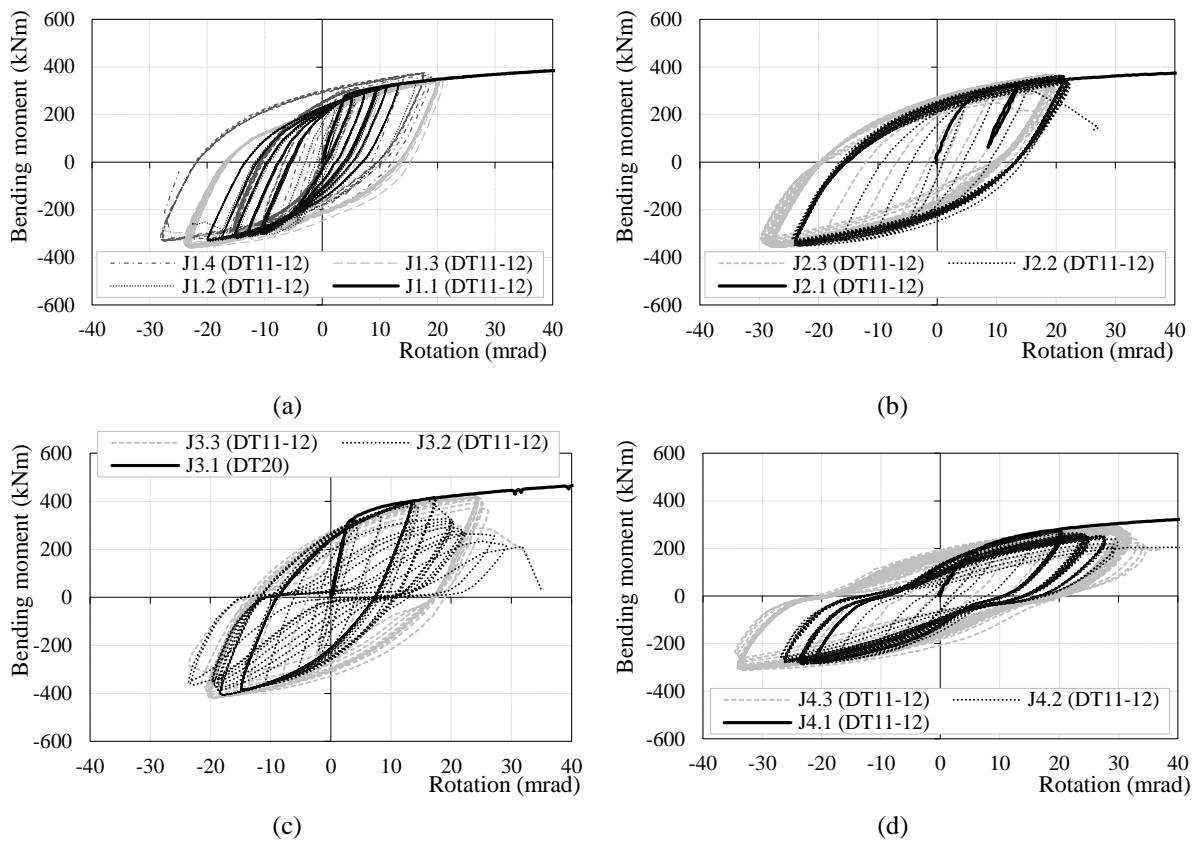


Figure 3.23: Experimental moment-rotation curves.

Table 3.12: Comparison between the experimental, numerical and analytical results.

	Experimental values		Numerical values			Analytical values				
	M_{pl} (kNm)	$S_{j,ini}$ (kNm/rad)	M_{pd} (kNm)	Error (%)	$S_{j,ini}$ (kNm/rad)	Error (%)	M_{pd} (kNm)	Error (%)	$S_{j,ini}$ (kNm/rad)	Error (%)
J1.1	335	71340	339	+1.2	60660	-15.0	354.5	+5.8	60246	-15.6
J3.1	395	95057	391	-1.0	77480	-18.5	389.3	-1.4	72950	-23.3
J4.1	304	38495	312	+2.6	34125	-11.4	270.5	-11.0	37865	-1.6

Table 3.13: Bolted beam-to-column double extended end-plate joints test programme.

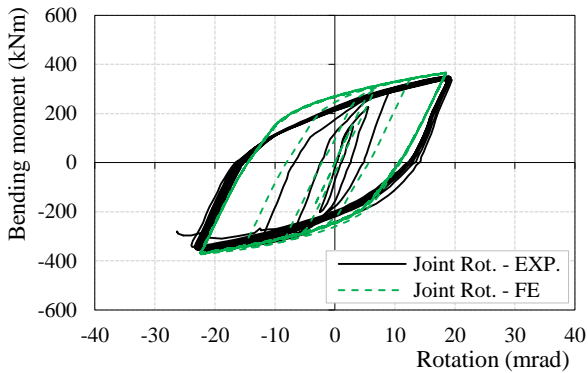
Test	Loading Strategy	Failure mode	- M_{min} (kNm)	+ M_{max} (kNm)	n.° of cycles	- θ_{min} (mrad)	+ θ_{max} (mrad)	Total energy (kNm×mrad)
J1.2	S1	weld	-335	+340	83	-23	+16	435156
J1.3	S2	weld	-362	+352	22	-28	+21	293979
J1.4	SA	cracking EP	-333	+378	28	-28	+19	201946
J2.2	S2	weld	-353	+365	27	-24	+22	368538
J2.3	S2	weld	-358	+368	27	-30	+21	382945
J3.2	S1	cracking EP	-408	+418	26	-19	+17	215156
J3.3	S2	weld	-421	+431	13	-21	+26	195075
J4.2	S1	weld	-290	+276	54	-27	+30	448850
J4.3	S2	weld	-310	+295	34	-35	+35	505611

Next the results from the numerical models are compared with some of the experimental test results previously described, one for each different geometry. Bending moments and rotations were determined according to the procedure described in Table 3.10. For the FE models, the reaction forces and the displacements of some predefined nodes were selected. The bending moments are computed at the face of the connected column flange $M=F*d$ using distance d and the forces applied in the tip of the beam. Rotations are computed using the relation between the displacements measured in LVDTs (or the displacements obtained in the pre-defined nodes in the FE mesh) and the distance between them, excluding the rotations due to the elastic deformation of the members and the rotations due to the support clearances ($\theta_{total} = \text{atan}((DT_i - DT_{i+1})/d_n) - \theta_{elast_column} - \theta_{block}$). To compute the total rotation of the joint, the column web contribution is added to the connection contribution, with the help of the crosshead, for experimental tests is used the Eq. (3.11), and for the FE models is used the Eq.(3.12).

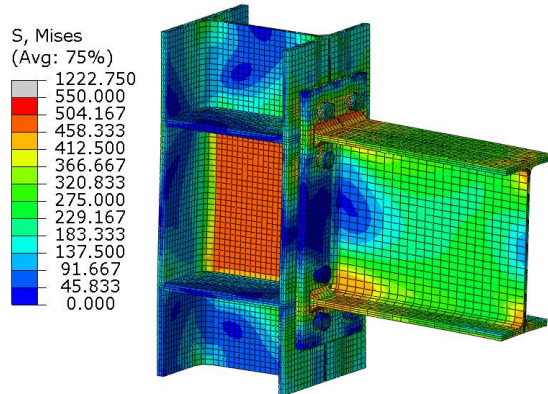
Figure 3.24 (a), (c) and (e), compare the experimental and the numerical moment-rotation curves for the three joints, J1.3, J3.2 and J4.3, respectively.

Figure 3.24(b), (d) and (f) represent the Von Mises stress distribution in the joint region for the 3 joints analysed, for the maximum rotation achieved in the joint, i.e., the largest rotation

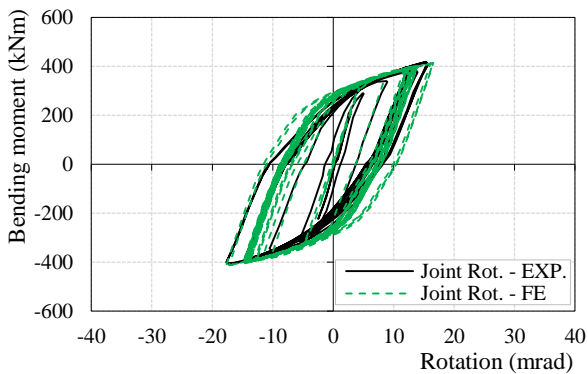
amplitude achieved during the loading protocol. The stress patterns are very similar for all joints, although for J4.3 it is possible to see higher stress concentration around the stiffeners in the opposite flange of the column, which is due to the smaller lever arm of the beam inducing larger rotations in the joint. The stress peak values occurred in the bolts, the stress scale was limited to a small range of stress values.



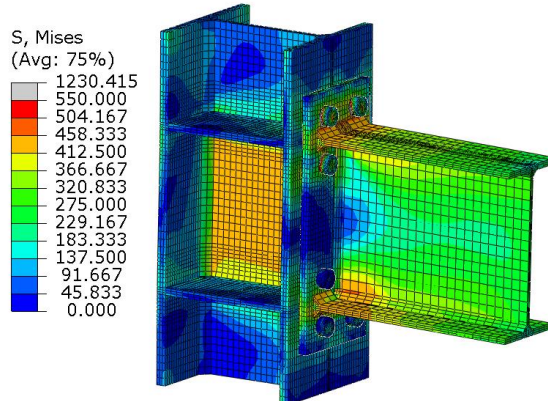
(a) J1.3 global response of the joint.



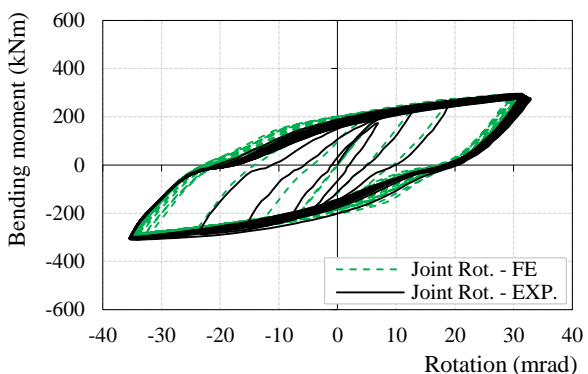
(b) J1.3 Mises distribution.



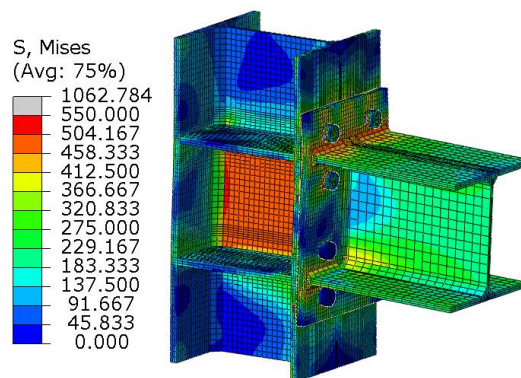
(c) J3.2 global response of the joint.



(d) J3.2 Mises distribution.



(e) J4.3 global response of the joint.



(f) J4.3 Mises distribution.

Figure 3.24: Global experimental and numerical results.

The comparisons between numerical and experimental results, including Table 3.14, allow to conclude that the extended end-plate joints FE models produce very accurate results when compared with the experimental data also for cyclic load cases.

From the detailed analysis of the cyclic behaviour, it is possible to identify the strength and stiffness degradation experimented by the joints, for the stable cycles, see Figure 3.25. The positive and negative stiffness are determined in the unloading branch of each positive and negative half-cycle, respectively. It is noted that the first positive and negative cycles were disregarded, because these include fictitious values provided by the beginning of the test not reflecting the true stiffness in the discharge. The positive and negative bending moments, depicted in the Figure 3.25, are the maximum and minimum moments in each half-cycle, respectively. It is possible to conclude that, for the group J1, degradation of stiffness is observed for all joints, but at different rates. In the case of J1.4, degradation only occurred in the last 7 cycles. Strength degradation is not noticeable in J1.2, but it occurs in J1.4 only in the last 7 cycles, after an amplitude increase. In the case of the group J2, a very similar behaviour was observed for both joints with some degradation of stiffness and strength occurring with the evolution of the loading protocol. J3.2 presents a very stable behaviour in terms of stiffness and strength. Similar to J3.2, the J3.3 joint exhibited very stable behaviour in terms of stiffness and strength, although after the 10th cycle it is possible to observe a strong degradation of stiffness and strength as a result of the damage observed in the welds between the end-plate and the beam. Similar to the group J2, the group J4 showed a similar behaviour for both joints in the group, with similar strength and stiffness degradation, although in this case the number of cycles achieved by J4.2 was 37% higher than for J4.3, the failure occurred by the beam-to-end-plate welds in both cases.

Table 3.14: Comparison of the strength and rotation extremes between the experimental and numerical results.

	- M_{min} (Exp.) (kNm)	- M_{min} (FE) (kNm)	Error (%)	+ M_{max} (Exp.) (kNm)	+ M_{max} (FE) (kNm)	Error (%)	- θ_{min} (Exp.) (mrad)	- θ_{min} (FE) (mrad)	Error (%)	+ θ_{max} (Exp.) (mrad)	+ θ_{max} (FE) (mrad)	Error (%)
J1.3	-362	-373	+2.9	+352	+364	+3.3	-24	-22.5	-6.3	+19	+18.5	-2.6
J3.2	-408	-416	+1.9	+418	+414	-1.0	-17.7	-17.7	0.0	+15.7	+16.6	+5.4
J4.3	-310	-298	-3.9	+295	+295	+0.0	-35	-35	+0.0	+32	+32	+0.0

The comparisons with the numerical results are quite good, although the numerical results for J1.3 are slightly lower than the correspondent obtained in the tests.

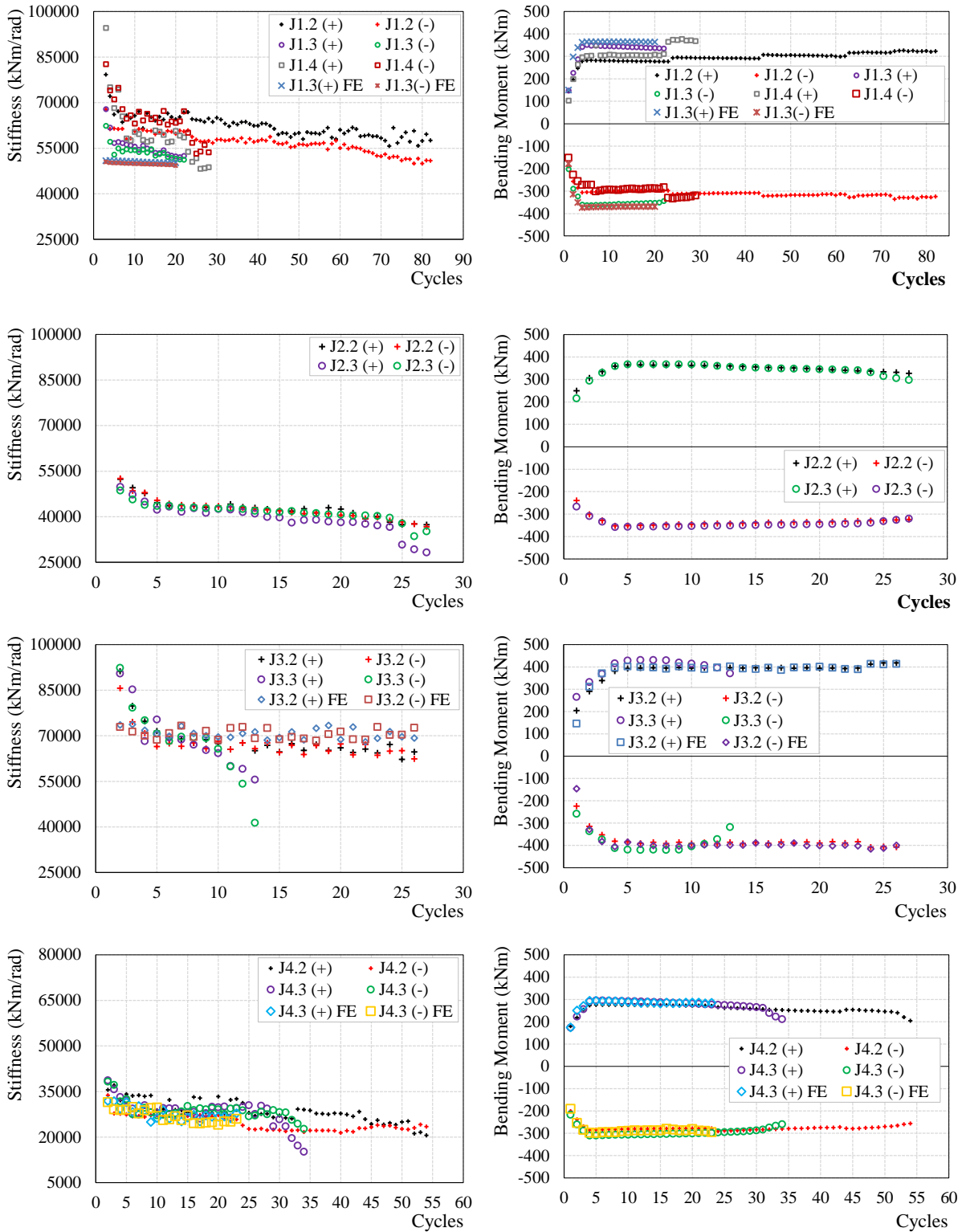


Figure 3.25: Stiffness and strength degradation during cycles.

3.2.4.4 COMPONENTS BEHAVIOUR

As already mentioned, the most dissipative components, in an end-plate bolted joint, are the end-plate and/or column flanges in bending and the column web panel in shear. In the particular case of the studied joints the continuity transverse web stiffeners limit the column flanges deformation, so the large contribution is provided by the other two components. The column web crossheads were used to determine the rotations of these components, so Eqs. (3.14) and (3.15) are used to determine the joints column web rotation, for the experimental and numerical models, respectively. Eqs. (3.16) and (3.17) are used to determine the end-plate contribution for the experimental and numerical models, respectively.

i) Joints under monotonic loading conditions

Figure 3.26 compares the moment-rotation curves for each joint and the two critical components, for the experimental and numerical results. For all tests, the column web panel in shear exhibits the largest contribution towards the deformability of the joint. The comparisons revealed the accuracy of the finite element models also at the components level.

Table 3.15 summarizes the experimental initial stiffness and resistance of the critical components end-plate in bending and column web panel in shear, comparing the experimental tests results with analytical models. The stiffness values of the components, obtained according to EC3-1-8 (EN 1993-1-8, 2005), are computed using only the equivalent stiffness coefficient k_{eq} , for all the bolt-rows in tension. The experimental results are compared with the analytical models using the same procedure illustrated in Figure 3.22(d), with the ones obtained with the Atamaz-Jaspart model (AJM) (Jaspart, 1990) and the Krawinkler model (Krawinkler *et al.*, 1975), described in detail in Chapter 2.

Figure 3.27 (a) represents the critical component end-plate in bending for the J1.1, J3.1 and J4.1 joints, also representing the moments achieved by each bolt-row, using for the lever arm the distance between each row to the middle of the compressed beam flange. It is possible to conclude that J4.1 is more ductile than J1.1, roughly twice and that the bending moments are well estimated by EN 1993-1-8. Figure 3.27 (b) shows the comparison of the column web rotation between the experimental test and the model proposed by Krawinkler as well as the Atamaz-Jaspart model. It is noted that the Krawinkler model considers that the post-yielding stiffness is developed up to the yielding of the column flanges assumed equal to four times the

yielding rotation (distortion). After the yielding of the flanges the hardening of the steel is 2% of the initial stiffness. The reference points for the AJM are: i) first yielding of the web; ii) strain-hardening in the web, γ_{st} , and plastic shear stress uniformly distributed in the whole panel, V_{ny} , iii) ultimate shear force, V_{nu} , followed by a plateau until the joint's rupture, see Figure 2.26(b) and Table 2.5 for more details.

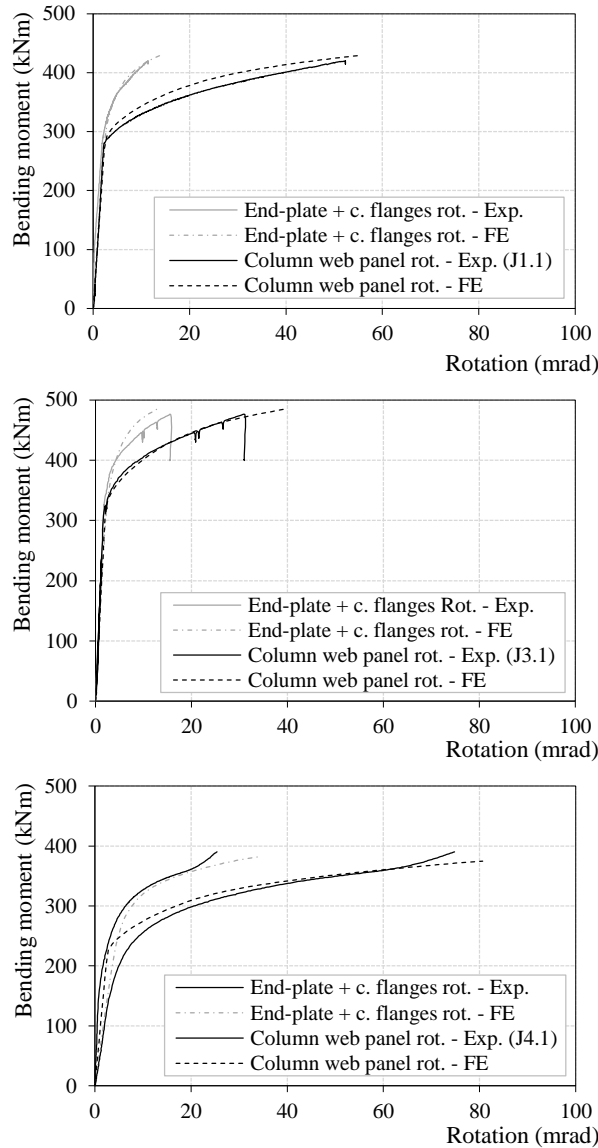


Figure 3.26: Comparison of the moment-rotation responses for the identified components.

From the figures it is possible to observe that for the J1.1 and J3.1 the initial stiffness obtained with the Atamaz-Jaspart model has a better adjustment to the experimental curve, while for the J4.1, the Krawinkler model provides a better adjustment. In terms of resistance,

both methods achieved good results, although the Krawinkler method seems to be more conservative than the Atamaz-Jaspart model.

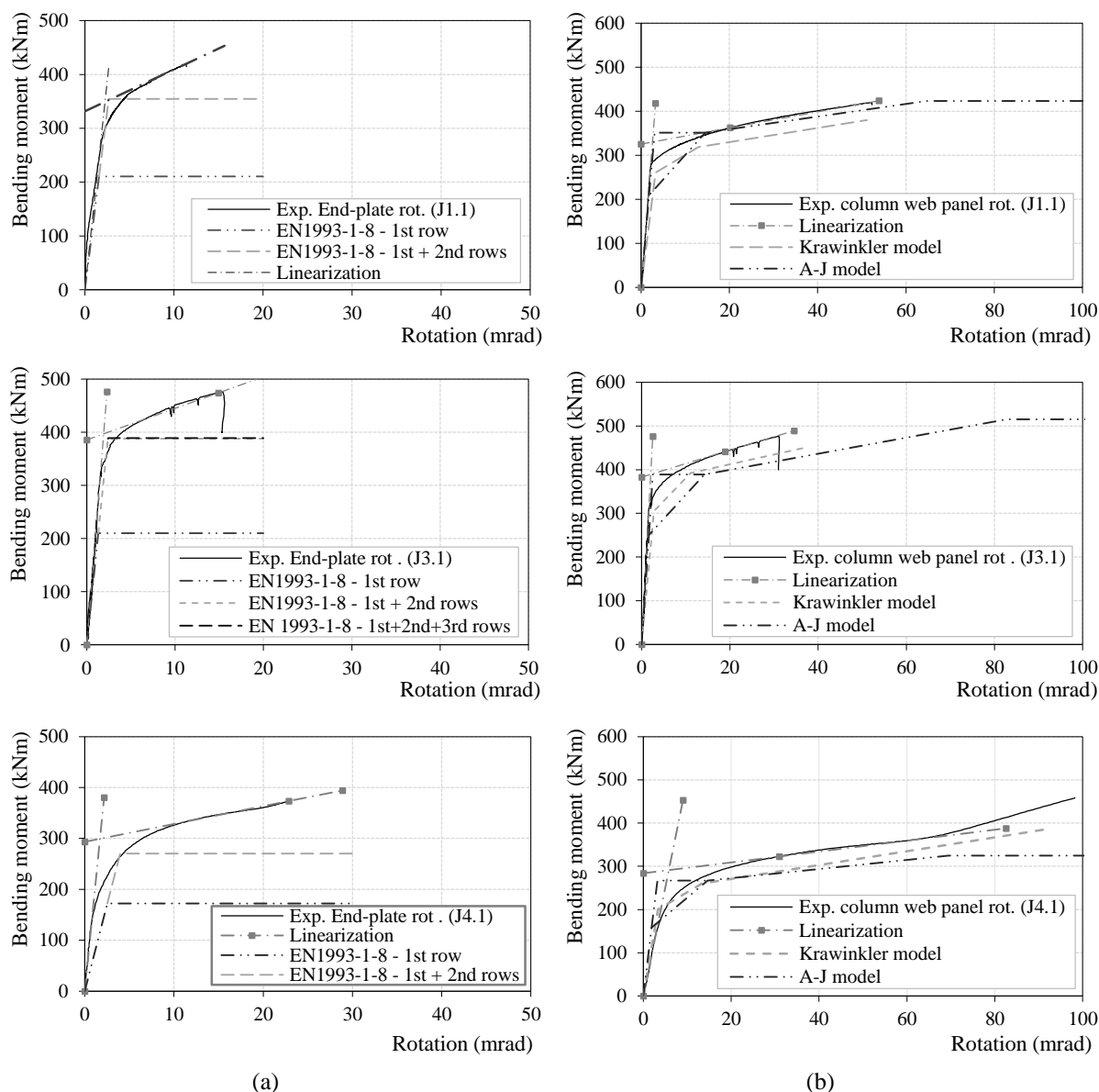


Figure 3.27: (a) End-plate and column flanges $M-\theta$ relationships, (b) Column web panel $M-\theta$ relationships for the J1.1, J3.1 and J4.1.

In the next chapter a procedure to extract the column web components is proposed based on the integration of the stress and displacements fields, as such it is appropriate also to validate the joints at the strains level in the column web. In Figure 3.28 is depicted a comparison between the top and bottom strain gauges, positioned in the column web at 60 mm from the stiffeners, and the logarithmic strain from the corresponding nodes in the FE models, revealing a good agreement. Note that strain gauges are very sensitive and are easily damaged by plastic

deformation. Thus, the comparison is performed mostly in the elastic range, observing a good agreement for all specimens.

Table 3.15: Strength and initial stiffness of the critical components

Test	End-plate in bending						
	Experimental			EN1993-1-8			
	K_{ij} (kNm/rad)	M_e (kNm)	M_{pl} (kNm)	K_{ij} (kNm/rad)	M_{1st} (kNm)	$M_{1st+2nd}$ (kNm)	$M_{1st+2nd+3rd}$ (kNm)
J1.1	155000	233	350	133416	210.4	354.5	354.5
J3.1	208000	267	400	160579	210.4	387.8	389.3
J4.1	175000	200	300	68003	172.3	270.5	270.5

Test	Distortion of the column web panel								
	Experimental			Krawinkler model			Atamaz-Jaspart model		
	K_{ij} (kNm/rad)	M_e (kNm)	M_{pl} (kNm)	K_{ij} (kNm/rad)	M_e (kNm)	M_{pl} (kNm)	K_{ij} (kNm/rad)	M_e (kNm)	M_{pl} (kNm)
J1.1	126000	220	330	80120	260.72	318.39	113954	209.2	351.4
J3.1	190500	260	390	110111	305.03	392.54	153122	250.4	388.9
J4.1	50500	193	290	60901	200.80	260.02	84325	158.6	267.1

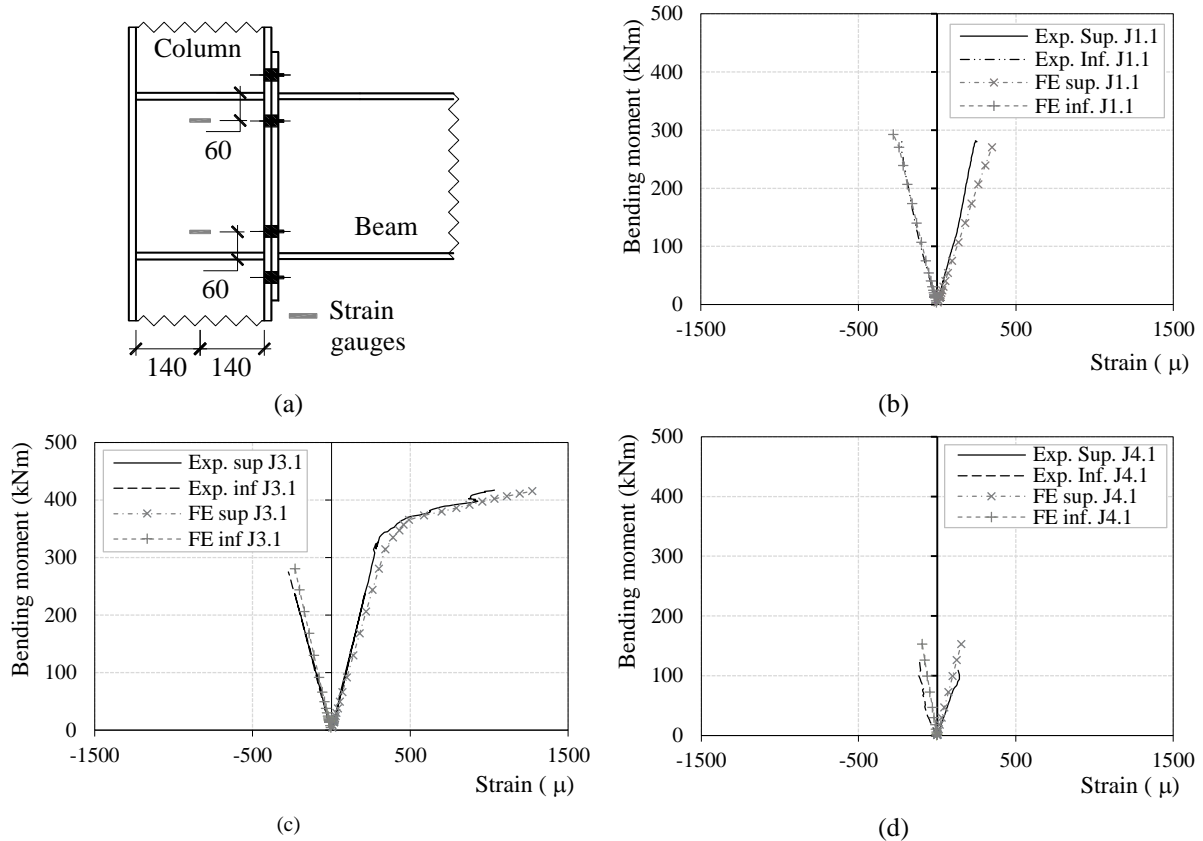


Figure 3.28: a) Strain gauges location (dimensions in mm); b), c) and d) comparison of the strains obtained in the column web panel, from the numerical and experimental results.

ii) Joints under cyclic loading conditions

The components behaviour of the cyclic loaded joints followed the same principles as for the monotonically loaded ones. Figure 3.29 compares the moment-rotation curves for each joint and the two critical components, both for the experimental and the numerical results. The comparisons revealed good agreement between the experimental and numerical results. The comparison also revealed once more the ability of the models to characterize accurately the joints components behaviour.

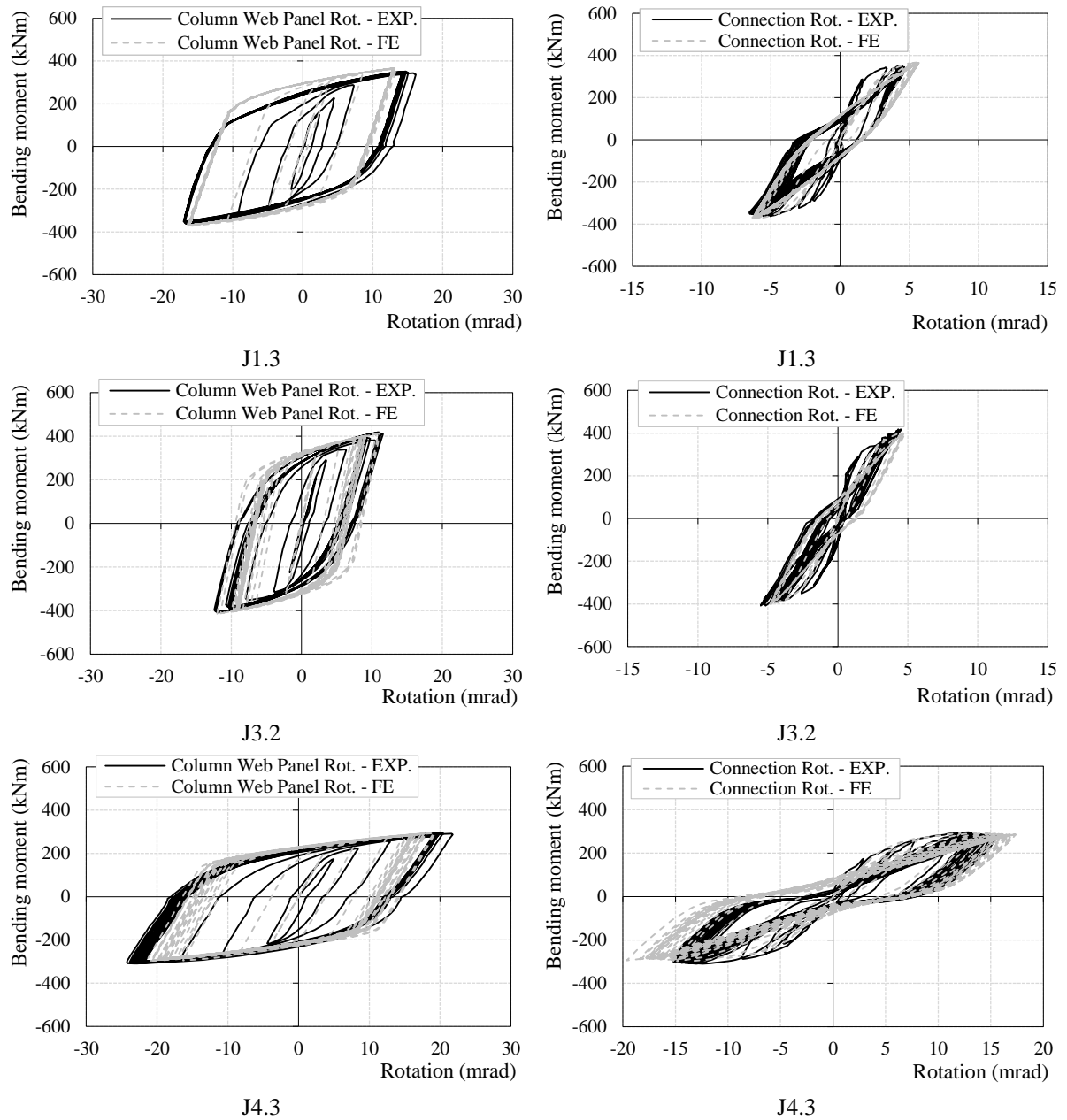


Figure 3.29: Comparison of the moment-rotation responses.

3.2.4.5 ENERGY DISSIPATION

If a load is applied to a body within its elastic limits, the body deforms and some work is done which is stored within the body in the form of internal energy or strain energy. Once the load is removed from the body it recovers the original form using the same energy stored. However, if the elastic limit is exceeded some permanent deformations remain in the body, because the particles of the material of the body slide one over another. In this case the work done is spent overcoming the cohesion of the particles and the energy is dissipated as heat in the strained material of the body (Rattan, 2008, chap.3).

Current seismic design philosophy relies on the energy dissipation, through plastic deformation of the structural members and/or connections, for a rational and economical design of steel structures. Plastic deformation allows the redistribution of forces throughout the structural members, reducing the demand and the required resistance of the members and joints, allowing for an optimum design. This research is focused on the behaviour of beam-to-column end-plate bolted joints and its capacity to dissipate energy during a seismic event as part of a moment resisting frame system. The capacity of the joints to dissipate energy depends on their dissipative components, provided that all other non-dissipative components are capacity designed. The identification of the responses of the components, obtained in the experimental tests and in the numerical models, allows the determination of the corresponding energy dissipation for each component, but also for the total energy dissipated by the joint. For that, the energy is assessed measuring the area beneath the moment-rotation relationship as illustrated in Figure 3.30 (a), or in the case of the cyclic loaded joints measuring the area of each cycle in the response curve.

Figure 3.30 illustrates the relative dissipation of energy for the two critical components, for the experimental and numerical results for the joints where a pushover analysis was performed. For all tests, the column web panel in shear exhibits the largest contribution towards the deformability of the joint (66% to 83%), while the end-plate in bending represents 17% to 34% of the overall energy dissipated. The remaining components have little contribution as they remain elastic.

Figure 3.31 compares the energy dissipated in the experimental tests with the one assessed in the FE models for the joints submitted to cyclic load protocols. The comparisons

are performed for the results where the joints presented stable behaviour, i.e., until the first fail was observed in the test. The comparisons reveal good agreement between the experimental and numerical results. For all tests, the column web panel in shear provided the largest contribution in terms of deformation and energy dissipation of the joint (78% to 83%), while the end-plate in bending represented 17% to 22% of the overall energy dissipated. As seen from the numbers, the remaining components have little contribution.

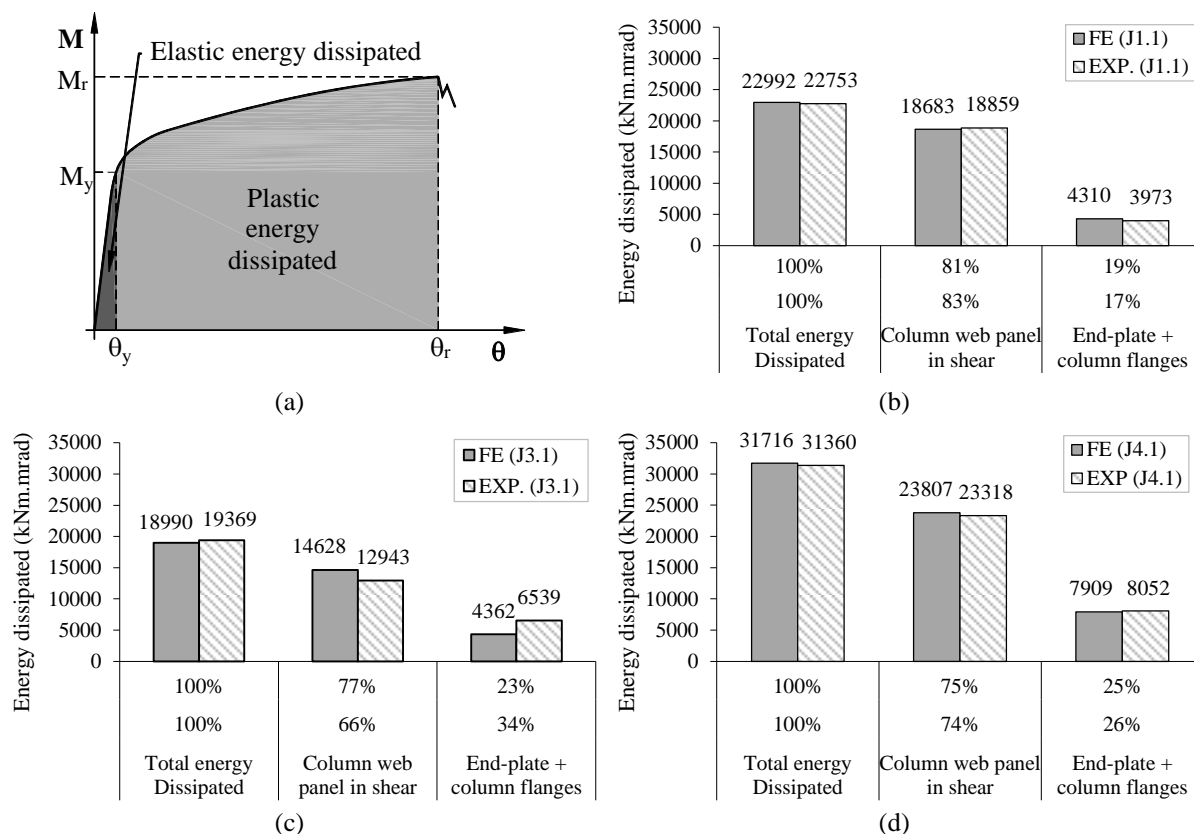


Figure 3.30: Comparison of the energy dissipated in the joints and in its components for the monotonic loaded joints.

From a design point of view, and according to the current European seismic design code (EN 1998-1, 2004), for steel moment-resisting frame possessing dissipative joints, the results of the analysed joints indicate that they could not be applied in seismic regions, because at least the mandatory clause 6.6.4(4): “(...) column web panel shear deformation should not contribute for more than 30% of the plastic rotation capability θ_p ” is not satisfied. The contribution of the column web panel is always much higher than the components in bending. Nevertheless, all joints presented stable cycles without considerable strength and stiffness degradation until the first failure has occurred.

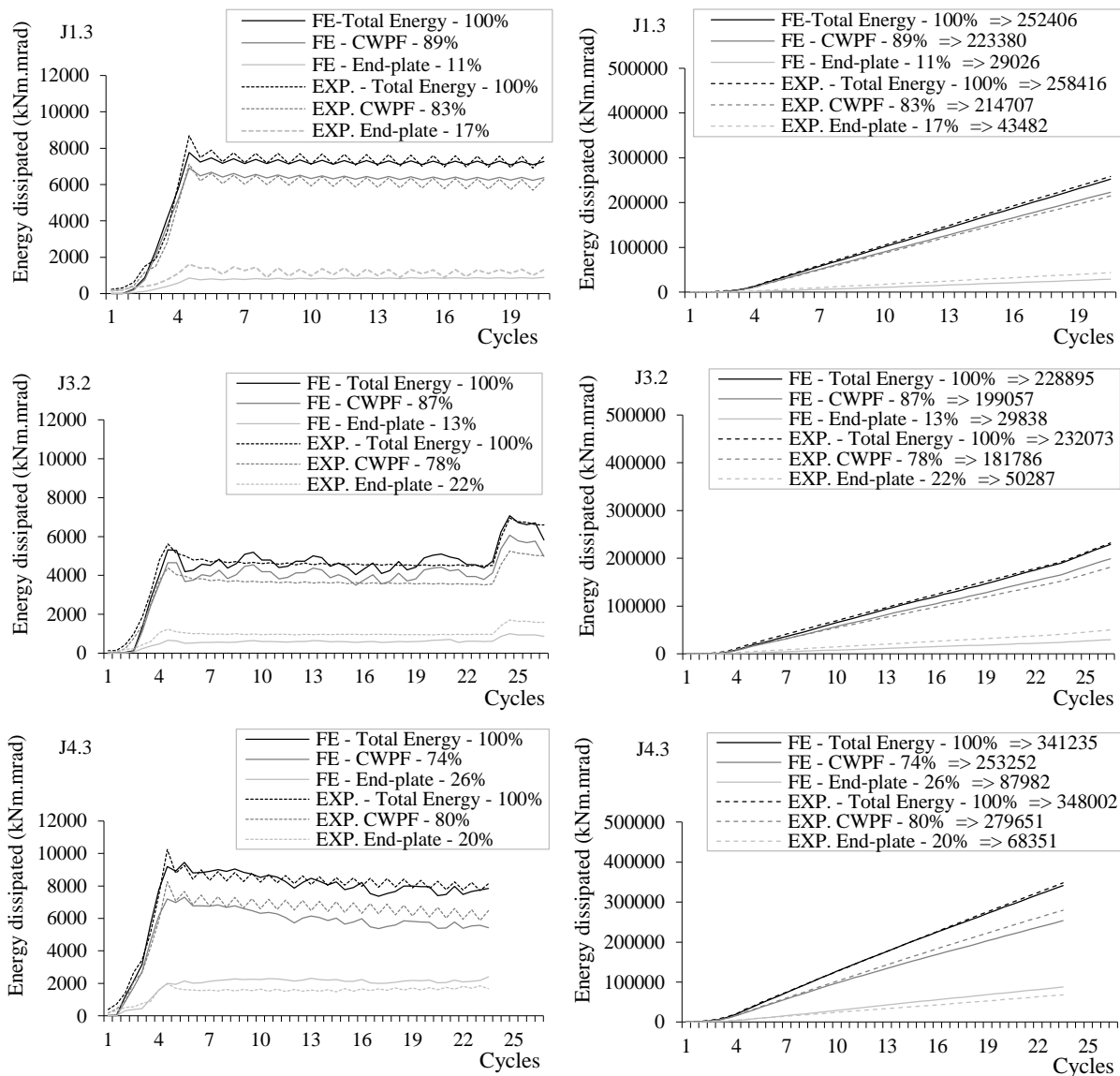


Figure 3.31: Comparison of the relative energy dissipation of the components for the joints loaded cyclically.

It is also important to take into account that the provisions, mentioned previously, were added to the code after the brittle damage found in steel welded joints due to the Northridge (1994) and Kobe (1995) earthquakes. The studies that followed the events found that the excessive rotations provided by the column web panel, among other problems, induced cracks in the less ductile welded zones of the joints. Therefore, the solution was to limit the contribution of the column web panel to the joint rotation. In fact, the European practice is quite different than the USA practice or Japanese practice, welded joints on site is far less used solution in Europe. The demand in the welds of bolted end-plate joints, when large rotations in the panel zone occur, can be considerably different than the joints where the beam is welded

directly to the column flanges. Thus, the code requirements may be too severe for this solution. This discussion falls outside the scope of this thesis. Nevertheless, it is intended in this research to characterize the column web panel components behaviour, a task that can be more efficient in weak column web panel joints.

The results obtained from FE analysis show good agreement with the experimental ones and it is therefore concluded that the numerical models for the groups J1, J3 and J4 are representative of the real behaviour.

From the results presented here, it is possible to state that the developed numerical models are reliable to predict the stiffened beam-to-column end-plate bolted joints behaviour.

3.3 END-PLATE BEAM-TO-COLUMN JOINT MODELS WITH UNSTIFFENED COLUMNS

3.3.1 EXPERIMENTAL TESTS USED IN THE NUMERICAL MODELS VALIDATION

To complement the extensive calibration / validation of the FE models, provided by the experimental tests presented above, also a comparison with a bolted end-plate connection with unstiffened column is performed. For that purpose, the SERICON (SEmi-RIgid CONnection) databank developed at the University of Aachen in Germany (SERICON, 1995; Weynand, 1992) was used. The chosen joint has the reference code 101.004 and it was tested at the University of Liege in 1987.

The specimen is a single-extended end-plate external beam-to-column steel moment-resisting joint, included in a sub-assembly representative of a moment-resisting frame structure. The joint is composed by an asymmetrical end-plate with three bolt rows of M16 bolts with the grade 10.9, two rows interior to the beam flanges and one row exterior, making the end-plate extended only in one side of the connected beam. Contrary to the previous specimens, the steel grade of the beam and column is S235 and the column does not possess transverse web stiffeners. The connection details are illustrated in Figure 3.32. The bolts were subjected to a pre-stress of $0.8f_{yb}$, and a monotonic load was imposed to the beam.

The test was performed with the column in the horizontal position, thereby adjusting the materialization of the external boundary conditions with the layout and the equipment available in the laboratory. The test instrumentation is detailed in Jaspert and Maquoi (1990), and it was set up so that the measurements allow for determining the amplitude of the joint deformability at any level of the loading.

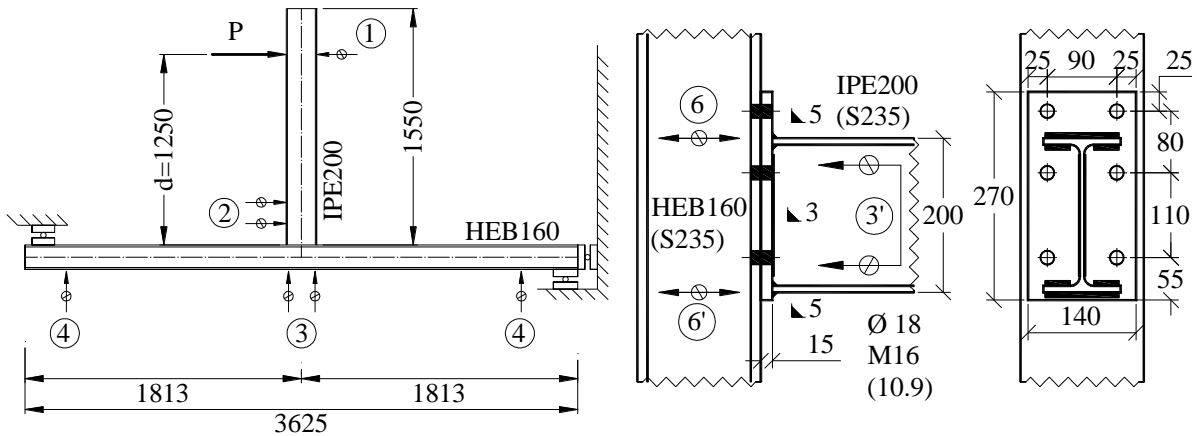


Figure 3.32: Detail of the 101.004 joint (dimensions in *mm*) (images based on (Jaspert and Maquoi, 1990; Jaspert, 1991)).

3.3.2 FE MODEL DESCRIPTION

The model geometry and mesh discretization is depicted in Figure 3.33 and defined according to the scheme of Figure 3.34. The numerical model follows the test setup and geometry described above, including the boundary conditions and the load protocol adopted, as well as the geometry and arrangement of the connection.

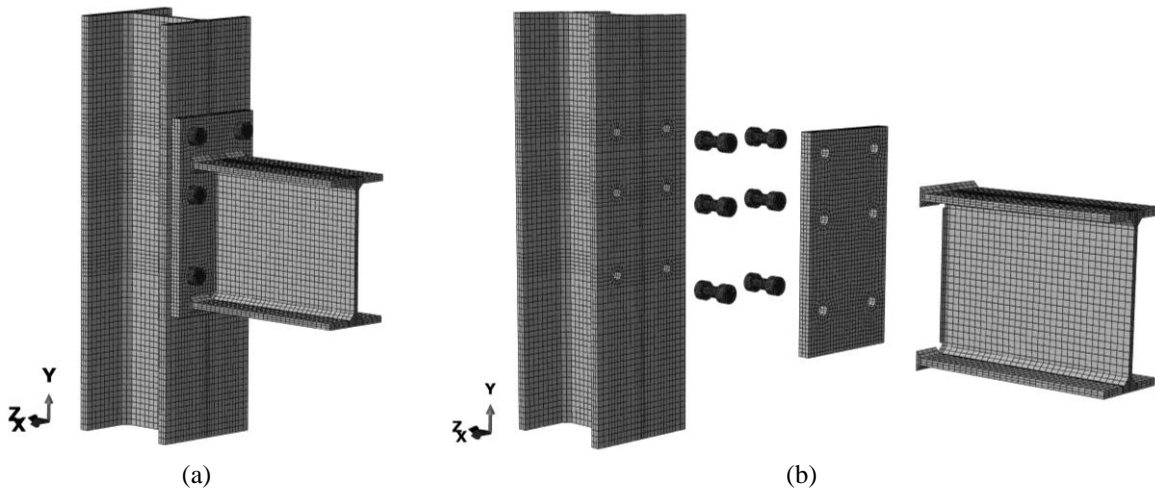
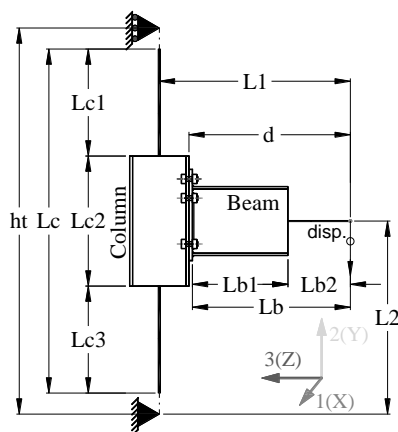


Figure 3.33: (a) FE model for the 101.004 joint and (b) mesh discretization of the solid parts that form the joint.

To build the finite element model the same modelling approach, described in Section 3.2.3, was adopted, including the use of two types of elements (beam and solid), the elements type, the boundary conditions, constraint and interactions between the parts.



Column	HEB160
Beam	IPE200
ht (mm)	3625
Lc (mm)	3425
Lc1 (mm)	1428
Lc2 (mm)	570
L1 (mm)	1331
L2 (mm)	1813
Lb1 (mm)	258
d (mm)	1250

Figure 3.34: Geometrical properties of the sub-assembly.

The material properties available in SERICON are listed in Table 3.16. As for the previous models, the constitutive material options are in line with the procedure described in Section 3.2.3. Unfortunately, the information in SERICON was incomplete with regard to the strains measured in the coupon tests, for the stages reported in Table 3.16. Therefore, in this case typical strains are adopted to build the stress-strain curves. The true stress-true strain curves obtained are depicted in Figure 3.35 and the obtained values are summarized in Table 3.16. These relationships are used directly in ABAQUS for the beam and column parts constituted by beam elements

Table 3.16: Mechanical properties of steel tested.

Sections	Component	Yield stress (MPa) f_{ym}	Nominal yield (MPa) f_y	Δ (%)	Young's modulus (GPa) E_m	Nominal value (GPa) E	Ultimate stress (MPa) f_{um}	Nominal value (MPa) f_u	Δ (%)
IPE200	Flanges	351.0	235	+33.0	-	210	456.0	360	+21.1
	Web	371.0	235	+36.7	-	210	477.0	360	+24.5
HEB160	Flanges	280.0	235	+16.1	-	210	422.3	360	+14.8
	Web	298.8	235	+21.4	-	210	422.0	360	+14.7
	End-plate 270x140x15	370.0	235	+36.5	-	210	556.0	360	+35.3

Similar to what was done for previous models, for the solid parts, a combined isotropic kinematic hardening constitutive material model is used for the plastic material properties. A summary of the kinematic hardening calibration parameters, for the member of the joints, are

shown in Table 3.18, and in Figure 3.36 is depicted the curve-fit of the backstress curves to the experimental values, using the assessed C_1 and γ_1 values.

Table 3.17: True stress true strain main material properties.

Joint members	Elastic modulus (GPa)	Yield true stress (MPa)	Yield true strain (%)	Ultimate true stress (MPa)	Ultimate true strain (%)	Ultimate true plastic strain (%)	True stress at rupture (MPa)	True strain at rupture (%)	True plastic strain at rupture (%)	
		f_{y_tru}	ϵ_{y_tru}	f_{u_tru}	ϵ_{u_tru}	ϵ_{u_pl}	$f_{r_tru}^*$	ϵ_{r_tru}	ϵ_{r_pl}	
IPE200	Flanges	210.53	351.59	0.167	547.20	18.232	17.972	583.86	27.763	27.486
	Web	210.56	371.65	0.177	572.40	18.232	17.960	610.75	27.763	27.473
HEB160	Flanges	210.42	280.37	0.133	506.76	18.232	17.991	540.71	27.763	27.506
	Web	210.45	299.22	0.142	506.40	18.232	17.992	540.33	27.763	27.507
End-plate	210.56	370.65	0.176	667.20	18.232	17.915	711.90	27.763	27.425	
Welds	210.53	440.91	0.206	659.88	20.049	19.740	687.20	23.111	22.790	
Bolts	211.35	903.85	0.428	1011.00	1.094	0.616	1061.9	3.343	2.841	

* - f_r values were achieved reducing f_u values by 3%.

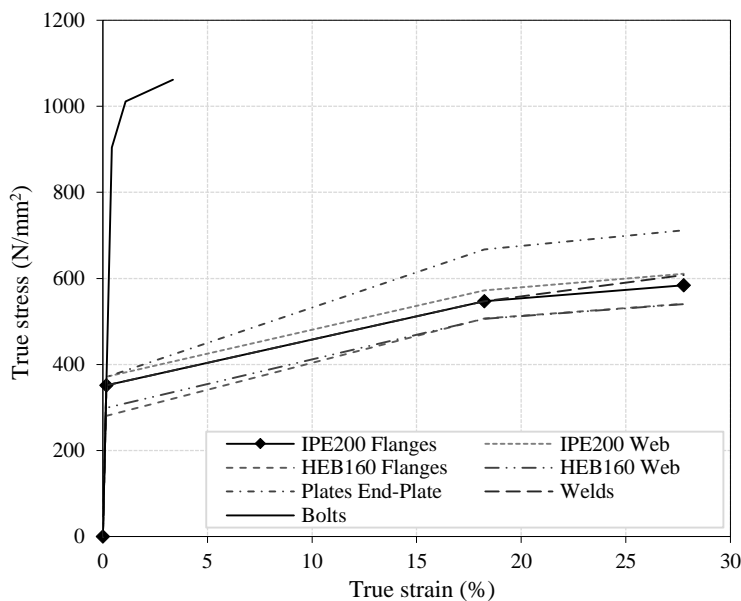
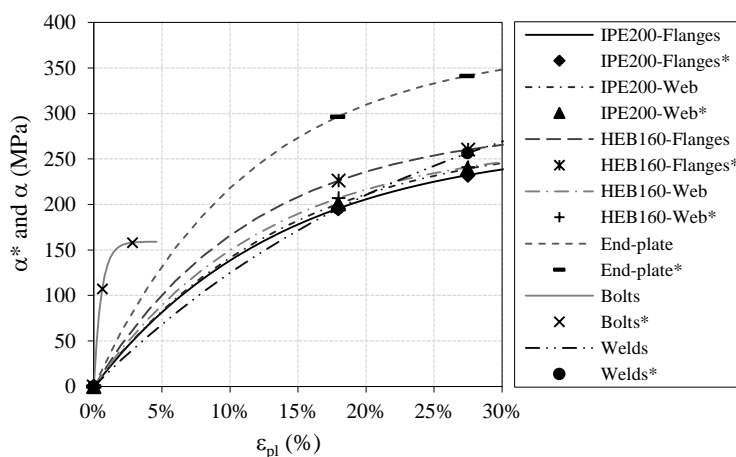


Figure 3.35: Idealized tri-linear true stress vs true strain constitutive material models.

The models were loaded following the tests procedure. An imposed displacement was applied to the beam end according to the scheme shown in Figure 3.34. The load applied to the specimen was only monotonic, being the extended part of the connection always in tension.

Table 3.18: Kinematic hardening calibration.

Joint members	f_y (MPa)	f_{u_tru} (MPa)	ϵ_{pl}	α^* (MPa)	α (MPa)	$(\alpha^*-\alpha)^2$	$\Sigma(\alpha^*-\alpha)^2$	C_1	γ_1	C_1/γ_1	
		351.586	0.000	0.000	0.000	0.00E+00					
IPE200	Flanges	351.6	547.200	0.180	195.614	195.613	1.43E-06	1.80E-06	1939.896	7.196	269.572
			583.862	0.275	232.276	232.276	3.70E-07				
			371.655	0.000	0.000	0.000	0.00E+00				
IPE200	Web	371.7	572.400	0.180	200.745	200.744	1.02E-06	1.39E-06	1974.588	7.077	279.024
			610.751	0.275	239.096	239.095	3.73E-07				
			280.373	0.000	0.000	0.000	0.00E+00				
HEB160	Flanges	280.4	506.760	0.180	226.387	226.384	1.10E-05	1.21E-05	2481.171	8.647	286.937
			540.713	0.275	260.340	260.341	1.16E-06				
			299.225	0.000	0.000	0.000	0.00E+00				
HEB160	Web	299.2	506.400	0.180	207.175	207.172	7.74E-06	7.84E-06	2183.307	8.072	270.467
			540.329	0.275	241.104	241.104	9.75E-08				
			370.651	0.000	0.000	0.000	0.00E+00				
End-plate	End-plate	370.7	667.200	0.179	296.549	296.549	2.12E-09	6.22E-09	3260.344	8.667	376.172
			711.902	0.274	341.251	341.251	4.11E-09				
			903.849	0.000	0.000	0.000	0.00E+00				
Bolts	Bolts	903.8	1011.00	0.006	107.151	107.151	1.95E-07	3.13E-07	28945.163	182.080	158.970
			1061.92	0.028	158.069	158.069	1.18E-07				
			351.586	0.000	0.000	0.000	0.00E+00				
Welds	Welds	351.6	547.200	0.180	195.614	195.612	5.06E-06	5.89E-06	1498.936	3.774	397.177
			607.939	0.275	256.353	256.354	8.32E-07				

Figure 3.36: Curve-fit representation for the assessed C_1 and γ_1 parameters.

3.3.3 VALIDATION OF THE FE MODELS USING EXPERIMENTAL EVIDENCE

To compute the responses of the experimental test and the numerical model is necessary to work with the measurements obtained from both experimental and numerical procedures. It

is easily understood that the data measured in the experimental test can only be extracted where some instrumentation was applied. That is why, normally, the tests setup present some redundancy in the instrumentation to measure a specific parameter. This serves two purposes, the first is related to the possible failure of some measure equipment, and in this case there are other ways to get results for this property. The second purpose is to guarantee that measurements from distinct measure equipment's are consistent increasing confidence in results. On the other hand, in the numerical model the results are available throughout the model, being easier to obtain the property specific results and compared to the experimental ones.

The response of the experimental test can be obtained by the displacement transducer 1 or the group of displacement transducers 2 and 3, and the forces are assessed directly by the load cell where the load P is applied, and consequently the bending moment at the connection level can be computed multiplying the force P by the length d , according to Eq. (3.6). It is necessary to remove the contribution of the system elastic deformation. To obtain the response for the numerical models Eq. (3.7) was used to compute the bending moment and the Eq. (3.21) was used to compute the rotation of the joint and θ_{elast_column} and θ_{elast_beam} are obtained from the Eqs. (3.18) and (3.19), respectively. $DT23$ and $DT24$ are identified in Figure 3.21. By measuring the rotations in the beam it is possible to capture also the beam deformations near the connection, including the beam web and flange in compression plastic deformation, which is captured by Eq. (3.21).

$$\theta_{total} = \arctan\left(\frac{DT23U3 - DT24U3}{DT23DT24}\right) - \theta_{elast_coluna} - \theta_{elast_beam} \quad (3.21)$$

Figure 3.37 shows a comparison between the response of the experimental test and the results obtained with the numerical model. An inspection to the figure allows concluding that the extended end-plate connection models can also produce very accurate results when compared with the experimental data, for unstiffened columns. In this case, the comparisons are performed only at the global joint rotation level, because no additional information could be found in the available literature regarding the components under assessment.

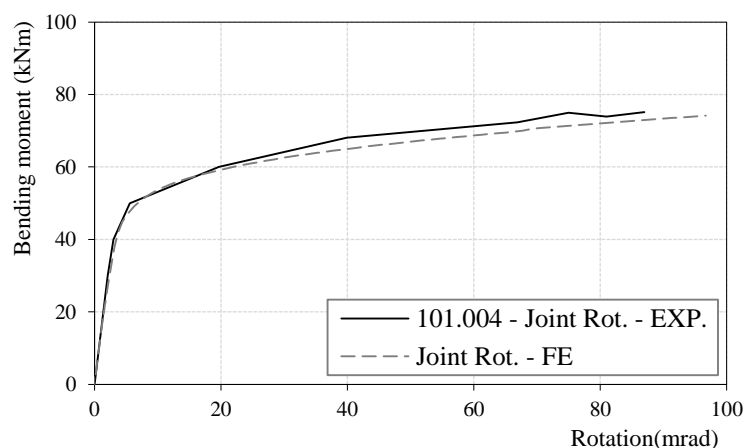


Figure 3.37: Comparison of the responses of the experimental and numerical results.

3.4 PARAMETERIZATION OF THE BEAM-TO-COLUMN END-PLATE JOINT MODEL

3.4.1 INTRODUCTION TO PYTHON AND ABAQUS INTERACTION

The characterization of joints behaviour can be obtained with a reasonable level of accuracy by finite element models, as discussed in the previous sections. In fact, when properly validated (by experimental evidence), numerical models can be an added value in the research to characterize the behaviour of joints.

Experimental tests proved to be so far the most accurate way to obtain the response of the joints behaviour. However, there are some limitations in obtaining all the data necessary for the proper characterization of the individual components that contribute to the joints behaviour. Finite element models provide the opportunity to complement the experimental test data, due to their discretised nature, providing all the relevant information in any element, and even providing data that is often unavailable from experimental tests, like contact or friction forces. Despite the fact that experimental tests are the most accurate way of determining the joints behaviour, their nature (needed infrastructures, highly qualified technicians and cost) limits their use. On the other hand, finite element models are the most sophisticated and precise tool to characterize the joints behaviour. In this perspective of complementarity between the experimental and numerical results, where the numerical models are an extension to the experimental ones, it is possible to develop large parametric studies, after the proper

calibration/validation of the FE models. Even though the evolution of commercial finite element software packages eased considerably this task, and despite being a method with increasingly wide acceptance, it is still very time consuming and cumbersome task modelling and analyse complex (but also in simple) finite element models, presenting frequently convergence and calibration difficulties (Gentili *et al.*, 2014). The task can be eased using scripting languages that can be compiled by the software, so repetitive and extensive parametric analysis can be performed, normally using a script. In the particular case of ABAQUS interface scripts are Python scripts. This implies of course to learn a programming language, but the user does not need to be a programming expert to use these tools, because there are some utilities that really makes this task easy to perform, as it will be explained hereafter. There is also available plenty of literature about the Python programming language, but in this particular case I would recommend the explanations and examples of Puri (2011), a manual directed to the use of Python scripts in ABAQUS from the first steps to far more complex tasks.

3.4.2 SCRIPT FOR THE EXTERNAL BEAM-TO-COLUMN FINITE ELEMENT MODEL

3.4.2.1 OBJECTIVE

The main objective of scripting is to save time in repetitive tasks, or the automation of tasks. In the context of this research, the objective was to build a tool capable of being versatile enough to deal with several end-plate bolted joints configurations, with several types of loading (quasi-static and dynamic) and capable of performing successive analysis for parametric studies. For that, the script contains all the needed variables to build the finite element model, to define the load protocol (static or dynamic), to define the type of analysis and information about the fields and history output requests. In addition to the modelling and analysis structure of the script, a post-processing statement was included, responsible to extract the relevant results, according to the user choices. The results are then grouped and exported to a text file, formatted according to the needs.

3.4.2.2 MAIN BODY OF THE SCRIPT

The main body of the script is divided in several parts, organized according to the steps taken in the ABAQUS GUI environment for the creation of the FE model, analysis and processing of the results. Firstly, a set of variables are defined, that takes into account the geometry of the model, meshing options, constitutive material options, analysis and convergence options and load options. Note that, from a parametric point of view, all variables are first of all *Lists*, whose length is defined by the number of joints to analyse (in the parametric study). Python *Lists* are defined in brackets separated by commas, and can contain *Numbers*, *Strings*, other *Lists*, *Tuple*, etc. Whenever possible, the name of the variables assigned to parameters are intuitive, often using familiar designations.

After all variables are identified, the beam-to-column finite element model is defined, starting with the creation of the model parts, including the wire and solid parts. After that, the material properties are created, considering that various materials may be assigned to distinct zones of each solid part, like in the case of having different material properties in the flanges and web of a profile. Then it is necessary to define the model profiles and sections and assign them to the corresponding parts. In the wire sections it is necessary to define the orientations. Following the creation of the model parts, and the assignment of mechanical properties to it, it is possible to define the type and shape of the mesh, as well the definition of the mesh generation for each part. The parts are then assembled according to the joints geometry. It is important at this stage to define sets of pre-defined mesh points, where the results are extracted in the post-processing phase. This step is crucial and the sets should be carefully chosen. The sets cannot be created after the analysis is completed, and they are needed to define the results extraction points in the script. After the assemblage of the model the steps are created. As explained in the previous sections, a step represents a phase in the model history, like a load change from a magnitude to another, an initial pre-stress operation of a part of the structure, or the change of a boundary condition in the model, and even the type of analysis. In this script, the solution of the problem is obtained in 3 steps according to what was mentioned in the loading part of Section 3.2.3.2. The choices for the field and history output request are also incorporated in the script. It is here that the user defines what results (stress, strain, displacements, forces, etc.) should be written to the output results file (.odb). These options are only available before the analysis. After that, the boundary conditions are defined, simulating the relations to the rest of

the frame. Thereafter it is possible to define the loads to apply to the sub-assembly containing the joint. In this case, the script allows the application of static and dynamic loads. For the static loads, a displacement is imposed to the beam, and for the dynamic an acceleration record should be provided and also an additional mass in the beam should be defined. The parts interact with each other by constraints and interactions, constraints are used, in this case, for the welded parts of the joint or to define the continuity between the solid and wire parts, and the interactions are used for the parts that are in contact, like the end-plate and the connected column flange. Finally, the job is created defining if possible the multiprocessor option available in ABAQUS.

So far, the script is able to create and run the beam-to-column model, next the post-processing options are defined according to the type of the analysis (frequency analysis, monotonic or cyclic static analysis and dynamic analysis). According to the user choice, the results are written to the output results file (*.odb*), for all nodes in the mesh or only for the pre-defined sets. At the end of the process, a text file with the chosen results is saved and converted to a *.csv* file in order to facilitate its manipulation in a worksheet.

A complete description of the steps needed to develop the script can be found in Annex B.

3.5 ISOLATED T-STUB FE MODELS

3.5.1 THE IMPORTANCE OF THE T-STUB MODEL

The study of joints behaviour discussed in the Chapter 2 allowed to clearly identify the components that can, or should, contribute to the energy dissipation, or to the rotation in the plastic domain. In a ductile extended end-plate joint, it is expected that the most dissipative components are the end-plate and/or column flanges in bending and the column web panel in shear. As discussed earlier, the energy dissipation associated to the column web panel in shear is, in most codes of practice, limited to a percentage of the joint rotation. In the case of the EC8 (EN 1998-1, 2004), this component cannot contribute more than 30% of the global joint plastic rotation. The validity of this rule can be discussed in more detail later. The issue here is that this limitation transfers to the other dissipative components the requirement to dissipate much of the energy. In this case, the equivalent T-stub concept, that is a simplified model with

practical interest, and which is used in the component method, can be the most useful tool, from a codification point of view, to characterize the behaviour of the components end-plate and/or column flanges in bending. With that in mind and since in beam-to-column end-plate bolted connections, several isolated T-stub models can be identified to characterize the connection behaviour, a set of isolated T-stub finite element models were developed in order to characterize their behaviour and plastic mechanisms associated to the several failure modes, identified in the EC3-1-8 (EN 1993-1-8, 2005). This will allow further to set considerations about the influence of these failure modes, for instance, in the equivalent viscous damping assessment for partial-strength joint or to understand better the phenomena involved in the interaction of the several elements that constitute the T-stubs, namely the T bending plates, the bolts and the interactions between them.

In the following paragraphs the developed isolated models will be explained, analysed and validated by the results of experimental tests available in the literature.

3.5.2 EXPERIMENTAL TESTS USED IN THE NUMERICAL MODELS VALIDATION

To understand the cyclic behaviour of the dissipative components of the partial-strength connections, it is important to study and calibrate each component separately. A set of models of isolated bolted T-Stubs that represent the flange of the column and the end-plate in bending were developed to calibrate their behaviour. The numerical models are in accordance with the experimental tests performed by Piluso and Rizzano (2008) at the Material and Structures Laboratory of the Department of Civil Engineering of Salerno University. Furthermore, the authors kindly provided the results of the coupons materials tests for use in this study. The objective is to calibrate the three typical bolted T-Stub failure modes, reviewed in Section 2.2.2.2 and shown in Figure 2.21, and also to calibrate the hysteretic behaviour of those connections.

Two types of “T” were used, namely laminated and welded as shown in Figure 3.38. For the laminated profiles, half HEA180 and HEB180 profiles were used and for the welded profiles, plates with thicknesses of 18mm for the flanges and 12mm for the webs were used. The bolts were M20 (class 8.8) in all cases, and the geometrical properties are listed in Table 3.19.

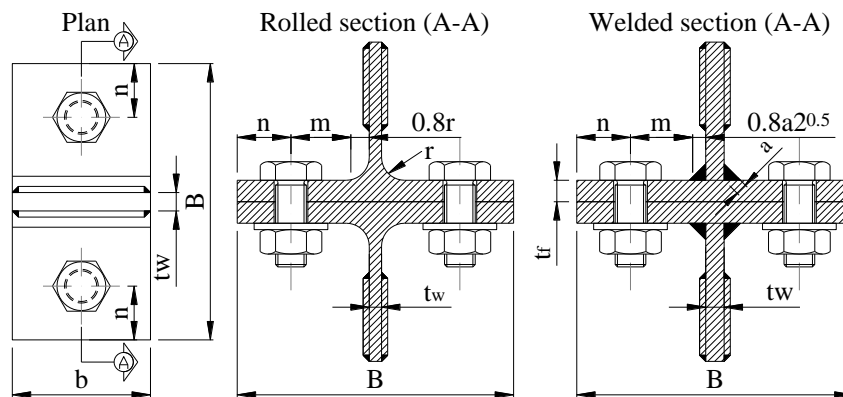


Figure 3.38: Geometry of bolted T-Stubs (Adapted from Piluso and Rizzano (2008)).

Two types of loading protocol were used in these models: monotonic and cyclic loading. It is recognised that the material property definition needs to be different to account for the difference in behaviour associated with the cyclic plasticity, as discussed in the previous sections.

Table 3.19: Measured geometrical properties of tested specimens.

Series	Test	B (mm)	b (mm)	t _f (mm)	t _w (mm)	r (a) (mm)	m (mm)	n (mm)
A: HEA 180	A1	181.25	158.75	9.71	6.78	15.00	37.39	37.85
	A2	181.75	158.25	9.68	6.83	15.00	37.23	38.24
B: HEB 180	B1	180.00	159.00	14.14	8.10	15.00	36.76	37.19
	B7	180.00	158.25	14.19	8.15	15.00	36.71	37.21
D: W18	D1	231.00	90.25	18.64	12.25	7.50	52.31	51.07

For the HEA 180, HEB 180 and plates, the material stress-strain data from Piluso and Rizzano (2008) were adopted and for the bolts, the nominal values for the 8.8 class were used, according to the EC3-1-8 (EN 1993-1-8, 2005), given the lack of information concerning the characterization of the bolt materials. Table 3.20 shows the coupons tests material properties, which reports values in terms of true stress and true strain.

Table 3.20: Measured mechanical properties of tested specimens.

Series	A ₀ (mm ²)	ε _u (%)	f _y (MPa)	f _u (MPa)
A: HEA 180	207.82	98.28	334.67	530.62
B: HEN 180	106.28	109.92	280.10	464.56
D: W18	373.13	98.32	307.34	464.94

3.5.3 DESCRIPTION OF THE NUMERICAL MODELS

As in the previous complete joint models T-stub behaviour is a three dimensional problem. Although, in this case, due to the lower complexity associated to this simpler models, a 2D representation can more easily obtain reasonable results with affordable deviations from the real results. Nevertheless, and in line with previous sections, the FE models use solid three-dimensional finite elements, contact elements and, additionally, geometrical and material non-linearity are also taken into account. The numerical models intend to translate the geometry of the connections, namely the T elements sections and the bolts, and the interaction between them, in an accurate way, the choice of the elements type and size, the proper material stress and strain relationships and also the proper analysis procedures are crucial to obtain the expected behaviour of the models. The essentials of the options taken in the FE development and analysis are much in line with what was described before in Section 3.2.3 for the joint solid part. However, the main options for the T-stub models will be briefly recalled here. The models geometry and mesh discretization is depicted in Figure 3.39.

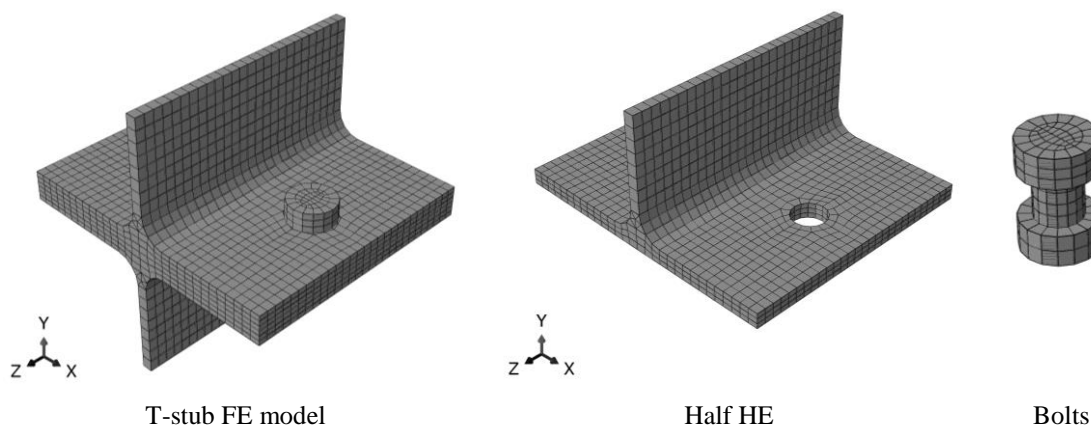


Figure 3.39: T-stub meshed parts of the FE model.

In general the standard volume elements of ABAQUS were used. Mainly the quadrilateral and hexahedra C3D8RH element is used, which is an 8-node linear brick element, with a hybrid formulation, featuring constant pressure, reduced integration and hourglass control. However, in specific situations where the hexahedra formulation was not possible to use, element C3D6H was used which is a 6-node linear triangular prism, hybrid and constant pressure element. To avoid the hourglass problem at least three layers were considered in the thickness of the plates in bending of the connections members, and the hourglass control formulation was activated for the elements. The elements chosen also have a hybrid formulation because severe plastic

deformation is expected, and the rate of total deformation becomes incompressible as the plastic deformation starts to dominate the response (ABAQUS, 2014).

The models are composed by several parts as shown in Figure 3.39, which interact with each other through constraints or interactions. The interactions between the bolts and the T-stub plates are achieved using the general contact algorithm based on “hard contact” formulation that acts in the normal direction to resist penetration and also accounts for tangential behaviour considering the friction between surfaces.

3.5.4 CONSTITUTIVE MODELS (MATERIAL OPTIONS)

An important feature in a numerical model is the material definition using constitutive stress-strain models. These models can be more or less elaborated depending on the material behaviour and generally, for sharp knee material types, bi-linear idealisations can be used without impairing accuracy. The use of theoretical stress-strain relationships for the material definition, and their validation through real tests, revealed to be an important help in the standardisation of the data collected from the several experimental tests. The lower complexity of the T-stub models allows a discussion on the choice of the main constitutive models available for the characterization of material properties, when the specimen is subjected to monotonic loading. Three theoretical expressions were used in the T-Stub models: a bilinear approach, the Ramberg-Osgood non-linear model for materials of round-house type at yielding and the Menegotto-Pinto non-linear model for materials of sharp-knee type at yielding. To define each expression the following material properties have been used: the yielding strength, f_y , ultimate strength, f_u and Young’s modulus, E . According to the formulation described in Section 2.2.3.2, the several stress-strain relationships were derived for the three approaches mentioned. Figure 3.40 illustrates the stress-strain relationships for the models adopted for the A1, B1 and D1 tests, under monotonic loading.

As for the beam-to-column end-plate joints, for the cyclic models, the combined isotropic/kinematic model available in ABAQUS was used for the simulation of the material hardening when subjected to cyclic loads, see Section 3.2.3.2 iii). Likewise, C_k and γ_k parameters of the kinematic component of the combined model, were determined by adjusting the kinematic analytical curve by the known points of the true stress-true strain curve, according to Figure 3.17, minimising the error between the points and the analytical kinematic expression.

Table 3.21 lists the procedure for the A2 and B7 tests and Figure 3.41 a) and b) illustrate the adjustment for the A2 and B7 tests, respectively.

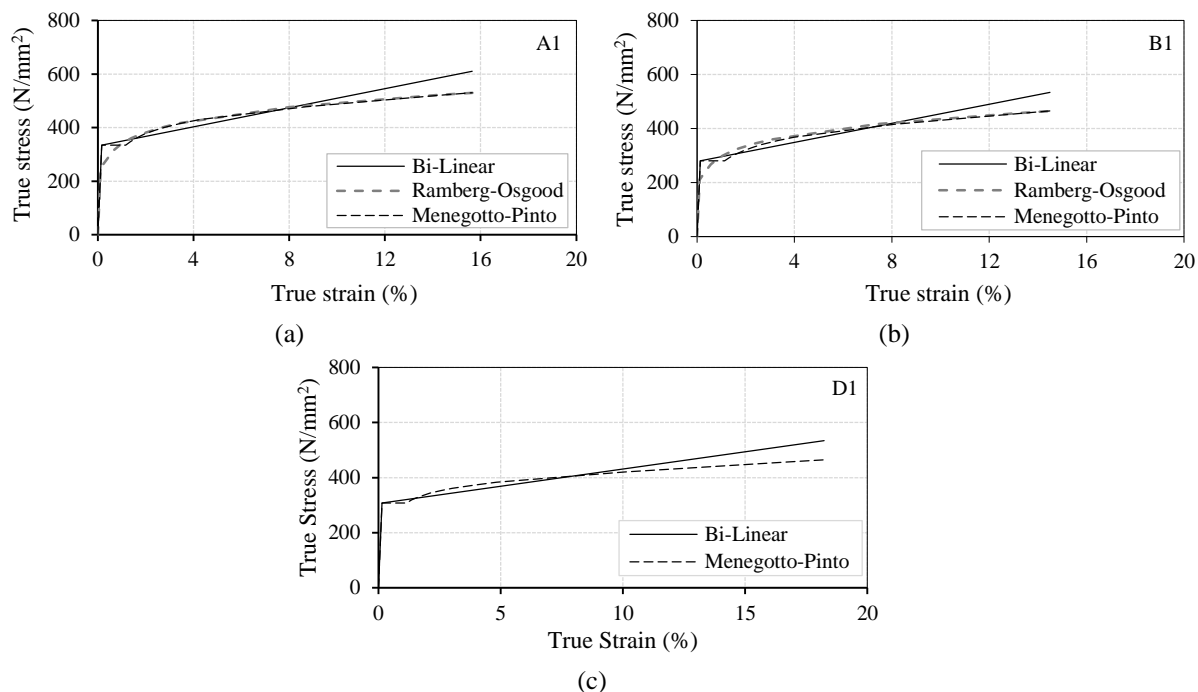


Figure 3.40: Stress-strain relationships for: a) test A1, b) test B1 and d) test D1.

Table 3.21: Kinematic hardening calibration.

	f_y (MPa)	f_{u_tru} (Mpa)	ϵ_{pl}	α^* (MPa)	α (MPa)	$(\alpha^*-\alpha)^2$	$\Sigma(\alpha^*-\alpha)^2$	C_1	γ_1	C_1/γ_1
A2	334.7	334.675	0.000	0.000	0.000	0	4.75E-04	3179.401	14.472	219.687
		478.084	0.073	143.410	143.388	4.57E-04				
		530.674	0.154	195.999	196.003	1.81E-05				
B7	265.0	265.4389	0.000	0.000	0.000	0	8.29E-10	1807.498	3.746	482.484
		387.1348	0.078	121.696	121.696	9.94E-11				
		464.5617	0.142	199.123	199.123	7.29E-10				

The determined relationships were introduced in ABAQUS in order to simulate the experimental tests results, for the several failure modes defined in EC3-1-8.

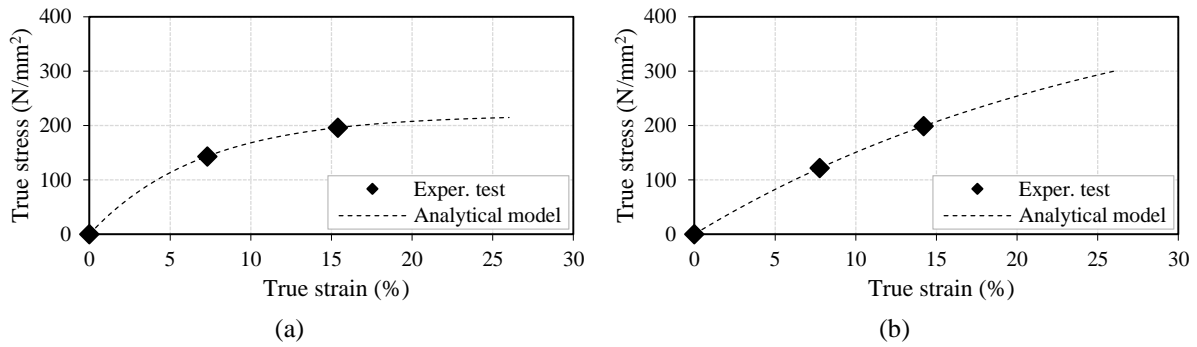


Figure 3.41: Lemaitre and Chaboche (1990) model for kinematic hardening for: a) A2 test and b) B7 test.

3.5.5 RESULTS OF THE FE MODELS AND EXPERIMENTAL TESTS

The models were loaded following the tests procedure. An imposed displacement was applied in the boundary conditions defined in the T-stubs. The solution of the problem is obtained in 3 steps. The first step is used to formulate the boundary conditions and the interactions defined previously. The second step corresponds to the pre-loading of the bolts using the adjust length option and determining the length magnitude by the elastic elongation needed to produce the required amount of force in the bolts, normally a percentage of the ultimate strength, but in this case only 80% of the bolt yield axial force was used. It is in the third step that the pushover analysis begins.

For the monotonic loaded specimens, the experimental tests results are depicted in Figure 3.42. As stated before, the objective of the monotonic study was to calibrate the various failure modes of bolted T-stubs, according to EC3-1-8 (EN 1993-1-8, 2005). Thus, the A1 tests exhibited failure mode 1, the B1 tests showed failure mode 2 and the D1 tests presented a failure mode 3, according to Figure 2.21.

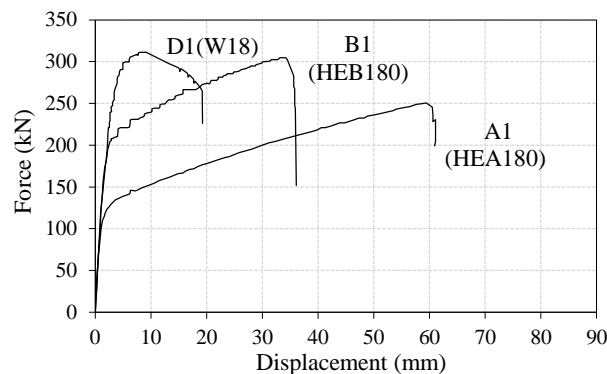


Figure 3.42: Monotonic Force-displacement experimental results (Piluso and Rizzano, 2008).

The numerical models incorporated several available constitutive models to simulate the material properties, in order to analyse the ones that produce the closest results to the experimental tests response.

The numerical results are compared with the experimental test results in terms of force-displacement relationship. Only the relevant part of the chart will be presented in Figure 3.43. The numerical results are presented in dashed lines and the experimental results are depicted in solid lines. In Figure 3.44, the Von Mises stresses are plotted, highlighting the development of the three failure modes previously outlined. For the A1 test, it is possible to observe the formation of the complete yielding of the flange, which is characteristic of the first mode plastic mechanism. In the case of the B1 test, the second mode plastic mechanism can be observed with the yielding of the plates and bolts. For the D1 test, the early yielding of the bolts indicates failure mode 3 behaviour.

A closer look in the comparisons, depicted in Figure 3.43, allows to conclude that the bi-linear approach achieved a good agreement with the experimental results. For the Ramberg-Osgood approach the agreement was not so good, and the best correlation was achieved with the Menegotto-Pinto model, due to its similarities with the measured stress-strain relationship (sharp knee material type). This fact proves that the adoption of more realistic models have advantages over simplified models in terms of accuracy of the results. However, it is necessary to evaluate whether the benefits, which are obtained with the use of a constitutive model more complex (non-linear model) are actually balanced by the increase of accuracy of the results. Consider this particular case where a bi-linear approach was used, for the material properties description, and a more refined non-linear approach was also used (Menegotto-Pinto). The obtained results are very similar in all the analyses performed. Despite the Menegotto-Pinto model is closer to the actual results the gain in accuracy is not worth the increased complexity of the analysis. That is the reason to use linear constitutive models whenever is possible in this research. It is important to mention that the analyses performed were all under monotonic loading and, as discussed in Section 2.2.3.2, when reversal load occurs a different approach should be used, because the cyclic plasticity is dependent on the load history.

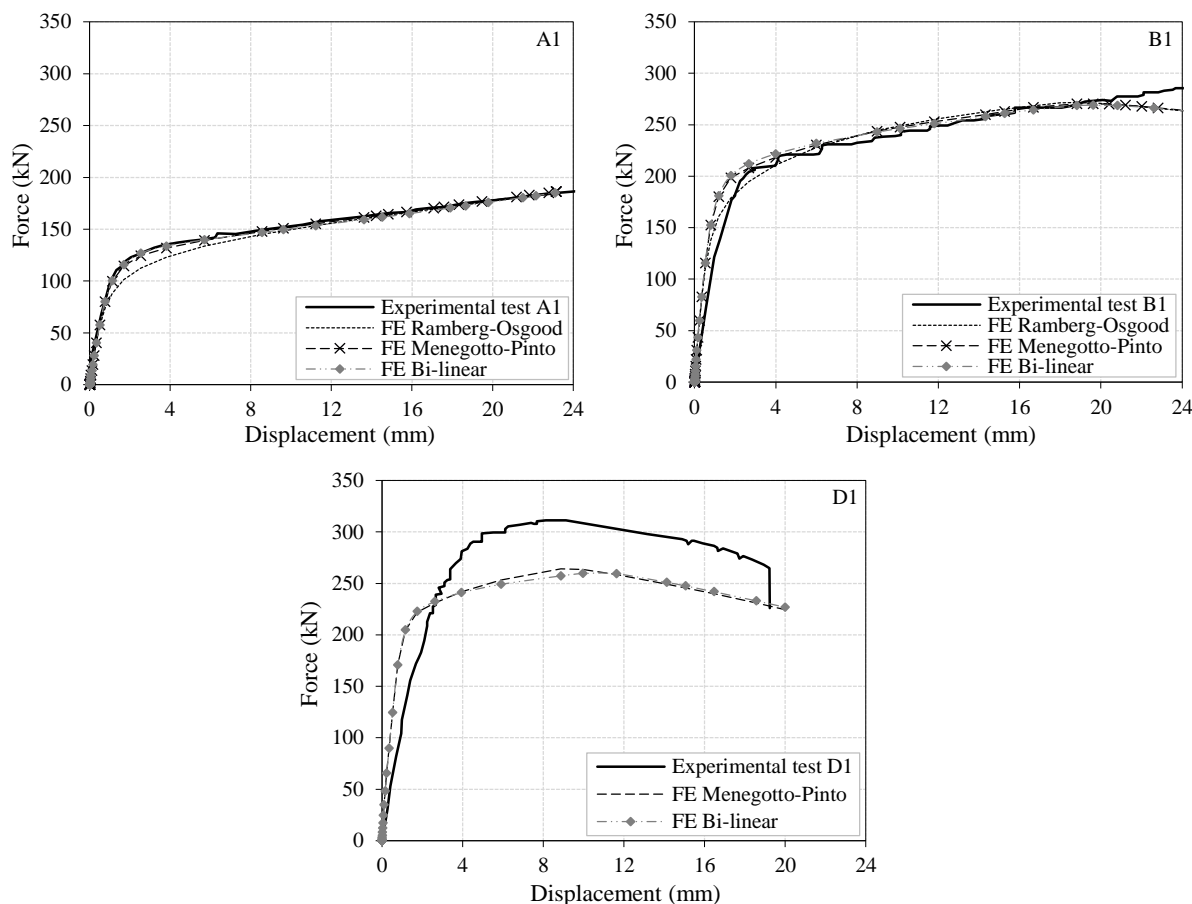


Figure 3.43: Results comparison with different material characterisations for models A1, B1 and D1.

For the D1 simulation, the numerical model did not fit well with the experimental results. According to EC3-18(EN 1993-1-8, 2005), this connection should exhibit failure mode type 2 but the test revealed a type 3 mode of failure, as observed also by the Piluso and Rizzano (2008) who remarked:

“The application of the formulations suggested by Eurocode 3, for predicting the resistance and the collapse mechanism of bolted T-stubs, provides for such specimens a type-2 collapse mechanism, i.e. flange yielding with bolt fracture. However, it is important to underline that, according to experimental evidence, W18 specimen exhibits a type-3 collapse mechanism, i.e. bolt fracture only.”

A further objective of the present study is the calibration of the cyclic hysteretic behaviour of the bolted T-Stubs for the two dissipative failure modes type 1 and type 2.

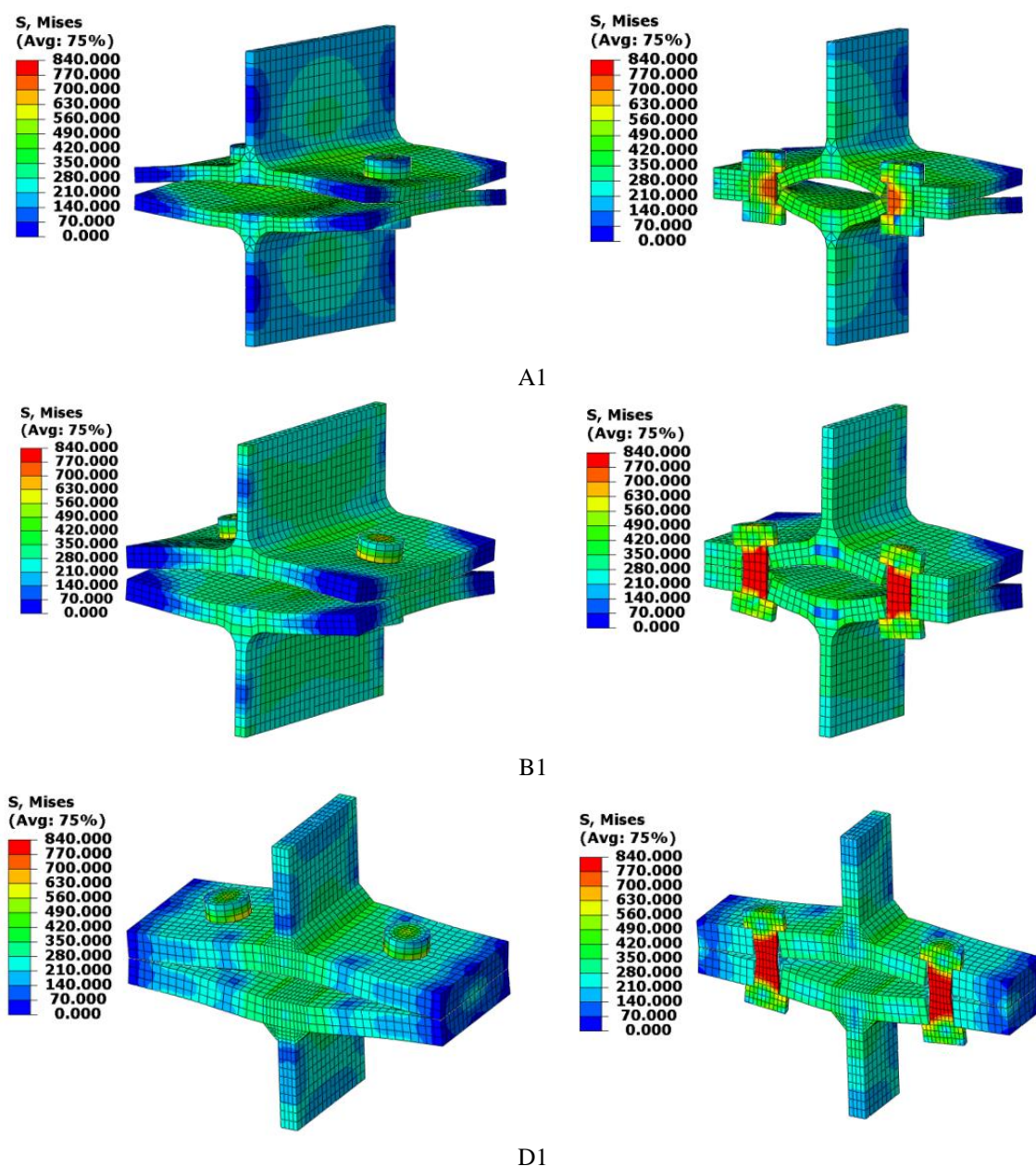


Figure 3.44: Von Mises stress results for a 20mm displacement for the FE models A1, B1 and D1.

The loading histories applied to both the tests and models consisted of 57 cycles of constant amplitude (10 mm) for the A2 test and 13 cycles of constant amplitude (20 mm) for the B7 test, which were applied to the upper support of the web.

For the cyclic response, the numerical results show good agreement with the experimental results, mainly in the A2 tests. For the B7 tests, the results were acceptable, but with less agreement. The comparison of results observed in Figure 3.45 and Figure 3.46 show good agreement between the numerical and experimental behaviour.

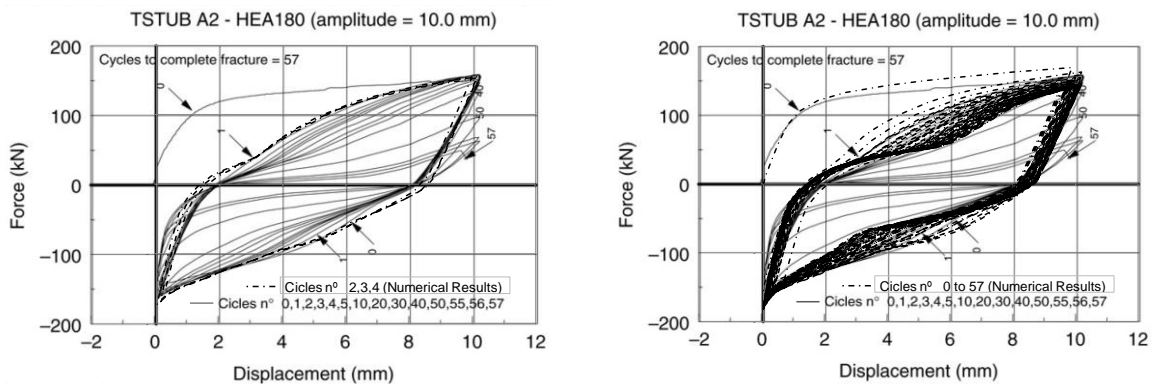


Figure 3.45A2 model results comparison, on the left only cycles 2 to 5 and on the right the complete results.

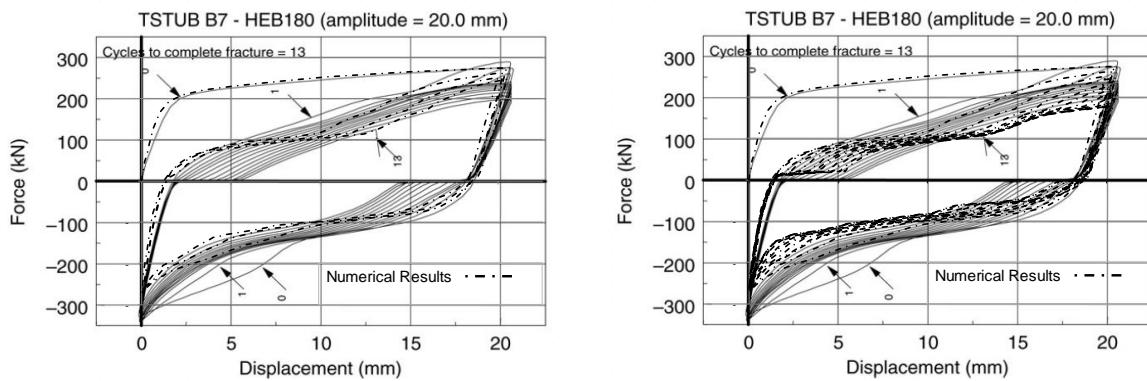


Figure 3.46: A7 and B7 model results comparison, on the left the first 3 cycles and on the right the complete results.

In the previous sections the discussion on the development of the finite element models, both for the complete sub-assemblages possessing beam-to-column end-plate bolted joints, and for the characterization of isolated T-stub models, revealed that numerical simulations revealed to be a powerful tool for the characterization of the joints behaviour and its components, whether determined directly in the complete model whether modelled separately.

3.6 MAIN CONCLUSIONS

This chapter described the development of a finite element model capable of representing the behaviour of extended end-plate joints classified as partial-strength according to Eurocode 3, but is also able to represent equal and full-strength joints. The model developed in ABAQUS uses solid (or continuum) elements in the connection zone. For computational efficiency, beam elements were used in the column and beam regions located away from the connection. The

model considers non-linear material and geometrical behaviour, non-linear contacts, re-contacts and slip. A material model combining both isotropic and kinematic hardening was employed.

The model was calibrated against experimental tests carried out at the University of Coimbra on double extended end-plate beam-to-column joints, and with others found in literature. The experimental tests were extensively detailed, and the results were analysed, globally and at the component level, and they were compared with the analytical values obtained using the EC3-1-8 (EN 1993-1-8, 2005) and other methodologies, namely the Krawinkler model for the column web distortion. The excellent agreement between the experimental data and the numerical results allowed concluding that the model is capable of simulating with accuracy the behaviour of end-plate beam-to-column joints, and that it can be used for detailed analyses of the components behaviour.

Additionally, isolated T-stub components models were also developed in ABAQUS, with the objective of characterizing the behaviour of the different failure modes according to the EC3-1-8. Several constitutive material models were investigated for the monotonically loaded models, revealing that the linear ones have sufficient accuracy to be used in further analysis.

Both end-plate models and isolated components models were subjected to monotonic and cyclic loading protocols, according to the tests procedures, revealing a good agreement between the numerical results and the experimental ones, either at the response level, or at the energy dissipation level.

A practical procedure to extract the moment-rotation relationships from the experimental and numerical models was also presented, both for the global behaviour and also at the components level.

4

DEVELOPMENT OF A METHODOLOGY FOR THE CHARACTERIZATION OF THE JOINT COMPONENTS USING THE FE MODELS

4.1 INTRODUCTION

The prediction of joint behaviour relies on experimental and numerical tests that provide accurate information for the characterization of the various joint components.

Partial-strength joints subject to static monotonic loading are well characterized in modern codes of practice, such as EC3-1-8 (EN 1993-1-8, 2005) within the framework of the component method. However, in the presence of cyclic load reversals there is no direct and easy approach to characterize their cyclic behaviour and energy dissipation, as discussed in Chapter 1. When this demand results from the seismic action, the cyclic behaviour of the dissipative members and joints play an important role defined by their ductility, tenacity, rotation capacity and energy dissipation.

As highlighted in the objectives of this research (Section 1.2) it is intended, with this research, to contribute to the development of an analytical design method, based on the component method, which takes directly into account the cyclic behaviour of each dissipative component, given that an adequate overstrength is assured for the non-dissipative components (capacity design). This analytical procedure allows the idealized behaviour of the joint to be included in the global analysis of the frame structure.

The load reversals bring additional complexity, because it is necessary to account for phenomena such as kinematic strain-hardening, Bauschinger effect, possible pinching effect, among others. Nevertheless, as realised by Shen and Astaneh-Asl (1999), when properly designed, bolted joints may exhibit high ductility and good energy-dissipation capacity under cyclic loading, provided that proper overstrength is available for the brittle components. With that in mind the discussion in this chapter aims to contribute to the mechanical characterization of the components in double-extended beam-to-column joints using a detailed parametric numerical model developed in ABAQUS (2014). The detailed numerical model described and validated in Chapter 3 will be used, taking also advantage of the Python programming language to develop a scripting interface for ABAQUS, as described in detail in Appendix B. The model is applied to end-plate beam-to-column joints and considers a three dimensional detailed representation of the various joint components taking into account the several phenomena involved in the connection behaviour, namely the nonlinearities related to the geometry, contact, slip and material properties. To deal with cyclic loading, a combined isotropic and kinematic material-hardening model is also included in order to characterize the connection behaviour under load reversal.

In the following sections, the cyclic behaviour of the joints is characterized, both globally and also in terms of the critical components, comparing the results with available analytical models and with advanced methodologies. A detailed procedure is described to isolate the column web components under cyclic loading, namely the column web panel in shear and the column web in transverse compression or tension, and to identify their mechanical behaviour analysing the stress and deformation fields in the FE models. At the connection level, a procedure is also proposed, based on the components deformation shape, and using the insights gained in the assessment of the column web components. Also, the response of the components in bending and bolts in tension is assessed.

4.2 CHARACTERIZATION OF THE COLUMN WEB COMPONENTS

4.2.1 FRAMEWORK

This section presents a methodology to characterize the behaviour of column web panel components from experimental results and/or FE models under monotonic and cyclic loading conditions.

Figure 4.1 shows a double-extended end-plate beam-to-column steel joint and two possible component models. The active components are the following:

- (1) column web panel in shear;
- (2) column web in transverse compression;
- (3) column web in transverse tension;
- (4) column flange in bending;
- (5) end-plate in bending;
- (7) beam flange and web in compression;
- (8) beam web in tension;
- (10) bolts in tension
- and (19) welds.

The characterization of the components behaviour under cyclic loading conditions is a complex task. To ease the process, and to analyse in detail each component behaviour, the identified components were grouped according to their location in the joint as follows: components of the column web (1, 2 and 3), components of the connection (4, 5, 10 and 19) and components of the beam (7 and 8). The components of the beam (7 and 8) and the welds (19) will not be analysed in this document. These components (7, 8, and 19) must be designed with sufficient overstrength.

When the joint is subjected to load reversal, it is necessary to take into account the added complexity of exhibiting tensile and compressive stresses within the same location of the joint. With reference to Figure 4.1, this added complexity mostly results from the fact that the load-introduction points, in the column web, vary as the stresses change from tension to compression. When transferring tension from the beam to the column, the load-introduction in the column web panel depends of the position of the bolt rows in tension, while compression is more evenly

distributed around the compression centre, with the peak maximum compressive stress aligned with the compressed beam flange, as it will be shown later in Figure 4.18.

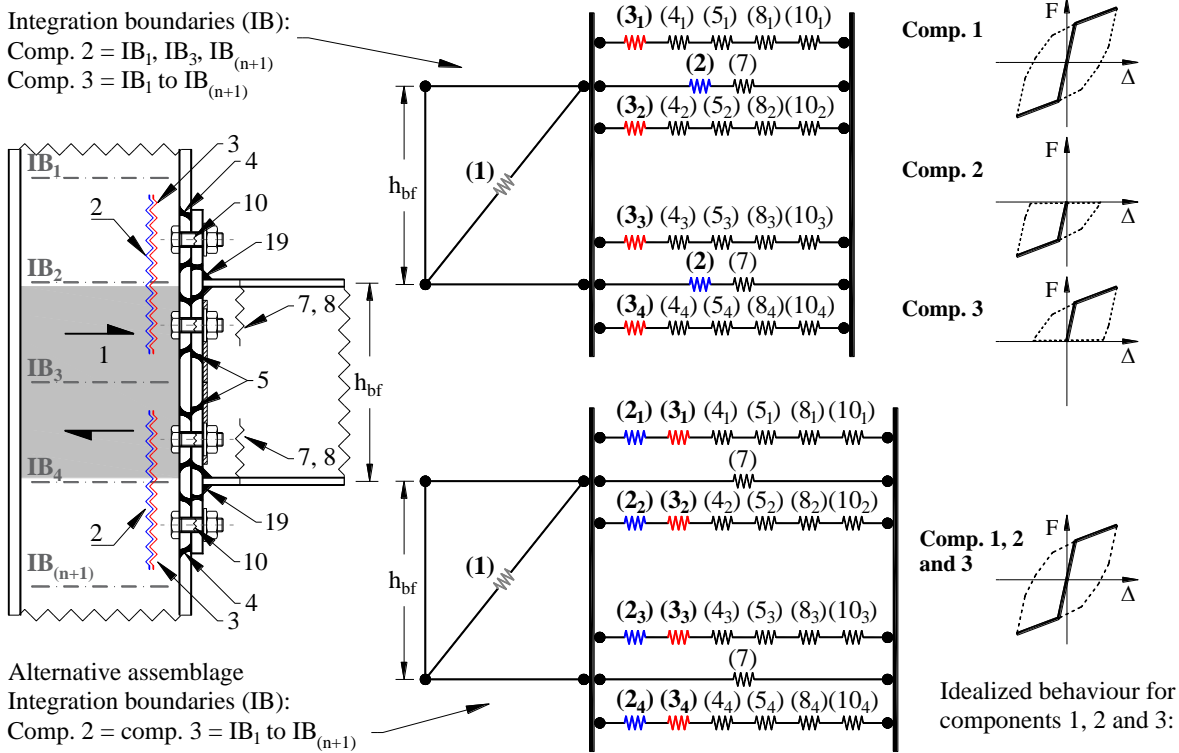


Figure 4.1: From left to right: Identification of the components in the joint and definition of possible integration boundaries (IB); assemblage of the identified components according to the integration boundaries chosen; idealized response of the column web components 1, 2 and 3.

In line with the main assumptions of the component method (EN 1993-1-8, 2005), the joint is discretized according to the bolt rows and the centre lines of the beam flanges, as shown in Figure 4.1, using appropriate effective widths. Consequently, the characterization of the components in the column web panel depends on the assumed simplifications of the component model. Nevertheless, it is possible to lump some of the components lines of action in order to simplify the problem, as shown in the alternative assemblage of Figure 4.1. This procedure aligns the load-introduction tensile and compressive components in the column web panel, allowing to combine the force-deformation response of these two components into one single force-deformation curve. However, this comes at the expense of losing consistency with the component characterization of EC3-1-8 for static monotonic conditions, as it can be seen in the idealized $F-\Delta$ response of the components for the alternative assemblage presented in Figure 4.1.

In the following section, a general extraction procedure is described that allows for the arbitrary consideration of any component model. Therefore, the choice is freely left to the user to implement any component model and to easily convert the component characterization of the column web panel components across different models such as those shown in Figure 4.1.

4.2.2 COMPONENTS IDENTIFICATION METHODOLOGY

In this section a methodology is presented to extract the column web panel components behaviour, due to the load-introduction effect and the shear effect. It is based on the results provided by the FE models and allows the derivation of force-displacement and shear-distortion curves of the components. This methodology was developed using numerical integration of the stress fields obtained from FE models in order to characterize the component column web panel in shear and the component column web in transverse compression/tension. The methodology is based on considerations presented in Jordão *et al.* (2013) for welded joints, the formulation is summarized in Table 4.1 and illustrated in Figure 4.2 to Figure 4.5 for the load-introduction effect and for the shear effect. The forces (F_c and F_t) are obtained through integration of the stress field according to Eq. (4.1) for the load-introduction effect and from Eq. (4.2) due to the shear effect. In these equations, σ_{33} (or σ_{zz}) is the normal horizontal stress in the column web along path PI , integrated over the lengths h_c for compression and h_t for tension (Eq. (4.1)). Furthermore τ_{23} (or τ_{yz}) is the shear stress in the column web along path $P3$, integrated over the corresponding lengths (Eq. (4.2)), t_{fc} and t_{wc} are the column flange and web thicknesses, respectively, and t_l is the thickness according to the shear area represented in Figure 4.5(b).

It is noted that this procedure is quite flexible in defining the integration boundaries (IB in Figure 4.2) to calculate the forces. The assessment of the forces will depend on the idealized mechanical model, and the procedure can be easily adapted to the two examples presented before or to any other compatible mechanical model. Moreover in the case of the shear evaluation other integration boundaries can be considered; in this case, the EC3-1-8 (EN 1993-1-8, 2005) shear area definition was used to set the boundaries for integration. The procedure is also applicable to joints with transverse web stiffeners, as depicted in Figure 4.3, for negative or positive bending.

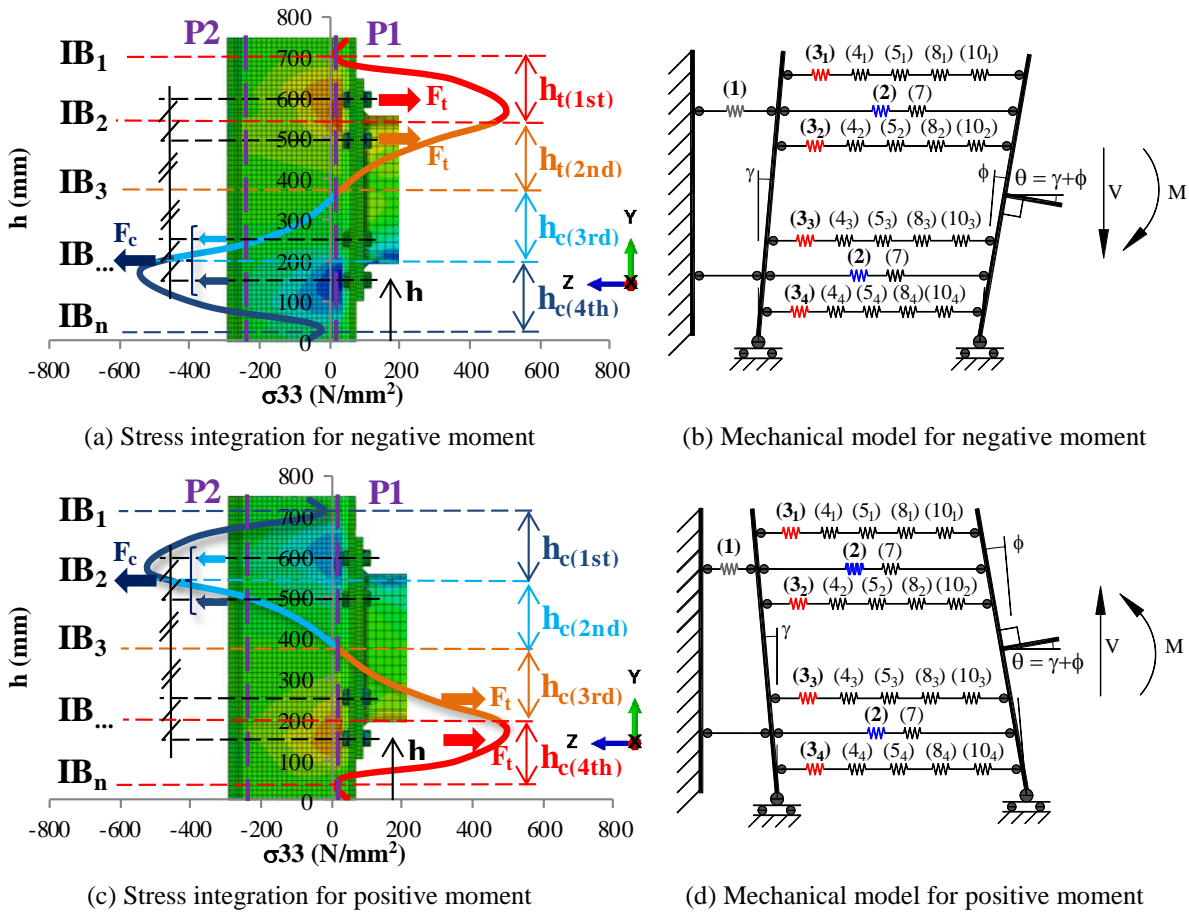


Figure 4.2: Procedure to obtain the forces in the column web in transverse tension and compression components, (a) and (c), under negative and positive bending moment; and in (b) and (d) the same components are identified in the global assembly of the joint components, also for negative and positive moment, respectively.

$$F_c = \left(\int_{h_{c,i}} \sigma_{33} dy \right) \cdot t_{wc} \quad \text{or} \quad F_{t,i} = \left(\int_{h_{t,i}} \sigma_{33} dy \right) \cdot t_{wc} \quad (4.1)$$

The paths P1 and P2, along which the normal stress diagrams are evaluated to compute the compression and tension forces and the normal displacements are evaluated, are located in the column web beyond the root radius, as identified in Figure 4.4 (b). This allows the identification of the forces introduced by the beam into the web and avoids the stress perturbation observed in the corner.

To determine the shear force (V_n) in the web panel, the stress field is evaluated at a cross section of the column aligned with the mid-height of the connected beam, where the stresses reach their maximum values (at bending neutral axis), using the middle elements of the web to extract the shear stresses. The stresses in the column web panel are assumed to be uniformly

distributed due to the action of the column flanges, as proposed by Jaspart (1991). Therefore, the shear stresses are only extracted along path P3, see Figure 4.5 (a).

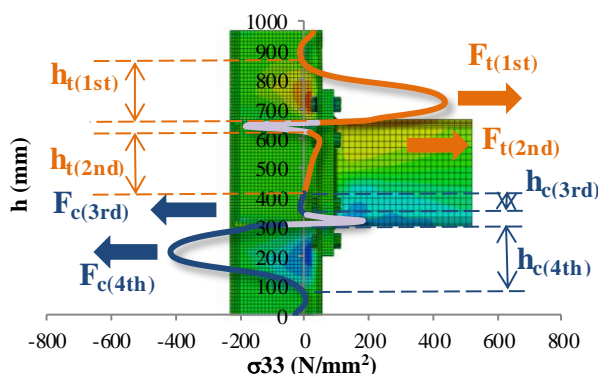


Figure 4.3: Particular case for joints with transverse web stiffeners, determined for positive bending moment.

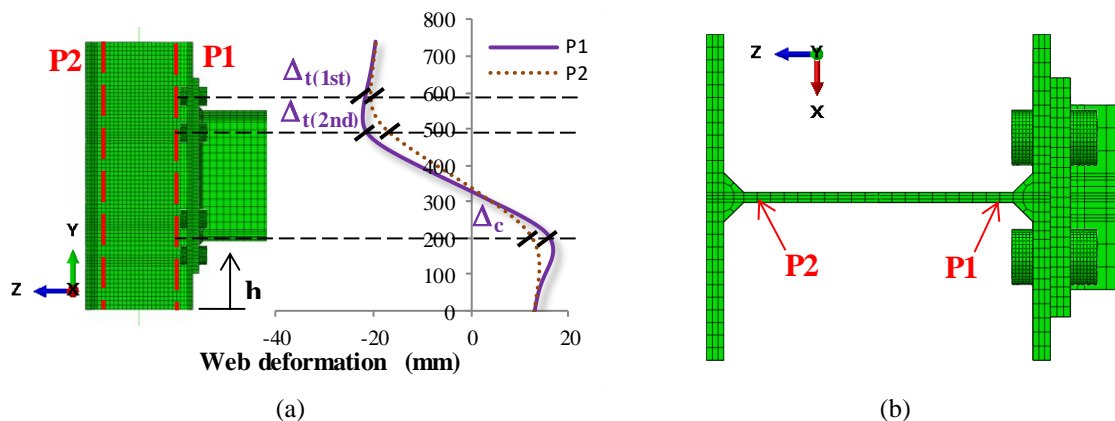


Figure 4.4: (a) Procedure to obtain the web deformation of the column web in transverse tension and compression components; (b) location of the paths P1 and P2.

The deformation and rotation corresponding to the load-introduction effect and shear effect, respectively, are obtained from the displacement fields. In the case of the load-introduction effect, the displacements are extracted from paths P1 and P2, see Figure 4.4, and the deformation is determined as the difference between the nodes in the paths aligned with the element that causes the deformation, e.g. bolt rows, flanges, etc., see Figure 4.4 (a) for negative bending moment. For the rotation due to the shear effect, the displacements are extracted from the predefined nodes indicated in Figure 4.5 (a) and computed according to Eq. (4.5).

Whenever transverse stiffeners are present, the additional shear strength is included, which is provided by the moment resisting frame formed by the column flanges and the transverse stiffeners aligned with the beam flanges. This is done assuming a plastic mechanism whereby the plastic hinges will occur in the column flanges due to the higher stiffness and

strength of the stiffeners. The stresses are extracted at a section near the flanges maxima normal stresses, σ_{22} , as depicted in Figure 4.6. Subsequently, Eq. (4.3) is used to determine the bending moment in the flanges, and Eq. (4.4) is used to obtain the additional shear strength V_c .

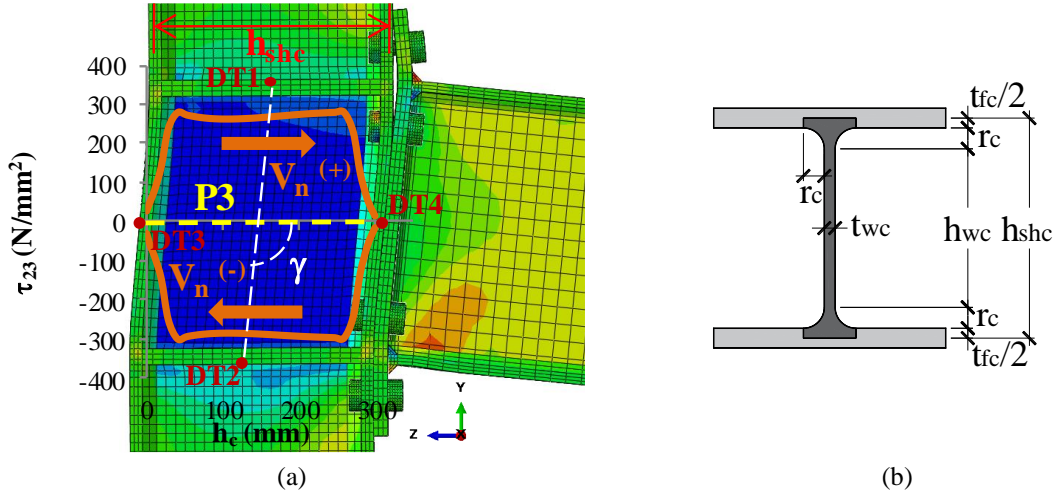


Figure 4.5: Procedure to obtain the shear force of the column web panel in shear component.

$$V_n = \left(\int_{(t_{fc}/2+r)_{back}}^{(t_{fc}/2+r)_{front}} \tau_{23} dz \right) \cdot t_1 + \left(\int_{h_{wc}} \tau_{23} dz \right) \cdot t_{wc} + \left(\int_{(t_{fc}/2+r)_{front}} \tau_{23} dz \right) \cdot t_1 \quad (4.2)$$

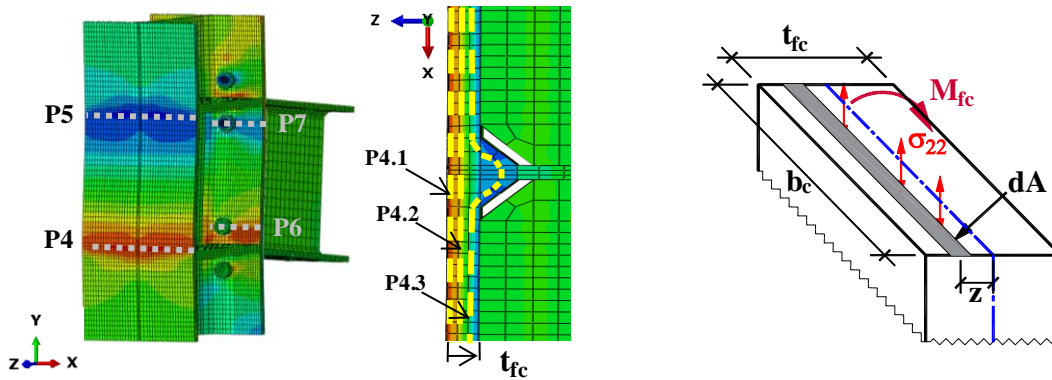


Figure 4.6: Determination of the bending moment in the flanges through stress integration.

$$M_{fc} = \int_{-t_{fc}/2}^{t_{fc}/2} z(\sigma_{22} dA) , \quad dA = b_c \cdot dz \quad (4.3)$$

$$V_c = \frac{M_{fc(P4)} + M_{fc(P5)} + M_{fc(P6)} + M_{fc(P7)}}{h_b - t_s} \quad (4.4)$$

For simplification, it is considered that the stresses are uniform along the width of the column flanges. Therefore, the integration of the stresses along each path results in a single

force at that strip. The bending moment is obtained by multiplying the force at each layer by the distance to the neutral axis. The bending moment can be computed with the forces determined in the two outer paths (P4.1 and P4.2). However, and because it is necessary to determine the neutral axis position, due to the presence of axial force in the column, a third path (P4.3) is required to determine the location where the stresses are equal to zero, the neutral axis position is sensitive to the back and forward from the cycles. It is also important to note that the third path should cross the radius and web elements so that the integrated forces and the neutral axis evaluation takes that into account.

The formulation used in the procedure to build the $F-\Delta$ curves for the column web components are summarized in Table 4.1.

Table 4.1: Equations for the extraction of the F-Δ relationships from the numerical results.

Component	Resistance (F)	Deformation (Δ)
Column web panel in shear	$V_n = \left(\int_{(t_{fc}/2+r)_{back}}^{(t_{fc}/2+r)_{front}} \tau_{23} dz \right) \cdot t_1 + \left(\int_{t_{wc}}^{h_{wc}} \tau_{23} dz \right) \cdot t_{wc} + \left(\int \tau_{23} dz \right) \cdot t_1$	$\gamma = \arctan\left(\frac{DT1_{U3} - DT2_{U3}}{h_b}\right) + \arctan\left(\frac{DT3_{U2} - DT4_{U2}}{h_c}\right)$
Column web panel in shear with stiffeners	$M_{fc} = \int z(\sigma_{22} dA), \quad dA = b_c \cdot dz$ $V_c = \frac{M_{fc(P4)} + M_{fc(P5)} + M_{fc(P6)} + M_{fc(P7)}}{h_b - t_s}$	$\Delta_c = (\delta_{P1} - \delta_{P2})_{comp_beam_fl}$
	$V = V_n + V_c$	$\Delta_{t,i} = (\delta_{P1} - \delta_{P2})_{row_i}$
Column web In transverse compression	$F_c = \left(\int \sigma_{33} dy \right) \cdot t_{wc}$	$\Delta_c = (\delta_{P1} - \delta_{P2})_{comp_beam_fl}$
Column web in transverse tension	$F_{t,i} = \left(\int \sigma_{33} dy \right) \cdot t_{wc}$	$\Delta_{t,i} = (\delta_{P1} - \delta_{P2})_{row_i}$

4.2.3 APPLICATION TO THE JOINTS

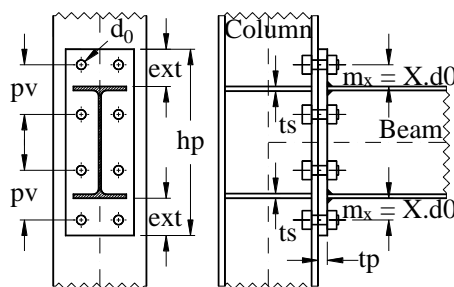
4.2.3.1 JOINTS LOADED MONOTONICALLY

The methodology described above was applied to the calibrated FE models for test J1.1. The force-deformation ($F-\Delta$) and shear-distortion ($V-\gamma$) relationships of the column web panel components were determined for use in a mechanical model capable of characterizing the contribution of these components to the joint rotation.

Some variants of the original test specimen were considered in order to assess the sensitivity of the methodology to the presence of transverse column web stiffeners, see Table 4.2. For the steel mechanical properties adopted in the analyses the nominal values in Eurocode 3 part 1-1 (EN 1993-1-1, 2005) were used ($E = 2.10E^5 \text{ N/mm}^2$; $f_y = 355 \text{ N/mm}^2$; $f_u = 490 \text{ N/mm}^2$) even for the 40 mm plate.

Table 4.2: Joints analysed.

Joints based on J1.1			
	tp = 18mm	tp = 40mm	
	pv = 100mm	pv = 120mm	
ts (mm)	mx = 40mm	mx = 50mm	
	hp = 540mm	hp = 560mm	
	M24 (10.9)	M30 (10.9)	
Without stiffeners.	J1_1_pv1_tp18_ts0	J1_1_pv2_tp40_ts0	
20	J1_1_pv1_tp18_ts20	J1_1_pv2_tp40_ts20	



The main design properties, according to EC3-1-8, are shown in Table 4.3. Notice that J1_1_pv2_tp40 was designed so that the weakest components are the column web in tension and compression. The 40 mm thick end-plate was adopted to be sufficiently stiff to allow the column web to be the main source of plastic deformation.

Table 4.3: Main design properties of the joints according to EN1993-1-8.

Model	Global prop.		Component prop.													
	S _{j,ini} (kNm/rad)	M _{pl,Rd} (kNm)	Shear comp. V _{wp,Rd} (kN)	Compr. comp.					Tension comp.							
				F _{c,wc,Rd} (kN)	F _{c,fb,Rd} (kN)	1st Row				2nd Row						
						F _{t,wc,Rd} (kN)	F _{t,fc,Rd} (kN)	F _{lep,Rd} (kN)	F _{t,wb,Rd} (kN)	F _{t,Rd} (kN)	F _{t,wc,Rd} (kN)	F _{t,fc,Rd} (kN)	F _{lep,Rd} (kN)	F _{t,wb,Rd} (kN)	F _{t,Rd} (kN)	
J1_1_pv1_tp18ts0	45394	212	759	566	1042	646	507	459	-	459	646	507	520	781	<u>107</u>	
J1_1_pv1_tp18ts20	61274	290	832	-	1042	671	515	459	-	459	662	512	520	781	<u>373</u>	
J1_1_pv2_tp40ts0	48676	228	759	581	1042	528	536	910	-	528	528	536	1010	763	<u>52</u>	
J1_1_pv2_tp40ts20	64003	300	832	-	1042	528	536	910	-	528	528	536	1010	763	<u>304</u>	

i) Load Introduction Effects

Two components, defined in EC3-1-8 (EN 1993-1-8, 2005), are directly associated to the load-introduction effect: column web in transverse tension and column web in transverse compression. As already highlighted, the introduction of the loads in the column web, due to the beam force couple, is different in tension and in compression as tension is transferred by the bolt rows and compression is transferred directly from the contact of the beam flanges to the column web.

The stress and deformation fields are represented in Figure 4.7. By analysing the stress fields in the joint, it can be concluded that the maximum stresses evolve from a more or less symmetric configuration, which is located in the two tension bolt rows in the elastic range with identical stress values for the external and internal row, to a configuration in the plastic range where a single maximum stress occurs for the two tension bolt rows between the external line of bolts and the beam flange. This is due to the fact that the introduction of the loads in the web is not completely horizontal due to the shear in the beam. It is also important to realise that the maximum web elongations occur aligned with the second bolt row under the beam flange because of the higher stiffness of the second bolt row in tension.

By applying the methodology described before it is possible to compare the numerical $F-\Delta$ results with the Atamaz-Jaspart model (AJM) (Jaspart, 1990; Jaspart, 1991) and the EC3-1-8 (EN 1993-1-8, 2005) design procedure, see Figure 4.8. The computed $F-\Delta$ relationship was, in general, slightly stiffer than the analytical predictions, although the initial stiffness is well adjusted to the AJM for the isolated behaviour of the two tension bolt rows. In terms of resistance, for the column web in compression there is a good agreement between the AJM and the numerical $F-\Delta$ relationship, although for the model with $t_p=18\text{mm}$ the ultimate force obtained in the numerical simulation is slightly larger than the analytical prediction. For the tension component, grouping the first and second bolt rows, the AJM predicts well the first yielding resistance and the ultimate resistance of the component, although the Δ_u prediction in the AJM model occurs for an elongation larger than in the $F-\Delta$ relationship. This can be related to the stiffness of the hardening branch that depends on the steel uniaxial relationship, as in the AJM a multi-linear approach is used and in the FE model a nonlinear relationship is used. In the case of the isolated rows behaviour it is possible to see that the $F-\Delta$ relationship obtained for the first bolt row is different from the second bolt row, mainly for the model with $t_p=40\text{mm}$. This difference can be explained by analysing the stress fields depicted in Figure 4.9.

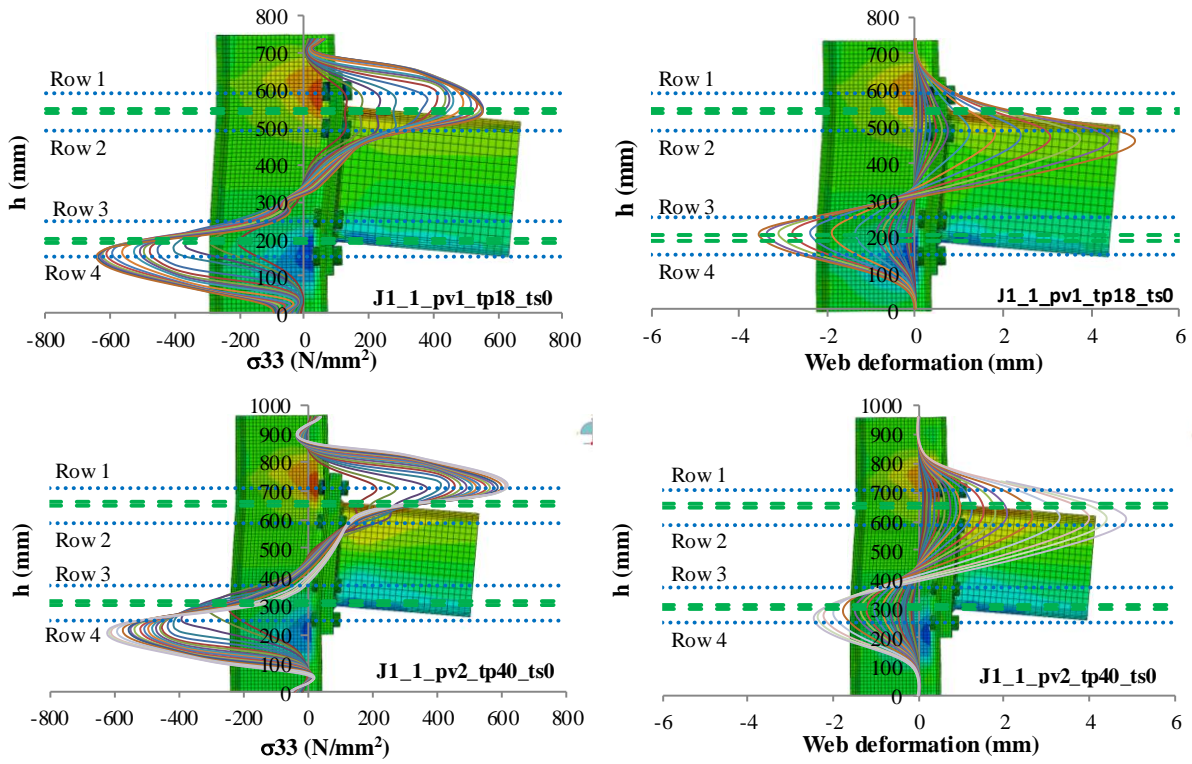


Figure 4.7: Stress fields (left), and web deformation fields (right), for increasing levels of bending moment.

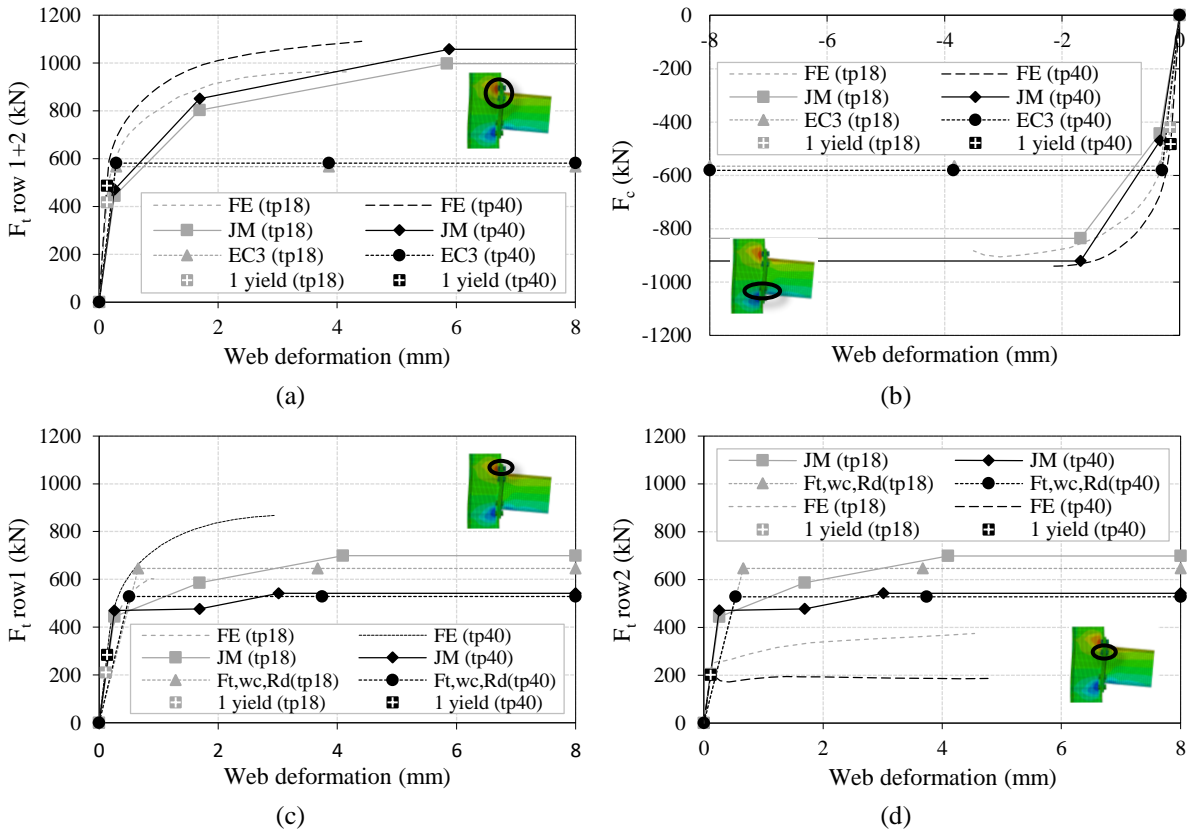


Figure 4.8: F- Δ behaviour for joints without stiffeners: (a) for the tension zone bolt rows 1 and 2 together, (b) for the compression zone, (c) and (d) for the tension zone bolt rows 1 and 2, respectively.

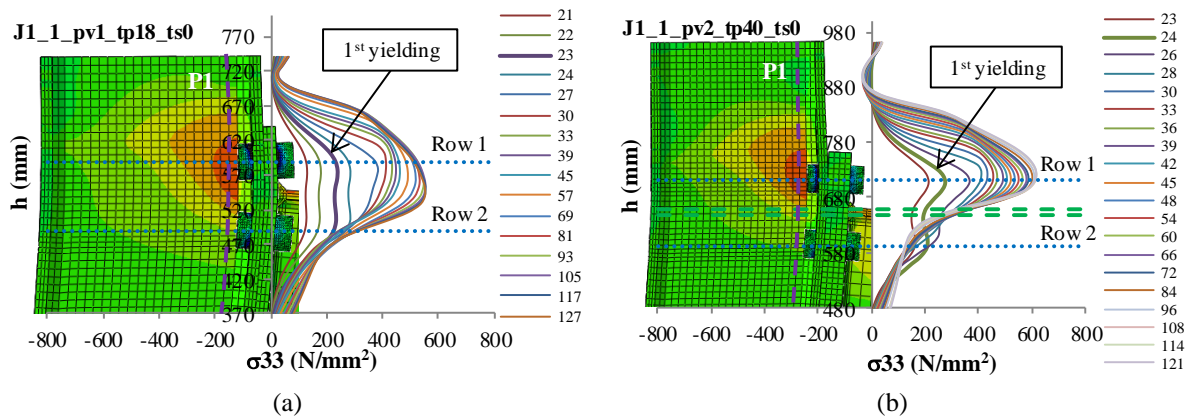


Figure 4.9: Detailed stress fields for the column web in tension.

ii) Shear Effects

By applying the methodology described before it is possible to obtain the $V-\gamma$ relationship. The stress fields for the joints with and without column web stiffeners are quite similar, as shown in Figure 4.10.

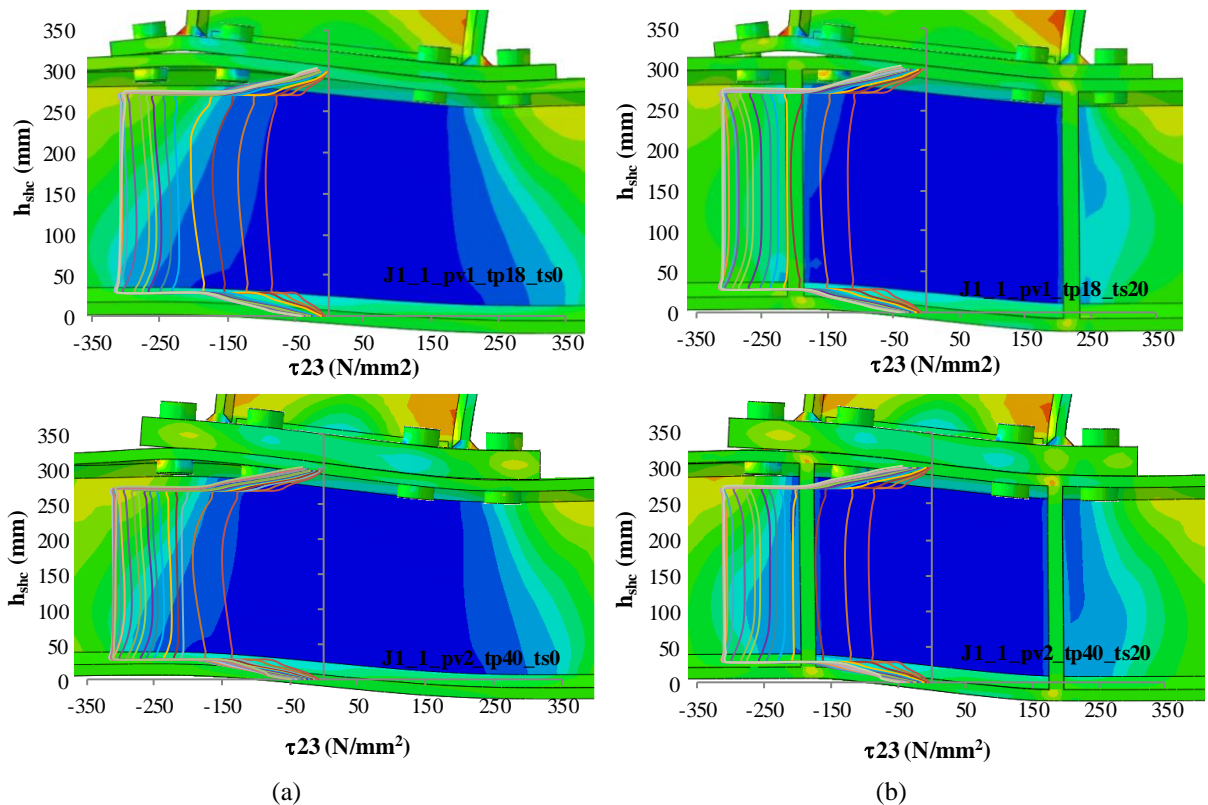


Figure 4.10: Shear stress fields for increasing levels of bending moment (a) for the unstiffened column web and (b) for the stiffened web.

Figure 4.11 compares the numerical results with the AJM and the EC3-1-8 model. It is possible to conclude that there is a good agreement between the numerical $V-\gamma$ relationship and

the AJM and, consequently, with the EC3-1-8 model. The prediction of the web panel shear contribution, in the AJM, (dash line) achieves a slightly better agreement, than the prediction of the sum of the web panel and stiffeners contribution together (solid line).

The additional shear resistance provided by the stiffeners is achieved by the frame action developed by the column flanges and the stiffeners, as the bare column web shear resistance is similar with or without stiffeners. From the numerical $F-\Delta$ curve a good agreement can be seen for the additional shear strength, due to the stiffeners, between the proposed procedure and the EC3-1-8 and the AJM. The differences found can be justified by the partial hinges observed in the column flanges of the FE models, as can be seen in Figure 4.12.

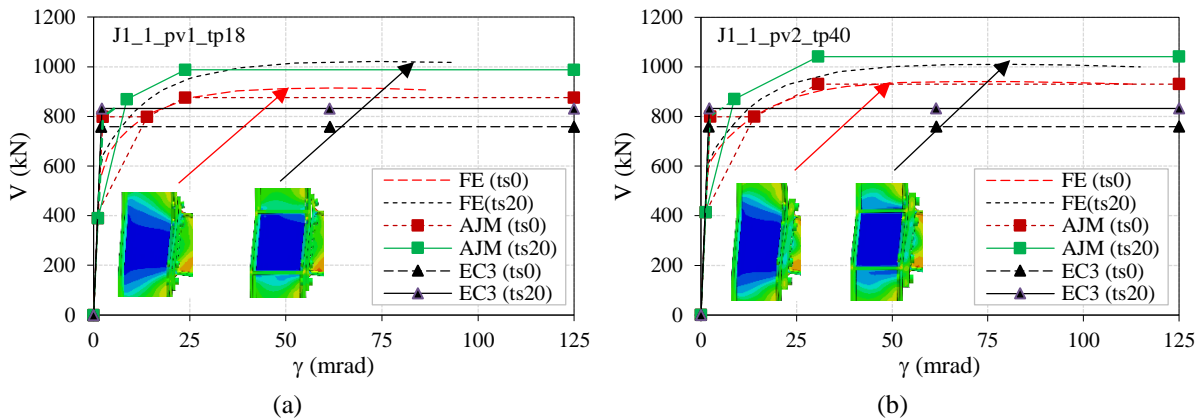


Figure 4.11: V- γ behaviour for the shear load.

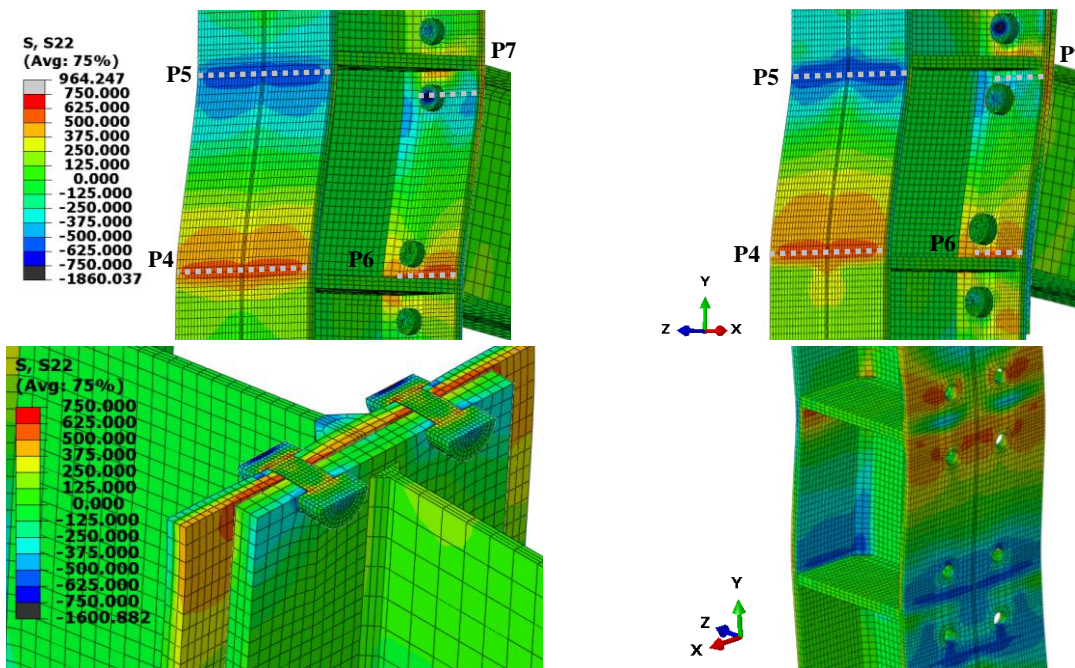


Figure 4.12: σ_{yy} stress distribution comparison for the J1_1_pv1_tp18_ts20 on the left and J1_1_pv2_tp40_ts20 on the right.

The influence of the transverse stiffeners on the joints strength and deformation can be neglected in the elastic range and increases with the yielding of the column flanges, as shown in Figure 4.13. Figure 4.13(b) represents the relative reduction of the rotation due to the stiffeners. This is obtained through the difference in the rotation achieved for the same level of strength, at each load increment, taking as reference the maximum rotation imposed in the joints, leading to a reduction of the rotation of 55% for J1_1pv1_tp18 and 41% for J1_1pv2_tp40.

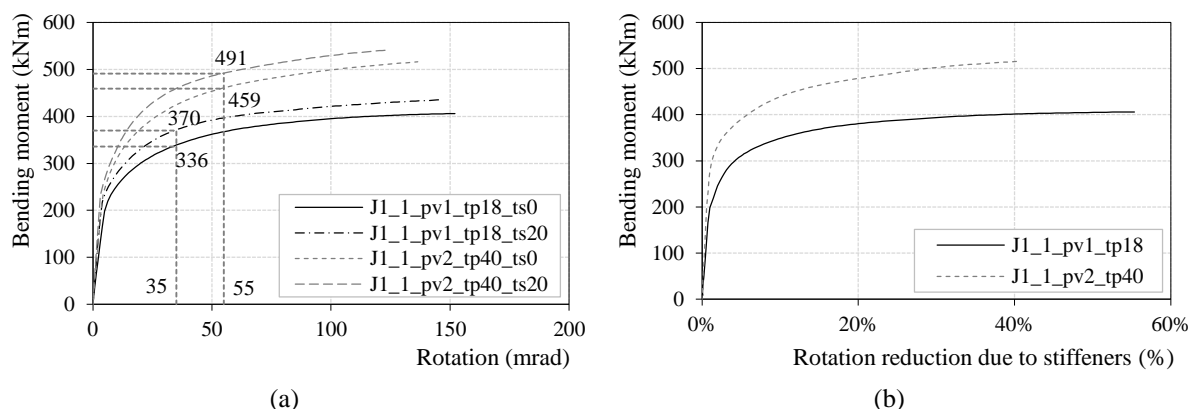


Figure 4.13: Influence of the column web stiffeners in the joints strength and deformation.

The evolution of the flanges bending moment (M_{fc}) vs the web rotation is depicted in Figure 4.14a) and (b) for the two joints with transverse stiffeners. Note that the stress distribution of M_{fc} near the bolt row in tension is affected by the presence of the holes in the flange. The stress field is also affected by the bolt forces transferred to the column flange, as can be seen in Figure 4.12, resulting in a shift of the position of the plastic hinge towards the bolt row alignment.

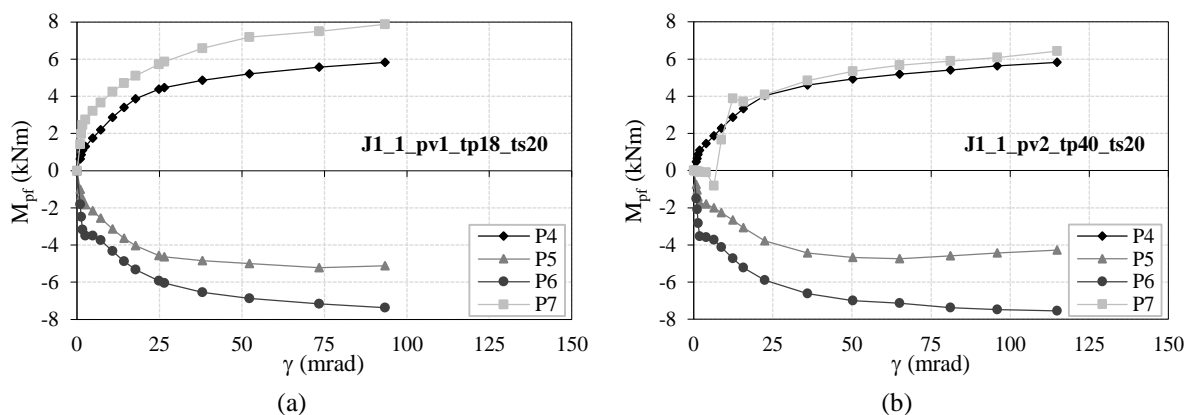


Figure 4.14: Evolution of the bending moments in the column flanges.

4.2.3.2 CYCLICALLY LOADED JOINTS

For the joints loaded cyclically, the proposed procedure was applied to some of the variants of J1.1, with and without stiffeners, presented above. The procedure was also extended to other geometries developed using the same principles. These joints are also studied in Chapter 5. The geometrical properties are described in Table 4.4, with reference to the scheme of Figure 3.9. The first two geometries correspond to joint J1.1, with and without transverse web stiffeners. The last two joints are also double-extended end-plate joints with stronger beam and column profiles, IPE600 and HEB500, respectively, with six bolt rows, with four inner rows, bolt size M36 in grade 10.9, with and without transverse web stiffeners. The E3-TB-E-M3-ts30 joint was designed according to EC3-1-8, to reach a strength level similar to the beam plastic moment. The geometry of the joint is plotted in Figure 4.15(a). In the design of the joints without stiffeners, the governing component, on the compression side, was the column web in transverse compression. In the tension side, the governing component, for the external bolt rows, was, in both geometries (J1.1 or E3), the end-plate in bending. For the inner bolt rows, the strength of the compression component limited the development of the full resistance of the tension components. In the case of the J1.1 joint, the component that governed the design was the column flange in bending and in the E3 joint was the end-plate in bending. In the latter case, the third bolt row was inactive. In the presence of transverse web stiffeners, the governing component, in the compression side, was the column web panel in shear. On the tension side, the behaviour was similar to the joints without stiffeners, but due to the higher strength of the compression component, it was possible to reach higher values in the tension components for the inner bolt rows.

Table 4.4: Geometrical properties of the FE models.

	Column	Beam	h_t (mm)	L_c (mm)	L_{c1} (mm)	L_{c2} (mm)	L_1 (mm)	L_2 (mm)	L_{b1} (mm)	d (mm)
J1_1-pv1_tp18_ts0	HEA320	IPE360	3220	3000	1395	720	1331	1355	467	1175
J1_1-pv1_tp18_ts20	HEA320	IPE360	3220	3000	1395	720	1331	1355	467	1175
E3-TB-E-M3-ts0	HEB500	IPE600	3500	3200	995	1210	2600	1750	780	2350
E3-TB-E-M3-ts30	HEB500	IPE600	3500	3200	995	1210	2600	1750	780	2350

See also the scheme of Figure 3.9.

The steel mechanical properties adopted in these analyses correspond to the nominal values in Eurocode 3 part 1-1 (EN 1993-1-1, 2005) ($E = 2.10E^5 \text{ N/mm}^2$; $f_y = 355 \text{ N/mm}^2$; $f_u =$

490 N/mm^2) for the joints based on J1.1. For the remaining joints, the stress-strain relationship depicted in Figure 4.15 (b) was considered.

Two different loading protocols were used: ECCS (1986) was adopted for the joints based on J1.1, and the protocol specified in the ANSI/AISC 341-10 (2010) was employed for the remaining joints. The ECCS loading protocol is defined as follows: i) one cycle in the ranges: $\theta_y/4$; $2\theta_y/4$; $3\theta_y/4$ and θ_y ; ii) three cycles in the ranges: $2\theta_y$; $(2+2n)\theta_y$ where $n = 1, 2, \dots$. The assessment of the elastic limit, θ_y , is based on the bi-linearization of the nonlinear monotonic response of the joints, see Figure 4.16 (a). In case of AISC 341-10, the procedure is conducted by controlling the inter-storey drift, θ , imposed to the test specimen, six cycles in the ranges $0.00375rad$, $0.005rad$, $0.0075rad$, four cycles in the range $0.01rad$ and two cycles in the ranges $0.015rad$, $0.02rad$, $0.03rad$, $0.04rad$. The loading is applied with increments of $0.01rad$, with two cycles of loading for each step. In the analysis, the vertical beam deflection is the controlled parameter. Thus, when defining the load function in ABAQUS, the amplitude δ is used and it is defined by Eq. (4.11), according to Figure 4.16 (b).

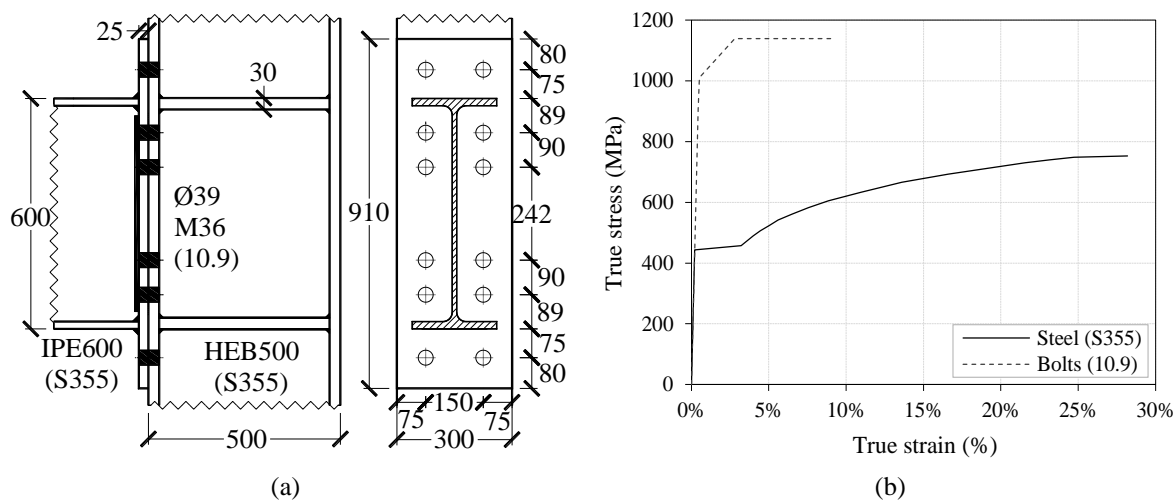


Figure 4.15: (a) Geometry of the E3-TB-E-M3-ts30 (dimensions in mm) and (b) true stress – true strain curves of the materials adopted.

$$\theta = \frac{\delta}{L_b} \Leftrightarrow \delta = \theta \cdot L_b \quad (4.11)$$

Table 4.5 lists the stiffness and strength values for the basic components, identified in the end-plate bolted joints, when the procedure prescribed in EC3-1-8 is applied to the selected joints. For the tension components, the first 3 bolt rows were considered for the joints based on the J1.1 and for the E3 joints. Although for the J1.1 joints the third bolt row is closer to the

compression centre then the tension side, this bolt row does not contribute to the negative bending moment resistance. On the other hand, for the E3 joints, the fourth and fifth bolt rows were not represented in the table, because they are located on the compression side (for negative bending moments), although their strength and stiffness values can easily be identified in the table using the second and third bolt rows values, due to the symmetry of the joint.

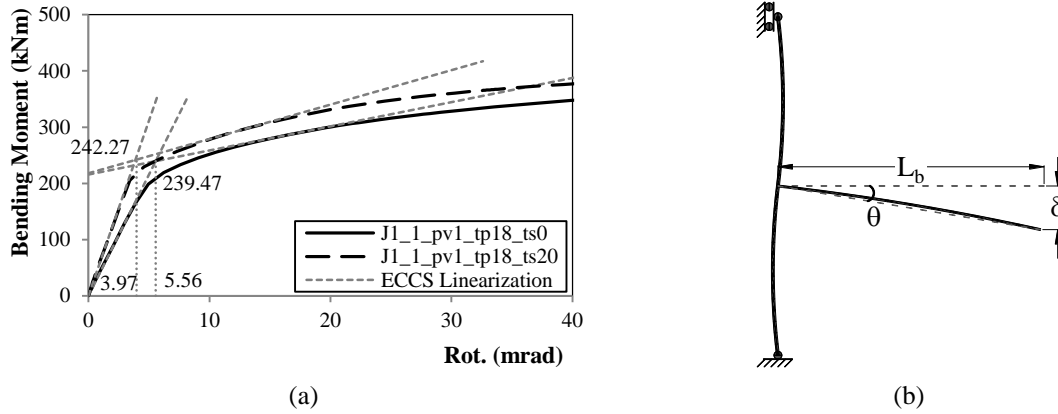


Figure 4.16: (a) Determination of the elastic limit based on the nonlinear monotonic behaviour of the joints; (b) geometrical properties for the AISC 341-10 load protocol.

Table 4.5: Stiffness and strength of the basic components according to the EC3-1-8 (EN 1993-1-8, 2005).

Force type	Location	Comp.	J1_1_pv1_tp18_ts0		J1_1_pv1_tp18_ts20		E3-TB-E-M3-ts0		E3-TB-E-M3-ts30	
			$F_{Rd,i}$ (kN)	k_i (mm)	$F_{Rd,i}$ (kN)	k_i (mm)	$F_{Rd,i}$ (kN)	k_i (mm)	$F_{Rd,i}$ (kN)	k_i (mm)
Shear	Column web panel	1 CWS	758.70	4.733	832.37	4.716	2071.06	6.205	2238.39	6.197
Compression	Column web	2 CWC	565.91	8.264		∞	1423.28	9.247		∞
	Beam	7 BFWC	1041.59		1041.59		2682.36		2682.36	
Tension	1 st row	3 CWT	646.37	4.681	671.05	5.084	1593.98	5.756	1661.10	7.547
		4 CFB	506.69	23.212	514.72	25.213	1119.90	44.457	1308.51	58.285
		5 EPB	459.41	31.295	459.41	31.295	590.31	6.026	590.31	6.026
		3 CWT	646.37	4.681	661.90	5.084	1593.98	3.305	1673.77	5.276
		4 CFB	506.69	23.212	511.71	25.213	1119.90	25.527	1313.37	40.748
	2 nd row	5 EPB	520.50	18.741	520.50	18.741	1016.31	13.383	1174.47	14.354
		8 BWT	780.72		780.72		2054.92		2054.92	
		3 CWT	646.37	5.084	661.90	5.084	1593.98	4.320	1593.98	4.320
		4 CFB	506.69	25.213	511.71	25.213	1119.90	33.366	1283.30	33.366
		5 EPB	520.50	18.741	520.50	18.741	982.26	8.710	1140.41	8.710
3 rd row	8 BWT	780.72		780.72		1872.53		1872.53		
	Bolts	10 BT	317.70	11.184	317.70	11.184	735.30	16.547	735.30	16.547
	Welds	19 Welds	1057.91		912.18		-		-	

i) Load Introduction Effects

Figure 4.17 shows the stress, along the path PI , and deformation fields, $\Delta_{P1}-\Delta_{P2}$, for the joints defined in Table 4.4, for several load increments. Globally, the stress distribution is very similar in tension and in compression, especially for the joints without transverse web stiffeners. However, some differences are noted. The first load increments, depicted in Figure 4.18, show that the differences between tension and compression are more evident in the elastic range, with local maxima stresses perfectly aligned with the position of the bolts rows for tensile stresses, and with the position of the beam flanges for compressive stresses. After yielding of the web is reached, both tension and compression diagrams become similar and the maximum stresses deviate from the position of the bolt rows.

Regarding the web deformation, the differences between tension (positive) and compression (negative) are more notorious. For the joints without transverse web stiffeners, the maximum deformation in compression is aligned with the beam flanges, while in tension the maximum deformation is aligned with the inner bolt row, revealing the stiffer behaviour of those bolt rows. The transverse web stiffeners, aligned with the beam flanges, prevent the deformation of the column web in compression in the inner bolt row.

The application of the methodology described in Section 4.2.2 allows obtaining the numerical $F-\Delta$ curves for the components. The procedure is general in the sense that it allows to obtain force resultants and deformations for any selected tributary area between two integration limits, both for the column web in tension or in compression. Note that, in the comparisons presented next, not all charts have the same scales, in order to allow for a more detailed view of the depicted curves.

Figure 4.19 shows the cyclic force-deformation behaviour for the load-introduction in the column web panel for the four joints. A single lumped component is considered for the top and bottom zones. Consequently, and with reference to Figure 4.2, the integration limits are defined between points of zero or near zero normal stress σ_{33} for the top and bottom zones, respectively. It is noted that these limits will not necessarily coincide for positive and negative bending moments, neither between different load cycles. However, Figure 4.17 shows that they are stable and hence it is possible to assume constant limits of integration for all loading cycles. Concerning the deformation, the web deformation aligned with the beam flanges in tension and compression is selected. It should be noted that the maximum deformation values will not

necessarily occur at that section. Typically, the maximum web deformation in compression is observed at the level of the beam flange while in tension it often develops aligned with one of the bolt rows.

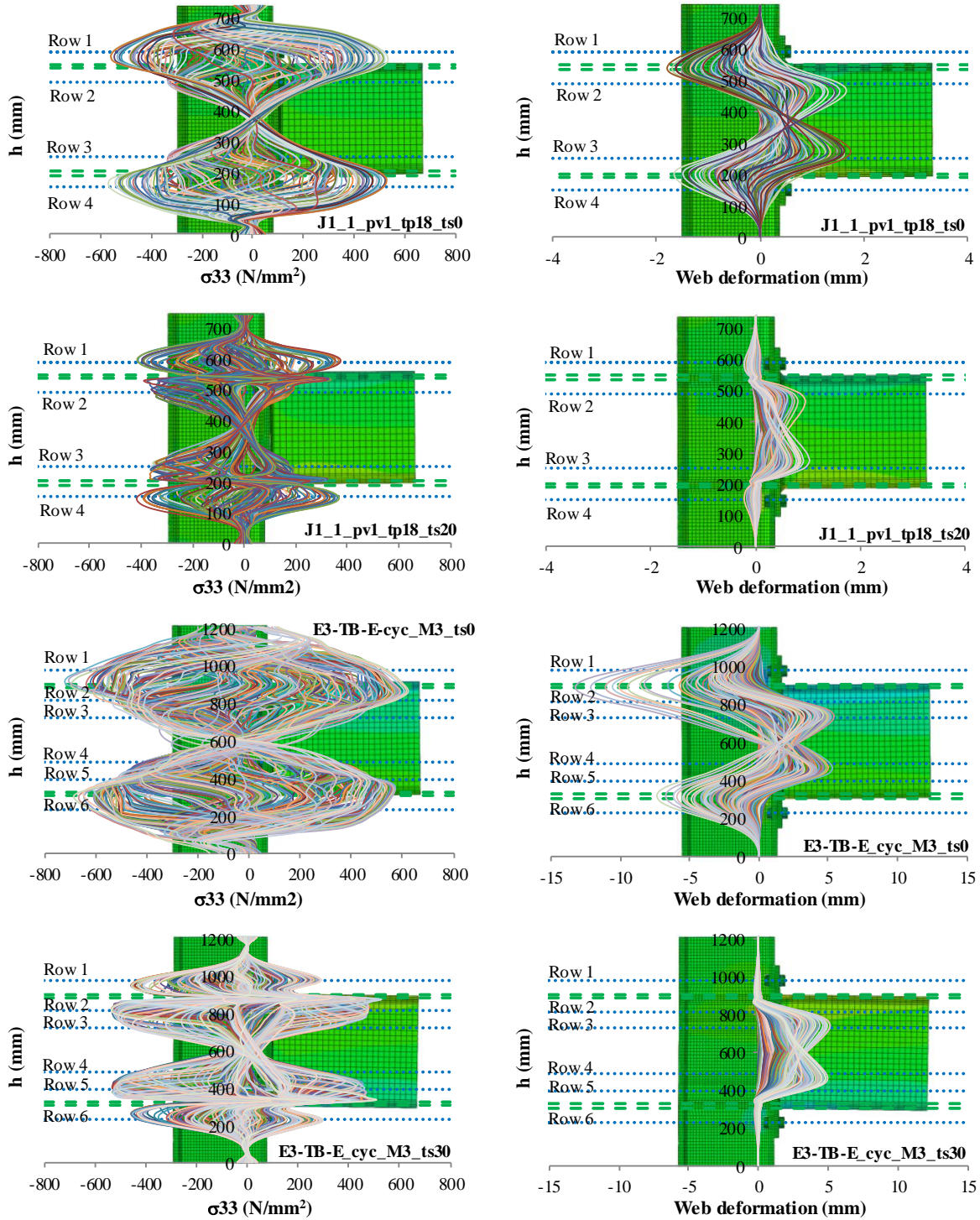


Figure 4.17: Stress fields (left), and web deformation fields (right), for increasing levels of bending moment.

Figure 4.20 and Figure 4.21 represent the force-deformation cyclic curves for joints J1.1 and E3, respectively, according to the alternative component model shown in Figure 4.1, i.e., with the load-introduction components (tension and compression) positioned according to the bolt rows. In this case, for the top and bottom zones, the integration limits for each bolt row are established based on the effective widths of the components. The deformation, in this case, is measured aligned with the corresponding bolt row.

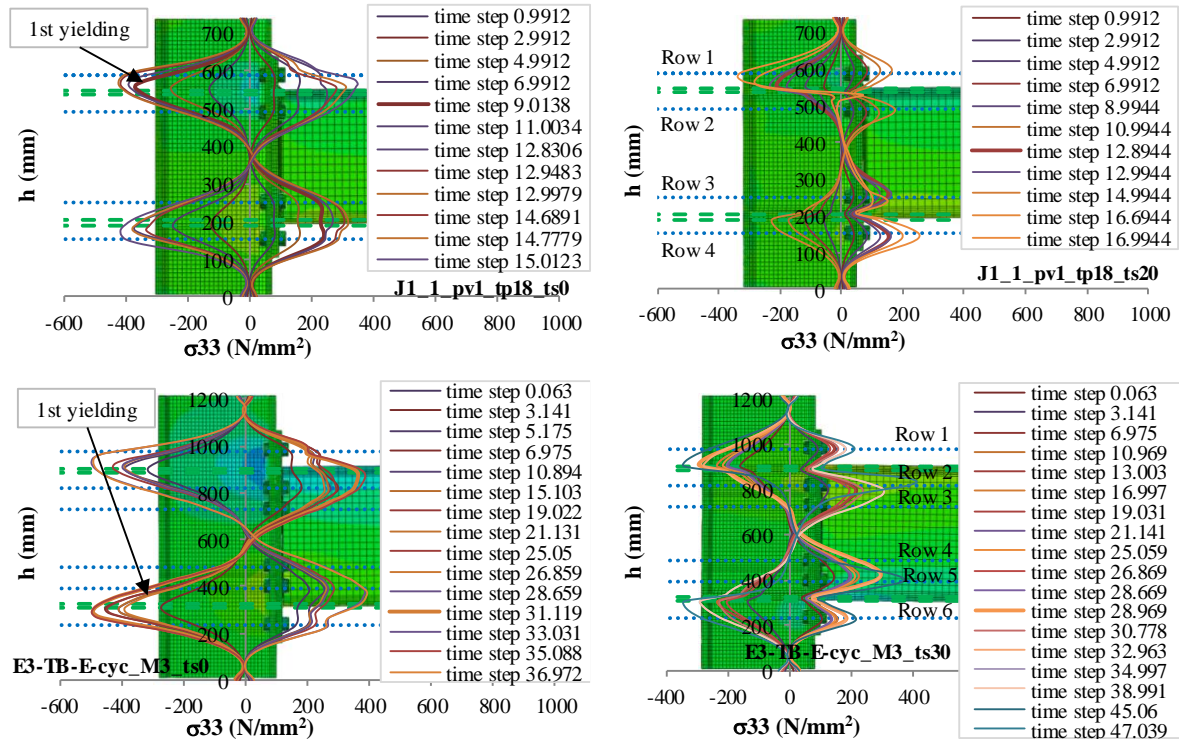


Figure 4.18: Stress fields for the first load increments, and first yielding identification.

The component model illustrated in Figure 4.1 reflects the definition of the individual components in accordance with EC3-1-8 (EN 1993-1-8, 2005). It further highlights that the effective width of the column web panel in compression is clearly distinct from the corresponding effective widths of the column web panel in tension components for each bolt row in tension. Hence, the integration limits in tension and in compression should be different. Figure 4.22 illustrates the cyclic behaviour of the column web panel in compression, referenced to the beam flange level, while Figure 4.23 depicts the cyclic force-deformation curves for the column web panel in tension for each bolt row.

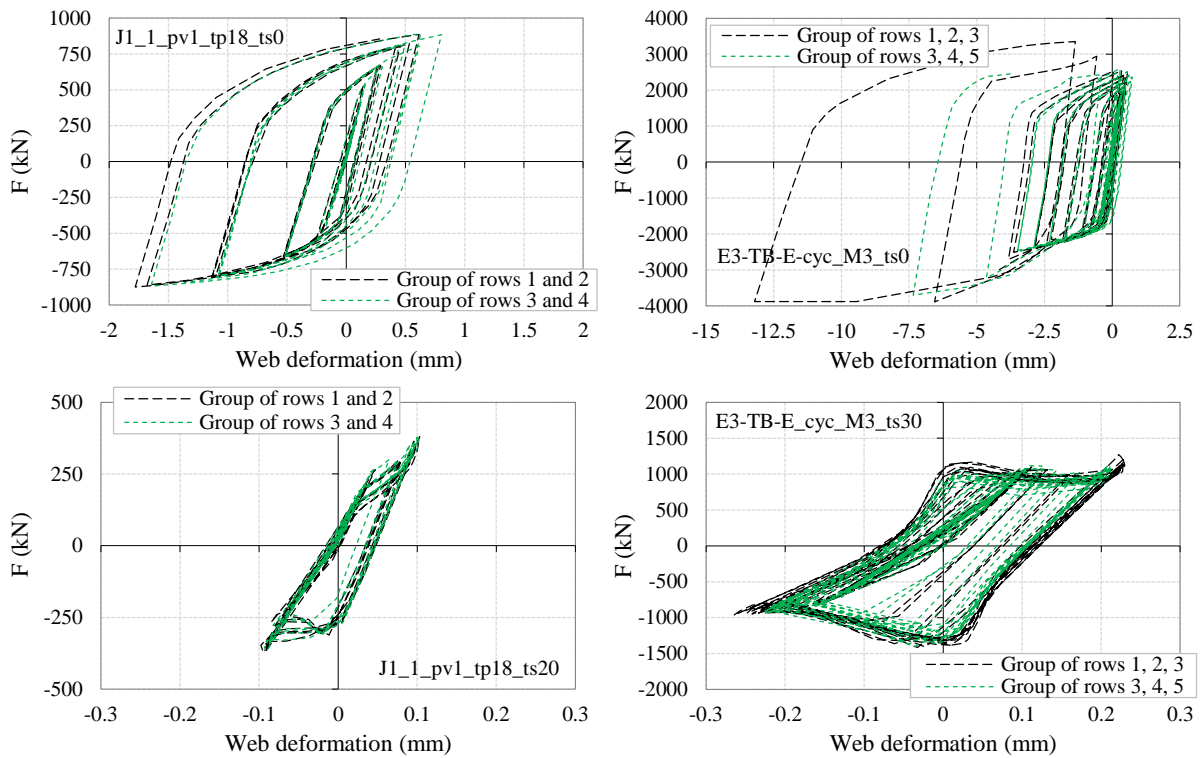


Figure 4.19: F- Δ curves for the components due to the load-introduction effect considering the group of bolts around the beam flanges.

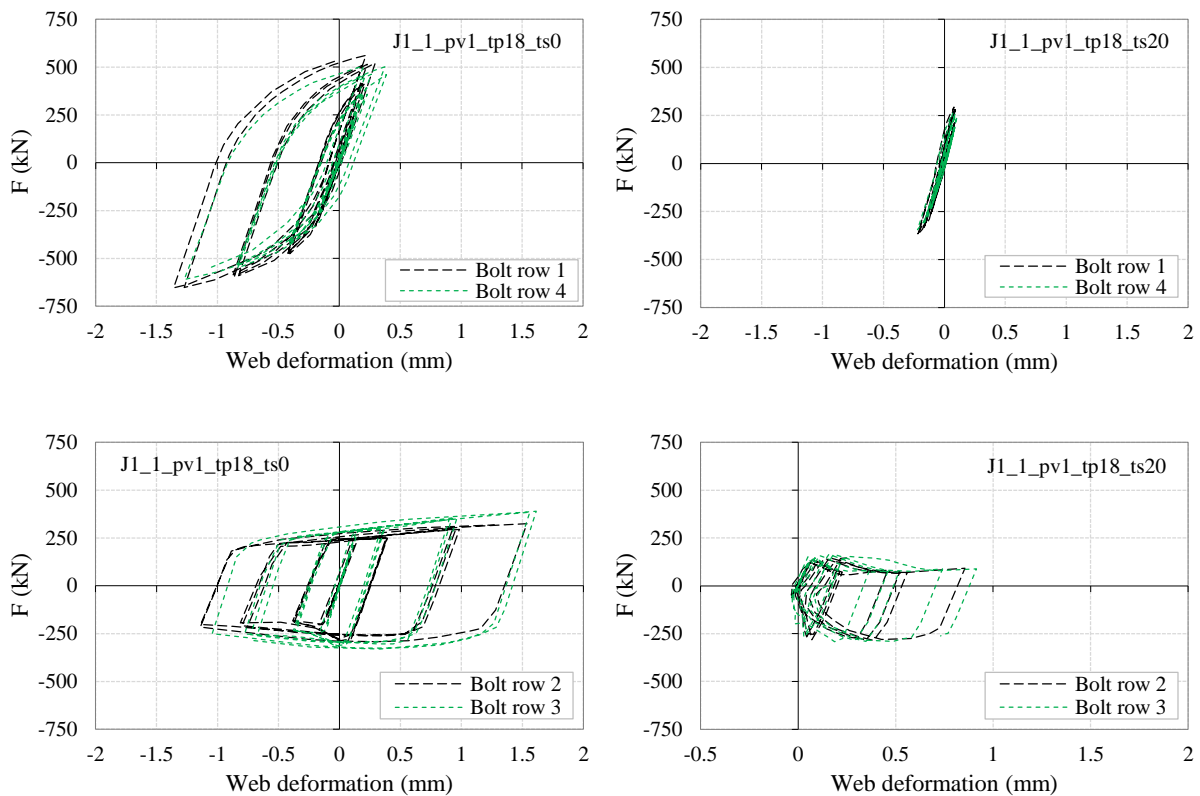


Figure 4.20: F- Δ curves for the components due to the load-introduction effect for each bolt row, for the J1.1 joints, according to the alternative mechanical model depicted in Figure 4.1.

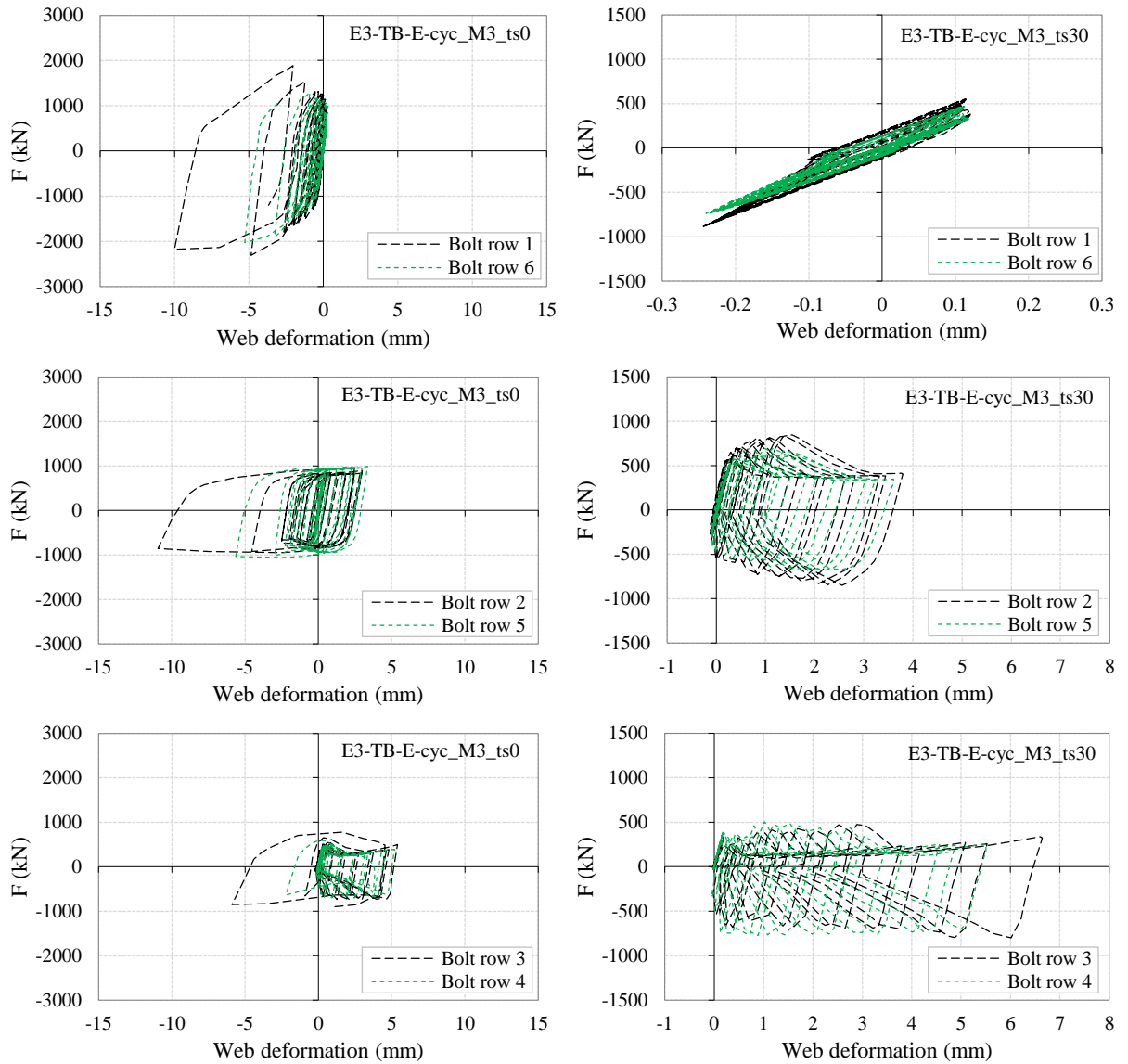


Figure 4.21: F-Δ curves for the components due to the load-introduction effect for each bolt row, for E3 joints, according to the alternative mechanical model depicted in Figure 4.1.

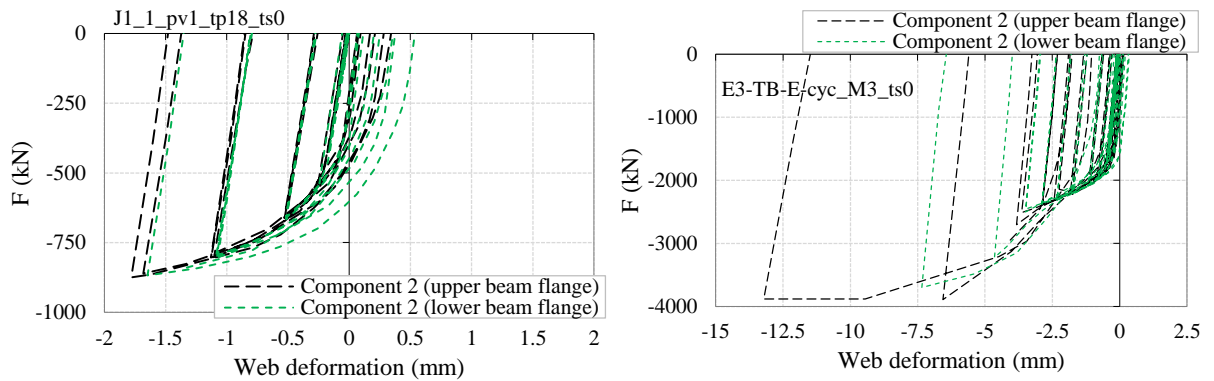


Figure 4.22: F-Δ behaviour for component (2) due to the load-introduction effect, compression side of the previous relationships.

The comparison of the results obtained for the stiffened and unstiffened joints shows that the transverse web stiffeners have a major influence on the amplitude and shape of the force-displacement curves. Whilst the compression force is transmitted directly to the stiffeners without causing transverse deformation in the column web, tensile force causes deformation in the column web aligned with the bolt rows. The examination of the behaviour of the inner bolt rows, see Figure 4.21, reveals a ratcheting effect after yielding, mainly in the third and fourth rows of the E3-TB-E_cyc_M3 joints, due to the migration of the normal stresses (σ_{33}) across the web with the increase of bending moment, see Figure 4.26. This phenomenon can be associated with the interaction with the shear stress (τ_{23}) that progressively increases the normal stress beyond the line of the beam flanges alignment.

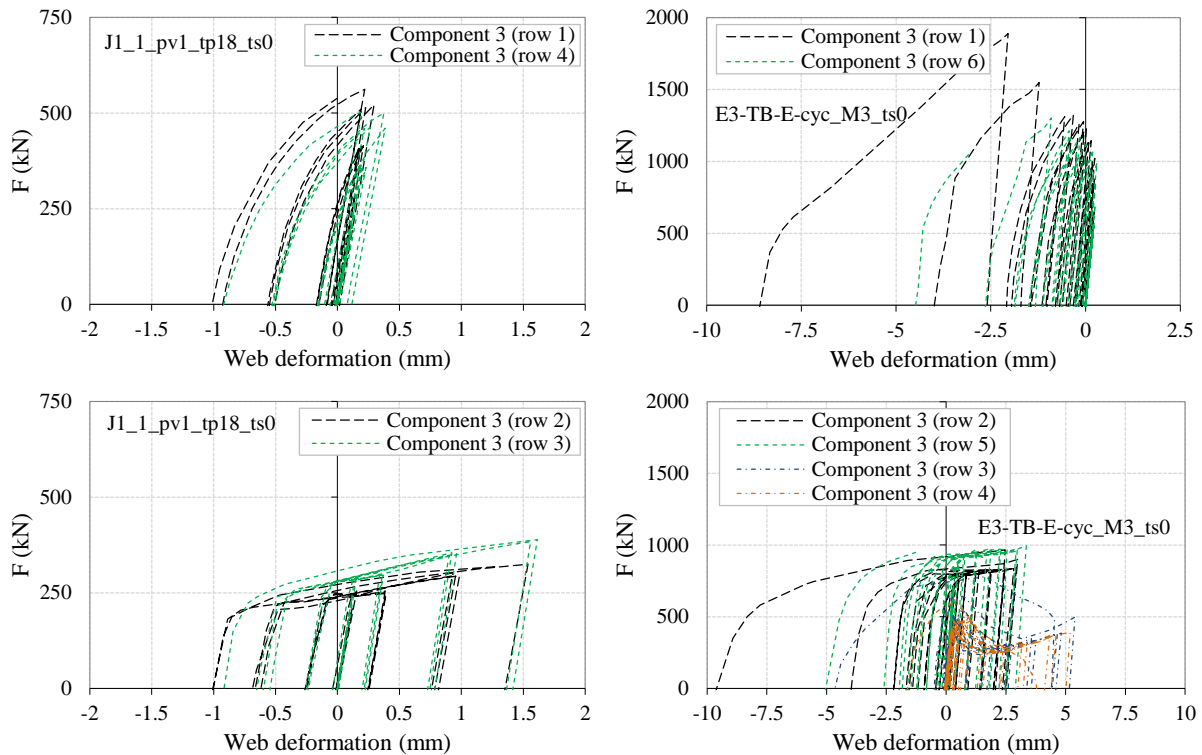


Figure 4.23: F- Δ curves for component (3) due to the load-introduction effect, tension side of the previous relationships.

The joints without stiffeners may exhibit out-of-plane deformations, as illustrated in Figure 4.24. This phenomenon is captured in the derived $F-\Delta$ relationships, represented by the last cycles with larger amplitude, for the joint E3-TB-E_cyc_M3_ts0, visible in the response of the external and in the internal bolt rows, see Figure 4.21 or Figure 4.23. The transverse web stiffeners may prevent this undesired phenomenon, as shown in both figures.

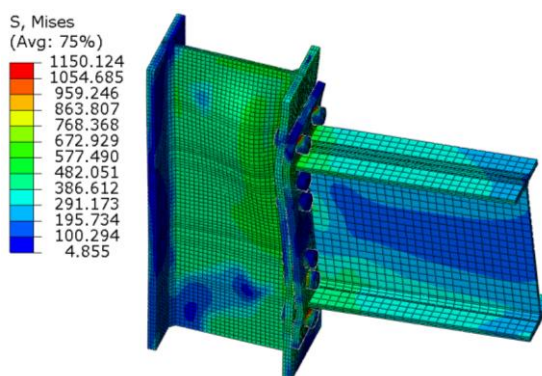


Figure 4.24: Mises stress distribution with out-of-plane column web deformation, for a global rotation of 84mrad.

Table 4.6 summarises the main results for the column web panel in tension and compression $F-\Delta$ relationships. In general, the initial stiffness of the achieved $F-\Delta$ relationships, is lower for the joints without stiffeners, although for the E3 joints this is not verified in some bolt rows, as highlighted in the table. Regarding the maximum strength achieved in the component, it is clear that the joints without stiffeners present the highest values in comparison with the joints with stiffeners. This results from the fact that the transverse web stiffeners directly transfer the compression forces to shear in the column web.

The joints were also subjected to different loading protocols, ECCS (1986) and ANSI/AISC 341-10 (2010), resulting in different demands, see Figure 4.25. ECCS is clearly more severe than the AISC loading protocol. Note that the ECCS loading protocol imposes four cycles in the elastic range, while the AISC protocol may involve a significant number of cycles in the elastic range before the yield resistance of the joint is reached. This difference is related to the fact that the ECCS protocol has a pre-processing procedure to assess the elastic limit of the joint, relating the amplitudes of the cycles with the assessed value, unlike the AISC load protocol that specifies fixed values for the amplitudes. In the plastic range, the ECCS loading protocol is also more severe than the AISC protocol, as it doubles the deformation amplitude between sets of cycles after yielding. In contrast, AISC increases the deformation amplitude by 150% between sets of cycles after yielding. Although the yield rotations for both geometries (J1.1 and E3) are similar, in terms of beam displacement amplitude, E3 needs approximately double the amplitude of the J1.1, due to the higher beam length, a fact that was considered in the comparisons of the two load protocols. The evolution of the two protocols reveals that ECCS always reached higher amplitudes earlier than AISC. This evidence can lead to higher

degradation levels in the joints subjected to the ECCS loading protocol (see Figure 4.25). The lower amplitudes obtained with AISC protocol allow the joints to sustain more cycles before failure. However, the specimens are prone to very-low cycle fatigue effects.

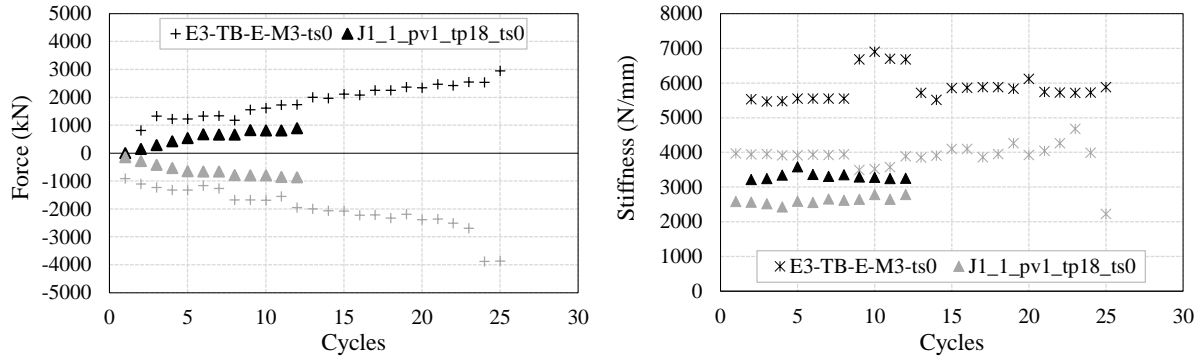


Figure 4.25: Comparison of the strength and stiffness degradation for the F-Δ relationship for the group of bolt rows 1, 2 and 3.

Table 4.6: Main features of the achieved F-Δ relationships.

Joint		S_{ini} (kN/mm)	Δ_{max} (mm)	Δ_{min} (mm)	F_{max} (kN)	F_{min} (kN)
J1_1_pv1_tp18_ts0	Group 1, 2	2575	0.62	-1.78	887.1	-874.9
	Group 3, 4	3304	0.80	-1.65	891.4	-867.6
	Row 1	1847	0.30	-1.36	562.1	-654.8
	Row 2	1551	1.54	-1.14	325.0	-297.0
	Row 3	2011	1.61	-1.04	388.9	-330.7
	Row 4	1669	0.39	-1.27	502.5	-610.9
J1_1_pv1_tp18_ts20	Group 1, 2	3519	0.10	-0.10	380.5	-373.0
	Group 3, 4	5726	0.10	-0.09	377.2	-369.7
	Row 1	2126	0.09	-0.22	293.1	-367.9
	Row 2	1718	0.86	-0.03	147.6	-284.7
	Row 3	2277	0.92	-0.03	165.0	-292.4
	Row 4	2055	0.10	-0.22	263.7	-344.3
E3-TB-E_cyc_M3_ts0	Group 1, 2, 3	3971	0.56	-13.21	3349.7	-3888.6
	Group 4, 5, 6	5530	0.74	-7.35	2599.7	-3697.6
	Row 1	2991	0.24	-10.00	1888.2	-2308.0
	Row 2	2000	2.99	-10.94	965.4	-949.3
	Row 3	948	5.39	-5.90	778.9	-901.7
	Row 4	1739	5.19	-2.22	593.7	-708.9
	Row 5	2150	3.36	-5.64	994.2	-1052.2
Row 6	2525	0.30	-5.27	1301.7	-2029.2	
E3-TB-E_cyc_M3_ts30	Group 1, 2, 3	4963	0.23	-0.27	1272.7	-1415.9
	Group 4, 5, 6	9766	0.21	-0.23	1123.8	-1368.9
	Row 1	3241	0.12	-0.24	554.5	-882.5
	Row 2	2764	3.79	-0.12	845.4	-851.3
	Row 3	607	6.64	-0.03	475.8	-801.1
	Row 4	2288	5.50	-0.05	503.9	-772.3
	Row 5	2029	3.60	-0.10	697.3	-689.1
Row 6	2813	0.12	-0.24	477.7	-740.9	

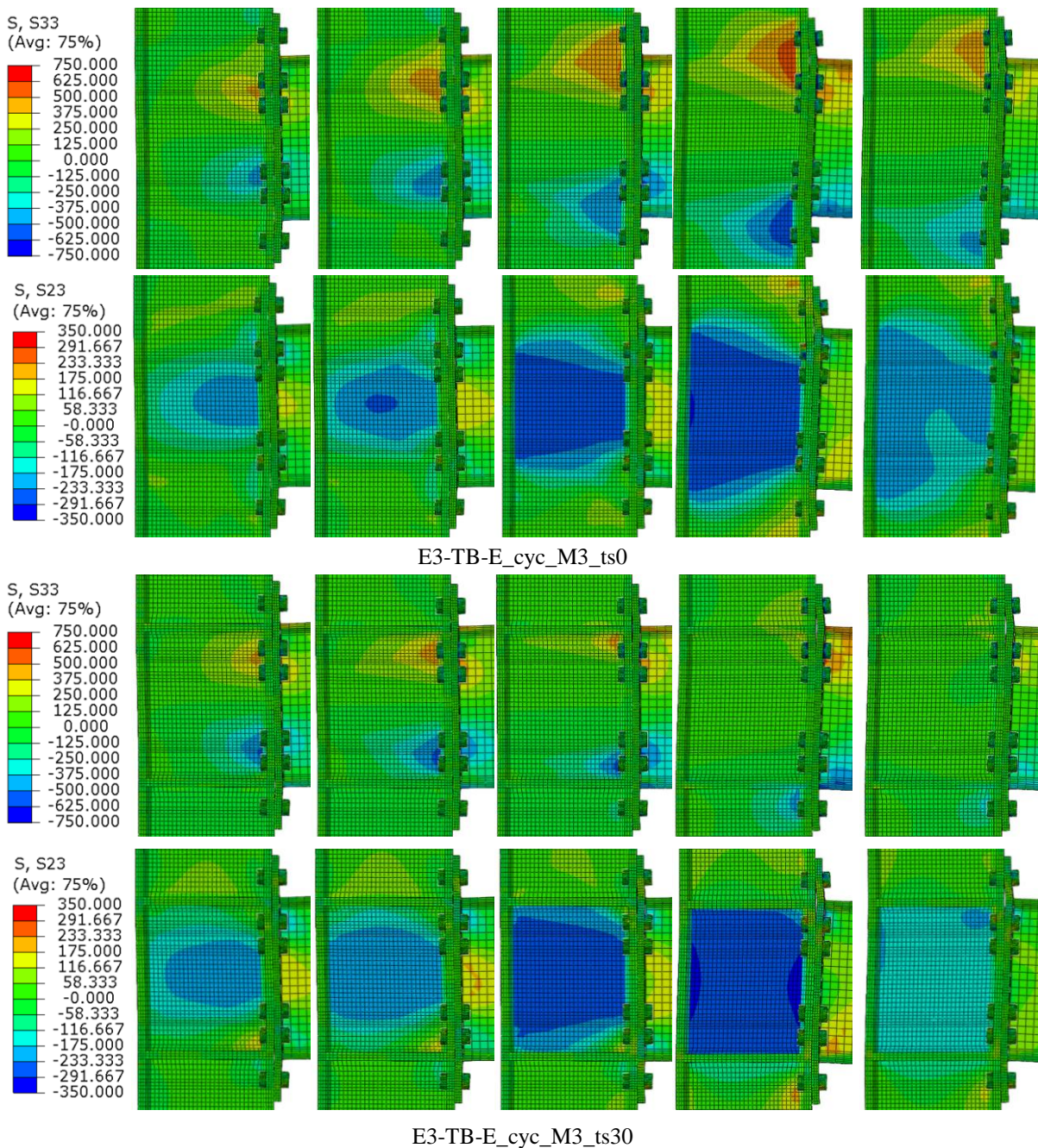


Figure 4.26: Evolution of the normal (σ_{33}) and shear (τ_{23}) stress for a half-cycle.

ii) Shear Results

Similar to the previous section, it is possible to obtain the shear-distortion ($V-\gamma$) relationships by applying the methodology described Section 4.2.2. As shown in Figure 4.27, the stress fields for the joints with and without column web stiffeners are quite similar, although, in the presence of the transverse web stiffeners, the shear stress is confined by the stiffeners and the flanges, while it is more spread in the case of the unstiffened column web.

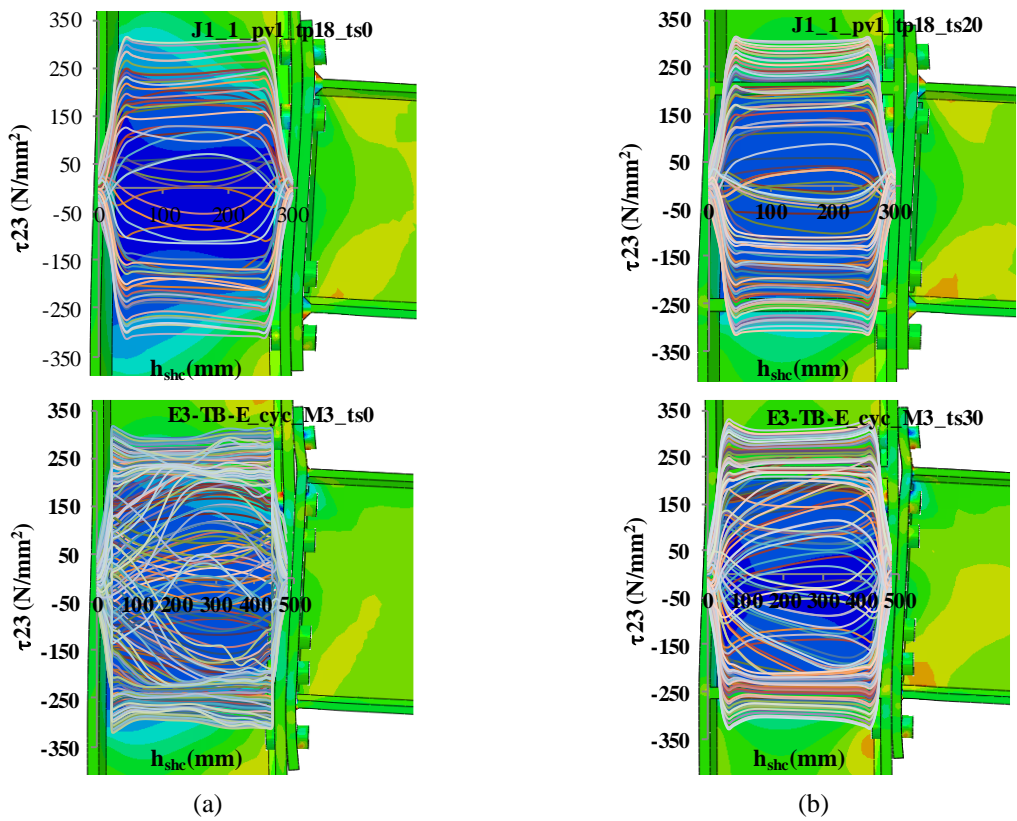


Figure 4.27: Shear stress fields for increasing levels of bending moment (a) unstiffened and (b) stiffened column web.

Figure 4.28 depicts the derived relationships and compares the results with and without transverse web stiffeners. Note that, in the case of the E3-TB-E_cyc_M3_ts0 joint the out-of-plane deformation is also noticeable, preventing the web to reach the same level of distortion and shear strength as the joint with stiffeners. These out-of-plane deformations detected in the column web, after a global rotation of 35mrad , have a strong influence in the degradation of the shear strength on the column web.

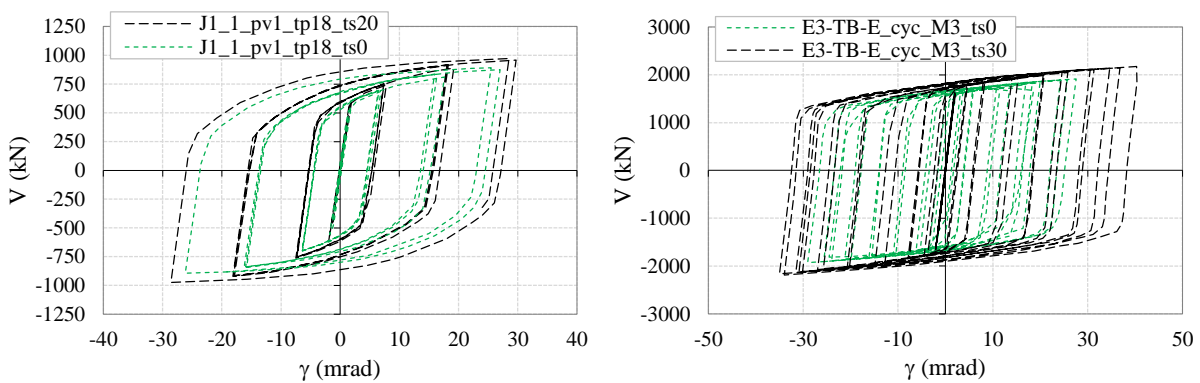


Figure 4.28: V- γ behaviour for the shear load.

The column web panel in shear also exhibits differences in behaviour due to the loading protocol applied to the joints. The ECCS protocol is more severe so the difference between stable cycles is larger than in the joints subjected to the AISC protocol. Figure 4.29 represents the evolution of the peak strength and stiffness (measured in the unloading branch) for the stiffened joints. The results show that no degradation is detected and that the ECCS loading protocol is more severe than AISC protocol in the first cycles. Conversely, a small degradation of stiffness can be observed in the E3 joint. The behaviour in positive and negative shear stress is similar, as expected, due to the symmetry of the joints.

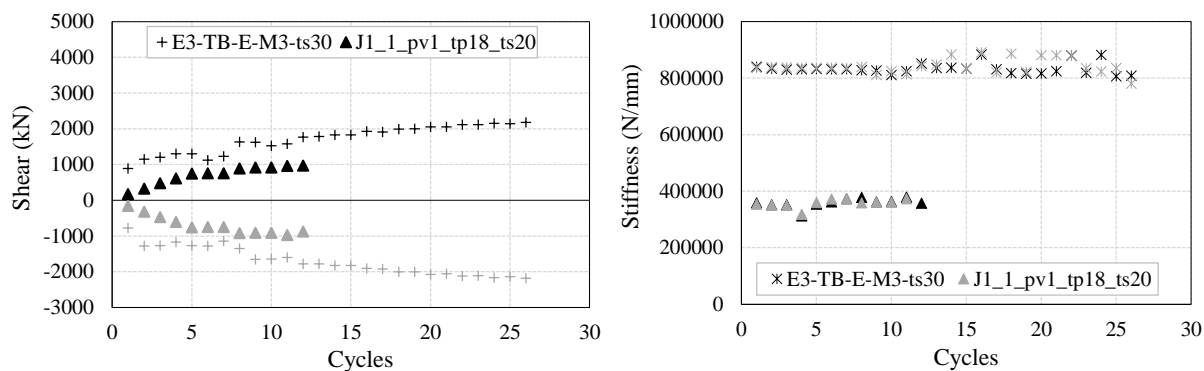


Figure 4.29: Comparison of the strength and stiffness degradation for the V- γ relationship.

Since the shear resistance of the column web panel is independent of the presence of transverse web stiffeners, the additional resistance that is observed is a result from the contribution of the frame action provided by the column flanges and the transverse web stiffeners.

The evolution of the bending moment (M_{fc}) in the flanges against the web rotation is depicted in Figure 4.30. Note that the stress distribution near the bolts row in tension and compression is influenced by the presence of the holes in the flange, resulting in a shift of the position of the plastic hinge towards the bolts row alignment. For that reason, paths *P6* and *P7* are considered aligned with the bolts holes, although in the transition between tension and compression this shift is not so notorious, as observed in Figure 4.31.

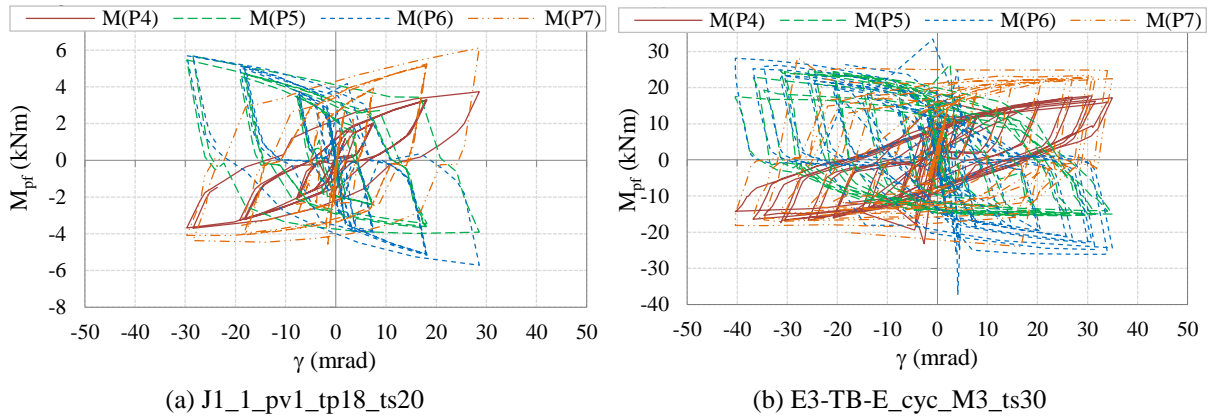


Figure 4.30: Evolution of the flanges bending moment (M_{fc}) vs the web distortion (γ).

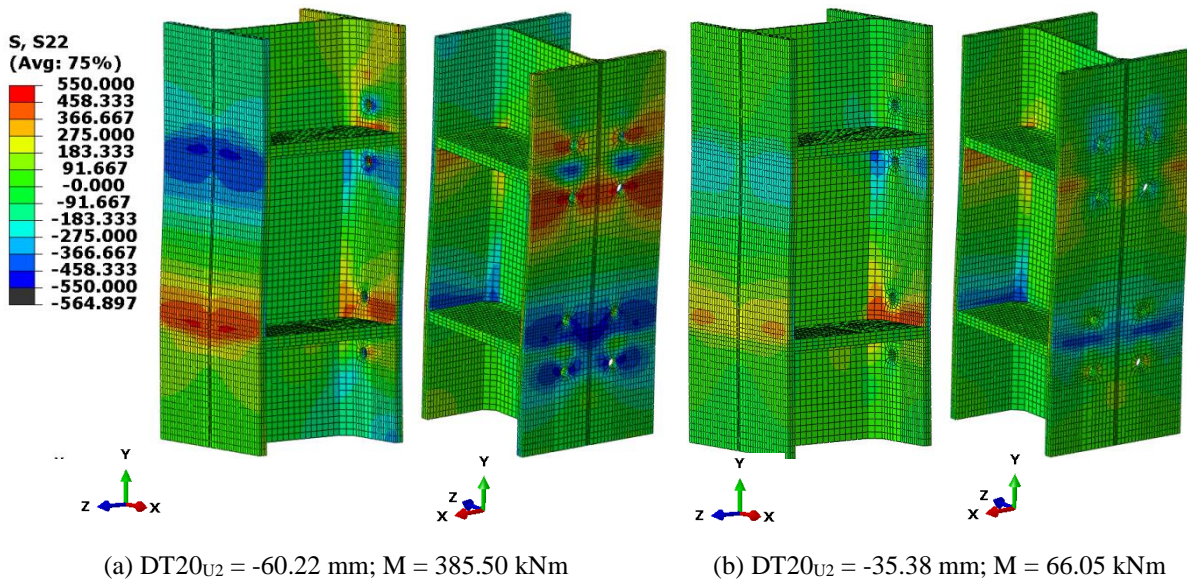


Figure 4.31: Normal stress fields in the column flanges for different levels of bending moment.

4.3 CHARACTERIZATION OF THE CONNECTION COMPONENTS

4.3.1 INTRODUCTION

The contribution of each isolated component for the global joint deformation depends both on stiffness (tangent and effective) and on ductility (the capability to sustain plastic deformation). Components governed by bending, like the column flange and the end-plate in bending, have the ability to form plastic hinges and dissipate energy. Normally these components have lower stiffness when related to the components in tension or compression or even in shear, depending on the length to thickness ratio of the plates involved. As referred

earlier, bending components are the most suitable for energy dissipation in the context of seismic applications. The components that contribute to the connection deformation, referred to in Chapter 3 the contribution of the connection component to the joint deformation, identified in J1 to J4 series, are actually five components, which are: column flange in bending, end-plate in bending, bolts in tension, column web in transverse tension and column web in transverse compression. However, the two last components were already characterized in the last section. Hence, only the first three components will be studied here.

In the comparisons made in Chapter 3, the limitations in the instrumentation setup of the experimental tests did not allow isolating the contribution of each basic component. Nevertheless, due to the presence of continuity column web stiffeners, the major contribution for the deformability is associated to the contribution of the component end-plate in bending. This assumption is only valid if effectively the deformation of the two components is in fact much smaller than the component end-plate in bending. In the absence of the transverse web stiffeners this assumption will not be fulfilled.

4.3.2 METHODOLOGY TO ASSESS THE ISOLATED CONTRIBUTION OF THE CONNECTION COMPONENTS TO THE JOINT ROTATION

A procedure to assess the contribution of the three most significant basic components to the connection rotation and to determine the force-deformation relationships needed for a component based mechanical model is presented here. The procedure isolates the deformation of each component relating the relative displacements of pre-defined nodes in the FE mesh. For that, several additional predefined nodes in the mesh were identified, see Figure 4.32. The deformation mechanisms, in the tension zone of the connection, are depicted in Figure 4.33. In the figure, the deformations obtained in the FE model are amplified, so that it can be observed in detail the specific mechanisms that contribute to the connection rotation. The major contributions arise from the relative deformations around the bolts holes in relation to the column or beam webs, for both components column flange in bending and end-plate in bending. It is also required to consider the flip of the extended part of the end-plate as well as the elongation of the bolts. Although, the deformation in the column flanges is quite different in the presence or absence of transverse web stiffeners, the deformation mechanism that contributes to the connection rotation is very similar, i.e., the deformation around the bolts holes is

responsible for the displacement of the tension flange of the beam caused by the deformation of the column flanges. Although the amplitude of the deformation is very different with and without transverse web stiffeners. Each deformation mechanism, associated to the corresponding basic component, is studied separately. The several mechanisms are analysed in detail hereafter.

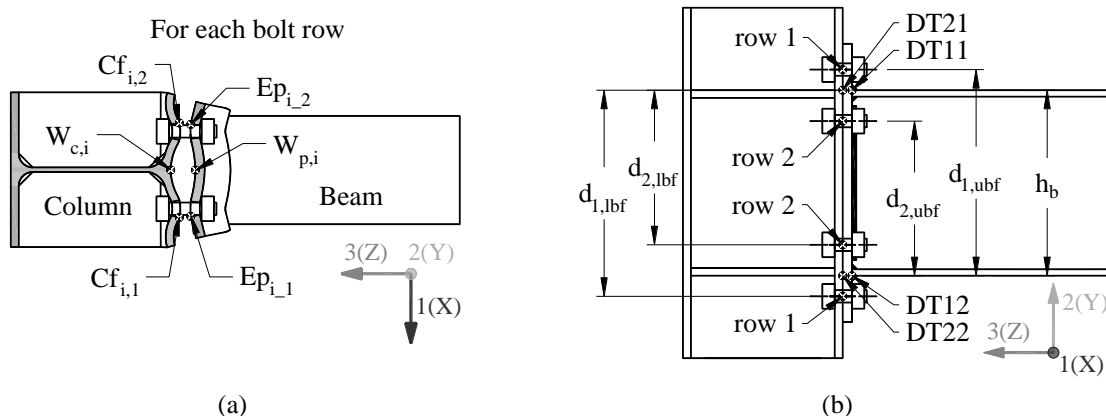


Figure 4.32: Predefined nodes where the displacements are extracted.

The connection rotation is obtained from the relative displacements measured in the nodes $DT11$ and $DT12$, according to Eq. (4.12). The gap formed between $DT11$ and $DT21$, see Figure 4.33 c), or $DT12$ and $DT22$, when the upper or the lower beam flange are in tension, respectively, can be consider the responsible for the connection rotation. The amplitude of the gaps depends on the deformation of the column flanges in bending, the elongation of the bolts in tension and the deformation of the end-plate in bending. The rotation of the connection can be computed using the relative displacements provided by the gap in tension and the displacement of the column flange in compression. For the bolt row located immediately above and beneath the tensioned beam flange the contribution of each component for the gap is determined using the equations described in Table 4.7 to Table 4.10. Table 4.7 describes the procedure to assess the contribution of the column flange in bending for the connection rotation. For that, the average of the displacements measured in the first and second bolts holes of the column flange ($Cf_{i,1,U3}$ and $Cf_{i,2,U3}$) is determined first, see Eq. (4.13); after that, the deformation is determined by computing the relative displacement between the previous displacement and the displacement measured in the column web ($W_{c,i,U3}$), see Eqs. (4.14) and (4.15). After computing the column flange deformation for each bolt row, the value of the deformation at the beam flange level is interpolated according to Eq. (4.16).

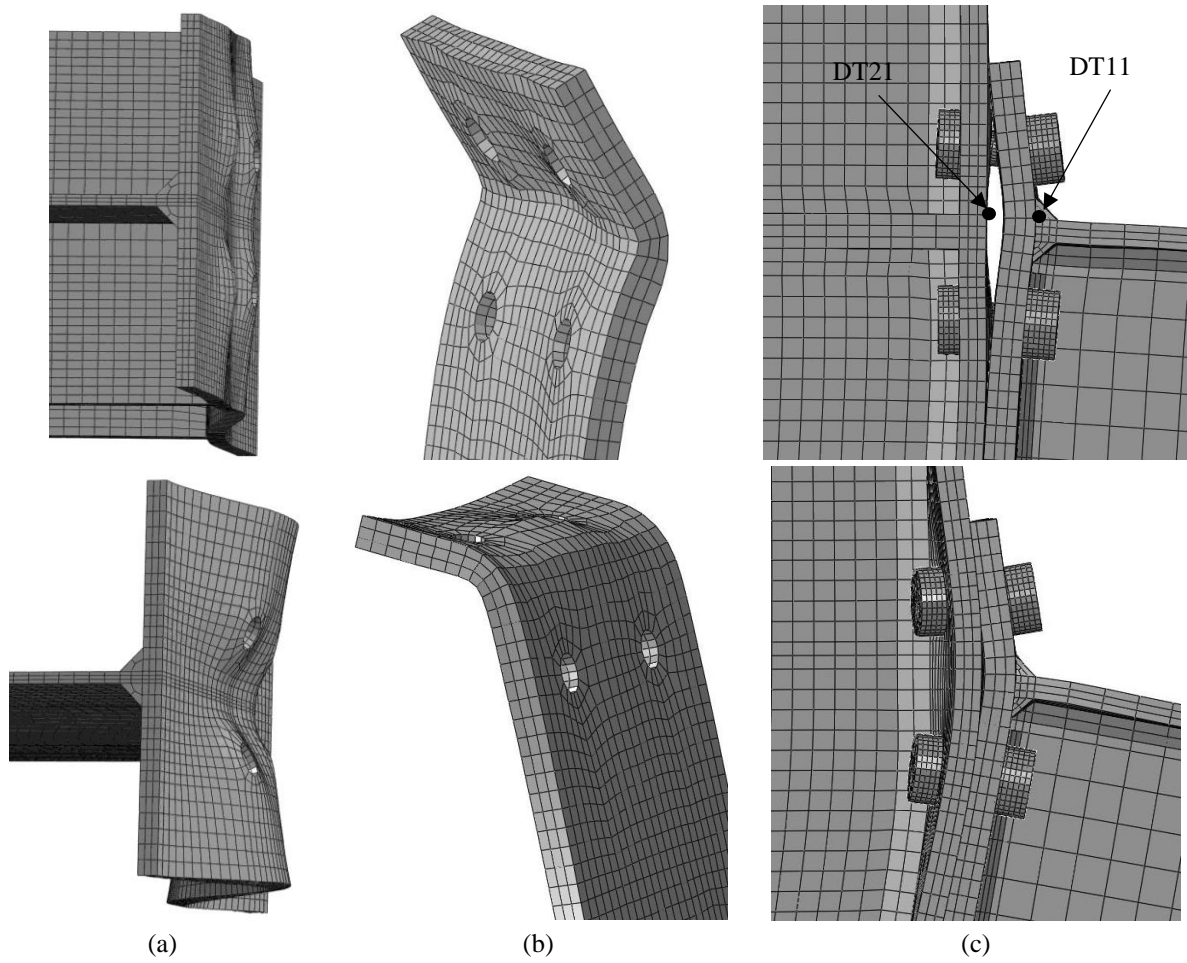
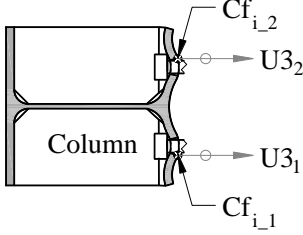
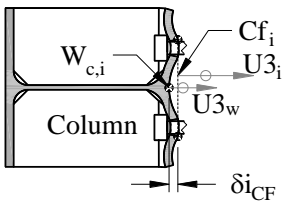
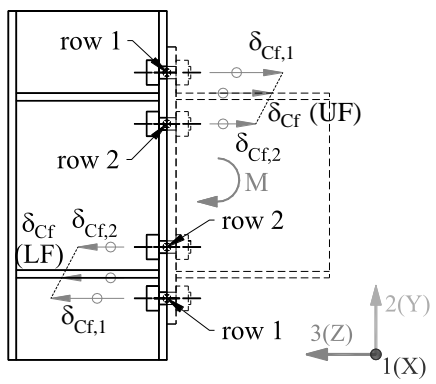


Figure 4.33: Amplified deformation details in the tension zone for stiffened and unstiffened joints.

$$\theta_{connection} = \arctan\left(\frac{DT11_{U3} - DT12_{U3}}{DT11DT12}\right) - \theta_{column_web} - \theta_{elastic_def_column} \quad (4.12)$$

To assess the contribution of the basic component bolts in tension to the connection rotation, the average of the displacements measured in the first and second bolts holes of the column flange (using $Cf_{i,1,U3}$ and $Cf_{i,2,U3}$) and in the end-plate (using $Ep_{i,1,U3}$ and $Ep_{i,2,U3}$) are firstly determined, see Eq. (4.13) and Eq. (4.17). Then, the difference between the average of the displacement found in the column flange ($Cf_{i,U3}$) and in the end-plate ($Ep_{i,U3}$) corresponds to the deformation installed in the bolts, see Eq. (4.18) and (4.19) for each bolt row around the beam flanges, as described in Table 4.8.

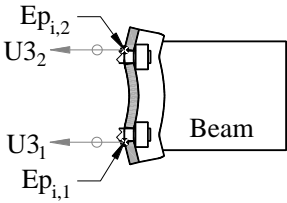
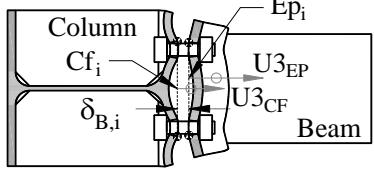
Table 4.7: Procedure to assess the contribution of the component column flange in bending to the connection rotation.

Step	Action / tools	Comments and illustrations
1	<p>Average of the displacements in $Cf_{i,1}$ and $Cf_{i,2}$ according to the direction U3.</p> $Cf_{i,U3} = (Cf_{i,1,U3} + Cf_{i,2,U3})/2 \quad (4.13)$	<p>For each bolt row</p> 
2	<p>External bolt row – determine the flange deformation in the bolts zone in relation to the column web.</p> $\delta_{Cf,1} = Cf_{1,U3} - W_{c,1,U3} \quad (4.14)$ <p>Internal bolt row - determine the flange deformation in the bolts zone in relation to the column web.</p> $\delta_{Cf,2} = Cf_{2,U3} - W_{c,2,U3} \quad (4.15)$	<p>For each bolt row</p> 
3	<p>Interpolation, between bolt rows, for the DT21 and DT22 zones (upper and lower beam flanges, respectively).</p> $\delta_{Cf} = -\frac{(\delta_{Cf,1} - \delta_{Cf,2})}{d_1 - d_2}(d_1 - h_b) - \delta_{Cf,1} \quad (4.16)$	

To determine the contribution for the connection rotation of the end-plate in bending, a similar procedure, to obtain the contribution of the column flange in bending, is firstly applied to the end-plate. The relative displacement between the bolts holes displacement (Ep_i) and the beam web alignment displacement ($W_{p,i}$) is determined, see Eqs. (4.21) and (4.22). However, for the unstiffened extended end-plate connections, the flip of the extended part of the end-plate normally represents the highest contribution of the end-plate to the connection rotation, see Figure 4.33 b). To determine the contribution of the flip to each one of the bolt rows deformation in the end-plate the following procedure is applied: first the contribution of each one of the connection components for the deformation, of each bolt row in tension, is determined ($\delta_{all,i}$), see Eqs. (4.23) and (4.24); then the gap between the end-plate and the column flange, at the beam flanges level (upper and lower beam flange), is determined using DT11,

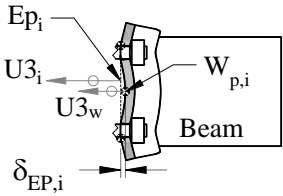
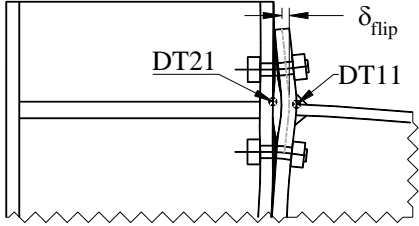
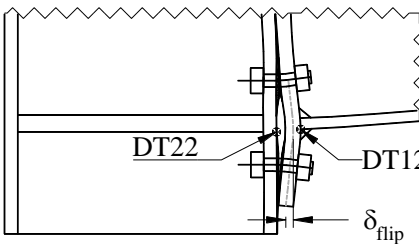
DT12, DT21 and DT22; through interpolation, the contribution of the deformation, computed at the bolt rows level, is determined for the upper and lower flange level ($\delta_{all,ubf}$ or $\delta_{all,lb}$), see Eq. (4.25); after that, the deformation provided by the flip of the end-plate is determined by subtracting the deformation provided by the computed contributions and the total amplitude of the gap, see Eqs. (4.26) and (4.27). The flip deformation can now be added to the interpolated deformation of the bolts holes for the beam flange levels, see Eq. (4.28). The procedure is fully described in Table 4.9.

Table 4.8: Procedure to assess the contribution of the component bolts in tension to the connection rotation.

Step	Action / tools	Comments and illustrations
4	<p>Average of the displacements $Ep_{i,1}$ and $Ep_{i,2}$ according to the direction U3.</p> $Ep_{i,U3} = (Ep_{i,1,U3} + Ep_{i,2,U3})/2 \quad (4.17)$	<p>For each bolt row</p> 
5	<p>External bolt row – determine the bolts deformation.</p> $\delta_{B,1} = Cf_{1,U3} - Ep_{1,U3} \quad (4.18)$ <p>Internal bolt row - determine the bolts deformation.</p> $\delta_{B,2} = Cf_{2,U3} - Ep_{2,U3} \quad (4.19)$	<p>For each bolt row</p> 
6	<p>Interpolation, between bolt rows, for the DT21 and DT22 zones (upper and lower beam flanges, respectively).</p> $\delta_B = -\frac{(\delta_{B,1} - \delta_{B,2})}{d_1 - d_2}(d_1 - h_b) - \delta_{B,1} \quad (4.20)$	<p>Similar to step 3 for bolts deformation.</p>

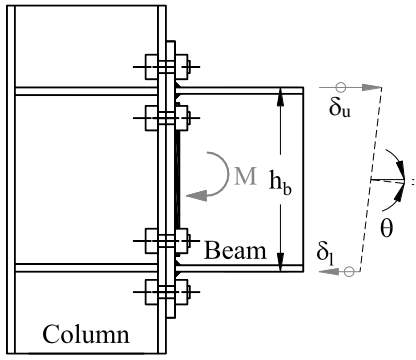
After computing the individual contribution of each component, the relative displacement given by the sum of all contribution, in the upper and lower beam flanges zones, see Eqs. (4.29) and (4.30) allows to determine the rotation of the connection, taking into account the high of the beam, see Eq. (4.31). The procedure is described in Table 4.10.

Table 4.9: Procedure to assess the contribution of the component end-plate in bending to the connection rotation.

Step	Action / tools	Comments and illustrations
7	External bolt row – determine the end-plate deformation in the bolts zone in relation to the beam web. $\delta_{Ep,1} = Ep_{1,U3} - W_{p,1,U3} \quad (4.21)$	For each bolt row 
	Internal bolt row - determine the end-plate deformation in the bolts zone in relation to the beam web. $\delta_{Ep,2} = Ep_{2,U3} - W_{p,2,U3} \quad (4.22)$	
8	External bolt row – sum of the contributions to the deformation until this step. $\delta_{all,1} = \delta_{Cf,1} + \delta_{B,1} + \delta_{Ep,1} \quad (4.23)$	For each bolt row
	Internal bolt row – sum of the contributions to the deformation until this step. $\delta_{all,2} = \delta_{Cf,2} + \delta_{B,2} + \delta_{Ep,2} \quad (4.24)$	For each bolt row
9	Interpolation, between bolt rows, for the DT21 and DT22 zones (upper and lower beam flanges, respectively). $\delta_{all} = -\frac{(\delta_{all,1} - \delta_{all,2})}{d_1 - d_2}(d_1 - h_b) - \delta_{all,1} \quad (4.25)$	Similar to step 3 for the sum of the deformations of CF, B and EP, determined so previously.
10	Determine δ_{flip_EP} for the DT11 zone (upper beam flanges) $\delta_{flip,ubf} = (DT11 - DT21) - (\delta_{all,ubf}) \quad (4.26)$	
11	Determine δ_{flip_EP} for the DT12 zone (lower beam flanges) $\delta_{flip,lbef} = (DT12 - DT22) - (\delta_{all,lbef}) \quad (4.27)$	3 
12	Interpolation, between bolt rows, for the DT21 and DT22 zones (upper and lower beam flanges, respectively). $\delta_{Ep} = -\frac{(\delta_{Ep,1} - \delta_{Ep,2})}{d_1 - d_2}(d_1 - h_b) - \delta_{Ep,1} + \delta_{flip} \quad (4.28)$	Similar to step 3 for end-plate deformation. Note that δ_{flip} is $\delta_{flip,ubf}$ or $\delta_{flip,lbef}$ for the upper and lower beam flange zones, respectively.

The rotation associated to each component is thus determined as a part of the total connection rotation. Note that this procedure produces approximated results, because of the linear interpolations between bolt rows, and because in the compression zone a similar procedure is used to allow for the cyclic behaviour assessment. To be more precise, the deformation aligned with the compression beam flange should be determined, but this would complicate the cyclic behaviour systematization, without significantly increasing the accuracy of the results.

Table 4.10: Procedure to assess the connection rotation.

Step	Action / tools	Comments and illustrations
13	Determine the total deformation for the DT11 zone (upper beam flanges). $\delta_u = \delta_{Cf,u} + \delta_{B,u} + \delta_{Ep,u} \quad (4.29)$	
	Determine the total deformation for the DT12 zone (lower beam flanges). $\delta_l = \delta_{Cf,l} + \delta_{B,l} + \delta_{Ep,l} \quad (4.30)$	
Determine the connection rotation		
14	$\theta = \arctan\left(\frac{\delta_u - \delta_l}{h_b}\right) \quad (4.31)$	

4.3.3 APPLICATION OF THE METHODOLOGY TO THE JOINTS

The previous procedure was applied to the joints used in Section 4.2.3.2 under monotonic and cyclic loading conditions. The geometrical properties of the models are described in Table 4.4.

The response of the J1.1 joints is depicted in Figure 4.34, both for the monotonic and cyclic behaviour. By using the premises of Chapter 3 the contribution of the column web and connection for the joint rotation are depicted in Figure 4.35 and Figure 4.36, for the J1.1 and E3 joints, respectively. It is possible to observe that the J1.1 joints have a wide contribution from the column web panel, with stable behaviour, and that the connection components present

also a considerable contribution to the joint rotation, however much smaller than the column web panel, confirming previous conclusions. In the case of the E3 joint, a more balanced behaviour can be observed between the column web panel and the connections components. Furthermore, in the joint E3-TB-E-M3-ts0 it is possible to observe that the out-of-plane deformation, after a global rotation of 35mrad , illustrated in Figure 4.24, is responsible for the degradation of the shear strength in the column web. This phenomenon affects the connection response, due to the equation used to determine the rotation, Eq. (3.17). This equation uses the rotation of the joint and subtracts the web rotation. The out-of-plane deformation is a local phenomenon that increases the global deformation of the joint. However, the shear deformation of the web remains constant or even decreases, giving the idea that is the connection the responsible for the increase of the rotation.

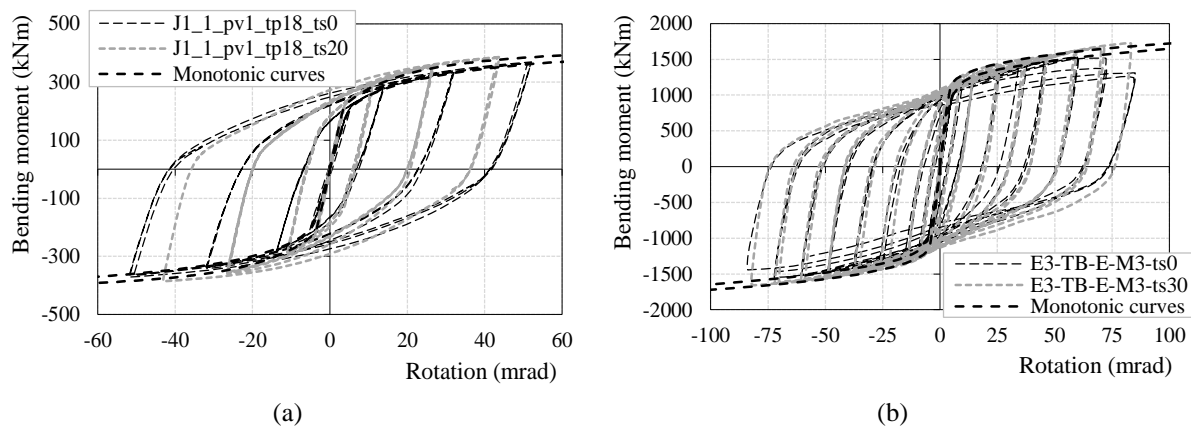


Figure 4.34: Joints response both for monotonic and cyclic loading.

The application of the previous methodology allows to refine the contribution of each individual component to the connection rotation, even when out-of-plane deformation is detected. It also allows having a clear understanding of the behaviour of the connection components, namely the column flange in bending (CFB), end-plate in bending (EPB) and bolts in tension (BT). Figure 4.37 and Figure 4.38 depict the moment-rotation relationships for the three components mentioned above, both for the joints loaded monotonically and cyclically. Considerable differences in behaviour of the three components were detected when transverse stiffeners are added to the joint, both in case of monotonic and cyclic loading. A difference justified by the contribution of the component column flanges in bending, and by the changes in stiffness provided to the connection.

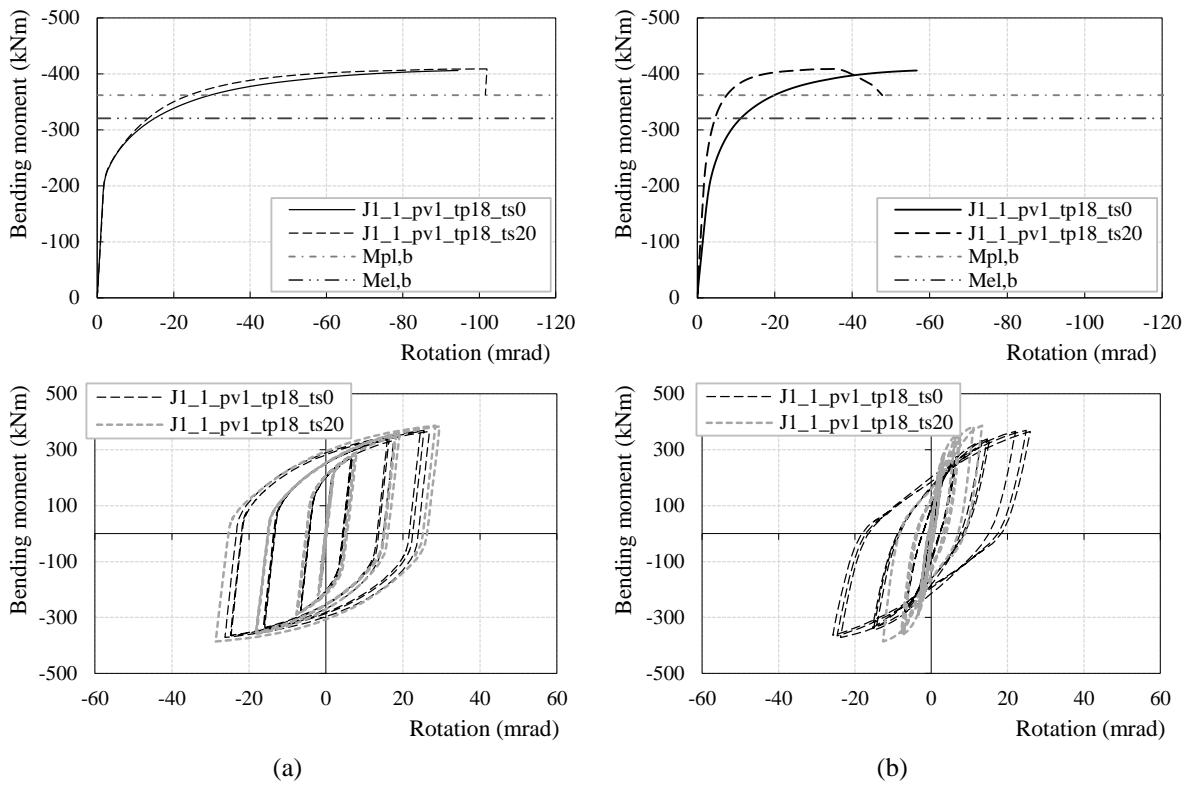


Figure 4.35: (a) Column web panel components and (b) connection components, according to the premises adopted in Chapter 3, for the J1.1 joints.

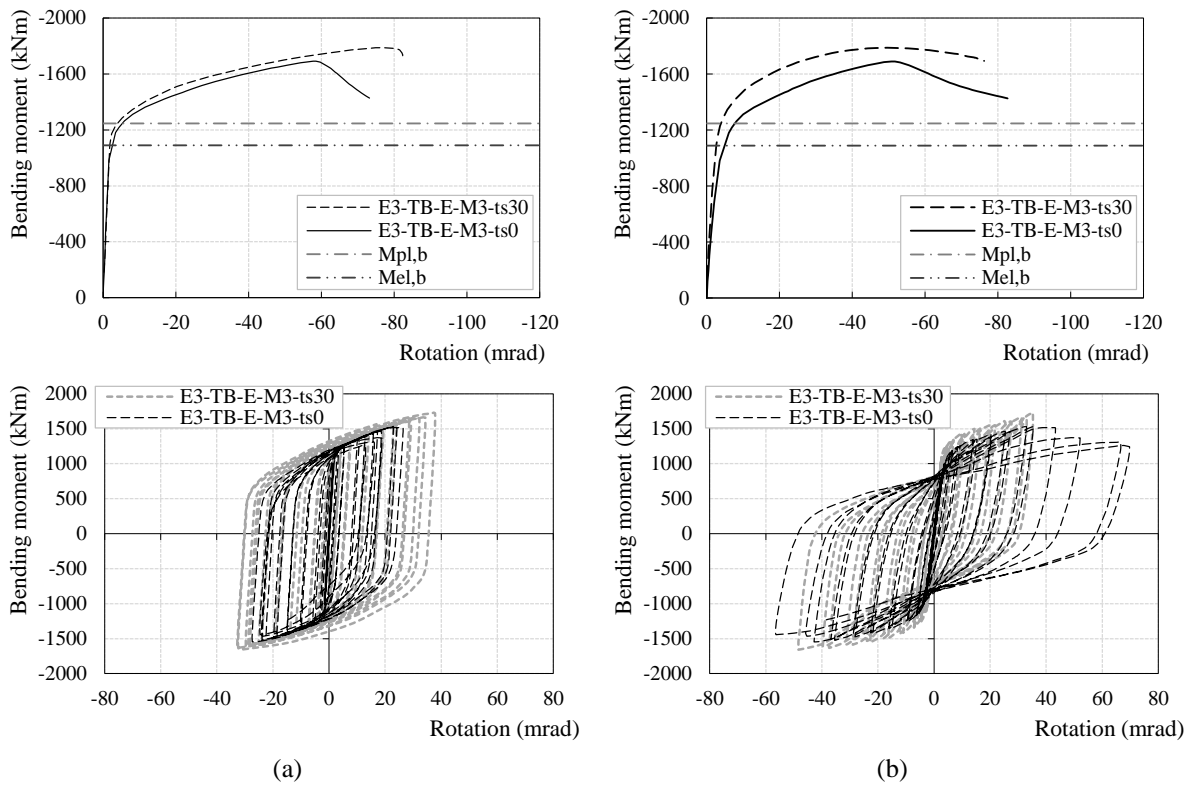


Figure 4.36: (a) Column web panel components and (b) connection components, according to the premises adopted in Chapter 3, for the E3 joints.

The contribution of the component column flanges in bending can be neglected in the presence of the transverse web stiffeners but it has a remarkable influence in the absence of the transverse web stiffeners, as observed in the comparisons depicted in the Figure 4.37 and Figure 4.38. This effect is clearly more notorious in the joints based on J1.1, because the column flange thickness is smaller than the end-plate thickness, which is not the case in the E3 joints. In the E3 joints the column flange in bending remains practically elastic during the analysis, as observed in Figure 4.38. The higher stiffness detected, in the presence of transverse web stiffeners, causes larger deformations due to tension in the bolts.

The proposed procedure proved to be capable of characterizing the contribution of the components of connection.

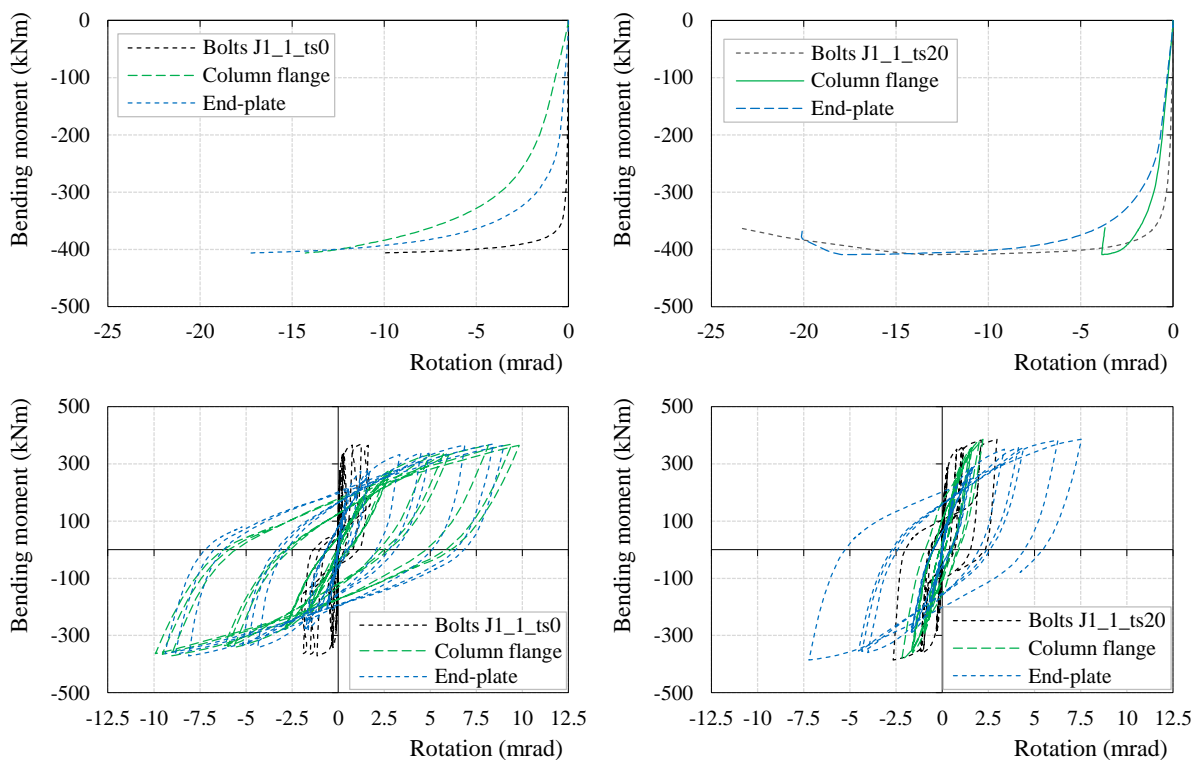


Figure 4.37: Moment-rotation relationships of the components associated to the connection zone, for the J1.1 joints.

By knowing the contribution of each component to the joint rotation, it is possible to determine the energy dissipated during the analyses. In Figure 4.39 and Figure 4.40 are depicted the energy dissipation of the joints under monotonic and cyclic loading, respectively. For the joints loaded monotonically, the accumulated energy was determined until a global rotation of 100mrad was reached. For the cyclic loaded joints the same number of cycles were consider

for the joints in comparison. As discussed in Chapter 3, the accumulated energy dissipated is obtained by computing the area beneath the moment-rotation curve, in the monotonic case, or the some of the areas of the cycles in the moment –rotation relationship, for the cyclically loaded joints. An inspection of the figures allows confirming, quantitatively, the observations made for the moment-rotation curves, depicted before.

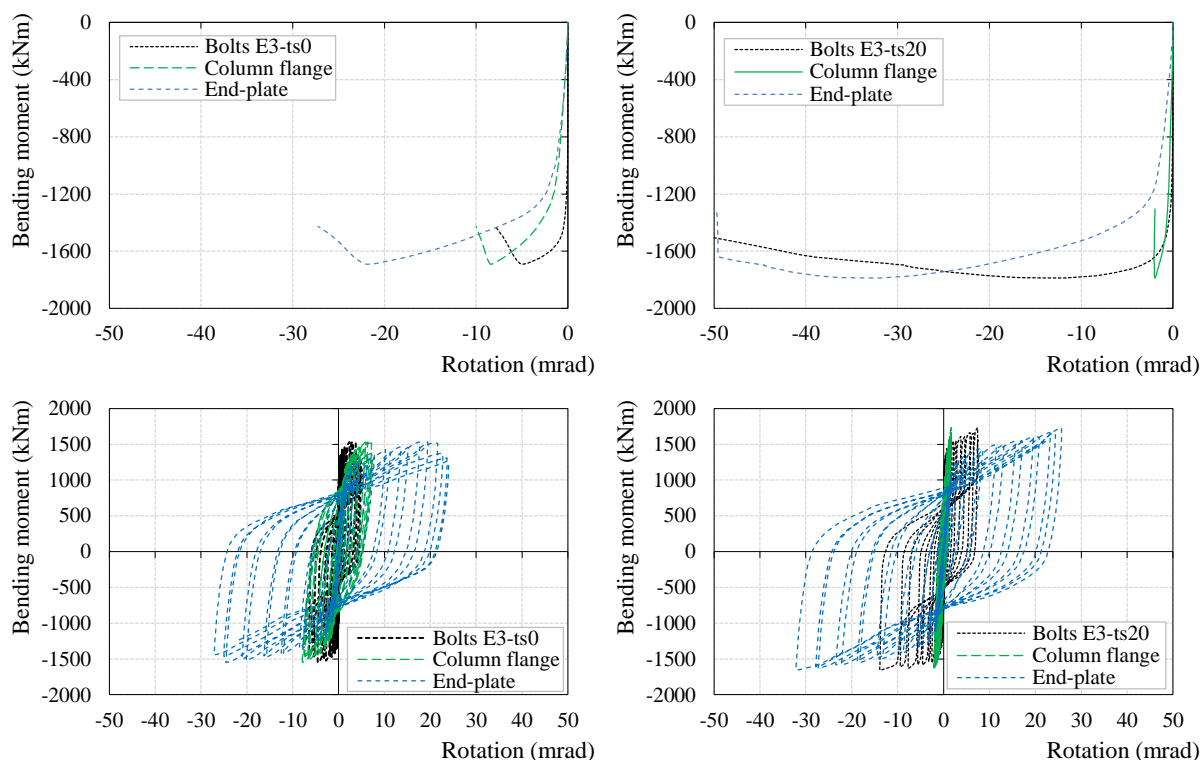


Figure 4.38: Moment-rotation relationships of the components associated to the connection zone, for the E3 joints.

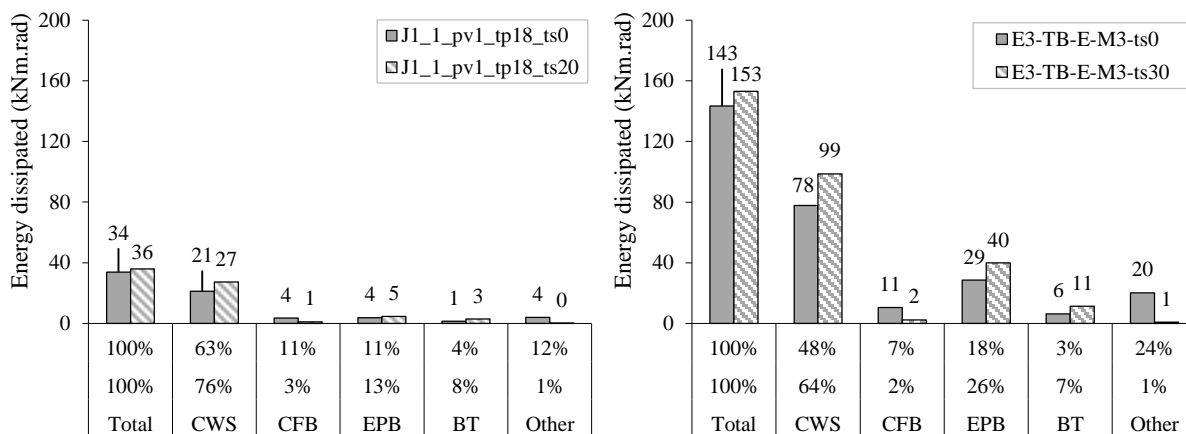


Figure 4.39: Energy dissipated in the joints loaded monotonically.

The major contribution to the energy dissipation is obtained in the column web panel in shear (CWS). This can be a matter of concern in a seismic application following the current codes of practice, like the EC8 (EN 1998-1, 2004) that limits the column web panel contribution to the global rotation. Nevertheless, the J1.1 joints were not designed to fulfil this criterion. The contribution of the connection components is more relevant in the E3 joints, although in the J1.1 joints there is balance between the column flange and the end-plate in bending distribution of energy dissipated, for the unstiffened joint, due to the approximate thicknesses of the column flange and end-plate. The influence of the transverse web stiffeners is evident in the comparisons, especially in the component column flange in bending, leading to a higher demand in the component end-plate in bending.

It is also possible to observe that, for the joints without transverse web stiffeners, the other contributions are always higher than in the stiffened joints. A fact justified by the activation of other components, like the column web in transverse tension or the column web in transverse compression, that are not accounted for in the proposed procedure in the connection components. This conclusion confirms the accuracy of the proposed procedure to isolate the connection components.

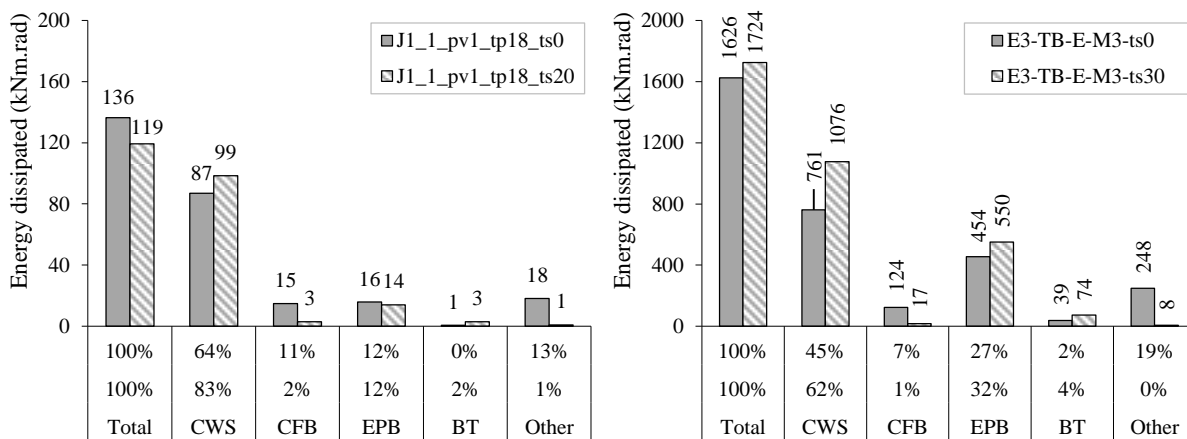


Figure 4.40: Energy dissipated in the joints loaded cyclically.

4.3.4 METHODOLOGY TO EXTRACT THE FORCE-DISPLACEMENT RELATIONSHIPS OF THE CONNECTION COMPONENTS

In the previous section a methodology to determine the contribution to the joint rotation of the three components identified in the connection zone was presented. In this section, the extension of that methodology to extract from the numerical models the force-displacement (F -

4) relationships of the three identified components: column flange in bending, bolts in tension and the end-plate in bending, is presented. These relationships can be used directly in component based models, as those presented in Figure 4.1.

The proposed methodology uses the displacements, in predefined nodes of the FE mesh of the numerical model of the joint, to determine the deformation due to the components according to the bolt rows location. The deformation at the beam flanges level is then computed, by linear interpolation. Additionally, for unstiffened extended end-plates, it is necessary to consider the deformation of the extended part of the end-plate in bending (flip). In this procedure that deformation is computed directly at the level of the beam flanges. It is, therefore, necessary to distribute this deformation among the bolts rows, to be possible to determine the $F-\Delta$ relationships. Thus, the procedure remains unchanged for steps 1, 2, 4, 5, 7, 8, 10 and 11, in the assessment of the deformation according to the bolt rows. Then it is necessary to distribute the contribution of the end-plate flip deformation. Following the concept of the component method defined in the code (EN 1993-1-8, 2005), bolt rows are associated to springs working in parallel, according to the bolt rows location in the joints. These springs are connected by rigid links that assure a linear relationship of the spring's displacements, as shown in Figure 4.41.

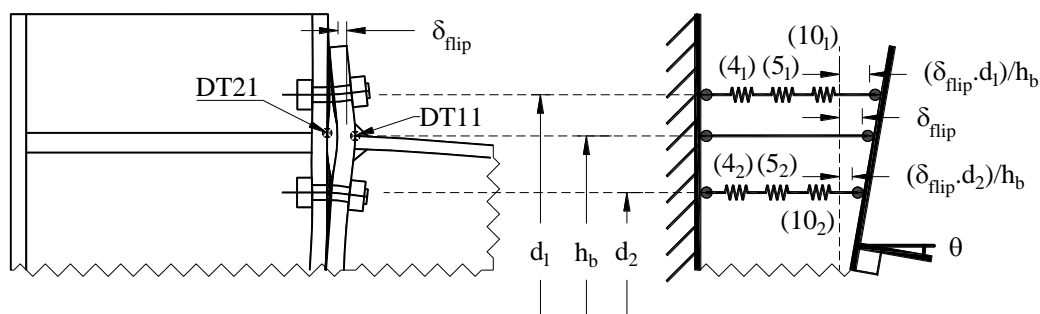


Figure 4.41: Association of the connection components in a mechanical model.

After the calculation of the deformations associated to each component, identified in the connection, it is necessary to determine the corresponding forces. A methodology was proposed in Section 4.2 to assess the force-displacement relationships for the components of the column web, namely the column web in transverse compression or tension components. The resulting equations (Eq. (4.7) and Eq. (4.9)) capture the forces that enter in the column web, transmitted by the bolt rows, in the tension side, and by the direct contact of the end-plate with the column flange in the compression side. It is then possible to associate the forces transmitted to the

column web with the ones developed in the components under investigation. This hypothesis is valid because, in the mechanical model, the springs representative of the connection components are associated in series and therefore the force is the same in all springs in the bolt row. Table 4.11 summarizes the procedure to extract the F - Δ relationships for each component of the connection. Eq. (4.32) represents Eq. (4.7) and Eq. (4.9) used alternately.

Table 4.11: Equations for the extraction of the F- Δ curves from the numerical results.

Component	Force (F)	Deformation (Δ)
Column flange in bending	$F_i = \left(\int \sigma_{33} dy \right) \cdot t_{wc}$ (4.32)	$Cf_{i,U3} = (Cf_{i,1,U3} + Cf_{i,2,U3})/2$ (4.13)
		$\delta_{Cf,i} = Cf_{i,U3} - W_{c,i,U3}$ (4.33)
Bolts in tension	$F_i = \left(\int \sigma_{33} dy \right) \cdot t_{wc}$ (4.32)	$Ep_{i,U3} = (Ep_{i,1,U3} + Ep_{i,2,U3})/2$ (4.17)
		$\delta_{B,i} = Cf_{i,U3} - Ep_{i,U3}$ (4.34)
		$\delta_{Ep,i} = Ep_{i,U3} - W_{p,i,U3}$ (4.35)
		$\delta_{all,i} = \delta_{Cf,i} + \delta_{B,i} + \delta_{Ep,i}$ (4.36)
End-plate in bending	$F_i = \left(\int \sigma_{33} dy \right) \cdot t_{wc}$ (4.32)	$\delta_{flip,ubf} = (DT11 - DT21) - (\delta_{all,ubf})$ (4.26)
		$\delta_{flip,lbf} = (DT12 - DT22) - (\delta_{all,lbf})$ (4.27)
		$\delta_{i,ubf} = \delta_{Ep,i} + (\delta_{flip,ubf} \cdot d_i)/h_b$ (4.37)
		$\delta_{Ep,i,lbf} = \delta_{Ep,i} + (\delta_{flip,lbf} \cdot d_i)/h_b$ (4.38)

Similar to the procedure proposed for the extraction of the behaviour of the components of the column web, see Section 4.2.2, the definition of the boundary conditions for the stress integration depends on the mechanical model adopted. If the alternative procedure in Figure 4.1 is used, the forces and displacements are computed for the influence area of each bolt row. In this case, the integration boundaries for the assessment of tension and compression forces are the same, and the response captures the behaviour of the component both in tension and in compression. However, these components are only activated on the tension side of the joint. Therefore, only the tension part of the response should be considered, in line with the main assumptions of the component method (EN 1993-1-8, 2005), as shown in Figure 4.1. The procedure can be directly applied to unstiffened joints, where the transverse stresses in the web can be associated to the bending moment transmitted by the beam. On the other hand, in the presence of transverse web stiffeners, the bending moment from the beam is distributed not only to the web, but also to the stiffeners which, in turn, transmit them to the web panel in the

form of shear. This is a drawback in the extraction of forces for the component response according to the proposed procedure. To overcome this problem, it is proposed that, in these cases, the tension forces should be determined directly in the bolts of each bolt row. Figure 4.42 illustrates the proposed procedure. The stresses are integrated along the path P8 in the area of the bolts section, according to Eq. (4.39). Due to the symmetry of the joint, and for the joints subjected to simple bending, the force in the bolt row can be taken as the double of the derived forces in one bolt of the row. The forces are then associated to the deformations whose determination remains unchanged, i.e. in Table 4.11 the Eqs. (4.7) and (4.9) are replaced by Eq. (4.39). This procedure will be used in Chapter 5.

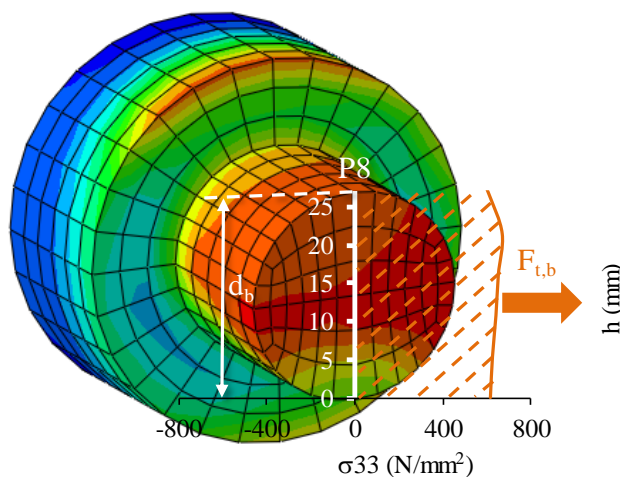


Figure 4.42: Procedure to obtain the tension force of the bolts by stress integration.

$$F_{t,b} = \int_0^{d_{b,i}} \sigma_{33} dA \quad (4.39)$$

It should be highlighted that these procedures used to extract the forces follow a different approach than the component method defined in EC3-1-8 (EN 1993-1-8, 2005), which uses the concept of T-stub with equivalent effective width, with three possible failure modes depending on the expected plastic mechanisms. Here, a displacement-based approach is adopted to determine the mechanisms developed in the joint when applying the load protocol, which can be extracted from the finite element model, thereby enabling to obtain the cyclical behaviour of the component. However, the type of failure mode is not automatically identified by the procedure, but can still be identified using EC3-1-8 (EN 1993-1-8, 2005).

4.3.5 APPLICATION OF THE METHODOLOGY TO THE JOINTS

The previous procedure was applied to some of the joints analysed in Section 4.3.3, using the results obtained in Section 4.2.3.2, for the forces entering in the web, in the components column web in transverse tension or compression.

Figure 4.43 and Figure 4.44 represent the force-deformation cyclic curves for the J1_1_pv1_tp18_ts0 and E3-TB-E-M3-ts0, respectively, according to the alternative component model shown in Figure 4.1, i.e., with the load-introduction components (tension and compression) positioned according to the bolt rows. In this case, the integration boundaries for each bolt row are established based on the effective widths of the components. The deformation mechanisms are determined according to the proposed procedure and the associated forces were computed by taking advantage of the results obtained in Section 4.2.3.2. It should be noted that the deformation scale in the charts of EPB, in Figure 4.44, is three times larger than for the other components.

If a formulation more in line with the component method is required, Figure 4.1, only the tension side of the response of each component is needed and can be achieved isolating the curves in the first and second quadrants of the previous charts.

The analysis of the figures reveals that the individual behaviour of each bolt row is in line with the findings reported in Section 4.3.3, for the joint rotation. The J1.1 joints exhibit a balanced response between the components column flange in bending and the end-plate in bending, due to the similar stiffness of the column flanges and end-plate in bending. On the other hand, E3-TB-E-M3-ts0 is governed by the component end-plate in bending, presenting deformations two to three times higher than the component column flange in bending. As expected the bolt rows closer to the beam flanges have higher demand than the other inner rows. This is a result of the concentration of forces in the beam flanges, resulting from decomposition of the bending moment, present as a force binary at the beam end. The inner rows closer to the beam flanges exhibit stable cycles without pinching, unlike the external rows, which clearly are affected by that phenomenon. In terms of the component bolts in tension, their behaviour was almost elastic, although in the last cycles some plastic deformation can be observed.

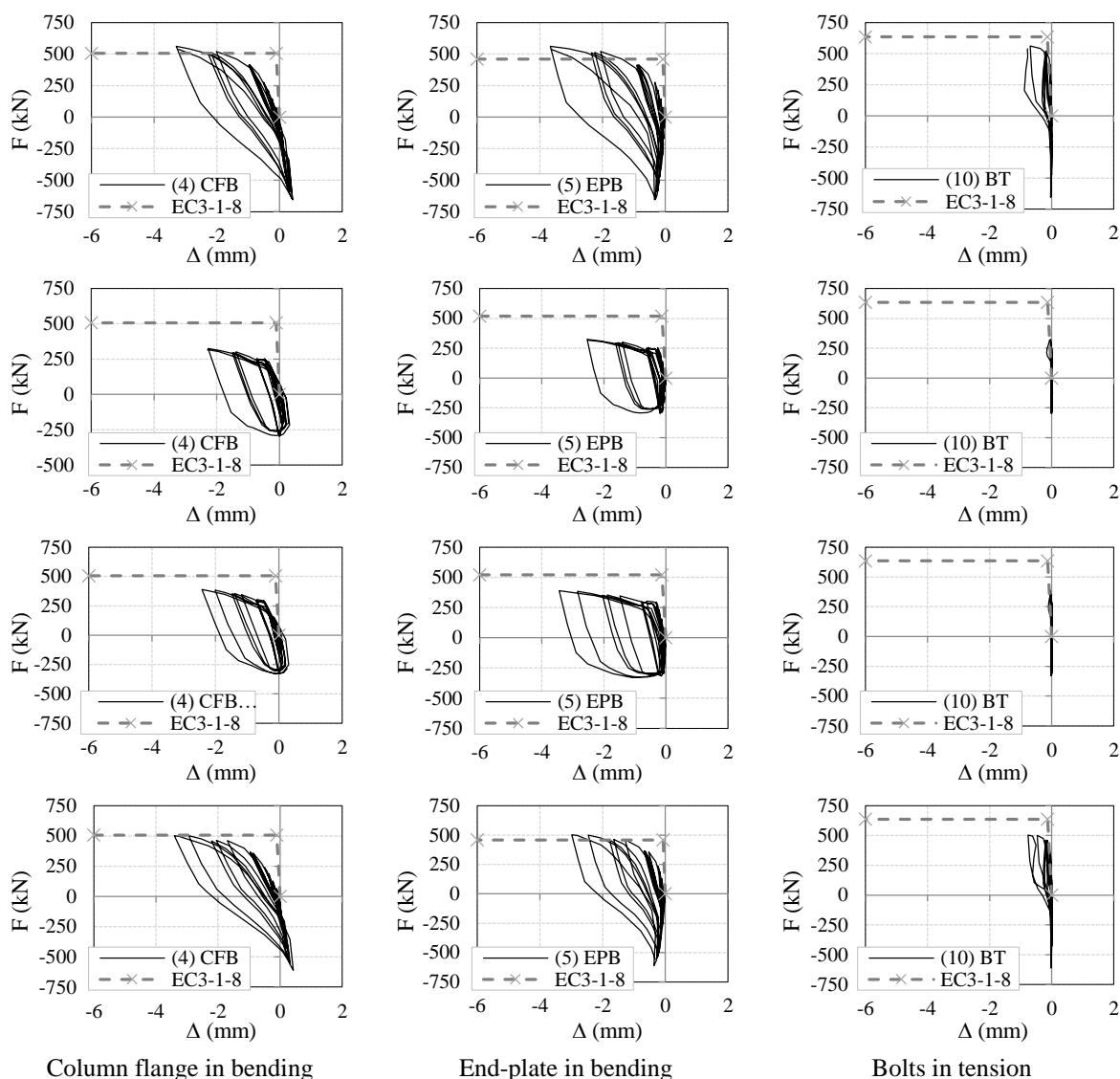


Figure 4.43: F-Δ curves for the connection components for each bolt row, for J1_1_pv1_tp18_ts0 joint, according to the alternative mechanical model of Figure 4.1. From top to bottom row 1 to 4.

The comparisons with EC3-1-8 (EN 1993-1-8, 2005) reveal a good agreement, in terms of strength of the basic components, mainly in the rows closer to the centre of tension and compression, i.e. the beam flanges location. In terms of stiffness, the components column flange in bending and end-plate in bending present normally lower initial stiffness in the cyclic behaviour, when compared with the analytical assessment provided by the formulation in the EC3-1-8. The only exception is in the component bolts in tension where the initial stiffness is closer to that computed analytically.

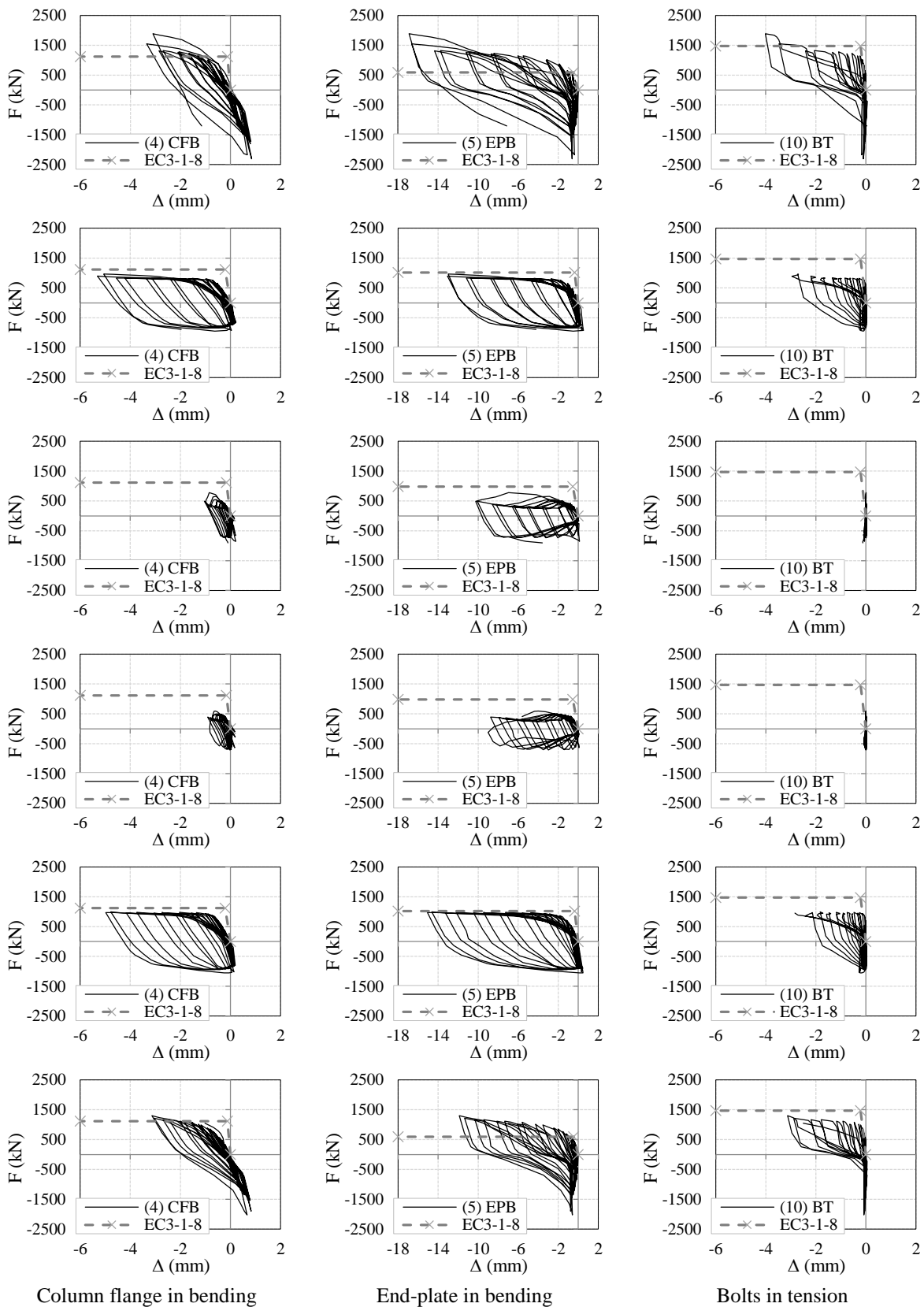


Figure 4.44: F- Δ curves for the connection components for each bolt row, for E3-TB-E-M3-ts0 joint, according to the alternative mechanical model of Figure 4.1. From top to bottom row 1 to 6.

This procedure prosed in this chapter reveals to be effective for the assessment of the force-deformation behaviour of the connection components, especially for joints loaded cyclically. The obtained responses can be directly applied to a component model such as the one illustrated in Figure 4.1.

4.4 METHODOLOGY WALKTHROUGH

A methodology to extract the column web components and connection components response was presented and explained in the previous sections, which was applied to several joints. The objective of this section is to summarize the proposed methodology in a walkthrough Table 4.12 summarizes the steps required for the application of the methodology.

Table 4.12: Methodology overview.

Step	Action	Tools / Comments
1	Development of the FE model of the joint	ABAQUS or other similar software
1.1	Validation of the model	Experimental results or proper benchmark
1.2	Selection of the component model and active components	
2	Extraction of the components column web in tension and compression	
2.1	Definition of the stress paths P1 and P2	Defined in the column web after the flange to web radius, see also Figure 4.4 (b)
2.1.1	P1	Near the connected flange
2.1.2	P2	Opposite flange
2.2	Extraction of the normal stresses (σ_{zz}) along P1	For the selected load increments of the FE analysis
2.2.2	Determination of the integration boundaries (IB ₁ to IB _n)	According to the mechanical model, see also Figure 4.2
2.2.1	Determination of the forces through integration of σ_{zz} over the lengths h_c for compression and h_t for tension	$F_c = \left(\int \sigma_{33} dy \right) \cdot t_{wc} \quad \text{or} \quad F_{t,i} = \left(\int \sigma_{33} dy \right) \cdot t_{wc}$ (Eq. (4.1))
2.3	Extraction of the displacements fields along P1 and P2	For the selected load increments of the FE analysis
2.3.1	Determination of the deformation of the web	$\Delta_{cw} = \delta_{P1} - \delta_{P2}$ (usually aligned with the element rows that causes the deformation, e.g. bolt rows, flanges, etc.)

Step	Action	Tools / Comments
2.4	Derivation of the force-deformation curve for the integration boundaries chosen	For each selected load increment relate the calculated forces with the computed deformation $F-\Delta_{cw}$
3	Extraction of the component column web panel in shear	
3.1	Definition of the stress path P3	See Figure 4.5 (a)
3.2	Extraction of the shear stresses (τ_{yz}) in P3	For the selected load increments of the FE analysis
3.2.2	Determination of the integration boundaries	According to the shear area adopted (for the EC3 shear area see also Figure 4.5 (b))
3.2.1	Determination of the shear forces by integration of τ_{yz} over the lengths defined for the shear area.	$V_n = \left(\int_{(t_{fc}/2+r)_{back}}^{(t_{fc}/2+r)_{front}} \tau_{23} dz \right) \cdot t_1 + \left(\int_{(t_{fc}/2+r)_{front}}^{h_{wc}} \tau_{23} dz \right) \cdot t_{wc} + \left(\int_{(t_{fc}/2+r)_{back}}^{(t_{fc}/2+r)_{front}} \tau_{23} dz \right) \cdot t_1$ <p style="text-align: right;">(Eq. (4.2))</p>
3.3	Extraction of the displacements in four orthogonal points in the web	For the selected load increments of the FE analysis, see also Figure 4.5 (a)
3.3.1	Determination of the horizontal rotation of the web	$\theta_h = a \tan((DT1_{U3} - DT2_{U3})/h_b)$
3.3.2	Determination of the vertical rotation of the web	$\theta_v = a \tan((DT3_{U3} - DT4_{U3})/h_c)$
3.3.3	Determination of the distortion of the web	$\gamma = \theta_h + \theta_v$
3.4	In the presence of transverse web stiffeners	Account for the additional shear strength
3.4.1	Definition of the hinges location in the column flanges P4, P5, P6 and P7	See Figure 4.6
3.4.1.1	Definition of the extraction paths P4.1, P4.2, P4.3, P5.1, P5.2, P5.3, P6.1, P6.2, P6.3 and P7.1, P7.2, P7.3	
3.4.2	Extraction of the normal stresses (σ_{yy}) in each path	For the selected load increments of the FE analysis
3.4.2.1	Determination of the neutral axis using paths Pi.2 and Pi.3	Interpolating between the paths Pi.2 and Pi.3 where the stress becomes zero.
3.4.2.2	Determination of the bending moments by integration of σ_{yy} over the width of the column flanges	$M_{fc} = \int z(\sigma_{22} dA), \quad dA = b_c \cdot dz$ <p style="text-align: right;">(Eq. (4.3))</p>
3.4.3	Determination of the additional shear stress	$V_c = \frac{M_{fc(P4)} + M_{fc(P5)} + M_{fc(P6)} + M_{fc(P7)}}{h_b - t_s}$ <p style="text-align: right;">(Eq. (4.4))</p>

Step	Action	Tools / Comments
3.5	Derivation of the force-deformation curve for the integration boundaries chosen	For each selected load increment relate the achieved shear forces with the achieved distortion
4	Extraction of the component column flange in bending; bolts in tension and end-plate in bending	
4.1	Evaluate the need of transverse web stiffeners.	
4.2	If the stiffeners are not required, the forces determined for the components column web in transverse tension and compression should be used for the three components CFB, BT and EPB, see 2.2.1	$F_c = \left(\int \sigma_{33} dy \right) \cdot t_{wc} \quad \text{or} \quad F_{t,i} = \left(\int \sigma_{33} dy \right) \cdot t_{wc}$ <p style="text-align: center;">(Eq. (4.1))</p>
4.3	If the joint requires transverse web stiffeners, the forces should be obtained in the bolts.	
4.3.1	Definition of the stress paths P8.	Defined in the bolts shank section, vertical position, see also Figure 4.42.
4.3.2	Extraction of the normal stresses (σ_{zz}) along P8.	For the selected load increments of the FE analysis.
4.3.3	Determination of the forces through integration of σ_{zz} over the lengths d_b , according to the area of the shank section. The forces are the same for the three components CFB, BT and EPB, because they are associated in series.	$F_{t,b} = \int_0^{d_{b,i}} \sigma_{33} dA$ <p style="text-align: center;">(Eq.(4.39))</p>
4.4	Determination of the deformations of the components	
4.4.1	Extraction of the displacements of pre-defined nodes in the FE model for each bolt row. $Cf_{i,1,U3}$, $Cf_{i,2,U3}$, $W_{c,i,U3}$, $Ep_{i,1,U3}$, $Ep_{i,2,U3}$, $W_{p,i,U3}$, DT11, DT12, DT21 and DT22	For the selected load increments of the FE analysis. See also Table 4.7, Table 4.8 and Table 4.9
4.4.2	Determination of the deformation of the component column flange in bending	$\delta_{Cf,i} = Cf_{i,U3} - W_{c,i,U3}$ <p style="text-align: center;">(Eq.(4.33)) See also Table 4.11</p>
4.4.3	Determination of the deformation of the component bolts in tension	$\delta_{B,i} = Cf_{i,U3} - Ep_{i,U3}$ <p style="text-align: center;">(Eq.(4.34)) See also Table 4.11</p>

Step	Action	Tools / Comments
4.4.3	Determination of the deformation of the end-plate in bending	For this component is also necessary to consider the flip of the unstiffened extended part of the end-plate.
4.4.3.1	Deformation of the bolt zone in relation to the beam web alignment	$\delta_{Ep,i} = Ep_{i,U3} - W_{p,i,U3}$ (Eq.(4.35)) See also Table 4.11
4.4.3.2	Deformation regarding the flip of the unstiffened extended part of the end-plate	$\delta_{i,ubf} = \delta_{Ep,i} + (\delta_{flip,ubf} \cdot d_i) / h_b$ $\delta_{Ep,i,lbf} = \delta_{Ep,i} + (\delta_{flip,lbf} \cdot d_i) / h_b$ (Eqs.(4.37) and (4.38)) See also Table 4.11
4.5	Derivation of the force-deformation curve for each component	For each selected load increment relate the achieved forces with the achieved deformations

4.5 MAIN CONCLUSIONS

In this chapter a detailed study of the components behaviour of double-extended end-plate bolted joints was carried out, in order to characterize the behaviour of individual components, particularly in cyclic loaded joints. Several components were analysed, with particular emphasis on the components of the column web panel, when the joint is subjected to bending moment.

A versatile and efficient methodology for the extraction of the monotonic and cyclic behaviour of the web panel components from experimental tests and numerical simulations was presented, applicable to bolted end-plate joints, but extensible to other joint configurations. The methodology uses the integration of stress fields from the FE models of the joints, namely the column web panel in shear and the column web in transverse compression or tension components. The accuracy of the methodology depends on the column web element size and the number of stress fields analysed from the available load increments. Finally, it was highlighted that the procedure is very flexible in terms of the definition of the integration boundaries; in particular, and in line with the definition of the components in EC3-1-8 (EN 1993-1-8, 2005), the boundaries may be different for tension or compression, therefore generating tension or compression cyclic $F-\Delta$ curves only.

Double-extended end-plate joints were analysed and used to assess the proposed methodology. The numerical results for the joints subjected to monotonic loads were compared with the results obtained from EC3-1-8, the Atamaz-Jaspart and the Krawinkler models. The numerical results and the proposed methodology generally confirm the accuracy of the Atamaz-Jaspart model and the EC3-1-8 design model, further allowing to explain in a detailed way the load transfer from the beam to the column. The force-deformation relationship of the components can be implemented in a spring's model assembled according to the joints geometry, or used directly in frame analysis and design.

The double-extended end-plate joints, with and without transverse web stiffeners, subjected to different cyclic load protocols (ECCS and AISC 341-10) were analysed and used to validate the proposed methodology. The results allowed concluding that the procedure is able to capture the behaviour of the column web under tension and compression, for both groups of bolts and isolated bolt rows, as well as the shear-rotation behaviour, including the additional shear resistance provided by the stiffeners and achieved by the frame action developed by the column flanges and the stiffeners. The direct comparison of the behaviour of the joints, with and without stiffeners, shows that the procedure is able to capture the influence of these designs in the amplitude and shape of the force-displacement relationships.

A practical and efficient methodology for the extraction of the behaviour of the basic components in the connection zone in the numerical simulations was proposed, which is applicable to bolted end-plate beam-to-column joints. The connection components that were studied are the column flange in bending, the end-plate in bending and the bolts in tension. The methodology is displacement-based as it uses the relative displacements, of predefined nodes in the finite element model, to assess the deformation mechanisms in the components. These deformation mechanism are then associated to the forces obtained by integration of the stress fields, according to the previous methodology to assess the tension and compression forces that enter in the column web, which are directly transmitted by the connection components. The methodology can be applied to determine the contribution of the individual components to the joints global rotation, or to extract the force-deformation response curves of each individual components.

The procedure was applied to the previous joints, both loaded monotonically and cyclically, allowing to refine the contribution of each individual component to the connection

rotation, even when out-of-plane deformation is detected. Its application allows a better understanding of the behaviour of the connection components. Considerable differences in behaviour, of the three components, were detected when transverse stiffeners are added to the joint, both in case of monotonic and cyclic loading. A difference justified by the changes in stiffness provided to the connection.

As expected, the bolt rows closer to the beam flanges have higher demand than the other inner rows, as a result of the concentration of forces in the beam flanges, coming from decomposition of the bending moment, present at the beam end, as a binary of forces. The inner rows closer to the beam flanges present stable cycles without pinching, unlike the external rows, which clearly are affected by that phenomenon. In terms of the component bolts in tension their behaviour was almost elastic although in the last cycles some plastic deformation could be observed, which contributed to the joint rotation.

Even though the double-extended end-plate steel joints analysed in this chapter fall out of the scope of Eurocode 8, due to the excessive contribution of the column web panel to the plastic deformation of the joint, the specific characteristics of the joints allowed to analyse and characterize in detail the cyclic behaviour of the column web components. The force-displacement relationships obtained revealed a cyclic stable behaviour and high energy dissipation capacity, mostly provided by the column web panel in shear. The proposed procedures revealed to be an excellent tool to obtain the isolated behaviour of the components of the joint, and it can be extended to other components such as the beam and column flange in compression or the beam web in tension.

5

APPLICATION OF THE DEVELOPED METHODOLOGIES TO DOUBLE-EXTENDED END-PLATE JOINTS

5.1 INTRODUCTION

As highlighted in previous chapters, double-extended end-plate joints, are widely used in European countries due to their excellent mechanical properties and low manufacturing cost. In those chapters this type of joints was investigated by reviewing past experimental, numerical and analytical methodologies and by further developing new numerical and analytical procedures to characterise the behaviour of the joints when subjected to reversal loading, at both global and components level. To achieve these main goals a comprehensive set of numerical models were developed and calibrated using the finite element modelling and analysis technics. In this chapter the methodologies developed in Chapters 3 and 4 are applied to a set of double-extended end-plate joints and their behaviour is analysed for both monotonic and cyclic loading conditions.

In the context of a European research project (Landolfo *et al.*, 2017) several beam-to-column double-extended end-plate joints were designed to be tested and analysed by detailed finite element models. The joint selection was based on steel frame building structures designed for seismic resistance using current European state-of-practice structural typologies of low to medium rise buildings, designed according to the EC8-1 (EN 1998-1, 2004). Both exterior and interior beam-to-column joints configurations were investigated including extended end-plate joints with partial-strength partial-rigid connection, which were chosen to be analysed here using the developed methodologies. The connections were designed to achieve equal and partial

strength, according to the connected beam resistance and the EC3-1-8 (EN 1993-1-8, 2005) criterion to classify partial-strength joints.

The geometry and design of the joints will be briefly addressed followed by finite element analyses that include a parametric study carried out to analyse the sensitivity to key parameters affecting the joint response. Furthermore, the methodologies developed in Chapter 4 to extract the individual force-displacement behaviour of the components response will be applied.

The numerical characterization of the bolted end-plate beam-to-column joints behaviour presented in this chapter, is based on the procedures presented in Chapter 3, namely the finite element modelling options and validation using the FE software ABAQUS (2014).

This numerical study was partly conducted before experimental tests were performed on the same joints by others and results were available. However, when test results were already available, they were used to calibrate the FE models using the updated material relationships obtained from the coupon tests.

5.2 BEAM-TO-COLUMN JOINTS CONFIGURATION

5.2.1 REQUIREMENTS

A set of joints configuration representative of such present in portal frames (see Figure 5.1) is constituted by external beam-to-column joints: E2 – IPE450 – HEB340 and E3 – IPE600 – HEB500.

For each configuration three different connections were designed, according to their level of strength (designated as Full, Equal and Partial) in relation to the beam strength. The joints designed for Full-strength should develop the plastic hinges on the beam, in the case of the Equal-strength joints the plastic deformations should occur in both beam and joint simultaneously, and in the case of the Partial-strength joint it is expected that the main source of plasticity is concentrated in the joint. The partial-strength joints were designed to achieve a strength level of approximately 60% of the beam strength.

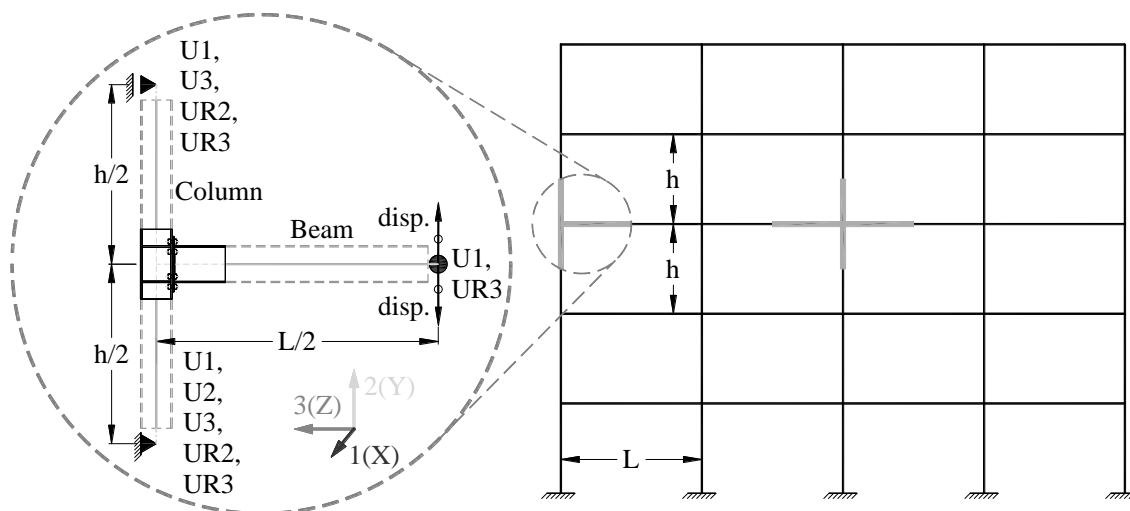


Figure 5.1: Scheme of the beam-to-column sub-assembly extracted from the portal frames.

5.2.2 CONFIGURATION AND DESIGN OF THE JOINTS

Four categories of unstiffened end-plate joints were designed characterized by different relative strength levels of the connection zone and in the web panel zone, in relation to the beam resistance (Jaspart *et al.*, 2014):

Equal strength joints: $M_{p,b} \approx M_{p,con}$;

Partial strength joints: $M_{p,b} > M_{p,con}$;

Balanced web panel joints: $M_{p,wp} \approx \min(M_{p,b}, M_{p,con})$;

Weak web panel joints: $M_{p,wp} < \min(M_{p,b}, M_{p,con})$.

Were $M_{p,b}$ is the plastic capacity of the beam section, $M_{p,con}$ is the plastic capacity of the connection (end-plate, bolts, column flanges and column web) and $M_{p,wp}$ is the plastic capacity of the web panel in shear due to the bending moment transmitted by the beam. It is important to refer that the joint classification was performed using the nominal material properties for all the elements in the joint.

In Table 5.1 are listed the specimens that will be addressed in this section, the joints classification according to their strength and the expected weakest component. The type of the sub-assembly and the code assigned to each one of the joints is also presented. From the code name is possible to identify the configuration of the sub-assembly (TB or XW), the

classification of the joint E (equal) or P (partial) and the beam-to-column cross section (E2 or E3).

Table 5.1: Specimens of the unstiffened joints.

Specimen name	Members involved	Type	Description
E2-TB-E	HEB340-IPE450	T	Balanced web panel, equal strength
E2-TB-P	HEB340-IPE450	T	Balanced web panel, partial strength (0.6)
E2-XW-P	HEB500-IPE450	X	Weak web panel, partial strength (0.8)
E3-TB-E	HEB500-IPE600	T	Balanced web panel, equal strength
E3-TB-P	HEB500-IPE600	T	Balanced web panel, partial strength (0.6)
E3-XW-P	HEB500-IPE600	X	Weak web panel, partial strength (0.8)

When dealing with partial and equal strength joints it is expected that some plastic mechanisms will form in the connection zone or in the members. There are three possible zones where the plastic mechanisms can developed: near the beam ends, the connection and in the column web panel. As discussed in Section 2.2.2.3, and demonstrated in literature, the column web panel and the beam are two elements with high ductility, currently addressed in design codes (EN 1998-1, 2004) for energy dissipation, although some limitations are imposed to the column web plastic contribution to the joint rotation (30%). As in a context of partial-strength joints is not expect to have severe plastic deformations in the beam, the ductility of the connection zone assumes an important role. With that in mind some ductility criterion were defined, based on the T-stub representation of the connection components in bending, and the three failure modes associated to it (Landolfo, 2014). The two ductility levels were defined and are represented in the Figure 5.2.

Ductility level 1: $\beta \leq 1$ (accounting $\gamma_{ov} = 1.25$ for the plates), applied for the partial-strength joints (with balance or strong web panel). This condition means that the failure mode 1 or the failure mode 2 (but very close the mode 1) are expected, the ductility is therefore enough.

Ductility level 2: $\eta \leq 0.95$ (accounting $\gamma_{ov} = 1.25$ for the plates), applied for the equal-strength joints or the partial-strength joints (but with weak web panel). This condition means that the failure mode 2 (but not too close the mode 3) is expected, the brittle failure is therefore avoided.

β and η are defined in Figure 5.2 and by the Eq. (2.9). Further explanation on the above criterions can be found in Section 2.2.2.2, or with deeper detail in Jaspart (1997).

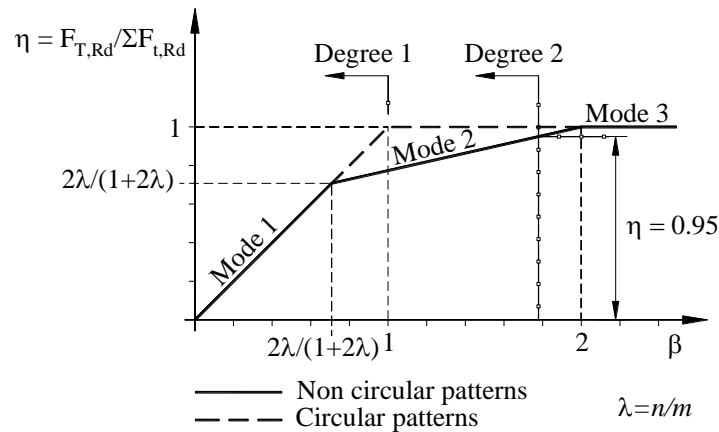


Figure 5.2: Ductility criterion based on the three failure modes found in T-stub.

The selected joints were analysed both in monotonic and cyclic conditions, and their geometric characteristics are presented in Table 5.2 and in Figure 5.3. In the table, $S_{ini,pw}$ is the initial stiffness of the column web panel; $S_{ini,c}$ is the initial stiffness of the connection (end-plate, bolts, and column flange and web); $S_{ini,pw+c}$ is the initial stiffness of the joint (column web panel and connection).

The finite element models followed the experimental tests setup depicted in the Figure 5.1, where the total height h is equal to 3.5 meters and the total length L is 5.5 meters.

Table 5.2: Main design properties of the joints according to EC3-1-8 (EN 1993-1-8, 2005) from Jaspart *et al.* (2014).

	E2-TB-E	E2-TB-P(0.6)	E2-XW-P(0.8)	E3-TB-E	E3-TB-P(0.6)	E3-XW-P(0.8)
$M_{p,b}$ (kNm)	604.2	604.2	604.2	1246.8	1246.8	1246.8
$M_{p,con}$ (kNm)	545.4	392.7	469.6	1129.6	736.4	913.2
$M_{p,wp}$ (kNm)	549.6	549.6	432.7	1217.5	1217.5	825.8
$M_{p,j}/M_{p,b}$	0.9	0.65	0.78	0.91	0.59	0.73
$M_{p,wp}/M_{p,con}$	1.0	1.4	0.92	1.07	1.65	0.90
β (bolt row 2)	1.58	1.00	1.34	0.96	0.62	0.75
η (bolt row 2)	0.92	0.75	0.85	0.77	0.62	0.72
$S_{ini,wp}$ (kNm/rad)	210620	211440	168440	436350	436350	295550
$S_{ini,con}$ (kNm/rad)	280250	195440	224150	468840	364130	376670
$S_{ini,j}$ (kNm/rad)	120250	101560	96170	226010	197940	165610
EI_b/L_b (kNm/rad)	12883	12883	12883	35158	35158	35158
k_b	9.3	7.9	7.5	6.4	5.6	4.7

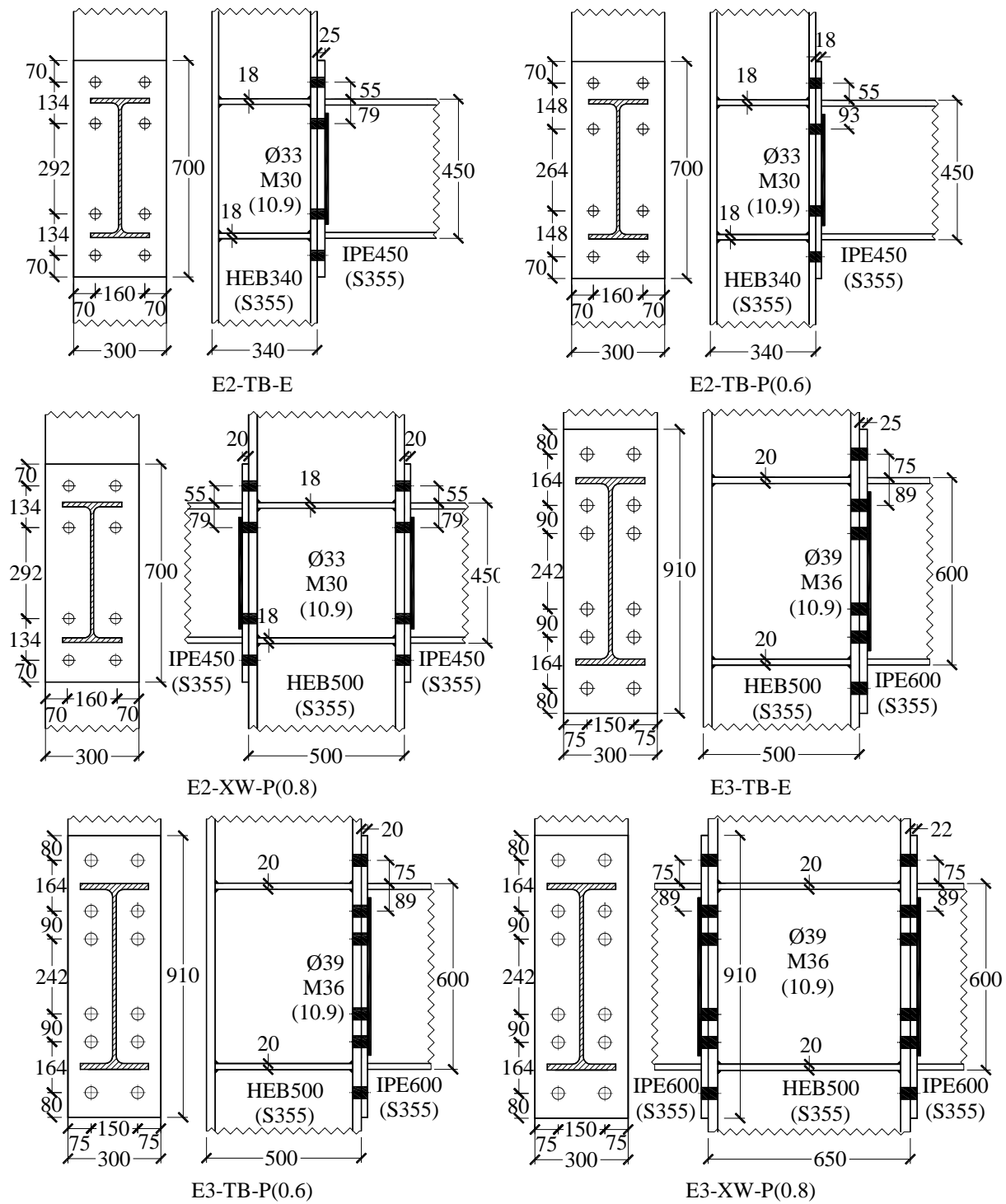


Figure 5.3: Geometrical properties of the selected joints (dimensions in mm).

5.2.3 FINITE ELEMENT MODELLING

In this section the scripting tools developed in Section 3.4 and Annex B were used to build the FE models. The models were developed according to the finite elements options

defined in Chapter 3. The 3D models of the joints are composed of several parts (solid and wire instance parts) identified in Figure 5.4.

Similar to the joints E3-TB-E-M3 analysed in Section 4.2.3.2 the same stress-strain relationships are used, see Figure 4.15 (b), in the preliminary models developed to set the bases of the experimental tests. Likewise the overstrength factor $\gamma_{ov} = 1.25$ proposed by the EC8-1 (EN 1998-1, 2004) was considered for the base material properties (M-3), for the steel grade adopted, S355, to tackle the overstrength normally found in the mechanical properties of current steel elements belonging to a steel grade.

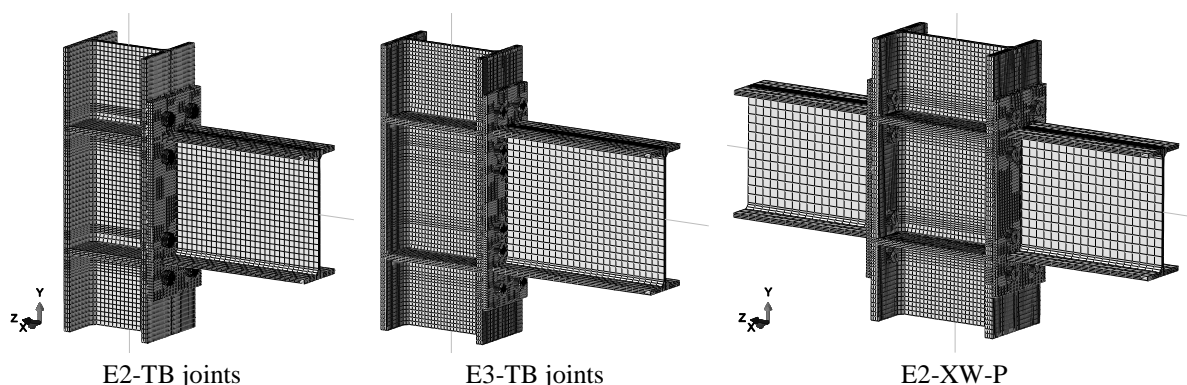


Figure 5.4: Joint FE models typologies.

5.2.4 LOAD PROTOCOL ADOPTED

For the cyclic loaded joints (E2-TB-E/P and E3-TB-E/P) the load protocol adopted was ANSI/AISC 341-10 (2010). This procedure is conducted by controlling the inter-storey drift, θ , imposed on the test specimen, as defined in Section 4.2.3.2, six cycles in the ranges $0.00375rad$, $0.005rad$, $0.0075rad$, four cycles in the range $0.01rad$ and two cycles in the ranges $0.015rad$, $0.02rad$, $0.03rad$, $0.04rad$. The loading is continued at increments of $\theta = 0.01rad$, with two cycles of loading at each step, as defined in Figure 5.5.

The deformation control parameter (inter-story drift angle θ) is defined as inter-story displacement divided by the story height. In the test specimen this angle is defined as the beam deflection δ divided by the beam span (to the column centreline L_b). So the amplitude δ is defined by the Eq. (4.11) according to the Figure 4.16 (b).

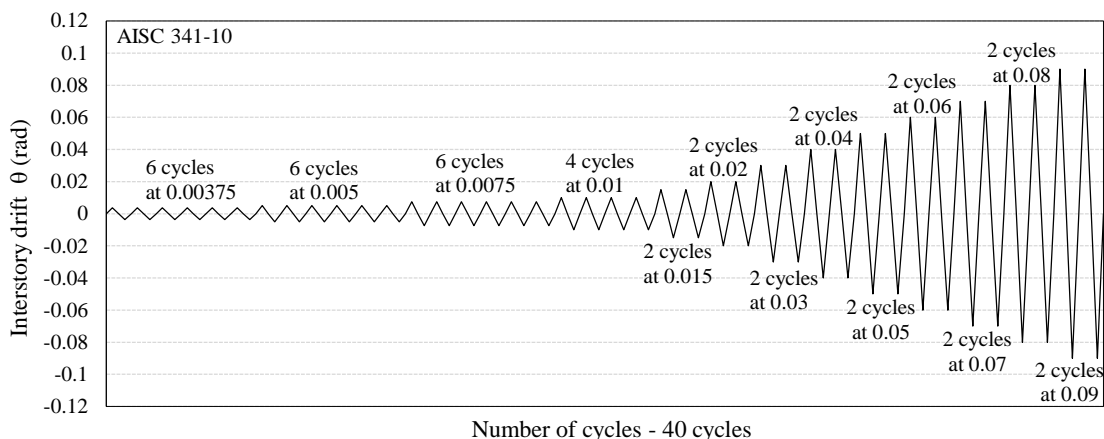


Figure 5.5: ANSI / AISC 341-10 cyclic loading procedure (figure from (ANSI/AISC 341-10, 2010)).

5.3 ANALYTICAL VS NUMERICAL RESULTS

5.3.1 FRAMEWORK

The analytical design of the joints, according to the EC3-1-8 (EN 1993-1-8, 2005), predicted the joint main properties, in terms of stiffness, strength and ductility, summarised in Table 5.2. Next a comparison of the analytical predictions with the results of the FEM analysis is undertaken and discussed. Furthermore, in the case of the FEM results, to obtain the global rotations in the joints, Eq. (3.7) was used to compute the bending moment and the Eq. (3.21) was used to compute the rotation of the joint and θ_{elast_column} and θ_{elast_beam} are obtained from the Eqs. (3.18) and (3.19), respectively. *DT23* and *DT24* are identified in Figure 3.21.

5.3.2 MOMENT-ROTATION RELATIONSHIPS

The moment-rotation relationships obtained in the FEM are depicted in Figure 5.6 for the E2 and E3 joints geometries, along with the analytical response obtained using the EC3-1-8 (EN 1993-1-8, 2005) formulation, the beam plastic capacity to bending moment ($M_{j,b}$) and the design moment expected for the joint ($M_{j,Ed}$).

In the case of the external joints, with equal-strength classification, the analytical predictions seems to have a closer agreement with the nonlinear response obtained in the FEM. On the contrary the FEM response of the partial-strength external joints behaviour is always much higher than the analytical predictions obtained by the code.

For the internal joints the comparison between the connection results and the analytical predictions revealed to be well adjusted for both E2 and E3 joints.

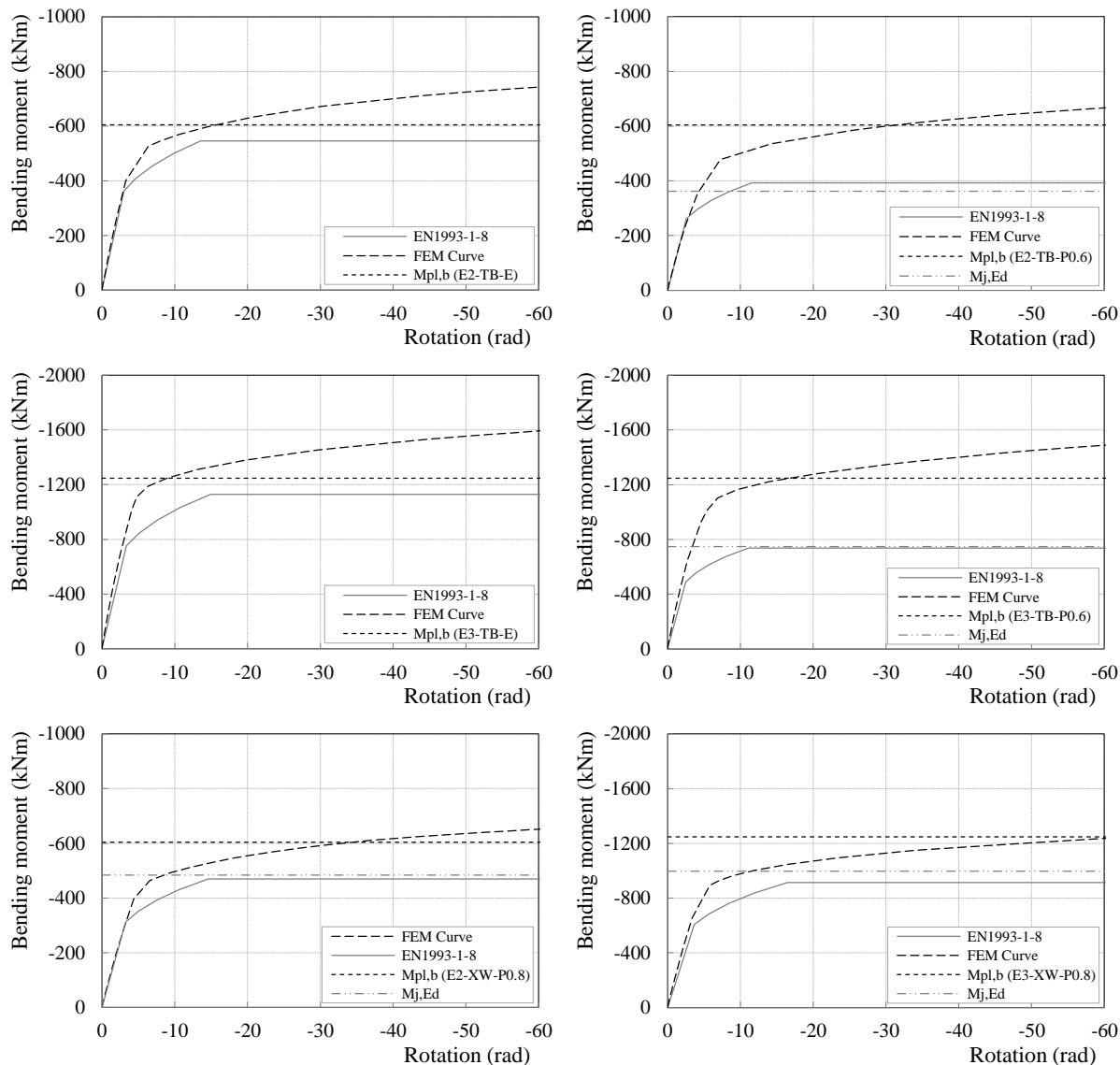


Figure 5.6: Moment-rotation relationships in the joints.

A closer look to the initial stiffness of the joints, see Table 5.3, allows to conclude that the analytical predictions compared with the FEM results present better results, in the case of the E2 joints (with IPE450 in the beam) than in the case of E3 joints (with IPE600 in the beam). The last present larger differences in the initial stiffness, between 14 and 19%, being always higher in the FEM.

The degree of strength predicted for the joints ($M_{j,Ed}$) in relation to the beam plastic resistance ($M_{j,b}$) was captured in a better way by FEM in the E2 joints geometries. It seems that

the analytical predictions, provided by the code, produced closer results for more compact connections. It is important to notice that the connections, with E3 configurations, are almost 30% larger than the connections with E2 configurations. E3 also has two additional inner bolt rows, whose resistance may influence differently the global joint response, in the FEM and in the analytical predictions. In the next section a parametric study is undertaken, changing some relevant properties of the connections, which will contribute to this discussion.

Table 5.3: Comparison of the initial stiffness obtained by the EC3-1-8 and by the FEM.

	E2-TB-E	E2-TB-P(0.6)	E2-XW-P(0.8)	E3-TB-E	E3-TB-P(0.6)	E3-XW-P(0.8)
$S_{ini,j}$ (kNm/rad)	120250	101560	96170	226010	197940	165610
$S_{ini,j,FEM}$ (kNm/rad)	132000	95600	96300	278900	235300	192800
Δ (%)	-9.8	+5.8	+0.13	-19.0	-15.9	-14.1

5.3.3 STRESS AND PLASTIC STRAIN ANALYSIS

The Von Mises stress distribution and the equivalent plastic strain (PEEQ), in the numerical analysis, for the external joints, are depicted in Figure 5.7, for a rotation of $60mrad$.

An inspection to the figures reveals that the stresses and the plastic strain, in the column web panel are more sever in the equal-strength joints than in the partial-strength ones. In the case of the partial-strength joints there is a balance between the stresses in the connection zone and in the column web panel zone, due to the slender end-plate.

For the internal joints the Von Mises stress distribution and the equivalent plastic strain (PEEQ), in the numerical analysis are depicted in Figure 5.8, also for a rotation of $60mrad$.

In this case the stress and accumulated plastic strain patterns are quite similar in both configurations of joints (E2 and E3). Although in the E2 joints higher plastic strains zones were achieved in the column web panel zone.

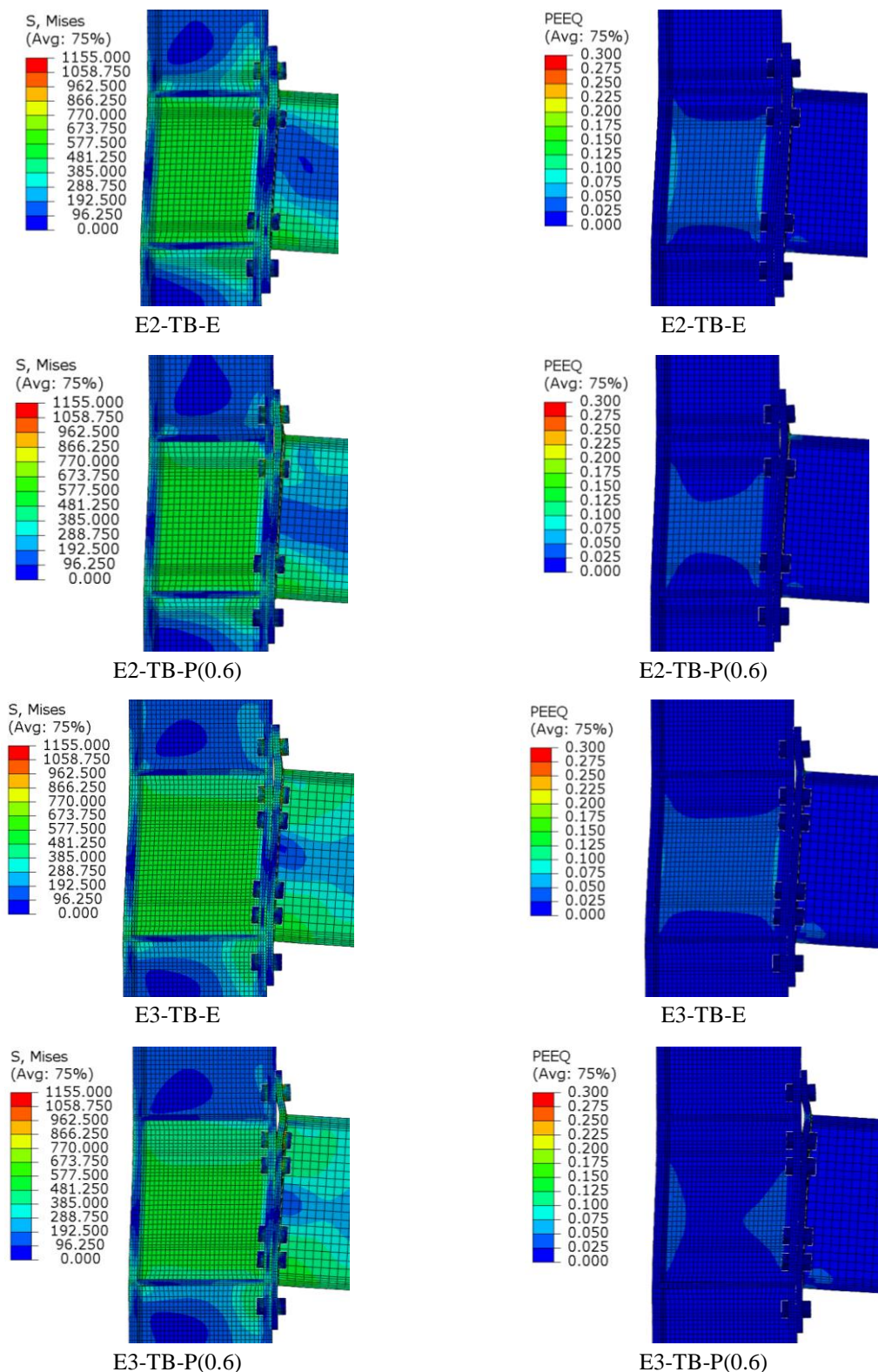


Figure 5.7: Von Mises stress and equivalent plastic strain (PEEQ) patterns for the external joints.

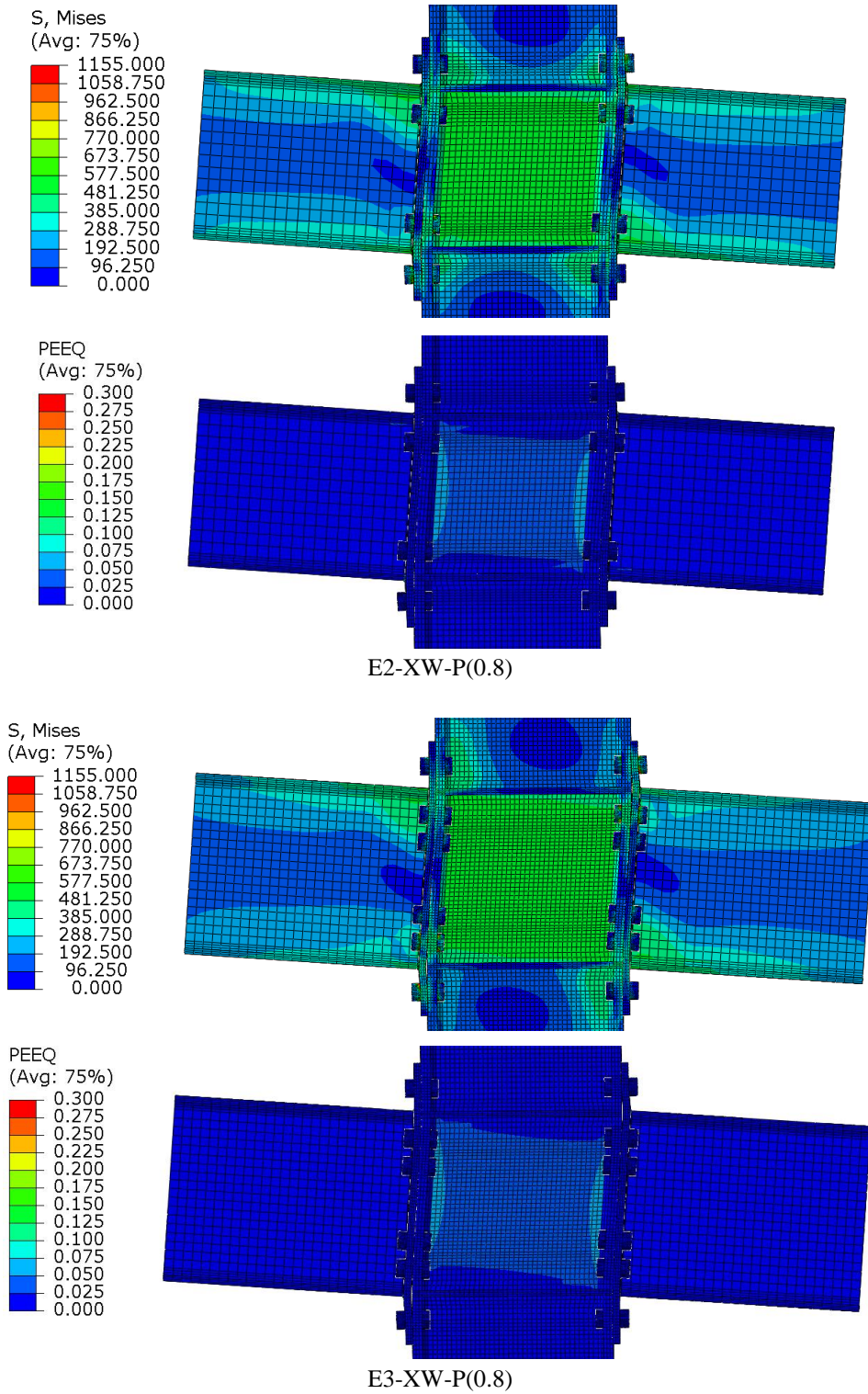


Figure 5.8: Von Mises stress and PEEQ patterns for the internal joints.

5.3.4 FINAL REMARKS ON THE DESIGN AND ANALYSIS OF THE SELECTED JOINTS

The analytical results of the joints were compared with the results of the corresponding finite element models, in terms of the moment-rotation relationships. The Von Mises stresses and equivalent plastic strains (PEEQ) patterns, obtained in the FEM, were also analysed and compared. The comparisons revealed that the design predictions from the EC3-1-8 (EN 1993-1-8, 2005) are well adjusted with the numerical models results, in the case of external joints, which present similar plastic resistance as the connected beam (designated equal-strength joints) and in the internal joints. However for the external joints with partial-strength classification the results of the FEM were considerably higher than the analytical ones. The stress patterns are quite similar in equal and partial-strength joints, although some differences may be found in the beam.

A quantitative comparison of the initial stiffness of the joints, using the analytical and numerical approaches, was performed. The results revealed that the analytical predictions present closer results, to the ones achieved with the FEM results, in the case of the E2 joints (with IPE450 in the beam). In the case of E3 joints (with IPE600 in the beam) the differences in the initial stiffness are bigger, between 14 and 19%, being always higher in the case of the FEM.

For the Von Mises stress and equivalent plastic strain (PEEQ) patterns obtained by the numerical simulations it is possible to state that, for the external joints, the stresses, and consequently plastic strain, in the column web panel are more severe in the equal-strength joints than in the partial-strength ones. In the case of the Partial strength joints there is a balance between the stresses in the connection zone and in the column web panel zone, due to the slender end-plate. On the other hand for the internal joints no significant differences were found in stress and strain distribution.

5.4 PARAMETRIC STUDY

5.4.1 DEFINITION OF THE PARAMETERS

5.4.1.1 FRAMEWORK

It is intended in this section to perform a sensitivity analysis of the beam-to-column end-plate bolted joints, to several parameters that can affect the joints behaviour. For that reason the designed joints were modified according to the following key parameters that have the potential to influence the joint response.

Four main parameters were studied:

- The influence of the continuity column web stiffeners;
- The influence of a middle bolt row
- The influence of two bolt rows in the extended part of the end-plate
- The sensitivity to the material properties of the end-plate ($\gamma_{ovM1} = 0.88$; $\gamma_{ovM2} = 1.00$; $\gamma_{ovM3} = 1.25$; $\gamma_{ovM4} = 1.63$);

Next this four parameters will be described and the expected influence in the joints is discussed.

5.4.1.2 INFLUENCE OF THE CONTINUITY COLUMN WEB STIFFENERS

As observed in the previous chapter the influence of the continuity column web stiffener is noticed in the overall joint resistance, in the stress distribution and also in the initial stiffness of the joint. It has a direct influence on the behaviour of the basic components of the joints, namely in the column web panel in shear, column web in transverse compression and/or tension and the column flange in bending. In the presence of the stiffeners there is an increase of the resistance of the component column web panel in shear due to the frame action developed by the column flanges and the stiffeners, as the bare column web shear resistance is similar with or without stiffeners. In the case of the components, according to the conclusions from Chapter 4, a direct influence in the behaviour is expected in column web in transverse tension and compression, and column flange in bending, changing the deformation pattern of these components.

It is intended in this study to analyse the influence of the continuity stiffener in the two external beam-to-column geometries (E2 and E3) when subjected to monotonic loading and also to cyclic loading. For that the models response with continuity column web stiffeners are compared with the models without column web stiffeners, see Figure 5.9. The models are identified by the termination “ts0” added to the joints name, t_s represents the transverse web stiffeners thickness.

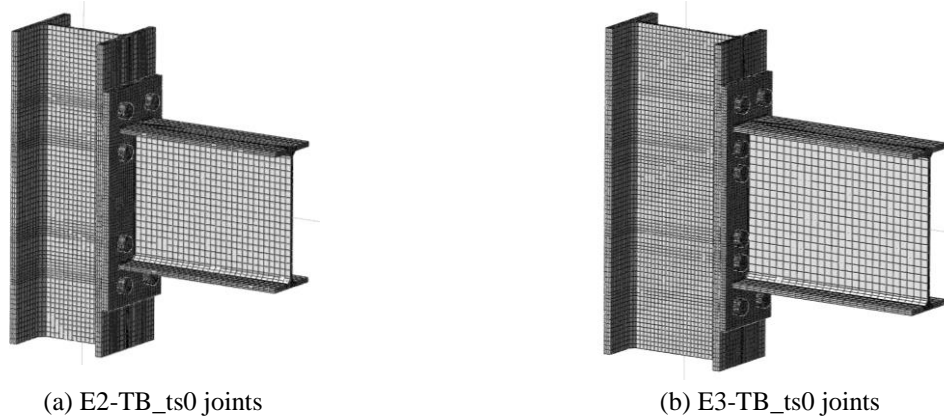


Figure 5.9: FE models for the joints without continuity column web stiffeners.

5.4.1.3 INFLUENCE OF THE MIDDLE BOLT ROW

In this case it is intended to analyse the influence of an additional bolt row positioned at the axis of symmetry of the joints. Generally, secondary bolt rows positioned far from the tension beam flange are less effective for the connection bending moment resistance. A fact justified by the smaller lever arm that this row will have compared to the ones closer to the tension centre. Nevertheless, this approach can be rational to the connection shear resistance, when the joint is subjected to cyclic loading. The fact that this bolt row is less affected by the tension forces, due to the symmetric positioning in relation to the connection, allows for a more constant tension stress state due to the pre-stress and consequently to the shear resistance.

In order to avoid buckling of slender plates and because of durability concern the additional bolt row is recommended in the EC3-1-8 (EN 1993-1-8, 2005). When larger distance is left between bolt rows the contact between the bolted plates cannot be assured and, according to the exposure to corrosive agents, durability may be shortened.

To study the influence of the middle bolt row in the response of the joints analysed additional models were developed with an additional middle bolt row, see Figure 5.10. The models are identified by the termination “mid” added to the joints name.

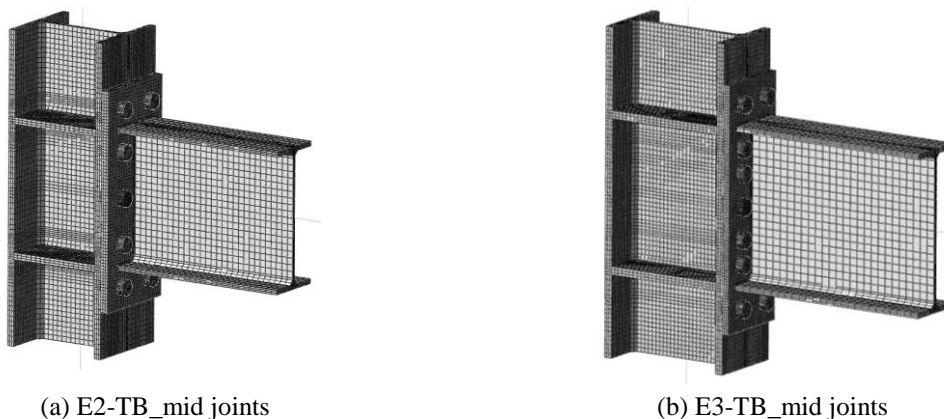


Figure 5.10: FE models for the joints with an additional bolt row aligned with the symmetry axis.

5.4.1.4 INFLUENCE OF TWO BOLT ROWS IN THE EXTENDED PART OF THE END-PLATE

The influence of additional bolt rows to the extended part of the end-plate is analysed here, i.e., existence of two bolt rows in the extended part of the end-plate, instead of one. The bigger lever arm of those rows could indicate an important contribution to the bending moment resistance. However, without an effective load distribution to those rows performed by a rib stiffener, their inclusion may be ineffective. Although this situation is out of the scope of this thesis, the influence of having two external bolt rows to the beam flanges are investigated and additional models are developed and analysed, which include the additional bolt rows and a longer end-plate, as depicted in Figure 5.11. The models are identified by the termination “2ext” added to the joints name.

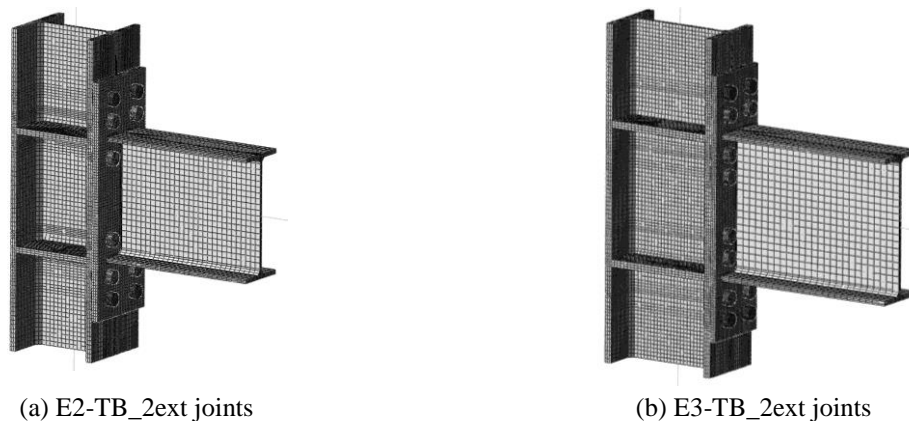


Figure 5.11: FE models for the joints with additional bolt rows in the extended part of the end-plate.

5.4.1.5 SENSITIVITY TO THE MATERIAL PROPERTIES OF THE END-PLATE

In seismic design of steel structures, the variability of the steel mechanical properties must be taken into account in the overstrength.

To assess the effect of the variability of the material properties a set of four different stress-strain relationships were assigned to the end-plate, trying to capture the variability detected in practice. The different relationships are expressed in the backstress strain kinematic hardening determined according to Eq. (3.5), see Figure 5.12.

- M-1 – 70% of M-3 $\rightarrow \gamma_{ovM1} = 0.88$;
- M-2 – 80% of M-3 $\rightarrow \gamma_{ovM2} = 1.00$;
- M-3 (base) material $\rightarrow \gamma_{ovM3} = 1.25$;
- M-4 – 130% of M3 $\rightarrow \gamma_{ovM4} = 1.63$.

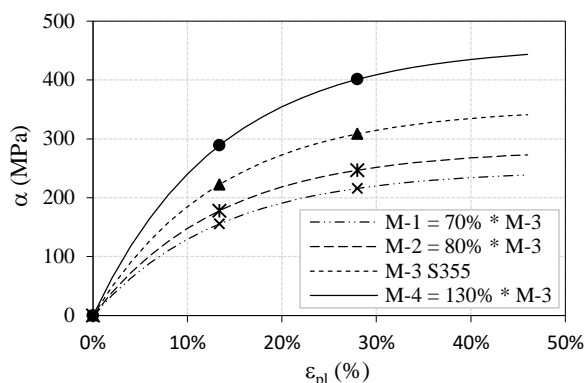


Figure 5.12: Plastic true stress – true strain relationships for the backstresses used in the end-plate material properties.

The variation, of the material properties, is performed only in the end-plate where a significant contribution to the total energy dissipated is expected.

5.4.1.6 FINITE ELEMENT MODELS

The set of finite element models for this parametric study comprised 56 models. The main details of each model are summarised in Table 5.4. The combination of the several parameters described in the previous section, along with the four external beam-to-column joints typologies and the two load protocols, monotonic and cyclic, totals 56 study cases.

Table 5.4: Set of finite element models.

Analysis code	Column		Beam		End-plate		Bolts		Stiffener		Material		Load protocol	
	Section	L _c (mm)	Section	h _p (mm)	t _p (mm)	Size	Class	Nbr. of rows	t _s (mm)	σ-ε	γ _{ov}	name	Amp (mm)	
E2-TB-E_mon_M3	HEB340	3200	IPE450	700	25	30	10.9	4	22	M-3 S355	1.25	Monot.	-800	
E2-TB-P06_mon_M3	HEB340	3200	IPE450	700	18	30	10.9	4	22	M-3 S355	1.25	Monot.	-800	
E3-TB-E_mon_M3	HEB500	3200	IPE600	910	25	36	10.9	6	30	M-3 S355	1.25	Monot.	-800	
E3-TB-P06_mon_M3	HEB500	3200	IPE600	910	25	36	10.9	6	30	M-3 S355	1.25	Monot.	-800	
E2-TB-E_cyc_M3	HEB340	3200	IPE450	700	25	30	10.9	4	22	M-3 S355	1.25	AISC	1	
E2-TB-P06_cyc_M3	HEB340	3200	IPE450	700	18	30	10.9	4	22	M-3 S355	1.25	AISC	1	
E3-TB-E_cyc_M3	HEB500	3200	IPE600	910	25	36	10.9	6	30	M-3 S355	1.25	AISC	1	
E3-TB-P06_cyc_M3	HEB500	3200	IPE600	910	25	36	10.9	6	30	M-3 S355	1.25	AISC	1	
E2-TB-E_mon_M3_ts0	HEB340	3200	IPE450	700	25	30	10.9	4	0	M-3 S355	1.25	Monot.	-800	
E2-TB-P06_mon_M3_ts0	HEB340	3200	IPE450	700	18	30	10.9	4	0	M-3 S355	1.25	Monot.	-800	
E3-TB-E_mon_M3_ts0	HEB500	3200	IPE600	910	25	36	10.9	6	0	M-3 S355	1.25	Monot.	-800	
E3-TB-P06_mon_M3_ts0	HEB500	3200	IPE600	910	25	36	10.9	6	0	M-3 S355	1.25	Monot.	-800	
E2-TB-E_cyc_M3_ts0	HEB340	3200	IPE450	700	25	30	10.9	4	0	M-3 S355	1.25	AISC	1	
E2-TB-P06_cyc_M3_ts0	HEB340	3200	IPE450	700	18	30	10.9	4	0	M-3 S355	1.25	AISC	1	
E3-TB-E_cyc_M3_ts0	HEB500	3200	IPE600	910	25	36	10.9	6	0	M-3 S355	1.25	AISC	1	
E3-TB-P06_cyc_M3_ts0	HEB500	3200	IPE600	910	25	36	10.9	6	0	M-3 S355	1.25	AISC	1	
E2-TB-E_mon_M3_mid	HEB340	3200	IPE450	700	25	30	10.9	5	22	M-3 S355	1.25	Monot.	-800	
E2-TB-P06_mon_M3_mid	HEB340	3200	IPE450	700	18	30	10.9	5	22	M-3 S355	1.25	Monot.	-800	
E3-TB-E_mon_M3_mid	HEB500	3200	IPE600	910	25	36	10.9	7	30	M-3 S355	1.25	Monot.	-800	
E3-TB-P06_mon_M3_mid	HEB500	3200	IPE600	910	25	36	10.9	7	30	M-3 S355	1.25	Monot.	-800	
E2-TB-E_cyc_M3_mid	HEB340	3200	IPE450	700	25	30	10.9	5	22	M-3 S355	1.25	AISC	1	
E2-TB-P06_cyc_M3_mid	HEB340	3200	IPE450	700	18	30	10.9	5	22	M-3 S355	1.25	AISC	1	
E3-TB-E_cyc_M3_mid	HEB500	3200	IPE600	910	25	36	10.9	7	30	M-3 S355	1.25	AISC	1	
E3-TB-P06_cyc_M3_mid	HEB500	3200	IPE600	910	25	36	10.9	7	30	M-3 S355	1.25	AISC	1	
E2-TB-E_mon_M3_2ext	HEB340	3200	IPE450	860	25	30	10.9	6	22	M-3 S355	1.25	Monot.	-800	
E2-TB-P06_mon_M3_2ext	HEB340	3200	IPE450	860	18	30	10.9	6	22	M-3 S355	1.25	Monot.	-1000	
E3-TB-E_mon_M3_2ext	HEB500	3200	IPE600	1090	25	36	10.9	8	30	M-3 S355	1.25	Monot.	-800	
E3-TB-P06_mon_M3_2ext	HEB500	3200	IPE600	1090	25	36	10.9	8	30	M-3 S355	1.25	Monot.	-800	
E2-TB-E_cyc_M3_2ext	HEB340	3200	IPE450	860	25	30	10.9	6	22	M-3 S355	1.25	AISC	1	
E2-TB-P06_cyc_M3_2ext	HEB340	3200	IPE450	860	18	30	10.9	6	22	M-3 S355	1.25	AISC	1	
E3-TB-E_cyc_M3_2ext	HEB500	3200	IPE600	1090	25	36	10.9	8	30	M-3 S355	1.25	AISC	1	
E3-TB-P06_cyc_M3_2ext	HEB500	3200	IPE600	1090	25	36	10.9	8	30	M-3 S355	1.25	AISC	1	
E2-TB-E_mon_M1	HEB340	3200	IPE450	700	25	30	10.9	4	22	M-1 = 70% * M-3	0.88	Monot.	-800	
E2-TB-P06_mon_M1	HEB340	3200	IPE450	700	18	30	10.9	4	22	M-1 = 70% * M-3	0.88	Monot.	-800	
E3-TB-E_mon_M1	HEB500	3200	IPE600	910	25	36	10.9	6	30	M-1 = 70% * M-3	0.88	Monot.	-800	
E3-TB-P06_mon_M1	HEB500	3200	IPE600	910	25	36	10.9	6	30	M-1 = 70% * M-3	0.88	Monot.	-800	
E2-TB-E_cyc_M1	HEB340	3200	IPE450	700	25	30	10.9	4	22	M-1 = 70% * M-3	0.88	AISC	1	
E2-TB-P06_cyc_M1	HEB340	3200	IPE450	700	18	30	10.9	4	22	M-1 = 70% * M-3	0.88	AISC	1	
E3-TB-E_cyc_M1	HEB500	3200	IPE600	910	25	36	10.9	6	30	M-1 = 70% * M-3	0.88	AISC	1	
E3-TB-P06_cyc_M1	HEB500	3200	IPE600	910	25	36	10.9	6	30	M-1 = 70% * M-3	0.88	AISC	1	
E2-TB-E_mon_M2	HEB340	3200	IPE450	700	25	30	10.9	4	22	M-2 = 80% * M-3	1.00	Monot.	-800	
E2-TB-P06_mon_M2	HEB340	3200	IPE450	700	18	30	10.9	4	22	M-2 = 80% * M-3	1.00	Monot.	-800	
E3-TB-E_mon_M2	HEB500	3200	IPE600	910	25	36	10.9	6	30	M-2 = 80% * M-3	1.00	Monot.	-800	
E3-TB-P06_mon_M2	HEB500	3200	IPE600	910	25	36	10.9	6	30	M-2 = 80% * M-3	1.00	Monot.	-800	
E2-TB-E_cyc_M2	HEB340	3200	IPE450	700	25	30	10.9	4	22	M-2 = 80% * M-3	1.00	AISC	1	
E2-TB-P06_cyc_M2	HEB340	3200	IPE450	700	18	30	10.9	4	22	M-2 = 80% * M-3	1.00	AISC	1	
E3-TB-E_cyc_M2	HEB500	3200	IPE600	910	25	36	10.9	6	30	M-2 = 80% * M-3	1.00	AISC	1	
E3-TB-P06_cyc_M2	HEB500	3200	IPE600	910	25	36	10.9	6	30	M-2 = 80% * M-3	1.00	AISC	1	
E2-TB-E_mon_M4	HEB340	3200	IPE450	700	25	30	10.9	4	22	M-4 = 130% * M-3	1.63	Monot.	-800	
E2-TB-P06_mon_M4	HEB340	3200	IPE450	700	18	30	10.9	4	22	M-4 = 130% * M-3	1.63	Monot.	-800	
E3-TB-E_mon_M4	HEB500	3200	IPE600	910	25	36	10.9	6	30	M-4 = 130% * M-3	1.63	Monot.	-800	
E3-TB-P06_mon_M4	HEB500	3200	IPE600	910	25	36	10.9	6	30	M-4 = 130% * M-3	1.63	Monot.	-800	
E2-TB-E_cyc_M4	HEB340	3200	IPE450	700	25	30	10.9	4	22	M-4 = 130% * M-3	1.63	AISC	1	
E2-TB-P06_cyc_M4	HEB340	3200	IPE450	700	18	30	10.9	4	22	M-4 = 130% * M-3	1.63	AISC	1	
E3-TB-E_cyc_M4	HEB500	3200	IPE600	910	25	36	10.9	6	30	M-4 = 130% * M-3	1.63	AISC	1	
E3-TB-P06_cyc_M4	HEB500	3200	IPE600	910	25	36	10.9	6	30	M-4 = 130% * M-3	1.63	AISC	1	

The results are grouped and compared according to the main property being studied. Comparisons are performed between the results of the reference set of models (E2-TB-E_M3, E2-TB-P06_M3, E3-TB-E_M3 and E3-TB-P06_M3), in terms of geometry and mechanical properties, described in Section 5.2, and the results from the modified models, described in the previous section. For each parameter in study, monotonic and cyclic loaded joints are analysed separately. For both monotonic and cyclic loaded joints first the moment-rotation capacity curves are presented, using the same equations as in the previous section (5.3). When relevant also the relationship of the bending moment with the individual contribution of each one of the main dissipative components, to the connection rotation, is presented. For the component column web panel in shear (CWS) the $M-\theta$ curves were determined using Eq. (3.15). For the connection components, column flange in bending (CFB), end-plate in bending (EPB) and bolts in tension (BT), the proposed methodology presented in Section 4.3.2 was applied to extract the $M-\theta$ response curves. In the monotonic case it is also depicted in the figures the elastic and plastic bending moment of the connected beam, designated as $M_{el,b}$ and $M_{pl,b}$, respectively, considering $f_y = 355\text{Mpa}$.

Next the energy dissipation of each set of joints according to the beam-to-column profiles E2 or E3 is depicted. It is also included in the figures the energy dissipation of the most dissipative components involved in the joint, namely the column web panel in shear, the column flange in bending, end-plate in bending, bolts in tension and other contributions, inclusive from the beam plastic deformation. Then the initial stiffness of the joints is compared. The procedure presented in the Figure 3.22 (d) is used to determine the initial stiffness from the monotonic curves, it is estimated by adjusting a straight line between the point of zero loading and the elastic moment of the joint (M_{el} , first yield in the joint).

Lastly, the Von Mises stresses and if relevant the equivalent plastic strain (PEEQ), for the reference and modified models are depicted for comparison.

5.4.2 RESULTS AND DISCUSSION

5.4.2.1 INFLUENCE OF THE CONTINUITY COLUMN WEB STIFFENERS

In Figure 5.13 is depicted the response of the joints when subjected to monotonic loading.

i) Monotonic loaded Joints

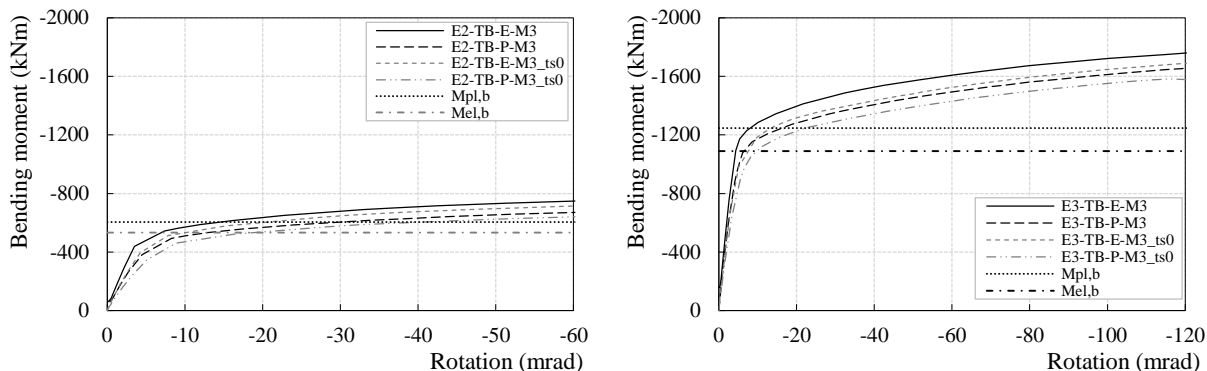


Figure 5.13: Moment-rotation relationships for joints subjected to monotonic loading.

The energy dissipated during the joints loading is depicted in Figure 5.14, until a rotation of 100mrad has been reached, following the procedure described in Section 3.2.4.5. In Figure 5.15 is depicted the Von Mises stress patterns distribution in the joints. The initial stiffness of the joints is depicted in Figure 5.16, for the joints in study, it is also depicted in the figure the analytical values of the initial stiffness, when the EC3-1-8 (EN 1993-1-8, 2005) procedure is applied to the joints, and also the rigid limit set by the EC3-1-8.

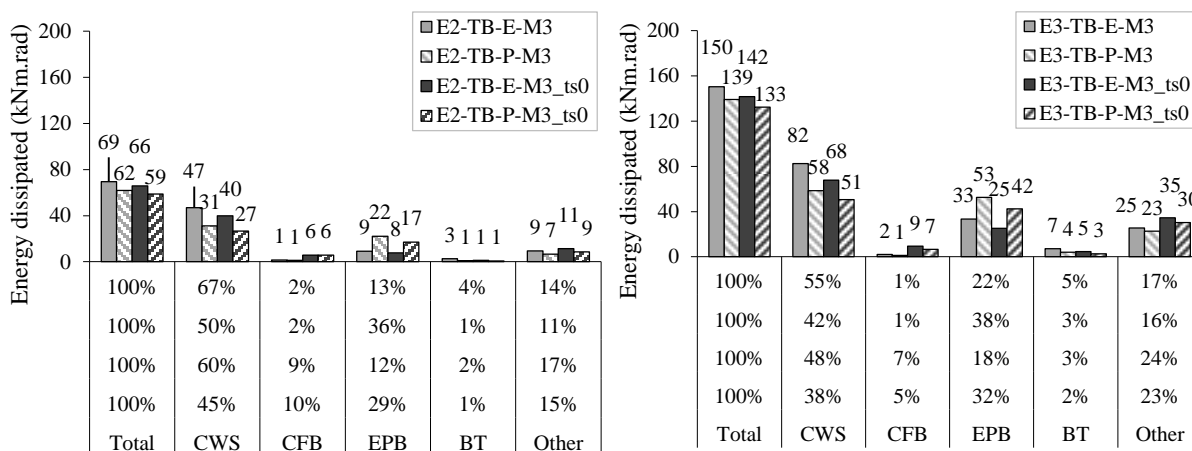


Figure 5.14: Energy dissipation in the joints until a rotation of 100mrad has been reached.

The comparisons between the stiffened and the unstiffened joints confirmed the influence of the transverse web stiffeners, both in terms of strength and initial stiffness of the joints. The higher strength of the equal-strength joints led to a higher energy dissipation, when compared with the corresponding partial-strength joints. The column web panel in shear was the main dissipative component with values between 38 and 67% of the total energy dissipated. In the partial-strength joints a higher balance was found between the main dissipative components, end-plate in bending and column web panel in shear, due to the slender end-plate.

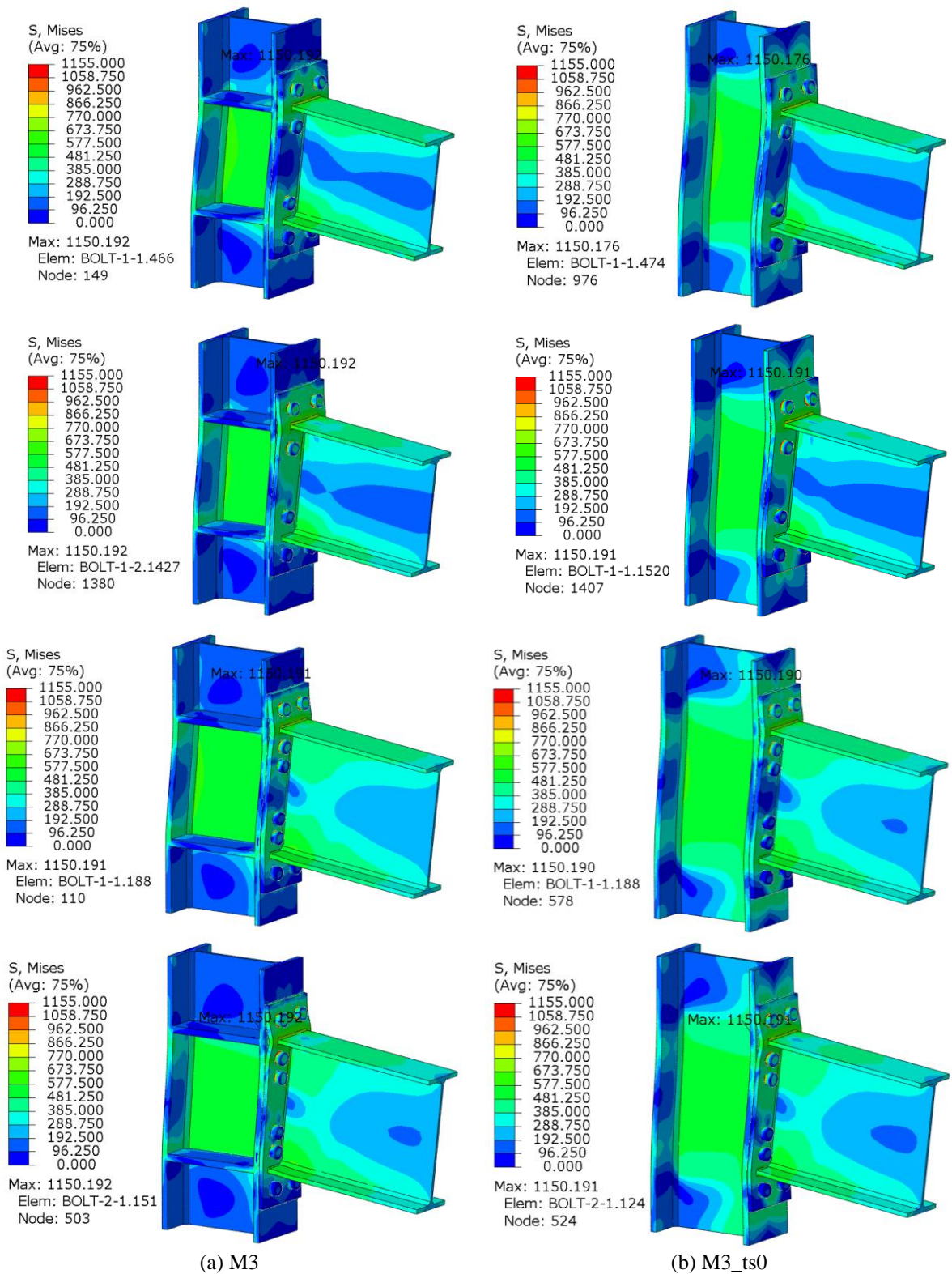


Figure 5.15: Von Mises stress patterns for a rotation of 100mrad, from top to bottom: E2-TB-E-, E2-TB-P-, E3-TB-E-, E3-TB-P-.

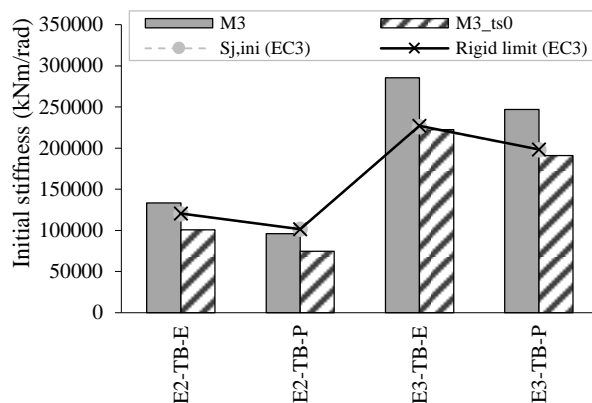


Figure 5.16: Comparison of the initial stiffness of the joints.

Without the transverse web stiffeners the component column flange in bending contributes more significantly to the joint rotation and also to the energy dissipated. The presence of the transverse web stiffeners has the effect of confining almost all the plastic stresses between the column flanges and the stiffeners. The level of stress in the column web panel revealed to be similar in both models with and without stiffeners. Apparently, the stress patterns in the end-plate, indicate that the unstiffened joints have lower demand, when compared with the stiffened joints. The lower contribution of the component column flange in bending to the rotation of the joint, due to the transverse web stiffeners, may contribute to the higher demand on the end-plate.

ii) Cyclic Loaded Joints

In Figure 5.17 is depicted the response of the joints when subjected to cyclic loading.

At the components level the response of joints is depicted in Figure 5.18, for the column web in shear, Figure 5.19 for the column flange in bending and Figure 5.20 for the end-plate in bending.

The energy dissipated is depicted in Figure 5.21, until the 36th cycle has been reached, following also the procedure described in Section 3.2.4.5.

The previous results revealed that the equal-strength joints present more stable cycles when compared to the partial-strength ones. The slender end-plate of the partial-strength joints makes them more prone to pinching. It is noticed that in the case of unstiffened joints the pinching effect is amplified specially in the joints with lower beam height (E2) and slender

column flanges. This fact can be justified by the additional contribution of the plastic deformation of the column flanges. The strength degradation, of the response of equal-strength joints for higher demands, is apparently more pronounced in the unstiffened joints due to the higher plastic deformations detected in the column flanges. In the case of partial-strength joints, with slender end-plates, the differences detected in the joints behaviour are smaller, even for higher demands. These joints are more dependent of the end-plate deformation, and less influenced by the column flanges. A detailed analysis of the response of the components further supports the previous observations, namely the higher contribution of the column flanges deformation to the joints rotation in the unstiffened joints.

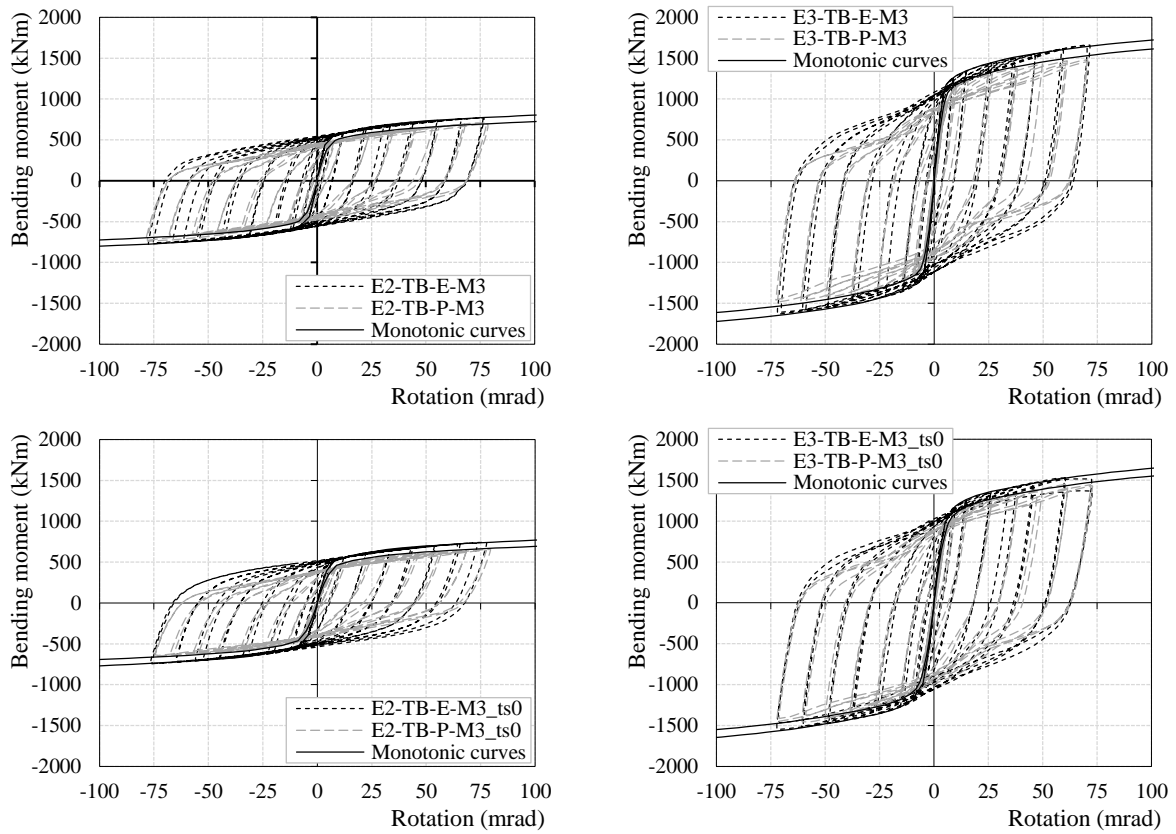


Figure 5.17: Moment-rotation relationships for joints subjected to cyclic loading.

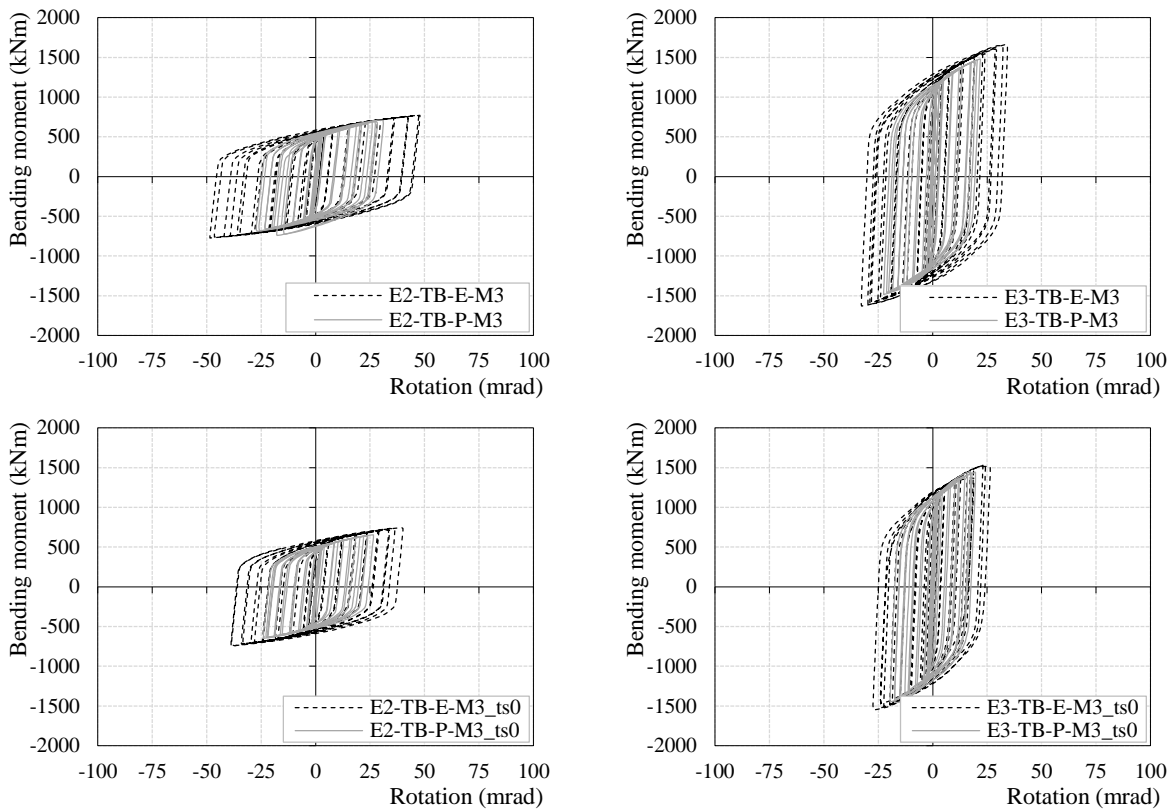


Figure 5.18: Moment-rotation relationships for component column web panel in shear.

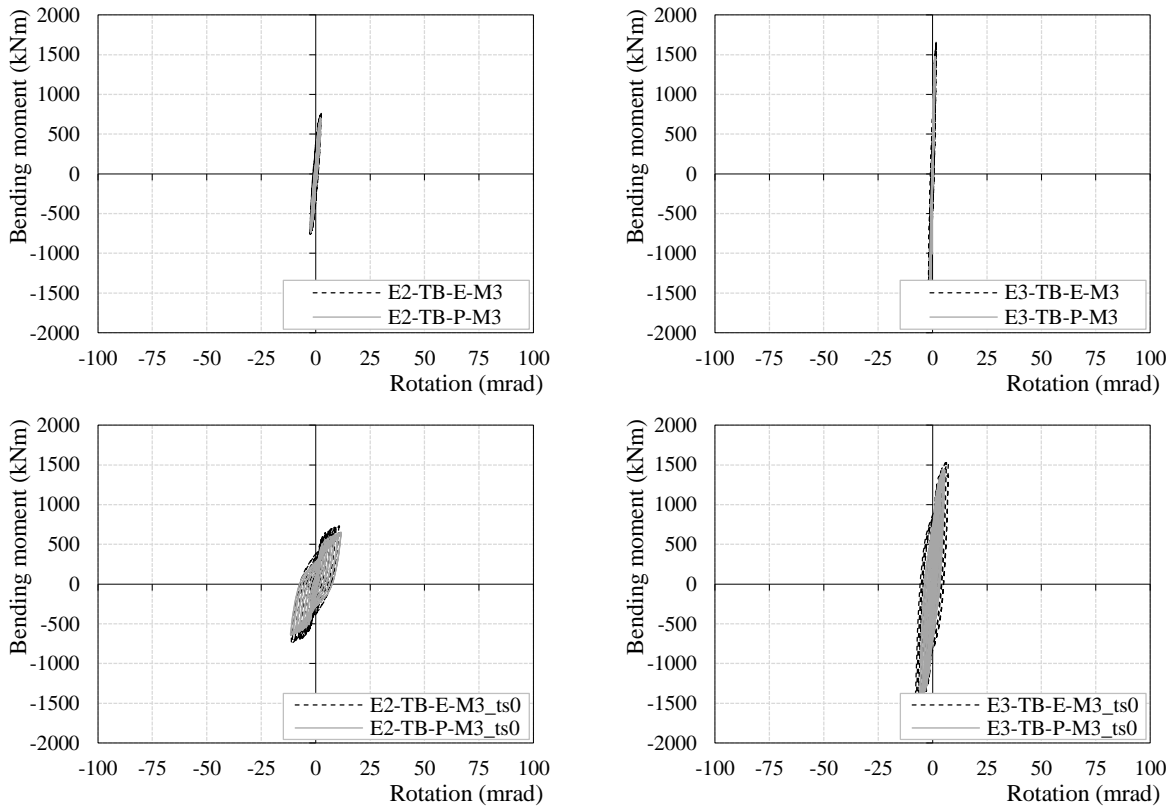


Figure 5.19: Moment-rotation relationships for component column flange in bending.

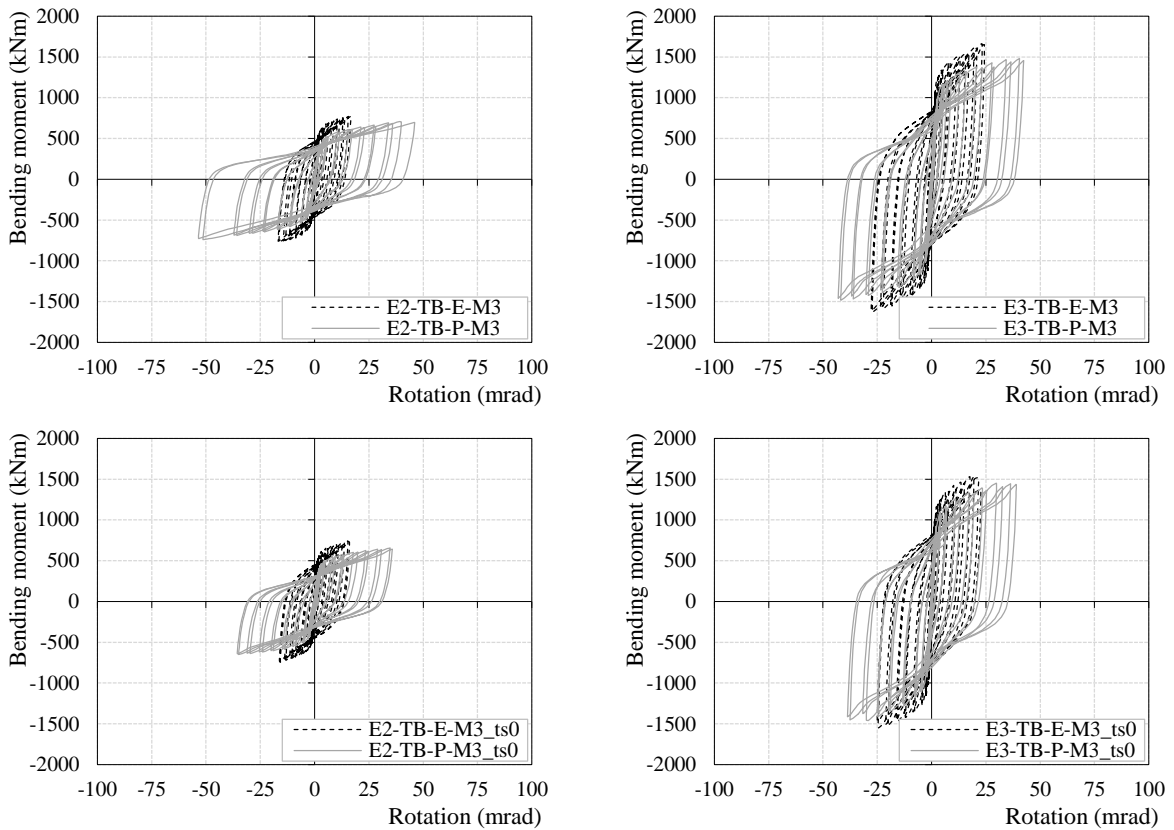


Figure 5.20: Moment-rotation relationships for component end-plate in bending.

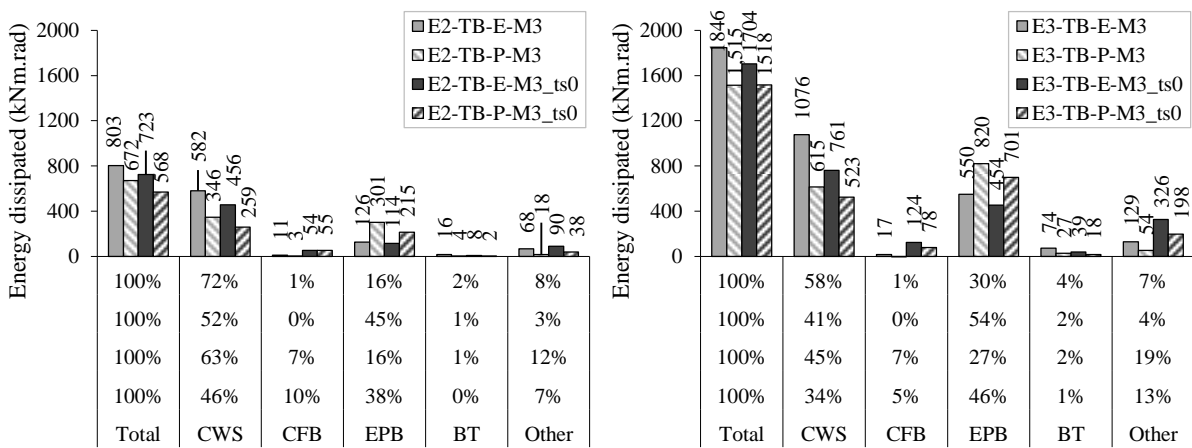


Figure 5.21: Comparison of the accumulated energy dissipation per component until the 36th cycle is reached.

The analysis of the energy dissipation confirms the previous observations related to the absence of the transverse web stiffeners, which increases the energy dissipation of the component column flange in bending and decreases the contribution of the component end-plate in bending, especially for joints with slender column flanges (E2). It is also observed that the energy dissipation of the component column web panel in shear increases for the stiffened joints.

5.4.2.2 INFLUENCE OF THE MIDDLE BOLT ROW

The results of the reference models are compared with the geometrically modified models, when an additional bolt row was added to the geometrical centre of the connection.

i) **Monotonic loaded Joints**

In Figure 5.22 is depicted the response of the joints when subjected to monotonic loading.

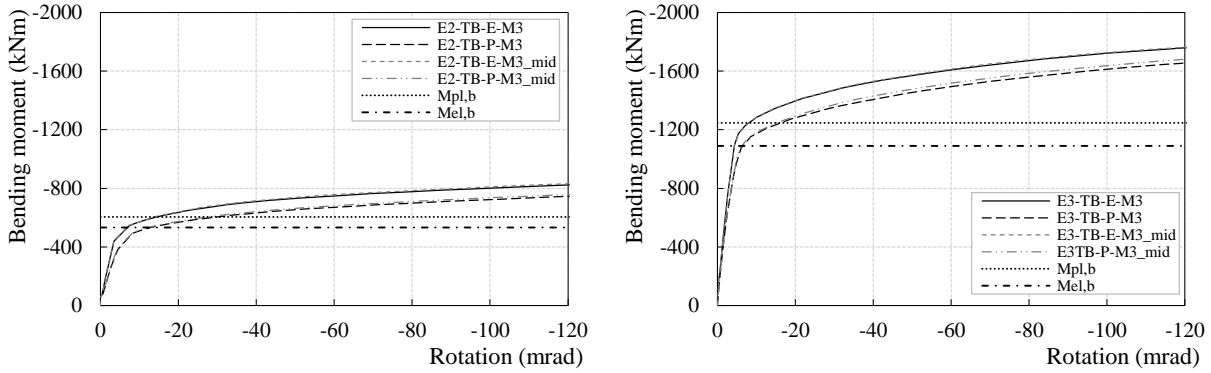


Figure 5.22: Moment-rotation relationships for joints subjected to monotonic loading.

The energy dissipated is depicted in Figure 5.23, until a rotation of 100mrad has been reached.

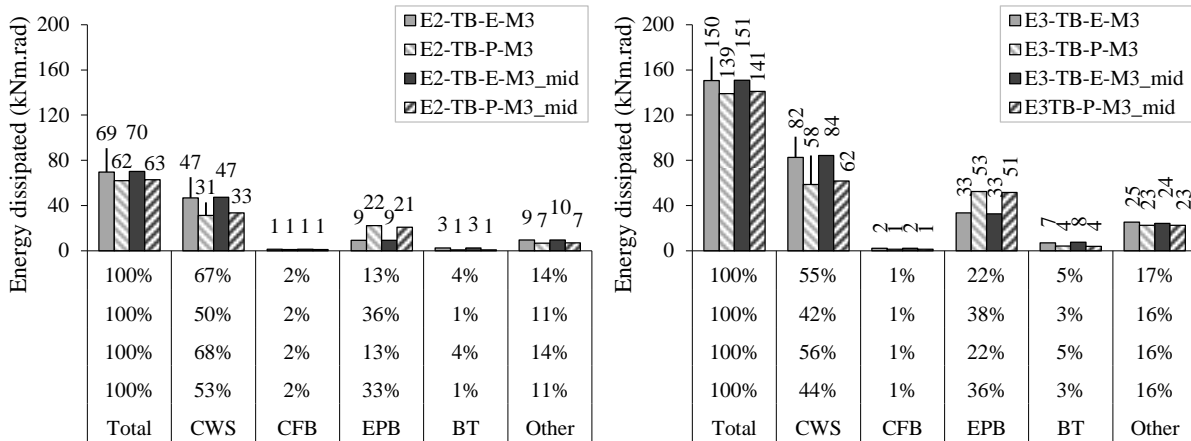


Figure 5.23: Energy dissipation in the joints until a rotation of 100mrad has been reached.

In Figure 5.24 is depicted the Von Mises stress patterns distribution in the joints.

Finally the numerical and analytical (EC3-1-8) initial stiffness of the joints is depicted in Figure 5.25.

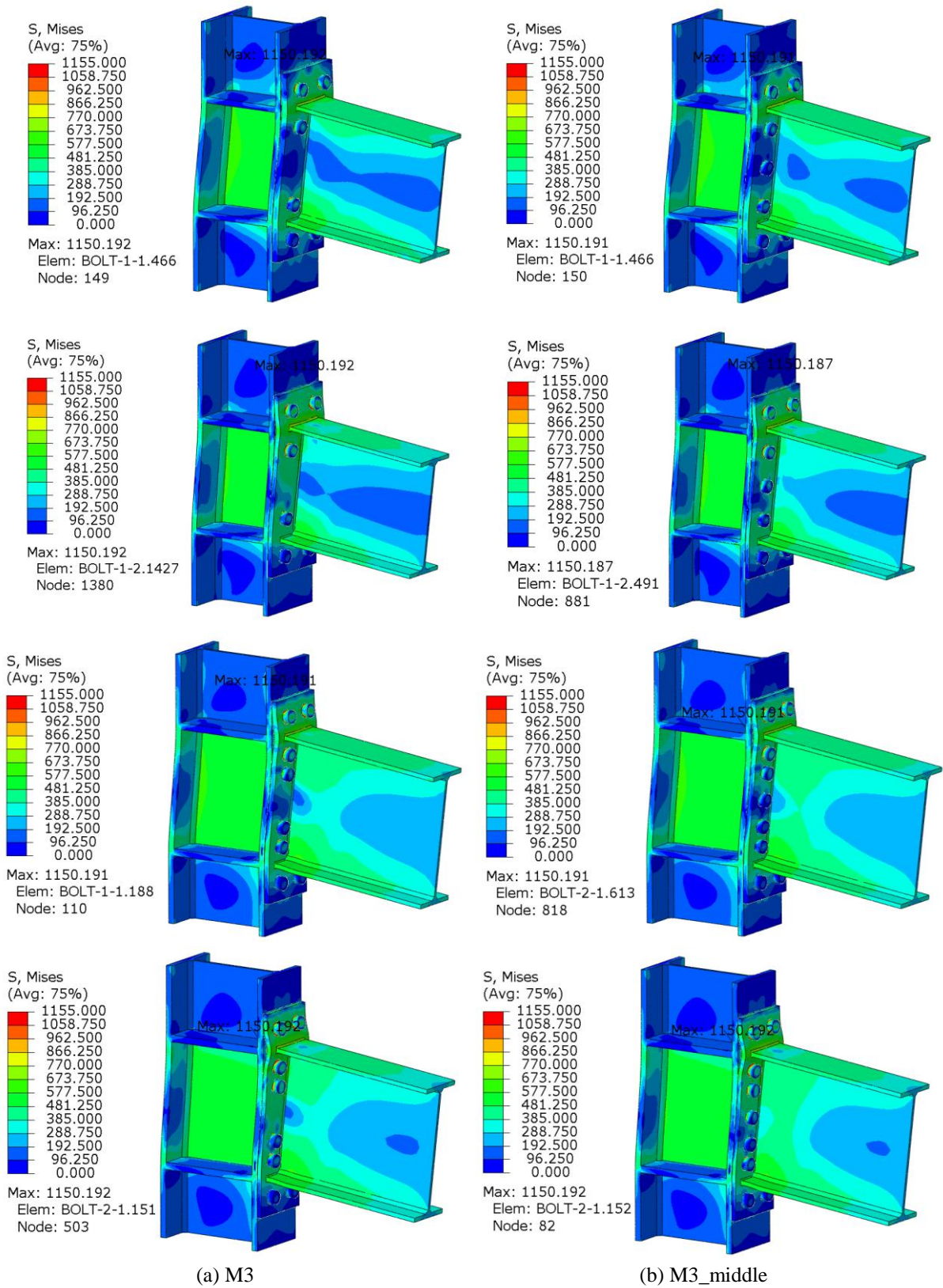


Figure 5.24: Von Mises stress patterns for a rotation of 100mrad, from top to bottom: E2-TB-E-; E2-TB-P-, E3-TB-E-, E3-TB-P-.

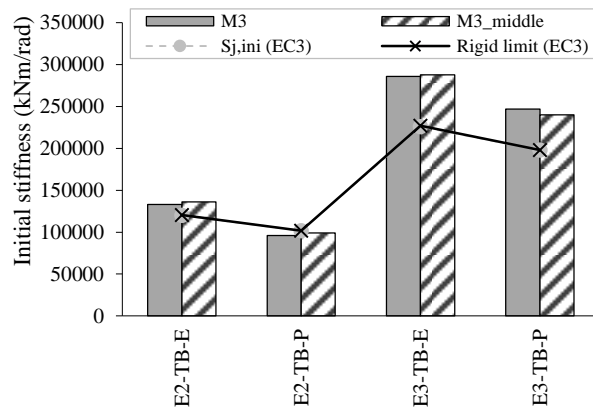


Figure 5.25: Comparison of the initial stiffness of the joints.

The results revealed that there is no apparent influence of the additional bolt row for the joints behaviour. Only some minor differences can be observed in the stress patterns of the end-plate, more notorious in the partial-strength joints, with slender end-plates. This is also noticed in the beam stress patterns presents near the additional middle bolt row.

ii) Cyclic Loaded Joints

In Figure 5.26 is depicted the response of the joints when subjected to cyclic loading.

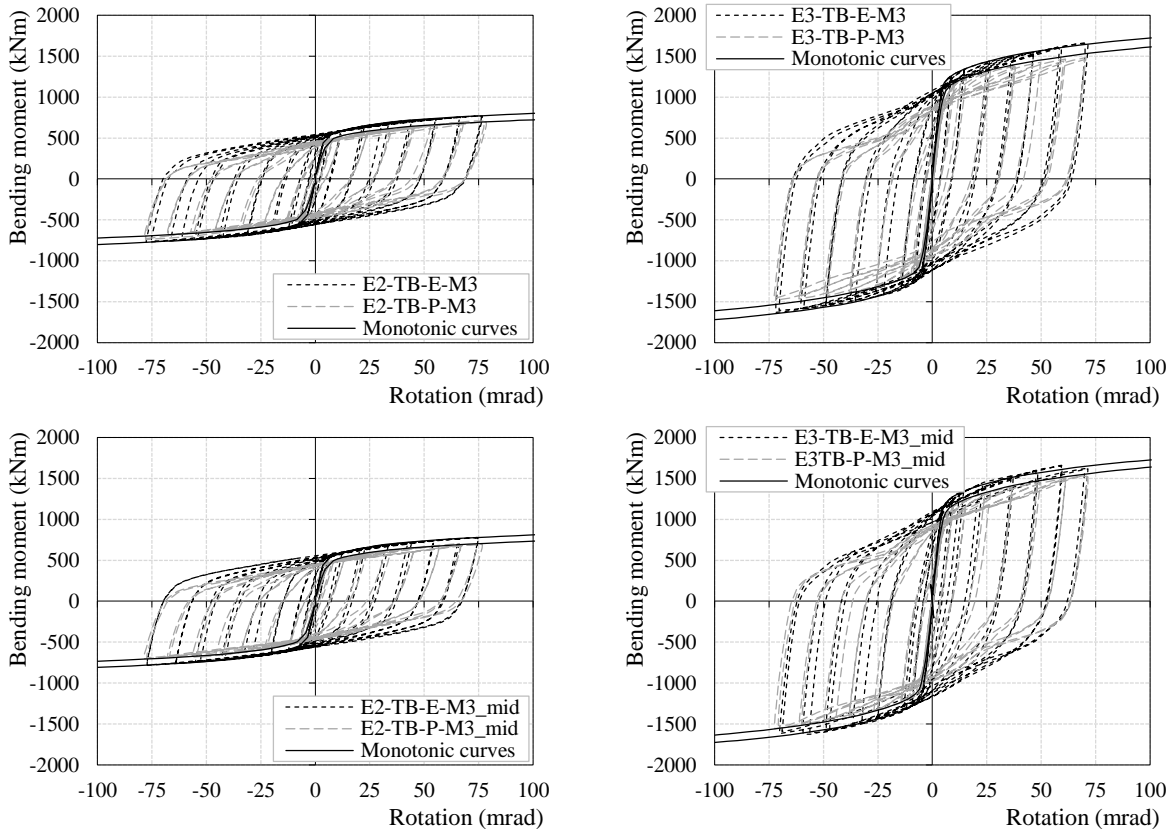


Figure 5.26: Moment-rotation relationships for joints subjected to cyclic loading.

The energy dissipated is depicted in Figure 5.27, until the 36th cycle has been reached.

As for the joints loaded monotonically, the previous results show that there is no apparent influence of the additional bolt row in the joints behaviour. Although in the joints with a higher beam section (IPE600) the moment-rotation response presents some differences. Possibly due to the higher lever arm of the middle bolt row in this case, that may contribute more significantly.

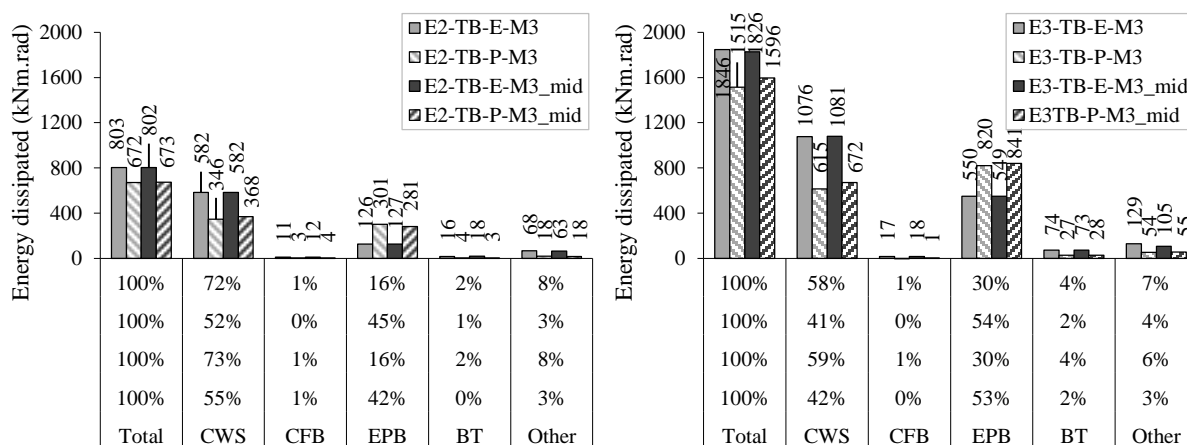


Figure 5.27: Comparison of the accumulated energy dissipation per component until the 36th cycle is reached.

5.4.2.3 INFLUENCE OF TWO BOLT ROWS IN THE EXTENDED PART OF THE END-PLATE

The results of the reference models are compared with the geometrically modified models, when an additional bolt row was added to each extended part of the end-plate.

i) Monotonic loaded Joints

In Figure 5.28 is depicted the response of the joints when subjected to monotonic loading.

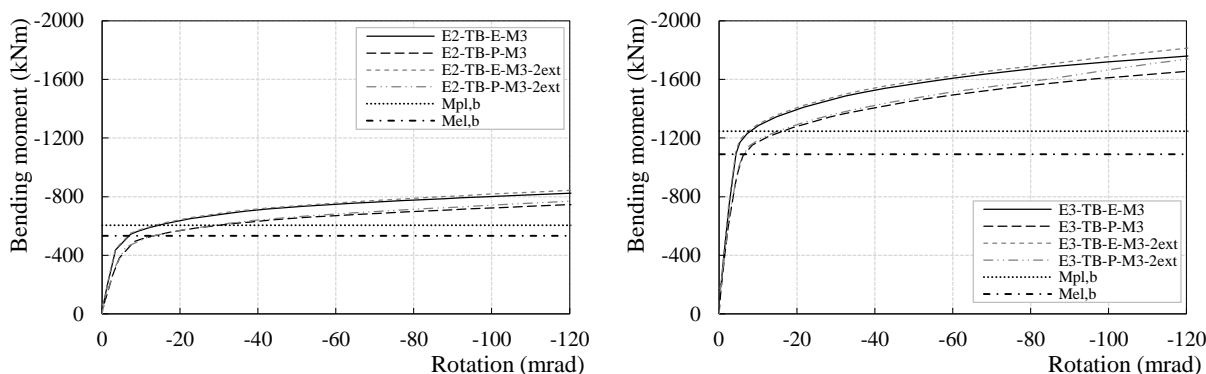


Figure 5.28: Moment-rotation relationships for joints subjected to monotonic loading.

The energy dissipated during the joints loading is depicted in Figure 5.29, until a rotation of 100mrad has been reached.

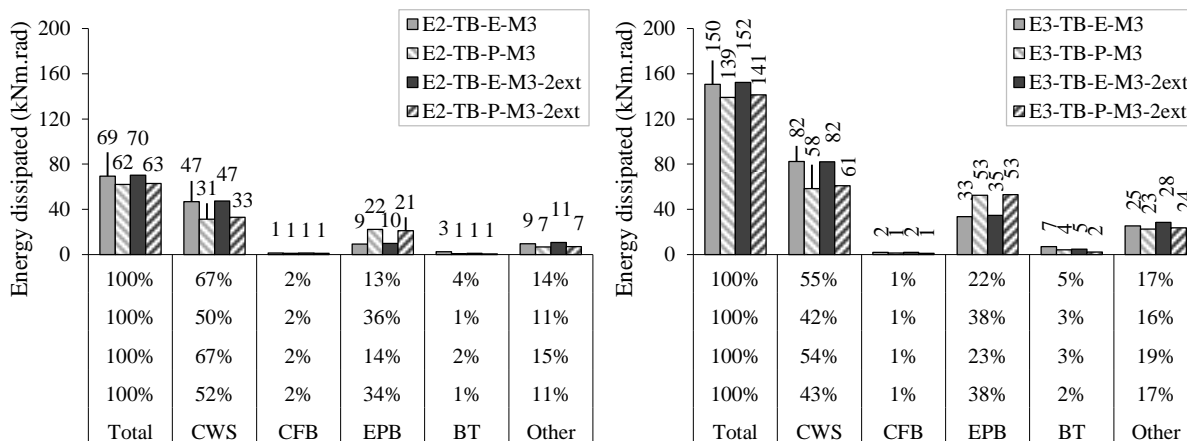


Figure 5.29: Energy dissipation in the joints until a rotation of 100mrad has been reached.

Finally the numerical and analytical (EC3-1-8) initial stiffness of the joints is depicted in Figure 5.30.

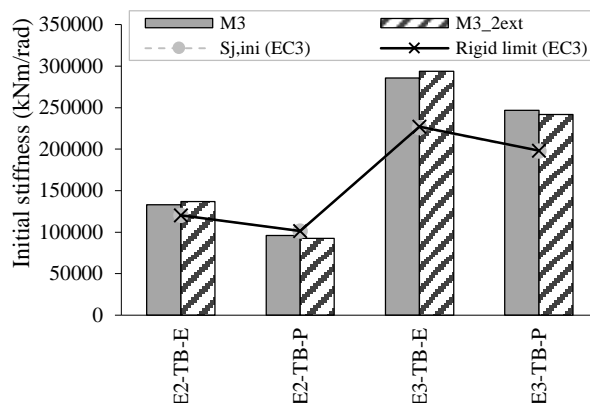


Figure 5.30: Comparison of the initial stiffness of the joints.

Finally in Figure 5.31 is depicted the Von Mises stress patterns distribution in the joints.

An inspection to the results revealed that the influence of second external bolt row is only notorious for larger rotations, after 80mrad. After the first external bolt row suffers plastic deformation the second bolt row becomes active. Some changes in the plastic mechanism of the end-plate can justify the increase of strength after that rotation. Some new hinges can developed in the end-plate conferring additional strength. Also the presence of a second bolt row may enhance the membrane effect in the end-plate for larger rotations. The initial stiffness is not affected by the additional rows. In terms of stress distribution, no apparent influence can be detected, apart from the previous mentioned.

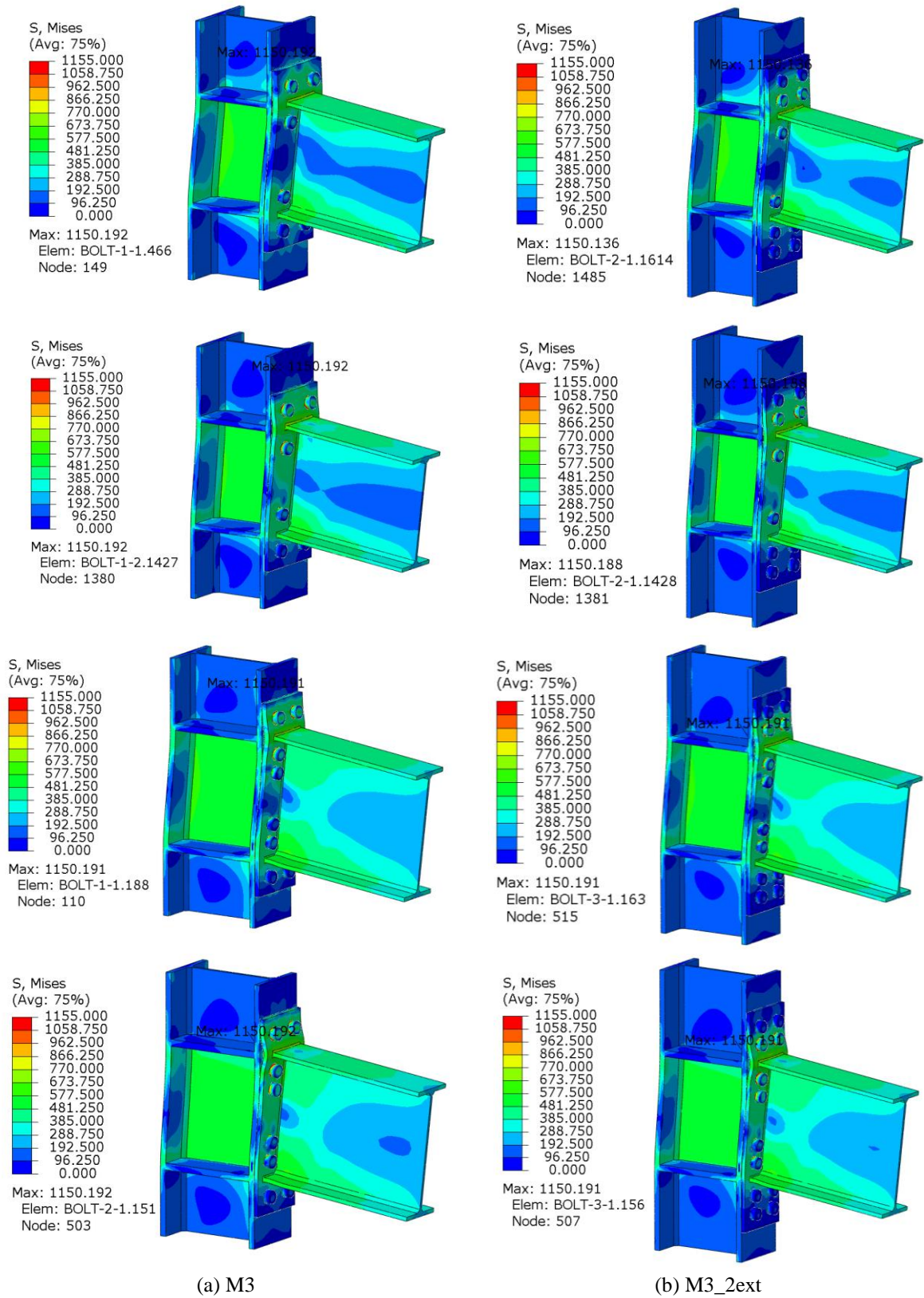


Figure 5.31: Von Mises stress patterns for a rotation of 100mrad, from top to bottom: E2-TB-E-; E2-TB-P-, E3-TB-E-, E3-TB-P-.

ii) Cyclic Loaded Joints

In Figure 5.32 is depicted the response of the joints when subjected to cyclic loading.

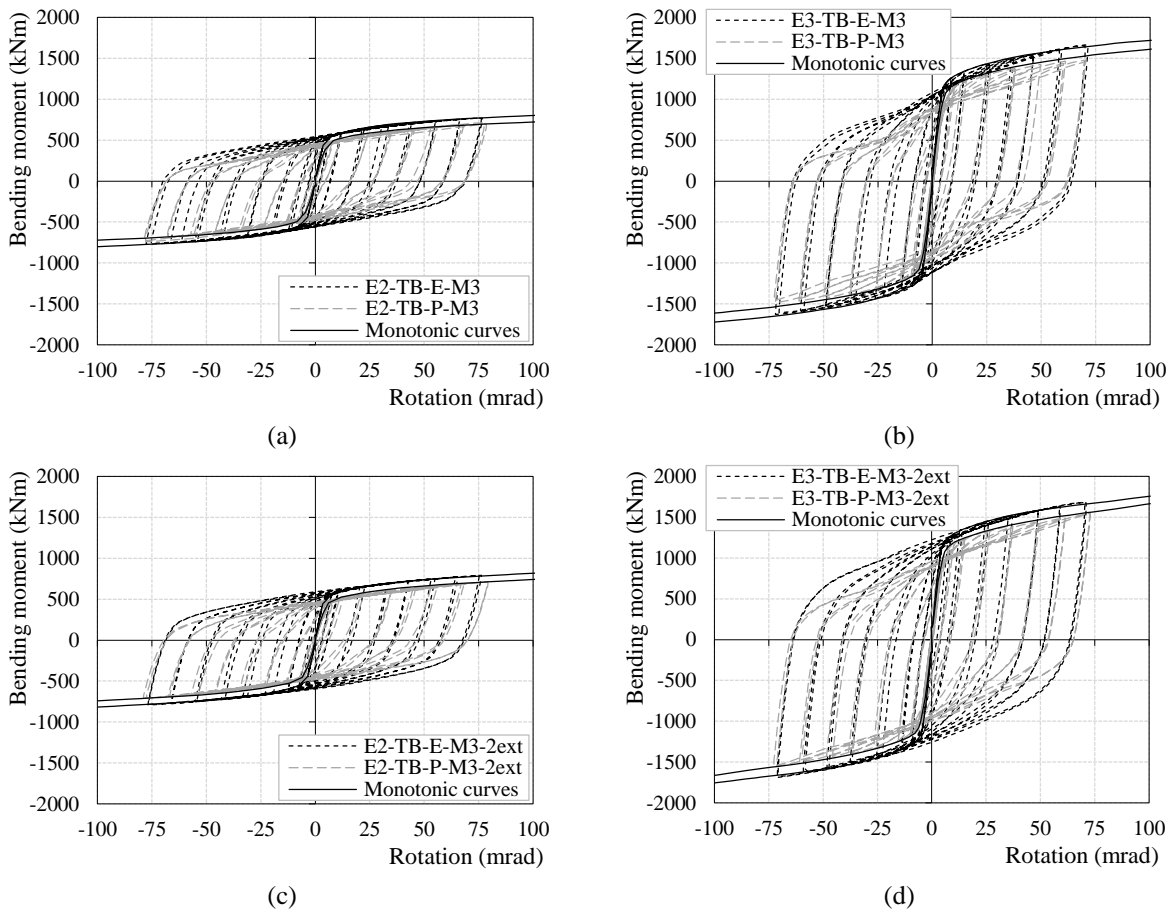


Figure 5.32: Moment-rotation relationships for joints subjected to cyclic loading.

At the components level the joints response is depicted in Figure 5.33, for the components column web panel in shear, and in Figure 5.35 for the components column flange in bending and end-plate in bending.

The energy dissipated is depicted in Figure 5.34, until the 36th cycle has been reached.

The previous results revealed that the influence of second external bolt row is more notorious in the component end-plate in bending response, for partial-strength joints with smaller beam section (IPE450). This reveals that the additional bolt rows condition the end-plate deformation capacity. In line with what was observed in the response of the joints, the energy dissipation revealed that the joints with the additional bolt rows present higher dissipation capacity. The increase of strength provided by the end-plate contributed to this increase.

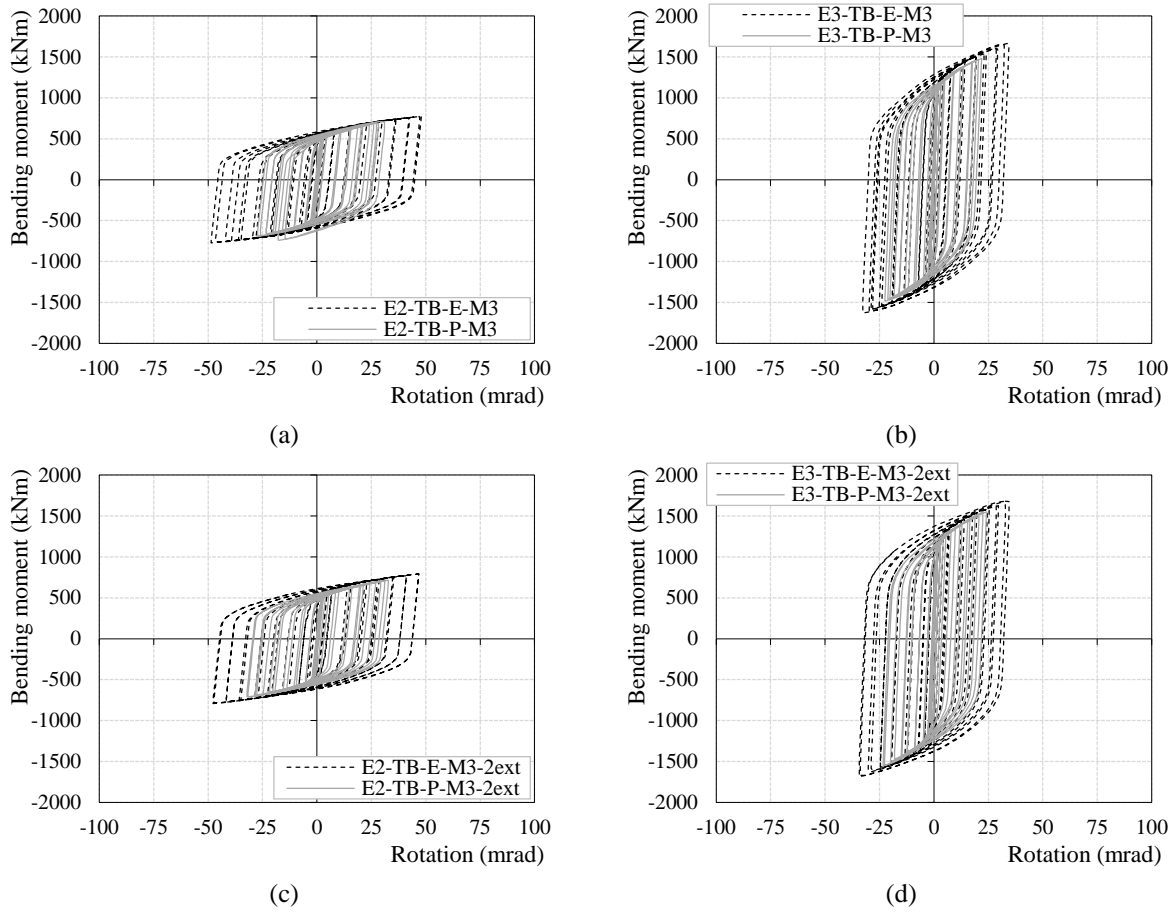


Figure 5.33: Moment-rotation relationships for component column web panel in shear.

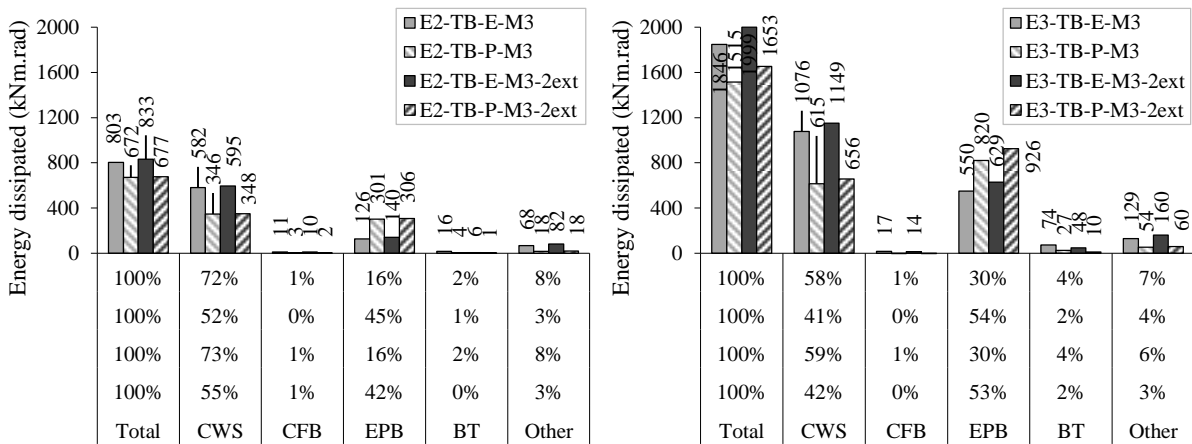


Figure 5.34: Comparison of the accumulated energy dissipation per component until the 36th cycle is reached.

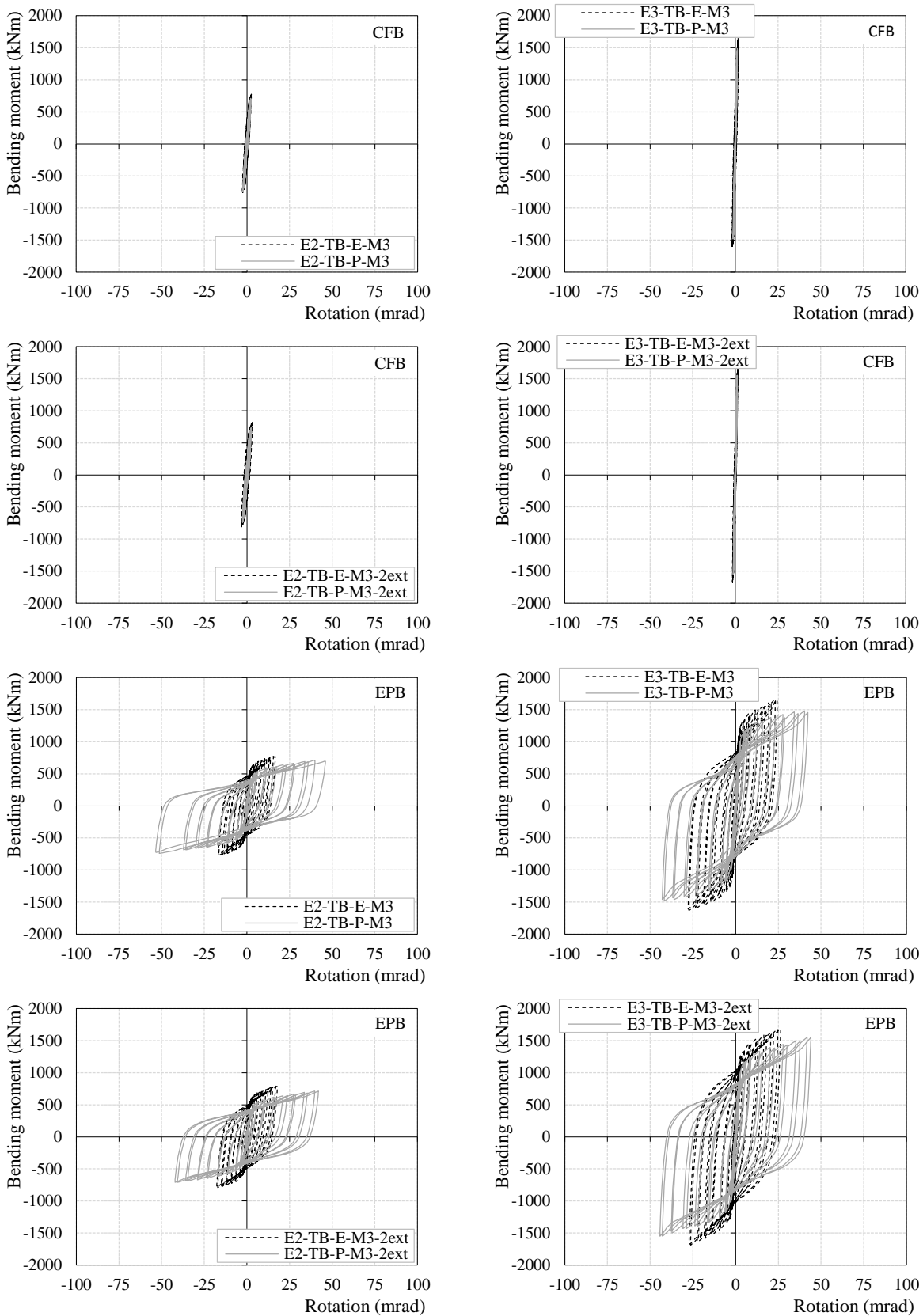


Figure 5.35: Moment-rotation relationships for components column flange in bending (CFB) and end-plate in bending (EPB).

5.4.2.4 SENSITIVITY TO THE MATERIAL PROPERTIES OF THE END-PLATE

The results of the reference models are compared with the mechanically modified models when the material properties of the end-plate are varied, using increasing overstrength factors applied to the nominal stress-strain relationships of the structural steel S355.

iii) Monotonic loaded Joints

In Figure 5.36 is depicted the response of the joints when subjected to monotonic loading.

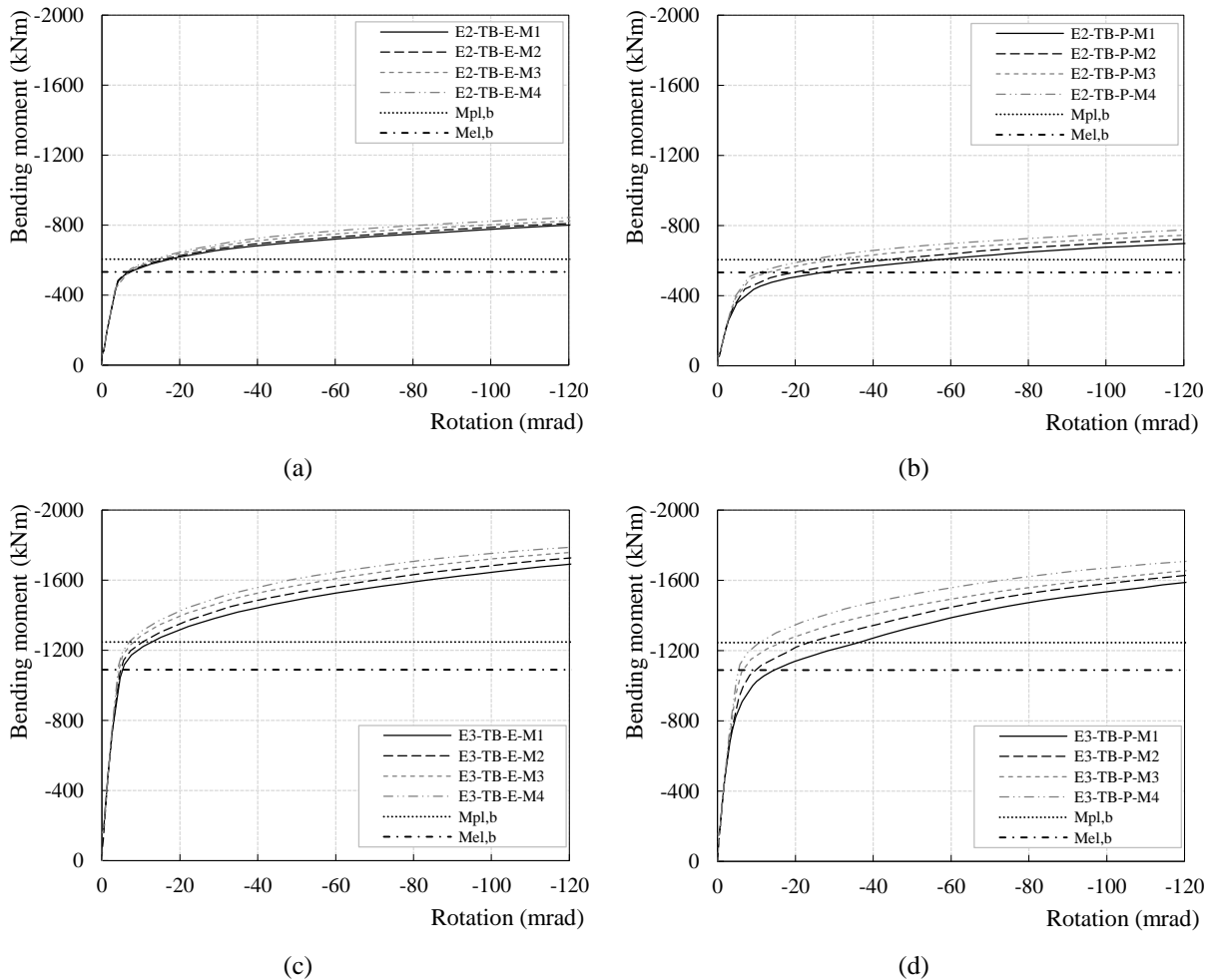


Figure 5.36: Moment-rotation relationships for joints subjected to monotonic loading.

The energy dissipated is depicted in Figure 5.37, until a rotation of 100mrad has been reached.

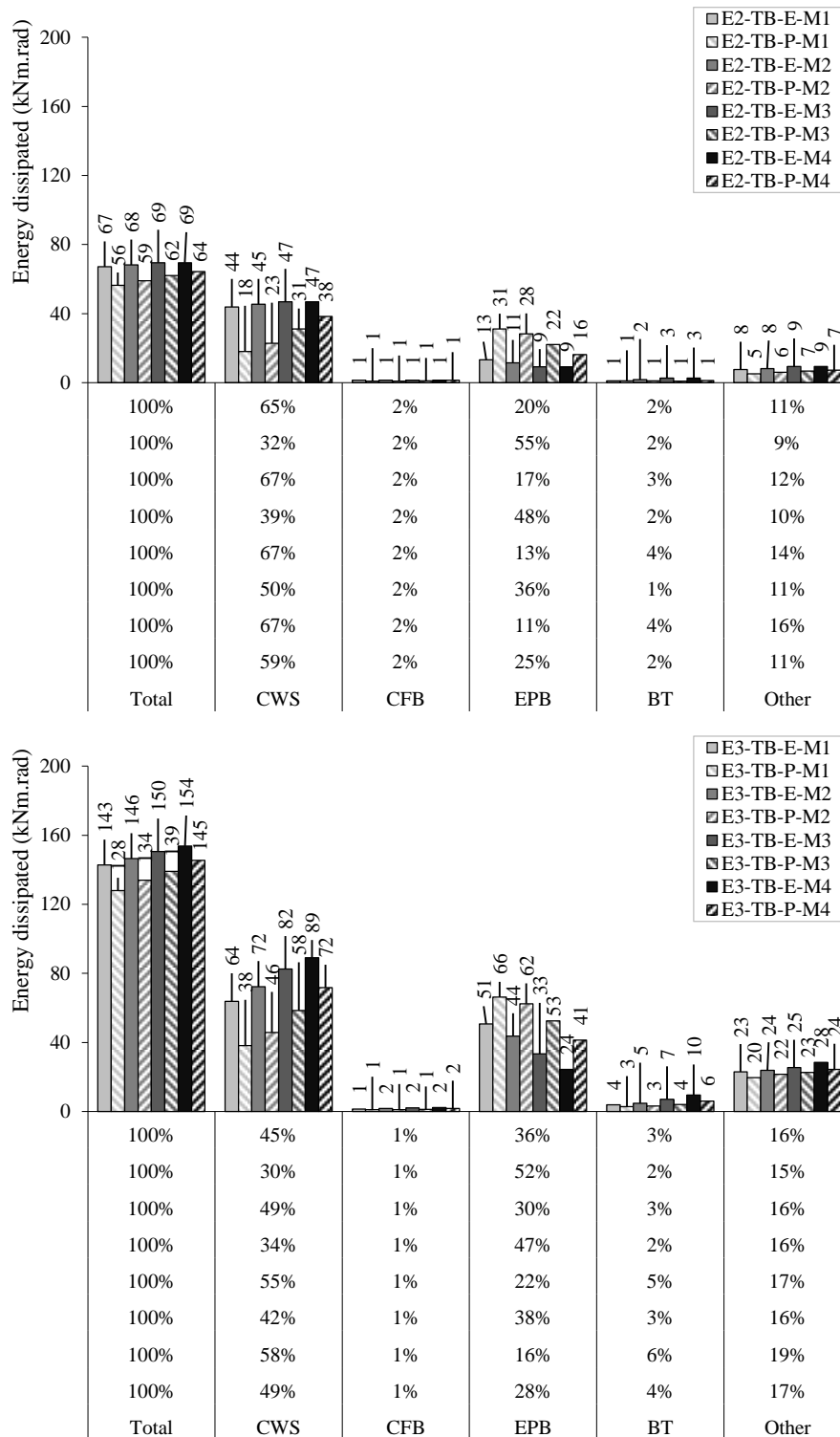


Figure 5.37: Energy dissipation in the joints until a rotation of 100mrad has been reached.

The initial stiffness of the joints is depicted in Figure 5.38, for the joints in study, it is also depicted in the figure the analytical values of the initial stiffness, when the EC3-1-8 (EN 1993-1-8, 2005) procedure is applied to the joints, as well the rigid limit set by the EC3-1-8.

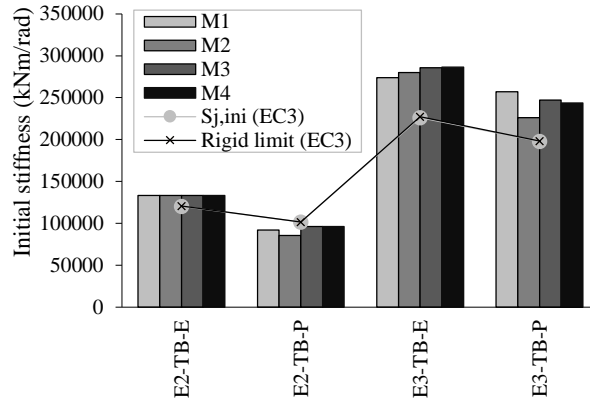


Figure 5.38: Comparison of the initial stiffness of the joints.

Finally in Figure 5.39 is depicted the Von Mises stress patterns distribution in the joints.

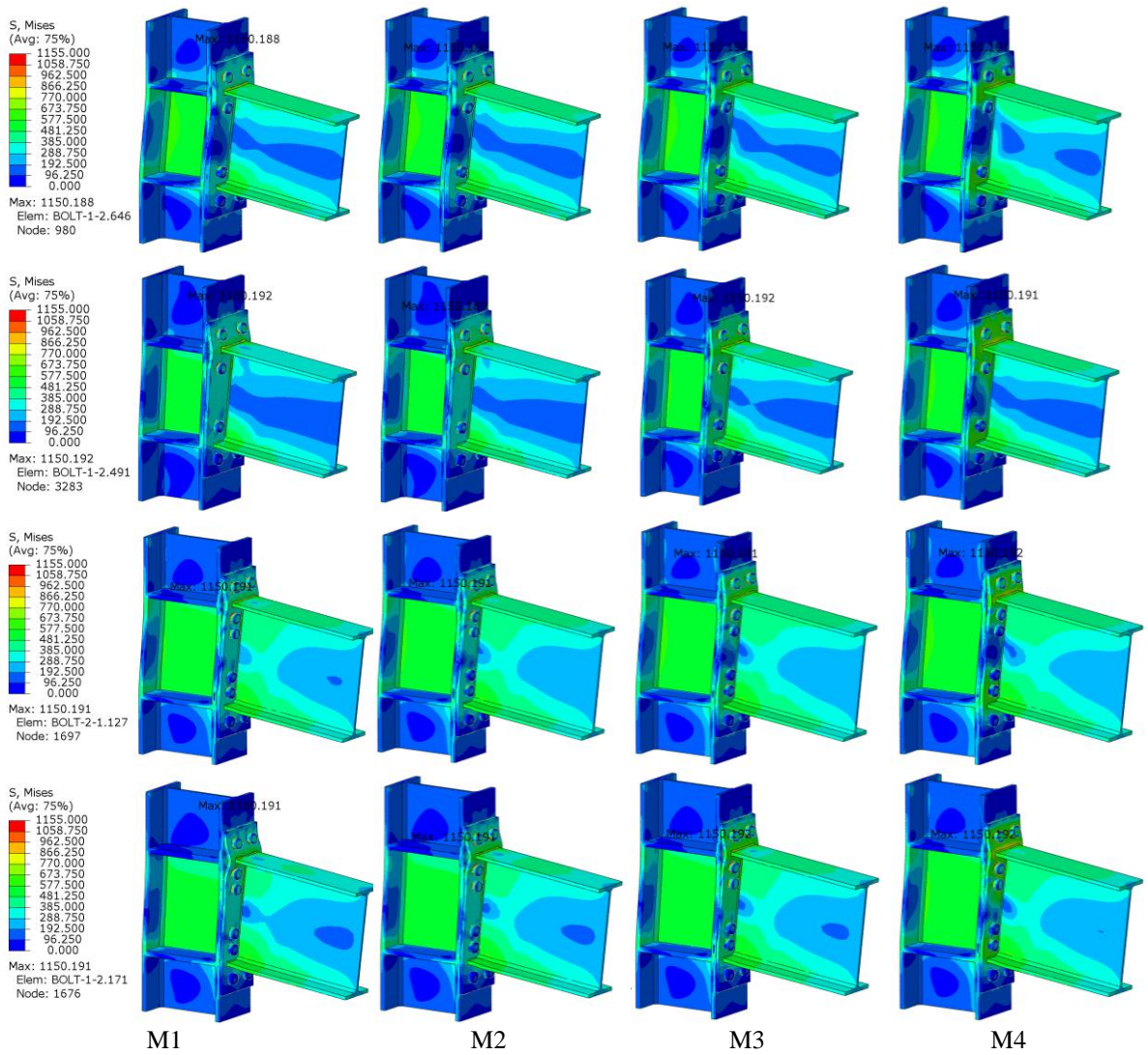


Figure 5.39: Von Mises stress patterns for a rotation of 100mrad, from top to bottom: E2-TB-E-, E2-TB-P-, E3-TB-E-, E3-TB-P-.

The analysis of the results allows the conclusion that there is a remarkable influence of the end-plate material properties in the global response of the joints. This fact can be justified by the substantial contribution that the component end-plate in bending has to the joints strength and stiffness. This influence is clearly more notorious in the joints with slender end-plates, i.e., partial-strength joints, due to the higher contribution of this component to the behaviour and energy dissipation of the joints. For the joints with deeper beams (IPE600) the influence of the end-plate mechanical properties is more notorious, even for the equal-strength joints. The fact that these joints possess stronger columns can also contribute to this effect, impairing more load to the end-plate.

The analysis of the energy dissipated confirms the earlier conclusion, i.e. the influence of the end-plate resistance is more notorious in the joints with deeper beams (IPE600). Consequently, there is a reduction of the contribution of the component column web panel in shear for the global energy dissipation in the joint.

Apparently, the initial stiffness is not significantly affected by the end-plate mechanical properties, although in the joints with a higher contribution from the end-plate, this influence is more notorious.

The mechanical properties of the end-plate has a direct impact on the stress patterns of the joints. Particularly the end-plate stress distribution, with the increase of the mechanical properties of the end-plate a lower distribution of stresses is observed. The stresses patterns in the column are quite similar and in the beam only small changes can be noticed.

iv) Cyclic Loaded Joints

In Figure 5.40 is depicted the response of the joints when subjected to cyclic loading.

At the components level the response of joints is depicted in Figure 5.41, for the component column web panel in shear, Figure 5.42 for the component column flange in bending and Figure 5.43 for the component end-plate in bending.

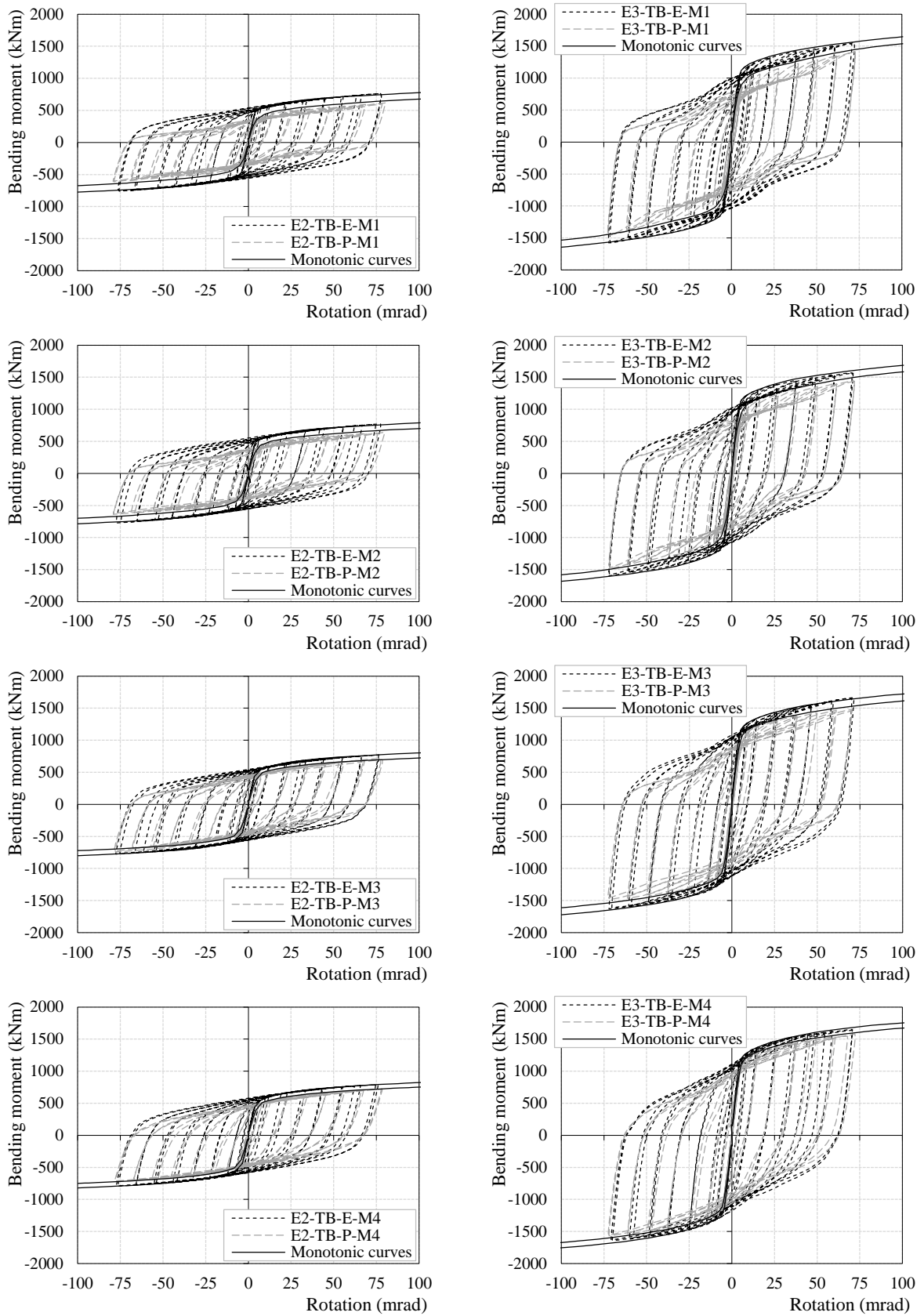


Figure 5.40: Moment-rotation relationships for joints subjected to cyclic loading.

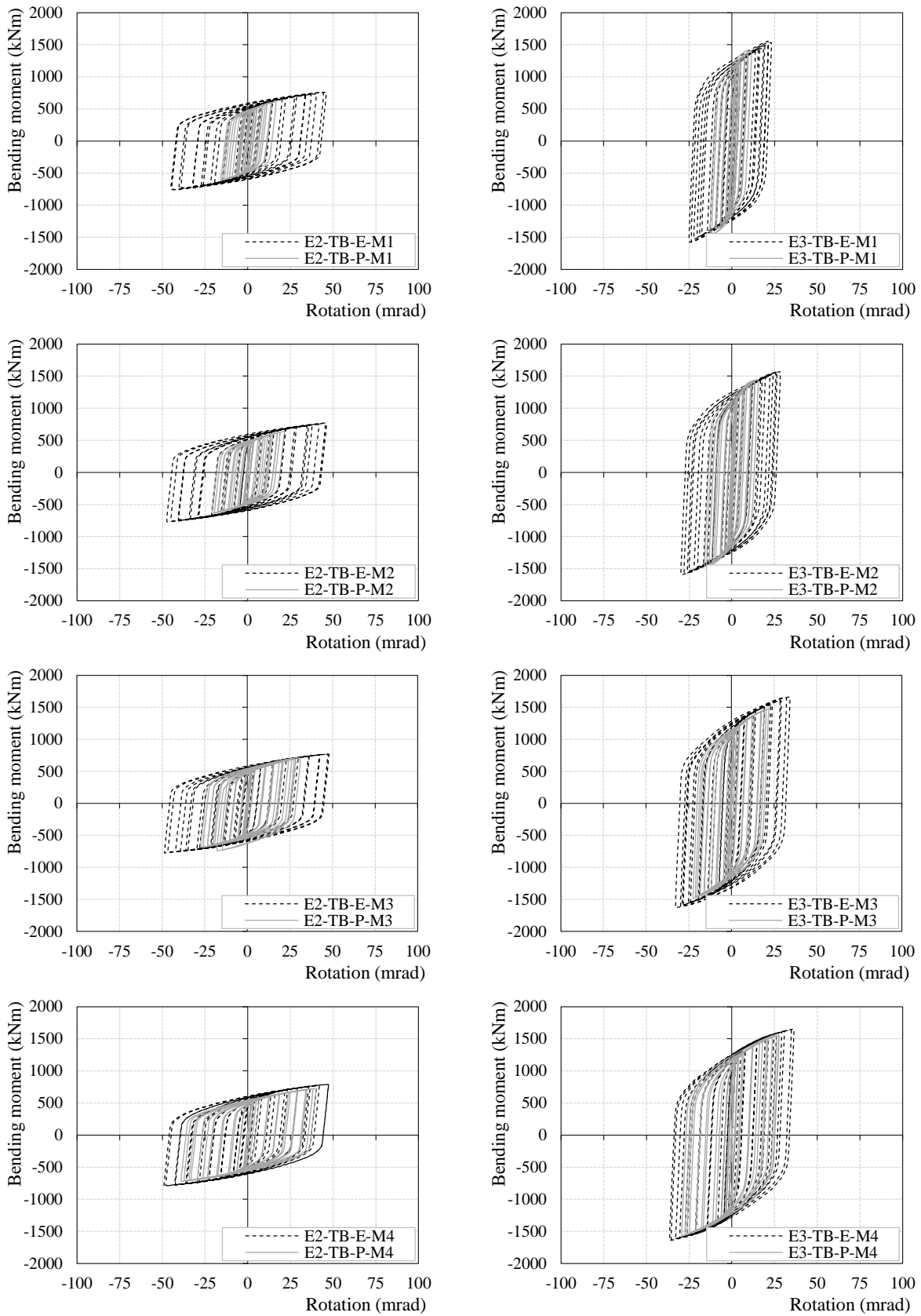


Figure 5.41: Moment-rotation relationships for component column web panel in shear.

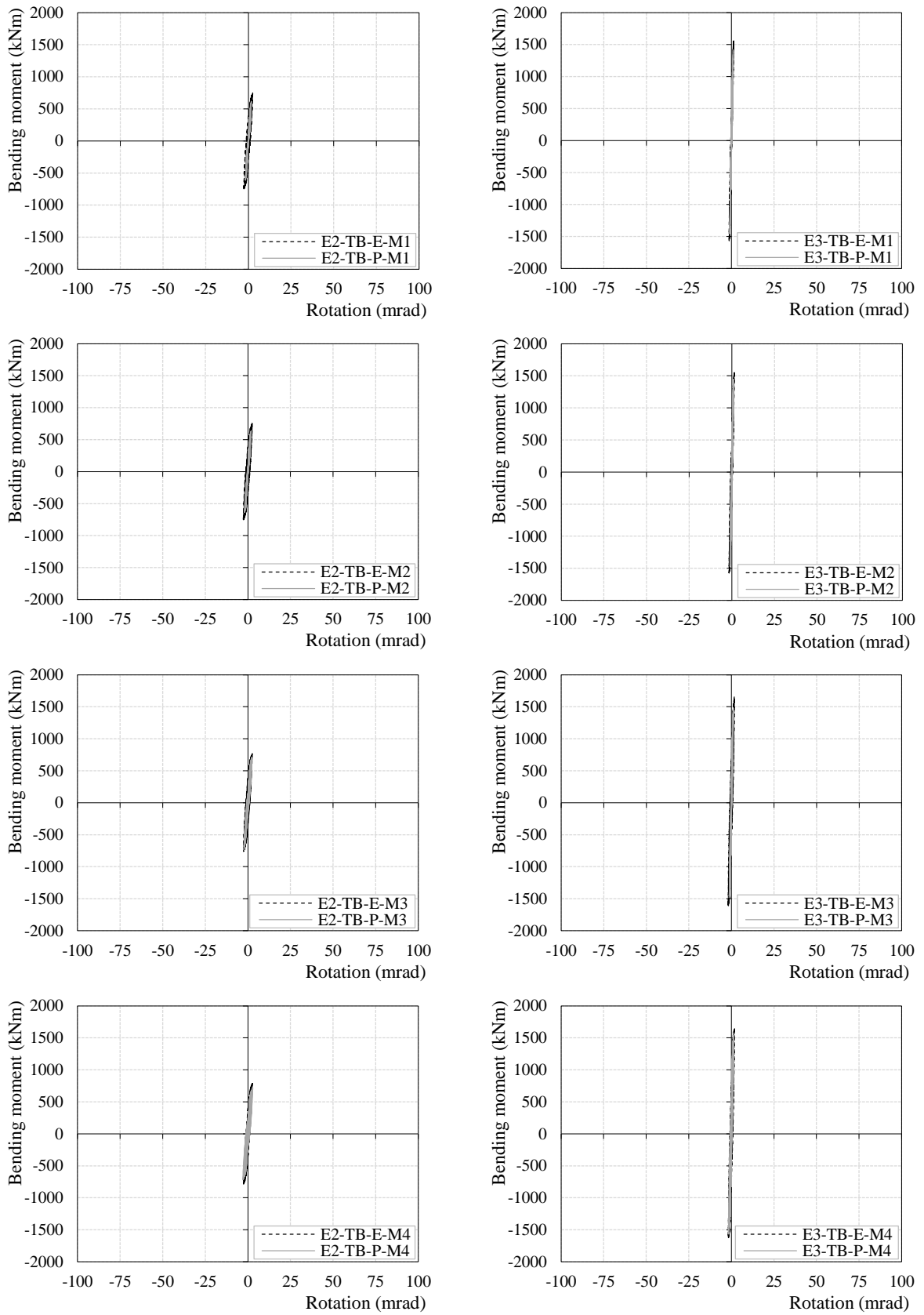


Figure 5.42: Moment-rotation relationships for component column flange in bending.

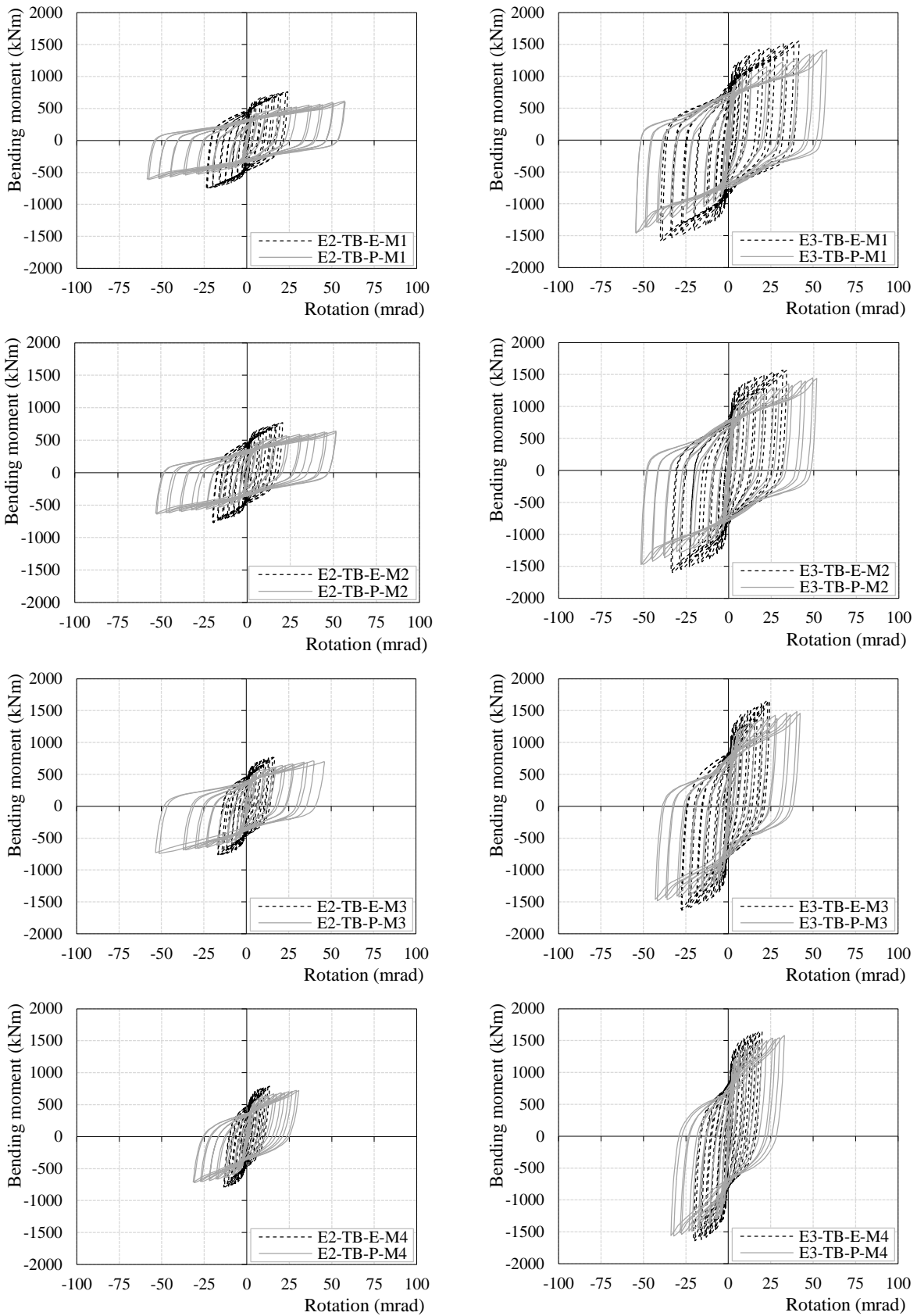


Figure 5.43: Moment-rotation relationships for component end-plate in bending.

The energy dissipated during the joints loading is depicted in Figure 5.44, until the 36th cycle has been reached.

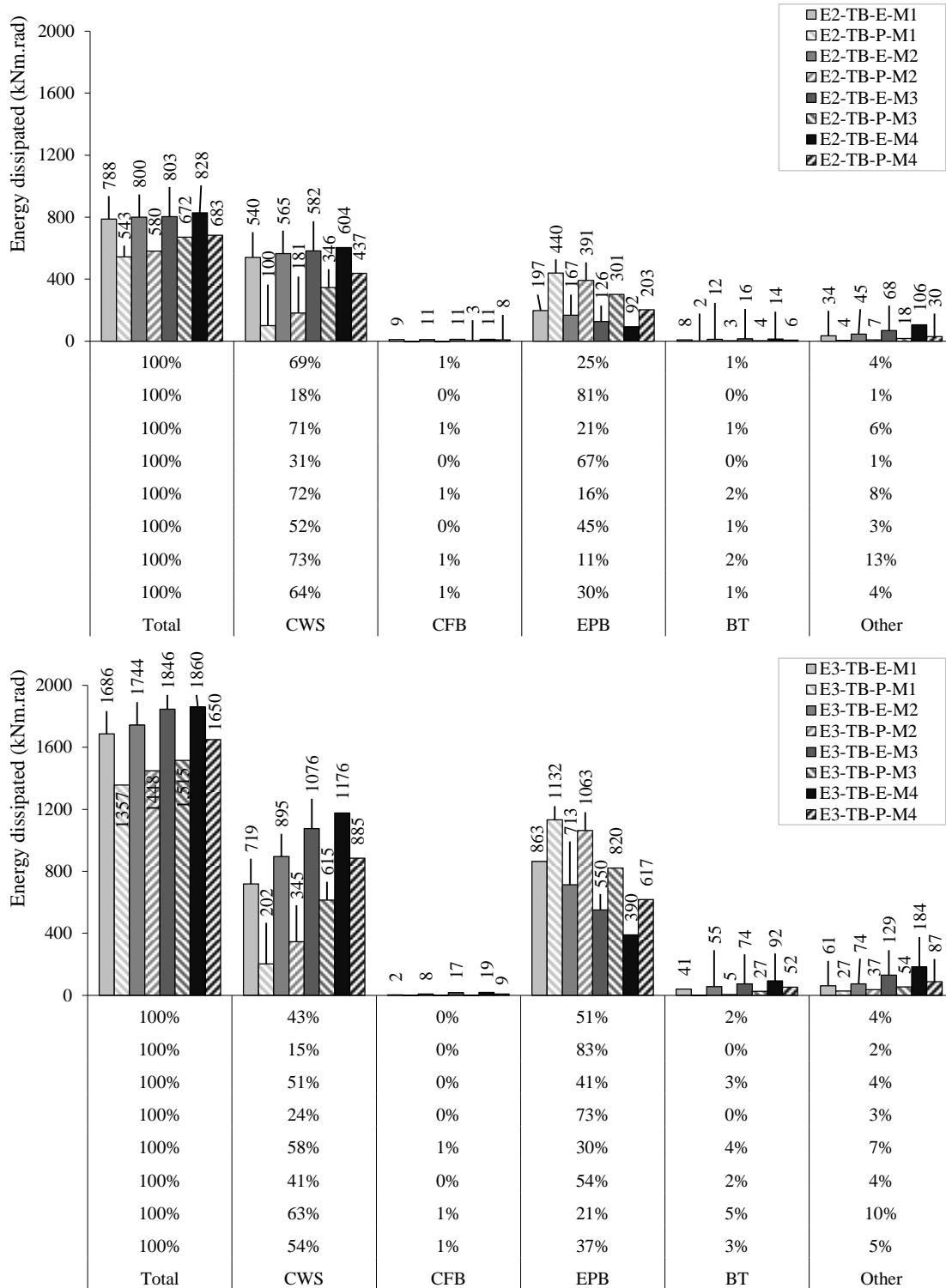


Figure 5.44: Comparison of the accumulated energy dissipation per component until the 36th cycle is reached.

As in the monotonic results the response of the joints subjected to cyclic loading also revealed the influence of the mechanical properties of the end-plate. This influence is more evident in the partial-strength joints, due to their slender end-plates. Some pinching effect can be detected in the joints with lower material stress-strain relationships, namely with the M1 material properties, where the plastic deformation in the end-plate was reached for a lower demand. A detailed analysis of the components responses revealed that the contribution of the component column web panel in shear to the global response increases with increasing material properties in the end-plate. On the other hand the contribution of the component end-plate in bending, for the global response of the joint, decreases with the increase of the mechanical properties of the end-plate. This conclusion is also reflected in the energy dissipation accumulated, with the contribution of the component column web panel to the global energy dissipation, growing and the contribution of the component end-plate in bending decreasing.

5.4.3 FINAL REMARKS ON THE PARAMETRIC STUDY

In this study a set of finite element models were developed using the ABAQUS software package to characterize the behaviour of the external beam-to-column bolted end-plate joints. The parametric study was based on the variation of some geometrical and mechanical properties in the joints that have the potential to influence their behaviour. The presence of the continuity stiffeners in the column web; the influence of an additional bolt row located in the axis of symmetry of the joints or two additional bolt rows in the extended parts of the end-plate and the sensitivity to the end-plate mechanical properties were the parameters considered in the study.

- i) Influence of the continuity column web stiffeners.

The presence of column transverse web stiffeners increases the initial stiffness and resistance of the joints. In the unstiffened joints the component column flange in bending gained some relevance in the contribution to the global energy dissipated. The continuity stiffeners in the column web and the column flanges confine the major plastic deformations in the column web panel. The absence of transverse web stiffeners amplifies the pinching effect, mainly in the partial-strength joints.

- ii) Influence of middle bolt row.

No influence of the additional middle bolt row in the joints behaviour was detected.

- iii) Influence of two bolt row in the extended part of the end-plate.

The influence of second external bolt row is only evident for larger rotations, after the external bolt row, closer to the beam flange, suffers plastic deformation. The plastic mechanism of the end-plate, for large rotations, may change allowing for a new plastic hinge in the end-plate, conferring additional strength, combined with the membrane effect.

- iv) Sensitivity to the Mechanical Properties of the End-Plate.

The mechanical properties of the end-plate have a direct impact in the response of the joints, especially in the partial-strength joints, due to their slender end-plates. There is an increase of the pinching effect with the decrease of the end-plate mechanical properties and thickness. With the increase of the mechanical properties of end-plate the contribution of the component column web panel in shear, to the global energy dissipation grows and the contribution of the component end-plate in bending decreases.

5.5 COMPARISON WITH THE EXPERIMENTAL TESTS RESULTS

5.5.1 RESULTS AND DISCUSSION

The available results from experimental tests performed on the joints (Landolfo *et al.*, 2017) analysed in the previous section are used to validate the numerical models updated with the actual material behaviour from coupon tests. The material properties are summarized in Table 5.5. It is also included in the table a comparison with the adopted nominal mechanical properties used in the previous FEM. It is important to highlight that an overstrength factor of $\gamma_{ov} = 1.25$ was considered for the base material properties (M-3) according to EC8 (EN 1998-1, 2004). From the table it is possible to observe that this option is, in most cases, on the unsafe side for the seismic design of structures. The real variation factor is found to be, in most cases, higher than the proposed material overstrength factor (γ_{ov}). The largest differences were found in the flanges of the column HEB340 and in the end-plates and stiffeners with thickness of 20mm.

Table 5.5: Average mechanical properties of steel tested (true stress values).

Section size	Component	Engineering yield stress (MPa) f_{ym}	True yield stress (MPa) f_{ym}	Nominal yield (MPa) f_y	Real variation factor ($\gamma=f_{ym}/f_y$)	Young's modulus (GPa) E_m	Nominal value (GPa) E	Δ (%)
IPE450	Flange	445.6	446.61	355.00	1.26	206.76	210	-1.6
	Web	466.2	467.25	355.00	1.32	204.82	210	-2.5
IPE600	Flanges	475.8	477.03	355.00	1.34	184.87	210	-13.6
	Web	461.9	462.91	355.00	1.30	207.83	210	-1.0
HEB340	Flanges	509.0	510.25	355.00	1.44	204.38	210	-2.8
	Web	455.3	456.26	355.00	1.29	208.88	210	-0.5
HEB500	Flanges	446.8	428.01	355.00	<u>1.21</u>	223.34	210	+6.0
	Web	434.8	435.72	355.00	<u>1.23</u>	213.13	210	+1.5
18 mm	End-plate, Stiffeners	417.9	418.83	355.00	<u>1.18</u>	196.83	210	-6.7
20 mm	End-plate, Stiffeners	509.3	510.53	355.00	1.44	212.02	210	+1.0
25 mm	End-plate	459.8	460.80	355.00	1.30	216.72	210	+3.1

The FE models were updated with the new material properties. The results were compared with those from previous models using nominal values and are shown in Figure 5.45 for the joints subjected to monotonic loads and in Figure 5.46 for the joints subjected to cyclic loads.

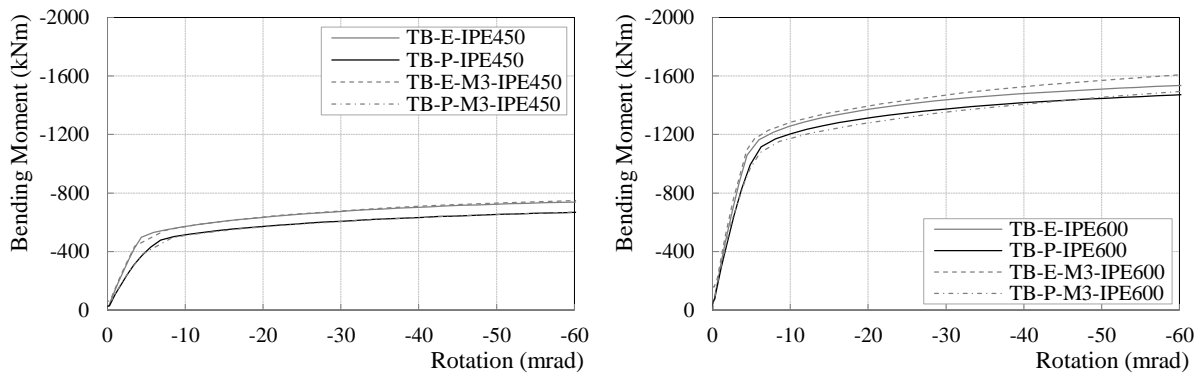


Figure 5.45: Comparison between the FEM with M3 material properties and the FEM with the material properties based on the coupon tests, for the joints subjected to monotonic loads.

The previous results are quite similar to the ones obtained with the steel properties based on the coupon tests results. This adjustment is better in the joints loaded monotonically.

The response of the joints were compared with the analytical values using the real material properties obtained in the coupon tests (engineering stress), see Table 5.6 and Figure 5.47. The analytical results are now closer to the numerical results, due to the use of the same material properties. In the case of the equal-strength joints the relation between the design

bending moment and the beam plastic moment decreased, the joint is now closer to a partial-strength joint with 80% of the beam resistance. In the case of the partial-strength joints the relations remain almost unchanged, around 60% of the beam plastic resistance. The relation between the strength of the column web and the joint strength increased in all joints except for the E3-TB-P(0.6). In terms of the ductility criteria it is possible to realize that the ductility level 1 ($\beta \leq 1$) is fulfilled for the partial-strength joints. However, for the second criterion, ductility level 2 ($\eta \leq 0.95$) the joint E2-TB-E presents a value of $\eta = 0.97$ slightly higher than the requested, i.e. still having a failure mode type 2 but too close to the failure mode type 3.

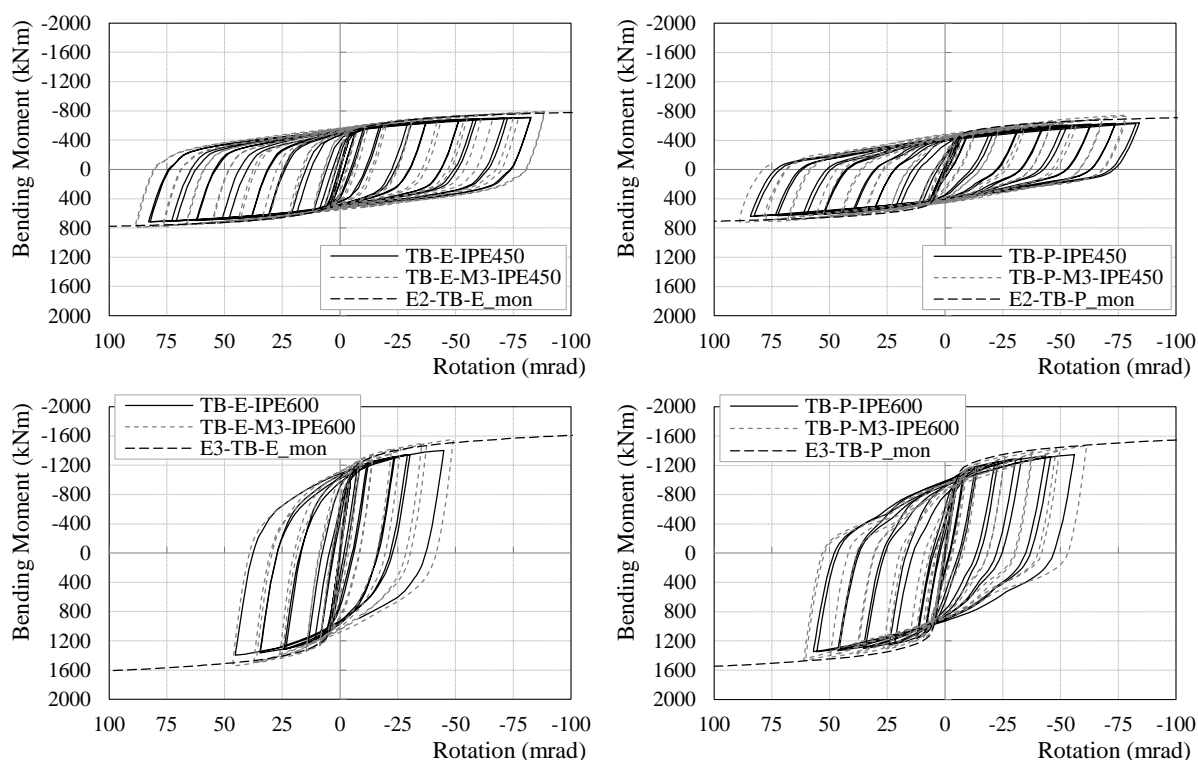


Figure 5.46: Comparison between the FEM with M3 material properties and the FEM with the material properties based on the coupon tests, for the joints subjected to cyclic loads.

Table 5.6: Main design properties of the joints according to EC3-1-8 (EN 1993-1-8, 2005).

	Nominal values				Updated values			
	E2-TB-E	E2-TB-P(0.6)	E3-TB-E	E3-TB-P(0.6)	E2-TB-E	E2-TB-P(0.6)	E3-TB-E	E3-TB-P(0.6)
$M_{p,b}$ (kNm)	604.2	604.2	1246.8	1246.8	765.4	765.4	1660.0	1660.0
$M_{p,j}$ (kNm)	545.4	392.7	1129.6	736.4	612.3	484.6	1341.3	1123.9
$M_{p,wp}$ (kNm)	549.6	549.6	1217.5	1217.5	703.4	703.4	1499.6	1499.6
$M_{p,j}/M_{p,b}$	0.9	0.65	0.91	0.59	0.8	0.63	0.8	0.68
$M_{p,wp}/M_{p,j}$	1.0	1.4	1.07	1.65	1.15	1.45	1.12	1.33
β (bolt row 2)	1.58	1.00	0.96	0.62	1.82	0.95	1.02	0.72
η (bolt row 2)	0.92	0.75	0.77	0.62	0.97	0.75	0.78	0.72

The new FEM results, taking into account the updated material properties, were compared with the available results of the joints experimental tests, see Figure 5.49. Table 5.7 summarizes the experimental tests performed for comparison. Note that several experimental tests were performed for each joint configuration, designated by C1, C2 and P_C. The later comprises a treatment to improve the beam-to-end-plate welds behaviour.

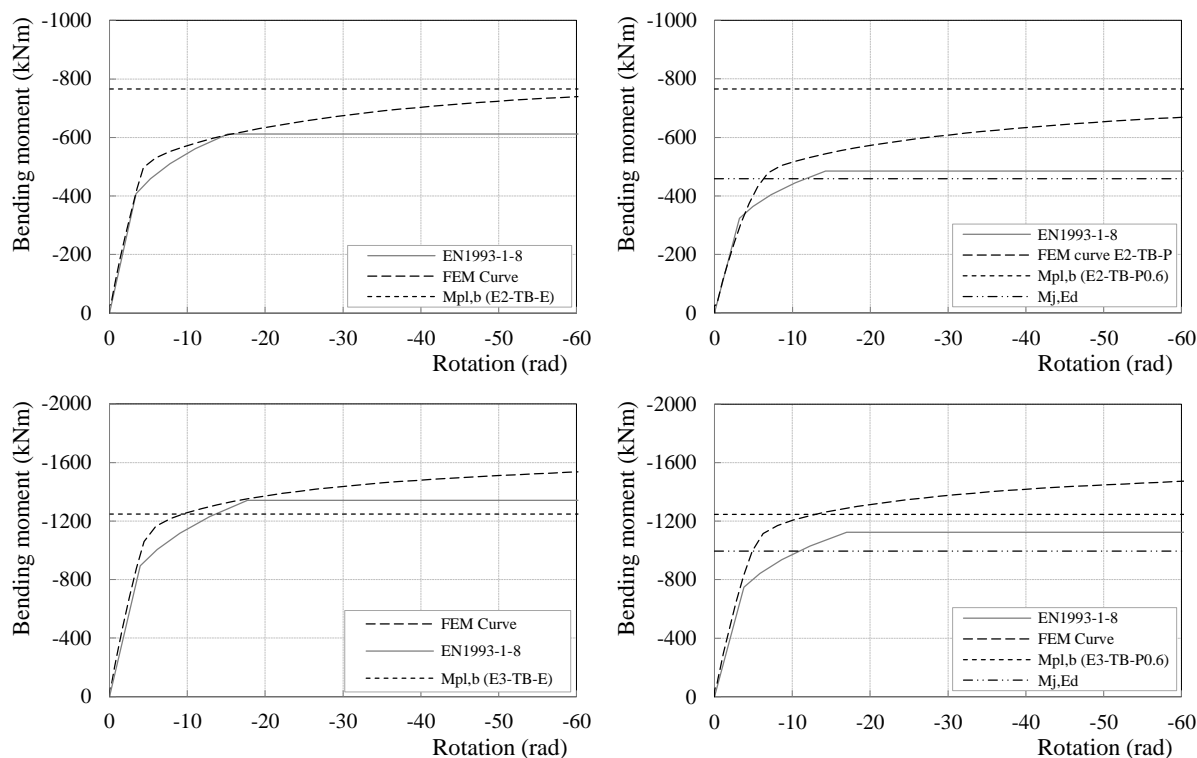


Figure 5.47: Moment-rotation relationships in the joints.

Table 5.7: Tested specimens in Liège.

Specimen name	Column	Beam	End-plate thickness (mm)	Loading protocol
E2-TB-E_C1	HEB340	IPE450	25	AISC
E2-TB-E_C2	HEB340	IPE450	25	AISC
E2-TB-P_C1	HEB340	IPE450	18	AISC
E2-TB-P_C2	HEB340	IPE450	18	AISC
E2-TB-PP_C	HEB340	IPE450	18	AISC
E3-TB-E_C1	HEB500	IPE600	25	AISC
E3-TB-E_C2	HEB500	IPE600	25	AISC
E3-TB-P_C1	HEB500	IPE600	20	AISC
E3-TB-P_C2	HEB500	IPE600	20	AISC

As in the previous sections, the joints moment-rotation relationship, for the numerical models, were obtained by the Eq. (3.7) and Eq. (3.21) supported by Eqs. (3.18) and (3.19). In the case of the experimental tests the instrumentation layout was slightly different from the

Nogueiro's tests (Nogueiro, 2009). The instrumentation layout is depicted in Figure 5.48. In order to obtain the bending moments, Eq. (3.6) was used. To obtain the rotations a modification to Eq. (3.9), supported by Eqs. (3.18), (3.19) and (3.20), was used, see Eq. (5.1) and (5.2).

$$\theta_{total} = 0.5 \left(\frac{B_2 - B_1 + C_2 - C_1}{70} \right) - \theta_{elast_beam} - \theta_{elast_column} - \theta_{block} \quad (5.1)$$

$$\theta_{block} = a \tan \left(\frac{M_1 - F_1}{M_1 F_1} \right) \quad (5.2)$$

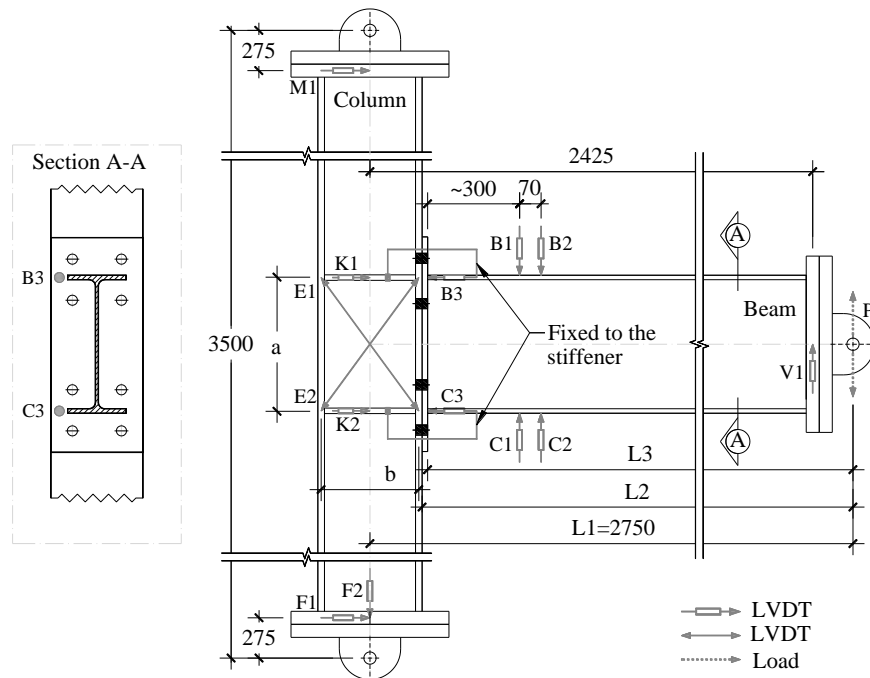


Figure 5.48: Experimental tests setup for the sub-assembly containing the joints in study (dimensions in *mm*).

The results revealed an excellent agreement between the numerical results and the envelope of the several experimental results available for each joint typology. The comparisons demonstrate the accuracy of the developed finite element model and of the procedures to extract the responses of the joints behaviour for different geometries. The moment-rotation response of the joints present a stable behaviour without strength degradation, although it is possible to observe some degradation of stiffness for the larger cycles, with higher demand, which is a phenomenon well captured by the numerical models. For the partial-strength joints, some pinching effect can be identified in the response, both for E2 and E3 joints geometries.

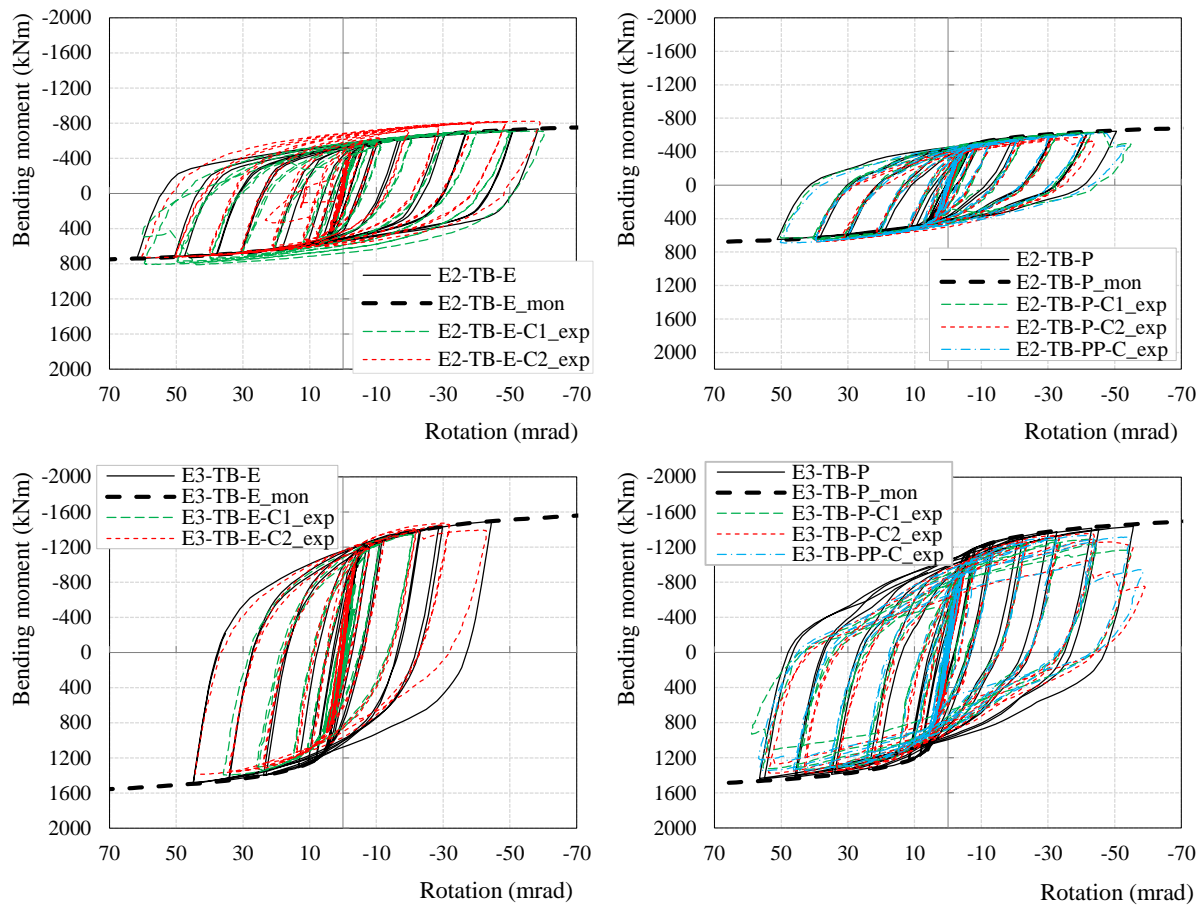


Figure 5.49: Moment-rotation relationships between the numerical and experimental results.

5.5.2 FINAL REMARKS ON THE COMPARISONS WITH THE EXPERIMENTAL TESTS RESULTS

The developed finite element models (FEM) of external nodes were updated with the mechanical properties found in the coupon material tests. The results revealed that the adoption of a overstrength factor ($\gamma_{ov} = 1.25$) in the material properties used in the preliminary FEM, to tackle the variability of the mechanical properties generally found in the current steels grade used in construction, is slightly on the unsafe side. The real variation factor is found to be, in most cases, higher than the material overstrength factor (γ_{ov}) proposed in the EC8 (EN 1998-1, 2004).

The comparisons of the preliminary results and the ones obtained with material properties based on the coupon tests results, have shown a good agreement. However, some differences were found in the analytical results, obtained using the procedures found in the EC3-1-8 (EN 1993-1-8, 2005), when the nominal steel grade or the average results of the coupon tests is used

for the mechanical properties of the steel. These results revealed that the initial assumptions can change significantly the design of the joints, namely the failure modes behaviour. In the case of the joint E2-TB-E the ductility criteria was no longer satisfied, using the new mechanical properties, approaching the T-stub failure mode type 3. This conclusion alert to the need of carrying out design verifications of joints and members considering the actual properties of steel involved, especially in structures located in seismic regions, where members and joints are expected to dissipate energy by plastic deformation.

The comparisons of the moment-rotation relationships obtained from FEM, updated with the mechanical properties of the coupon tests, and the envelope of the results of the joints experimental tests performed, revealed an excellent agreement. The comparisons demonstrate the accuracy of the developed finite element model and the validity of the procedures to extract the joints behaviour, also for different joint geometries. It was also verified that the response of the joints present a stable behaviour without strength degradation, although it is possible to observe some degradation of stiffness for the larger cycles, with higher demand.

5.6 COMPONENT'S BEHAVIOUR EXTRACTION

5.6.1 FRAMEWORK AND DEFINITIONS

The proposed methodology to characterize the behaviour of the basic components, presented in Chapter 4, was applied to the finite element models representative of the joints tested experimentally and identified in Table 5.6. Only the joints under cyclic loading conditions will be studied in this section.

The walkthrough to extract the force-deformation relationships, described in Table 4.12, is used to determine the response of the basic components (1 – CWS, 2 – CWC, 3 – CWT, 4 – CFB, 5 – EPB and 10 - BT), using the integration of stress and displacement fields.

All joints in study are provided with transverse web stiffeners. This will increase the shear strength due to the moment resisting frame formed by the column flanges and the transverse web stiffeners. This will also reduce the contribution to the joint rotation of the components 2, 3 and 4.

5.6.2 RESULTS AND DISCUSSION

5.6.2.1 COLUMN WEB COMPONENTS

The presentation of the results will follow the considerations taken on Section 4.2.3.2. For the component column web panel in shear (1) the force – displacement ($F-\Delta$) relationships are obtained directly by applying the extraction procedure. For components column web in transverse compression (2) and column web in transverse tension (3) the $F-\Delta$ relationships are calculated according to the integration boundaries of the alternative mechanical model of Figure 4.1. Tension and compression are combined together, in the same $F-\Delta$ relationship for each bolt row, according to the alternative procedure in Figure 4.1. Nevertheless, from those curves, it is possible to extract the $F-\Delta$ relationships according to the specifications of EC3-1-8 (EN 1993-1-8, 2005), defined in the top mechanical model depicted in Figure 4.1. For that the response of the component column web in transverse compression (2) corresponds to the compression side of the group of rows around each beam flange. On the other hand the component column web in transverse tension (3) is achieved isolating the tension side of the curves determined individually for each bolt row.

i) Component Column Web Panel in Shear

Figure 5.50 shows the stress fields for increasing levels of bending moment. The stress patterns and levels are very similar for all the joints analysed, revealing a similar distribution of stress in the equal and partial-strength joints. Figure 5.51 shows the derived relationships for the component behaviour, taking into account the addition shear strength provided by the moment resisting frame formed by the transverse web stiffeners and the column flanges. All joints present stable behaviour and high ductility. E2-TB-E is the joint that reaches the highest ductility achieving a web rotation of more than $40mrad$.

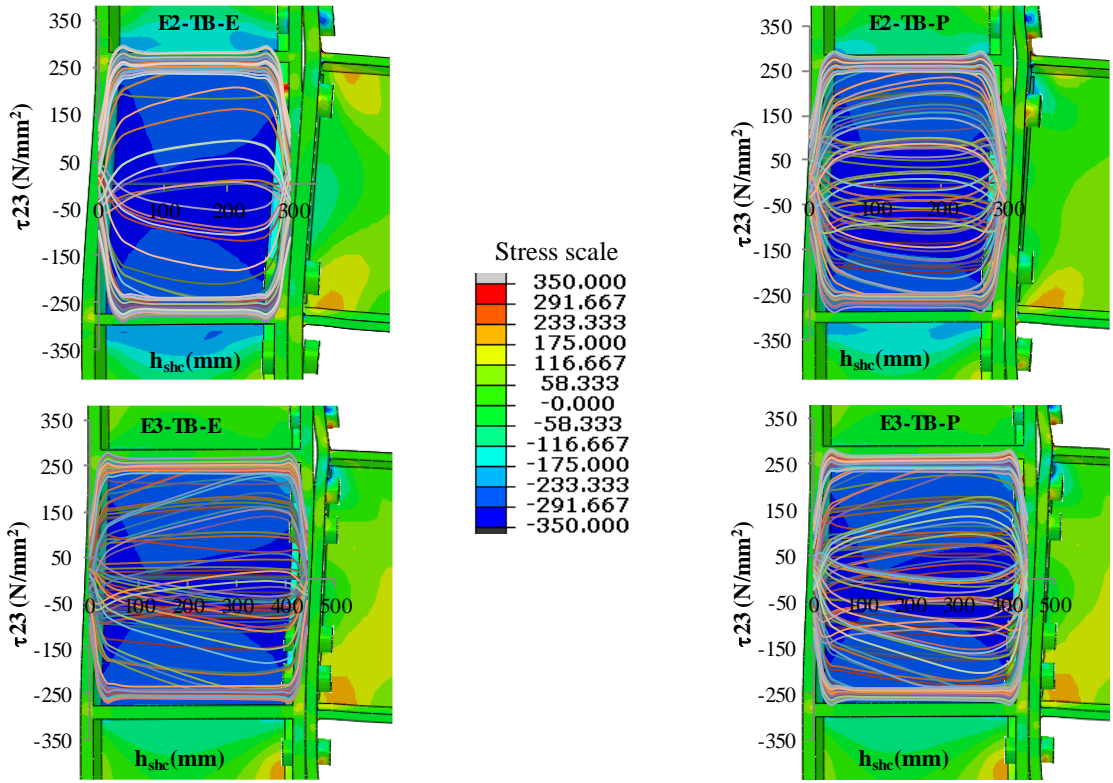


Figure 5.50: Shear stress fields for increasing levels of bending moment.

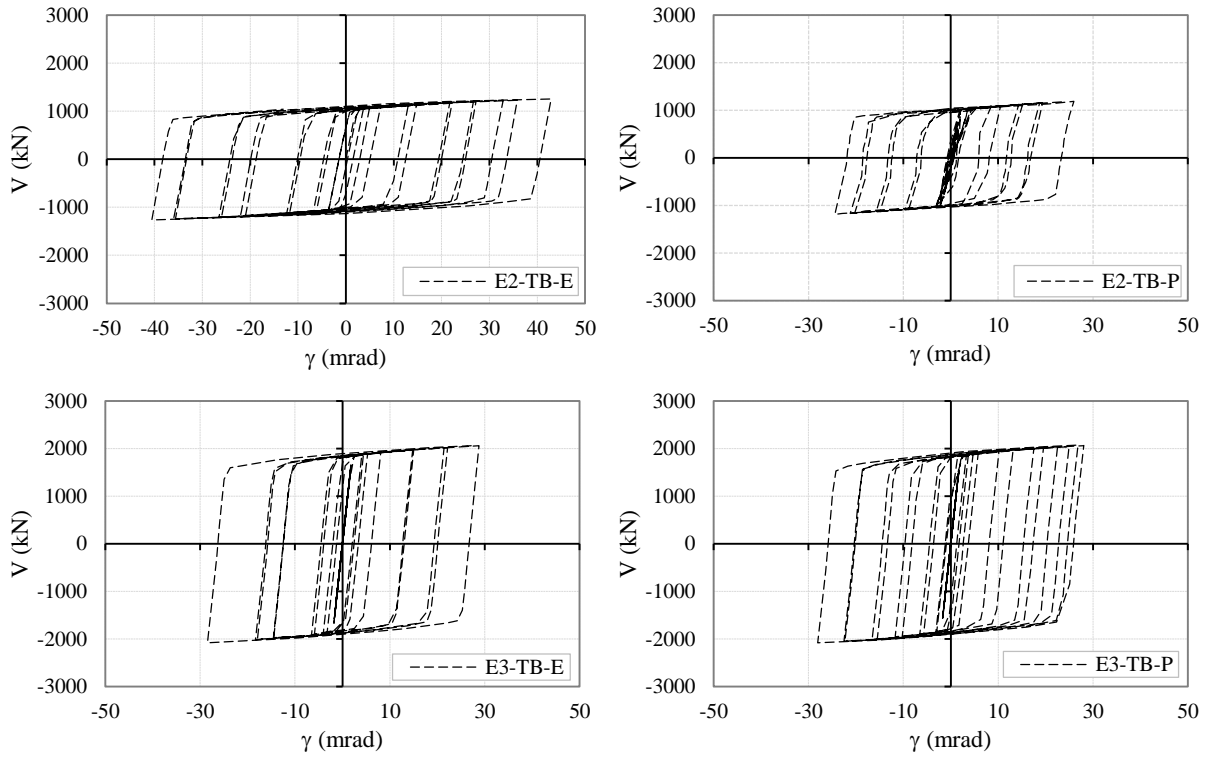


Figure 5.51: V- γ relationships for the shear load.

ii) Components Column Web in Transverse Compression / Tension

Figure 5.52 shows the stress and deformation fields for increasing levels of bending moment. The stress fields in the joints followed approximately the same stress distribution, although it is possible to observe that in the E3 joints the stresses reached higher values, due to the stronger beam and column. The displacement fields revealed that the deformation in the column web was considerably higher in the E3 joints, when compared with the E2 joints. This is possibly due to the contribution of the additional inner bolt rows to the deformation. For the outer bolt rows, located in the extended part of the end-plate, the deformation of the column web is considerably smaller when compared with the inner bolt rows, due to the lower stiffness of the extended part of the end-plate. This phenomenon is more pronounced in the presence of transverse web stiffeners. This was also observed in the $F-\Delta$ relationships presented in the Figure 5.53, where it can be seen that the relationship was nearly elastic for the first and last bolt rows. On the other hand the inner bolt rows present a more ductile responses, although some ratcheting is noticed with the evolution of the loading, in accordance with the findings in Chapter 4. Note that the scale of the axes of the charts is not the same, for a more detail view of the $F-\Delta$ relationships with very lower deformations.

Figure 5.54 presents the $F-\Delta$ relationships for the group of bolts close to the beam flanges. The component column web in transverse compression can be obtained by isolating only the part of the curves in compression. Due to the presence of the transverse web stiffeners, the load-introduction binary originated by the beam bending moment is transferred in compression side, partially by the column transvers web stiffeners to the web panel shear and partially directly by the column web in transverse compression, which is captured by the response curves. Notice that those curves present a very low deformation, under $0.5mm$, remaining almost elastic, because the transverse stiffeners conditions significantly the transverse deformation of the column web.

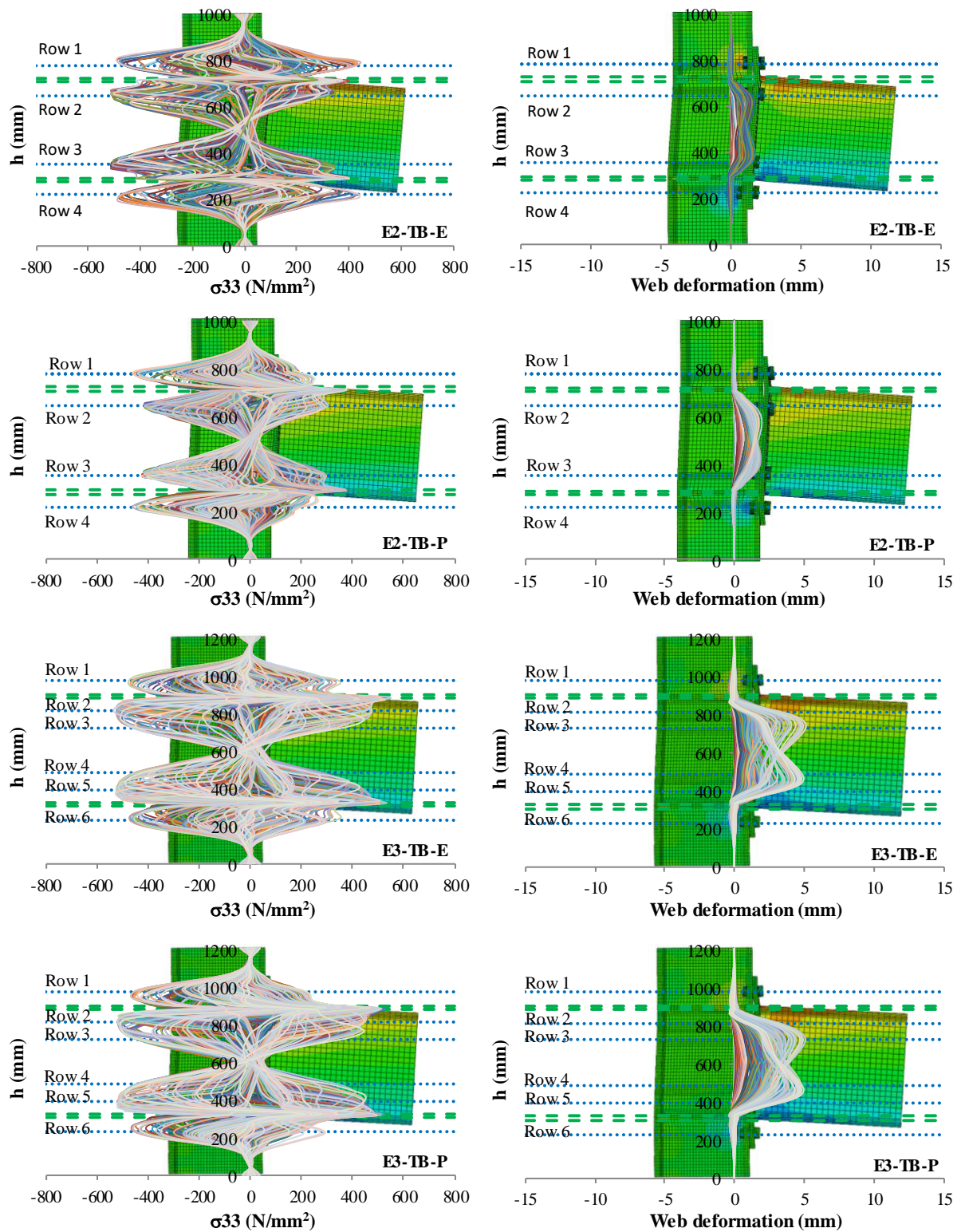


Figure 5.52: Stress fields (left), and web deformation fields (right), for increasing levels of bending moment.

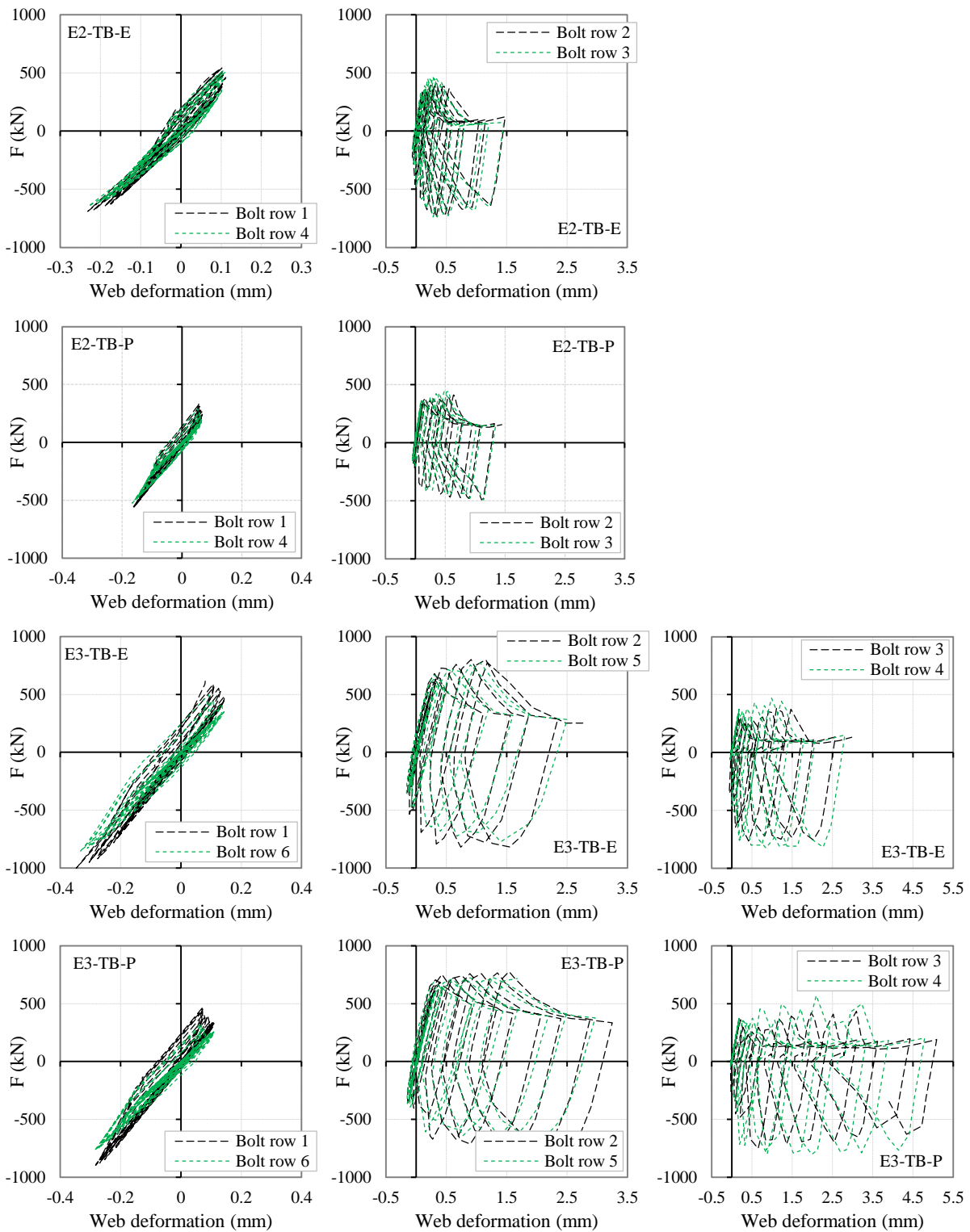


Figure 5.53: F-Δ curves for the components due to the load-introduction effect for each bolt row.

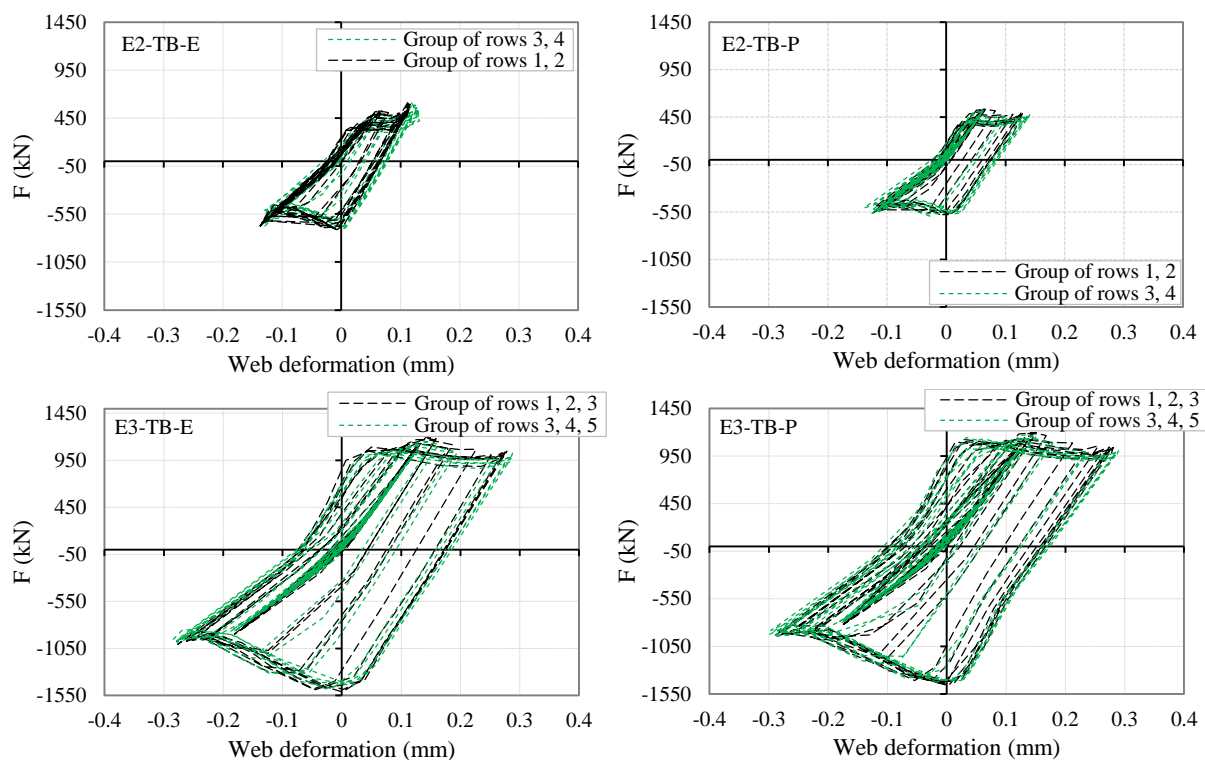


Figure 5.54: F- Δ curves for the components due to the load-introduction effect considering the group of bolts around the beam flanges.

5.6.2.2 CONNECTION COMPONENTS

In this section the connection components response will be analysed, namely the column flange in bending (4 - CFB), end-plate in bending (5 - EPB) and the bolts in tension (10 - BT). All of these components are activated in the tension side of the joint. The transverse web stiffeners significantly influences the deformation of the connected column flange, and it is expected that this component remains in the elastic domain. Also due to the presence of the stiffeners the corresponding forces cannot be directly assessed using the forces that enter in the column web. In this case the forces were directly obtained by integration from the bolts, according to Section 4.3.4, Eq. (4.39).

First the contribution of each component to the joint rotation is compared, using the methodology proposed in Section 4.3.2. Then the force-displacement relationships are determined and compared, using the procedure in Section 4.3.4. Note that the computed curves can be applied in a component based approach following the EC3-1-8 (EN 1993-1-8, 2005) provisions, and/or the mechanical models proposed in Figure 4.1.

i) Contribution of Each Basic Component to the Joint Rotation

Figure 5.55 shows the contribution of each basic component to the joint moment-rotation relationship, using the methodology proposed in Section 4.3.2. As expected, the relationships show that the biggest contribution to the connection rotation comes from the end-plate in bending, in all joints analysed. Nevertheless, the partial-strength joints with thinner end-plates clearly demonstrated to have higher contributions. This observation reinforces the statements made in Chapter 4, since in the presence of transverse web stiffeners the major contribution to the connection rotation is provided by the end-plate in bending.

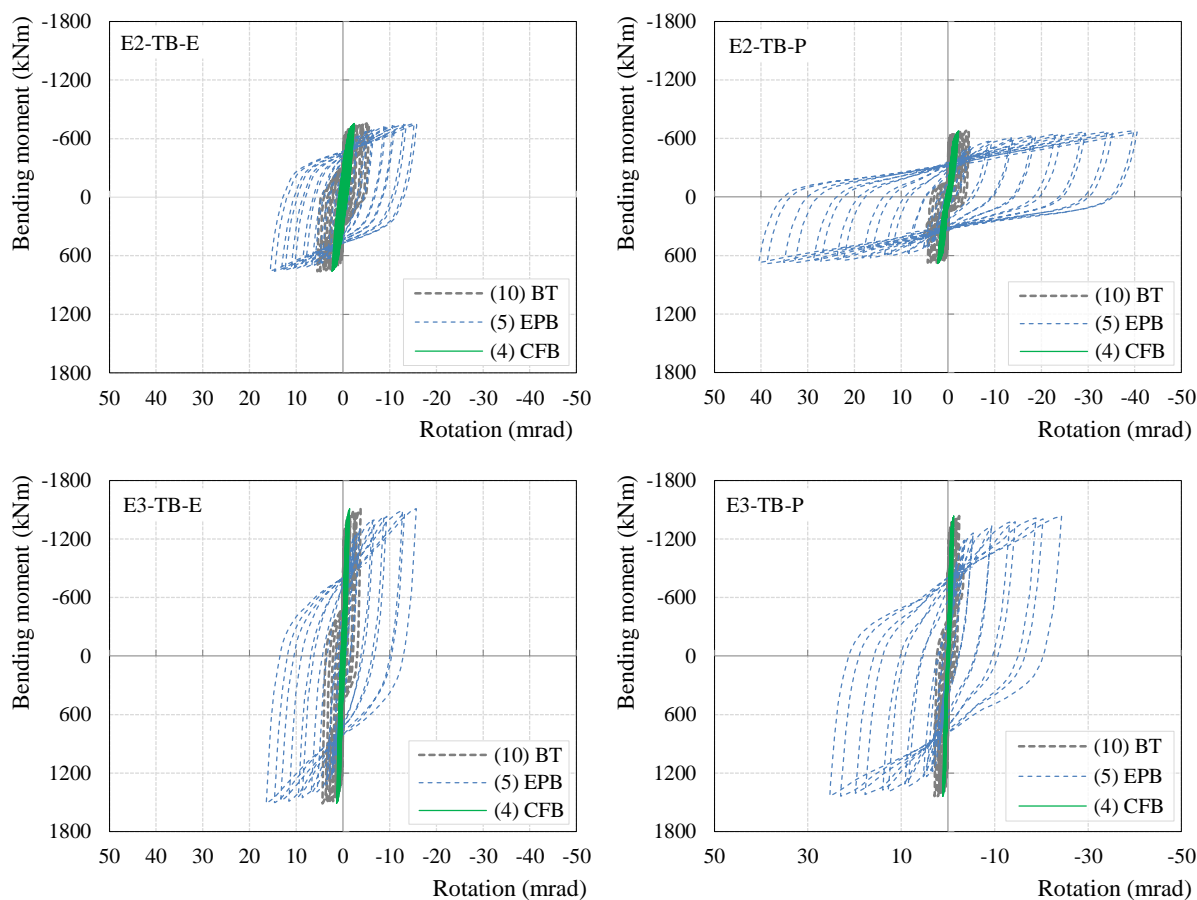


Figure 5.55: Moment-rotation relationships of the components associated to the connection zone.

In all joints the contribution of component 4 (CFB) was very small, due to the presence of the stiffeners. This component may actually be assumed to be elastic, in this situation. The lack of deformability of the column flange results in a higher demand of the bolts, due to the higher stiffness of the column flanges. The partial-strength joint E2-TB-P is the only joint where the contribution of the end-plate is clearly higher than the contribution of the column web panel

in shear (see Figure 5.51). However, this is not enough to comply with the EC8 (EN 1998-1, 2004) Section 6.6.4(4) requirement, where the contribution of the column web panel to the plastic deformation cannot exceed 30% of the plastic rotation capacity of the joint. The contribution of the bolts in tension is higher in the equal-strength joints, due to the stronger end-plates.

ii) Force-Displacement Relationships of the Basic Component of the Connection

For each bolt row the force-displacement ($F-\Delta$) relationships of the components of the connection were extracted from the FE models, using the proposed procedure in Section 4.3.4. Figure 5.56 to Figure 5.59 show the derived $F-\Delta$ relationships for the components: column flange in bending (4 - CFB), end-plate in bending (5 - EPB) and the bolts in tension (10 - BT). From the figures is possible to observe that the component end-plate in bending is the only that can be considered as dissipative. In fact, as observed earlier, the basic component column flange in bending remains nearly elastic in all bolt rows and in all joints. The component related to bolts in tension show incursions in the plastic range in the external bolt rows of the E2 joints configuration, as well as in the external and internal bolt rows, closer to the beam flanges, of the E3 joints configuration. Due to the fragile nature of bolts, this ductility should not be considered in the behaviour of the spring used to characterize this component.

A careful analysis to the end-plate in bending relationships indicate that the initial pre-load applied to the bolts influences the curves. The first elastic cycles start already with some force, corresponding to the pre-load installed in the bolts. With the transition to the plastic deformation, this load starts to decrease with the increase of plastic deformation. In some bolt rows this reduction can completely nullify the force of the pre-load, as observed in the external rows (first and fourth) of the E2-TB-E joint. In most cases some residual force of the pre-load force remains in the bolts. That explains why the curves do not reach zero force in the discharge. Some ratcheting effect is also notice in the response of the basic component end-plate in bending, possibly due to the plastic deformation of the bolts along with the plastic deformation of the end-plate. The steep backbone curve, of the first cycles in the plastic range, smooths with the increase of the plastic deformations. In Figure 5.60 is shown the incremental evolution of the forces in the bolt rows 1, 2 and 3 of the E3-TB-E joint. Confirming the previous statement,

in the beginning of the analysis bolts present already some level of force, due to the pre-loading of the bolts. After the elastic range (more or less at time step 30 seconds) bolts start to develop some plastic deformation and the force due to the pre-load start to decrease, reaching in some bolt rows the zero force, as in the first bolt row. On the other hand, in the second bolt row some residual force remains in the bolts. In the third bolt row the force due to the pre-load remains constant during the analysis. The small demand of this bolt row is shown in the $F-\Delta$ relationships of the E3 joints. This is more evident in the E3-TB-E joint due to the stronger end-plate, in the case of the E3-TB-P the end-plate reaches the plastic deformation of the end-plate sooner redistributing forces faster to the innermost bolt rows, leading to a higher demand of this bolt rows.

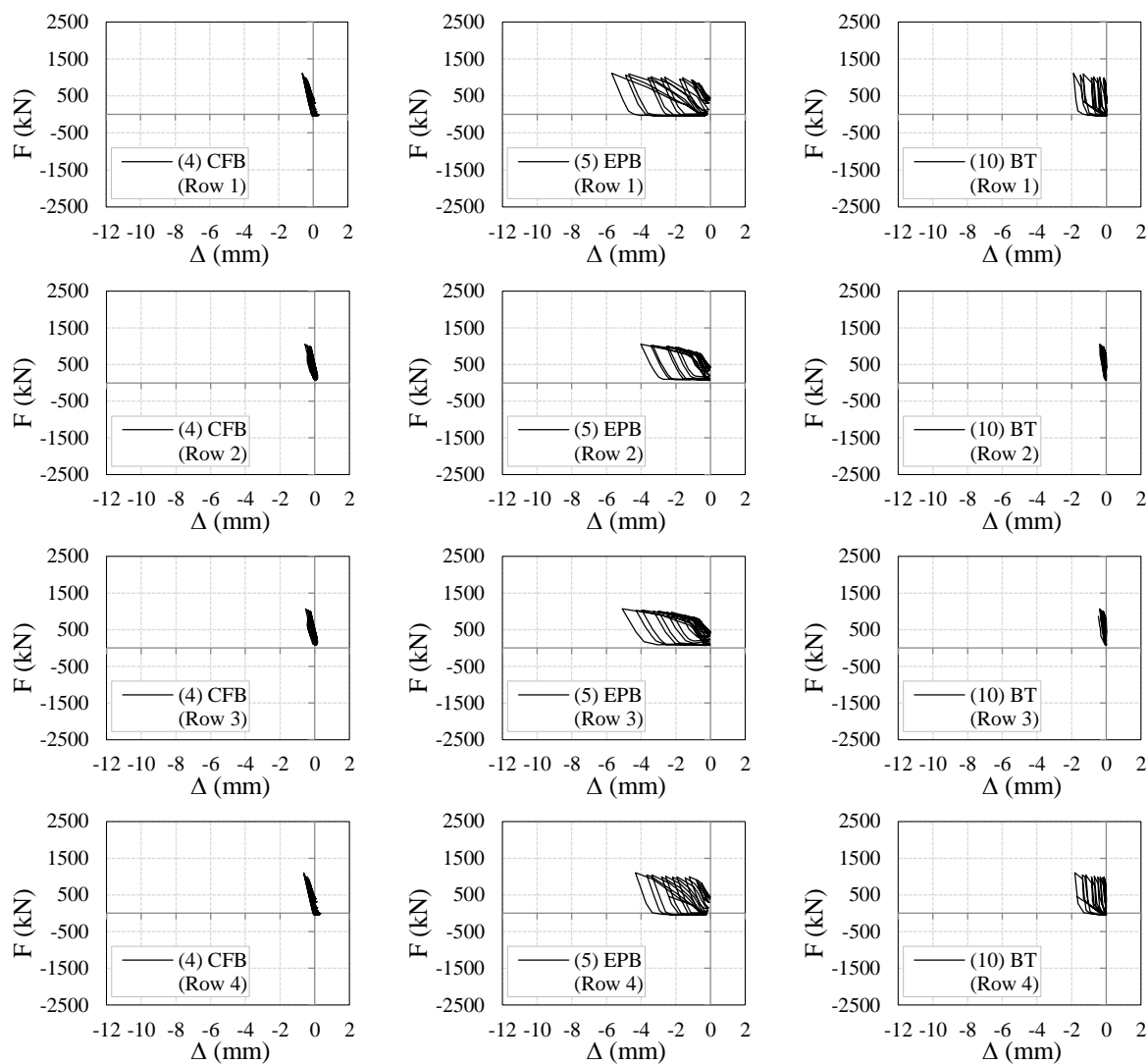


Figure 5.56: $F-\Delta$ curves for the connection components for each bolt row, for E2-TB-E joint.

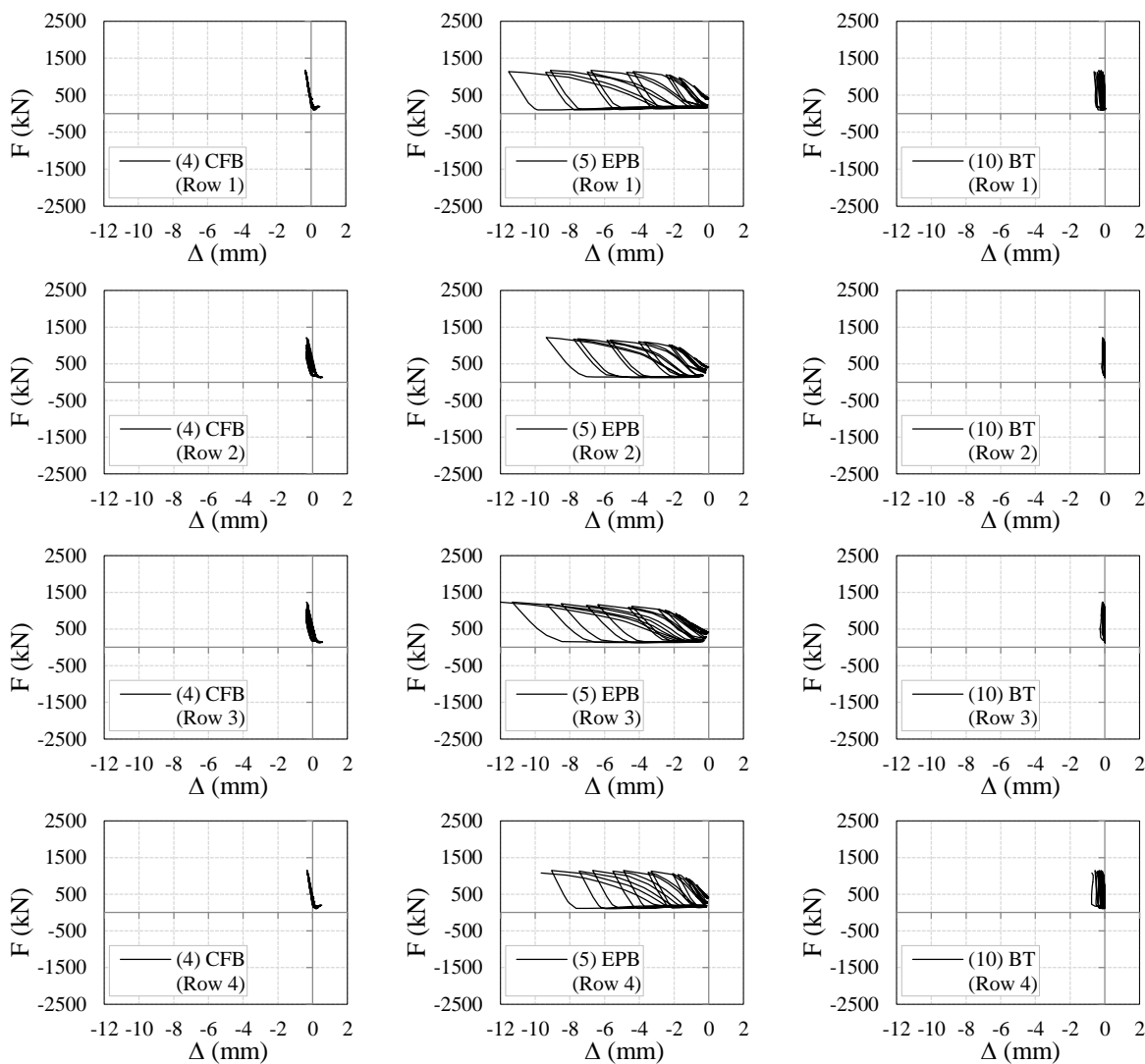


Figure 5.57: F-Δ curves for the connection components for each bolt row, for E2-TB-P joint.

5.7 MAIN CONCLUSIONS

In this chapter the proposed methodologies developed in Chapters 3 and 4 were applied to a set of joints designed according to the EC3-1-8 (EN 1993-1-8, 2005). The joint selection was defined in the context of an European research project (Landolfo, 2014). The study cases include internal and external beam-to-column joints, designed as equal and partial-strength joints, according to the strength of the joint in relation to that of the connected beams.

Preliminary finite element models (FEM) of the selected joints were developed, using nominal values for the steel grade chosen (S355), using though the material overstrength factor, proposed in the Eurocode 8, to take into account the variability of the steel properties.

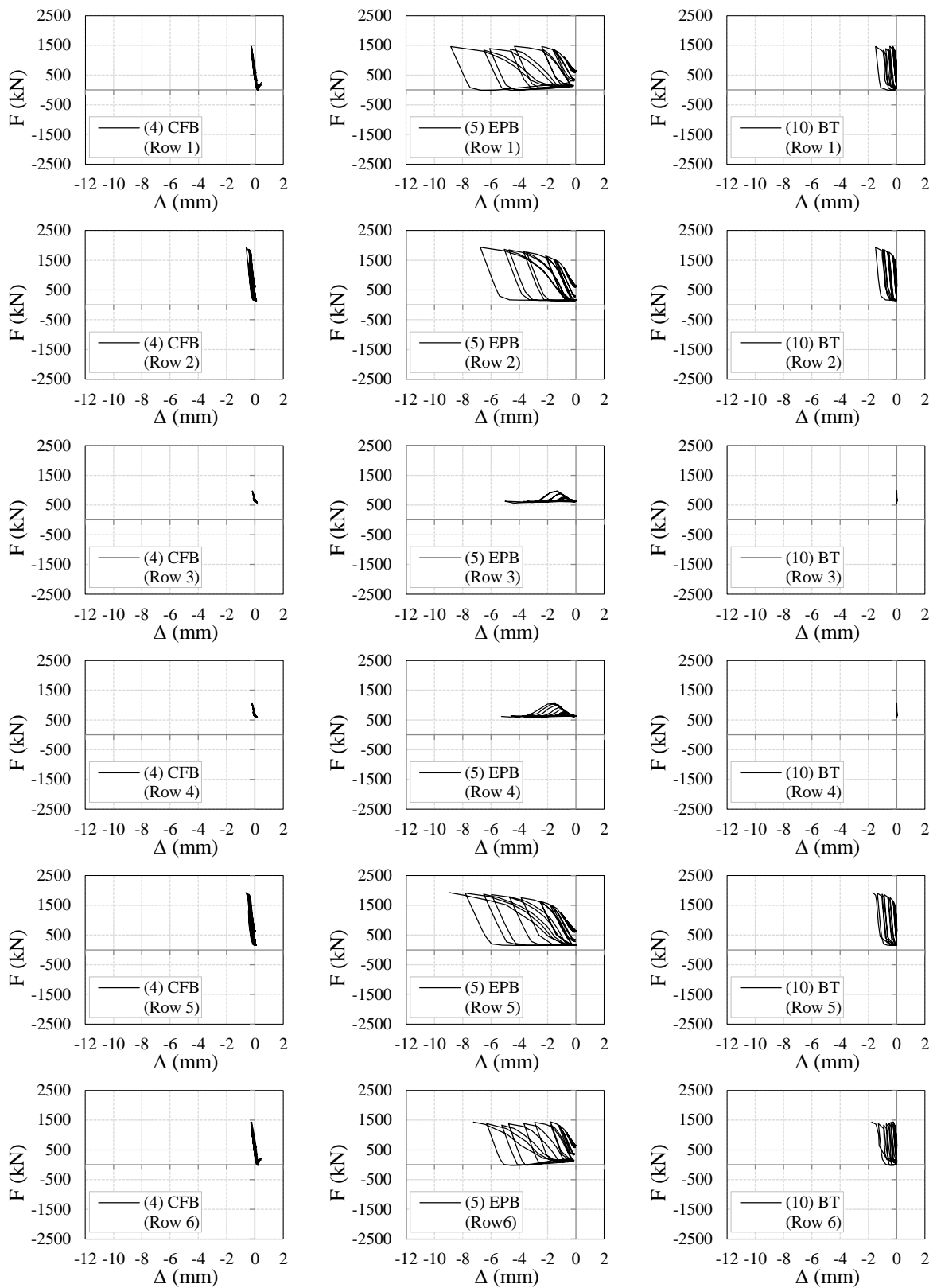


Figure 5.58: F- Δ curves for the connection components for each bolt row, for E3-TB-E joint.

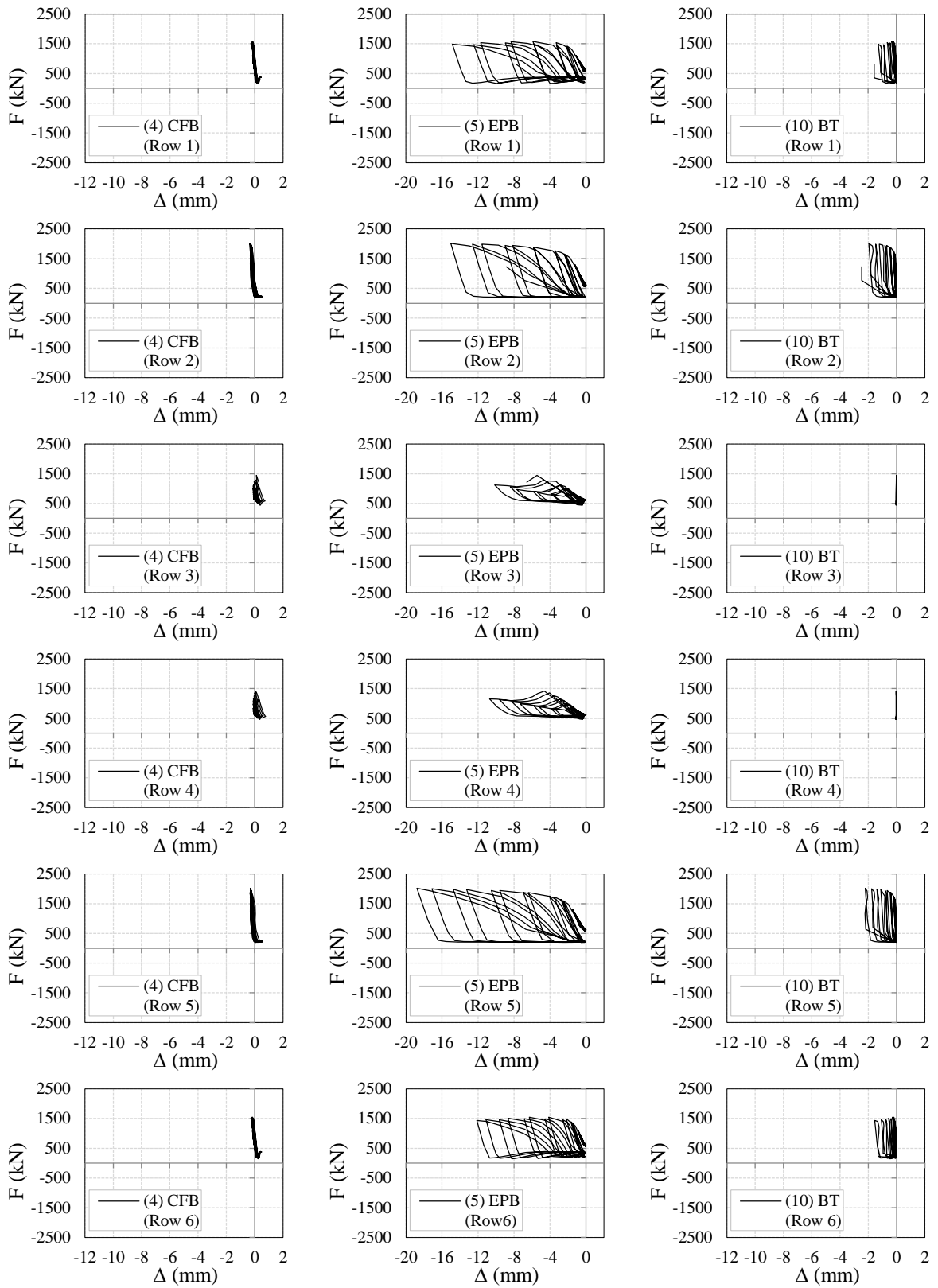


Figure 5.59: F- Δ curves for the connection components for each bolt row, for E3-TB-P joint.

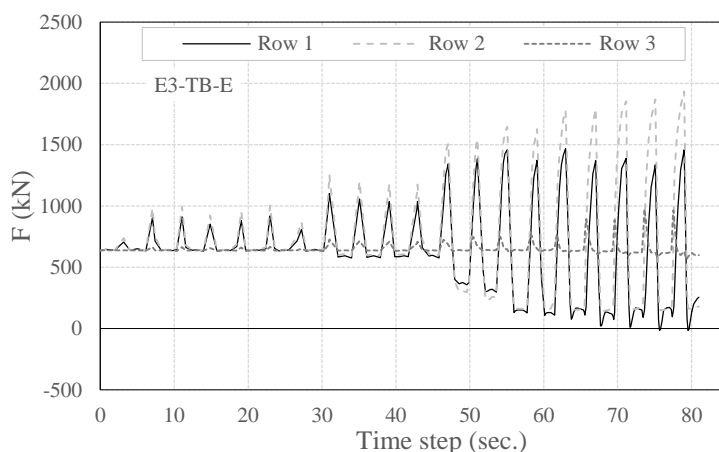


Figure 5.60: Evolution of the forces in the three top bolt rows, with the time step, of the E3-TB-E joint.

The comparisons revealed that the design predictions from the EC3-1-8 (EN 1993-1-8, 2005) fitted very well the numerical models results, in the case of both external equal-strength joints and internal partial-strength joints. However, for the external partial-strength joints the results of the FEM were considerably higher than the corresponding analytical ones. In terms of the initial stiffness comparison, for the case of the E2 joints with smaller beam section (IPE450), the analytical predictions presented closer results to the ones achieved with the FEM results. In the case of E3 joints, with higher beam section (IPE600) the differences in the initial stiffness are considerably higher, achieving differences between 14% and 19%, being always higher in the case of the FEM response.

A parametric study was undertaken using finite element models. The objective was to study some geometrical and mechanical properties in the joints that have the potential to influence the joints behaviour. The chosen parameters were: the presence of the continuity column web stiffeners; the influence of an addition bolt row located in the axis of symmetry of the joints; the influence of two additional bolt rows in the extended part of the end-plate; and the sensitivity to the end-plate mechanical properties.

The presence of transverse web stiffeners increases the initial stiffness and resistance of the joints. In the unstiffened joints an additional component gain some relevance, the column flange in bending, in the global response of the joint and in the accumulated energy dissipated. The transverse web stiffeners and the column flanges confine the major plastic deformations of the column web panel in shear, which is an advantage to control the plastic damage. For the unstiffened joints the pinching effect was more notorious, mainly in the partial-strength joints.

There is no apparent influence of the additional middle bolt row for the joints behaviour to bending moment. The influence of second external bolt row is only notorious for larger rotations, after the first external bolt row suffers plastic deformation the second bolt row becomes active.

The response of the joints is significantly affected by the mechanical properties of the end-plate, especially in the partial-strength joints, due to their slender end-plates. There is an increase of the pinching effect with the decrease of the end-plate mechanical properties and thickness. With the improvement of the mechanical properties of end-plate the contribution of the component column web panel in shear, to the global energy dissipation, grows and the contribution of the component end-plate in bending decreases.

The parametric study allowed to conclude that the variability often detected in the steel structures can affect significantly the joints behaviour, and the idealized design principles. The contribution of the column web stiffeners to the joints strength, stiffness and stability makes their use recommended. The additional bolt rows were not as effective as expected and their used should be balanced with economical gain and with other aspects like the durability or the redundancy in case of accidental actions, or even to avoid instability problems in slender plates.

The preliminary developed finite element models for the external beam-to-column joints were updated with the mechanical properties, obtained from the coupon tests and compared with the results of the available experimental tests results of the joints. A comparison of the nominal properties of the steel grade adopted for the joints members and plates, with the average of the ones found in the material tests, revealed that the adoption of the material overstrength factor recommended by the Eurocode 8 ($\gamma_{ov} = 1.25$) is in this case on the unsafe side. The real variation factor is found to be, in most cases, higher than the proposed material overstrength factor (γ_{ov}). The joints were redesigned with the updated mechanical properties, revealing that the initial assumptions can change significantly the design of the joints, namely the failure modes behaviour. The comparisons between the moment-rotation relationships obtained from the FEM, updated with the mechanical properties of the coupon tests, and the envelope of the experimental tests results revealed an excellent agreement. It was also verified that the response of the joints present a stable behaviour without strength degradation, although it is possible to observe some degradation of stiffness for the larger cycles.

Finally, the basic components of the external beam-to-column end-plate joint were extracted from the finite element models created, using the procedures developed in Chapters 3 and 4. The joints were divided into two zones: column web zone and the connection zone, where the basic components were identified, according to the EC3-1-8 definition. The components extracted are the following: column web panel in shear (1); column web in transverse compression; (2) and column web in transverse tension (3). For the column web panel zone. And for the connection zone the components are: column flange in bending (4), end-plate in bending (5) and bolts in tension (10).

The basic component column web panel in shear presented a stable behaviour for all joints. For the components column web in transverse tension and compression the transverse web stiffeners significantly condition their response. In the compression side the response was almost elastic and in the tension side only the internal bolt rows presented a substantial contribution to the joint rotation, the external ones also remained almost elastic.

For the connection components only the end-plate in bending contributed significantly to the joint non-linear rotation, the other connection components remaining elastic. The extraction of the forces of the basic connection components was obtained by the integration of the stress fields in the bolts section, due to the presence of transverse web stiffeners. It was found that the initial pre-load applied to the bolts influenced the force-deformation responses. Furthermore, it was observed that the force due to the pre-load of the bolts decreases with the increase of the plastic deformations in the bolts. The analysis of the force-deformation curves led to the conclusion that the derived relationships, for the component end-plate in bending, presents some ratcheting effect. Possibly due to the plastic deformation of the bolts along with the plastic deformation of the end-plate. It was also found that the steep backbone curve of the first cycles in the plastic range, of the end-plate in bending curves for each bolt row, smooths with the increase of the plastic deformations.

The proposed methodologies developed in Chapters 3 and 4 were able to extract the basic components behaviour of the finite element models of the beam-to-column end-plate joints under cyclic loading conditions. The results can be applied directly in a mechanical model scheme similar to the one presented in Figure 4.1.

6

EQUIVALENT VISCOUS DAMPING ASSESSMENT IN MRF WITH END-PLATE PARTIAL-STRENGTH JOINTS

6.1 INTRODUCTION

In the framework of a research project (Calvi *et al.*, 2015), a study was conducted to determine ductility-equivalent viscous damping relationships (μ -EVD) for steel moment-resisting frames (MRF) with partial-strength end-plate bolted joints. The main objective of the project was to develop a displacement-based seismic design procedure for steel MRF structures capable of considering the contribution of the beam-to-column joint behaviour, since the joint selection may significantly affect the seismic behaviour and the building costs.

In the case of steel MRF structures with partial-strength beam-to-column joints, there may be a shift of the energy dissipation mechanism from the beams to the joints during a seismic event. Hence, it is of paramount importance to accurately assess the joints behaviour and how they affect the ductility-equivalent viscous damping relationship, which is a key parameter in the context of application of displacement-based seismic design procedures.

The parametric numerical model of the joints developed in Chapter 3 was the ideal tool to obtain the required relationships. Therefore, a large parametric study was undertaken, on sub-assemblages (see Figure 6.1 a) representative of MRF structures having partial-strength joints and subjected to several real earthquake records, representative of two different ground motions. Different elastic periods of the sub-assemblage could be considered by changing the system mass. Furthermore, the system was targeted for several ductility levels.

A series of representative bolted end-plate partial-strength joints covering the different features of their behaviour were designed and are described and characterized. To this end, the script presented in Annex B was developed using programming language Python. This script allows the easy parametric generation of FE models for the bolted end-plate partial-strength joints, which were validated against monotonic and cyclic experimental data in Chapter 3. The beam-to-column sub-assembly shown in Figure 6.1 a) uses the generated joint models and was employed to carry out non-linear time-history (NLTH) analyses, acted by real seismic records scaled to achieve several levels of ductility. A new procedure is then applied to the NLTH analyses results for the derivation of ductility-equivalent viscous damping relationships to be used in the Direct Displacement-Based Design (DDDB) method (Priestley *et al.*, 2007). In this context, the knowledge acquired in the joints modelling and calibration was successfully used to obtain the needed μ -EVD relationships in that method. Furthermore, a comparison and discussion is undertaken between the results obtained in the parametric study with those obtained from available expressions recommended by Priestley *et al.* (2007) for several hysteretic shapes.

6.2 PROCEDURE DEVELOPED FOR THE ASSESSMENT OF EQUIVALENT VISCOUS DAMPING

A procedure was developed to derive the ductility-equivalent viscous damping relationships for MRF with partial-strength bolted joints. A set of sub-assemblages representing SDOF systems with hysteretic characteristics representative of partial-strength joints were analysed using the NLTH procedure for a wide range of ductility levels and effective periods. The sub-assemblages were subjected to sets of accelerograms with different levels of intensity, in order to achieve different levels of system ductility. The calibration was carried out by identifying, for a given record, the level of damping that resulted in the same displacement demand of an elastic system with effective period T_e as an inelastic system with the partial-strength flexible joint hysteretic characteristics and with elastic viscous damping only. The procedure is illustrated in Figure 6.1.

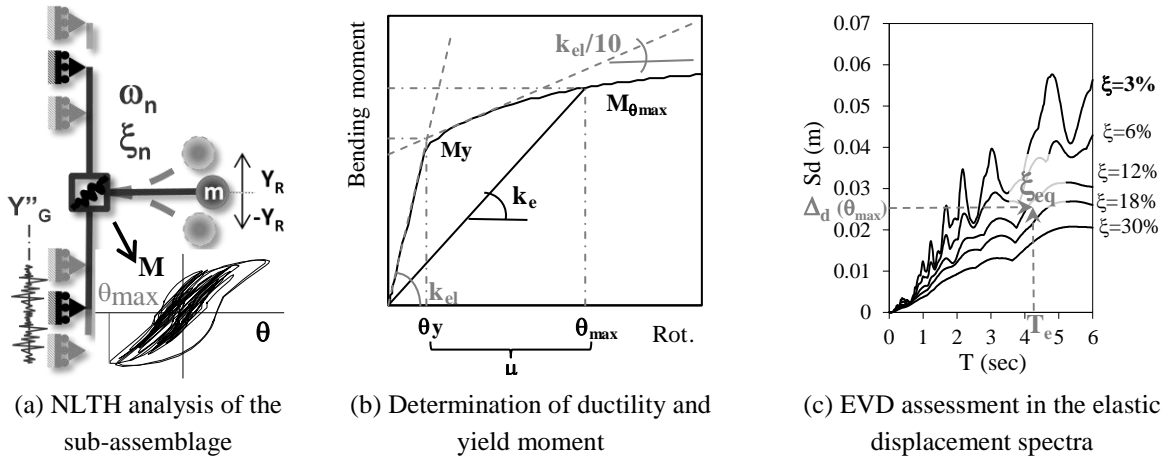


Figure 6.1: Procedure to determine the equivalent viscous damping.

The linearization of the inelastic response of the partial-strength end-plate connection is obtained by applying the developed procedure as follows:

- from the NLTH analysis using a given record, for a given mass, m , elastic period, T_{el} , and setting the level of elastic viscous damping ξ_{el} (see Figure 6.1 (a)) the maximum response of the FE model sub-assembly is determined;
- the yield point ($\theta_y; M_y$) is then determined by the linearization of the monotonic response curve previously obtained (Figure 6.1 (b)) using the ECCS (1986) procedure, and the achieved ductility μ is calculated by evaluating the ratio between the maximum displacement (rotation) and the yield displacement (rotation), given by:

$$\mu = \theta_{\max} / \theta_y \quad (6.1)$$

using the monotonic response curve (pushover) of the connection, the bending moment corresponding to the maximum rotation is obtained and the secant stiffness, k_e , and the effective period T_e are determined using the following expressions:

$$k_e = \frac{M_{\theta_{\max}}}{\theta_{\max}} \quad (6.2)$$

$$T_e = \frac{2\pi}{\sqrt{k_e/m}} \quad (6.3)$$

- the displacement spectra of the record under consideration are determined for several values of viscous damping (ξ) (Figure 6.1 (c)); in this study, the SeismoSignal (2012) software package was used to determine the displacement spectra. With the effective

period, T_e , and the target displacement, Δ_d , (corresponding to the max rotation, θ_{max}) the equivalent viscous damping, ξ_{eq} , is determined interpolating a more precise value in the displacement spectra.

The procedure described above is applied to a wide range of periods and ductility demands. It is possible to determine the ductility-EVD relationships for the different joints behaviours found in engineering practice, namely the ones that lead to the several failure modes according to Eurocode 3 Part 1-8 (EN 1993-1-8, 2005). These relationships can then implemented in the DDBD procedures for MRF structures with partial-strength joints, as illustrated in Figure 6.2.

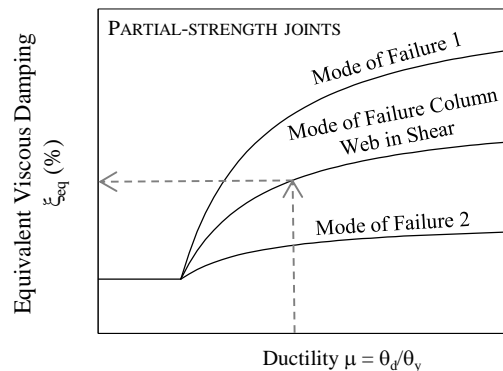


Figure 6.2: Example of μ -EVD relationship chart.

6.3 DESIGN AND CHARACTERIZATION OF THE END-PLATE JOINTS

6.3.1 JOINTS DESCRIPTION

A set of representative partial-strength joints covering the different features of their behaviour are numerically simulated. The criteria adopted allow the connections to exhibit the following features:

- Similar properties to those already studied and analysed.
- Partial-strength behaviour.
- One of the following:
 - post-elastic behaviour governed by column panel zone in yielding;

- post-elastic behaviour governed by yielding of the end-plate in bending – plastic mechanism according to failure mode 1;
- post-elastic behaviour governed by yielding of the end-plate in bending – plastic mechanism according to failure mode 2.

Five different joints were chosen to fulfil the previous criteria. Table 6.1 summarises the details of each connection.

Table 6.1: Connections description.

Connection	% of beam moment resistance	Description
C1	~90%	J3.2 used in Chapter 3
C2	~120%	Modified to fulfil the EC3 requirements, strengthening the web and the end-plate
C3	~75%	Based on the C2, reduction of the column strength (HEB320 to HEA320)
C4	~75%	Based on the C2, reduction of the end-plate, failure mode 1 according to the EC3
C5	~75%	Based on the C2, reduction of the end-plate, reduction of the bolts diameter and strength class, failure mode 2 according to the EC3

The J3.2 model used in the validation, Chapter 3, was selected to be the reference joint specimen, named C1. The C2 connection is a full-strength full-rigid joint, due to the presence of web stiffeners and end-plate thickness, being a control connection for the partial-strength ones. The geometry of the C2 joint will be changed, in the next joints, to achieve the required strength level and failure modes desired. The other three connections are designed to achieve the same level of strength, but with different governing failure modes, in order to understand their influence. C3 is a partial-strength connection governed by yielding of the column web panel zone. To ensure the web column panel yielding, the column was changed to an HEA 320 and the column stiffeners were removed. On the other hand, C4 and C5 connections have the same level of strength as C3, but in this case, the governing plastic mechanism is the end-plate in bending. A smaller end-plate thickness ensures the plastic mechanism type one according to the EC3-1-8 (EN 1993-1-8, 2005) for the C4 connection. In addition, a balanced reduction of the end-plate thickness, bolt diameter and bolt class ensures a plastic mechanism type two for the C5 connection. The sub-assembly with the joint's geometrical properties, for the FE model are described in Table 6.2 summarising the geometrical details of each joint, according to Figure 6.3.

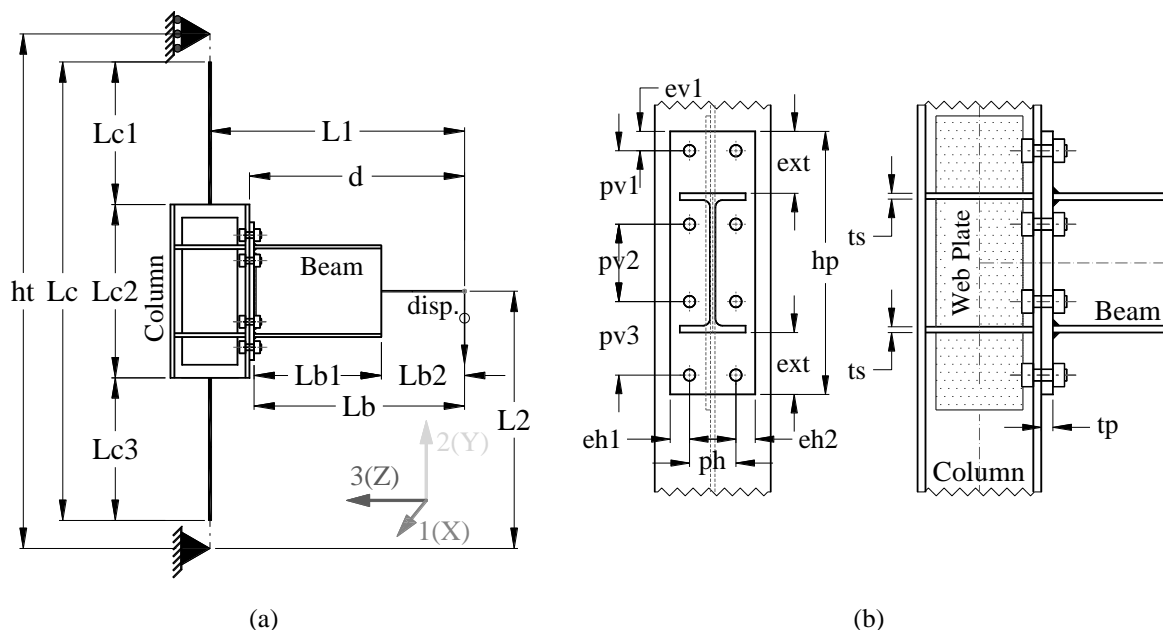


Figure 6.3: (a) Sub-assembly geometric properties (b) joint geometry.

Table 6.2: Geometrical properties of the FE models and joints.

	ht	Lc	Lc1	Lc2	L1	L2	Lb	Lb1	d	hp	bp	tp	pv1	pv2	pv3	eh1	ph	eh2	db	bclass	ext	ts	twp
C1	3229	3009	1207	840	1338	1492	1160	468	1178	540	220	18	100	240	100	55	110	55	24	10.9	90	15	no
C2	3500	3250	1290	920	1320	1625	1100	468	1160	680	220	60	190	200	190	50	120	50	30	10.9	160	15	12
C3	3500	3250	1260	980	1315	1625	1100	468	1160	680	220	60	190	200	190	50	120	50	30	10.9	160	no	no
C4	3500	3250	1290	920	1278	1625	1100	468	1118	680	215	18	190	200	190	50	115	50	30	10.9	160	15	12
C5	3500	3250	1290	920	1287	1625	1100	468	1127	680	220	27	190	200	190	50	120	50	24	8.8	160	15	12

Dimensions in mm;
ev1 = 50mm.

6.3.2 ANALYTICAL AND NUMERICAL RESULTS

The connections were calculated analytically, according to the rules prescribed in EC3-1-8 (EN 1993-1-8, 2005) and also numerically using ABAQUS models. Table 6.3 summarises the results obtained from analytical calculations. The analytical calculations were performed assuming the partial safety factors $\gamma_M = 1.00$ in order to be possible to compare with the numerical calculations. For the stiffness classification, a beam length of 7.5m was considered. The steel properties were kept equal for all the specimens, even for the 40mm thicker plates, using the ductility requirements of Eurocode 3 Part 1.1 (clause 3.2.2) (EN 1993-1-1, 2005) for the S355 steel grade. It is worth mentioning that the requirements of clause 6.2.7.2(9) of EC3-1-8 were disregarded, in order to ensure a better comparison with the FE models.

Table 6.3: Analytical results according to EC3 part 1-8.

	C1	C2	C3	C4	C5
M_{j,Rd} (kNm)	337.0	438.0	263.9	255.6	281.6
S_{j,ini} (kNm/rad)	74464	105733	55499	52525	71516
Stiffness classification	Semi-rigid (65%)	Semi-rigid (93%)	Semi-rigid (49%)	Semi-rigid (46%)	Semi-rigid (63%)
Class of strength:	Partial strength (93%)	Full strength (121%)	Partial strength (73%)	Partial strength (71%)	Partial strength (78%)
Dominant comp. / shear components:	BFWC: F _{c,fb,Rd} 1041.6 (kN)	BFWC: F _{c,fb,Rd} 1041.6 (kN)	CWT: F _{c,wc,Rd} 592.1 (kN)	BFWC: F _{c,fb,Rd} 1041.6 (kN)	BFWC: F _{c,fb,Rd} 1041.6 (kN)
	Bolts row 1	Bolts row 1	Bolts row 1	Bolts row 1	Bolts row 1
	EPB: F _{t1,Rd} 459.4 (kN)	CFB: F _{t1,Rd} 805.0 (kN)	CFB: F _{t1,Rd} 535.9 (kN)	EPB: F _{t1,Rd} 123.9 (kN)	EPB: F _{t1,Rd} 264.7 (kN)
	Mode 2	Mode 2	Mode 1	Mode 1	Mode 2
	Bolts row 2	Bolts row 2	Bolts row 2	Bolts row 2	Bolts row 2
Dominant tension components:	EPB: F _{t2,Rd} 520.5 (kN)	CFB: F _{t2,Rd} 236.6 (kN)	CFB: F _{t2,Rd} 56.2 (kN)	EPB: F _{t2,Rd} 652.8 (kN)	EPB: F _{t2,Rd} 508.3 (kN)
	Mode 2	Mode 2	Mode 1	Mode 1	Mode 3
	Bolts row 3	Bolts row 3	Bolts row 3	Bolts row 3	Bolts row 3
	EPB: F _{t3,Rd} 61.7 (kN)	CFB: F _{t3,Rd} 0 (kN)	CFB: F _{t3,Rd} 0 (kN)	EPB: F _{t3,Rd} 265.0 (kN)	EPB: F _{t3,Rd} 268.6 (kN)
	Mode 2	Mode 2	Mode 1	Mode 1	Mode 3
BFWC	Beam or column flange and web in compression EC3-1-8 (6.2.6.7)				
CWT	Column web in transverse compression EC3-1-8 (6.2.6.2)				
EPB	End-plate in bending EC3-1-8 (6.2.6.5)				
CFB	Column flange in bending EC3-1-8 (6.2.6.4)				

Connection C1 is governed by the end-plate in bending, which corresponds to a type 2 failure mode, i.e. bolt failure with yielding of the column flange. Due to the lower lever arm, the third bolt row cannot develop its full resistance. On the compression side, the governing component is the beam flange or web in compression. In the case of the C2 connection, it is the beam that governs the connection strength. On the tension side, the first bolts-row is governed by the component column flange in bending, with a failure mode type 2. The resistance of the second bolt-row has to be reduced to avoid exceeding the resistance associated to the beam flange or web in compression. The third bolt row is inactive. For the C3 connection, the first bolt-row is governed by the column flange in bending in a failure mode of type 1, consisting of complete yielding of the flange. Concerning the second bolt-row, the resistance of the column web in transverse compression limits the resistance and hence the third bolt-row is inactive. In the C4 connection, the end-plate in bending governs the first two bolts-rows, in a failure mode of type 1. The third bolt row cannot develop its full resistance, due to the lower lever arm. On

the compression side, the governing component is the beam flange or web in compression. Finally, in the C5 connection, the two first bolt rows on the tension side are governed by the component end-plate in bending (type 2 failure mode for the first bolt row and type 3 for the second bolt row). The third bolt row cannot develop its full resistance, due to the lower lever arm. On the compression side, the governing component is the beam flange or web in compression.

For the monotonically loaded models, the moment-rotation relationship is plotted in Figure 6.4. The relationships were obtained using Eq. (3.7) for the moments and Eq. (3.12) for the rotations. A comparison of the analytical results and the moment-rotation envelope obtained with clause 6.3.1(6) of EC3-1-8 is also performed. The plastic mechanisms identified in the numerical models of the joints through the analysis of the stress patterns, during the monotonic analysis, are depicted in Figure 6.5. From the figure, it is possible to state that connection C1 exhibited a plastic mechanism similar to the type 2 failure mode, showing a plastic hinge line near the lower beam flange and plastic hinges in the bolts in tension that may lead to rupture. It is also possible to observe plastic deformation in the column web panel. As expected, connection C2 responded in the elastic range with a plastic hinge forming in the beam. Connection C3 was clearly governed by the column web panel in shear, but also showing higher stress concentrations in transverse tension and transverse compression in the web, due to the absence of the transverse web stiffeners, confirming the design predictions. Connection C4 exhibited a type 1 plastic mechanism, with the formation of three plastic hinges in the end-plate before the bolts yield in tension. Connection C5 exhibited a type 2 plastic mechanism, similar to that developed in connection C1, but with a clearly lower rotation capacity due to the stiffened column web. The response of the components is shown in Figure 6.6. It allows the comparison of the main dissipative components in the joints, determined using the Eq. (3.7) for the bending moment assessment Eq. (3.15) to determine the rotations associated to the component column web panel in shear and Eq. (3.17) to assess the rotation associated to the connection. From the figures it is possible to observe that joints C1 and C3 are governed by the column web panel behaviour, presenting a column web rotation roughly twice the rotation due to the end-plate deformation. In the remaining joints the response in the column web panel is apparently elastic, due to the additional column web plates consider. Joints C4 and C5 are

governed by the component end-plate in bending, although C4 is clearly more ductile than the C5.

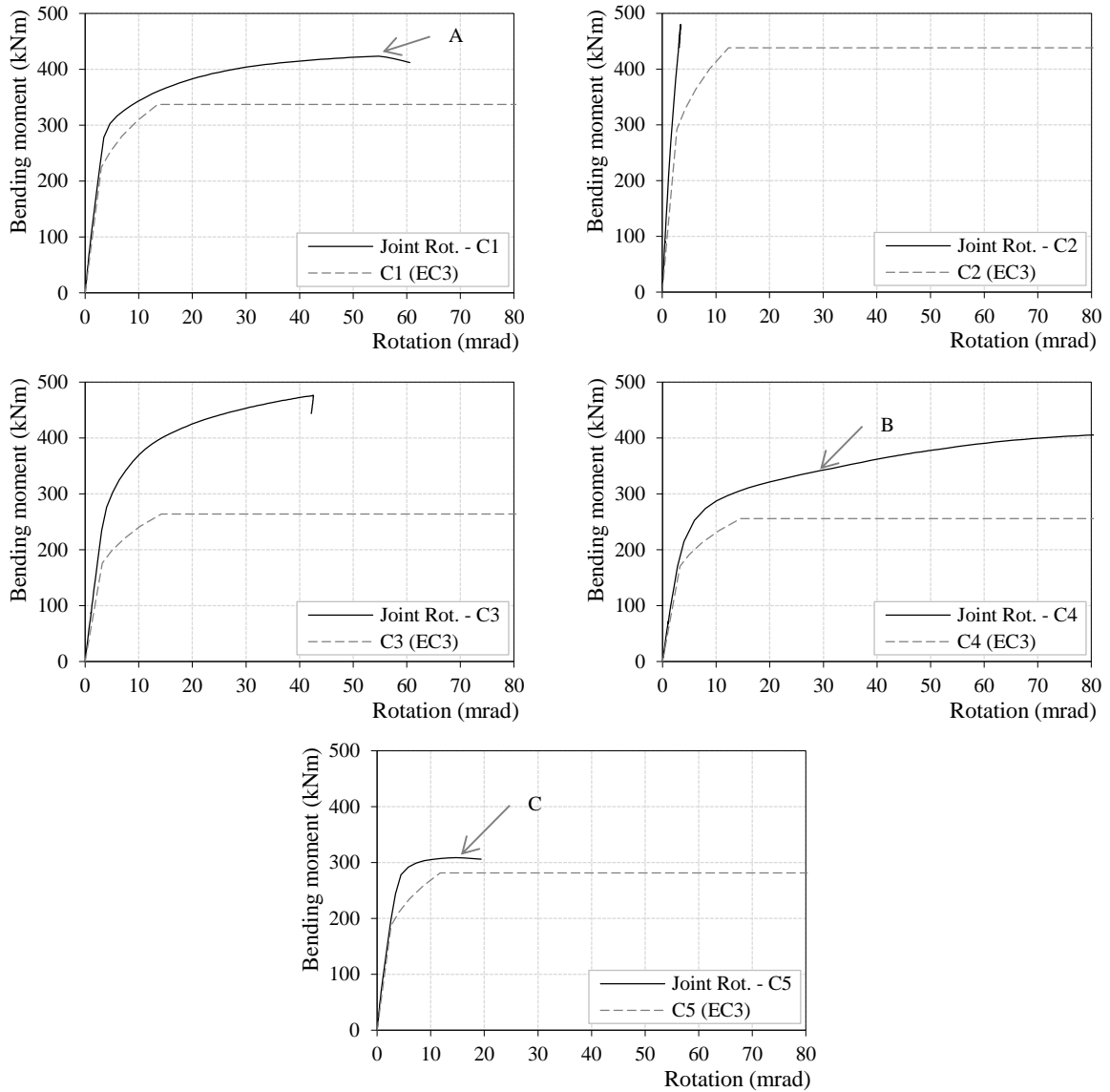


Figure 6.4: Monotonic results for the C1 to C5 joints.

To perform an analytical comparison of the results, the ECCS (1986) procedure was applied to the numerical results to assess the joints strength (M_y) and stiffness (k_{el}), as illustrated in Figure 6.1 (b) and exemplified in Figure 6.9 (a) for the C1 connection. The comparison between the analytical and numerical responses reveals, on one hand, a balanced agreement in terms of strength and in the case of the initial stiffness and, on the other hand, an apparent difficulty of the EC3-1-8 to reach the higher values obtained in the ECCS procedure when applied to the numerical approach. The comparisons are presented in Table 6.4 and in

Figure 6.7. The most significant differences occurred in joints C2 and C3 in terms of stiffness, with differences of around 40% and for the other joints, the differences were lower than 15%. In terms of strength, the C3 joint presented the most obvious difference where an increase of around 23% was observed with the numerical model, which could be justified by the higher non linearity of the C3 joint as it is essentially governed by the column web in shear, which makes the determination of the yield point difficult to assess. The C1 joint also showed considerable difference of over 12%, but in this case, a lower strength value in the numerical response was recorded. The strength results obtained for the joints C4 and C5 revealed good agreement between the numerical and the analytical results.

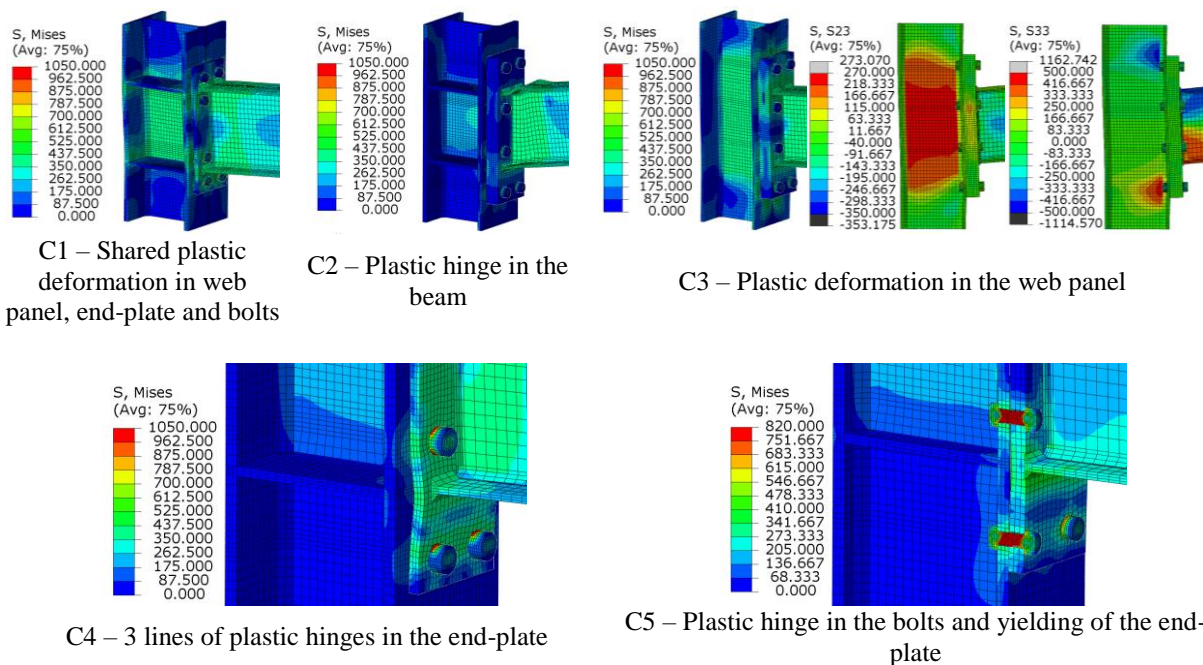


Figure 6.5: Plastic mechanisms identification through the analysis of the stress patterns.

The cyclic loading cases were analysed using the same joint geometry and material properties (adopting the combined isotropic/kinematic hardening model as in Chapter 3) and using the loading protocol depicted in Figure 6.8. The yield rotation (θ_y) was derived from the monotonic results employing the ECCS (1986) procedure, which is illustrated for the C1 joint in Figure 6.9, allowing also to determine the initial stiffness, $S_{j,ini}$, and the yield moment, here assumed as the joint strength, $M_{j,Rd}$. The yield rotation and the beam tip relative displacement

(Δ_y) can be also observed in the same figure, disregarding the elastic deformation of the column and beam.

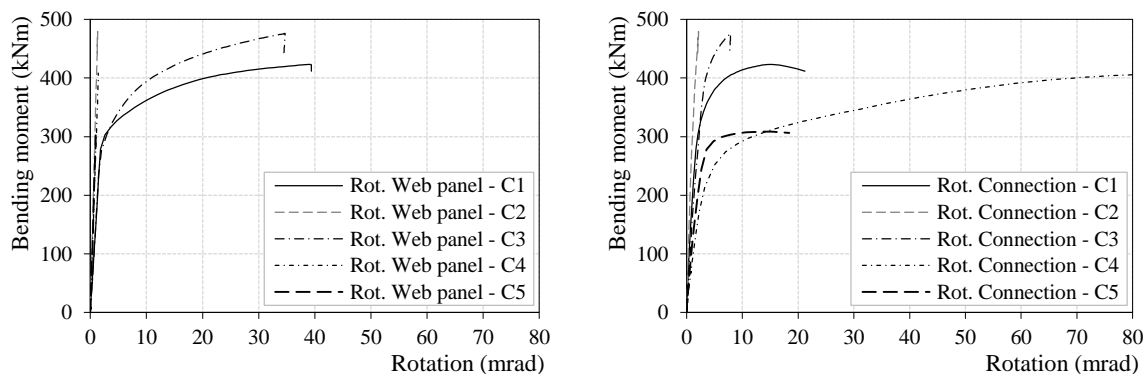


Figure 6.6: Monotonic results for the components of the joints C1 to C5.

The results can be seen in Figure 6.10, for the global joint rotation and for the main dissipative components column web in shear and the end-plate in bending. The results from the cyclic analyses confirm that the model is capable of representing different types of behaviour governed by the main dissipative components in the connections, namely the end-plate in bending and the column web panel in shear.

Table 6.4: Analytical results summary.

Joints	Joints results			Classification			Failure mode		
	$M_{J,Rd}$ (kN.m)	$S_{j,ini}$ (kN.m)	$S_{j,ini}$ Rigid limit	Strength	Stiffness	Weakest Comp.	Failure mode (EC3)		
Analytical calculations									
C1	337	74464	113890	Partial-strength	93%	Semi-rigid	65%	End-plate	2
C2	438	105733	113890	Full-strength	121%	Semi-rigid	93%	Column flange	2
C3	264	55499	113890	Partial-strength	73%	Semi-rigid	49%	End-plate	1
C4	256	52525	113890	Partial-strength	71%	Semi-rigid	46%	End-plate	1
C5	282	71516	113890	Partial-strength	78%	Semi-rigid	63%	End-plate	2
Numerical calculations									
C1	294	83384	113890.00	Partial-strength	81%	Semi-rigid	73%	End-plate	2
C2	480	143340	113890.00	Full-strength	133%	Rigid	126%	Beam	-
C3	325	78480	113890.00	Partial-strength	90%	Semi-rigid	69%	Web-panel	-
C4	253	59925	113890.00	Partial-strength	70%	Semi-rigid	53%	End-plate	1
C5	273	78814	113890.00	Partial-strength	75%	Semi-rigid	69%	End-plate	2

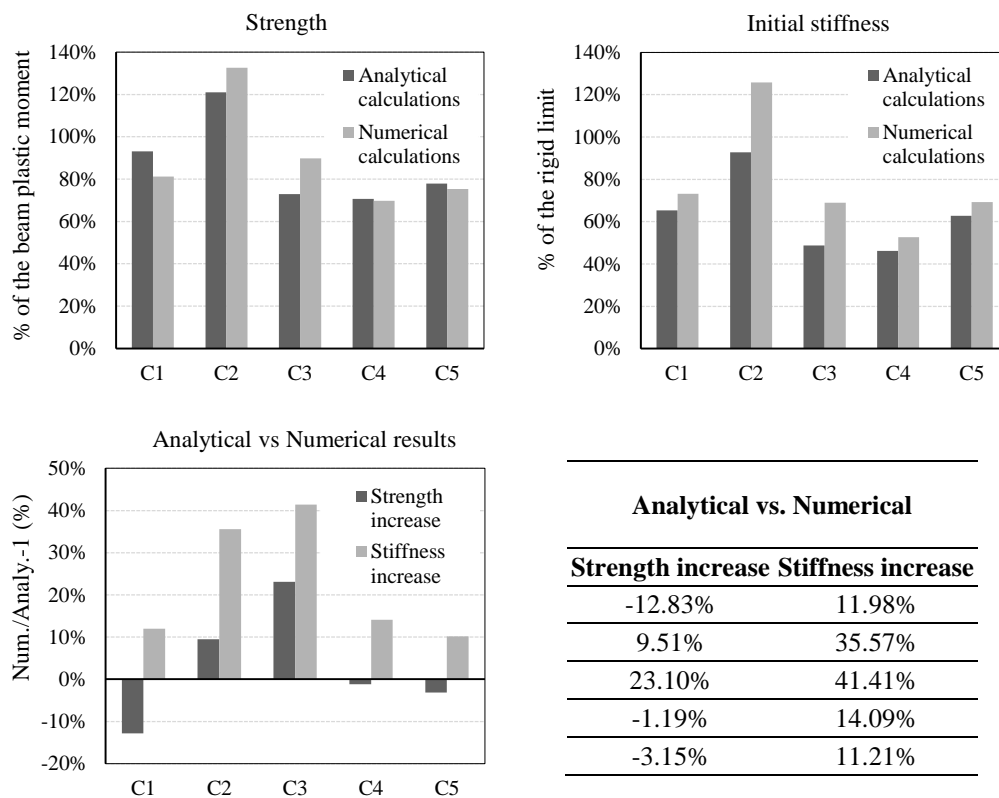


Figure 6.7: Comparison of strength and stiffness results.

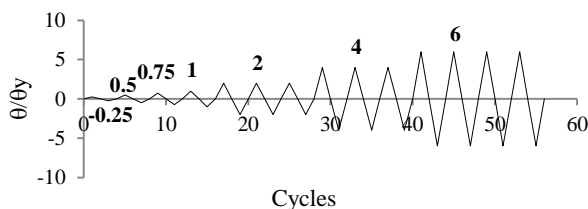


Figure 6.8: ECCS load protocol.

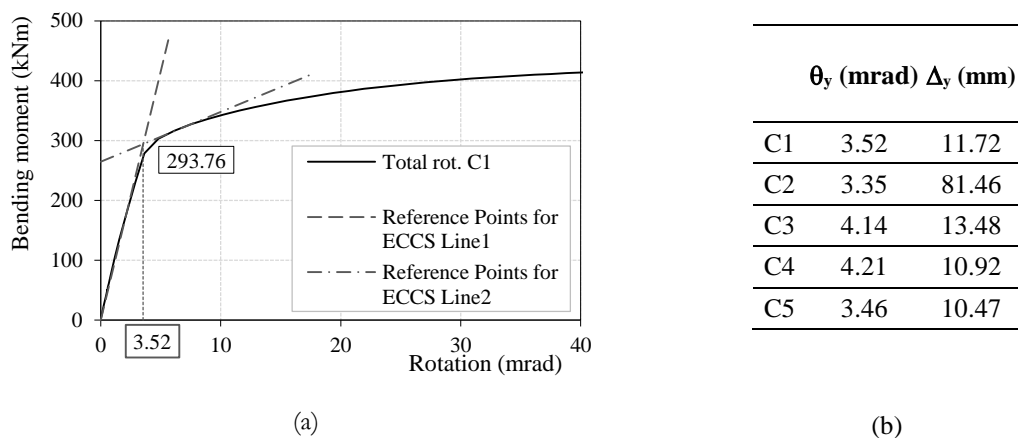
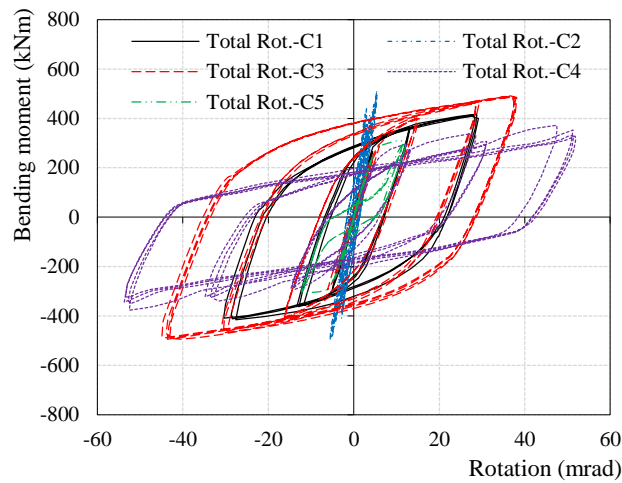
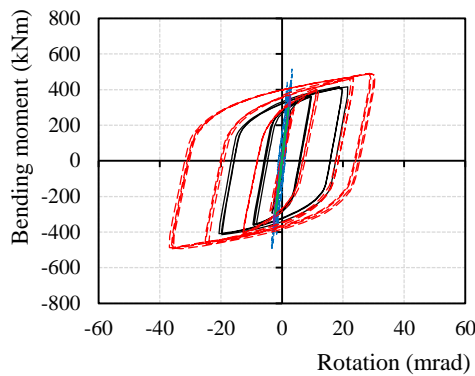


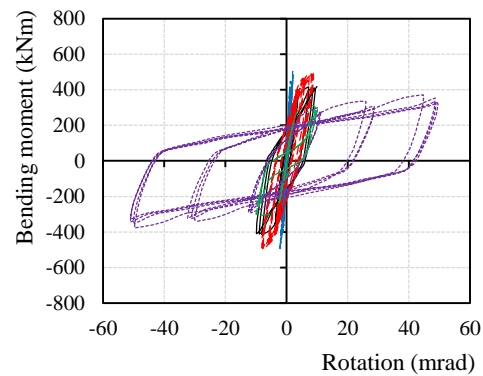
Figure 6.9: (a) Example of the assessment of the θ_y according to the ECCS procedure for the C1 joint, and (b) the results for the remaining joints.



(a) Rotation of the joint.



(b) Rotation of the column web panel.



(c) Rotation of the connection.

Figure 6.10: Cyclic response comparison for the joints C1 to C5.

6.3.3 FINAL REMARKS

With the objective of defining several end-plate bolted joints representative of partial-strength joints with several failure modes identified in the EC3-1-8, a set of joints were designed using the procedure proposed in EC3-1-8 and also using the finite element simulation of the joints to support the design. A comparison between the numerical and analytical results, obtained by means of the component method prescribed in EC3-1-8, revealed a good agreement in terms of the failure modes obtained as well as a reasonable agreement in the strength achieved for each joint. However, concerning the initial stiffness, some discrepancies were found on the results, which indicates some possible limitations regarding the application of the component method to determine the initial stiffness of the joints. This was mainly observed for the joints governed by yielding of the web column in shear, C3, and the ones that exhibited elastic behaviour, C2.

In terms of the cyclic loaded models, it became evident from the results obtained that the FE models are capable of representing different types of behaviour governed by the main dissipative components in the connections, namely the end-plate in bending and the column web panel in shear.

The designed joints will be used in the following section to perform a parametric study aiming at the assessment of ductility-equivalent viscous damping relationships.

6.4 DUCTILITY-EQUIVALENT VISCOUS DAMPING RELATIONSHIPS

6.4.1 JOINT SELECTION

Within the previous designed partial-strength joints four were chosen to assess the ductility-equivalent viscous damping relationships, namely C1, C3, C4 and C5. As explained before, the connections were designed to develop different plastic mechanisms corresponding to the various failure modes defined in EC3-1-8 (EN 1993-1-8, 2005), where C1 and C5 are governed by the plastic mechanism type 2, C4 is governed by the plastic mechanism type 1 due to the reduced end-plate thickness and C3 is governed by the column web in shear plastic mechanism. C1 has the same geometry as the J3.2 used in the FE models validation, in Chapter 3, where the contribution of the column web in shear is also significant in this joint.

In the procedure presented in the Section 6.2, the monotonic behaviour of the joints is used firstly to determine the elastic deformation limit, θ_y , and secondly, to determine the corresponding bending moment for the maximum rotation achieved in the NLTH analysis. For each joint, the monotonic response for positive and negative bending moment was determined, imposing a positive or negative displacement on the beam end, and the yield rotations were derived from the monotonic results employing the ECCS (ECCS, 1986) procedure, which is illustrated in Figure 6.1 (b). The main results are presented in Table 6.5. The bending moments were obtained with Eq. (3.7), and the rotations were obtained using Eq. (3.13), modified to consider the elastic deformation of the column, since it is intended to study the equivalent viscous damping of the system (MRF structures) with partial-strength joints. In the table are also presented the bending moments, rotations and displacements, determined using

the ECCS procedure for the yielding point, for the joints ($M_{y(j)}$ and $\theta_{y(j)}$) and for the global system ($M_{y(sys)}$, $\theta_{y(sys)}$ and $\Delta_{y(sys)}$).

For the generation of significant inertia force and, consequently, bending moments and rotations at the connection during the NLTH analyses it was necessary to consider a concentrated mass, m , to the model, applied in the beam end. The masses were determined in an iterative process using frequency analyses in the several joints, see Figure 6.11 for the period $T_{el} = 1.0s$, in order to obtain, for the elastic periods of the system, $T_{el} = 0.5s$, $T_{el} = 1.0s$ and $T_{el} = 2.0s$. The masses considered are also provided in Table 6.5. Note that in this iterative procedure a tolerance is set for the period. In this case the tolerance was defined to be 0.1%. This is a very precise methodology to assess the required periods.

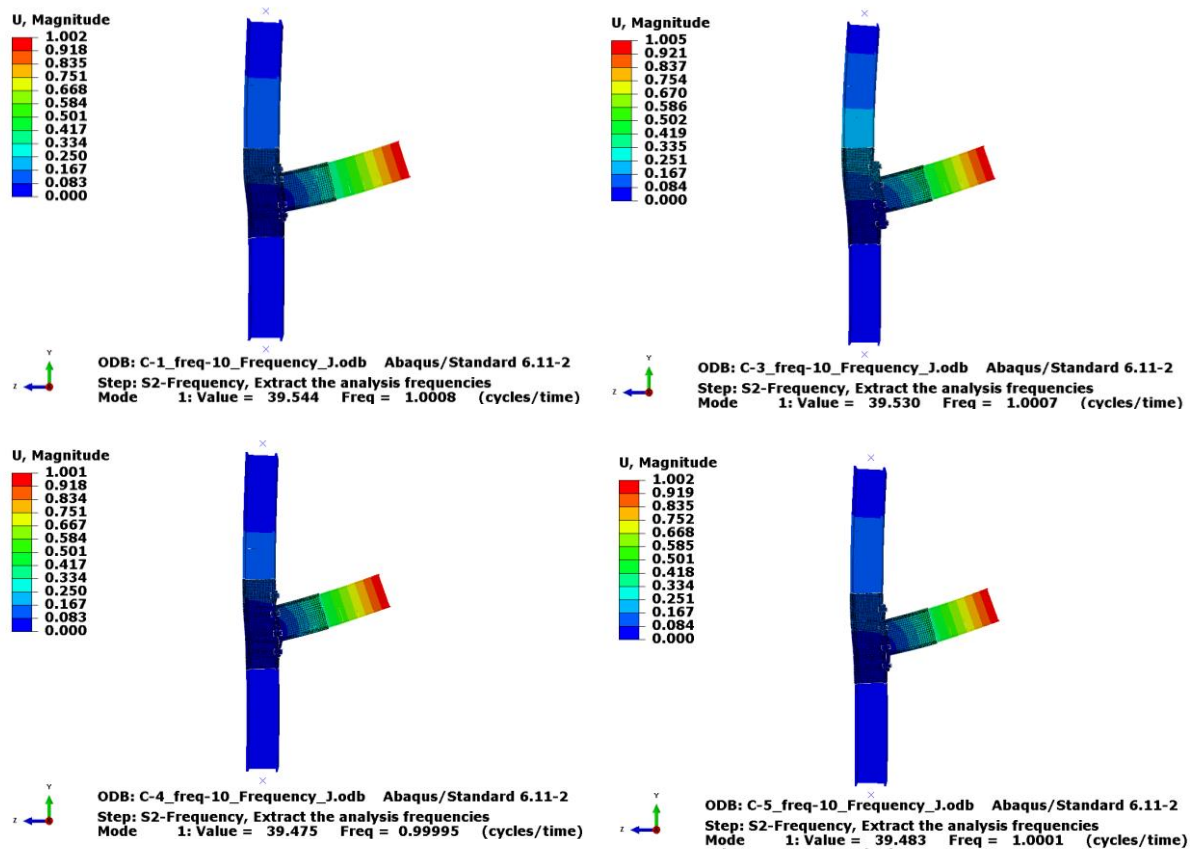
Table 6.5: Connections properties for the EVD assessment.

	$M_{y(j)}^+$	$M_{y(sys)}^+$	$\theta_{y(j)}^+$	$\theta_{y(sys)}^+$	$\Delta_{y(sys)}^+$	$M_{y(j)}^-$	$M_{y(sys)}^-$	$\theta_{y(j)}^-$	$\theta_{y(sys)}^-$	$\Delta_{y(sys)}^-$	Mass		
											$T_{el} = 0.5$	$T_{el} = 1.0$	$T_{el} = 2.0$
C1	294	303	3.52	4.91	11.72	-293	-302	-3.49	-4.86	-11.57	159.375	637.500	2560.00
C3	327	349	4.28	6.70	13.71	-325	-346	-4.22	-6.62	-13.61	158.750	634.375	2550.00
C4	253	260	4.22	5.53	10.92	-253	-262	-4.12	-5.47	-10.87	136.250	545.313	2180.00
C5	273	276	3.46	4.77	10.51	-273	-279	-3.60	-4.96	-10.79	174.063	696.875	2787.50

Bending Moments in kNm, rotations in mrad, displacements in mm, periods in seconds and mass in tones.

The elastic damping, ξ_{el} , is incorporated in the models through the use of Rayleigh damping with a value of 3% of critical damping. Stiffness-proportional damping according to Eq. (6.4) was used and applied to the first elastic period, which is determined with a modal analysis performed in ABAQUS ($T_{el} \approx 0.5s$, $T_{el} \approx 1.0s$ and $T_{el} \approx 2.0s$).

$$\beta_k = \frac{T_{el} \xi_{el}}{\pi} \quad (6.4)$$

Figure 6.11: Frequency analyses for $T_{el} = 1.0s$.

6.4.2 SEISMIC INPUT

A set of twenty records obtained from real earthquakes were used, which are spectral compatible with the EC8 (EN 1998-1, 2004) spectra defined for soils type A (LA1r to LA10r) and soils type C (LC1r to LC10r), see Table 6.6. The LA record set, see Figure 6.12, was selected to be compatible with the EC8 spectrum for soil type A, and the LC record set, see Figure 6.13, was selected to be compatible with the EC8 spectrum for soil type C. For further information see Maley *et al.* (2013). Note that, to save some computational time, the records were cut in the time domain by eliminating the initial or the tail part with lower seismic activity when possible, while still maintaining the original acceleration and displacement spectra. The differences obtained from the original spectra and the reduced ones were lower than 1%. The acceleration and displacement spectra, for $\xi_{el} = 3\%$, are represented in Figure 6.14.

The equal displacement rule was adopted to estimate the scaling factor to consider for each record and for each target ductility, at most 5, to achieve in the NLTH analyses the

expected spectral displacement. For that the displacement spectra, for the corresponding elastic period T_{el} and $\xi_{el} = 3\%$, of each record and the previously determined displacement at elastic limit values ($\Delta_{y(sys)}$) for each joint were used. For each record and joint configuration the five scale factors are achieved.

Table 6.6: Record description.

	Earthquake	Station Name	Earth. mag.	ClstD (km)	Vs30 (m/s)	Scaling factor ⁺	Time step (sec)	Max accel. (g)
LA1	Denali, Alaska	R109 (temp)	7.9	43	964	6.5	0.01	0.387
LA2	Chi-Chi, Taiwan	TCU085	7.62	58	1000	5.8	0.005	0.339
LA3	Chi-Chi, Taiwan	TAP065	7.62	122	1024	6.1	0.005	0.140
LA4	Chi-Chi, Taiwan	KAU003	7.62	114	914	5.2	0.004	0.094
LA5	Darfield	Rata Peats	7.1	93**	-	13.4	0.02	0.490
LA6	Loma Prieta	So. San Francisco, Sierra Pt.	6.93	63	1021	7.2	0.005	0.402
LA7	Loma Prieta	So. San Francisco, Sierra Pt.	6.93	63	1021	6.8	0.005	0.715
LA8	Irpinia, Italy-01	Auletta	6.9	10	1000	7.9	0.0029	0.457
LA9	Northridge-01	Sandberg - Bald Mtn	6.69	42	822	6.2	0.01	0.483
LA10	Northridge-01	Antelope Buttes	6.69	47	822	12.7	0.02	0.580
LC1	Chi-Chi, Taiwan	CHY082	7.62	36	193.69	2.1	0.005	0.143
LC2	Kocaeli	KOERI Botas	7.51	127	274.5	7.9	0.005	0.596
LC3	Landers	CDMG 14368 Downey – Co Maint Bldg	7.28	157	271.9	4.0	0.02	0.206
LC4	Hector	Mecca - CVWD Yard	7.13	92	345.4	2.9	0.01	0.294
LC5	St Elias, Alaska	USGS 2728 Yakutat	7.54	80	274.5	1.5	0.005	0.089
LC6	Loma Prieta*	USGS 1028 Hollister City Hall	6.93	28	198.8	1.8	0.005	0.451
LC7	Northridge-01	Neenach - Sacatara Ck	6.69	52	308.6	5.8	0.01	0.251
LC8	Superstition Hills-02	Westmorland Fire Sta	6.54	13	193.7	2.3	0.005	0.485
LC9	Imperial Valley-06	El Centro Array #1	6.53	22	237.33	5.1	0.005	0.643
LC10	Chi-Chi, Taiwan-03*	TCU061	6.2	40	272.6	5.6	0.005	0.373

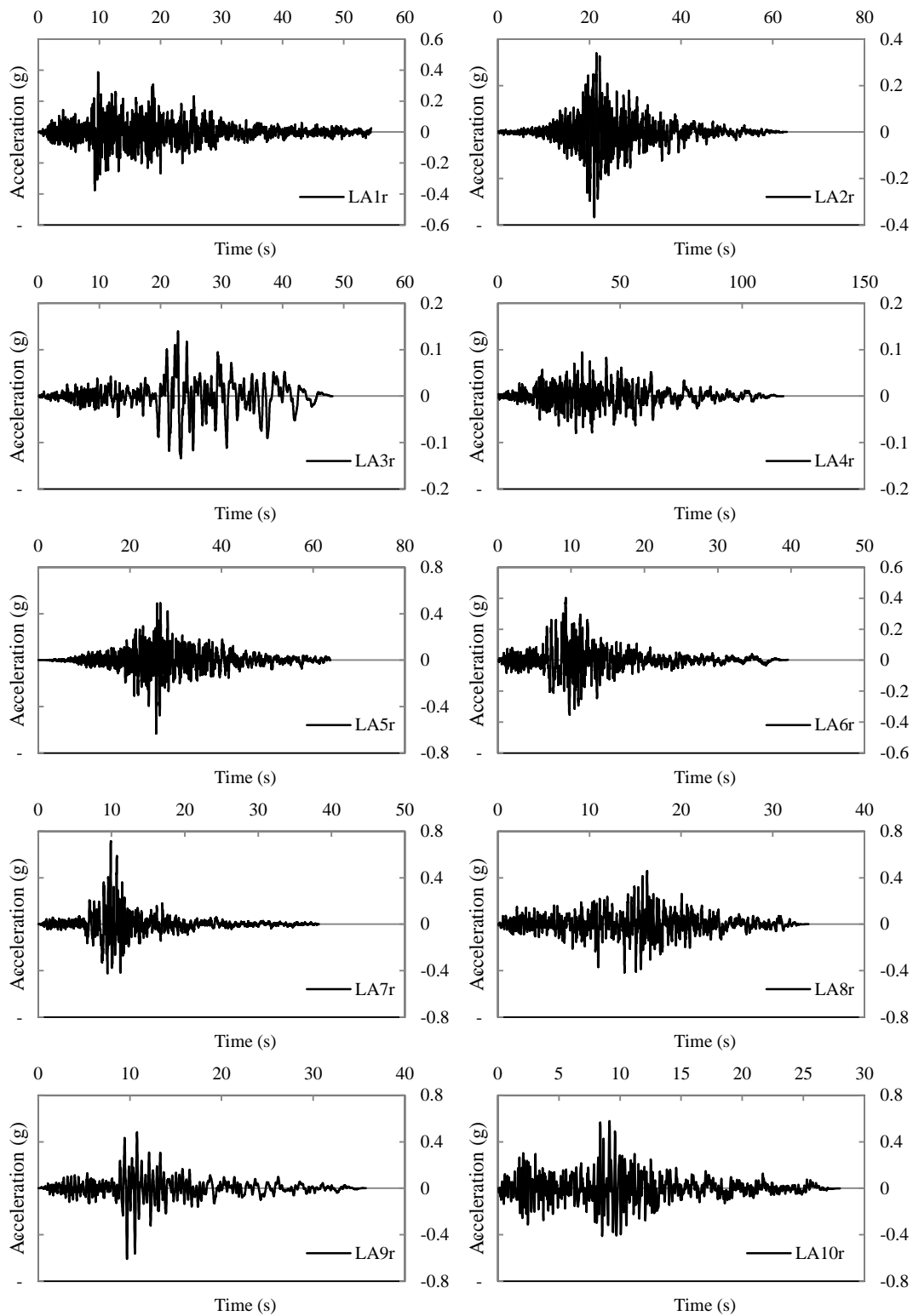


Figure 6.12: Records for the soil type A.

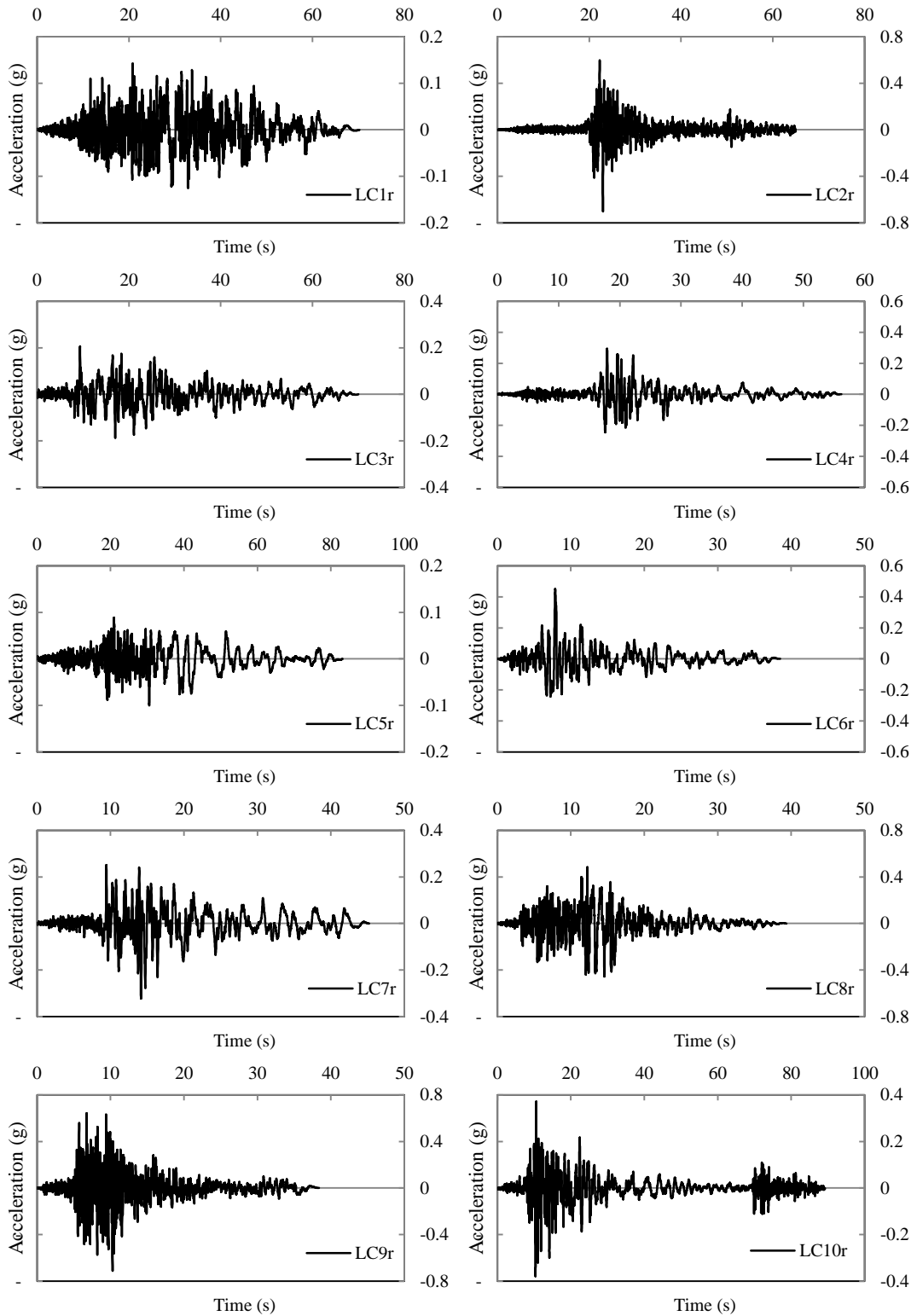


Figure 6.13: Records for the soil type C.

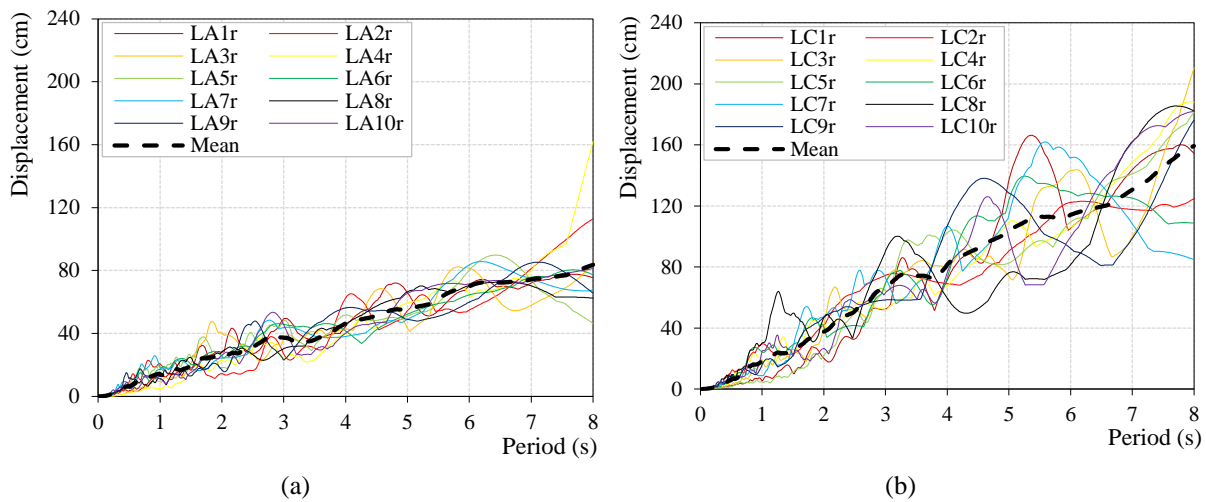


Figure 6.14: Displacement response spectra for: (a) LA set; and (b) LC set.

6.4.3 ANALYSIS PROCEDURE

Using the developed FE models for the joints C1, C3, C4 and C5 a large parametric study was undertaken. The study comprised 1000 NLTH analyses with complete FE models with up to 87313 elements and 295915 equations to solve. For this task a powerful computation and automation system was used. As explained earlier, to generate specific elastic and effective periods it was necessary to add a concentrated mass to the system applied at the beam tip. The masses were determined, using frequency analyses, in order to achieve three levels of system initial elastic periods ($T_{el,1} = 0.5s$, $T_{el,2} = 1.0s$, $T_{el,3} = 2.0s$). An elastic damping, ξ_{el} , of 3% was adopted in all the analyses. Rayleigh stiffness-proportional damping coefficient associated to the steel material properties was considered. Finally, the ductility-equivalent viscous damping relationships are obtained applying the proposed procedure described in Section 6.2 to the NLTH analyses results.

Figure 6.15 shows some additional information about the analyses performed in the parametric study, namely the number of analyses used for the equivalent viscous damping assessment, the interval of imposed ductility levels and the effective periods achieved for each connection and record type.

It is important to mention that, although all the connections have been analysed for the same range of parameters (ductility levels, records and initial elastic period), not all combinations of parameters analysed resulted in valid solutions for the EVD procedure, due to convergence and ductility limitations. Nevertheless, an inspection of the figure allows

concluding that joint C5 presents the lower rate of success, with an average of 10 analyses against 13 achieved for the other joints. A fact that can be justified by the lower ductility achieved with this joint, directly related to driving component plastic mechanism (mode 2), bolts and the end-plate plastic deformation acting together, that could easily lead to exceed the resistance of the joint, for more demanding cases. The range of ductility levels achieved revealed that the initial estimates, which were based on the adoption of scaling factors estimated based on the equal displacement rule, were, in most cases, very far from the ones actually obtained in the analyses. In some cases the ductility levels achieved were three times higher than those initially defined. The joint configuration for which the rule performed better was joint C3 which, on average, achieved an interval between 1.2, for the lowest ductility level, and 5.9 for the highest, against the 1 and 5 initially defined. On the other hand, joint C1 was the one where the rule presented the highest discrepancy, demonstrated by the mean values of the lowest ductility level, 1.5 instead of 1, and the higher value 11.9 instead of 5. Regarding the effective periods achieved, it is possible to conclude that the expected values (between 0.5s and 5s), and those effectively achieved were very similar, since the effective period, unlike the ductility, is less sensitive to the uncertainties associated with the adoption of the equal displacement rule to estimate the scaling factors.

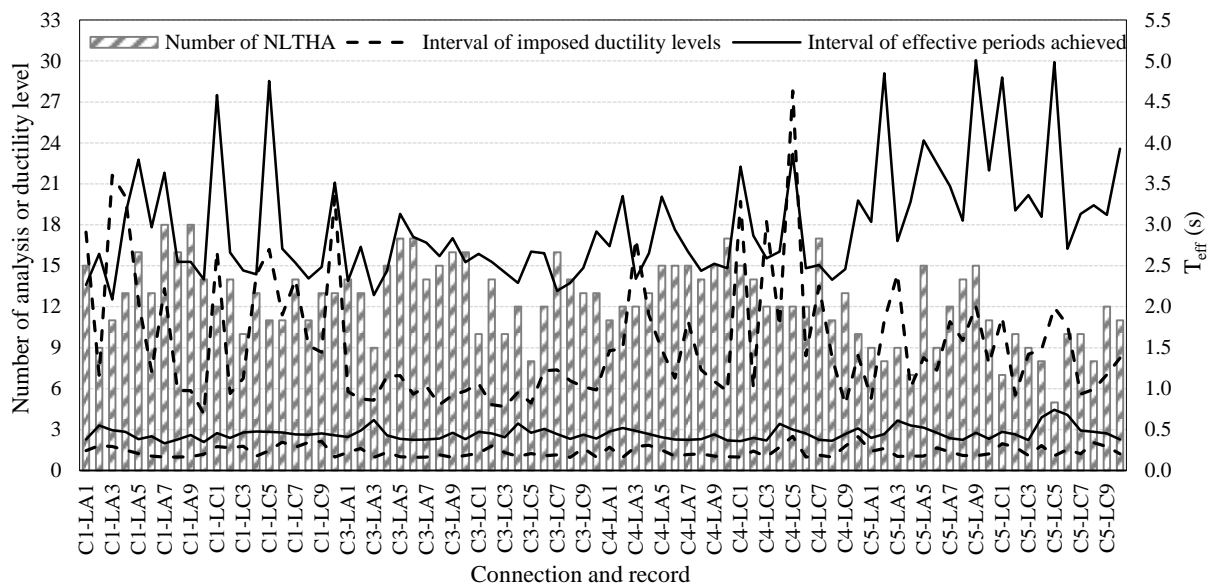


Figure 6.15: Additional information about the analyses.

Following the work of Priestley *et al.* (2007) and Dwairi *et al.* (2007), a modification to Eq. (2.33) will be proposed in the next section, taking the form of Eq. (6.5), which will take

into account a value of 3% for elastic damping, and the constant C will be derived using the ordinary least squares method fitting the EVD curves to the NLTH analyses results achieved.

$$\xi_{eq} = 0.03 + C \left(\frac{\mu - 1}{\mu\pi} \right) \quad (6.5)$$

6.4.4 DUCTILITY-EVD RELATIONSHIPS

The pairs of values between the ductility levels and the EVD are shown in Figure 6.16. Each point in the figure represents the application of the EVD procedure to a given joint typology, an effective period, a given record and a given ductility demand. In Figure 6.17 (a) are also depicted the mean EVD values, represented by the solid line, along with the standard deviation in dashed lines, quantitatively demonstrating the wide range of variation between the obtained results and the mean values. A closer look to the results is provided in Figure 6.17 (b), for the range of ductility levels with more prevalence. The Priestley *et al.* (2007) expressions are also represented in the figures.

The scatter detected in the results reveals that the relationship between the ductility and the EVD cannot be easily translated by a single curve; it is however interesting, from a codification point of view, to determine which correlations fit best the results obtained. It is also possible to observe that the expression proposed by Priestley *et al.* (2007) for steel MRF buildings, which is based on the assumption of the Ramberg-Osgood (RO) hysteresis rule, is not adequate for partial-strength joints. A fact that is not surprising for the reasons presented in Section 2.4.2.3. The existing curve is closer to an upper bound of the results obtained, whereas a considerable number of simulations revealed to have lower EVD values, a fact that is more evident for ductility levels between 1 and 6, see Figure 6.17 (b). The use of hysteretic rules more adequate to represent the pinching effect in end-plate joints, like the Takeda-Thin (TT) or even Takeda-Fat (TF), revealed also some inadequacy with the μ -EVD results, although the TT expression represents a clear improvement to the RO equation for partial-strength joints. The inadequacy of the existing expressions points out to the need for the development of a new expression for μ -EVD that is applicable for steel MRF with partial-strength end-plate joints.

An inspection of the figures allows concluding that there is a considerable number of simulations that resulted in EVD values lower than 3%, even for high ductility levels. Such behaviour was also identified by Penucci *et al.* (2011), which is justified by the jagged shape of

the response spectrum. This issue has an influence on the application of the procedure proposed in Section 6.2.

Looking at the global results, for the level of ductility equal to one, in the transition between the elastic and plastic range, the mean EVD value achieved is 2.5%, see Figure 6.17(b), which is very similar to what was expected, since the elastic damping adopted in the NLTHA was $\xi_{el} = 3\%$, proving that the accuracy of the input data.

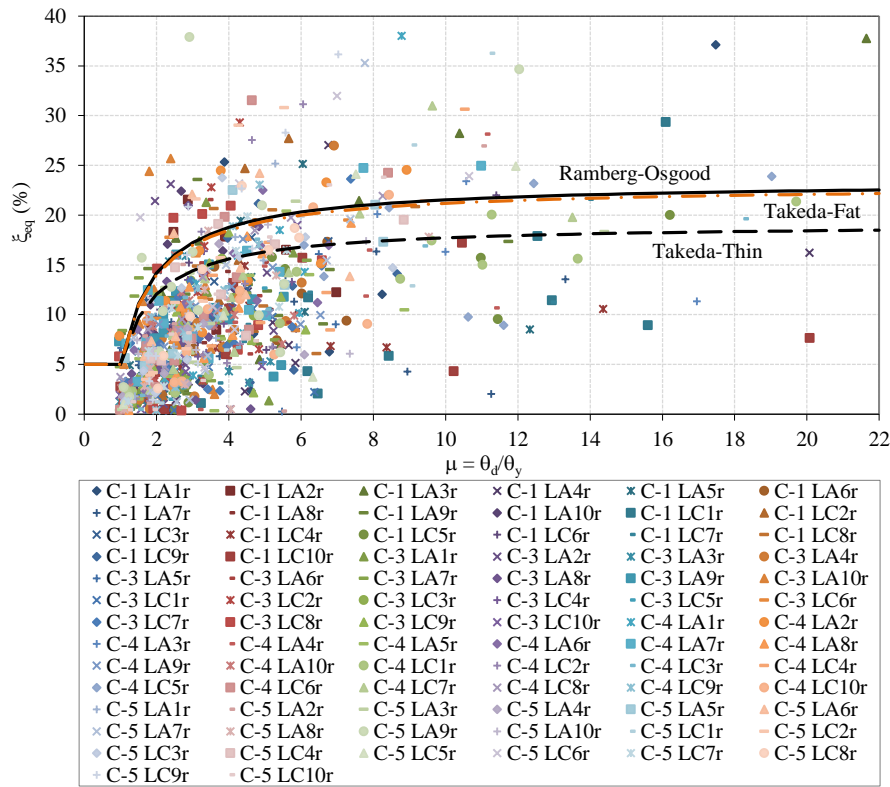


Figure 6.16: Comparison of the EVD results with the proposed expressions Priestley *et al.*(2007).

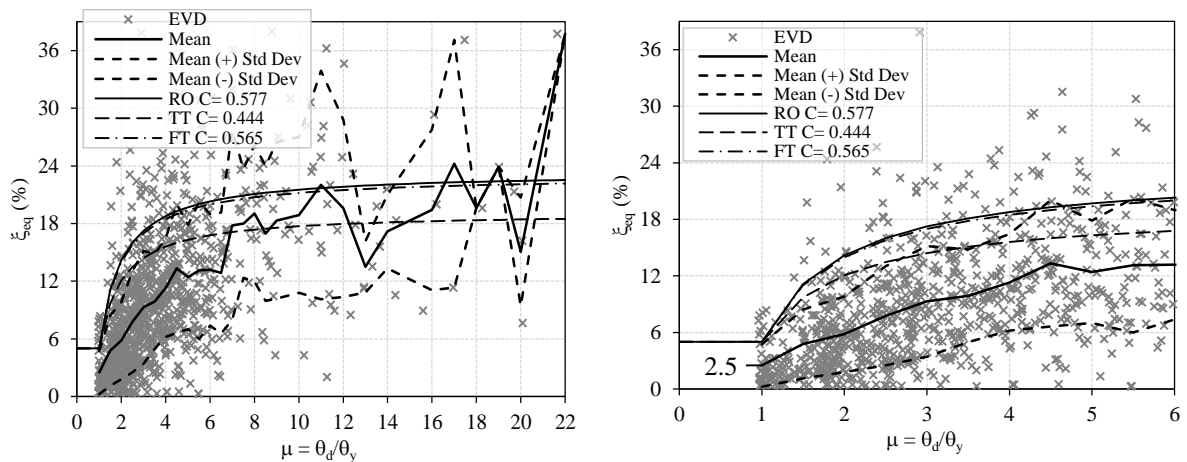


Figure 6.17: Equivalent viscous damping results mean curve: a) for all ductility levels; b) for ductility levels between 1 and 6.

6.5 DISCUSSION OF THE RESULTS

6.5.1 INFLUENCE OF THE JOINT MECHANISMS ON THE DUCTILITY-EVD RELATIONSHIPS

For each joint typology, Eq.(6.5) is calibrated to fit the obtained results by determining the constant C that minimises the error between the EVD values (for that joint type) and the ones obtained with the proposed expression. The curves are plotted in Figure 6.18 along with the procedure results. Note that, in this way, the derived equations cannot be changed to apply for different values of elastic damping, since the C coefficient is only valid for the adopted value of ξ_{el} . In Figure 6.18 it is also plotted the mean EVD values, for each set of results associated to each joint, along with the +/- standard deviation from the mean, as a measure of dispersion of the results.

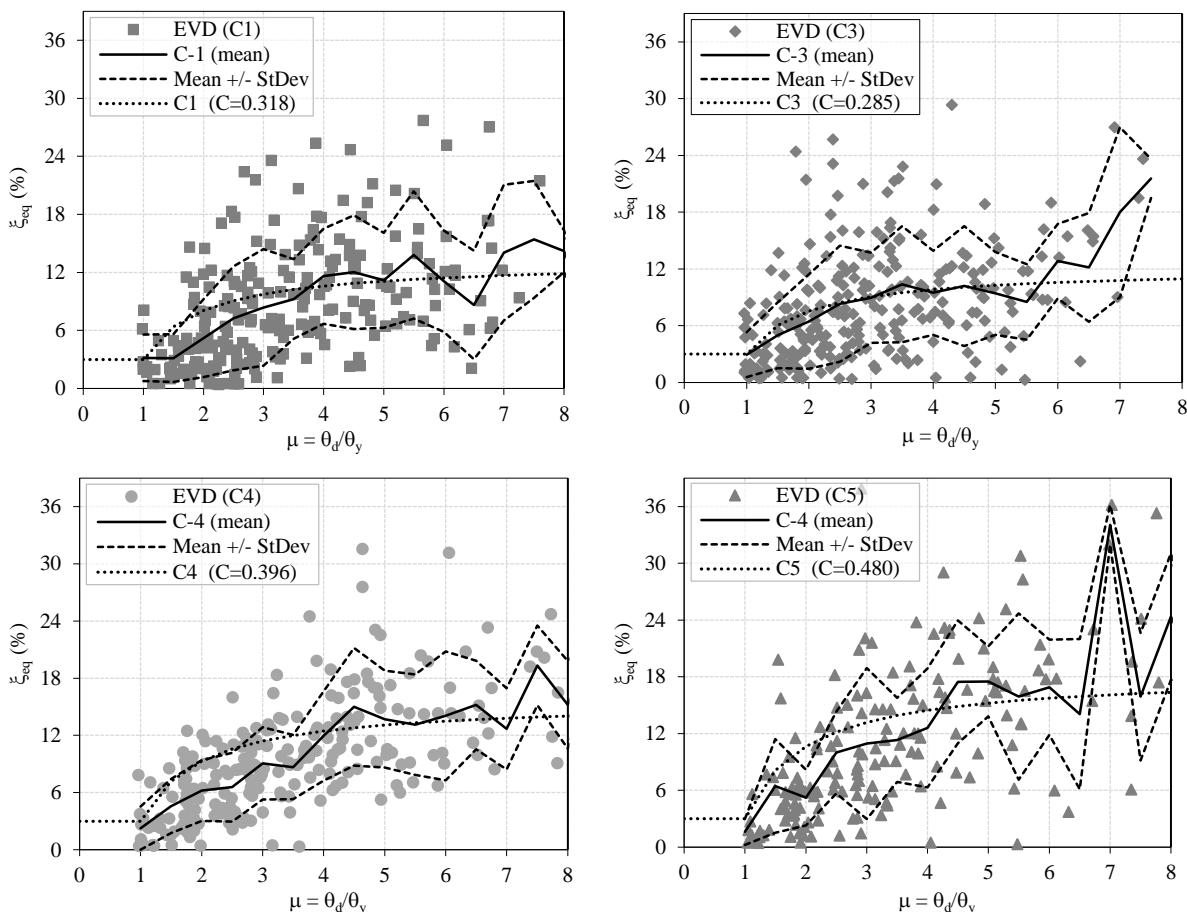


Figure 6.18: Average of the equivalent viscous damping values isolated for the four analysed joints.

The comparison between the analytical curves and the average of the EVD values allows concluding that the proposed expression provides good fit of the pairs of ductility-EVD data, particularly for larger levels of ductility. Notwithstanding the large scatter of results, the different values of the C parameter obtained for the four joints confirms that the complexity of the joints plastic mechanisms has an influence on the damping values. By analysing each joint in detail, it is interesting to note that, for $\mu = 1.0$, the average values of EVD achieved, 3.2% for C1, 2.9% for C3, 2.3% for C4 and 1.6% for C5, with the exception of the joint C5, possibly affected by the lower number of analyses, are very close to the elastic viscous damping adopted, i.e., 3%, confirming the good approximation achieved at the individual joint level. It is also possible to observe that joint C4 is the one presenting less scatter of results. On the other hand, the best adjustment between the mean curves from the numerical values and the analytical expressions is obtained for joint C3, which is governed by a plastic mechanism characterized by shear of the column web panel. Nevertheless, joint C5 also presented a good adjustment for ductility levels between 1 and 6. This is a joint governed by type 2 plastic mechanism, i.e., the end-plate in bending, with limited ductility, and with the higher scatter of results. Consequently, this limitation causes a reduced number of analyses with ductility levels higher than 5, severely influencing the mean values, as observed in Figure 6.19 by the peaks of the C5 mean curves. This behaviour clearly influenced the determination of the C coefficient.

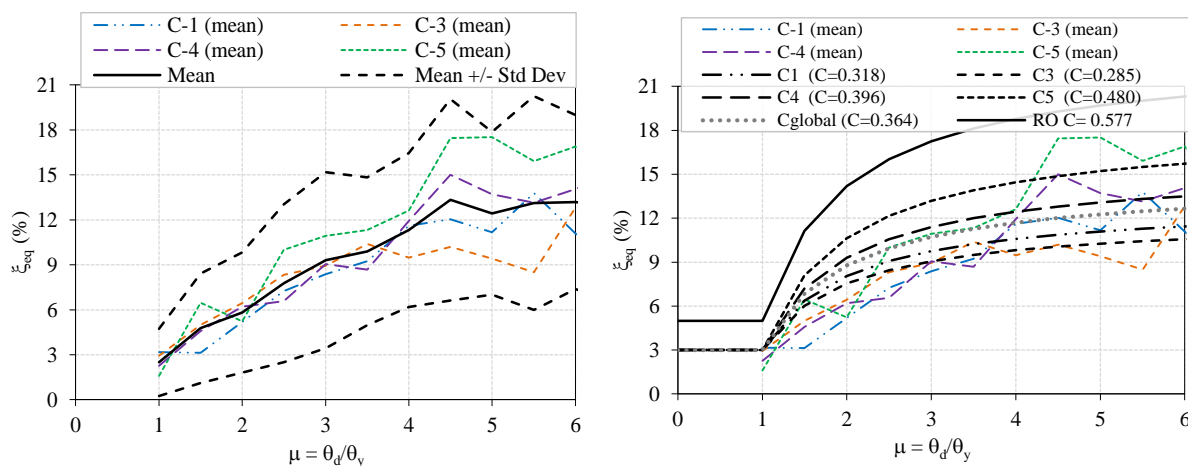


Figure 6.19: Comparison of the average EVD results and the proposed analytical expressions for the derived coefficients for the Eq. (6.5).

Analysing closely the average results of the EVD and the analytical expressions derived from it, see Figure 6.19, for a range of reasonable ductility levels, it is possible to conclude that, up to a ductility of around 3.5, the apparent influence of the plastic mechanism developing in

the joints is quite negligible, according to the average values recorded. Only the C5 joint shows some deviation from the average. Comparing the analytical expressions derived and the mean EVD curves achieved, it is possible to note that, for a ductility level of 1 the 3% damping value is in agreement with the initial assumption adopted in the FE analyses. For higher ductility levels, the analytical expressions and the numerical data follow different paths up to a ductility level of around 4, with lower values of EVD for the numerical curves.

In Figure 6.20 (a) it is also possible to observe that all the derived expressions conduct to significantly lower values of equivalent viscous damping, reinforcing the conclusion drawn earlier that, for steel frame buildings with partial-strength joints, the assumption of the Ramberg-Osgood hysteresis rule, is not adequate.

The discussion made in the previous paragraphs reveals the difficulty in establishing a direct dependence between the plastic mechanism and the ductility-EVD relationship. Moreover, it is possible to state that the influence is only significant for ductility levels higher than 4. The following proposed relationship between EVD and ductility (Eq.(6.6)) represents an improvement of the existing analytical expressions (Priestley *et al.*, 2007) and takes into account all joints behaviours analysed, for MRF structures with end-plate partial-strength beam-to-column joints.

$$\xi_{eq} = 0.03 + 0.364 \left(\frac{\mu - 1}{\mu\pi} \right) \quad (6.6)$$

It is important to refer that Pennucci *et al.* (2011) concluded that an EVD expression cannot be specified independently of a damping-dependent spectral scaling expression (i.e. the expression used to scale a design spectrum from 3% damping to other levels of damping). In Section 6.5.4, the applicability of several expressions available in the literature to scale the response spectrum for other levels of damping are tested to the set of records used in this study. The most accurate scaling is obtained with the equation prescribed in a previous version of EC8 (EN 1998-1, 1994). Similar levels of accuracy have been also achieved with the application of the expression proposed in the current version of the EC8 (EN 1998-1, 2004), see Section 6.5.4. Therefore, it is recommended that the ductility-EVD expression proposed in Eq. (6.5) should be used in combination with the current damping-related expression provided in EC8 for scaling response spectra, since that is the one currently in use and hence familiar to practitioners.

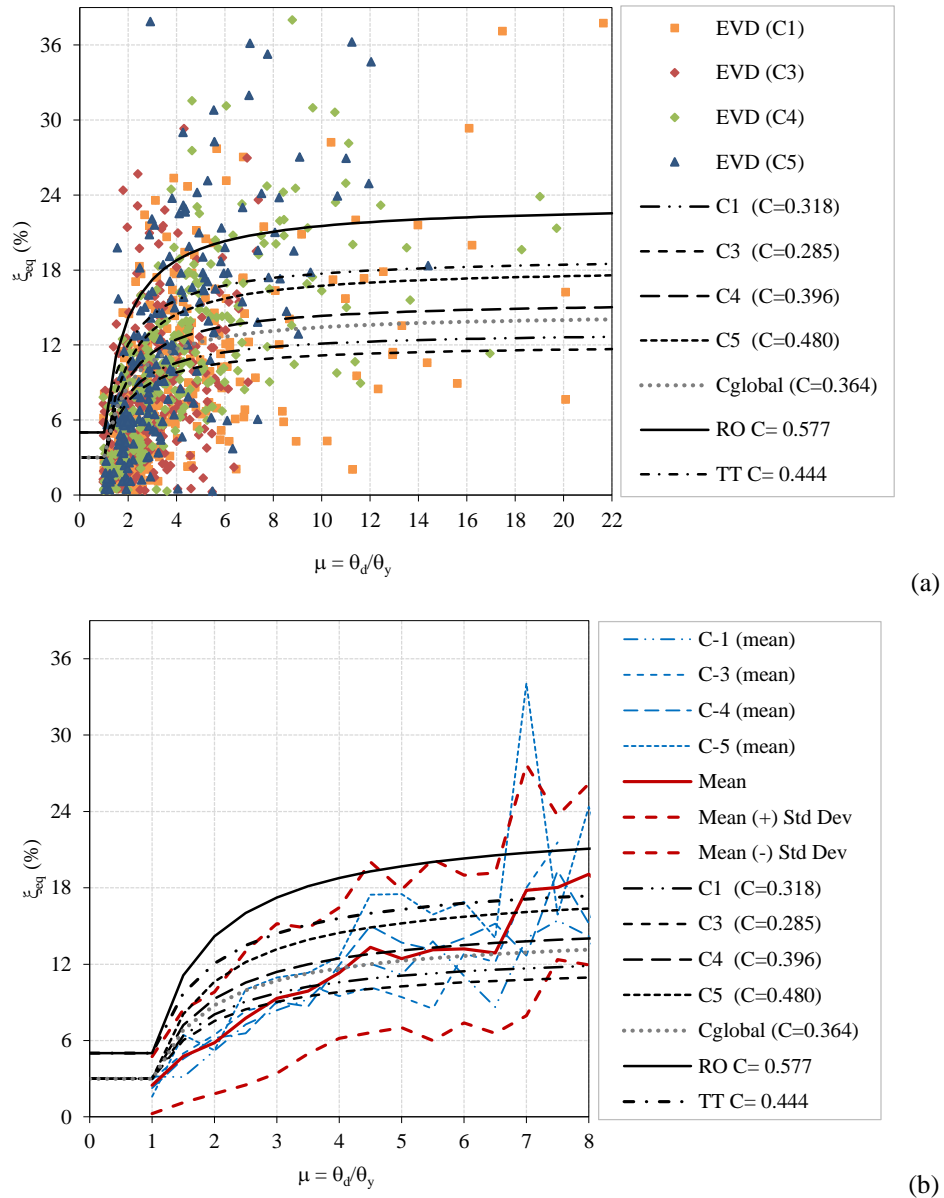


Figure 6.20: EVD results and proposed curves for the derived coefficients for the Eq. (6.5).

6.5.2 INFLUENCE OF THE ELASTIC PERIOD OF VIBRATION OF THE SYSTEM ON THE DUCTILITY-EVD RELATIONSHIP

Figure 6.21 shows the pairs of ductility-EVD obtained in this study grouped according to the initial elastic period of the sub-assembly. In the figures it is also represented the results obtained with the proposed expression (Eq. (6.5)) with a value of the C parameter equal to 0.364, calibrated based on the global set of results. It becomes clear from the figures that the results are not dependent on the initial elastic period of the system, for elastic periods above unity. However, the scatter is lower for the systems with initial period equal to 0.5s, and the

average curve also reveals some dependency of the EVD results. If this dependency of the EVD with the elastic period of the structure was confirmed, it could increase the complexity of the direct formulation of the DDBD procedure, since the elastic period depends on the initial stiffness of the structure, and in that case an iterative process would be required. In Figure 6.21(d) the three mean curves are compared with the proposed expression, showing that the analyses conducted for $T_{el} = 1.0s$ resulted in a closer match of the mean curve with the proposed expression.

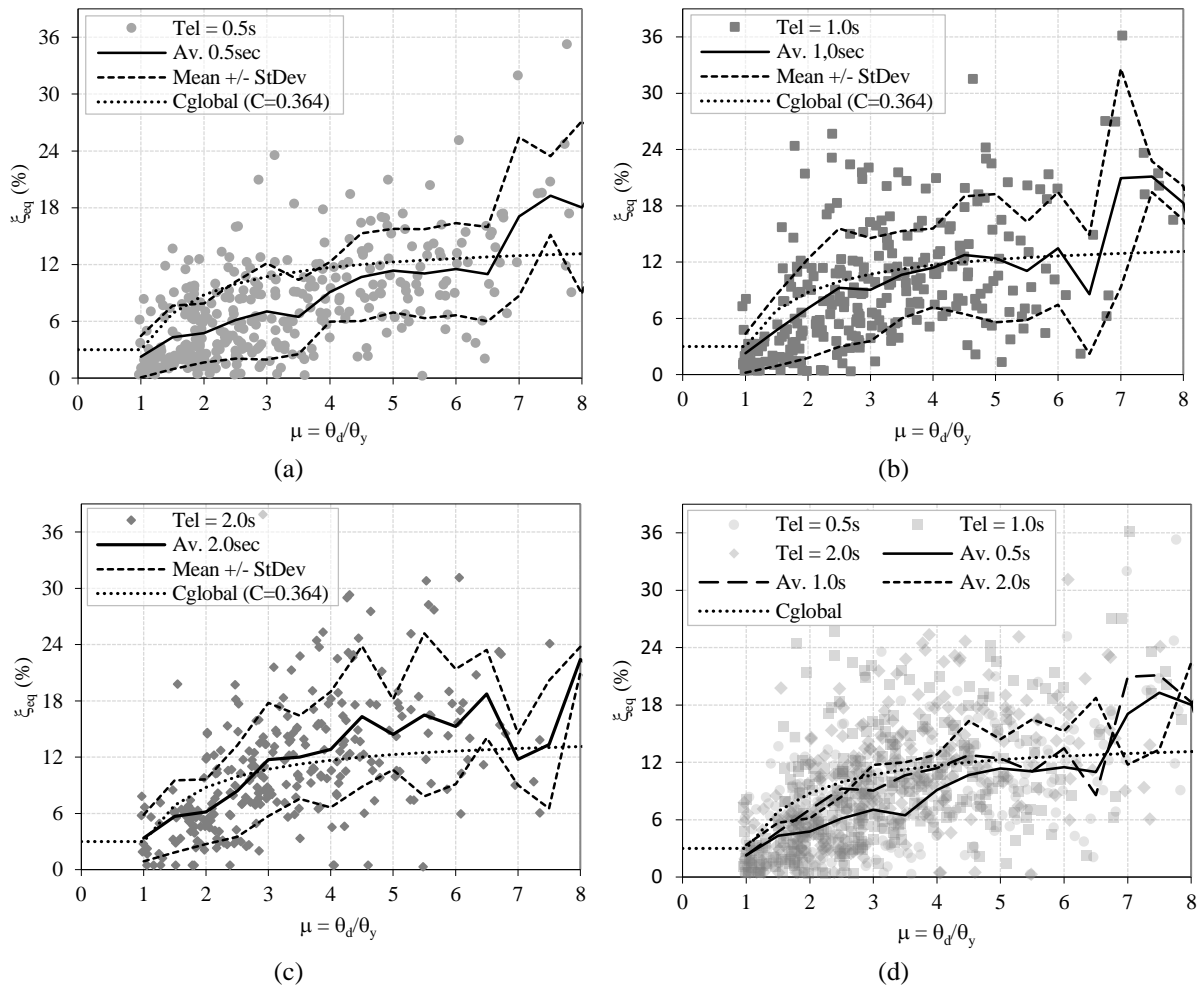


Figure 6.21: Influence of the elastic period of vibration on the ductility-EVD relationship.

6.5.3 INFLUENCE OF THE SOIL TYPE ON THE DUCTILITY-EVD RELATIONSHIPS

Figure 6.22 a) and b) show the distribution of the two sets of results grouped by the records type A and type C. The figures suggest that there is no dependency of the results on the record type. Nevertheless, the analyses conducted with the LA records produced closer results

between the proposed expression and the mean curve, for ductility levels between 1 and 5. A similar observation cannot be extracted for the analyses conducted with the LC records. The mean values of ductility-EVD obtained for each set are plotted in Figure 6.22 c), along with the results obtained with the proposed expression. The plot confirms once again the reduced influence of the soil type on the ductility-EVD relationship and also the adequacy of the proposed expression to fit the mean results obtained with each record set.

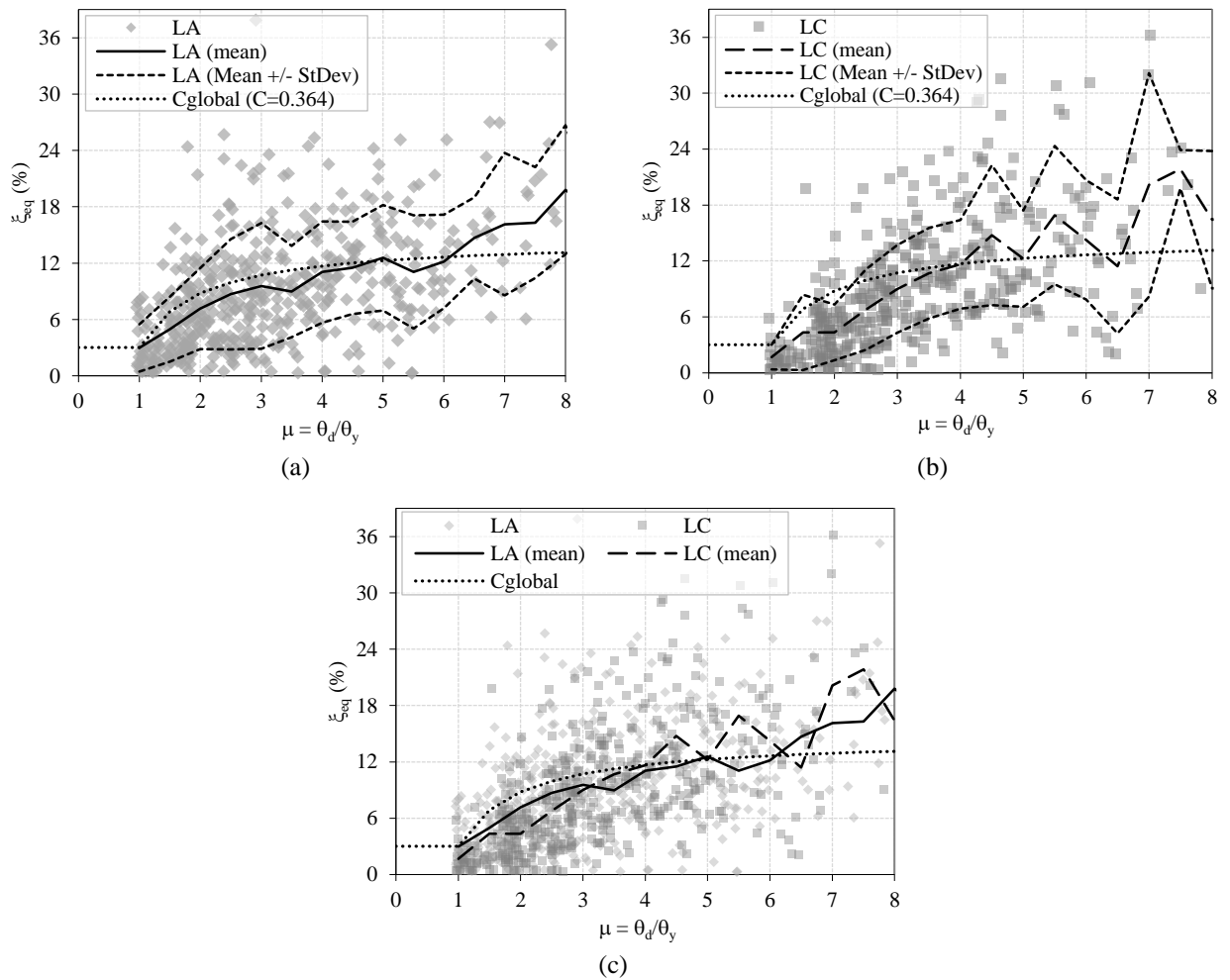


Figure 6.22: Influence of the soil type on the ductility-EVD relationship.

6.5.4 MODIFICATION FACTOR FOR THE SPECTRAL DISPLACEMENT RESPONSE

As observed in Section 2.4.2.3 is necessary to apply a modification factor R_ξ to the elastic displacement response spectrum to account for ductile response in the DDBD procedure (Priestley *et al.*, 2007). This fact is related to the use of the effective period for the representation

of the structural response in the DDBD procedure. In Section 2.4.2.3 several proposals of damping modifier R_ξ , available in literature, were revised. The relevant expressions are summarized in the Table 6.7. The accuracy of the expressions will be analysed using the equivalent viscous damping values determined, for the set of records used in this study.

Table 6.7: Available modification factor expressions for the spectral displacement response.

EC8-1 (EN 1998-1, 1994)	$R_\xi = (0.07/(0.02 + \xi))^{0.5} \geq 0.7$	(6.7)
EC8-1 (EN 1998-1, 2004)	$R_\xi = (0.1/(0.05 + \xi))^{0.5} \geq 0.55$	(6.8)
Newmark and Hall (1982)	$R_\xi = (1.31 - 0.19 \ln(100\xi))$	(6.9)
Priestley (2003)	$R_\xi = (0.07/(0.02 + \xi))^{0.25}$	(6.10)

To determine the displacement reduction factor, the ratio between the inelastic displacement (Δ_{in}) and the elastic displacement for the same effective period ($\Delta_{el,Te}$) is computed as follows:

$$\eta = \frac{\Delta_{in}}{\Delta_{el,Te}} \quad (6.11)$$

Figure 6.23 show the comparison of the results using Eq. (6.11), from NLTH analyses to determine the maximum inelastic displacement (Δ_{in}), and using the elastic displacement spectra with 3% of elastic damping to determine the elastic displacement ($\Delta_{el,Te}$) with the analytical expressions found in literature and presented previously. Note that the analytical expressions were used without the limitations imposed in the codes, i.e., only the first part of Eqs. (6.7) and (6.8) were used in the next comparisons. Figure 6.24 present the ratio between the reduction factors obtained from the NLTH analyses and the reduction factors obtained using Eqs. (6.7) to (6.10).

From a detailed inspection of the figures, it is possible to conclude that the most accurate analytical values are obtained with Eq. (6.7), although the predictions obtained with the expression proposed in the current version of the EC8 (EN 1998-1, 2004) are also reasonable. In the case of Eqs. (6.9) and (6.10), the poor correlation of the results indicates some inadequacy to deal with partial-strength joints and hence, they are not recommended to be used with the derived equivalent viscous damping expression.

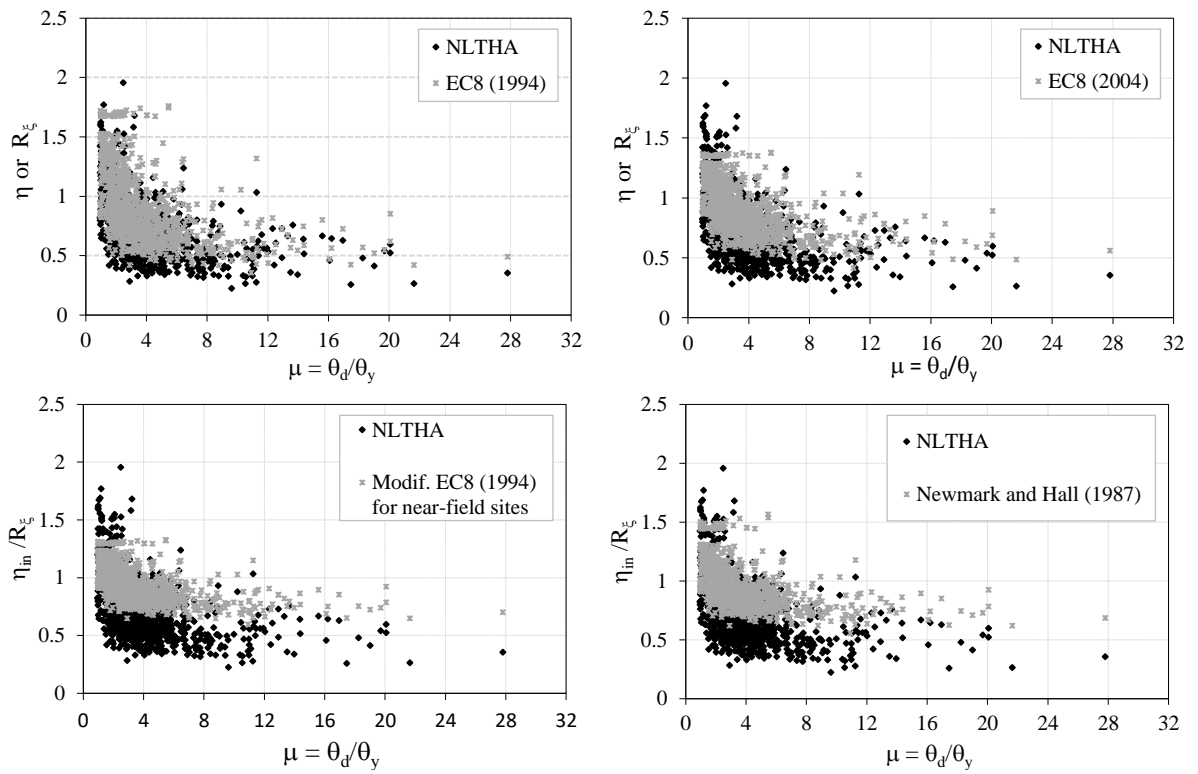


Figure 6.23: Damping modifier comparison.

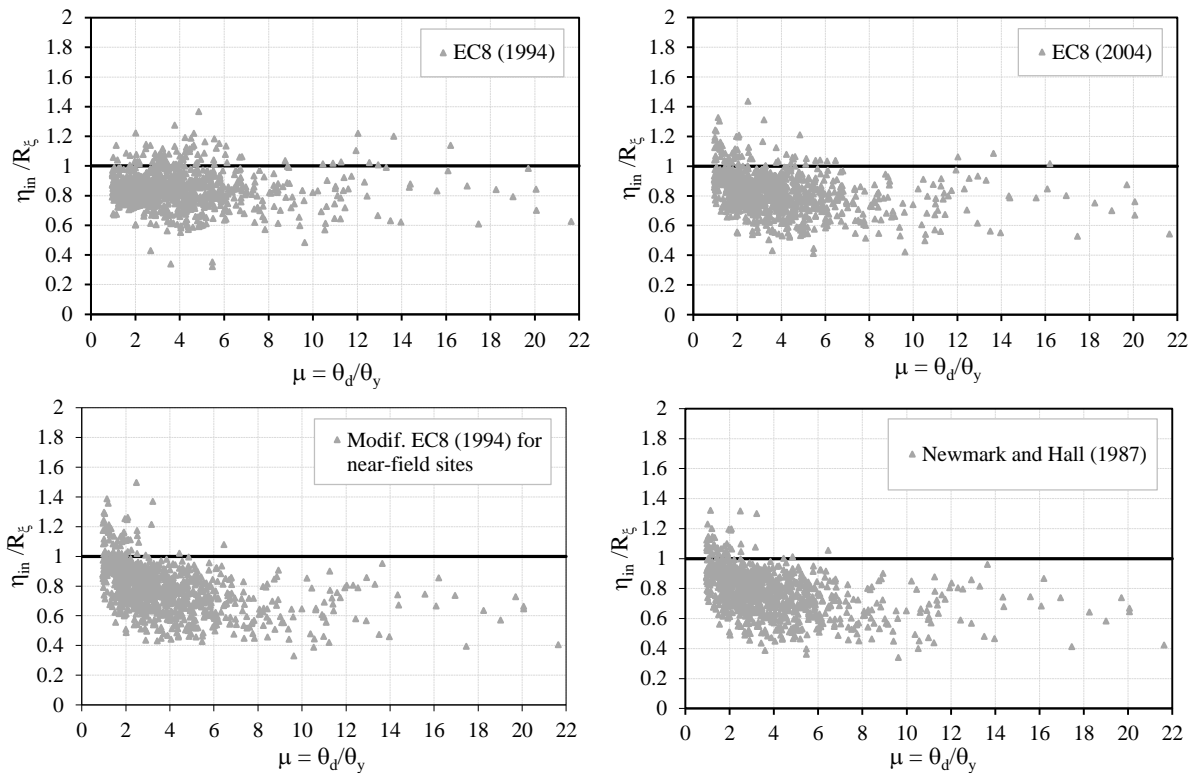


Figure 6.24: Deviation from the numerical and analytical reduction factors.

6.6 MAIN CONCLUSIONS

With the objective of contributing to the development and improvement of displacement based design procedures a large parametric study was carried out based on FE models developed in ABAQUS. The models are representative of sub-assemblages of moment-resisting frames with partial-strength bolted end-plate beam-to-column joints, which were generated using a script developed in Python for ABAQUS developed and validated in Chapter 3. The models were subjected to nonlinear time history (NLTH) analyses using real records scaled to achieve several levels of ductility.

A proposed procedure was then employed to the sub-assemblages with the objective of determining the ductility-equivalent viscous damping relationships. The procedure consists of linearizing the non-linear responses obtained in the NLTH analyses, using an elastic single degree of freedom structure and the elastic displacement spectra with secant stiffness at maximum displacement.

The results allowed concluding about the accurateness of the existing expressions proposed by Priestley *et al.* (2007). These expressions generally overestimates the levels of equivalent viscous damping (EVD), which is justified with the fact that it was derived assuming an hysteretic behaviour based on the Ramberg-Osgood constitutive law, for MRF structures having full-strength joints and plastic rotations smaller than limits producing strength deterioration. In fact, the expression based on the Takeda-Thin hysteretic rule, revealed to be closer to the average of the EVD results, but still overestimate the results obtained. The hysteresis loops of partial-strength joints indicate that the behaviour characterization should be closer to rules like Takeda-Thin in part due to the pinching effect detected in some of the analysed joints.

A detailed analysis of the numerical results obtained in the study revealed no clear dependency of the ductility-EVD relationships on the plastic mechanism of the joint type, on the elastic period of vibration of the system and on the soil type. An improved ductility-equivalent viscous damping relationship was derived based on the full set of results. The proposed expression represents an improvement in relation to the existing analytical expressions proposed by Priestley *et al.* (2007). The new expression is applicable to steel moment-resisting frames with partial-strength beam-to-column joints and can be directly used in the direct displacement-based seismic design (DDBD).

7

GENERAL CONCLUSIONS AND FUTURE WORK

7.1 FINAL REMARKS AND MAIN CONCLUSIONS

The research described in this thesis is part of the work developed by the author in the scope of two European research projects, *DiSTEEL* (RFSR-CT-2010-00029) and *EQUALJOINTS* (RFSR-CT-2013-00021). Chapters 2, 3 and 6 reflect the work developed within the first project, which had, as main objective, the development of a set of practical performance-based design guidelines for seismic design of steel moment-resisting frame structures using a displacement-based design procedure. Chapters 4 and 5 reflect the research developed within the scope of the second project, which had, as main objective, the seismic pre-qualification of steel beam-to-column joints in steel structures and the contribution to the improvement of the European design code concerning the joint design under cyclic and seismic loading

Chapter 1 introduces the subject and the objectives of the thesis. In Chapter 2 a literature review is performed on the subject focused on the recent developments in this field. Available experimental data from research experimental programs was collected and catalogued. Several models to characterize the joints behaviour or its components, available in literature, were analysed. The insights acquired in this chapter strengthened the basis of knowledge, which supported the rest of the research reported in this thesis.

Chapter 3 deals with the development, calibration and validation of the finite element model of the beam-to-column end-plate joint. The model can be considered a cornerstone in the research since the subsequent studies were based on this model. The experimental tests used in

the model calibration/validation were analysed both globally and at the component level. Furthermore, they were compared with the analytical values obtained using the EC3-1-8 and other available methodologies, namely the Krawinkler model for the column web panel behaviour. The excellent agreement between the experimental and numerical results allowed concluding that the model is capable of simulating, with accuracy, the behaviour of end-plate beam-to-column joints and their components. A practical procedure to extract the moment-rotation relationships from the experimental and numerical models was also proposed, both for the global behaviour and for the components.

Chapter 4 presents the methodologies to extract, from the FE model, the relevant force-displacement relationships of the basic components, as identified in the Eurocode 3. Two versatile and efficient methodologies were presented, according to the component location in the joint (column web or connection), for the extraction of the monotonic and cyclic behaviour of the bolted end-plate joints basic components. Those relationships can be applied directly in the springs of a mechanical model to assist in the joint design. For the assessment of the forces, for each basic component, the developed methodologies uses the integration of stress fields of predefined paths of the finite element models of the joints. To compute the deformations the relative displacements, of predefined nodes in the finite element model, are used to assess the deformation mechanisms of the components. The procedure is repeated for several load increments, until the complete characterization of the force-deformation curve of the basic component is obtained. The methodologies are applicable to the following basic components: column web panel in shear, column web in transverse compression or tension, column flange in bending, end-plate in bending and bolts in tension, however it can be extended to other components. The procedures are very flexible in terms of the definition of the integration boundaries to assess the force-displacement relationships. The mechanical model chosen will determine the integration boundaries, even because, as verified previously, the boundary conditions may be different for tension or compression forces. Double-extended end-plate joints were analysed and used to assess the proposed methodologies. The results allowed concluding that the procedure is able to capture the behaviour of the column web under transverse tension and compression, both for groups of bolts and for isolated bolt rows. Furthermore, the shear-rotation behaviour of the column web panel can be assessed, including the additional shear resistance provided by the transverse web stiffeners and achieved by the

frame action developed by the column flanges and the stiffeners. In the case of the connection components, namely the column flange in bending, end-plate in bending and bolts in tension, the procedure is also able to capture well the behaviour. Considerable differences in the behaviour of the three components were detected when transverse web stiffeners are added to the joint, both in case of monotonic and cyclic loading. The column flange in bending is the most affected component by the transverse web stiffeners. The component contribution may be neglected in the presence of the stiffeners. However, its contribution cannot be neglected in the absence of the transverse web stiffeners. As expected, the bolt rows closer to the beam flanges have higher demand than the other inner rows, as a result of the concentration of forces in the beam flanges. The inner rows closer to the beam flanges present stable hysteretic cycles without pinching, unlike the external rows, which clearly are affected by that phenomenon. Regarding the bolts in tension, their behaviour was almost elastic although in the last cycles some plastic deformation can be observed.

In Chapter 5 the methodologies developed in Chapters 3 and 4 were applied to a set of internal and external beam-to-column end-plate joints. These joints are characterized by different levels of strength according to the resistance of the connected beams, designated by equal-strength when the strength resistance of the joint and the beam are similar, and partial-strength for a resistance of the joint approximately 60% of the beam's resistance. The numerical results were also compared with available experimental tests results of the joints. To help in the design of the joints, a preliminary parametric study was conducted using finite element models of the selected geometries. The nominal values of the steel grade S355 were used, with an overstrength factor of $\gamma_{ov} = 1.25$ (proposed in the Eurocode 8). A parametric study was performed varying some geometrical and mechanical properties in the joints that have the potential to influence the joints behaviour. The main parameters included the presence of the continuity column web stiffeners, the influence of an additional bolt row located in the axis of symmetry of the joints, the influence of two additional bolt rows in the extended part of the end-plate and the sensitivity to the end-plate mechanical properties. This study led to the conclusion that the presence of column transverse web stiffeners influences the behaviour of the basic components of the joints, and confirmed previous studies conclusions regarding the increases of the initial stiffness and resistance of the joints provided by the presence of the transverse web stiffeners. In the absence of stiffeners, the column flange in bending gains some

relevance, contributing significantly to the global response of the joint and to the energy dissipated by the component. Furthermore, without transverse web stiffeners the pinching effect is amplified, mainly in partial-strength joints. The additional bolt rows do not seem to have a significant influence on the response of the joints. Only in the case of the addition of a second external bolt row seems to have some influence, however, only notorious for larger rotations, after the first external bolt row suffers plastic deformation. The influence of the mechanical properties of the end-plate is notorious in the response of the joints, especially in the partial-strength joints, due to their slender end-plates. There is an increase of the pinching effect with the decrease of the end-plate mechanical properties and thickness. Finally, this study allowed concluding that the contribution of the column web stiffeners to the joints strength, stiffness and stability makes their use recommended. The additional bolt rows were not as effective as expected and their use should be balanced with economical gain and with other aspects like the durability or the redundancy in case of accidental actions, or even to avoid stability problems in slender plates under compression.

The preliminary developed finite element models, for the set of designed joints, were then updated with the mechanical properties obtained in the coupon material tests and compared with the results of the available experimental tests results. A comparison of the nominal properties of the steel grade adopted for the joints members and plates, with the average of the ones found in the material tests, revealed that the adoption of the recommended value of the material overstrength factor of the Eurocode 8 ($\gamma_{ov} = 1.25$) is in this case on the unsafe side. The real variation factor was found to be, in most cases, higher than the proposed material overstrength factor (γ_{ov}). The joints were then redesigned with the updated mechanical properties, revealing that the initial assumptions can change significantly the design of the joints, namely the failure modes. It was observed that the response of the joints presented a stable behaviour without strength degradation, although it is possible to observe some degradation of stiffness for the last cycles. This phenomenon was well captured by the numerical models

Towards the end of the chapter the procedures proposed in Chapter 4 were applied to the joints to extract the behaviour of the basic components from the finite element models. The basic component column web panel in shear presented a stable behaviour for all joints. For the components column web in transverse tension and compression the transverse web stiffeners

significantly control their behaviour. On the compression side, the behaviour is almost elastic, and on the tension side only the internal bolt rows presented a substantial contribution to the joint non-linear rotation. The external bolt rows remained almost elastic. For the connection components, only the end-plate in bending significantly contributes to the joint non-linear rotation, the other connection components remained almost elastic. The extraction of the forces of the basic connection components was obtained through the integration of the stress fields in the bolts section, due to the presence of transverse web stiffeners. It was found that the initial pre-load applied to the bolts influenced the derived force-deformation responses. Furthermore, it was observed that the force due to the pre-load of the bolts decreases with the increase of the plastic deformations in the bolts. The analysis of the curves led to the conclusion that the derived relationships for the end-plate in bending presents some ratcheting effect, possibly due to the plastic deformation of the bolts along with the plastic deformation of the end-plate.

The proposed methodologies developed in Chapters 3 and 4 were able to extract the basic components behaviour of the finite element models of the beam-to-column end-plate joints under cyclic loading conditions. The derived relationships can be applied directly in the behaviour of the springs assembled in a mechanical model, compatible with the beam-to-column end-plate joint geometry, and in line with Eurocode 3 requirements for the monotonically loaded joints.

Chapter 6 is dedicated to the study of end-plate beam-to-column partial-strength joints in the context of moment-resisting frame structures, designed for seismic loading conditions. The aim is to improve existing displacement-based seismic design procedures, namely the direct displacement-based seismic design method, developed by Priestley *et al.* (2007), to take into account partial-strength joints as the main dissipative mechanism in the moment-resisting steel frame structure, using the concept of equivalent viscous damping. For that, a large parametric study was carried out based on finite element models developed in ABAQUS, following the same principles discussed in Chapter 3. The models were subjected to non-linear time history (NLTH) analyses using real records scaled to achieve several levels of ductility.

A proposed procedure was then employed to the sub-assemblages with the objective of determining the ductility-equivalent viscous damping relationships. The procedure consists of linearizing the non-linear responses obtained in the NLTH analyses, using an elastic single degree of freedom structure and the elastic displacement spectra with secant stiffness at

maximum displacement.

The results allowed concluding about the limitation of using the existing expression proposed by Priestley *et al.* (2007) which generally overestimates the levels of equivalent viscous damping. This is justified with the fact that it was derived assuming a hysteretic behaviour based on the Ramberg-Osgood constitutive law, for MRF structures having full-strength joints and plastic rotations smaller than limits producing strength deterioration. In fact, the expression based on Takeda-Thin constitutive law, revealed to be closer to the average of the equivalent viscous damping results, although continues to overestimate the results. The hysteresis loops of partial-strength joints indicate that the behaviour characterization should be closer to rules like Takeda-Thin in part due to the pinching effect detected in some of the joints analysed.

A detailed analysis of the numerical results obtained in the study revealed no clear dependency of the ductility-EVD relationships on the plastic mechanism of the joint type, on the elastic period of vibration of the system and also on the soil type. An improved ductility-equivalent viscous damping relationship was therefore derived based on the full set of results. The proposed expression represents a clear improvement in relation to the existing analytical expressions proposed by Priestley *et al.* (2007). The new expression is applicable to steel moment-resisting frames with partial-strength beam-to-column joints and can be directly used in seismic design procedures such as the direct displacement-based seismic design (DDBD). The developments presented in this research contribute to a more reliable application of DDBD to steel moment-resisting frames.

7.2 SUMMARY OF THE MAIN OUTCOMES

This document describes the research conducted on the numerical and analytical characterization of the behaviour of beam-to-column partial-strength joints under cyclic and seismic loading conditions.

For monotonic conditions, the characterization of the behaviour of steel joints is well established and codified through the implementation of the component method prescribed in Eurocode 3. However, for cyclic and dynamic loading conditions, still no general analytical procedure allows the direct characterization of the behaviour of the steel joints. Therefore, the

first goal of this study has been the development and calibration of FE models for beam-to-column partial-strength joints under cyclic loading. These models were further employed in derivation of analytical procedures for joint design and in the determination of the ductility-equivalent viscous damping relationships for displacement-based seismic design of steel moment-resisting frames.

Two main contributions of this work to the advance of knowledge can be summarized as follows:

- i) The development, calibration and validation of practical methodologies, capable of extracting the behaviour of the relevant basic components of beam-to-column joints. The derived force-displacement relationships of the components can be directly used in a mechanical model, composed by springs and rigid-links, to design and assess the global behaviour of joints. These methodologies are consistent with the component method prescribed in EC3 and represent a generalization to the cyclic behaviour of steel joints.
- ii) Based on the calibrated FE models of the joints, the ductility-equivalent viscous damping relationships are assessed using a proposed new methodology. It consists of linearizing the non-linear responses obtained in the NLTH analyses, using an elastic single degree of freedom structure and the elastic displacement spectra with secant stiffness at maximum displacement. It is thus possible to propose an improvement of the existing expressions for displacement-based seismic design methodologies, for steel moment-resisting frame structures with dissipative partial-strength joints, namely the ones proposed by Priestley *et al.* (2007).

The developments presented in this document, on the joint behaviour characterization, under cyclic and dynamic conditions, contribute to an improvement in knowledge in these areas. Furthermore, the methodologies developed, to assess the behaviour of the basic joint components, could be used directly in the analysis of the behaviour of steel beam-to-column joints, or directly in the analysis of the global frame with the response of the joints integrated in its formulation. These outcomes can also serve as a basis for future research, in order to create tools to assist the design of joints, under these conditions. The main outcomes of this research are identified in Table 7.1.

Table 7.1: Main outcomes of the research.

Outcome	Specific information	Chapter	Relevant references
Recommendations to assess moment-rotation ($M - \theta$) relationships	For the joint and for the component CWS	3	Table 3.10
	For the connection components (CFB, EPB, BT)	4	Table 4.7 Table 4.8 Table 4.9
Extraction of the $F-\Delta$ curves of the basic components of the column web	CWS CWT CWC	4	Table 4.12
Extraction of the $F-\Delta$ curves of the basic components of the connection	CFB BT EPB	4	
Assessment of the equivalent viscous damping	ξ_{eq}	6	Section 6.2
Proposal for $\xi_{eq} - \mu$ relationship for MRF with partial-strength joints	$\xi_{eq} - \mu$	6	Eq. (6.6)
Recommendations for the modification factor for the spectral displacement response to be used	R_{ξ}	6	Section 6.5.4
CWS	basic component Column Web panel in Shear		
CWC	basic component Column Web in transverse Compression		
CWT	basic component Column Web in transverse Tension		
CFB	basic component Column Flange in Bending		
EPB -	basic component End-Plate in Bending		
BT	basic component Bolts in Tension		
ξ_{eq}	equivalent viscous damping		
μ	ductility level		
R_{ξ}	modification factor for the spectral displacement response		

7.3 FURTHER DEVELOPMENTS AND RECOMMENDATIONS FOR FUTURE WORK

The research carried out, and presented previously, responded to the proposed objectives, particularly on the characterization of the behaviour of partial-strength joints under monotonic cyclic and dynamic conditions, both globally and in terms of the critical components. Several detailed procedures were proposed and validated to identify and characterize the joints global behaviour as well as the isolated behaviour of the basic components, which can be directly applied to the spring's behaviour, representative of the components, of a mechanical model of the joint. Concerning further development of the analytical procedures for the design of partial-strength steel joints, capable of dealing with reversal loading, the following tasks can be identified:

- i) Extend the proposed procedures to internal joints, with two beams connected to both column flanges. A first approach was made to this subject on Chapter 5. The work is ongoing with already some results at the components level. And if for some components the developed methodologies can be applied directly to the internal joint, namely the components of the connection (column flange in bending, end-plate in bending and bolts in tension), the components of the column web need to deal now with the load-introduction of the two connected beams. For the components column web in transverse tension or compression the extraction of the forces follows the same principles of the proposed procedures, using the integration of the stress fields in the column web, for each connection side. In turn, the computation of the column web deformation should be now shared by the two connections. One solution is to define one more intermediate path in the column web between P1 and P2. Then the deformation is determined by the relative displacements of the path near the connection and the new intermediate path, thereby capturing the transverse deformation of the column web in the corresponding half of the connection under study. The assessment of the component column web panel in shear remained unchanged, taking into account that in the assembly of this component, only one spring should be considered, unless the height of the beams is different. In this case a deeper research should be developed.
- ii) Refine the extraction process of the forces for the components of the connection, column flange in bending, end-plate in bending and bolts in tension, for joints with transverse web stiffeners, which is not influenced by the initial pre-stress of the bolts. At the outset, two approaches may be followed in this attempt to refine the proposed procedure: a) attempt to remove the pre-stress installed in the bolts directly in the extracted force-deformation response; b) or integrate the stresses that enter in the column web, however the stresses distributed to the stiffeners must be taken into account. As observed previously in the first solution the pre-stress in the bolts changes with plastic deformation of the plates and bolts, so the pre-stress force removed from the component response should take that into

consideration. In the second solution, the paths where the stresses are integrated, over the column web thickness, should cover the stiffeners as well.

- iii) Derive the main parameters to the analytical characterization of the behaviour of each basic component, under cyclic loading. Calibration of a mathematical model capable of describing the behaviour of each component, based on the derived main parameters. This may require performing a parametric study that covers a variety of end-plate joints typologies, beam and column sizes and several connections configurations. This will allow identifying the possible relationships, and the parameters that best characterize them. In the end, a statistical validation should be performed, to establish a statistical background to the derived parameters.
- iv) Identify, for each basic component, the failure criteria according to its expected ductility and accumulated plastic strain. It is well known that ductile components can sustain large plastic deformations. However, as discussed previously, when reversal load occurs, the ductility can be affected, and the accumulated plastic strain, resulting from the back and forward of the cyclic load protocol, will lead to the failure of the component. The assessment of the amount of plastic deformation that the component can withstand is vital for the design of the joint under cyclic loading. In this way, a component based approach that takes into account reversal loading condition can be implemented in a code of practice. Furthermore, in this situation is opened the door to a performance-based design of joints, which is certainly the most ideal and economical solution.
- v) Development of a tool capable of incorporate a mechanical model according to the joints geometry, in which the behaviour of the springs are determined by the force-deformation relationships derived previously for each basic component. Assembled in such a way that is able of reproducing the global behaviour of the joint. This ongoing step will definitely contribute to the aim of having a component based approach procedure, for the design of partial-strength steel joints, capable of dealing with reversal loading. This will allow combining all the derived relationships into a single model for the design of partial-strength end-plate joints.

- vi) Calibrate and validate the response of the mechanical model using real experimental test data. The previous tool should be then calibrated and validated through experimental and numerical results. Until the results inspire enough confidence to be used in the current practice.

In this research it was also studied the dynamic behaviour of partial-strength joints, in the context of displacement-based seismic design procedures. The study allowed improving existing ductility-equivalent viscous damping relationships for moment-resisting frames having partial-strength beam-to-column joints. For that, a large parametric study was conducted and several procedures developed. However, the results were limited to the study of partial-strength beam-to-column joints. Concerning the application to the displacement-based seismic design procedures, other joint typologies (e.g. column bases) and other frame systems (braced, dual systems) with partial-strength joints should be investigated.

7.4 DISSEMINATION AND PUBLICATIONS

The research work described above has been disseminated in several written supports and events, resulting in the following publications:

- i) Book Chapters

Sullivan, T. J., O'Reilly, G. J., Morelli, F., Salvatore, W., Della Corte, G., Di Lorenzo, G., Landolfo, R., Augusto, H., Castro, J. M., Rebelo, C., Simões da Silva, L. (2014). Review of previous experimental investigations. In T. J. Sullivan & G. J. O'Reilly (Eds.), *Characterising the Seismic Behaviour of Steel Beam-Column Joints for Seismic Design* (pp. 13–168). Pavia, Italy: IUSS Press.

Augusto, H., Castro, J. M., Rebelo, C., Simões da Silva, L. (2014). Characterising partial-strength joints using finite element analysis. In T. J. Sullivan & G. J. O'Reilly (Eds.), *Characterising the Seismic Behaviour of Steel Beam-Column Joints for Seismic Design* (pp. 267–364). Pavia, Italy: IUSS Press.

- ii) Technical Reports

Calvi, G.M., Sullivan, T., Roldán, R., O'Reilly, G., Simões da Silva, L., Rebelo, C., Castro, J.M., Augusto, H., Landolfo, R., Della Corte, G., Terraciano, G., Slavatore, W., Morelli, F. ,(2015). *Displacement based seismic design of steel moment resisting frame structures (DiSTEEL), Final Report*, Brussels.

iii) International Journal Papers (ISI)

- Augusto, H., Simões da Silva, L., Rebelo, C., Castro, J. M. (2016). Characterization of web panel components in double-extended bolted end-plate steel joints. *Journal of Constructional Steel Research*, 116, pp. 271–293.
- Augusto, H., Simões da Silva, L., Rebelo, C., Castro, J. M. (2017). Cyclic behaviour characterization of web panel components in bolted end-plate steel joints. *Journal of Constructional Steel Research*, 133, pp. 310–333.
- Augusto, H., Castro, J. M., Rebelo, C., Simões da Silva, L. (2017). Ductility-equivalent viscous damping relationships for beam-to-column partial-strength steel joints. *Journal of Earthquake Engineering*, (waiting publication).

iv) Other Journals

- Augusto, H., Castro, J. M., Rebelo, C., Simões da Silva, L. (2014). Calibração de um modelo de elementos finitos de ligação metálica viga-pilar para validação dos modelos de cálculo do Eurocódigo 3. *Revista Da Estrutura de Aço, CBCA*, 3(2), pp. 128–147.

v) International and National Conferences

- Augusto, H., Serra, M., Rebelo, C., Simões da Silva, L. (2011). Calibration of Numerical Models for the Simulation of Partial Strength Steel Connections Subjected to Cyclic Loading. In *DiSTEEL Workshop - Displacement Based Seismic Design of Steel Moment Resisting Frame Structures* (pp. 57–67). Guimarães: CMM – Associação Portuguesa de Construção Metálica e Mista.
- Augusto, H., Castro, J. M., Rebelo, C., Silva, L. S. (2012). Modelling of the Dissipative Behaviour of Partial-Strength Beam-to-Column Steel Connections. In *15th World Conference on Earthquake Engineering*. Lisbon.
- Augusto, H., Castro, J. M., Rebelo, C., Simões da Silva, L. (2012). Determinação dos parâmetros relevantes para a caracterização de ligações metálicas de resistência parcial sujeitas a carregamento cíclico. In *Congresso Construção 2012*. Coimbra.
- Augusto, H., Castro, J. M., Rebelo, C., Silva, L. S. da. (2013b). Numerical simulation of partial-strength steel beam-to-column connections under monotonic and cyclic loading. In *CNM 2013 - Congress on Numerical Methods in Engineering* (pp. 121–140). Bilbao.
- Augusto, H., Castro, J. M., Rebelo, C., Silva, L. S. da. (2013a). Assessment of key parameters for displacement-based seismic design of steel moment frames with partial-strength connections. In *XXIV Giornate Italiane della Costruzione in Acciaio* (Vol. 2, pp. 613–620). Turin: CTA - Collegio dei Tecnici Dell'Acciaio.
- Augusto, H., Serra, M., Rebelo, C., Simões da Silva, L. (2013). Numerical Characterization of the Cyclic Behaviour of End-Plate Beam-to-Column Steel Connections. In *II DiSTEEL Workshop - Direct Displacement-Based Design of Steel MRF Structures - Recent Developments and Contributions for the Seismic Design Approaches for MRF Steel*

- Structures* (pp. 71–87). Porto: CMM - Associação Portuguesa de Construção Metálica e Mista.
- Augusto, H., Castro, J. M., Rebelo, C., Simões da Silva, L. (2013). Calibração de um modelo de elementos finitos de ligação metálica viga-pilar para validação dos modelos de cálculo do Eurocódigo 3. In *IX congresso de construção metálica e mista & I congresso luso-brasileiro de construção metálica sustentável* (pp. 467–476). Porto: CMM - Associação Portuguesa de Construção Metálica e Mista.
- Augusto, H., Castro, J. M., Rebelo, C., Simões da Silva, L. (2014). Dynamic simulation of beam-to-column partial-strength steel joints for the assessment of ductility-equivalent viscous damping relationships. In A. Cunha, E. Caetano, P. Ribeiro, & G. Muller (Eds.), *Proceedings of the 9th International Conference on Structural Dynamics, EURODYN 2014* (pp. 395–402). Porto.
- Augusto, H., Castro, J. M., Rebelo, C., Simões da Silva, L. (2014). Contribution To the Extension of the Component Method To Beam-To-Column Connections Subjected To Cyclic Loading. In R. Landolfo & F. M. Mazzolani (Eds.), *7th European Conference on Steel and Composite Structures - EUROSTEEL 2014* (pp. 603–604). Naples: ECCS – European Convention for Constructional Steelwork and Wiley.
- Augusto, H., Castro, J. M., Rebelo, C., Simões da Silva, L. (2014). Determinação da relação ductilidade-amortecimento viscoso equivalente em ligações viga-coluna de resistência parcial pertencentes a pórticos simples recorrendo a simulações dinâmicas. In *5as Jornadas Portuguesas de Engenharia de Estruturas, Encontro Nacional Betão Estrutural e 9º Congresso Nacional De Sismologia e Engenharia Sísmica* (pp. 3301–33016). Lisbon.
- Augusto, H., Castro, J. M., Rebelo, C., Simões da Silva, L., Martins, J. P. (2014). Determinação da resistência de ligações viga-coluna através da resposta linearizada de modelos de elementos finitos segundo o EC3. In *III Congresso Luso-Africano de Construção Metálica Sustentável* (pp. 83–92). Luanda.
- Augusto, H., Castro, J. M., Rebelo, C., Simões da Silva, L. (2015). Caracterização do comportamento cíclico das componentes de ligações viga-coluna com recurso a modelos avançados de elementos finitos. In *X Congresso de Construção Metálica e Mista - Reabilitação do Ambiente Construído* (p. II403-II412). Coimbra: CMM - Associação Portuguesa de Construção Metálica e Mista.
- Augusto, H., Castro, J. M., Rebelo, C., Simões da Silva, L. (2015). A Step Forward in the Cyclic Assessment of the F- Δ Components Using Complete Finite Elements Models of Beam-to-Column Steel End Plate Bolted Joints. In F. M. Mazzolani, G.-Q. Li, S. Chen, & X. Qiang (Eds.), *8th International Conference on Behavior of Steel Structures in Seismic Areas - STESSA 2015* (pp. 639–646). Shanghai: China Architecture & Building Press.
- Augusto, H., Castro, J. M., Rebelo, C., Simões da Silva, L. (2015). Derivation of Ductility-Equivalent Viscous Damping Relationships for Steel Moment-Resisting Frames With Partial Strength Joints. In F. M. Mazzolani, G.-Q. Li, S. Chen, & X. Qiang (Eds.), *8th International Conference on Behavior of Steel Structures in Seismic Areas - STESSA 2015* (pp. 1131–1138). Shanghai: China Architecture & Building Press.
- Augusto, H., Castro, J. M., Rebelo, C., Simões da Silva, L. (2015). Assessment of the F- Δ Relationships for the Web Components Using Detailed Finite Elements Models of Beam-

to-Column Steel Joints. In *Eight International Conference on Advances in Steel Structures - ICASS'2015* (pp. 1–18). Lisbon.

Augusto, H., Castro, J. M., Rebelo, C., Simões da Silva, L. (2016). Extração do comportamento cíclico das componentes da alma da coluna em modelos avançados de elementos finitos de ligações viga-coluna. In *10º Congresso Nacional de Sismologia e Engenharia Sísmica - SISMICA2016* (pp. 1–12). Ponta Delgada.

Simões da Silva, L., Shahbazian, A., Gentili, F., Augusto, H. (2016). Implementation of a component model for the cyclic behaviour of steel joints. In *Connections VIII: Eighth International Workshop on Connection in Steel Structures*. Boston, USA.

References

- ABAQUS ,(2014). Users, Theory and Scripting manuals. Providence, USA: ABAQUS, Inc., Dassault Systèmes Simulia Corp.
- Abolmaali, A., Kukreti, A.R., Razavi, H. (2003). Hysteresis behavior of semi-rigid double web angle steel connections. *Journal of Constructional Steel Research*, 59(8), pp.1057–1082.
- Ádány, S., Calado, L., Dunai, L. (2001). Experimental study on the cyclic behaviour of bolted end-plate joints. *Steel and Composite Structures*, 1(1), pp.33–50.
- Ádány, S., Dunai, L. (2004). Finite element simulation of the cyclic behaviour of end-plate joints. *Computers and Structures*, 82(23–26), pp.2131–2143.
- Adey, B.T. (1997). *Extended End Plate Moment Connections Under Cyclic Loading*. MSc thesis, University of Alberta, p.216.
- Adey, B.T., Grondin, G.Y., Cheng, J.J.R. (1998). Extended end plate moment connections under cyclic loading. *Journal of Constructional Steel Research*, 46(1–3), pp.435–436.
- Ahmed, B., Li, T.Q., Nethercot, D.A. (1996). Modelling composite connection response. In R. Bjorhovde, A. Colson, & R. Zandonini, eds. *Connections in steel structures III: Behaviour, Strength and Design*. Trento, Italy, pp. 259–268.
- ANSI/AISC 341-10 (2010). Seismic Provisions for Structural Steel Buildings. *American Institute of Steel Construction*, (1), USA p.402.
- ASCE/SEI 41-13 (2014). Seismic evaluation and retrofit of existing buildings. *American Society of Civil Engineers*, Virginia, USA.
- Azizinamini, A., Bradburn, J.H., Radziminski, J.B. (1985). *Static and cyclic behaviour of steel beam-column connections*. *Structural Research Studies*, USA.
- Bahaari, M.R., Sherbourne, A.N. (1996). 3D simulation of bolted connections to unstiffened columns-II. Extended endplate connections. *Journal of Constructional Steel Research*, 40(3), pp.189–223.
- Bahaari, M.R., Sherbourne, A.N. (2000). Behavior of eight-bolt large capacity endplate connections. *Computers and Structures*, 77(3), pp.315–325.
- Bernuzzi, C. (1992). Cyclic response of semi-rigid steel joints. In *1st COST Workshop*. Strasbourg, France, pp. 194–209.
- Bernuzzi, C., Zandonini, R., Zanon, P. (1996). Experimental analysis and modelling of semi-rigid steel joints under cyclic reversal loading. *Journal of Constructional Steel Research*, 38(2), pp.95–123.
- Bhatti, M.A. (2005). *Fundamental Finite Element Analysis and Applications: with Mathematica and Matlab Computations*, John Wiley & Sons, Inc.

- Blandon, C.A., Priestley, M.J.N. (2005). Equivalent viscous damping equations for direct displacement based design. *Journal of Earthquake Engineering*, 9(SI 2), pp.257–278.
- Boorse, M.R. (1999). *Evaluation of the Inelastic Rotation Capability of Flush End-Plate Moment Connections*. MSc thesis, Virginia Polytechnic Institute and State University.
- Bravo, M.A., Herrera, R.A. (2014). Performance under cyclic load of built-up T-stubs for Double T moment connections. *Journal of Constructional Steel Research*, 103, pp.117–130.
- Broderick, B.M., Thomson, A.W. (2002). The response of flush end-plate joints under earthquake loading. *Journal of Constructional Steel Research*, 58(9), pp.1161–1175.
- Bursi, O.S., Ferrario, F., Fontanari, V. (2002). Non-linear analysis of the low-cycle fracture behaviour of isolated Tee stub connections. *Computers and Structures*, 80(27–30), pp.2333–2360.
- Bursi, O.S., Galvani, M. (1997). Low cycle behaviour of isolated bolted Tee stubs and extended end plate connections. In *CTA, Italian Conference on Steel Construction*. Ancona, Italy.
- Bursi, O.S., Jaspart, J.P. (1998). Basic issues in the finite element simulation of extended end plate connections. *Computers & Structures*, 69(3), pp.361–382.
- Bursi, O.S., Jaspart, J.P. (1997a). Benchmarks for finite element modelling of bolted steel connections. *Journal of Constructional Steel Research*, 43(1–3), pp.17–42.
- Bursi, O.S., Jaspart, J.P. (1997b). Calibration of a finite element model for isolated bolted end-plate steel connections. *Journal of Constructional Steel Research*, 44(3), pp.225–262.
- Calado, L. (1995). Experimental research and analytical modelling of the cyclic behaviour of bolted semi-rigid connections. In A. N. Kounadis, ed. *Steel Structures - Eurosteel 95*. Balkema, Rotterdam, pp. 197–204.
- Calado, L. (2003). Non-linear cyclic model of top and seat with web angle for steel beam-to-column connections. *Engineering Structures*, 25(9), pp.1189–1197.
- Calado, L., Castiglioni, C.A. (1996). Steel beam-to-column connections under low-cycle fatigue: Experimental and numerical research. In *XI World Conference on Earthquake Engineering, WCEE*. Acapulco, Mexico.
- Calado, L., Ferreira, J. (1994). A numerical model for predicting the cyclic behaviour of steel beam-to-column joints. In *10th European Conference on Earthquake Engineering*. Vienna, Austria.
- Calado, L., Mele, E. (2000). Cyclic Behavior of Steel Beam-To-Column Joints : Governing Parameters of Welded and Bolted Connections. In *Connections in Steel Structures IV: Steel Connections in the New Millennium, AISC*. pp. 194–204.
- Calvi, G.M., Sullivan, T., Roldán, R., O'Reilly, G., Simões da Silva, L., Rebelo, C., Castro, J.M., Augusto, H., Landolfo, R., Della Corte, G., Terraciano, G., Slavatore, W., Morelli, F. (2015). *Displacement based seismic design of steel moment resisting frame structures (DiSTEEL), Final Report*, Brussels.
- Castro, J.M., Elghazouli, A.Y., Izzuddin, B.A. (2005). Modelling of the panel zone in steel

- and composite moment frames. *Engineering Structures*, 27(1), pp.129–144.
- Chen, W.F., Matsuoka, K.G., Nomachi, S.G. (1988). Moment-rotation relation of top and seat angle with double web angle connections. In R. Bjorhovde, J. Brozzetti, & A. Colson, eds. *Connections in Steel Structures: Behaviour, strength and design*. London: Elsevier Applied Science.
- Clough, R.W., Johnston, S.B. (1966). Effect of stiffness degradation on earthquake ductility requirements. In *Proceedings of Second Japan National Conference on Earthquake Engineering*. pp. 227–232.
- Cofie, N.G., Krawinkler, H. (1985). Uniaxial Cyclic Stress-Strain Behavior of Structural Steel. *Journal of Engineering Mechanics*, 111(9), pp.1105–1120.
- Della Corte, G., Landolfo, R., Mazzolani, F.M. (2010). Displacement-based seismic design of braced steel structures. *Steel Construction*, 3(3), pp.134–139.
- Della Corte, G., De Matteis, G., Landolfo, R. (2000). Influence of connection modelling on seismic response of moment resisting steel frames. In F. M. Mazzolani, ed. *Moment resistant connections of steel frames in seismic areas – Design and reliability*. London: E&FN SPON, pp. 485–512.
- Della Corte, G., De Matteis, G., Landolfo, R., Mazzolani, F.M. (2002). Seismic analysis of MR steel frames based on refined hysteretic models of connections. *Journal of Constructional Steel Research*, 58(10), pp.1331–1345.
- Della Corte, G., Mazzolani, F.M. (2008). Theoretical Developments and Numerical Verification Of A Displacement-Based Design Procedure For Steel Braced Structures. In *14th World Conference on Earthquake Engineering (14WCEE)*. Beijing, China.
- D’Aniello, M., Tartaglia, R., Costanzo, S., Landolfo, R. (2017). Seismic design of extended stiffened end-plate joints in the framework of Eurocodes. *Journal of Constructional Steel Research*, 128, pp.512–527.
- Dafalias, Y.F. (1975). *On cyclic and anisotropic plasticity: (I) A general model including material behavior under stress reversals. (II) Anisotropic hardening for initially orthotropic materials*. PhD thesis, University of California, Berkeley.
- Danesh, F., Pirmoz, A., Daryan, A.S. (2007). Effect of shear force on the initial stiffness of top and seat angle connections with double web angles. *Journal of Constructional Steel Research*, 63(9), pp.1208–1218.
- Deng, C.G., Bursi, O.S., Zandonini, R. (2000). Hysteretic connection element and its applications. *Computers and Structures*, 78(1), pp.93–110.
- Dubina, D., Ciutina, A., Stratan, A. (2001). Cyclic tests of double-sided beam-to-column joints. *Journal of structural engineering*, 127(2), pp.129–136.
- Dubina, D., Ciutina, A., Stratan, A. (2000). Cyclic Tests on Bolted Steel Double-Sided Beam-to-Column Joints. In R. T. Leon, ed. *Connections in Steel Structures IV: Steel Connections in the New Millenium*, AISC. Roanoke, USA, pp. 170–180.
- Dunai, L., Kovács, N., Calado, L. (2004). Analysis of Bolted End-Plate Joints : Cyclic Test and Standard Approach. In F. S. K. Bijlaard, A. M. Gresnigt, & G. J. van der Vegte, eds. *Connections in Steel Structures V: Behaviour, Strength and Design*. Amsterdam,

Netherlands, pp. 191–200.

- Dunne, F., Petrinic, N. (2006). *Introduction to Computational Plasticity* second., Oxford University Press.
- Dwairi, H.M., Kowalsky, M.J., Nau, J.M. (2007). Equivalent Damping in Support of Direct Displacement-Based Design. *Journal of Earthquake Engineering*, 11(4), pp.512–530.
- ECCS (1986). *Recommended Testing Procedure for Assessing the Behaviour of Steel Elements under Cyclic Loads*, Brussels, Belgium.
- Elghazouli, A.Y. (2009). *Seismic design of buildings to Eurocode 8*, Spon Press. New York.
- Elnashai, A.S., Elghazouli, A.Y. (1994). Seismic behaviour of semi-rigid steel frames. *Journal of Constructional Steel Research*, 29(1–3), pp.149–174.
- Elnashai, A.S., Elghazouli, A.Y., Denesh-Ashtiani, F.A. (1998). Response of Semirigid Steel Frames to Cyclic and Earthquake Loads. *Journal of Structural Engineering, ASCE*, 124(8), pp.857–867.
- EN 1990 (2002). Eurocode - Basis of structural design. Brussels, Belgium: European Committee for Standardization.
- EN 1993-1-1 (2005). Eurocode 3: Design of steel structures – part 1-1: General rules and rules for buildings. Brussels, Belgium: European Committee for Standardization.
- EN 1993-1-1 (1992). Eurocode 3: General rules and rules for buildings. Brussels, Belgium: European Committee for Standardization.
- EN 1993-1-8 (2005). Eurocode 3: Design of steel structures – part 1-8: Design of joints. Brussels, Belgium: European Committee for Standardization.
- EN 1994-1-1 (2004). Eurocode 4: Design of composite steel and concrete structures - Part 1-1: General rules and rules for buildings. Brussels, Belgium: European Committee for Standardization.
- EN 1998-1 (2004). Eurocode 8: Design of earthquake resistance of structures – part 1-1: General rules – Seismic Actions and General Requirements for Structures. Brussels, Belgium: European Committee for Standardization.
- EN 1998-1 (1994). Eurocode 8. Design of structures for earthquake resistance — Part 1: general rules, seismic actions and rules for buildings. Brussels, Belgium: European Committee for Standardization.
- Faella, C., Piluso, V., Rizzano, G. (1997). A New Method to Design Extended End Plate Connections and Semirigid Braced Frames. *Journal of Constructional Steel Research*, 41(1), pp.61–91.
- Faella, C., Piluso, V., Rizzano, G. (2000). *Structural steel semirigid connections: Theory, design and software*, USA: CRC Press LLC.
- fib (2003). *Displacement-based seismic design of reinforced concrete buildings*, (No. Bulletin 25). *State-of-the-art report prepared by Task Group 7.2*. Fédération International du Béton.
- Filiatrault, A., Sullivan, T. (2014). Performance-based seismic design of nonstructural building components: The next frontier of earthquake engineering. *Earthquake*

- Engineering and Engineering Vibration*, 13(1), pp.17–46.
- Flanagan, D.P., Belytschko, T. (1981). A uniform strain hexahedron and quadrilateral with orthogonal hourglass control. *International Journal for Numerical Methods in Engineering*, 17(5), pp.679–706.
- Flejou, J.L., Colson, A. (1992). A general model for cyclic response of structural civil engineering connections. In *1st COST Workshop*. Strasbourg, France, pp. 419–430.
- Francavilla, A.B., Latour, M., Piluso, V., Rizzano, G. (2016). Bolted T-stubs: A refined model for flange and bolt fracture modes. *Steel and Composite Structures*, 20(2), pp.267–293.
- Francavilla, A.B., Latour, M., Piluso, V., Rizzano, G. (2015). Preliminary analysis and design of an experimental facility for the pseudodynamic earthquake test of a real scale steel moment resisting frame with partial strength joint. In F. M. Mazzolani et al., eds. *STESSA 2015, Behaviour of Steel Structures in Seismic Areas*. Shanghai: China Architecture & Building Press, p. 1665.
- Freeman, S.A. (1998). Development and Use of Capacity Spectrum Method. In *6th US National Conference on Earthquake Engineering*. Seattle, Washington, Paper 269.
- Freeman, S.A. (1978). Prediction of Response of Concrete Buildings to Severe Earthquake Motion. *ACI Journal*, 55(Special Publication), pp.589–606.
- Frye, M.J., Morris, G.A. (1975). Analysis of Flexibly Connected Steel Frames. *Canadian Journal of Civil Engineering*, 2(3), pp.280–291.
- Garcia, R., Sullivan, T.J., Della Corte, G. (2010). Development of a Displacement-Based Design Method for Steel Frame-RC Wall Buildings. *Journal of Earthquake Engineering*, 14(2), pp.252–277.
- Gentili, F., Costa, R.J.T., Simões da Silva, L. (2014). Development of a simplified model for joints in steel structures. In *9th Congresso Nacional de Mecânica Experimental*. Aveiro.
- Gerami, M., Saberi, H., Saberi, V., Daryan, A.S. (2011). Cyclic behavior of bolted connections with different arrangement of bolts. *Journal of Constructional Steel Research*, 67(4), pp.690–705.
- Gervásio, H., Simoes da Silva, L., Borges, L. (2004). Reliability assessment of the post-limit stiffness and ductility of steel joints. *Journal of Constructional Steel Research*, 60(3–5), pp.635–648.
- Ghobarah, A., Korol, R.M., Osman, A. (1992). Cyclic behavior of extended end-plate joints. *Journal of Structural Engineering, ASCE*, 118(5), pp.1333–1353.
- Girão Coelho, A.M. (2004). *Characterization of the ductility of bolted end plate beam-to-column steel connections*. PhD thesis, University of Coimbra.
- Grande, E., Rasulo, A. (2013). Seismic assessment of concentric X-braced steel frames. *Engineering Structures*, 49, pp.983–995.
- Grant, D.N., Blandon, C.A., Priestley, M.J.N. (2005). *Modelling inelastic response in direct displacement based design*, Pavia, Italy: IUSS Press.
- Gulkan, P., Sozen, M.A. (1974). Inelastic Responses of Reinforced Concrete Structure to

- Earthquake Motions. *ACI Journal Proceedings*, 71(12), pp.604–610.
- Guo, B., Gu, Q., Liu, F. (2006). Experimental Behavior of Stiffened and Unstiffened End-Plate Connections under Cyclic Loading. *Journal of Structural Engineering*, 132(9), pp.1352–1357.
- Hutton, D. V. (2003). *Fundamentals of Finite Element Analysis*, McGraw-Hill Science/Engineering/Math.
- Iannone, F., Latour, M., Piluso, V., Rizzano, G. (2011). Experimental Analysis of Bolted Steel Beam-to-Column Connections: Component Identification. *Journal of Earthquake Engineering*, 15(2), pp.214–244.
- Ibarra, L.F., Medina, R.A., Krawinkler, H. (2005). Hysteretic models that incorporate strength and stiffness deterioration. *Earthquake Engineering and Structural Dynamics*, 34(12), pp.1489–1511.
- Imaoka, S. (2008). Chaboche Nonlinear Kinematic Hardening Model. *ANSYS Release: 12.0.1, memo STI0805A*, May. Available at: http://ansys.net/tips_sheldon/STI0805_Chaboche.pdf.
- Jacobsen, L.S. (1930). Steady force vibration as influenced by damping. *Transactions of the American Society of Mechanical Engineers*, 52(15), pp.169–181.
- Jaspart, J.P. (1991). *Étude de la Semi-Rigidité des Noeuds Poutre-Colonne et son Influence sur la Resistence et la Stabilité des Ossatures en Acier*. PhD thesis, University of Liège, Belgium (in French).
- Jaspart, J.P. (1997). *Recent advances in the field of steel joints – columns bases and further configurations for beam-to-column joints and beam-splices*. Aggregation thesis, University of Liège, Belgium.
- Jaspart, J.P. (1990). *Shear and load-introduction deformability and strength of column web panels in strong axis beam-to-column joints - EC3 formulae: discussion and proposals for improvement, Internal report (No. 202)*.
- Jaspart, J.P., Demonceau, J.F., Hoang, V.L. (2014). *Design specifications and drawings of Joint specimens*, Liège. (No. D-WP1-5). *European pre-qualified steel joints (EQUALJOINTS) - Draft deliverable D-WP1-5*. Liège, Belgium.
- Jaspart, J.P., Maquoi, R. (1990). Investigation by testing of the structural response of semi-rigid joints. In *proceedings of the RILEM Workshop on “Needs in testing metals”, 29-31 of Mai*. Naples, pp. 53–63.
- Jaspart, J.P., Vandegans, D. (1998). Application of the component method to column bases. *Journal of Constructional Steel Research*, 48(2), pp.89–106.
- Jaspart, J.P., Weynand, K. (2016). *Design of Joints in Steel and Composite Structures: Eurocode 3: Design of Steel Structures. Part 1-8 Design of Joints. Eurocode 4: Design of Composite Steel and Concrete Structures*. Belgium: ECCS – European Convention for Constructional Steelwork and Wiley.
- Jordão, S., Simões da Silva, L., Simões, R. (2013). Behaviour of welded beam-to-column joints with beams of unequal depth. *Journal of Constructional Steel Research*, 91, pp.42–59.

- Kato, B., Aoki, H., Yamanouchi, H. (1990). Standardized mathematical expression for stress-strain relations of structural steel under monotonic and uniaxial tension loading. *Materials and Structures*, 23, pp.47–58.
- Kim, K.D., Engelhardt, M.D. (2002). Monotonic and cyclic loading models for panel zones in steel moment frames. *Journal of Constructional Steel Research*, 58(5–8), pp.605–635.
- Kishi, N., Ahmed, A., Yabuki, N., Chen, W.F. (2001). Nonlinear finite element analysis of top-and seat-angle with double web-angle connections. *Structural Engineering and Mechanics*, 12(2), pp.201–214.
- Kishi, N., Chen, W.F. (1987). Moment-rotation relations of semirigid connections with angles. *Journal of Structural Engineering, ASCE*, 116(7), pp.1813–1834.
- Komuro, M., Kishi, N., Chen, W.F. (2004). Elasto-plastic FE analysis on moment-rotation relations of top- and seat-angle connections. In F. S. K. Bijlaard, A. M. Gresnigt, & G. J. van der Vegte, eds. *Connections in Steel Structures V: Behaviour, Strength and Design*. Amsterdam, Netherlands, pp. 1101–1110.
- Komuro, M., Kishi, N., Hasan, R. (2003). Quasi-static loading tests on moment-rotation behavior of top- and seat-angle connections. In *Conference on Behaviour of Steel Structures in Seismic Areas, STESSA 2003*. Lisse, pp. 329–334.
- Korol, R.M., Ghobarah, A., Osman, A. (1990). Extended end-plate connections under cyclic loading: Behaviour and design. *Journal of Constructional Steel Research*, 16(4), pp.253–280.
- Krawinkler, H., Popov, E.P., Bertero, V.V. (1975). Shear behaviour of steel frame joints. *Journal of the Structural Division*, 101(11), pp.2317–2336.
- Krishnamurthy, N. (1978). A fresh look at bolted end-plate behaviour and design. *Engineering Journal, AISC*, 15(2), pp.39–49.
- Krishnamurthy, N., Graddy, D.E. (1976). Correlation between 2- and 3-Dimensional Finite Element Analysis of Steel Bolted End-Plate Connections. *Computers & Structures*, 6(4–5), pp.381–389.
- Kuhlmann, U., Davison, J.B., Kattner, M. (1998). Structural systems and rotation capacity. In *COST Conference on Control of the Semi-rigid Behaviour of Civil Engineering Structural Connections*. Liège, Belgium, pp. 167–176.
- Kukreti, A.R., Abolmaali, A.S. (1999). Moment-rotation hysteresis behavior of top and seat angle steel frame connections. *Journal of Structural Engineering, ASCE*, 125(8), pp.810–820.
- Kukreti, A.R., Murray, J.M., Abolmaali, A. (1987). End-plate connections moment-rotation relationship. *Journal of Constructional Steel Research*, 8, pp.137–157.
- Landolfo, R. (2014). *European pre-QUALified steel JOINTS (EQUALJOINTS), Mid-Term Report*, Brussels.
- Landolfo, R. (2016). European qualification of seismic resistant steel bolted beam-to-column joints : the equaljoints project. In *Connections VIII: Eighth International Workshop on Connection in Steel Structures*. Boston, USA.
- Landolfo, R., et al. (2017). *European pre-qualified steel joints (EQUALJOINTS)* (No. Final

- Report (No. RFSR-CT-2013-00021)), Brussels, Belgium. (In preparation).
- Latour, M., Piluso, V., Rizzano, G. (2011). Cyclic Modeling of Bolted Beam-to-Column Connections: Component Approach. *Journal of Earthquake Engineering*, 15(4), pp.537–563.
- Latour, M., Piluso, V., Rizzano, G. (2015). Free from damage beam-to-column joints: Testing and design of DST connections with friction pads. *Engineering Structures*, 85, pp.219–233.
- Latour, M., Rizzano, G. (2015). Experimental Analysis on the Cyclic Response of Beam to Column Joints: State-of-the-Art at Salerno University. *The Open Construction and Building Technology Journal*, 8(1), pp.227–247.
- Latour, M., Rizzano, G. (2013). A component approach for the cyclic modelling of exposed column base plate joints. In *IX Conference on Steel and Mixed Construction*. Porto, Portugal.
- Lemaitre, J., Chaboche, J.L. (1990). *Mechanics of solid materials*, Cambridge University Press.
- Leon, R.T., Hu, J.W., Schrauben, C. (2004). Rotational Capacity and Demand in Top-and-Seat Angle Connections Subjected To Seismic Loading. In F. S. K. Bijlaard, A. M. Gresnigt, & G. J. van der Vegte, eds. *Connections in Steel Structures V: Behaviour, Strength and Design*. Amsterdam, Netherlands, pp. 201–210.
- Lignos, D.G., Krawinkler, H. (2011). Deterioration Modeling of Steel Components in Support of Collapse Prediction of Steel Moment Frames under Earthquake Loading. *Journal of Structural Engineering*, 137(11), pp.1291–1302.
- Ling, Y. (1996). Uniaxial True Stress-Strain after Necking. *AMP Journal of Technology*, 5(1), pp.37–48.
- Madas, P.J., Elnashai, A.S. (1992). A component-based model for beam-to-column connections. In *10th World Conference on Earthquake Engineering*. Madrid, Spain.
- Maggi, Y.I., Goncalves, R.M., Calado, L. (2003). Numerical and experimental behavior of beam-to-column extended end plate connections. In *Stessa 2003: Behaviour of Steel Structures in Seismic Areas*. Naples, Italy, pp.343–349.
- Maggi, Y.I., Gonçalves, R.M., Leon, R.T., Ribeiro, L.F.L. (2005). Parametric analysis of steel bolted end plate connections using finite element modeling. *Journal of Constructional Steel Research*, 61(5), pp.689–708.
- Maley, T.J., Sullivan, T.J., Della Corte, G. (2010). Development of a Displacement-Based Design Method for Steel Dual Systems With Buckling-Restrained Braces and Moment-Resisting Frames. *Journal of Earthquake Engineering*, 14(S1), pp.106–140.
- Maley, T., Sullivan, T.J., Lago, A., Roldán, R., Calvi, G.M. (2013). *Characterising the Seismic Behaviour of Steel MRF Structures*, (No. Report 2013/02). EUCENTRE, IUSS press. Pavia, Italy.
- De Martino, A., Faella, C., Mazzolani, F.M. (1984). Simulation of beam-to-column joint behaviour under cyclic loads. *Costruzioni Metalliche*, 6, pp.346–356.
- De Martino, A., Landolfo, R., Mazzolani, F.M. (1990). The use of the Ramberg-Osgood law

- for materials of round-house type. *Materials and Structures*, 23(1), pp.59–67.
- Mazzolani, F.M. (1988). Mathematical model for semi-rigid joints under cyclic loads. In R. Bjorhovde, J. Brozzetti, & A. Colson, eds. *Connections in Steel Structures: Behaviour, strength and design*. London: Elsevier Applied Science, pp. 112–120.
- Nader, M.N., Astaneh-Asl, A. (1991). Dynamic behavior of flexible, semirigid and rigid steel frames. *Journal of Constructional Steel Research*, 18(3), pp.179–192.
- Nader, M.N., Astaneh-Asl, A. (1996). Shaking Table Tests of Rigid, Semirigid, and Flexible Steel Frames. *Journal of Structural Engineering*, 122(6), pp.589–596.
- Nemati, N., Le Houedec, D., Zandonini, R. (2000). Numerical modelling of the cyclic behaviour of the basic components of steel end plate connections. *Advances in engineering software*, 31(11), pp.837–849.
- Newmark, N.M., Hall, W.J. (1982). *Earthquake Spectra and Design*, Oakland, USA.: EERI Monograph.
- Nievas, C.I., Sullivan, T.J. (2015). Applicability of the direct displacement-based design method to steel moment resisting frames with setbacks. *Bulletin of Earthquake Engineering*, 13(12), pp.3841–3870.
- Nogueiro, P. (2009). *Comportamento Cíclico de Ligações Metálicas (Dynamic Behaviour of Steel Connections)*. PhD thesis, University of Coimbra (in portuguese).
- Nogueiro, P., Da Silva, L.S., Bento, R., Simões, R. (2009). Calibration of model parameters for the cyclic response of end-plate beam-to-column steel-concrete composite joints. *Steel and Composite Structures*, 9(1), pp.39–58.
- Nogueiro, P., Simões da Silva, L., Bento, R., Simões, R. (2006). Experimental behaviour of standardised European end plate beam-to-column steel joints under arbitrary cyclic loading. In *Stability and Ductility of Steel Structures*. Lisbon.
- Nogueiro, P., Simões da Silva, L., Bento, R., Simões, R. (2007). Numerical implementation and calibration of a hysteretic model with pinching for the cyclic response of steel joints. *Advanced Steel Construction*, 3(1), pp.459–484.
- O'Reilly, G.J., Sullivan, T.J. (2016). Direct Displacement-Based Seismic Design of Eccentrically Braced Steel Frames. *Journal of Earthquake Engineering*, 20(2), pp.243–278.
- Paulay, T., Priestley, M.J.N. (1992). *Seismic Design of Reinforced Concrete and Masonry Buildings* I. John Wiley & Sons, ed., New York.
- Pennucci, D., Sullivan, T.J., Calvi, G.M. (2011). Displacement Reduction Factors for the Design of Medium and Long Period Structures. *Journal of Earthquake Engineering*, 15(S1), pp.1–29.
- Piluso, V., Rizzano, G. (2008). Experimental analysis and modelling of bolted T-stubs under cyclic loads. *Journal of Constructional Steel Research*, 64(6), pp.655–669.
- Pirmoz, A., Ahadi, P., Farajkhah, V. (2016). Finite element analysis of extended stiffened end plate link-to-column connections. *Steel Construction*, 9(1), pp.46–57.
- Pirmoz, A., Daryan, A.S., Mazaheri, A., Darbandi, H.E. (2008). Behavior of bolted angle

- connections subjected to combined shear force and moment. *Journal of Constructional Steel Research*, 64(4), pp.436–446.
- Pirmoz, A., Khoei, A.S., Mohammadrezapour, E., Daryan, A.S. (2009). Moment-rotation behavior of bolted top-seat angle connections. *Journal of Constructional Steel Research*, 65(4), pp.973–984.
- Pirmoz, A., Mohammadrezapour, E. (2008). Behavior Of Bolted Top-Seat Angle Connections Under Combined Axial Tension and Moment Loading. In *14th World Conference on Earthquake Engineering (14WCEE)*. Beijing, China.
- Plumier, A., Agatino, M.R., Castellani, A., Castiglioni, C.A., Chesi, C. (1998). Resistance of steel connections to low-cycle fatigue. In *11th European Conference on Earthquake Engineering*. Balkema, Rotterdam, pp. 1–11.
- Plumier, A., Schleich, J.B. (1993). Seismic resistance of steel and composite frame structures. *Journal of Constructional Steel Research*, 27, pp.159–176.
- Popov, E., Pinkney, R. (1968). *Behavior of steel building connections subjected to inelastic strain reversals*, (No. Bull No. 14 (Nov.)), Berkeley.
- Pradhan, A.M., Bouwkamp, J.G. (1994). Structural Performance Aspects on Cyclic Behavior of the Composite Beam-column Joints. In F. M. Mazzolani & V. Gioncu, eds. *Behaviour of Steel Structures in Seismic Areas – STESSA 94*,. London: E & FN SPON, pp. 221–230.
- Priestley, M.J.N. (2003). *Myths and Fallacies in Earthquake Engineering, Rev*, Pavia: IUSS Press.
- Priestley, M.J.N. (1993). Myths and fallacies in earthquake engineering – conflicts between design and reality. *Bulletin of the New Zealand Society for Earthquake Engineering*, 26(3), pp.329–341. Available at: <http://www.nzsee.org.nz/publications/nzsee-quarterly-bulletin/vol-21-30/#jtabs-3>.
- Priestley, M.J.N., Calvi, G.M., Kowalsky, M.J. (2007). *Displacement-Based Seismic Design of Structures*, Pavia: IUSS Press.
- Priestley, M.J.N., Seible, F., Calvi, G.M. (1996). *Seismic Design and Retrofit of Bridges*, New York: John Wiley & Sons, Inc.
- Puri, G.M. (2011). *Python scripts for Abaqus : learn by example*, Charleston, S.C. Available at: <http://www.abaquspython.com/>.
- Ramberg, W., Osgood, W.R. (1943). Description of stress-strain curves by three parameters. *National Advisory Committee For Aeronautics*, Technical Note No. 902.
- Rattan, S.S. (2008). *Strength of materials*, New Delhi: Tata McGraw-Hill.
- Richard, R.M., Abbott, B.J. (1975). Versatile elastic-plastic stress-strain formula. *Journal of the Engineering Mechanics Division*, 101(4), pp.511–515.
- Roldán, R., Sullivan, T.J., Della Corte, G. (2016). Displacement-based design of steel moment resisting frames with partially-restrained beam-to-column joints. *Bulletin of Earthquake Engineering*, 14(4), pp.1017–1046.
- Rosenblueth, E., Herrera, I. (1964). Proceedings of the American Society of Civil Engineers.

- Journal of Engineering Mechanics Division ASCE - Proceedings of the American Society of Civil Engineers*, 90, pp.37–48.
- Ryan, J.C. (1999). *Evaluation of Extended End-Plate Moment Connections Under Seismic Loading*. Virginia Polytechnic Institute and State University.
- Salawdeh, S. (2012). *Seismic Design of Concentrically Braced Steel Frames*. PhD thesis, National University of Ireland, Galway.
- Del Savio, A.A., Nethercot, D.A., Vellasco, P.C.G.S., Andrade, S.A.L., Martha, L.F. (2009). Generalised component-based model for beam-to-column connections including axial versus moment interaction. *Journal of Constructional Steel Research*, 65(8–9), pp.1876–1895.
- SeismoSignal (2012). User's Manual. Pavia, Italy: SeismoSoft Ltd., Inc., Earthquake Engineering Software Solutions.
- SERICON (1995). International databank system for semi-rigid connections. RWTH Aachen Germany: ECCS TC10 and Cost C1, Version 1.5.
- Shen, J., Astaneh-Asl, a (1999). Hysteretic behavior of bolted-angle connections. *Journal of Constructional Steel Research*, 51(3), pp.201–218.
- Sherbourne, A.N., Bahaari, M.R. (1996). 3D simulation of bolted connections to unstiffened columns-I. T-stub connections. *Journal of Constructional Steel Research*, 40(3), pp.169–187.
- Sherbourne, A.N., Bahaari, M.R. (1994). 3D simulation of end-plate bolted connections. *Journal of Structural Engineering, ASCE*, 120(11), pp.3122–3136.
- Shi, G., Chen, X. (2017). Moment-rotation curves of ultra-large capacity end-plate joints based on component method. *Journal of Constructional Steel Research*, 128, pp.451–461.
- Shi, G., Shi, Y., Wang, Y. (2007). Behaviour of end-plate moment connections under earthquake loading. *Engineering Structures*, 29(5), pp.703–716.
- Shi, G., Shi, Y., Wang, Y., Bradford, M.A. (2008). Numerical simulation of steel pretensioned bolted end-plate connections of different types and details. *Engineering Structures*, 30(10), pp.2677–2686.
- Simões, R., Simões da Silva, L., Cruz, P.J.S. (2001). Cyclic behaviour of end-plate beam-to-column composite joints. *Steel and Composite Structures*, 1(3), pp.355–376.
- Simões da Silva, L. (2008). Towards a consistent design approach for steel joints under generalized loading. *Journal of Constructional Steel Research*, 64(9), pp.1059–1075.
- Simões da Silva, L., Rebelo, C., Mota, L. (2009). Extension of the component method to end-plate beam-to-column steel joints subjected to seismic loading. In *The Twelfth International Conference on Civil, Structural and Environmental Engineering Computing, Computational Science, Engineering and Technology Series 22*. pp.149–167.
- Simões da Silva, L., Santiago, A., Vila Real, P. (2002). Post-limit stiffness and ductility of end-plate beam-to-column steel joints. *Computers and Structures*, 80(5–6), pp.515–531.

- Simões da Silva, L., Shahbazian, A., Gentili, F., Augusto, H. (2016). Implementation of a component model for the cyclic behaviour of steel joints. In *Connections VIII: Eighth International Workshop on Connection in Steel Structures*. Boston, USA.
- Sivaselvan, M. V., Reinhorn, A.M. (2000). Hysteretic Models for Deteriorating Inelastic Structures. *Journal of Engineering Mechanics*, 126(6), pp.633–640.
- Song, J., Pincheira, J. (2000). Spectral Displacement Demands of Stiffness- and Strength-Degrading Systems. *Earthquake Spectra*, 16(4), pp.817–851.
- Steenhuis, M., Evers, H., Gresnigt, N. (1996). Conceptual design of joints in braced steel frames. In *IABSE Semi-Rigid Structural Connections Colloquium*. Istanbul, pp. 327–336.
- Sullivan, T.J. (2013). Direct displacement-based seismic design of steel eccentrically braced frame structures. *Bulletin of Earthquake Engineering*, 11(6), pp.2197–2231.
- Sullivan, T.J., Calvi, G.M., Priestley, M.J.N., Kowalsky, M.J. (2003). The Limitations and Performances of Different Displacement-Based Design Methods. *Journal of Earthquake Engineering*, 7(S1), pp.201–241.
- Sullivan, T.J., O'Reilly, G.J. (2014). *Characterising the Seismic Behaviour of Steel Beam-Column Joints for Seismic Design* T. J. Sullivan & G. J. O'Reilly, eds., Pavia, Italy: IUSS Press.
- Sullivan, T.J., Priestley, M.J.N., Calvi, G.M. (2012). *A Model Code for the Displacement-Based Seismic Design of Structures*, Pavia: IUSS Press.
- Sullivan, T.J., Quaini, M., Maley, T., Calvi, G.M. (2011). Deformed shapes of steel moment resisting frames. In *EUROSTEEL 2011*. Budapest, Hungary.
- Sullivan, T.J., Goggins, J. (2009). Displacement-based seismic design of SDOF concentrically braced frames. In F. Mazzolani, J. M. Ricles, & R. Sause, eds. *Behaviour of Steel Structures in Seismic Areas*. Philadelphia, USA: CRC Press, pp. 685–691.
- Sumner, E.A. (2003). *Unified design of extended end-plate moment connections subjected to cyclic loading*. PhD thesis. Virginia Polytechnic Institute and State University.
- Sumner, E.A., Murray, T.M. (2002). Behavior of extended end-plate moment connections subject to cyclic loading. *Journal of Structural Engineering*, 128(4), pp.501–508.
- Sun, E.Q. (2006). Shear Locking and Hourglassing in MSC Nastran, ABAQUS and ANSYS. In *MSC Software Users Conference*. pp. 1–9.
- Takhirov, S.M., Popov, E.P. (2002). Bolted large seismic steel beam-to-column connections part 2: Numerical nonlinear analysis. *Engineering Structures*, 24(12), pp.1535–1545.
- Tartaglia, R., Zimbru, M., D'Aniello, M., Costanzo, S., Landolfo, R., De Martino, A. (2015). Parametric analysis on the seismic response of bolted extended stiffened end-plate joints. In *XXV Congress C.T.A. (The Italian Steel Days)*. Salerno, Italy.
- Tsai, K., Popov, E.P. (1990). Cyclic behavior of end-plate moment connections. *Journal of Structural Engineering*, ASCE, 116(11), pp.2917–2930.
- Vasilopoulos, A.A., Beskos, D.E. (2006). Seismic design of plane steel frames using advanced methods of analysis. *Soil Dynamics and Earthquake Engineering*, 26(12), pp.1077–1100.

- Villaverde, R. (2004). Seismic Analysis and Design of Nonstructural Elements. In Y. Bozorgnia & V. V. Bertero, eds. *Earthquake Engineering: from Engineering Seismology to Performance Based Engineering*. Boca Raton: CRC Press, p. 976.
- Weynand, K. (1992). SERICON: databank on joints in building frames. In *1st COST C1 Workshop, October 28-30*. Strasbourg.
- Weynand, K., Jaspard, J.P., Steenhuis, M. (1998). Economy studies of steel building frames with semi-rigid joints. *Journal of Constructional Steel Research*, 46(1–3), p.85.
- Weynand, K., Jaspard, J.P., Steenhuis, M. (1996). The stiffness model of revised Annex J of Eurocode 3. In R. Bjorhovde, A. Colson, & R. Zandonini, eds. *Connections in steel structures III: Behaviour, Strength and Design*. Trento, Italy, pp. 441–452.
- Wijesundara, K.K., Nascimbene, R., Sullivan, T.J. (2011). Equivalent viscous damping for steel concentrically braced frame structures. *Bulletin of Earthquake Engineering*, 9(5), pp.1535–1558.
- Yang, C.-M., Kim, Y.-M. (2007a). Cyclic behavior of bolted and welded beam-to-column joints. *International Journal of Mechanical Sciences*, 49(5), pp.635–649.
- Yang, C.-M., Kim, Y.-M. (2007b). Cyclic behaviour of beam–column connections in steel portals. *Proceedings of the ICE - Structures and Buildings*, 160(5), pp.259–272.
- Yee, K.L., Melchers, R.E. (1986). Moment-rotation curves for bolted connections. *Journal of Structural Engineering, ASCE*, 112, pp.615–635.
- Yorgun, C., Bayramoğlu, G. (2001). Cyclic tests for welded-plate sections with end-plate connections. *Journal of Constructional Steel Research*, 57(12), pp.1309–1320.
- Ziomek, D., Tomana, A., Waszczyszyn, Z. (1992). Finite element modeling of end plate connection versus experimental results. In *Proceedings of 1st COST Workshop*. Strasbourg, France, pp. 433–442.
- Zoetemeijer, P. (1974). Design Method for the Tension Side of Statically Loaded, Bolted Beam-To-Column Connections. *Heron*, 20(1), pp.1–59.
- Zoetemeijer, P. (1975). *The influence of normal, bending and shear stresses on the ultimate compression force exerted laterally to European rolled sections*, Report 6-75-18. Delft.

Annexes

A CONSIDERATIONS ON THE LINEARIZATION OF JOINTS RESPONSE

A.1. INTRODUCTION

In Section 3.2.4.3 a procedure was proposed for the linearization of the non-linear monotonic responses of joints, with the aim of determine the strength and initial stiffness of the joints, thus enabling to compare with analytical values or safety requirements. The procedure is defined as the intersection of the two straight lines corresponding to the initial stiffness of the joint and a post-limit stiffness. The latter is established on a case-by-case basis, directly from the full $M-\theta$ curve, defined as the tangent to the $M-\theta$ curve with a slope given by $S_{j,ini}/h$, where h is adjusted for each case. However, in the procedure, the ability to predict the joint strength and stiffness, as defined in EC3-1-8 (EN 1993-1-8, 2005), is dependent of the definition of the parameter h , which is defined according to the joint response. It is possible to find in literature other methodologies that uses the same linearization procedure to determine the yielding point, namely the ECCS (1986) procedure. In this case the post-limit stiffness is determined as the tangent, to the non-linear curve, that as a slope defined by a fixed value for h , equal to 10. The yielding point determined is then used to set the amplitudes in the load protocol for cyclic loading. It is therefore apparent that the objective behind the method is not intended to determine a resistance to the joint, but rather to define the yield point. On the other hand EC3-1-8 (EN 1993-1-8, 2005) defines the joints strength on the basis of the resistances of its basic components, and allows the use of linear-elastic or elastic-plastic analysis in the design of the joints. In the later the initial stiffness of the joint is reduced to take into account the non-linear response of the joint, depending on the design bending moment, see Figure A.1. Therefore

determining the joints initial stiffness and resistance systematically in the response curve, aiming to design the joint following the EC3-1-8 criteria, can be a difficult to exercise.

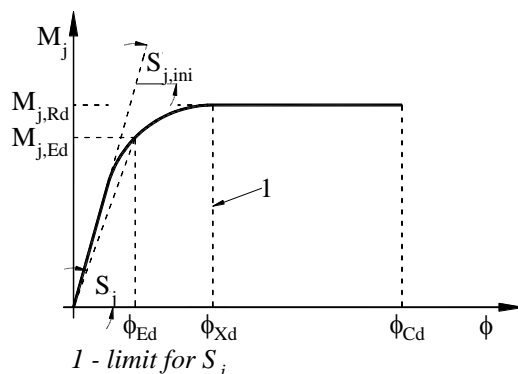


Figure A.1: Design moment rotations characteristics of a joint (extracted from EC3-1-8 (EN 1993-1-8, 2005)).

It is intended in this section to test the capability of the ECCS (1986) procedure, to predict the joint initial stiffness and strength according to the requirements of EC3-1-8 (EN 1993-1-8, 2005). For that a parametric study was undertaken comprising seventy finite element models (FEM) of the joints used in Chapter 3, in particular the J1.1 and J3.1, with modified geometries. The developed parametric script of the beam-to-column end-plate joint, developed in Chapter 3 and detailed in Appendix B, was also used in here.

A.2. FRAMEWORK AND INITIAL ASSUMPTIONS

Based on the FEM developed and validated in Chapter 3 for the J1.1 and J3.1, two parameters were studied: the distance of the external and internal bolt rows to the beam flanges (m_x) and the thickness of the end-plate (t_p), as defined in Figure A.2. The set of analysis presented in Table A.1, where the reference joints J1.1 and J3.1 are highlighted in bold. For the steel mechanical properties adopted in the analyses the nominal values in Eurocode 3 part 1-1 (EN 1993-1-1, 2005) were used ($E = 2.10E^5 \text{ N/mm}^2$; $f_y = 355 \text{ N/mm}^2$; $f_u = 490 \text{ N/mm}^2$). Using the minimum ductility requirements adopted in the EC3-1-1 for steel to build the stress-strain curve for the FEM, in particular the relationships defined by the Eqs. (A.1) and (A.2).

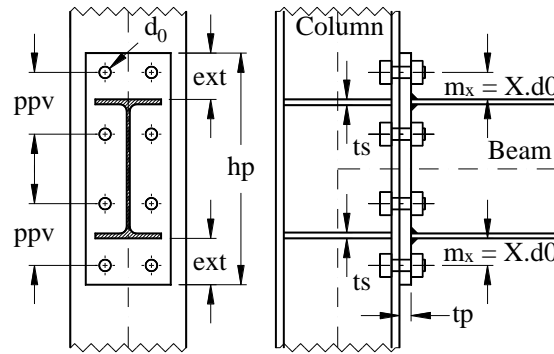


Figure A.2: Geometrical parameters varied in the parametric study.

$$\varepsilon_u / \varepsilon_y = 15 \quad (\text{A.1})$$

$$\varepsilon_r(\text{min}) = 0.15 \quad (\text{A.2})$$

Table A.1: Matrix of the joints in study.

	ppv (mm)	m _x (mm)	X	t _p (mm)				
				18	20	22	24	26
Joints based on J1.1	100	40	1.54	C1_1ppv1_tp0	C1_1ppv1_tp1	C1_1ppv1_tp2	C1_1ppv1_tp3	C1_1ppv1_tp4
	120	50	1.92	C1_1ppv2_tp0	C1_1ppv2_tp1	C1_1ppv2_tp2	C1_1ppv2_tp3	C1_1ppv2_tp4
	140	60	2.31	C1_1ppv3_tp0	C1_1ppv3_tp1	C1_1ppv3_tp2	C1_1ppv3_tp3	C1_1ppv3_tp4
	160	70	2.69	C1_1ppv4_tp0	C1_1ppv4_tp1	C1_1ppv4_tp2	C1_1ppv4_tp3	C1_1ppv4_tp4
	180	80	3.08	C1_1ppv5_tp0	C1_1ppv5_tp1	C1_1ppv5_tp2	C1_1ppv5_tp3	C1_1ppv5_tp4
	200	90	3.46	C1_1ppv6_tp0	C1_1ppv6_tp1	C1_1ppv6_tp2	C1_1ppv6_tp3	C1_1ppv6_tp4
	220	100	3.85	C1_1ppv7_tp0	C1_1ppv7_tp1	C1_1ppv7_tp2	C1_1ppv7_tp3	C1_1ppv7_tp4
Joints based on J3.1	100	40	1.54	C3_1ppv1_tp0	C3_1ppv1_tp1	C3_1ppv1_tp2	C3_1ppv1_tp3	C3_1ppv1_tp4
	120	50	1.92	C3_1ppv2_tp0	C3_1ppv2_tp1	C3_1ppv2_tp2	C3_1ppv2_tp3	C3_1ppv2_tp4
	140	60	2.31	C3_1ppv3_tp0	C3_1ppv3_tp1	C3_1ppv3_tp2	C3_1ppv3_tp3	C3_1ppv3_tp4
	160	70	2.69	C3_1ppv4_tp0	C3_1ppv4_tp1	C3_1ppv4_tp2	C3_1ppv4_tp3	C3_1ppv4_tp4
	180	80	3.08	C3_1ppv5_tp0	C3_1ppv5_tp1	C3_1ppv5_tp2	C3_1ppv5_tp3	C3_1ppv5_tp4
	200	90	3.46	C3_1ppv6_tp0	C3_1ppv6_tp1	C3_1ppv6_tp2	C3_1ppv6_tp3	C3_1ppv6_tp4
	220	100	3.85	C3_1ppv7_tp0	C3_1ppv7_tp1	C3_1ppv7_tp2	C3_1ppv7_tp3	C3_1ppv7_tp4

Plastic mechanism type 1, for the external bolt row, according to the EC3-1-8.

Plastic mechanism type 2, for the external bolt row, according to the EC3-1-8.

In the EC3-1-8 the strength of a joint is determined directly, on the basis of the resistances of its basic components. On the other hand in the numerical analysis it is necessary to identify in the moment-rotation curve, normally non-linear, where the representative strength value of the joint can be defined. The procedure defined in the ECCS (1986), originally defined to determine the yield point, is used to define the representative strength value of the joint. The procedure is illustrated in the Figure A.3. To determine the joints rotations the Eq. (3.21) was used, which considers also the plastic deformation of the beam web and flange in compression near the end-plate.

The failure modes associated to the T-stub models plastic mechanisms, representative of the components end-plate in bending and column flange in bending behaviour, for each bolt row, as defined in the EC3-1-8, are also identified in Table A.1. In particular the ductile ones: mode 1, characterized by the yielding of the plates (end-plate or column flange), considering that the bolts are sufficiently strong to resist to the applied axial tension forces, including the prying forces (Q), see Section 2.2.2.2; and the mode 2 characterized by a shared plastic deformation of the bolts and plates, although in the plates the full plastic mechanism is not reached. For the external bolt rows the different plastic mechanism modes (1 or 2) is highlight in the table, for the mode 1 in grey-shaded, and the mode 2 are the remaining. For the second and third inner bolt rows the mode 2 was always achieved. It is also important to refer that, in the application of the EC3-1-8 procedure to determine the joint resistance, the partial safety factors were all consider equal to 1.0.

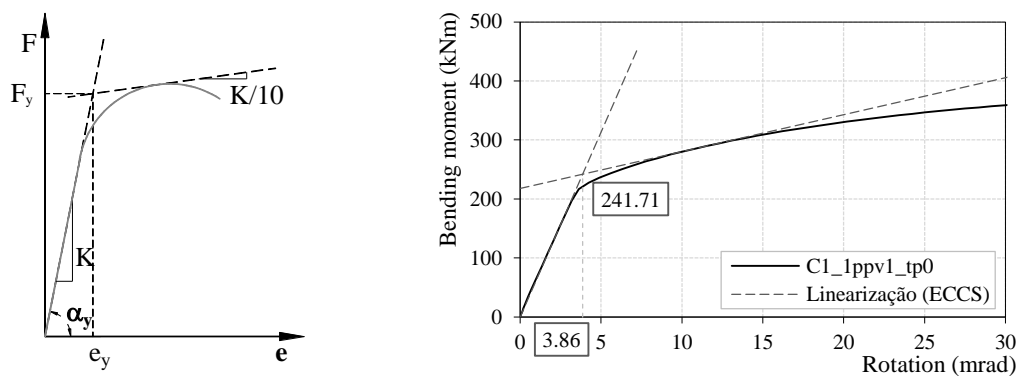


Figure A.3: ECCS (1986) procedure to determine the yielding point.

A.3. DISCUSSION OF THE RESULTS

In Figure A.4 and also in Figure A.5 are depicted the comparisons of the resistance of the joints in terms of the bending moment, for the joints based on the J1.1, between the resistance obtained by the EC3-1-8 and the ones obtained by the application of the ECCS procedure to the moment-rotation response obtained in the numerical models. In the Figure A.6 and also in Figure A.7, the same comparison is performed, but for the joints based on the J3.1.

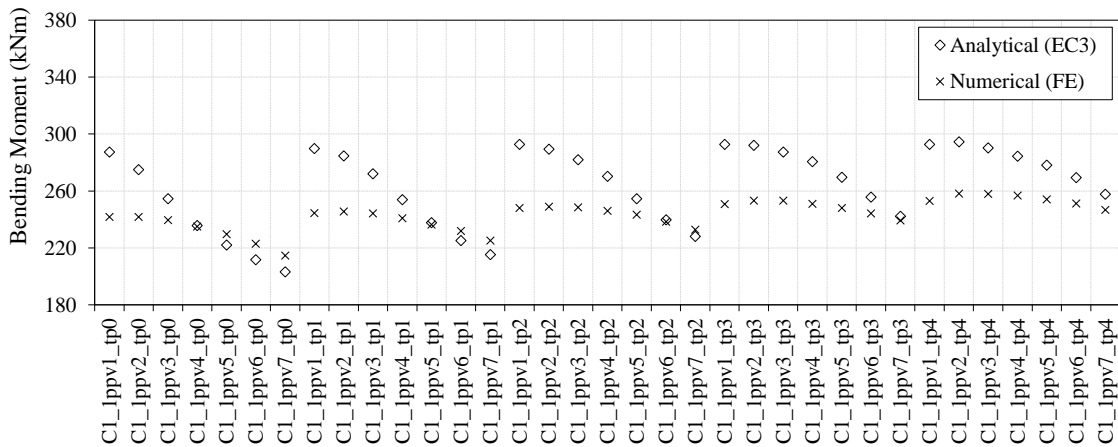


Figure A.4: Comparison of the joints strength, obtained with analytical and numerical procedures, ranging m_x and keeping t_p .

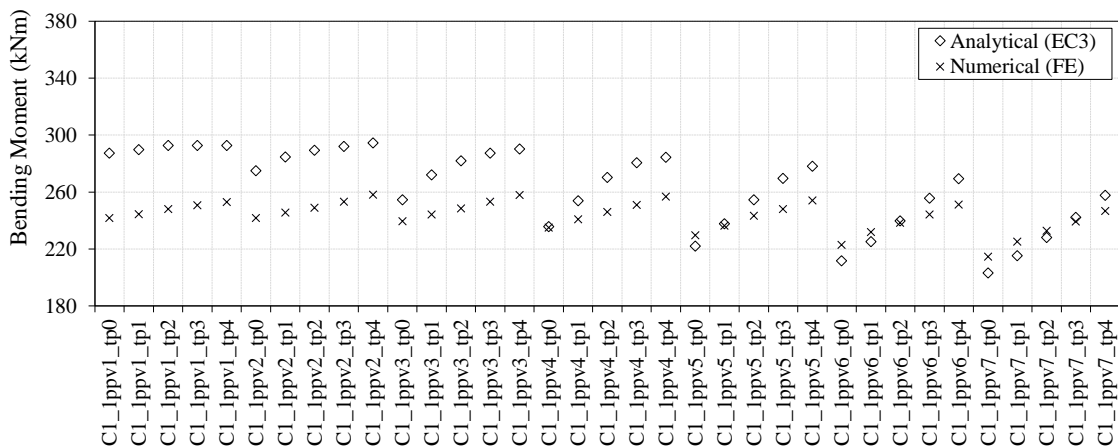


Figure A.5: Comparison of the joints strength, obtained with analytical and numerical procedures, ranging t_p and keeping m_x .

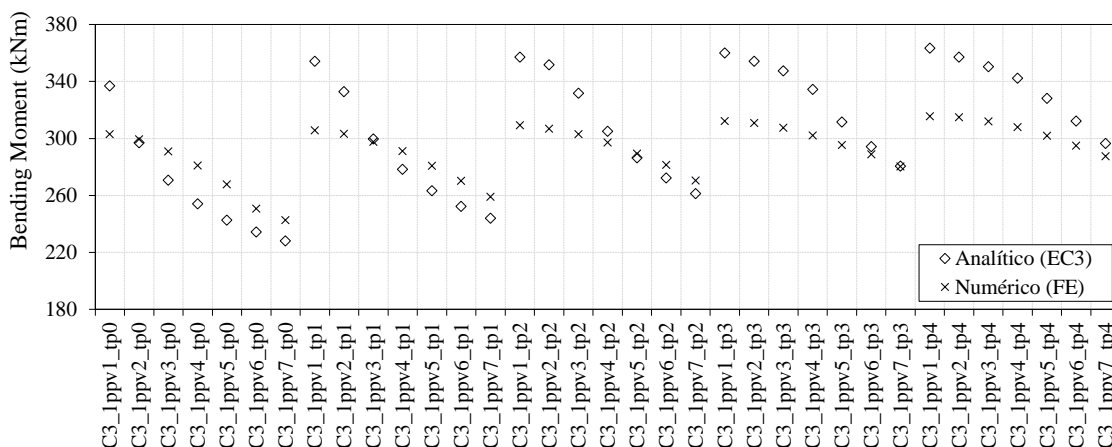


Figure A.6: Comparison of the joints strength, obtained with analytical and numerical procedures, ranging m_x and keeping t_p .

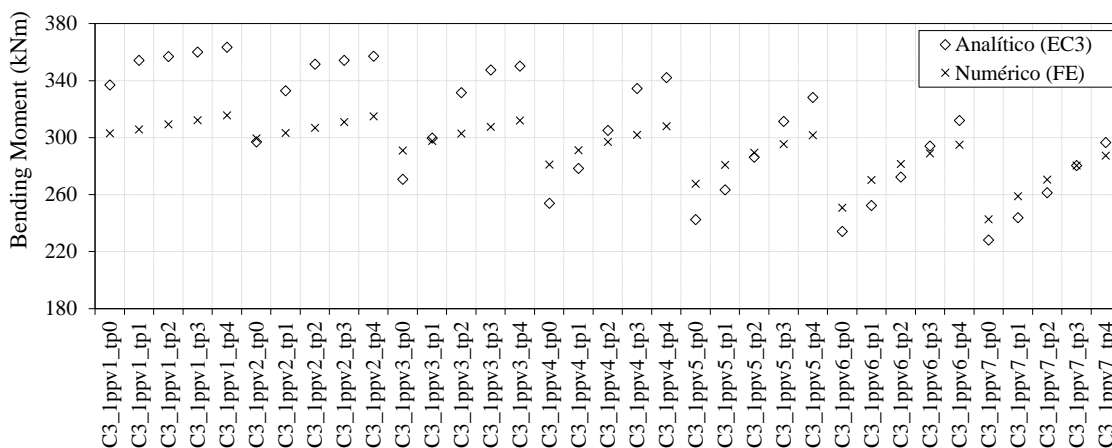


Figure A.7: Comparison of the joints strength, obtained with analytical and numerical procedures, ranging t_p and keeping m_x .

A careful analysis of the figures reveals that there are considerable differences between the strength values obtained by the analytical procedure available in the EC3-1-8 and the ECCS procedure applied to the FEM moment-rotation response. These differences are more significant in the joints based on J1.1, in which the resistance is more conditioned by component column web panel in shear. For the joints based on the J3.1, a good agreement, between the analytical and numerical results, was observed in the joints with $t_p = 18mm$, with the exception of the joint with $ppv = 100mm$, where the strength obtained analytically is considerably higher. It is also possible to realize that the difference between the analytical and numerical results grows with the thickness increase of the end-plate, and with the reduction of the distance between bolt rows.

From Figure A.8 to Figure A.11 the initial stiffness is compared when the analytical procedure, using the component method, and the numerical procedure, using the slope of the elastic branch of the ECCS methodology, as illustrated in Figure A.3, are adopted. In the Figure A.8, ranging m_x and fixing t_p values, and in the Figure A.9, ranging t_p and fixing m_x values, are depicted the comparisons for the joints based on J1.1. In the Figure A.10, ranging m_x and fixing t_p values, and in the Figure A.11, ranging t_p and fixing m_x values, are depicted the comparisons of the joints based on J3.1.

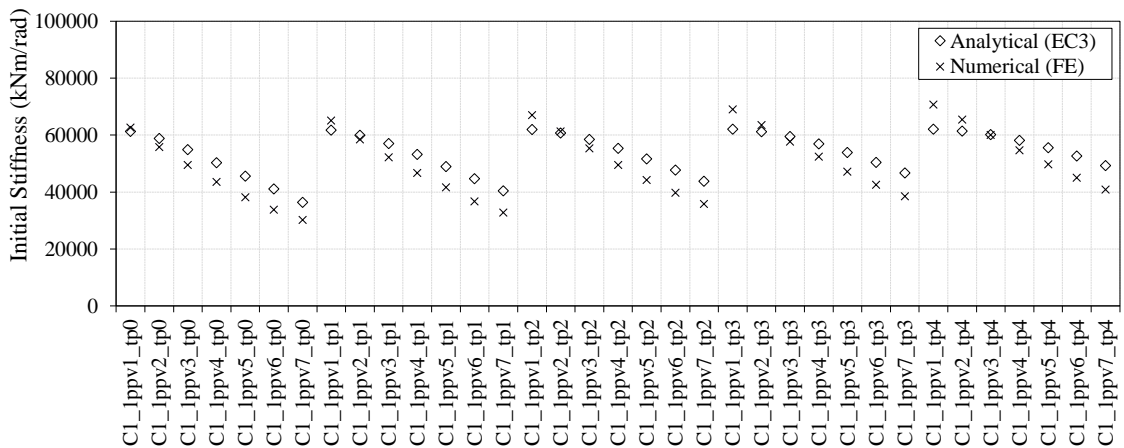


Figure A.8: Comparison of the joints initial stiffness, obtained with analytical and numerical procedures, ranging m_x and keeping t_p .

The comparisons revealed that, in general, the results have a good agreement, although it is noted that for joints with higher end-plate thicknesses, the variation of the initial stiffness, when the distance between bolt rows changes, is linear in the analytical results, however in the numerical approach the variation evolves slowly and with a non-linear shape.

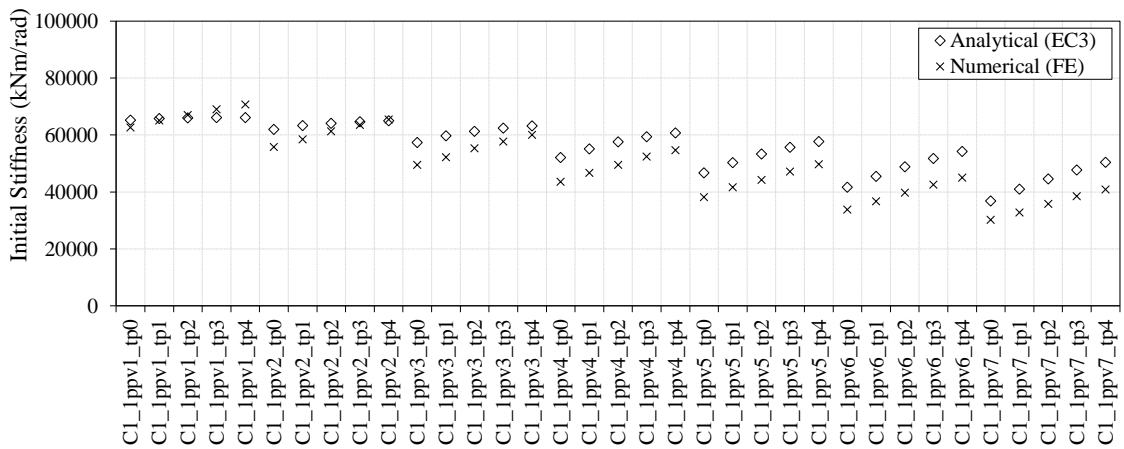


Figure A.9: Comparison of the joints initial stiffness, obtained with analytical and numerical procedures, ranging t_p and keeping m_x .

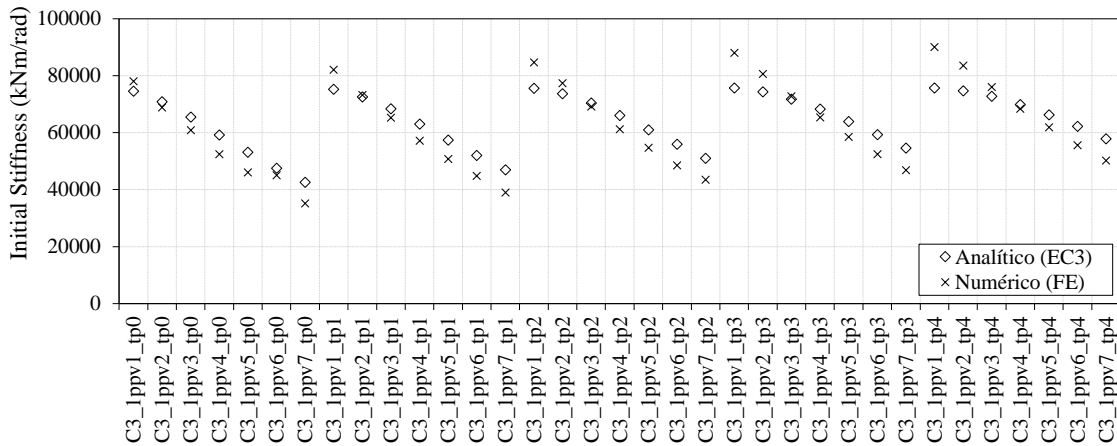


Figure A.10: Comparison of the joints initial stiffness, obtained with analytical and numerical procedures, ranging m_x and keeping t_p .

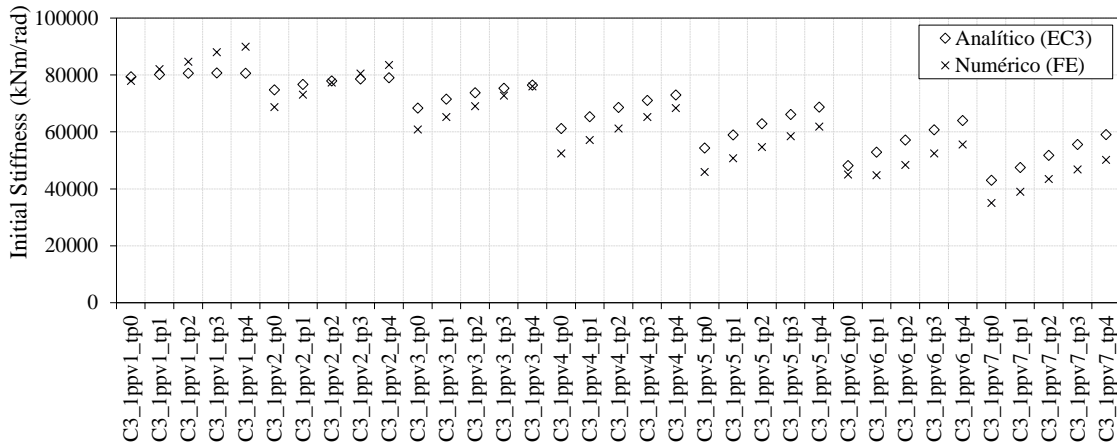


Figure A.11: Comparison of the joints initial stiffness, obtained with analytical and numerical procedures, ranging t_p and keeping m_x .

Table A.2 quantifies the differences when the analytical and numerical procedures are used to compute the joints strength in terms of bending moment. It is possible to observe that the biggest differences occur in the joints where the tensioned bolt rows falls in the failure mode 2. In fact there is a reduction of the differences found as the joints external bolt rows approach to the failure mode 1.

Table A.2: Differences between the joints strength determined analytically and numerically.

ppv (mm)		t_p (mm)				
		$t_{p0} = 18$	$t_{p1} = 20$	$t_{p2} = 22$	$t_{p3} = 24$	$t_{p4} = 26$
		$ M_{j,Rd}/M_{y(FE)} - 1 $	$ M_{j,Rd}/M_{y(FE)} - 1 $	$ M_{j,Rd}/M_{y(FE)} - 1 $	$ M_{j,Rd}/M_{y(FE)} - 1 $	$ M_{j,Rd}/M_{y(FE)} - 1 $
Joints based on J1.1	ppv ₁ = 100	18.88%	18.88%	17.94%	16.74%	15.76%
	ppv ₂ = 120	13.73%	15.96%	16.25%	15.31%	14.05%
	ppv ₃ = 140	6.23%	11.39%	13.51%	13.47%	12.53%
	ppv ₄ = 160	0.27%	5.43%	9.91%	11.74%	10.78%
	ppv ₅ = 180	3.35%	0.53%	4.58%	8.61%	9.45%
	ppv ₆ = 200	5.05%	2.87%	0.59%	4.77%	7.29%
	ppv ₇ = 220	5.34%	4.44%	1.98%	1.21%	4.41%
Joints based on J3.1	ppv ₁ = 100	11.17%	15.87%	15.41%	15.28%	15.11%
	ppv ₂ = 120	0.83%	9.76%	14.60%	13.94%	13.36%
	ppv ₃ = 140	6.96%	0.65%	9.47%	12.96%	12.24%
	ppv ₄ = 160	9.62%	4.42%	2.68%	10.73%	11.08%
	ppv ₅ = 180	9.39%	6.20%	1.08%	5.45%	8.72%
	ppv ₆ = 200	6.56%	6.61%	3.26%	1.83%	5.79%
	ppv ₇ = 220	6.03%	5.82%	3.38%	0.07%	3.14%

A.4. IMPROVING THE PERFORMANCE OF THE LINEARIZATION TO THE EC3 RESULTS

It is intended in this section to determine a better post-limit stiffness parameter (h) for the tangent to the M - θ curve defined by the slope given by $S_{j,ini}/h$. For that the parameter h was derived minimizing the some of the differences between the results obtained by the EC3-1-8 and the results obtained applying the ECCS procedure to the numerical results, according to the Eq. (A.3). As observed in Table A.2, the failure modes associated to the external bolt row of the joints, influences the agreement between the analytical and numerical results, being in the joints presenting mode 2 that the biggest differences were found. It is then expected that also different h parameters should be applied to joints governed by different failure modes. In this way the adjustment of the parameter h was determined separately for the joints presenting mode 1 and mode 2 in the external bolt row. For the joints based on the J1.1 a value of 12.37 (for the mode 1) and 18.72 (for the mode 2) was found for the parameter h_1 and h_2 , respectively. In the case of the joints based on the J3.1 the values found for the parameter h are: $h_1 = 9.54$ and $h_2 = 20.58$. From the average of the obtained values the following parameters are proposed for a better adjustment: $h_1 = 11$ and $h_2 = 20$. If the proposed values are applied to the numerical

results it is possible to observe that there is a considerable reduction in the differences found between the application of the two procedures, mainly in the joints presenting mode two in the external bolt row of the component end-plate in bending, see Table A.3. However for the joints with mode 1 the differences found in the strength did not change significantly, because the parameter h suffered only a small change. For that reason it is proposed the same value of h for the joints conditioned by the failure mode type 1.

$$\left| M_{j,Rd(EC3)} / M_{y(FE)} - 1 \right| * 100 \quad (\text{A.3})$$

Table A.3: Differences between the strength determined analytically and numerically for $h_1=11$ and $h_2 = 20$.

ppv (mm)		t_p (mm)				
		$t_{p0} = 18$	$t_{p1} = 20$	$t_{p2} = 22$	$t_{p3} = 24$	$t_{p4} = 26$
		$ M_{j,Rd}/M_{y(FE)} - 1 $	$ M_{j,Rd}/M_{y(FE)} - 1 $	$ M_{j,Rd}/M_{y(FE)} - 1 $	$ M_{j,Rd}/M_{y(FE)} - 1 $	$ M_{j,Rd}/M_{y(FE)} - 1 $
Joints based on J1.1	ppv ₁ = 100	1.66%	1.18%	0.48%	0.94%	2.27%
	ppv ₂ = 120	11.43%	13.60%	0.53%	1.41%	2.58%
	ppv ₃ = 140	4.06%	9.11%	11.17%	2.59%	3.55%
	ppv ₄ = 160	1.78%	3.22%	7.63%	9.42%	4.60%
	ppv ₅ = 180	5.34%	1.55%	2.42%	6.36%	5.30%
	ppv ₆ = 200	7.01%	4.89%	1.55%	2.59%	5.01%
	ppv ₇ = 220	7.37%	6.45%	4.04%	0.94%	2.21%
Joints based on J3.1	ppv ₁ = 100	2.04%	2.13%	1.85%	1.76%	1.59%
	ppv ₂ = 120	2.41%	8.01%	0.98%	0.54%	0.09%
	ppv ₃ = 140	8.45%	1.01%	7.72%	0.32%	1.00%
	ppv ₄ = 160	11.04%	5.99%	0.97%	8.91%	1.91%
	ppv ₅ = 180	10.85%	7.73%	2.72%	3.70%	3.57%
	ppv ₆ = 200	8.02%	8.10%	4.76%	0.27%	4.07%
	ppv ₇ = 220	7.49%	7.30%	4.89%	1.49%	1.53%

The comparisons of strength obtained with the new parameters, $h_1 = 11$ and $h_2 = 20$, can be seen, for joints based on the J1.1, in Figure A.12 ranging m_x and fixing t_p values, and in Figure A.13, ranging t_p and fixing m_x values. In turn, for joints based on the J3.1, the comparisons can be seen in Figure A.14, ranging m_x and fixing t_p values, and in Figure A.15, ranging t_p and fixing m_x values. The improvements in the adjustment of the two procedures is notorious, especially for joints presenting failure mode type 1. It is however evident that in the transition between using one parameter or another, for joints with slender end-plates, the improvement is not so notorious, as in the case of joints with thicker end-plates, particularly in the joints based on J1.1, possibly due to the higher dependency of these joints from the column web panel deformation.

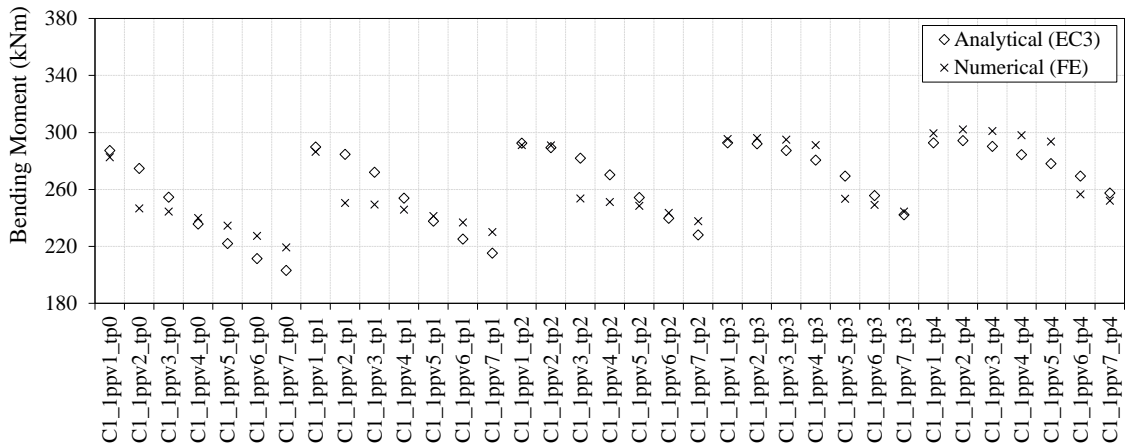


Figure A.12: Comparison of the joints strength, obtained with analytical and numerical procedures, ranging m_x and keeping t_p .

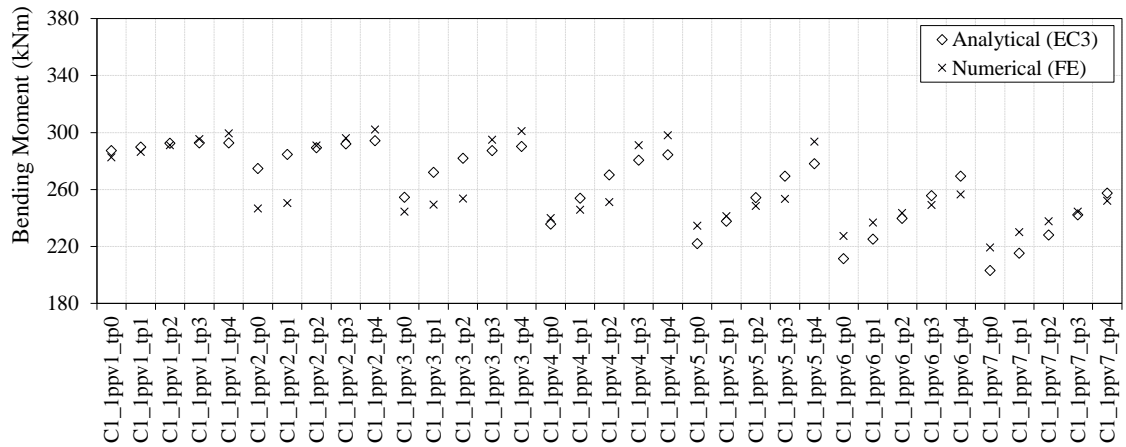


Figure A.13: Comparison of the joints strength, obtained with analytical and numerical procedures, ranging t_p and keeping m_x .

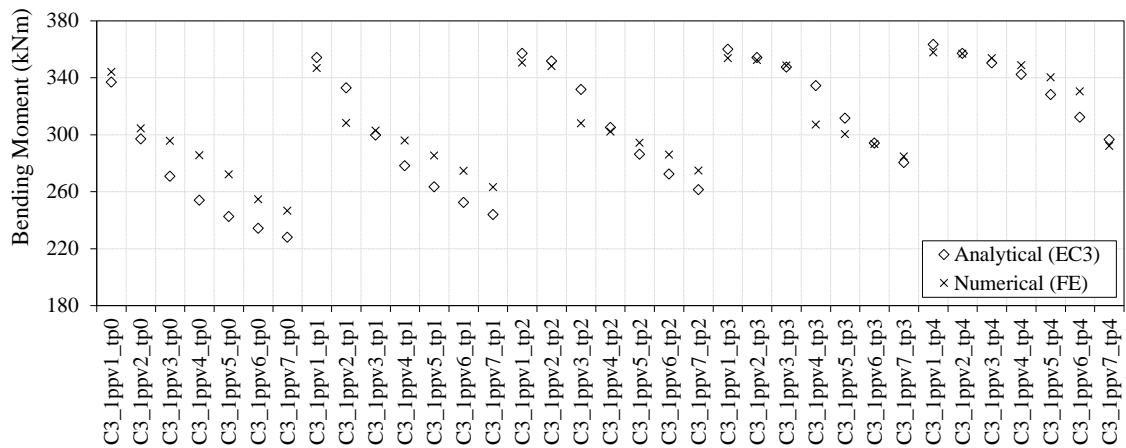


Figure A.14: Comparison of the joints strength, obtained with analytical and numerical procedures, ranging m_x and keeping t_p .

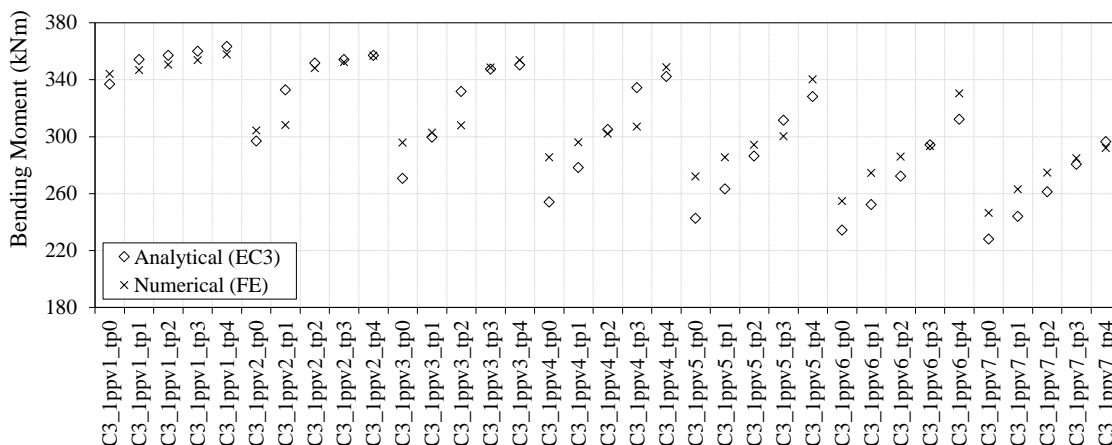


Figure A.15: Comparison of the joints strength, obtained with analytical and numerical procedures, ranging t_p and keeping m_x .

A.5. CONCLUSIONS ON THE LINEARIZATION OF JOINTS RESPONSE

A parametric study with seventy analyses was carried out, in joints based on the ones used to validate the models, taking advantage of the scripting potentialities of the finite element models of end-plate beam-to-column joints developed in Chapter 3. This study intends to investigate a systematic linearization procedure, that applied to the non-linear response of joints, could extract the proper strength and initial stiffness values comparable with the proposed values obtained using the analytical procedure available in the EC3-1-8 (EN 1993-1-8, 2005). For that the procedure proposed in the ECCS (1986) publication for the yielding point determination, using the linearization of the non-linear response of the joints, was analysed and the results compared with the EC3-1-8.

Several parameter were studied, namely: the distance of the external and internal bolt rows to the beam flanges, the high and thickness of the end-plate. These combinations allowed to have multiple joints governed by different failure modes according to the EC3-1-8. For the material properties the nominal values found in the EC3-1-1 (EN 1993-1-1, 2005) were used, in both analytical and numerical simulations, the partial safety factors were consider equal to 1.0. The results revealed that, generally, considerable differences can be found between the bending moment strength determined using the procedure proposed in the EC3-1-8, and using the ECCS linearization procedure applied to the results of the FEM of the joint. It was found that the differences are more pronounced in the joints where the column has more influence in

the behaviour. It is also possible to verify that the difference, between the analytical and numerical strength values, increase with the increase of the end-plate thickness and with the reduction of the distance between bolt rows around the beam flange, i.e. for stiffer T-stubs.

Furthermore, in the comparisons between the analytical and numerical results, it is also possible to observed that the joints conditioned by the failure mode 2, according to the EC3-1-8, in the tensioned external bolt row, are the ones that present the highest differences in the strength values, i.e. the ones that are characterized by a shared plastic deformation of the bolts and plates, although in the plates the full plastic mechanism is not reached. Analysing the joints according to their T-stub failure modes, in the end-plate, the joints based in the J3.1 are the ones where the differences are more notorious. Possibly because these joints are less influenced by the column web panel deformation, due to the stronger column.

In this study it was also possible to compare the initial stiffness of the joints using the component method available in the EC3-1-8 and the elastic stiffness obtained from the moment-rotation relationship of the FEM. The results allowed to conclude that the results between the two procedures are quite similar, however the stiffness variation clearly follows different patterns.

With the intension of improving the agreement between the two procedures (analytical and numerical) in the assessment of a representative strength value for the joints, new values were determined for the parameter that defines the slope of the post-limit stiffness branch in the ECCS procedure. The parameter was adjusted minimizing the sum of the differences between the strength values (determined with the EC3-1-8 and the ECCS procedure applied to the FEM results). Due to the earlier observation that the failure modes in the end-plate influences the agreement between the analytical and numerical results, the adjustment of the parameter was determined separately, according to the failure mode determined for the external bolt row of the end-plate (mode 1 or mode 2). The conclusions revealed that, for the joints governed by the mode 1 in the end-plate, the variation of the parameter of the post-limit stiffness branch proposed in the ECCS procedure, is adequate for the generality of the joints, the value obtained with the adjustment gave 11 instead of the 10 proposed. However for the mode 2 the values obtained with the adjustment were considerably different, yielding more or less twice the value proposed in the ECCS procedure, i.e., 20.

B

PARAMETERIZATION OF THE BEAM-TO-COLUMN END-PLATE JOINT MODEL

B.1. SCOPE AND DEFINITIONS

It is intended in this chapter to explain the structure of the script developed to generate and run the beam-to-column end-plate FE model in ABAQUS (2014) software package. The main steps of the script are explained, and the main capabilities and limitations are discussed. However, it is not intended in this chapter to break each line of code to explain it, due to its long length (more than 5000 lines of code), but rather give an oriented explanation, supported by examples, of a possible structure of the script. For further information please consult devoted literature to the subject (Puri, 2011).

ABAQUS interface scripts are Python scripts. When the graphical user interface (GUI) also called ABAQUS /CAE, is used to create or visualize a finite element model, Python commands are issued internally by ABAQUS/CAE after every operation. ABAQUS uses a Scripting Interface (ASI) that is an extension of the Python object-oriented programming language. ABAQUS is able to compile Python scripts to model, or modify an existing model, including parts, material properties, loads, steps, etc. To create, modify and submit analysis jobs. Extract results, read and write to an ABAQUS output database or view the results of an analysis (ABAQUS, 2014). Actually it is possible to do just about everything by a script that is possible to do in the GUI mode. With the advantage of having available all the versatile tools of the Python programming language. Like the possibility of making automated decisions in

the model creation, or automatically optimize a model design by performing successive analyses according to the results interpretation based on a pre-defined criterion.

In sum by using ABAQUS/CAE the actions performed in GUI generate commands in Python, and these are interpreted and sent to ABAQUS/CAE kernel which executes them. In other words, GUI is the interface between the user and the kernel, and the GUI and kernel communicate using Python commands, see Figure B.1. On the other hand, it is possible to use ASI (Abaqus Scripting Interface) to directly submit a Python script in a *.py* file and submit that to the ABAQUS/CAE kernel, without using the GUI interface (*noGUI* option), see Figure B.2. A really helpful tool for scripts that are able to generate the FE model, run the analysis and extract the required results, available in the output request. This is the case of the script developed for the beam-to-column sub-assembly, of a moment resisting frame (MRF) structure, with a bolted end-plate connection, and presented hereafter.

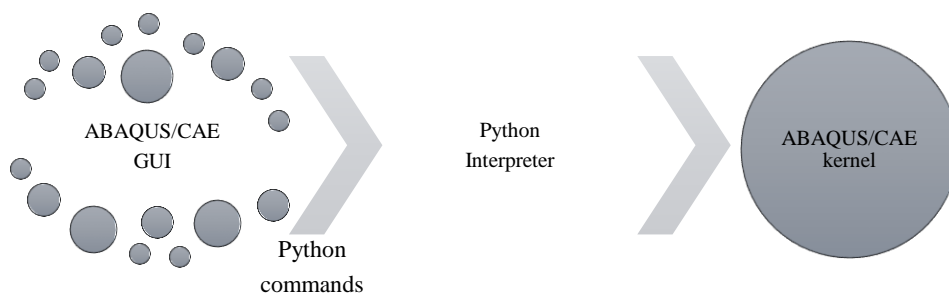


Figure B.1: Interface between ABQUS/CAE and ABAQUS kernel using Python Interpreter.

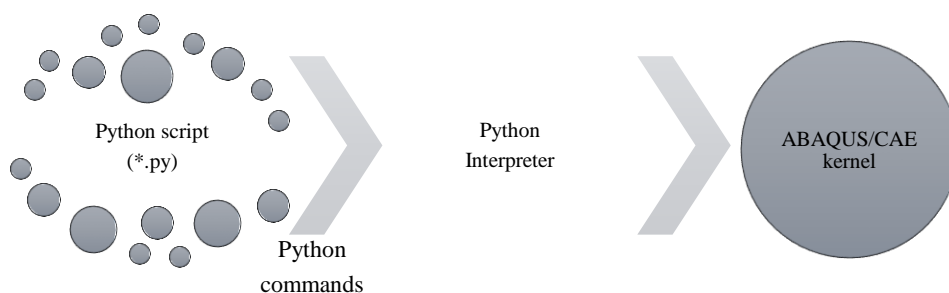


Figure B.2: Alternative approach submitting directly *.py* files to ABAQUS kernel using Python Interpreter.

From a practical point of view ABAQUS/CAE output files can really ease the scripting procedure, each time ABAQUS / CAE or Viewer is open a file called *abaqus.rpy* is created that

records, in Python programming language, all steps done in this session. There is also a file, generated when the ABAQUS/CAE model is saved for the first time, a journal file *.jnl*, which saves all steps made since the beginning of the project, in a Python programming language. Unlike *abaqus.rpy* this file records the information even for different sessions. Both files can easily be converted in a *.py* file, changing the file extension. Of course, due to the several interactions in the model the Python files still looks messy and it is a good exercise and habit to put some structure into it. So even without the complete understanding of the generated code lines, at the beginning, it is possible to develop a script, even if it is only the result of actions taken in GUI. The script can then be improved with the insertion of variables, loops, libraries, etc. which makes it even more powerful solving problem with the finite element method.

In the next sections the code structure for the beam-to-column end-plate joint FE model is explained. Particular attention is devoted to the variables required to define the model and the loads. Next the several parts of the script are identified and the main features are explained.

B.2. CROSS-SECTIONAL INFORMATION FOR ALL ABAQUS SCRIPTS

As in other programming languages Python is written in the form of code statements separated by different lines. In addition, statements in blocks of code need to be indented, that's the only way Python separate the blocks of code, for instance a statement inside a *For* loop. The code structure is case sensitive but inside of a statement the spaces left between the code pieces are not relevant. The variables in Python are generally not declared, it is the context that dictates the type of variable. Comments can be introduced in the code using the hash (#) symbol before the comment, it is important to use plain text, i.e., only English characters, even in the comments, to avoid undesirable errors. The script executes from top to bottom.

In the beginning of the script the first line should be saved for `# -*- coding: mbcs -*-` that assures this script will use Multibyte Character Sets (MBCS). This is an older approach to the need to support character sets, like Japanese and Chinese, which cannot be represented in a single byte, but are still recognized in ABAQUS interpreter.

Then is necessary to import the required modules, the code block dealing with this step is displayed bellow.

```
# -*- coding: mbcs -*-
#
# Import the required modules
import os
import math
import cmath
import copy

# Importing ABAQUS modules
from abaqus import *
from abaqusConstants import *
import regionToolset
from caeModules import *
from driverUtils import executeOnCaeStartup

executeOnCaeStartup()
session.viewports['Viewport: 1'].setValues(displayedObject=None)

import sketch
import part
import material
import section
import mesh
import assembly
import step
import job

# POST PROCESSING
from odbAccess import *
from visualization import*
import regionToolset
import displayGroupMdbToolset as dgm
import xyPlot
import displayGroupOdbToolset as dgo
```

The first group of modules are utilities, not directly related with ABAQUS, but with other Python operations, like the module *os* (operating system) is needed to deal with paths, operating, creating documents and folders, etc. Then the ABAQUS dedicated modules are imported, which makes the ABAQUS objects accessible to the script, makes the symbolic constants available and other necessary modules. Like the *regionToolset* module to access its methods through the script. The statement *session.viewports* cleans the viewport, which is the

window in GUI, and it allows ABAQUS to display information visually. Next the individual modules required to assemble the model are imported: sketch, part, material, section, mesh, assembly, step and job. The construction of each one of these tasks will be described later. Lastly, if necessary, the needed modules for the post processing phase to deal with the output results file (.odb).

After the assignment of all needed variables, as described in the next section it is necessary to include some code related to the coordinate system used in ABAQUS. By default, ABAQUS references to the coordinate system by its own codification language, not a very friendly language to work with. It is necessary to instruct ABAQUS to change the coordinate references to a more friendly language. To do that the next instruction should be given in the script, before any other modelling action.

```
session.journalOptions.setValues(replayGeometry=COORDINATE,
recoverGeometry=COORDINATE)
```

Common to all ABAQUS scripts is the definition of a name to the new model and the definition of a work directory. It is also necessary to instruct ABAQUS about the model type, i.e., which is the analysis that will be performed in the model. The next piece of code is related to these issues:

```
mdb.Model(name=m_name, modelType=STANDARD_EXPLICIT)

try:
    del mdb.models['Model-1']
except:
    pass

Jointmodel = mdb.models[m_name]

m_work_directory = os.path.split(m_path)[0]
os.chdir(m_work_directory)
```

The model name can be assigned directly in the code or automatically in the case of a sequence of analyses, for a parametric study.

The *try* function is used in case of using the GUI mode to run the script, by default ABAQUS names the first model as “Model-1”, and the function tries to delete it, in any other case the option is to *pass* this operation.

It is also recommended to assign a variable to `mdb.model[m_name]`, because this command is repeated in almost all code blocks that requires the definition of the model name, which hereinafter is substituted by *Jointmodel*.

B.3. INPUT VARIABLES FOR THE SCRIPT OF THE EXTERNAL BEAM-TO-COLUMN MODEL

B.3.1. PARAMETERS RELATED TO THE GEOMETRY OF THE MODEL

In Table B.1, supported by the Figure B.3 are defined the parameter and the corresponding Python variables related to the MRF sub-assembly and joint geometry. First the beam and column variables are assigned, defining the geometry of the beam and column sections. The notation is defined according to Eurocode 3-1-1 (EN 1993-1-1, 2005), with an index “b” and “c” to distinguish the beam and the column variables, respectively. To model the transition radius between the web and the flanges, of the beam and column sections profiles (I or H), a triangle is adopted instead of a quarter of a circle. This option intends to avoid distorted elements in the mesh. For that an equivalency between the areas of the triangle and the quarter of a circle is performed, according to Eq.(B.1), in relation to Figure B.4 a).

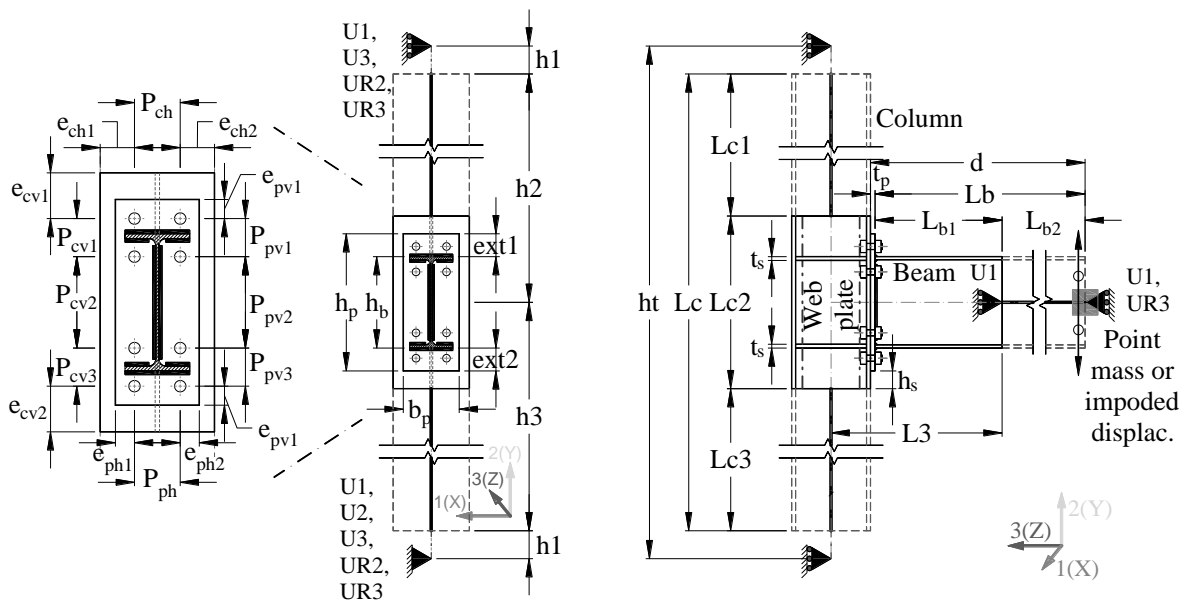


Figure B.3: Geometrical parameters of the beam-to-column FE models.

Table B.1: Parameters related to the geometry of the joint sub-assembly and the corresponding Python variables.

Parameters	Python variables							
	Type	Name	content					
Beam geometrical properties (mm)	List	Beam_prop	string [Beam name,	float hb,	float bb,	float tfb,	float twb,	float rb]
Column geometrical properties (mm)	List	Column_prop	string [Col. name,	float hb,	float bb,	float tfb,	float twb,	float rb]
Sub-assembly geometry (mm)	List	assembly_prop	float [Lb,	float Lc,	float h1,	float h2,	float hs]	
Type of connection	Int	Type	#	Extended end-plate = 0 ; Flush End-Plate = 1				
Bolts properties (mm, mm ² , N/mm ²)	List	bolt_prop	float [db,	float D1,	float D2,	float bh,	float As,	float fub]
Washer presence	Int	washer	#	Washers yes = 1; Washers no = 0				
Clearance of the bolts holes in the end-plate (mm)	float	bp_gap						
Clearance of the bolts holes in the column flange (mm)	float	bc_gap						
End-plate geometrical properties (mm)	List	end_plate_prop	float [hp,	float bp,	float tp]			
Horizontal eccentricity between the end-plate and the column axis (mm)	float	ecc_p	#	positive values => left; negative values => right				
Vertical spacing of the bolt rows (mm)	List	ppv	float [epv1,	float ppv1,	float ppv2,,	float ppv _n]	
Horizontal spacing of the bolt rows (mm)	List	pph	float [eph1,	float pph,	float eph2]			
Length of the extended parts of the end-plate (mm)	List	ext	float [ext1,	float ext2]				
End-plate to beam welds (mm)	List	welds	float [af,	float aw]				
Transverse web stiffeners (mm)	List	ts	float [ts1,	float ts2,	float ts3,,	float ts _n]	
Transverse web stiffeners not aligned with the beam flanges (mm)	List	h_stiff_b	float [h_s_b1,	float h_s_b2,	float h_s_b3,,	float h_s_bn]	
Thickness of the supplementary web plates (mm)	float	tswp	#	tswp is added to the thickness of the solid column web				

$$r_c^2 - \frac{\pi \cdot r_c^2}{4} = \frac{r_t^2}{2} \Leftrightarrow r_t = \sqrt{2r_c^2 - \frac{\pi \cdot r_c^2}{2}} = r_c \sqrt{\frac{4 - \pi}{2}} \cong 0.655r_c \quad (\text{B.1})$$

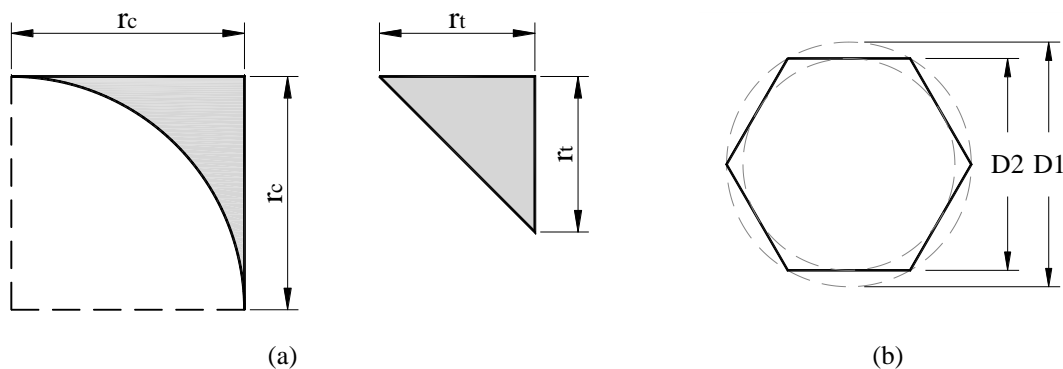


Figure B.4: (a) Equivalency between the areas of the web to flanges transition from a round approach to a straight line; (b) outer and inner diameter of the bolts head.

Next the sub-assembly variables are assigned defining the beam length (L_b), the column length (L_c), the relative position of the beam in the system (L_2) and the definition of the solid part of the joint. Note that the solid part of the sub-assembly, defined by L_{c2} , may be adjusted by the “user”, using h_s , to define the portion of solid column beyond the end-plate length. Or set automatically to cover the effective width of column web in compression, for a bolted end-plate connection, $b_{eff,c,wc}$, as defined in the EC3-1-8 (EN 1993-1-8, 2005) (clause 6.2.6.2).

After the definition of the MRF sub-assembly geometrical properties the connection properties are assigned, starting with the bolts, where d_b is the bolts diameter, D_1 and D_2 are the outer and inner radius inscribed in the bolts head, see Figure B.4 b). b_h and b_n define the thicknesses of the bolts head and nut, respectively. A_s is the shear area and f_{ub} the ultimate tensile strength of the bolt, as defined in EC3-1-8 (EN 1993-1-8, 2005). Bolts are modelled as a set of rollers, see Figure 3.10. To consider the threaded portion of the shank, the bolts diameter d_i is obtained by the nominal shear area A_s . The clearance of the bolts holes in the end-plate and in the column flange is also defined, and the presence of the washer is defined by a marker. The presence of the washer will affect the bolts head and nut diameter.

The end-plate geometrical properties are defined, assigning the end-plate dimensions, h_p and b_p and the thickness t_p . The end-plate can be positioned eccentrically to the axis of the column defining the horizontal eccentricity ecc_p . The relative position of the bolts in the plate are defined using the variables ppv and pph . The script is limited to two columns of bolts, however, it is prepared to accept any number of bolt rows, according to the geometry of the joint. The extended part of the end-plate, in relation to the beam flanges, is defined by the

variables ext_1 and ext_2 . The fillet welds throat between the end-plate and beam are defined by a_f and a_w , for the beam flanges and web, respectively.

The script is prepared to deal with some stiffening options in the column: Transverse web stiffeners or supplementary web plates. If the transverse web stiffeners are aligned with the beam flanges it is only necessary to define the corresponding thickness of the stiffeners t_s . However, it is possible to define any other position for the stiffeners. For that is necessary to define the number of stiffeners and their position, in relation to the beam lower flange using the list h_stiff_b , see Figure B.5. The user is responsible for avoiding collisions with the bolts rows position. In the case of the additional supplementary web plates to the column web, it is necessary to define the thickness of the additional plates t_{swp} . To ease the process, the thickness of the column web is increased, only in the solid part of the column, by the thickness defined to the supplementary web plates.

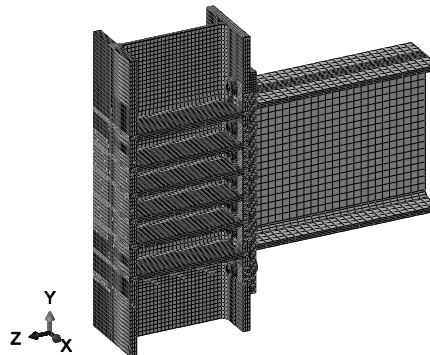


Figure B.5: Example of the versatility of the script to place stiffeners and bolt rows.

Other geometrical variables can easily be obtained from the input variables. This process is illustrated, for some of them, hereafter, see also Figure B.3.

```

h3 = Lc-h2
Lc2 = round(max(hp+2*hs, hb+(tfb+2.0*(2.0*af)**0.5+5.0*(tfc+rc)+2.0*tp)-tfb),0)
Lc1 = h2-(Lc2/2.0)
Lc3 = Lc-Lc1-Lc2
Lb1 = hb*1.3
Lb2 = Lb-Lb1
rtc = math.ceil(0.655*rc) # Rounds up to a integer
rtb = math.ceil(0.655*rb)
lb = float(tp+tfc)
di = (As*4.0/math.pi)**0.5 # Bolt nominal stress diameter
di = round(di,1)
dp0 = di+bp_gap

```

```

if washer == 0:      # Defining the diameter of the bolts head
    Df = D2          # Without washer it is consider the smaller diameter
elif washer == 1:
    Df = D1          # With washer it is adopted the external diameter
else:
    print "wrong value in the washer option!"

h_stiff = [0.0]*len(h_stiff_b)
h_stiff[0] = h_stiff_b[0]+Lc2/2.0-hb/2.0

for i in range (1, len (h_stiff_b)):
    h_stiff[i] = h_stiff_b[i]

epv1 = ppv[0]
epv2 = hp-sum (ppv)
eph1 = pph[0]
eph2 = pph[-1]      # Set the last element of the pph list
ech1 = eph1+(bc-bp)/2.0-ecc_p
ech2 = eph2+(bc-bp)/2.0+ecc_p
pch = [ech1, pph[1], ech2]
ecv1 = Lc2/2.0-hb/2.0-ext[0]+epv1
pcv = copy.deepcopy(ppv)      # To copy complex structures use 'deepcopy'
pcv[0] = ecv1
ppv_sum = 0.0

for i in range (1, len(ppv)):
    ppv_sum = ppv_sum + ppv[i]
ecv2 = Lc2-ecv1-ppv_sum
dc0 = di+bc_gap

# Define the position of the horizontal stiffeners
if all(v == 0 for v in h_stiff_b):
    h_stiff[0] = (Lc2-hb)/2.0
    h_stiff[1] = hb-ts[1]
else:
    h_stiff = h_stiff

```

B.3.1.1. PARAMETERS RELATED TO MESH OPTIONS

The parameters and associated variables, related to the mesh options, are described in Table B.2. For each part of the model is defined the approximate size of the elements, the deviation and size factors. Furthermore, the element type can be defined, according to the three automatic mesh generation options for three-dimensional element types *Hex*, *Wedge* and *Tet*,

i.e., brick elements, triangular prism elements or tetrahedron elements, respectively. For the parts constituted by plated elements, i.e., columns, beams and end-plate, it is possible to define the number of elements in the thickness, using the list *esf*, which defines the number of seeds in the thickness. This is useful to avoid hour glassing problems in reduced integration elements, see Section 3.2.3.2.

Table B.2: Parameters related to the mesh options of the joint sub-assembly and the corresponding Python variables.

Parameters	Python variables								
	Type	Name	content						
Approximate size of the element (mm)	List	ags	float [Wire bot. col.,	float wire top col.,	float wire beam,	float column,	float beam,	float end-plate,	float bolts]
Deviation Factor	List	df	float [wire bot. col.,	float wire top col.,	float wire beam,	float column,	float beam,	float end-plate,	float bolts]
Size Factor	List	sf	float [wire bot. col.,	float wire top col.,	float wire beam,	float column,	float beam,	float end-plate,	float bolts]
Element type	List	elem_code	string [wire bot. col.,	string wire top col.,	string wire beam,	string [col. hex,	string col. wedge,	string col. tet],	string [beam hex,
			string beam wedge,	string beam tet],	string [e-p hex,	string e-p wedge,	string e-p tet],	string [bolts hex,	string bolts wedge,
Seed number in the thickness of the plated members	List	esf	float [column,	float beam,	float end-plate]				

Definition of the variables for the joint J3.1:

```

ags = [300.0, 300.0, 150.0, 15.0, 20.0, 10.0, 3.0] # [mm]
df = [0.1, 0.1, 0.1, 0.1, 0.1, 0.1, 0.1]
sf = [0.1, 0.1, 0.1, 0.1, 0.1, 0.1, 0.1]
elem_code = ['B31', 'B31', 'B31', ['C3D8RH', 'C3D6H', 'C3D4H'],
['C3D8RH', 'C3D6H', 'C3D4H'], ['C3D8RH', 'C3D6H', 'C3D4H'], ['C3D8RH', 'C3D6H', 'C3D4H']]
esf = 3.0

```

B.3.1.2. PARAMETERS RELATED TO CONSTITUTIVE MATERIAL OPTIONS

The parameters related to the constitutive material options and the corresponding variables are described in the Table B.3. First the main properties of the material are defined: the steel density, the Young modulus or the Poisson ratio. For the dynamic analyses some

additional information regarding damping is also required, such as: the elastic material damping coefficient, normally defined as a percentage of the critical damping; and the material Rayleigh damping coefficient, which can vary for each material assigned.

Table B.3: Parameters related to the constitutive material options of the joint sub-assembly and the corresponding Python variables.

Parameters	Python variables												
	Type	Name	content										
Steel density (ton/mm ³)	float	steel_density											
Friction coefficient	float	friction_coeff											
Young modulus (N/mm ²)	List	young_m	float	float	float	float	float	float	float	float	float	float	[wire col., beam, flange, web, flange, web, plate, , stiffeners, welds]
Poisson ratio	List	poisson	float	float	float	float	float	float	float	float	float	float	[wire col., beam, flange, web, flange, web, plate, , stiffeners, welds]
Elastic damping coefficient (%)	float	el_damp_coef											
Rayleigh damping stiffness-proportional coefficient β_k	List	damping_Bk	float	float	float	float	float	float	float	float	float	float	[wire col., beam, flange, web, flange, web, plate, , stiffeners, welds]
Post yielding branch (N/mm ² , dimensionless)	List	plastic_t	float	float	float	float	float	float	float	float	float	float	[wire col., beam, flange, web, flange, web, plate, , stiffeners, welds]

For the definition of the post-elastic stress-strain relationship the combined isotropic/kinematic hardening model is used, for solid elements. The values of C and γ parameters of the kinematic hardening model and the corresponding yield stress, are required. For the beam elements a tri-linear approximation is used, as explained in Section 3.2.3.2. An example of the material properties definition, for the joint J3.1 is shown below. First the tri-linear material properties of the wire beam and column members are assigned. Then the parameters for the kinematic hardening model are introduced for the remaining parts. The values are in accordance with Table 3.7 and Table 3.8.

```
# (True stress, True plastic strain)
# (N/mm2, dimensionless)
plastic_t = (((394.6, 0.000),
              (609.2, 0.154), # wire column
              (656.6, 0.259)),
```



```

((430.9, 0.000),
 (637.3, 0.137),           # wire beam
 (672.0, 0.220)),

(394.6, 2486.86, 8.424),   # Column flanges
(399.6, 2663.698, 9.936),   # Column web
(430.9, 2947.485, 11.180),  # Beam flange
(449.1, 2459.437, 9.650),   # Beam web
(393.6, 3184.993, 12.593),  # End-Plate
(994.6, 65074.654, 262.366), # Bolts
(286.8, 3078.647, 10.089),  # Stiffeners
(440.9, 1321.347, 1.827)]  # welds

```

B.3.1.3. PARAMETERS RELATED TO THE ANALYSIS AND CONVERGENCE OPTIONS

For the numerical analysis is necessary to define some parameters related to the convergence, increment size, define the output record frequency, etc. The parameter related to this operations and the corresponding variables are described in Table B.4. First is necessary to define the type of analysis, the script is prepared to deal with Frequency analysis, Quasi-static analysis (monotonic / cyclic) or Dynamic (implicit) analysis. For that a flag 0 or 1 is requested. Then is necessary to define the time period of the step, the user should define the value that corresponds to the end of the analysis, for a monotonic analysis 1 is recommended. If a displacement of $100mm$ is applied to the beam, 1 represents the complete amount of load applied (displacement). On the other hand if a dynamic analysis is performed, using an acceleration record, it is recommended to set the time period as the amount of time of the record. Each step, in an ABAQUS analysis, is divided into multiple iterations and increments, and it is up to the user to decide whether to use automatic (automatic time incrementation) or user-specified fixed time incrementation. By default in this script is set automatic time incrementation. Nevertheless the initial increment must be defined by the user. The first increment should be smaller than the maximum increment, however very small increments can cause convergence problems. The user can also define the maximum number of increments, the analysis will stop if this maximum number is exceeded. It is recommended to have sufficient number of allowed increments in the analysis. The minimum increment size must be defined by the user. In the case of a frequency analysis the maximum frequency of interest should be defined (cycles/time). The maximum increment size can be specified either for the quasi-static analysis, or for the dynamic analysis.

ABAQUS/Standard allows for parallel execution, the problem is divided and analysed in different processors. The direct sparse solver supports both shared memory computers and computer clusters for parallelization.

Table B.4: Parameters related to the analysis options of the joint sub-assembly and the corresponding Python variables.

Parameters	Python variables						
	Type	Name	content				
Type of analysis	List	analysis_type	int [s2,	int s3,	int s4]	# S2 - Frequency; S3 - Monotonic/Cyclic; S4 - Dynamic (0 - OFF; 1 - ON)	
Time period for the step	float	time_period					
Initial increment size	float	initial_inc					
Maximum number of increments	int	max_numb_inc					
Minimum increment size	float	min_inc_size					
Maximum frequency of interest	float	max_numb_freq	# Only for the frequency analysis				
Maximum increment size in quasi-static analysis	float	max_inc_c	# Only for the mon/cyclic analysis				
Maximum increment size in Dynamic analysis for several records	List	max_inc	float [record1,	float record2,	float record3,	... recordn]	float
Time period of the record	float	time_period_dy					
Number of processors used in the calculations	int	number_processors					
Automatic stabilization for quasi-static analysis	List	stab_magnitude	float [stab. Magnitude,	float damping ratio]			
Output request option	int	output	# output request for the entire model (0) or only for the created sets of points (1)				
Time interval in which data is recorded	float	time_interval_rec					

ABAQUS/Standard provides an automatic mechanism for stabilizing unstable quasi-static problems through the automatic addition of volume-proportional damping to the model. The applied damping factors can be constant over the duration of a step, or they can vary with time to account for changes over the course of a step (ABAQUS, 2014). The latter, adaptive approach is the one adopted in this script. In this approach damping factor can vary spatially

and with time. In this case the damping factor is controlled by the convergence history and the ratio of the energy dissipated by viscous damping to the total strain energy. The adaptive damping ratio allows to control the ratio of the energy dissipated by viscous damping to the total strain energy. This accuracy tolerance is imposed on the global level for the whole model. Due to the virtual energy added to the system it is recommended to check if the viscous forces (*VF*) are relatively small compared with the overall forces in the model (*TF*). Furthermore, it is recommended to compare the viscous damping energy (*ALLSD*) with the total strain energy (*ALLIE*), and ensure that the ratio does not exceed the dissipated energy fraction or any reasonable amount.

The script is able to provide the option of saving the requested results in all nodes and elements of the mesh, or only to the ones specified in the pre-defined sets of points, some of those points are represented in the Figure 3.21 (b). This option can reduce significantly the size of the output file (*.odb*), and save storage space. It is also possible to define a time interval in which the data is recorded, also saving some storage space.

B.3.1.4. PARAMETERS RELATED TO THE LOADING OPTIONS

The options related to the loads applied to the joint, the parameters and the associated variables are identified in Table B.5. As mentioned in Section 3.2.3.2, for the quasi-static analyses, a displacement is imposed in the beam to generate bending moments in the joint. This displacement (yield displacement) can be defined as the total displacement required to generate the necessary bending moment. An option normally used for the monotonically loaded joints. Or, in the case of the cyclic loaded joints, used as a reference value, e.g. the yield displacement of the joint. The load history is defined in an additional *.txt* file with the corresponding amplitudes (*amp_file_name*). If bolts are pre-stressed the user should define the pre-stress as a percentage of the ultimate strength of the bolts.

For the dynamic analysis a point mass, assigned to the beam end, is necessary to give the problem significant mass to generate the necessary bending moments in the joint. If a specific frequency in the structure is required, the mass is defined using an algorithm. This algorithm runs successive frequency analysis until the target frequency is reached, in a pre-defined tolerance, using specific mass increments. Furthermore, the script is prepared to deal with

incremental dynamic analysis. For that a set of scale factors can be assign, according to the correspondent record. The number of accelerograms is defined by the user.

Table B.5: Parameters related to the load options of the joint sub-assembly and the corresponding Python variables.

Parameters	Python variables			
	Type	Name	content	
Yielding displacement (mm)	float	yield_disp		
Mass in the end of the beam (ton)	float	point_mass		
File with amplitudes corresponding to the load protocol	string	amp_file_name	# name of the text file with the extension *.txt	
Scale factors of the records amplitudes	List	scale_factor	float	float float ... float [record1, record2, record3, ..., recordn]
Pre-stress of the bolts (%)	float	pre_stress_str	# Percentage of the ultimate strength	
Predefined frequencies (1/sec)	float	target_frequencies	# Determine the point mass for a specific predefined frequency	
Increments of mass (ton)	float	increment		
Tolerance for the frequencies achieved	float	freq_tolerance		

B.4. MAIN BODY OF THE SCRIPT FOR THE BEAM-TO-COLUMN FE MODEL

B.4.1. CREATE THE MODEL PARTS

B.4.1.1. INTRODUCTION TO THE PARTS CREATION

The structure of the script, to define the finite element beam-to-column model, follows the same hierarchy identified in the ABAQUS/CAE model tree. It begins with the definition of the several parts that constitute the model. The model contains two reference points, in the top and bottom of the column, for the supports, three wire parts (bottom column, top column and beam), and four solid parts, column, beam, end-plate and bolts, as illustrated in Figure 3.10.

B.4.1.2. REFERENCE POINTS AND WIRE PARTS

First is created a reference point to apply the boundary conditions.

```
# Part => Support

p = Jointmodel.Part(name='Support', dimensionality=THREE_D, type=DEFORMABLE_BODY)
p.ReferencePoint(point=(0.0, 0.0, 0.0))
p = Jointmodel.parts['Support']
session.viewports['viewport: 1'].setValues(displayedObject=p)
```

Then the wire parts of the model are created using the *Sketch* menu to define the parts length. The process is repeated for: *Wire Bottom Column*, *Wire Top Column* and the *Wire Beam*.

```
s = Jointmodel.ConstrainedSketch(name='__profile__', sheetSize=2.0*Lc3)
s.Line(point1=(0.0, 0.0), point2=(Lc3, 0.0))
p = Jointmodel.Part(name=Column+'_Wire_Bot',
    dimensionality=THREE_D, type=DEFORMABLE_BODY)
p = Jointmodel.parts[Column+'_Wire_Bot']
p.BaseWire(sketch=s)
del Jointmodel.sketches['__profile__']
```

B.4.1.3. SOLID COLUMN PART

It is in the solid parts that the parametrization get more complex contours. In addition to the geometry of each of the solid parts is necessary to establish the proper relationships to define: the position of the bolts holes, definition of the transverse stiffeners, definition of the welds, and also create a set of partitions that guarantees a proper and regular mesh generation. Due to the large amount of code required to perform all these operations only some representative examples of the code will be displayed here.

The first solid part to be created is the column. Once again the *Sketch* menu is used to draw the column section. According to the variables defined in the list *Beam_prop*, the coordinates of the points that constitute the section are defined and stored. Then the section is extruded to the column length ($Lc2$).

```
# Part => Solid Column

s1 = Jointmodel.ConstrainedSketch(name='__profile__', sheetSize=2.0*hc)
s1.Line(point1=(0.0, 0.0), point2=(bc, 0.0))
s1.Line(point1=(bc, 0.0), point2=(bc, tfc))
s1.Line(point1=(bc, tfc), point2=(bc/2.0+twc/2.0+rtc, tfc))
s1.Line(point1=(bc/2.0+twc/2.0+rtc, tfc), point2=(bc/2.0+twc/2.0, tfc+rtc))
s1.Line(point1=(bc/2.0+twc/2.0, tfc+rtc), point2=(bc/2.0+twc/2.0, hc-tfc-rtc))
s1.Line(point1=(bc/2.0+twc/2.0, hc-tfc-rtc), point2=(bc/2.0+twc/2.0+rtc, hc-tfc))
s1.Line(point1=(bc/2.0+twc/2.0+rtc, hc-tfc), point2=(bc, hc-tfc))
s1.Line(point1=(bc, hc-tfc), point2=(bc, hc))
s1.Line(point1=(bc, hc), point2=(0.0, hc))
```

```

s1.Line(point1=(0.0, hc), point2=(0.0, hc-tfc))
s1.Line(point1=(0.0, hc-tfc), point2=(bc/2-twc/2-rtc, hc-tfc))
s1.Line(point1=(bc/2.0-twc/2.0-rtc, hc-tfc), point2=(bc/2.0-twc/2.0, hc-tfc-rtc))
s1.Line(point1=(bc/2.0-twc/2.0, hc-tfc-rtc), point2=(bc/2.0-twc/2.0, tfc+rtc))
s1.Line(point1=(bc/2.0-twc/2.0, tfc+rtc), point2=(bc/2.0-twc/2.0-rtc, tfc))
s1.Line(point1=(bc/2.0-twc/2.0-rtc, tfc), point2=(0.0, tfc))
s1.Line(point1=(0.0, tfc), point2=(0.0, 0.0))

p = Jointmodel.Part(name=Column, dimensionality=THREE_D, type=DEFORMABLE_BODY)
p = Jointmodel.parts[Column]
p.BaseSolidExtrude(sketch=s1, depth=Lc2)
del Jointmodel.sketches['__profile__']

```

The bolts holes in the column flange are arranged according to the position of the bolts holes in the end-plate, see Figure B.3. The number of bolt rows is defined by the user, there is no limitation to the number of rows, so a loop is used to determine how many rows exist in the joint and create the holes. The range of the loop is defined by the length of the variable *ppv*. The holes diameter is defined by the bolts diameter and clearance b_{c_gap} .

```

# Define the bolts holes

dist_sup=ecv1
Lenght_ppv=len (ppv)

for i in range(0,Lenght_ppv):
    pcvi=pcv[i]
    dist_sup=dist_sup+pcv[i]

    if pcvi>0:
        p = Jointmodel.parts[Column]
        f1, e = p.faces, p.edges
        p.HoleBlindFromEdges(plane=f1.findAt(coordinates=(bc/2.0, 0.0, Lc2/2.0)),
            edge1=e.findAt(coordinates=(bc/4.0, 0.0, Lc2)), edge2=e.findAt(
            coordinates=(0.0, 0.0, Lc2/3.0)), planeSide=SIDE1, diameter=dc0,
            distance1=dist_sup, distance2=ech1, depth=tfc)
        p = Jointmodel.parts[Column]
        f, e1 = p.faces, p.edges
        p.HoleBlindFromEdges(plane=f.findAt(coordinates=(bc/2, 0.0, Lc2/2.0)),
            edge1=e1.findAt(coordinates=(bc/4.0, 0.0, Lc2)), edge2=e1.findAt(

```

```

coordinates=(bc, 0.0, Lc2/3.0)), planeSide=SIDE1, diameter=dc0,
distance1=dist_sup, distance2=ech2, depth=tfc)

```

In the presence of transverse web stiffeners the column part is edited to accommodate them, using a *Sketch* transformation. The number and position of the stiffeners is defined by the variable *h_stiff*. Similarly to the definition of the column section the stiffeners are created, for each position. First the coordinates of the points that define the stiffeners in the column section are assigned, and then the section is extruded to the stiffeners thickness.

```

# Define the transverse stiffeners if they exist (ts>0)
if any(z > 0 for z in ts ):
    h_stiff_i=0

    for i in range(0, len(h_stiff)):

        h_stiff_i = h_stiff_i + h_stiff[i]

        if h_stiff[i] != 0:
            # Create a Datum Plane for the Stiffner position
            p = Jointmodel.parts[Column]
            datum_var[0] = p.DatumPlaneByPrincipalPlane(principalPlane=XYPLANE,
            offset=h_stiff_i)

            p = Jointmodel.parts[Column]
            e, d = p.edges, p.datums
            t = p.MakesSketchTransform(sketchPlane=p.datums[datum_var[0].id],
            sketchUpEdge=e.findAt(coordinates=(bc, tfc/2.0, Lc2)),
            sketchPlaneSide=SIDE1, sketchOrientation=RIGHT,
            origin=(bc/2.0, hc/2.0, h_stiff_i))

            s = Jointmodel.ConstrainedSketch(name='__profile__',
            sheetsize=5.0*hc, gridSpacing=5.0*hc/40.0, transform=t)

            p = Jointmodel.parts[Column]
            p.projectReferencesOntoSketch(sketch=s, filter=COPLANAR_EDGES)
            s.Line(point1=(-bc/2.0, -(hc/2.0-tfc)), point2=(-twc/2.0-rc, -(hc/2.0-tfc)))
            s.Line(point1=(-twc/2.0-rc, -(hc/2.0-tfc)),
            point2=(-twc/2.0, -(hc/2.0-tfc-rc)))

```

```

s.Line(point1=(-twc/2.0, -(hc/2.0-tfc-rc)),
point2=(-twc/2.0, hc/2.0-tfc-rc))
s.Line(point1=(-twc/2.0, hc/2.0-tfc-rc), point2=(-twc/2.0-rc, hc/2.0-tfc))
s.Line(point1=(-twc/2.0-rc, hc/2.0-tfc), point2=(-bc/2.0, hc/2.0-tfc))
s.Line(point1=(-bc/2.0, hc/2.0-tfc), point2=(-bc/2.0, -(hc/2.0-tfc)))
s.Line(point1=(bc/2.0, -(hc/2.0-tfc)), point2=(twc/2.0+rc, -(hc/2.0-tfc)))
s.Line(point1=(twc/2.0+rc, -(hc/2.0-tfc)),
point2=(twc/2.0, -(hc/2.0-tfc-rc)))
s.Line(point1=(twc/2.0, -(hc/2.0-tfc-rc)), point2=(twc/2.0, hc/2.0-tfc-rc))
s.Line(point1=(twc/2.0, hc/2.0-tfc-rc), point2=(twc/2.0+rc, hc/2.0-tfc))
s.Line(point1=(twc/2.0+rc, hc/2.0-tfc), point2=(bc/2.0, hc/2.0-tfc))
s.Line(point1=(bc/2.0, hc/2.0-tfc), point2=(bc/2.0, -(hc/2.0-tfc)))

p = Jointmodel.parts[Column]
e1, d2 = p.edges, p.datums
p.SolidExtrude(sketchPlane=p.datums[datum_var[0].id], sketchUpEdge=e.findAt(
coordinates=(bc, tfc/2.0, Lc2)), sketchPlaneSide=SIDE1,
sketchOrientation=RIGHT, sketch=s, depth=ts[i],
flipExtrudeDirection=OFF)
s.unsetPrimaryObject()
del Jointmodel.sketches['__profile__']
else:
break

```

The geometry of the solid part of the column is complete. Nevertheless, the geometry of the column is now much more complex, with several plate intersections, round holes and non-orthogonal intersections of the facets. The generation of an automatic mesh in this part will create an irregular mesh. In fact in this case, without further actions, is not possible to use hexahedra, for the elements shape, only tetrahedrons are available, see Figure B.6 (a). To force a regular mesh, in an automatic generation environment, it is necessary to limit the irregular zones, and create the conditions for hexahedra elements, as shown in Figure B.6 (b). ABAQUS offers a tool to divide the part and create several dependent zones where a regular mesh can be developed. Figure B.6 (c) illustrates the partitioning of the column part to obtain the regular mesh of elements with hexahedra shape. In addition the partitioning of the parts also allows the assignment of different material properties for the several divided zones.

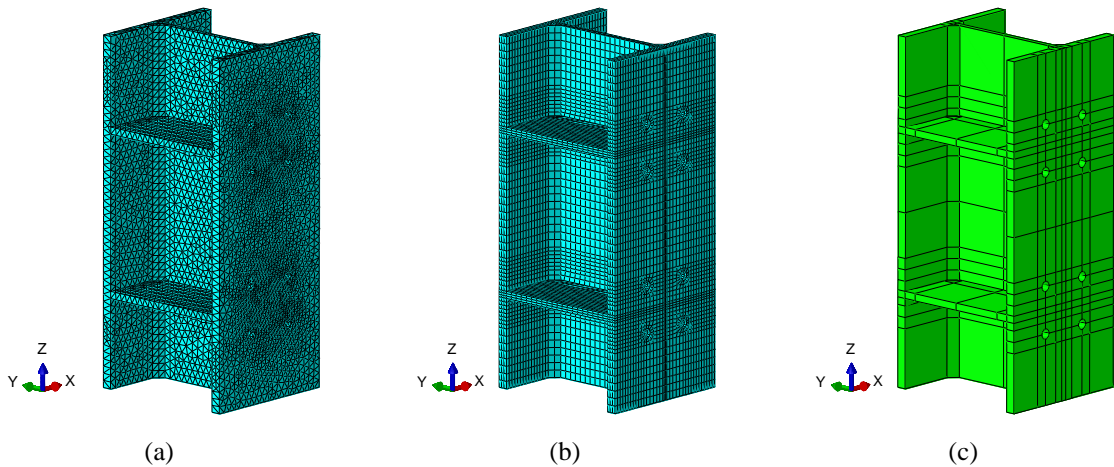


Figure B.6: Mesh generation: (a) without using partitions; (b) and (c) using partitioning in the part.

B.4.1.4. SOLID BEAM

A similar procedure is done for the solid beam part, first is necessary to draw the beam section, using the *Sketch* menu and the properties of the section stored in the variable *Beam_prop*. Then the section is extruded to the beam length ($Lb1$). Additionally the welds to the end-plate are modelled in the beam part, using the same principles as for the stiffeners. The section of the welds are defined, using a *Sketch* transformation, and then are extruded according to the corresponding welds length.

As in the solid column part also in this case is necessary to define a set of partitions that allows a regular mesh, and the assignment of the different material properties in the beam part. Partitions should be defined whenever an irregularity occurs, intersection of the plates, intersection of the welds, web-to-flange transition radius, etc.

```
# Part => Solid Beam
s1 = Jointmodel.ConstrainedSketch(name='__profile__',
    sheetSize=2.0*hb)
s1.Line(point1=(0.0, 0.0), point2=(bb, 0.0))
s1.Line(point1=(bb, 0.0), point2=(bb, tfb))
s1.Line(point1=(bb, tfb), point2=(bb/2.0+twb/2.0+rtb, tfb))
s1.Line(point1=(bb/2.0+twb/2.0+rtb, tfb), point2=(bb/2.0+twb/2.0, tfb+rtb))
s1.Line(point1=(bb/2.0+twb/2.0, tfb+rtb), point2=(bb/2.0+twb/2.0, hb-tfb-rtb))
s1.Line(point1=(bb/2.0+twb/2.0, hb-tfb-rtb), point2=(bb/2.0+twb/2.0+rtb, hb-tfb))
s1.Line(point1=(bb/2.0+twb/2.0+rtb, hb-tfb), point2=(bb, hb-tfb))
s1.Line(point1=(bb, hb-tfb), point2=(bb, hb))
```

```

s1.Line(point1=(bb, hb), point2=(0.0, hb))
s1.Line(point1=(0.0, hb), point2=(0.0, hb-tfb))
s1.Line(point1=(0.0, hb-tfb), point2=(bb/2.0-twb/2.0-rtb, hb-tfb))
s1.Line(point1=(bb/2.0-twb/2.0-rtb, hb-tfb), point2=(bb/2.0-twb/2.0, hb-tfb-rtb))
s1.Line(point1=(bb/2.0-twb/2.0, hb-tfb-rtb), point2=(bb/2.0-twb/2.0, tfb+rtb))
s1.Line(point1=(bb/2.0-twb/2.0, tfb+rtb), point2=(bb/2.0-twb/2.0-rtb, tfb))
s1.Line(point1=(bb/2.0-twb/2.0-rtb, tfb), point2=(0.0, tfb))
s1.Line(point1=(0.0, tfb), point2=(0.0, 0.0))

p = Jointmodel.Part(name=Beam,
    dimensionality=THREE_D, type=DEFORMABLE_BODY)
p = Jointmodel.parts[Beam]
p.BaseSolidExtrude(sketch=s1, depth=Lb1)
del Jointmodel.sketches['__profile__']

```

B.4.1.5. END-PLATE

The extrude option is used to create the end-plate part, using the list *end_plate_prop*. First the width and length of the plate is defined and then is extruded through the thickness. Similarly, to the column, the bolts holes position are defined by their distance to the plate edges. A loop is required to accommodate any number of bolt rows defined by the user. For a proper mesh generation, also in the end-plate is necessary to create partitions, due to the bolt holes irregularities.

```

# Part => Solid End-Plate
s = Jointmodel.ConstrainedSketch(name='__profile__',
    sheetSize=2*hp)
s.rectangle(point1=(0.0, 0.0), point2=(bp, hp))

p = Jointmodel.Part(name='End-Plate', dimensionality=THREE_D,
    type=DEFORMABLE_BODY)
p = Jointmodel.parts['End-Plate']
p.BaseSolidExtrude(sketch=s, depth=tp)
del Jointmodel.sketches['__profile__']

```

```

# Define the bolts holes
dist_sup_p = 0.0

for i in range(0, len(ppv)):
    dist_sup_p = dist_sup_p + ppv[i]

    if ppv[i] > 0:
        p = Jointmodel.parts['End-Plate']
        f1, e = p.faces, p.edges
        p.HoleBlindFromEdges(plane=f1.findAt(coordinates=(bp/2.0, hp/2.0, 0.0)),
            edge1=e.findAt(coordinates=(bp/2.0, hp, 0.0)), edge2=e.findAt(
            coordinates=(0.0, hp/3.0, 0.0)), planeSide=SIDE1, diameter=dp0,
            distance1=dist_sup_p, distance2=eph1, depth=tp)

        p = Jointmodel.parts['End-Plate']
        f, e1 = p.faces, p.edges
        p.HoleBlindFromEdges(plane=f.findAt(coordinates=(bp/2.0, hp/2.0, 0.0)),
            edge1=e1.findAt(coordinates=(bp/2.0, hp, 0.0)), edge2=e1.findAt(
            coordinates=(bp, hp/3.0, 0.0)), planeSide=SIDE1, diameter=dp0,
            distance1=dist_sup_p, distance2=eph2, depth=tp)

```

B.4.1.6. BOLTS

Due to the cylindrical shape of the bolts, this part, is programed to be generated by revolution. First half of a bolt section is defined, using a set of coordinates based on the geometry of the bolts provided by the list *bolt_prop*, according to the Figure B.7. After the generation of the bolt is necessary to define partitions, for a regular mesh, and also to define a plane required for the pre-stress of the bolts, see Figure 3.20.

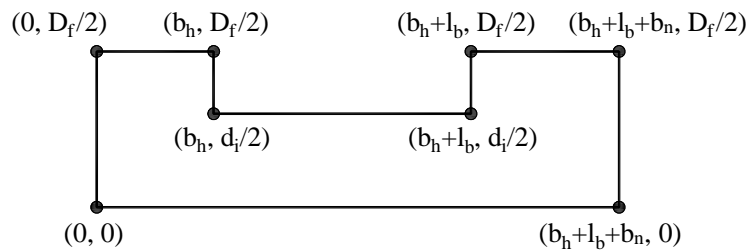


Figure B.7: Coordinates of the points for the half section of the bolt.

```
# Part => Solid Bolts
s1 = Jointmodel.ConstrainedSketch(name='__profile__',
    sheetSize=tp+tf+cb+bn)
s1.Line(point1=(0.0, 0.0), point2=(bh+lb+bn, 0.0))
s1.Line(point1=(bh+lb+bn, 0.0), point2=(bh+lb+bn, Df/2))
s1.Line(point1=(bh+lb+bn, Df/2), point2=(bh+lb, Df/2))
s1.Line(point1=(bh+lb, Df/2), point2=(bh+lb, di/2))
s1.Line(point1=(bh+lb, di/2), point2=(bh, di/2))
s1.Line(point1=(bh, di/2), point2=(bh, Df/2))
s1.Line(point1=(bh, Df/2), point2=(0.0, Df/2))
s1.Line(point1=(0.0, Df/2), point2=(0.0, 0.0))
s1.ConstructionLine(point1=(0.0, 0.0), point2=(bh+lb+bn, 0.0))

p = Jointmodel.Part(name='Bolt', dimensionality=THREE_D,
    type=DEFORMABLE_BODY)
p = Jointmodel.parts['Bolt']
p.BaseSolidRevolve(sketch=s1, angle=360.0, flipRevolveDirection=OFF)
del Jointmodel.sketches['__profile__']
```

B.4.1.7. FINAL REMARKS ON THE CREATION OF THE PARTS

All necessary parts of the MRF sub-assembly possessing the end-plate joint are covered in the code. It is recommended to define a list with the parts names, to be used in subsequent blocks of code, need for instance in the generation of the finite element mesh.

```
# Parts list
parts_list = [Column+'_Wire_Bot', Column+'_Wire_Top', Beam+'_Wire', Column, Beam,
    'End-Plate', 'Bolt']
```

B.4.2. CREATE THE MATERIAL PROPERTIES

As discussed in the Chapter 3 the material properties may be different even in the same member (beam or column). Normally, in an H or I section, the properties of the web are different from the flanges. A fact related to the lamination process. The material properties of the welded zones may also be different from the material properties of the connected plates. For the wire members it is not possible to assign different types of material on the same cross-section. Therefore an average of the material properties of the flanges and web should be assigned to

the parts. On the other hand, in the solid parts, the partitions created previously should allow the assignment of different material properties for different regions.

In ABAQUS the materials defined are not directly assigned to the parts of the FE model. They are first associated to a *Section*, where the type of element shape is defined (solid, shell or beam). In the case of a shell the thickness of the plate should also be defined, and in the case of a beam a *Profile* (cross-section) should also be assigned. First a list of the regions of the joint that have different material properties is defined, for a sequential generation of the material properties.

```
regions_name = [Column+'_Wire', Beam+'_Wire', Column+'_Flange', Column+'_Web',
                Beam+'_Flange', Beam+'_Web', 'End-Plate', 'Bolts', 'Stiffeners',
                'Welds']

# Materials => Wire Column and Wire Beam
for i in range(0,2):
    Jointmodel.Material(name=regions_name[i])
    Jointmodel.materials[regions_name[i]].Density(table=((steel_density, ), ))
    Jointmodel.materials[regions_name[i]].Elastic(table=((young_m[i],
                poisson[i]), ))
    Jointmodel.materials[regions_name[i]].Plastic(table=plastic_t[i])

# Materials => Remaining Regions
for i in range (2, len(regions_name)):
    Jointmodel.Material(name=regions_name[i])
    Jointmodel.materials[regions_name[i]].Density(table=((steel_density, ), ))
    Jointmodel.materials[regions_name[i]].Elastic(table=((young_m[i],
                poisson[i]), ))
    Jointmodel.materials[regions_name[i]].Plastic(hardening=COMBINED,
                dataType=PARAMETERS, table=(plastic_t[i], ))
    Jointmodel.materials[regions_name[i]].Damping(beta=damping_Bk[i])
```

B.4.3. CREATE THE MODEL PROFILES AND SECTIONS

B.4.3.1. CREATE THE WIRE PROFILES

As explained earlier the beam elements requires the definition of a cross-section for the wire. ABAQUS has already some predefined shapes that can be used, “I” shape is one of them.

It is also recommended in this case to define a list of a profiles for future use in further blocks of code.

```
# CREATE THE WIRE PROFILES
Jointmodel.IProfile(name=Column, l=hc/2.0, h=hc, b1=bc, b2=bc,
    t1=afc, t2=afc, t3=twc-tswp)
Jointmodel.IProfile(name=Beam, l=hb/2.0, h=hb, b1=bb, b2=bb,
    t1=afb, t2=afb, t3=twb)

profiles_list = [Column, Beam]
```

B.4.3.2. CREATE AND ASSIGN THE SECTIONS

For each different material property created a section is defined, taking into account the profiles created for the beam parts. Then the sections are assigned to each region. The assignment of the section depends on the number of the regions created, defined by the partitions. It is, therefore, important to guarantee that every region is selected and a section is assigned to it. This is probably the task that requires more attention, at least for the column and end-plate parts, remember that the partitions will depend on the number of bolt rows. For that reason a loop ranging all bolt rows is required, and probably some conditions should be formulated, depending on the spacing between the bolts rows and the number of partitions allowed on it. A few examples are described hereafter.

```
# CREATE SECTIONS
sections_name = [Column+'-Wire_S', Beam+'-Wire_S', Column+'-Flange_S',
    Column+'-Web_S', Beam+'-Flange_S', Beam+'-Web_S',
    'End-Plate_S', 'Bolts_S', 'Stiffeners_S', 'Welds_S']
for i in range (0, len(profiles_list)):
    Jointmodel.BeamSection(name=sections_name[i],
        integration=DURING_ANALYSIS, poissonRatio=0.0, profile=profiles_list[i],
        material=regions_name[i], temperatureVar=LINEAR,
        consistentMassMatrix=False)
for i in range (len(profiles_list), len(sections_name)):
    Jointmodel.HomogeneousSolidSection(name=sections_name[i],
        material=regions_name[i], thickness=None)

# Assignment of the sections
```

```

# Bottom wire column
p = Jointmodel.parts[Column+'_Wire_Bot']
e = p.edges
edges = e.findAt(((Lc3/3.0, 0.0, 0.0), ))
region = regionToolset.Region(edges=edges)

p = Jointmodel.parts[Column+'_Wire_Bot']
p.SectionAssignment(region=region, sectionName=sections_name[0], offset=0.0,
    offsetType=MIDDLE_SURFACE, offsetField='', thicknessAssignment=FROM_SECTION)

# Solid Column
# Determine the cells to assign the FLANGE regions
# For regions around the bolts
n_lines = 0
for i in range(0, len(pcv)):
    if pcv[i] > 0:
        n_lines = n_lines+1

z_level_f = [0.0, Lc2] # Level of the regions in the flanges
z_level_b = [0.0]*(len(h_stiff)+2)
count2 = -1.0
dist_sup = 0.0

for i in range(0, len(pcv)):
    dist_sup = dist_sup + pcv[i]
    if pcv[i] > 0:
        # Selects the regions immediately above the bolts
        z_level_f.append (Lc2-dist_sup + (datum_point_z_coor[i] -
            (Lc2-dist_sup))/2.0)
        # Selects the regions immediately below the bolts
        z_level_f.append (Lc2-dist_sup - ((Lc2-dist_sup) -
            datum_point_z_coor[i+n_lines])/2.0)
        # Selects the regions immediately after the upper partitions around bolts
        z_level_f.append (datum_point_z_coor[i] + ags[3]/10.0)
        # Selects the regions immediately after the lower partitions around bolts
        z_level_f.append (datum_point_z_coor[i+n_lines] - ags[3]/10.0)

```

(...)

B.4.4. DEFINE THE WIRE ORIENTATIONS

The local axes of the wire parts need to be defined, setting the corresponding orientation.

```
# WIRE PROFILES
# Bottom wire column
p = Jointmodel.parts[Column+'_Wire_Bot']
e = p.edges
edges = e
region=regionToolset.Region(edges=edges)

p = Jointmodel.parts[Column+'_Wire_Bot']
p.assignBeamSectionOrientation(region=region, method=N1_COSINES,
    n1=(0.0, 0.0, -1.0))
(...)
```

B.4.5. CREATE THE MESH

For each part an independent mesh should assigned. First is defined the element type, defined by the user in the list *element_code*. Then using the function *findAt* a point of the part is selected, and the approximate mesh size is determined using the lists *size*, *df* and *sf*. Finally the instruction to generate the mesh is given for each part. Remember that is necessary to guarantee the number of elements in the thickness of the plated regions of the sections, according to the list *esf*, defined by the user. Note that, after the mesh generation the round regions become polygons. This is particularly important for the bolts and the bolts holes. If the clearance of the hole is not enough the mesh of the bolts can intersect the mesh of the bolts, creating convergence difficulties. For that an algorithm was developed, that determines the number of seeds in the bolts holes to avoid geometrical intersections, according to the mesh of the parts. See the code examples:

```
# Mesh => Wire Top Column
p1 = Jointmodel.parts[Column+'_Wire_Top']
session.viewports['viewport: 1'].setValues(displayedObject=p1)
elemType1 = mesh.ElementType(elemCode=elem_code[1], elemLibrary=STANDARD)
p = Jointmodel.parts[Column+'_Wire_Top']
e = p.edges
edges = e.findAt(((Lc1/3.0, 0.0, 0.0), ))
```



```

pickedRegions =(edges, )
p.setElementType(regions=pickedRegions, elemTypes=(elemType1, ))
p = Jointmodel.parts[Column+'_Wire_Top']
p.seedPart(size=ags[1], deviationFactor=df[1], minSizeFactor=sf[1])
p = Jointmodel.parts[Column+'_Wire_Top']
p.generateMesh()

# Mesh => Solid Column
try:
    p = Jointmodel.parts[Column]
    c = p.cells
    pickedRegions = c
    p.setMeshControls(regions=pickedRegions, elemShape=HEX, technique=STRUCTURED)
except:
    print "Not all elements of the column are Hex!"

elemType1 = mesh.ElementType(elemCode=eval(elem_code[3][0]), elemLibrary=STANDARD)
elemType2 = mesh.ElementType(elemCode=eval(elem_code[3][1]), elemLibrary=STANDARD)
elemType3 = mesh.ElementType(elemCode=eval(elem_code[3][2]), elemLibrary=STANDARD)
p = Jointmodel.parts[Column]
c = p.cells
cells = c
pickedRegions =(cells, )
p.setElementType(regions=pickedRegions, elemTypes=(elemType1, elemType2,
    elemType3))

# Seed part
p = Jointmodel.parts[Column]
p.seedPart(size=ags[3], deviationFactor=df[3], minSizeFactor=sf[3])

# Seed edges
p = Jointmodel.parts[Column]
e = p.edges
pickedEdges = e.findAt(((0.0, tfc/3.0, Lc2), ),
    ((0.0, hc-tfc/3.0, Lc2), ),
    ((bc/2.0, tfc, Lc2), ))
p.seedEdgeByNumber(edges=pickedEdges, number=int(esf[0]), constraint=FINER)

```

B.4.6. ASSEMBLY OF THE MODEL PARTS

The script is now able to create, assign properties and mesh to the several parts that constitute the beam-to-column model. Now is necessary to perform the assembly of all the parts. For that is necessary to create *Instances* associated to each parts. The instances are rotated and positioned using the coordinate system. Note that is possible to create several instances of the same part, which is the case of the bolts, according to following example.

```
# Solid Bolts
dist_sup_c = 0.0
x_cir = (dp0/2.0)*math.cos(math.pi/4.0)
y_cir = (dp0/2.0)*math.sin(math.pi/4.0)

for i in range(0, len (pcv)):
    dist_sup_c = dist_sup_c + pcv[i]
    if ppv[i] > 0:
        dist_left_p = 0.0
        for j in range(0, len (pph)-1):
            dist_left_p = dist_left_p + pph[j]
            if pph[j] > 0:
                a = Jointmodel.rootAssembly
                p = Jointmodel.parts['Bolt']
                a.Instance(name='Bolt-'+str(i+1)+'-'+str(j+1), part=p,
                    dependent=ON)
                a = Jointmodel.rootAssembly
                a.rotate(instanceList=('Bolt-'+str(i+1)+'-'+str(j+1), ),
                    axisPoint=(0.0, 0.0, 0.0),
                    axisDirection=(0.0, 1.0, 0.0), angle=90.0)
                a = Jointmodel.rootAssembly
                v1 = a.instances['Bolt-'+str(i+1)+'-'+str(j+1)].vertices
                e1 = a.instances['End-Plate-1'].edges
                a.CoincidentPoint(movablePoint=v1.findAt(coordinates=(0.0,
                    0.0, -(bh+tf+tp))),
                    fixedPoint=a.instances['End-Plate-1'].InterestingPoint(
                    edge=e1.findAt(
                    coordinates=(bp/2.0+ecc_p-dist_left_p-x_cir,
                    h1+Lc3+Lc2-dist_sup_c+y_cir, -(hc/2.0+tp))), rule=CENTER))
```

```

        else:
            break
    else:
        break

```

B.4.7. CREATE THE PRE-DEFINED SETS

As described previously it is necessary to define several pre-defined nodes in the mesh, see Figure 3.21, where the displacements are extracted to determine the rotations and deformations of the joint and components. The code to generate the set for DT1 is described hereafter. Note that the sets are then saved in a list to be used in the post-processing phase. It is recommended to determine the relevant properties and distances, and save them in a text file to ease the data treatment.

```

# Create a set for DT1
list_sets_column = []

a = Jointmodel.rootAssembly
v1 = a.instances[Column+ '-1'].vertices
verts1 = v1.findAt(((twc/2.0, h1+h3+hb/2.0, 0.0), ))
a.Set(vertices=verts1, name='DT1-U3')
list_sets_column.append(((twc/2.0, h1+h3+hb/2.0, 0.0), ))

```

B.4.8. CREATE THE STEPS

The step *Initial* is generated automatically, where the initial boundary conditions are generated, see Section 3.2.3.2 point iv). The first step created is for pre-stressing the bolts. This step is common to all subsequent analysis. For each step created is necessary to indicate the previous one, in this case is the step *Initial*. The second step may be a frequency analysis, a static analysis (monotonic or cyclic) or a dynamic analysis. A condition is created to determine the type of analysis, according to the list *analysis_type*. In the case of a static analysis another condition is required to define the use of stabilization methods, according to the *stab_magnitude* instructions.

```

# Step 1 - Prestressing_bolts
Jointmodel.StaticStep(name='S1-Prestressing_bolts',
    previous='Initial', description='Bolts Prestressing',

```

```
maxNumInc=max_num_inc,  
initialInc=initial_inc,  
nlgeom=ON)  
session.viewports['Viewport: 1'].assemblyDisplay.setValues(  
step='S1-Prestressing_bolts')  
Jointmodel.steps['S1-Prestressing_bolts'].setValues(  
timePeriod=time_period, maxInc=time_period)  
  
# Step 2 - Extract the analysis frequencies  
if analysis_type[0] == 1:  
    Jointmodel.FrequencyStep(name='S2-Frequency',  
        previous='S1-Prestressing_bolts', description='Extract the analysis  
        frequencies', maxEigen=max_num_freq)  
    session.viewports['Viewport: 1'].assemblyDisplay.setValues(  
        step='S2-Frequency')  
  
# Step 3 - Monotonic/Cyclic analysis according to the loading protocol  
if analysis_type[1] == 1:  
    Jointmodel.StaticStep(name='S3-Cyclic',  
        previous='S1-Prestressing_bolts',  
        description='Cyclical analysis according to the loading protocol',  
        timePeriod=time_period  
        maxNumInc=max_num_inc,  
        initialInc=initial_inc,  
        minInc=min_inc_size,  
        maxInc=max_inc_c  
        nlgeom=ON)  
    session.viewports['Viewport: 1'].assemblyDisplay.setValues(step='S3-Cyclic')  
    if stab_magnitude[0] > 0:  
        Jointmodel.steps['S3-Cyclic'].setValues(  
            stabilizationMagnitude=stab_magnitude[0],  
            stabilizationMethod=DAMPING_FACTOR, continueDampingFactors=False,  
            adaptiveDampingRatio=stab_magnitude[1])  
  
# Step 4 - Dynamic analysis using records accelerograms  
if analysis_type[2] == 1:  
    Jointmodel.ImplicitDynamicsStep(name='S4-Dynamic',
```

```

previous='S1-Prestressing_bolts',
description='Dynamic analysis using records accelerograms',
timePeriod=time_period_dy,
maxNumInc=max_numb_inc,
initialInc=initial_inc,
minInc=min_inc_size,
maxInc=max_inc,
nohaf=OFF,
nlgeom=ON)

session.viewports['viewport: 1'].assemblyDisplay.setValues(step='S4-Dynamic')

```

B.4.9. DEFINE THE FIELD AND HISTORY OUTPUT REQUEST

ABAQUS requires the definition of the field output and history output request, for each step created, before the analyses. Otherwise the results are not recorded in the output file (*.odb). The script is prepared to collect the information in all nodes and elements or only in the sets defined previously. A condition should be defined with the instruction given by the variable *output*. An example is given for the step 1, hereafter.

```

# For step 1
Jointmodel.fieldOutputRequests.changeKey(fromName='F-Output-1',
toName='F-Output-S1')
if output == 0:
    Jointmodel.fieldOutputRequests['F-Output-S1'].setValuesInStep(
        stepName='S1-Prestressing_bolts', variables=('S', 'E', 'U'))
elif output == 1:
    regionDef=Jointmodel.rootAssembly.sets['ALL_DTS']
    Jointmodel.fieldOutputRequests['F-Output-S1'].setValues(
        variables=('S', 'E', 'U'), region=regionDef, sectionPoints=DEFAULT,
        rebar=EXCLUDE)
else:
    print "Wrong input in the 'output' value, should be 0 or 1"

```

B.4.10. CREATE THE BOUNDARY CONDITIONS

The boundary conditions are applied to the model, according to the scheme depicted in Figure B.3. As an example, for the bottom support, the code is as follows:

```

a = Jointmodel.rootAssembly
r1 = a.instances['Bot-Support'].referencePoints
refPoints1=(r1[1], )
region = regionToolset.Region(referencePoints=refPoints1)
Jointmodel.DisplacementBC(name='Sup_column_base',
    createStepName='Initial', region=region, u1=SET,
                                u2=SET,
                                u3=SET,
                                ur1=UNSET,
                                ur2=SET,
                                ur3=SET,
    amplitude=UNSET, distributionType=UNIFORM, fieldName='', localCsys=None)

```

B.4.11. DEFINE THE LOADS APPLICATION

The first load to be applied is the pre-stress of the bolts. The amount of pre-stress is determined by a percentage of the ultimate bolts force. The Hooke's law is used to determine the reduced length in the bolts required to achieve that stress state. Then is necessary to define for each subsequent step the *Fix Length* method.

For the static loading the boundary condition associated to the beam tip is modified and a displacement is imposed in the direction 2 (Y). This imposed displacement is associated to a history of amplitudes, defined in a tabular form. It is recommended to use an external *.txt* file with the required amplitudes. Then with a loop fill the amplitudes table.

For the dynamic analysis first is necessary to create a point mass, available in the menu engineering features. Note that in Chapter 6 the mass is determined using an algorithm that runs frequency analysis, with successive increments of mass, to determine the mass corresponding to specific predefined frequency. Then an additional boundary condition is created in the bottom support of the column. The boundary condition is of the type *Acceleration*. In the direction A2 the gravitational acceleration is defined, associated to an amplitude (defined previously in a tabular form) that corresponds to the selected accelerogram.

B.4.12. CREATE THE CONSTRAINTS AND INTERACTIONS

The several instances need to be connected to each other through *Constraints*, in the case of instances with continuity to others. The wire column are tied to the solid column, the beam is tied to the end-plate through the welds, etc. On the other hand, the instances can interact with each other by non-linear contact (*Interactions*). Bolts interact with the column flange and the end-plate, or the end-plate is in contact with the column flange. Both for constraints or interactions slave and master regions should be selected. The master surface should be the one with the biggest elements dimension or the hardest one. As in the assignment of the sections, also here, due to the several regions created by the partitions, the assignment of the master and slave regions should be carefully planned. The function *findAt* is the best tool to pick the region, by simply select a mesh point of that region.

To connect the wire instances to the solid ones the function *MPC* (multi point constraint) is used. For the connection of the end-plate to the beam the function *tie* is used.

For the interactions first is necessary to define the contact properties, normal and tangential. Then using the function *surface to surface contact* the slave and master regions are selected and the defined contact properties are assigned.

```
# Multi Point Constraint between the wire bottom column and the solid column
a = Jointmodel.rootAssembly
v1 = a.instances[Column+'_wire_Bot-1'].vertices
verts1 = v1.findAt(((0.0, h1+Lc3, 0.0), ))
region1=regionToolset.Region(vertices=verts1)
a = Jointmodel.rootAssembly
f1 = a.instances[Column+'-1'].faces
faces1 = f1.findAt(((bc/2-(bc/2.0-twc/2.0-rtc)/2.0, h1+Lc3, hc/2.0-tfc/2.0), ),
                  ((twc/2.0+rtc/2.0, h1+Lc3, hc/2.0-tfc/2.0), ),
                  (...),
                  ((-bc/2.0, h1+Lc3, -(hc/2.0-tfc/2.0)), ))
region2=regionToolset.Region(faces=faces1)
Jointmodel.MultipointConstraint(name='MPC_Bottom_Column',
                                controlPoint=region1, surface=region2, mpcType=BEAM_MPC,
                                userMode=DOF_MODE_MPC, userType=0, csys=None)

# Define the Interaction Properties
Jointmodel.ContactProperty('Hard_contact')
```

```
Jointmodel.interactionProperties['Hard_contact'].TangentialBehavior(  
    formulation=PENALTY, directionality=ISOTROPIC, slipRateDependency=OFF,  
    pressureDependency=OFF, temperatureDependency=OFF, dependencies=0, table=((  
    friction_coeff, ), ), shearStressLimit=None, maximumElasticSlip=FRACTION,  
    fraction=0.005, elasticSlipStiffness=None)
```

B.4.13. CREATE THE JOB

After all the previous steps are defined and tested is necessary to create a job to run the analyses. The model is saved. In the end ABAQUS is instructed to run the job. If post processing options are also included in the script it is necessary to instruct ABAQUS to wait for completion, before the rest of the script is compiled.

```
# Create the job  
mdb.Job(name=m_name+'_J', model=m_name, description='',  
    type=ANALYSIS, atTime=None, waitMinutes=0, waitHours=0, queue=None,  
    memory=90, memoryUnits=PERCENTAGE, getMemoryFromAnalysis=True,  
    explicitPrecision=SINGLE, nodalOutputPrecision=SINGLE, echoPrint=OFF,  
    modelPrint=OFF, contactPrint=OFF, historyPrint=OFF, usersSubroutine='',  
    scratch='', multiprocessingMode=DEFAULT, numCpus=number_processors,  
    numDomains=number_processors)  
  
# Save the CAE model created  
try:  
    mdb.saveAs(pathName=m_path+'.cae')  
except:  
    print "CAE model name already exists! It wasn't saved for this iteration!!"  
  
# Run the job  
mdb.jobs[m_name+'_J'].submit(consistencyChecking=OFF)  
  
# Do not return control till job is finished running  
try:  
    mdb.jobs[m_name+'_J'].waitForCompletion()  
except:  
    pass
```



```
# Save the CAE model
mdb.save()
```

B.5. POST PROCESSING OPTIONS

To ease the extraction of the results some post processing actions can be incorporated in the script. First the *.odb* file is assessed and the corresponding data is written to a *.txt* file. In the end, to ease the data treatment the *.txt* file is converted to *.csv* file reading each line of the *.txt* file and write it to the *.csv* file. As an example the next code describes the instructions for extracting the results of the reaction forces in the beam end, for the static analysis.

```
if analysis_type[1] == 1:
    odb = session.odbs[m_name+'_J.odb']
    odbName=session.viewports[session.currentViewportName].odbDisplay.name
    session.odbData[odbName].setValues(activeFrames=((('S3-Cyclic', ('0:-1', )), ))

    # Reaction on the beam end
    odb = session.odbs[m_name+'_J.odb']
    xyList = xyPlot.xyDataListFromField(odb=odb, outputPosition=NODAL, variable=((
        'RF', NODAL, ((COMPONENT, 'RF2'), )), ), nodeSets=('DT20(a)', ))

    RF2_DT20 = session.xyDataObjects[session.xyDataObjects.keys()
        [len (session.xyDataObjects) -1]]

    # Convert the results for 'text' files
    # appendMode=OFF => in this first set of results to clear the data
    session.writeXYReport(fileName=m_name+'-RESULTS_C.txt', appendMode=OFF,
        xyData=(RF2_DT20))

    while(len(session.xyDataObjects)>0):
        del session.xyDataObjects[session.xyDataObjects.keys()[0]]
    (...)
    # Close the odb file
    session.odbs[m_name+'_J.odb'].close()
```

B.6. MAIN CONCLUSIONS

In this annex were described and explained the main steps for the development of the Python script of the beam-to-column end-plate joint finite element model. Note that the script has more than 5000 lines of code. It would be very lengthy to explain all the lines of code in here. In turn it was tried to explain with examples the main steps and also the biggest difficulties to develop it.

This script was used intensively during the entire research. More than 1500 models were run automatically using this script. For that a second script was developed where the properties of the group of joints to be analysed were defined in *lists*. A loop was then defined to run each one of the analysis, calling the first script, designated from now on as main script. For that the main script is defined as a function, where the function variables are the pre-defined properties of the joints.

It was in the assessment of the equivalent viscous damping, performed in Chapter 3, that this script was used with greater intensity. A large parametric study was conducted using the previous scheme. In this case, the mass was determined running frequency analysis, until a target frequency was achieved, with in a pre-defined tolerance. Then each joint typology was combined with each one of the twenty accelerograms selected. In the end the pre-defined results were saved in a *.csv* files, and the data was treated using prepared excel sheets. For that a VBA script was prepared to copy all generated data to the prepared excel sheets, and determine the EVD value for each ductility demand. It would be very difficult to perform all the analysis without the help of the scripts developed. However it is necessary to balance well the required time to perform the script with the benefits obtained with it. In this case the large time spent in the development of the beam-to-column joint script, was well employed.